LIPID METABOLISM AND HUMAN DISEASES, 2nd Edition

EDITED BY: Da-wei Zhang, Xian-Cheng Jiang and Kai Yin

PUBLISHED IN: Frontiers in Physiology

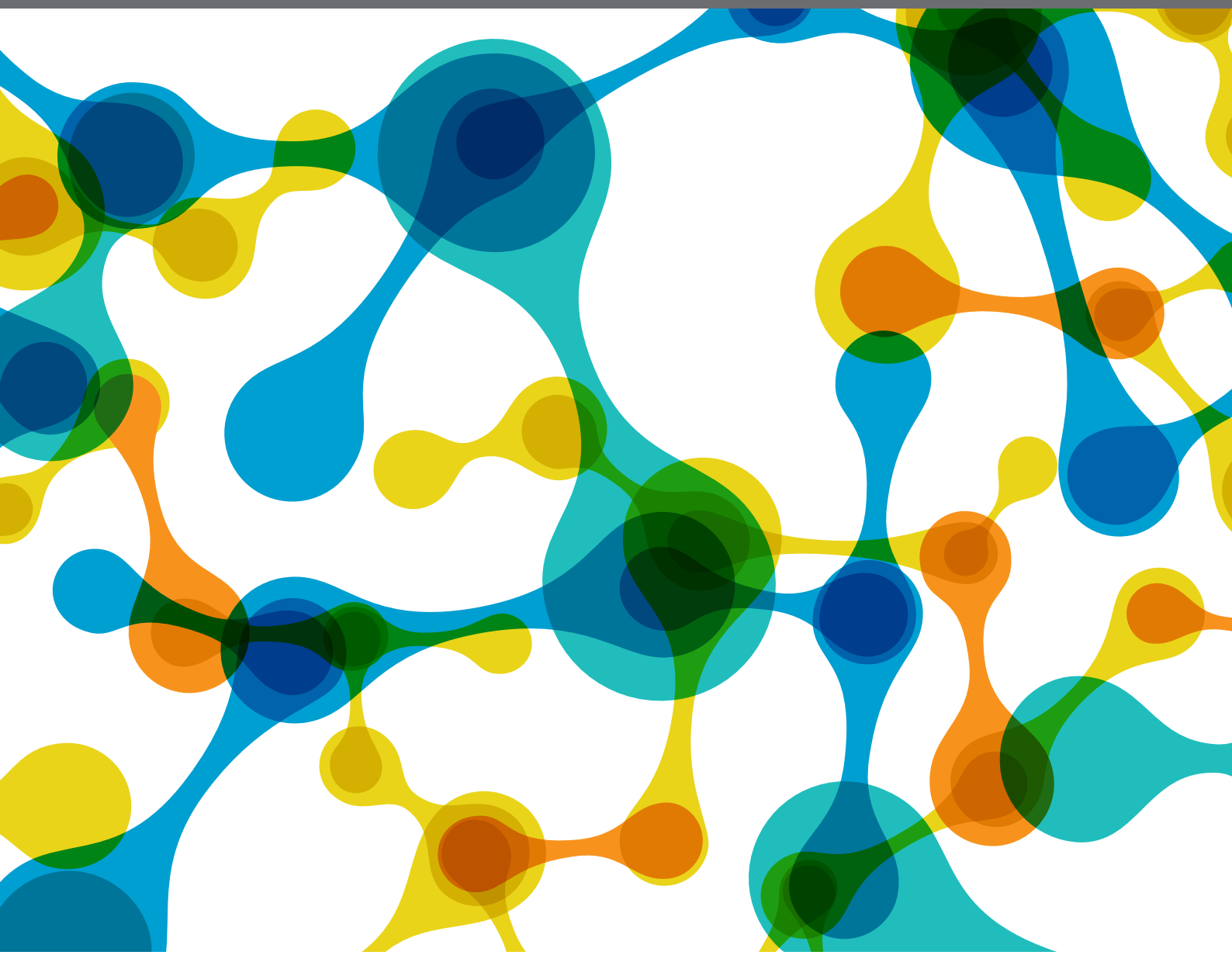

frontiers Research Topics

frontiers

ISSN 1664-8714
ISBN 978-2-8325-3624-7
DOI 10.3389/978-2-8325-3624-7

About Frontiers

Frontiers is more than just an open-access publisher of scholarly articles: it is a pioneering approach to the world of academia, radically improving the way scholarly research is managed. The grand vision of Frontiers is a world where all people have an equal opportunity to seek, share and generate knowledge. Frontiers provides immediate and permanent online open access to all its publications, but this alone is not enough to realize our grand goals.

Frontiers Journal Series

The Frontiers Journal Series is a multi-tier and interdisciplinary set of open-access, online journals, promising a paradigm shift from the current review, selection and dissemination processes in academic publishing. All Frontiers journals are driven by researchers for researchers; therefore, they constitute a service to the scholarly community. At the same time, the Frontiers Journal Series operates on a revolutionary invention, the tiered publishing system, initially addressing specific communities of scholars, and gradually climbing up to broader public understanding, thus serving the interests of the lay society, too.

Dedication to Quality

Each Frontiers article is a landmark of the highest quality, thanks to genuinely collaborative interactions between authors and review editors, who include some of the world's best academicians. Research must be certified by peers before entering a stream of knowledge that may eventually reach the public - and shape society; therefore, Frontiers only applies the most rigorous and unbiased reviews.
Frontiers revolutionizes research publishing by freely delivering the most outstanding research, evaluated with no bias from both the academic and social point of view. By applying the most advanced information technologies, Frontiers is catapulting scholarly publishing into a new generation.

What are Frontiers Research Topics?

Frontiers Research Topics are very popular trademarks of the Frontiers Journals Series: they are collections of at least ten articles, all centered on a particular subject. With their unique mix of varied contributions from Original Research to Review Articles, Frontiers Research Topics unify the most influential researchers, the latest key findings and historical advances in a hot research area! Find out more on how to host your own Frontiers Research Topic or contribute to one as an author by contacting the Frontiers Editorial Office: frontiersin.org/about/contact

LIPID METABOLISM AND HUMAN DISEASES, 2nd Edition

Topic Editors:
Da-wei Zhang, University of Alberta, Canada
Xian-Cheng Jiang, Downstate Health Sciences University, United States
Kai Yin, Guilin Medical University, China

Publisher's note: This is a 2nd edition due to an article retraction.

Citation: Zhang, D.-w., Jiang, X.-C., Yin, K., eds. (2023). Lipid Metabolism and Human Diseases, 2nd Edition. Lausanne: Frontiers Media SA.
doi: 10.3389/978-2-8325-3624-7

Table of Contents

frontiers | Frontiers in Physiology

TYPE Editorial
PUBLISHED 04 November 2022
DOI 10.3389/fphys.2022.1072903

OPEN ACCESS

EDITED AND REVIEWED BY
Nada A. Abumrad,
Washington University in St. Louis,
United States

*CORRESPONDENCE
Da-wei Zhang,
dzhang@ualberta.ca

SPECIALTY SECTION
This article was submitted to Lipid and Fatty Acid Research,
a section of the journal
Frontiers in Physiology

RECEIVED 18 October 2022
ACCEPTED 24 October 2022
PUBLISHED 04 November 2022

CITATION
Amadi PU, Gu H-M, Yin K, Jiang X-C and Zhang D-w (2022), Editorial: Lipid metabolism and human diseases.
Front. Physiol. 13:1072903.
doi: 10.3389/fphys.2022.1072903

Editorial: Lipid metabolism and human diseases

Peter U. Amadi[1], Hong-Mei Gu[1], Kai Yin[2], Xian-Cheng Jiang[3] and Da-wei Zhang[1]*

[1]Department of Pediatrics, Group on the Molecular and Cell Biology of Lipids, University of Alberta, Edmonton, AB, Canada, [2]Center for Diabetic Systems Medicine, Guilin Medical University, Guilin, China, [3]SUNY Downstate Health Sciences University, Brooklyn, NY, United States

KEYWORDS

low-density lipoprotein (LDL), metabolic-associated fatty liver disease, coronary artery ectasia, idiopathic pulmonary fibrosis (IDF), coronary artery ectasia (CAE), atherosclerotic cardiovascular disease (ASCVD)

Editorial on the Research Topic
Lipid metabolism and human diseases

The metabolism of lipids is crucial to several functional processes in the body, including the storage of energy, regulation of hormones, and transportation of nutrients. These processes are disrupted when lipids become dysregulated, leading to lipid disorders. The Research Topic, Lipid Metabolism and Human Diseases, presents a critical insight into the latest advances and progress made in cardiovascular disease research. The Research Topic featured eight original research articles and four reviews that advanced the understanding of how lipid metabolism contributes to metabolic disorders.

The biology of lipoproteins and their roles in the progression of cardiovascular disorders is well documented. Low-density lipoprotein (LDL) plays a central role during cardiovascular homeostasis and primarily mediates the initiation and progression of atherosclerotic cardiovascular disorders (ASCVD). LDL cholesterol (LDL-C) is the main biological marker for LDL and remains the clinical target for ASCVD treatment, despite the fact that ASCVD risks persist in some patients with moderate LDL-C levels (Cromwell et al., 2007). LDL-C stands for cholesterol content in LDL particles (LDL-Ps). Qiao et al., in their article, exhaustively discussed the preference and precision of LDL-Ps over LDL-C in the prognosis of ASCVDs. The prognostic accuracy of LDL-C is affected by variations in lifestyle and drug intervention among individuals, which is why traditional lipid-lowering drugs like statins significantly reduce LDL-C levels and less of LDL-P levels. The article by Qiao et al. further outlined the atherogenic mechanisms of the action of LDL by focusing on subclasses of LDL-Ps, including sdLDL and ox-LDL, summarized the analytical techniques used for their measurement, and examined the advances in using statins and PCSK9i as LDL-lowering therapies.

In addition to elucidating the molecular mechanisms of proteins and pathways relevant to lipid metabolism, this Research Topic also covered the metabolic roles of lipids in the pathogenesis of metabolism-associated fatty liver disease (MAFLD) (Jia et al.), Alcohol-Associated Fatty Liver (Ferdouse and Clugston), Coronary Artery Ectasias (Liu

et al.), Idiopathic Pulmonary Fibrosis (Geng et al.), and Prurigo Nodularis (Chu et al.). MAFLD, previously known as non-alcoholic fatty liver disease, occurs after significant accumulation of fats in the liver without any clear cause, like alcohol. Accumulation of triglycerides, impaired lipid metabolism, liver fibrosis and cirrhosis, non-alcoholic steatohepatitis (NASH), and in some cases, hepatocellular carcinoma are some common outcomes of MAFLD (Yki-Jarvinen et al., 2021). Of importance, MAFLD has been shown to share similar pathophysiological mechanisms with diabetes; however, establishing a common biomarker for both comorbidities has been arduous and inconclusive. Jia et al., in their study, have shown the suitability of monocyte to high-density lipoprotein cholesterol ratio (MHR) as a novel inflammatory biomarker. Through a rigorous and detailed study, they have established that T2DM patients with higher MHR have higher predisposition to be diagnosed with MAFLD.

Ferdouse and Clugston, in their article, proffered mechanistic insights on the mechanisms leading to ALD initiation, with a particular focus on hepatic lipid accumulation and the development of fatty liver. The article also strengthened the current understanding of how alcohol abuse impairs hepatic lipid metabolism. Lipid metabolism was reviewed in several transgenic models, including peroxisome proliferator-activated receptor γ (PPARγ) transgenic mice, and knockout mouse models of sterol regulatory element-binding protein 1 (Srebp1c), stearoyl–CoA desaturase-1 (SCD1), diglyceride acyltransferase (DGAT), and perilipin-2 (PLIN2). The article further highlighted the limitations associated with possible gender-based bias in earlier studies of AFD and other limitations like the use of low-fat/high carbohydrate Lieber-DeCarli (LDeC) liquid diet that may affect hepatic lipid accumulation pathways, and inducing whole body ablation of specific genes that may affect whole body lipid and hepatic lipid metabolism instead of liver specific knockouts.

Distinguishing the progression of coronary artery ectasia (CAE) from coronary artery disease (CAD) has been subject to extensive probing without any notable progress (Chou et al., 2022). However, Liu et al., in their study, used a targeted metabolomics approach to establish fatty acid biomarkers with high diagnostic performance for CAE progression from CAD. The study identified 35 promising metabolites of AA, EPA, and DHA that showed significant differences between CAE and CAD, out of which five of these biomarkers namely; 12-hydroxyeicosatetraenoic acid (12-HETE), 17(S)-hydroxydocosahexaenoic acid (17-HDoHE), EPA, AA, and 5-HETE, after rigorous screening showed the highest specificity for the diagnosis of CAE.

Idiopathic pulmonary fibrosis (IPF) is a fatal fibrotic disorder with no known cause (Sartiani et al., 2022). Geng et al. provided new insights into the role of fatty acid metabolism in the development of pulmonary fibrosis. The article provided extensive insights and expert opinions on the profibrotic processes that occur in distinct fibroblasts, macrophages, epithelial and lung cells. Aberrant fatty acid metabolism in the lungs and the contributory mechanisms leading to the overproduction of profibrotic lipids were well elucidated. The study further discussed the development of apoptosis and pro-fibrotic phenotypes in lung epithelial cells, and provided insights into the links between dysfunctional fatty acid metabolism and increased ER stress, macrophage polarization, and cytokines-induced fibroblast differentiation into myofibroblasts. In addition, some promising therapies that target the fatty acid metabolic pathway in idiopathic pulmonary fibrosis, and their possible mechanisms of action were well elucidated. Prurigo nodularis (PN), another chronic disease with unknown etiology, was also investigated by Chu et al. to understand how the severity of PN affects the levels of steroids. Using liquid chromatography-tandem mass spectrometry, they quantified the levels of cortisol, cortisone, testosterone, progesterone, and dehydroepiandrosterone (DHEA) in PN patients, matched to a control group. The study consistently showed a relationship between the levels of cortisol and cortisone and the severity of PN. This is the first study to demonstrate this relationship, therefore further studies can now target these biomarkers to achieve higher diagnostic accuracy for monitoring PN progression.

The study of Cao et al. investigated if the distribution of fatty acids in the sebum underpins the severity of acne among adolescents. It is well documented that inflammatory response and sebum production become elevated during acne. Earlier studies validated the hypothesis that variations in fatty acid distribution account for the inflammatory responses during acne (Zouboulis et al., 2014). However, until the study of Cao et al., the FA alterations in facial sebum remained to be clearly studied. The findings of the study showed the likelihood of the higher incidence of acne in females compared to males, may be due to the unique differences in fatty acid alteration in the facial sebum. Different anatomical sites in adult females showed altered fatty acid composition that inflamed the environment, mimicking the U-zone acne. These findings indicate that the development of gender- and site-specific therapeutic approaches for acne can target the levels of these specific fatty acids.

In conclusion, this Research Topic broadly covered various aspects of lipid metabolism and the consequences of impaired lipid metabolism. Expert insights were provided on the various pathophysiological mechanisms involved in the initiation and progression of different diseases associated with lipid metabolism, and in addition, current gaps in existing studies were highlighted. This Research Topic will thus become relevant in advancing both the current and future directions in providing new therapies for lipid disorders and the development of new diagnostic markers for lipid disorders.

Author contributions

PA wrote the first draft. H-MG, KY, and X-CJ provided helpful discussions and comments. D-wZ wrote the final version.

Funding

D-wZ was supported a grant from the Natural Sciences and Engineering Research Council of Canada (RGPIN-2016-06479), Canadian Institutes of Health Research (PS 178091, PS 155994), Grant-in-Aid from the Heart and Stroke Foundation of Canada (GIA G-22-0032022). PA was supported by a grant from Tertiary Education Trust Fund (TETFund, Nigeria - RES0059744).

Conflict of interest

The authors declare that the research was conducted in the absence of any commercial or financial relationships that could be construed as a potential conflict of interest.

Publisher's note

All claims expressed in this article are solely those of the authors and do not necessarily represent those of their affiliated organizations, or those of the publisher, the editors and the reviewers. Any product that may be evaluated in this article, or claim that may be made by its manufacturer, is not guaranteed or endorsed by the publisher.

References

Chou, E. L., Chaffin, M., Simonson, B., Pirruccello, J. P., Akkad, A. D., Nekoui, M., et al. (2022). Aortic cellular diversity and quantitative genome-wide association study trait prioritization through single-nuclear RNA sequencing of the aneurysmal human aorta. *Arterioscler. Thromb. Vasc. Biol.* 42 (11), 1355–1374. doi:10.1161/ATVBAHA.122.317953

Cromwell, W. C., Otvos, J. D., Keyes, M. J., Pencina, M. J., Sullivan, L., Vasan, R. S., et al. (2007). LDL particle number and risk of future cardiovascular disease in the framingham offspring study - implications for LDL management. *J. Clin. Lipidol.* 1, 583–592. doi:10.1016/j.jacl.2007.10.001

Sartiani, L., Bartolucci, G., Pallecchi, M., Spinelli, V., and Cerbai, E. (2022). Pharmacological basis of the antifibrotic effects of pirfenidone: Mechanistic insights from cardiac *in-vitro* and *in-vivo* models. *Front. Cardiovasc. Med.* 9, 751499. doi:10.3389/fcvm.2022.751499

Yki-Jarvinen, H., Luukkonen, P. K., Hodson, L., and Moore, J. B. (2021). Dietary carbohydrates and fats in nonalcoholic fatty liver disease. *Nat. Rev. Gastroenterol. Hepatol.* 18, 770–786. doi:10.1038/s41575-021-00472-y

Zouboulis, C. C., Jourdan, E., and Picardo, M. (2014). Acne is an inflammatory disease and alterations of sebum composition initiate acne lesions. *J. Eur. Acad. Dermatol. Venereol.* 28 (5), 527–532. doi:10.1111/jdv.12298

frontiers in Physiology

ORIGINAL RESEARCH
published: 19 November 2021
doi: 10.3389/fphys.2021.770223

Metabolomic Characterization of Fatty Acids in Patients With Coronary Artery Ectasias

Tianlong Liu[1,2†], Yingying Sun[1†], Hao Li[1], Haochen Xu[1], Ning Xiao[1], Xuliang Wang[1], Li Song[1], Congxia Bai[1], Hongyan Wen[1], Jing Ge[1], Yinhui Zhang[1], Weihua Song[3] and Jingzhou Chen[1]**

[1] State Key Laboratory of Cardiovascular Disease, Fuwai Hospital, National Center for Cardiovascular Diseases, Chinese Academy of Medical Sciences and Peking Union Medical College, Beijing, China, [2] Department of Pharmacy, Affiliated Hospital of Inner Mongolia Medical University, Hohhot, China, [3] Department of Cardiology, Fuwai Hospital, National Center for Cardiovascular Diseases, Chinese Academy of Medical Sciences and Peking Union Medical College, Beijing, China

OPEN ACCESS

Edited by:
Dawei Zhang,
University of Alberta, Canada

Reviewed by:
Andrew Carley,
The Ohio State University, United States
Paul "Li-Hao" Huang,
Fudan University, China

***Correspondence:**
Weihua Song
songweihua926@163.com
Jingzhou Chen
chendragon1976@aliyun.com

[†] These authors have contributed equally to this work

Specialty section:
This article was submitted to Lipid and Fatty Acid Research, a section of the journal Frontiers in Physiology

Received: 03 September 2021
Accepted: 21 October 2021
Published: 19 November 2021

Citation:
Liu T, Sun Y, Li H, Xu H, Xiao N, Wang X, Song L, Bai C, Wen H, Ge J, Zhang Y, Song W and Chen J (2021) Metabolomic Characterization of Fatty Acids in Patients With Coronary Artery Ectasias. Front. Physiol. 12:770223. doi: 10.3389/fphys.2021.770223

Background: We used a targeted metabolomics approach to identify fatty acid (FA) metabolites that distinguished patients with coronary artery ectasia (CAE) from healthy Controls and patients with coronary artery disease (CAD).

Materials and methods: Two hundred fifty-two human subjects were enrolled in our study, such as patients with CAE, patients with CAD, and Controls. All the subjects were diagnosed by coronary angiography. Plasma metabolomic profiles of FAs were determined by an ultra-high-performance liquid chromatography coupled to triple quadrupole mass spectrometric (UPLC-QqQ-MS/MS).

Results: Ninety-nine plasma metabolites were profiled in the discovery sets (n = 72), such as 35 metabolites of arachidonic acid (AA), eicosapentaenoic acid (EPA), and docosahexaenoic acid (DHA), 10 FAs, and 54 phospholipids. Among these metabolites, 36 metabolites of AA, EPA, and DHA showed the largest difference between CAE and Controls or CAD. 12-hydroxyeicosatetraenoic acid (12-HETE), 17(*S*)-hydroxydocosahexaenoic acid (17-HDoHE), EPA, AA, and 5-HETE were defined as a biomarker panel in peripheral blood to distinguish CAE from CAD and Controls in a discovery set (n = 72) and a validation set (n = 180). This biomarker panel had a better diagnostic performance than metabolite alone in differentiating CAE from Controls and CAD. The areas under the ROC curve of the biomarker panel were 0.991 and 0.836 for CAE versus Controls and 1.00 and 0.904 for CAE versus CAD in the discovery and validation sets, respectively.

Conclusions: Our findings revealed that the metabolic profiles of FAs in the plasma from patients with CAE can be distinguished from those of Controls and CAD. Differences in FAs metabolites may help to interpret pathological mechanisms of CAE.

Keywords: plasma metabolomic profiles, coronary artery ectasia, biomarkers, coronary artery disease, fatty acid metabolites

BACKGROUND

Coronary artery ectasia (CAE) is characterized as a diffuse, saccular, irregular, or fusiform dilation of the coronary arteries exceeding 1.5-fold the diameter of the normal adjacent vessel (Eitan and Roguin, 2016). The incidence of CAE was estimated to be 0.5–5%, with male predominance (Yetkin and Waltenberger, 2007). Previous studies reported that coronary luminal enlargement was considered an important reason for angiographic stigmata of impaired blood flow, such as sluggish circulation, swirling, strikingly slow, and scattered clearance of contrast material (Kruger et al., 1999). Indeed, some authors illustrated evidence of stable angina, positive treadmill test, increased levels of biochemical markers, or even myocardial infarction in isolated CAE without obstructive coronary artery disease (CAD), 38.7% of patients with isolated CAE were reported as having a history of myocardial infarction in the corresponding myocardial territory (Demopoulos et al., 1997; Sayin et al., 2001; Manginas and Cokkinos, 2006). More recently, in 2017, Takahito Doi's study found that the patients with isolated CAE had a significantly higher risk for cardiovascular events than patients without CAE (Doi et al., 2017). Besides, massive enlargement of the coronary artery cannot only result in compression of adjacent structures, vasospasm, thrombosis, and dissection, but also aneurysm rupture, albeit rare can cause acute cardiac tamponade (Kawsara et al., 2018). Therefore, it is clear that CAE, especially the giant ones, is not a benign disease.

Management of patients with CAE remained significant challenge for several reasons: the pathogenesis of CAE is largely unknown. Previous studies showed that 70–80% of CAE were attributed to atherosclerosis and genetic factors, whereas only 10–20% of CEA were associated with inflammatory or connective tissue diseases. Although degradation of the extracellular matrix, nitric oxide dysfunction, and abnormal matrix metalloproteinase activity was recognized as causes of CAE, detailed pathological mechanism still remains unclear (Bergman et al., 2007; Eitan and Roguin, 2016). Also, most CAEs are clinically silent and are only detected incidentally during coronary angiography or CT, while clinically symptomatic isolated CAE-induced myocardial infarction needs to perform percutaneous coronary interventions (Yip et al., 2002). Besides, no specific biomarker for CAE has yet been found, which also represents a huge barrier for further understanding of the mechanisms of CAE (Li et al., 2009).

Fatty acids (FAs) and metabolites played a critical role in the pathogenesis of CAE. Usama Boles's study found that serum FA metabolites were different in isolated CAE compared to atherosclerosis in mixed CAE, which suggested potentially specific pathophysiology in isolated CAE (Boles et al., 2017). Besides, abnormal FA metabolisms in plasma suggested alterations in lipid signaling in patients with CAE, especially in arachidonic acid (AA) and its metabolites (Zhang et al., 2014). Lipid signaling in the AA cascade is important for regulating some important biological processes, such as inflammation, blood flow, and plaque formation (Buczynski et al., 2009; Watkins and Hotamisligil, 2012). In addition to lipid signaling, FA metabolites, as a component of the phospholipid membrane, play an important role in cell signal transduction (Zeldin, 2001). Furthermore, a previous study showed that polyunsaturated FAs from P-450 metabolites of FAs could also regulate cardiac function and vascular tone (Roman, 2002).

Based on the important roles of FA metabolites in CAE formation, a targeted metabolomics approach was used to discover and subsequently validate the metabolic signatures of these FAs in plasma and to assess the performance of a biomarker signature to distinguish patients with CAE from healthy Controls and patients with CAD, which provided a theoretical basis for further interpreting pathological mechanism of CAE.

MATERIALS AND METHODS

Detailed methods are available in the online-only data **Supplementary Material**.

RESULTS

Study Design and Baseline Patient Characteristics

Two hundred and fifty-two participants were enrolled in the discovery and validation sets. The discovery sets included 72 participants, i.e., 24 participants with CAE and 48 sex-, age- and body mass index (BMI)-matched Controls and participants with CAD. For patients with CAD, the percentages of single-, double-, and multiple-vessel CAD were 29.16, 8.33, and 20.83%, respectively. The patients with CAE were diagnosed by coronary angiography, and CAE was defined as a localized dilatation in the diameter of a coronary artery segment that exceeded the luminal area of the adjacent normal coronary vessels by 1.5-fold. Controls were determined to not have CAE by coronary angiography. The baseline characteristics of the discovery sets are shown in **Table 1**. Validation sets included 180 participants, and the baseline characteristics of the participants are shown in **Supplementary Table 2**. The workflow of the study is presented in **Figure 1**.

Metabolic Profiles of Fatty Acids in Plasma From Different Subjects

To evaluate differences in FA metabolisms between subjects with CAE versus Controls or patients with CAD, we first performed metabolic profiling of FAs in plasma from different subjects. In total, 99 plasma metabolites were profiled in the discovery sets (n = 72), such as 35 metabolites of AA, eicosapentaenoic acid (EPA), and docosahexaenoic acid (DHA), 10 FAs, and 54 phospholipids (**Figure 2A**). For 35 metabolites of AA, EPA, and DHA, a total of 28 and 29 metabolites were significantly different between CAE versus Controls and CAE versus CAD, respectively ($P < 0.05$), although no significantly different metabolites were found between CAD versus Controls (**Figure 2B** and **Supplementary Table 3**). A total of 10, 5, and 3 phospholipids were significantly different between CAE versus Controls, CAE versus CAD, and CAD versus Controls, respectively ($P < 0.05$; **Supplementary Table 4**). A total of 3 and 4 FAs were significantly different between CAE versus Controls and CAE

TABLE 1 | Baseline characteristics of patients in the discovery sets.

	Controls	CAD	CAE	*p* Value for trend
n	**24**	**24**	**24**	
Age, yrs	54.42 ± 10.15	53.96 ± 11.17	54.58 ± 9.86	0.484
Men, %	66.7	66.7	66.7	
BMI, kg/m^2	26.25 ± 2.83	26.08 ± 3.11	26.67 ± 2.87	0.272
SBP, mm Hg	124.6 ± 14.86	128.2 ± 17.56	131.6 ± 20.46	0.350
DBP, mm Hg	79.29 ± 9.26	77.656 ± 12.36	82.38 ± 13.18	0.264
TC, mmol/L	4.19 ± 0.94	4.00 ± 1.09	4.15 ± 1.34	0.260
TG, mmol/L	1.41 ± 0.55	1.67 ± 1.08	1.53 ± 0.63	0.0043
HDL-C, mmol/L	1.12 ± 0.48	1.18 ± 0.87	0.99 ± 0.30	<0.0001
LDL-C, mmol/L	2.67 ± 0.90	2.52 ± 0.84	2.77 ± 1.17	0.248
Glucose, mmol/L	5.62 ± 1.55	5.83 ± 1.35	5.38 ± 1.08	0.240
Cigarette smoking, %				0.153
Never	39.13	62.5	37.5	
Current	60.89	37.5	62.5	
Alcohol intake, %				0.252
Never	52.17	79.17	60.54	
Current	47.83	20.83	39.46	
Hypertension history, %	66.67	62.50	70.83	0.829
DM history, %	12.50	12.50	8.33	0.869

Age, body mass index (BMI), Systolic (SBP) and diastolic (DBP) blood pressure, glucose, and TC values are given as means (±SD); TG values are medians (range), and the number of individuals (n) with percentage (n/N) are indicated. DM indicates Diabetes Mellitus. Body mass index is calculated as individual's body weight divided by the square of individual's height.

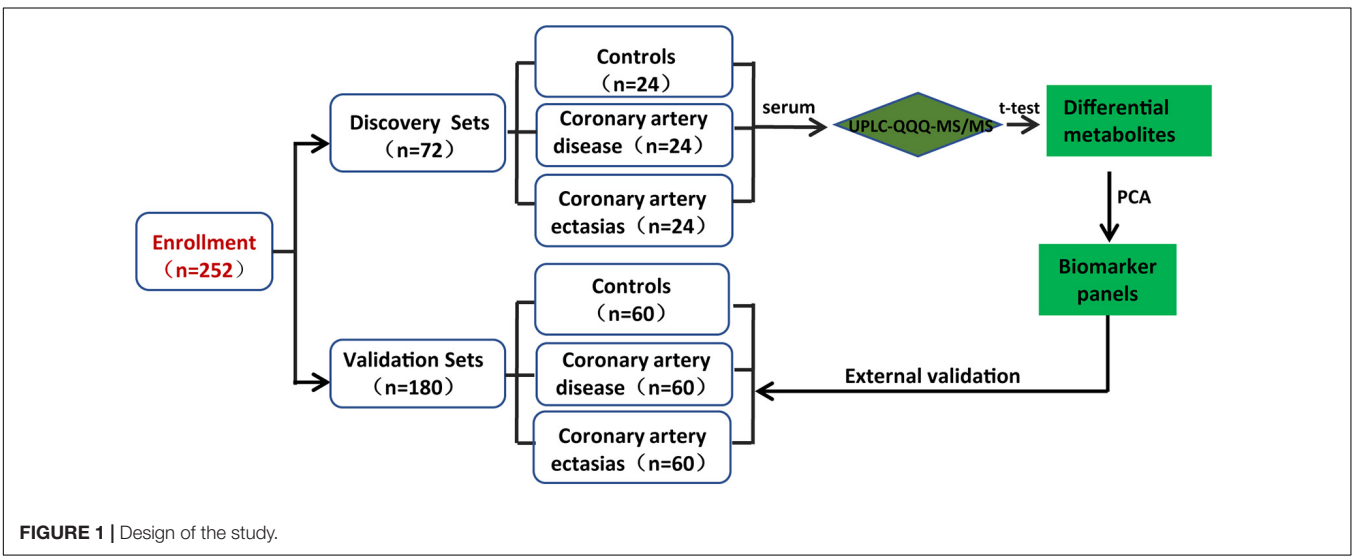

FIGURE 1 | Design of the study.

versus CAD, respectively ($P < 0.05$), however, no significantly different metabolites were found between CAD versus Controls (**Supplementary Table 5**). Therefore, 35 metabolites of AA, EPA, and DHA were emerged as the metabolites with the most significant differences between CAE and Controls or CAE and CAD compared with phospholipids and FAs.

Defining of a Potential Metabolic Biomarker for Coronary Artery Ectasia

Principal component analysis (PCA) score plots revealed that subjects with CAE were separated from Controls and subjects with CAD (**Figure 3A**). Fourteen and 15 metabolites with VIP (variable importance in projection) value > 1 on two principal components were found as important metabolites for distinguishing CAE from Controls and CAD, respectively (**Figure 3B** and **Supplementary Table 6**). Eight metabolites were screened as biomarker candidates via overlapping VIP value and *P*-value (**Figure 3C**). These metabolites were significantly increased in serum of patients with CAE compared with patients with CAD and Controls (**Figure 3D**). To further validate the eight biomarker candidates screened from the discovery sets, an independent validation set ($n = 180$) was used, and these

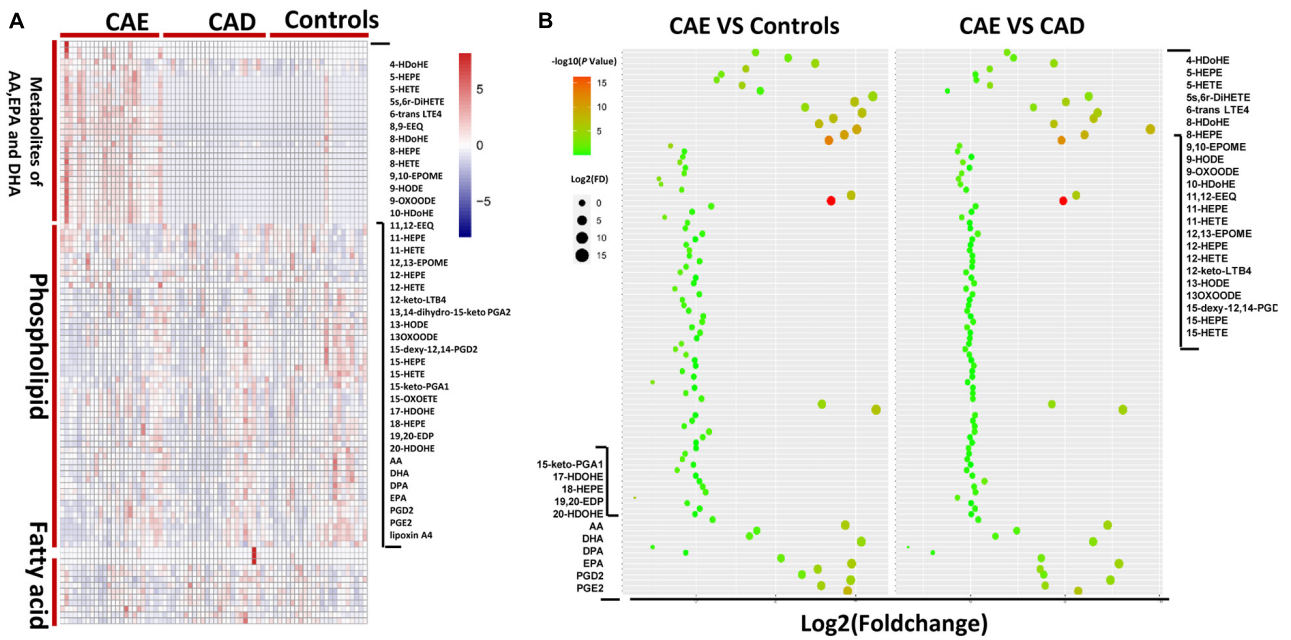

FIGURE 2 | Metabolic profiles of lipids in plasma from different subjects. **(A)** Comparison of 99 plasma metabolites concentrations in 72 discovery sets. **(B)** Fold change of 99 plasma metabolites in 72 discovery sets.

metabolites were detected by target metabolomics. The following criteria were satisfied to screen useful biomarkers: (1) $P < 0.05$ for CAE versus Controls and CAE versus CAD, respectively; and (2) having the same change trend as the discovery sets. Finally, five metabolites were screened: 12-hydroxyeicosatetraenoic acid (12-HETE), 17(*S*)-hydroxydocosahexaenoic acid (17-HDoHE), EPA, AA, and 5-HETE (**Supplementary Table 7**).

Validation of the Diagnostic Performance of the Biomarker Panel for Coronary Artery Ectasia

To further validate the diagnostic performance of the biomarker panel for CAE, a validation set (n = 180) was used. The serum concentrations of the biomarker panel are shown in **Figure 4A**. Biomarker panels were used to validate the diagnostic performance via a logistical regression model. The results showed that the biomarker panel had better diagnostic accuracy than signal metabolites for CAE. The areas under the ROC curve of the biomarker panel were 0.991 and 0.836 for CAE versus Controls, 1.00 and 0.904 for CAE versus CAD in the discovery and validation sets, respectively (**Figure 4B** and **Table 2**).

DISCUSSION

In our study, a target metabolomics approach was employed to analyze the metabolic profile characteristics of FAs in patients with CAE. PCA analysis showed good discrimination of CAE from Controls or CAD in the discovery sets by using 36 metabolites of AA, EPA, and DHA. Overall, a biomarker panel, such as 12-HETE, 17-HDoHE, EPA, AA, and 5-HETE, was identified for distinguishing CAE from Controls and CAD in the discovery. The diagnostic activity of the biomarker panel for distinguishing CAE from CAD and Controls was verified in the validation sets.

Although approximately half of CAE occurred due to atherosclerosis, a minority of cases was observed in the absence of a significant atherosclerotic lesion (Bilik et al., 2015). Patients with isolated CAE exhibited distinct clinical characteristics, such as more frequent involvement of the right coronary artery and a lower frequency of stent implantation (ElGuindy and ElGuindy, 2017). Moreover, patients with CAE coexisting with CAD had no additional risk of cardiovascular events compared to those with CAD only, however, even patients with isolated CAE had a significantly increased risk for cardiovascular events due to slow coronary blood flow, microemboli or thrombosis (Yetkin and Waltenberger, 2007). Besides, Usama Boles's study found that serum lipid profiles were different in isolated CAE compared to atherosclerosis in mixed CAE, which suggested potentially specific pathophysiology in isolated CAE (Boles et al., 2017). Therefore, it is not fully justified to conclude that CAE is a subtype of coronary atherosclerosis. However, the clinical presentation of CAE and CAD was similar, such as ischemic cardiomyopathy, unstable angina, and myocardial infarction. Therefore, healthy subjects and patients with CAD as Control were enrolled in our study, which was helpful to improve the accuracy and specificity of our results.

Unsaturated FAs and metabolites as potent endogenous mediators were involved in regulating various biological processes, such as inflammation, pain, and blood coagulation (Schuchardt et al., 2013). AA (C20:4) as omega-6 FAs, EPA (20:5 n-3), and DHA (22:6 n-3) as omega-3 FAs were essential

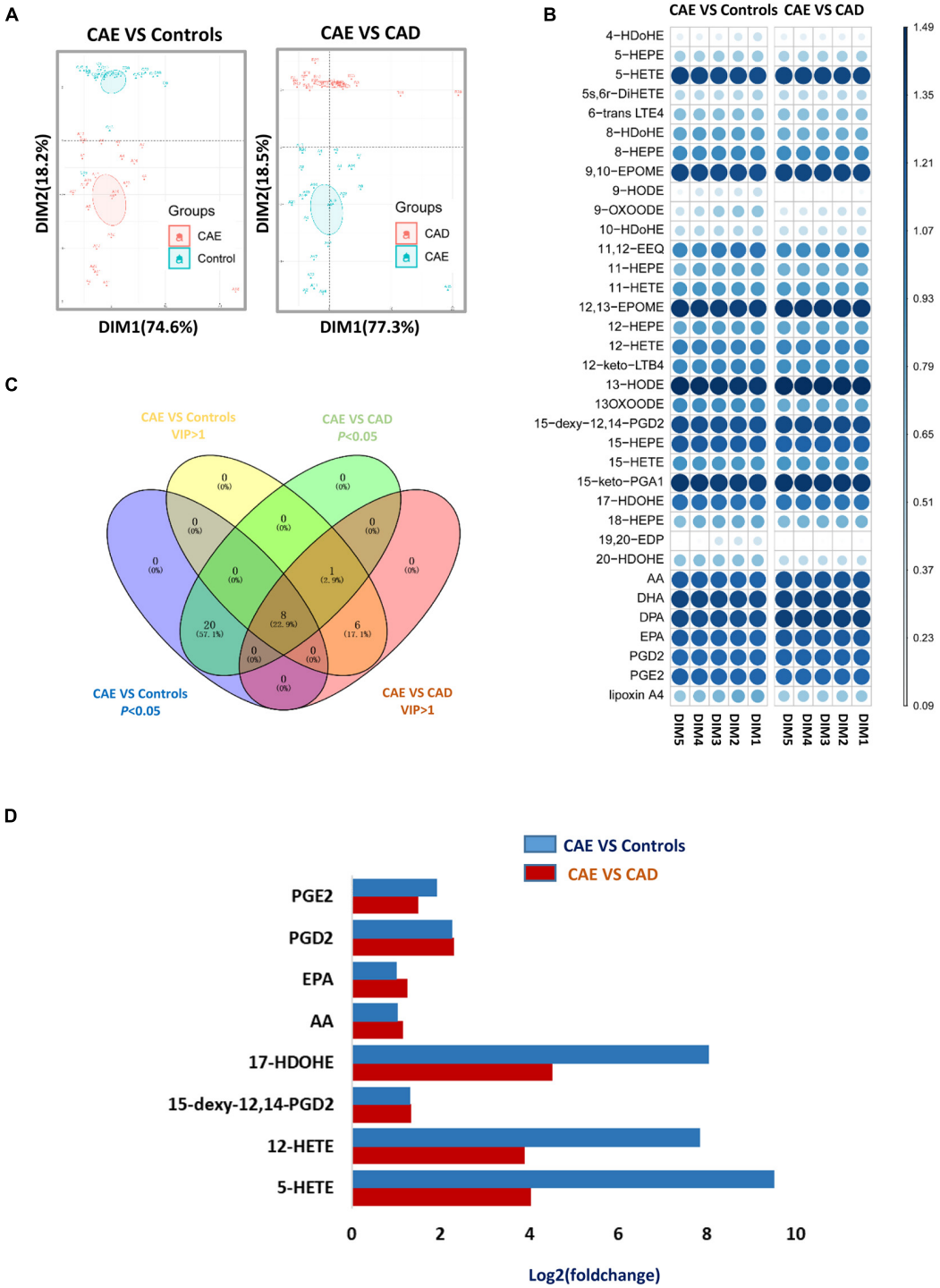

FIGURE 3 | Defining of a potential metabolic biomarker for CAE. **(A)** Score plot of the first (PC1) and second (PC2) PCs (horizontal and vertical axes, respectively) from principal component analysis of arachidonic acid metabolites in discovery sets. **(B)** VIP value of metabolites from PCA analysis in discovery sets. **(C)** Venn diagram shows an overlap between metabolites with VIP value > 1 and *P*-value < 0.05. **(D)** Fold change of eight serum metabolites from C in discovery sets. CAE, coronary artery ectasia; PCA, principal component analysis.

polyunsaturated FA and rely largely on the dietary intake for low conversion rate in adult (Brenna et al., 2009). AA, DHA, and EPA were catalyzed by lipoxygenases to form regio- and stereo-selective hydroperoxides and then were reduced to HETEs, HDoHE, and HEPEs (hydroxy-6E,8Z,11Z,14Z,17Z-eicosapentaenoic acid), respectively (Brash, 1999). Previous

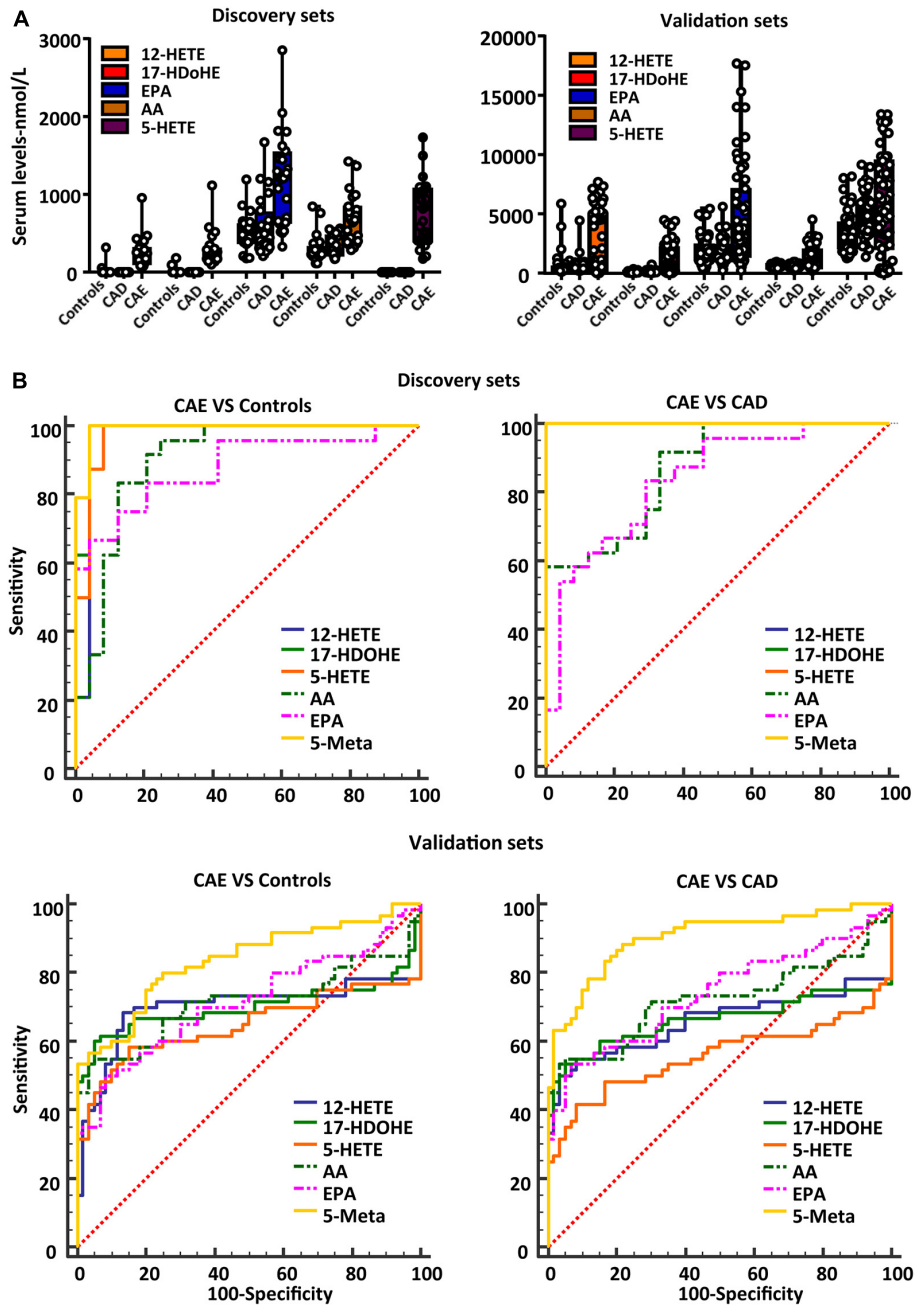

FIGURE 4 | Validating the diagnostic performance of the biomarker panel for CAE. **(A)** Serum concentrations of a defined biomarker panel in the discovery and validation sets. **(B)** ROC curves of biomarker panel and signal metabolites in discovery sets and validation sets. CAE, coronary artery ectasia.

studies showed that those oxylipins not only serve as precursors for leukotrienes and hepoxylins that played a critical role in regulating inflammation reaction and coagulation process, but also themselves and downstream products, such as oxo-ETE (oxo-6E,8Z,11Z,14Z-eicosatetraenoic acid) from HETEs could regulate various biological processes via G protein-coupled receptors pathway (Powell and Rokach, 2013). In our study, a significant increase in serum 12-HETE, 17-HDoHE, EPA, AA, and 5-HETE level was found in patients with CAE compared with patients with CAD and Controls, moreover, those metabolites as biomarker panel could be used to distinguish CAE from Controls and CAD in the discovery and validation sets.

Local alteration in coronary tone was involved in the pathological process of CAE (Yetkin and Waltenberger, 2007). Previous studies showed that vessel endothelial cells could synthesize and release CYP450-derived FA metabolites as endothelium-derived hyperpolarizing factors led to the

TABLE 2 | Results of measurement of the serum metabolite panel in the diagnosis of CAE.

	Discovery sets (*n* = 72)			Validation sets (*n* = 180)		
	AUC (95% CI)	**Sensitivity (%)**	**Specificity (%)**	**AUC (95% CI)**	**Sensitivity (%)**	**Specificity (%)**
CAE versus Controls						
12-HETE	0.967 (0.870–0.997)	100	98.5	0.698 (0.608–0.778)	68.3	86.7
17-HDoHE	0.984 (0.898–1.000)	100	95.8	0.703 (0.613–0.783)	60.0	96.7
AA	0.901 (0.780–0.968)	95.8	75.0	0.714 (0.624–0.793)	55.0	95.0
EPA	0.88 (0.754–0.956)	83.3	79.2	0.715 (0.625–0.793)	50.0	91.7
5-HETE	0.974 (0.881–0.999)	100	91.7	0.648 (0.555–0.733)	58.33	85.00
5-Meta	0.991 (0.910–1.000)	100	95.83	0.836 (0.757–0.897)	80.00	75.00
CAE versus CAD						
12-HETE	1 (0.926–1.000)	100	100	0.658 (0.566–0.742)	55.0	91.7
17-HDoHE	1 (0.926–1.000)	100	100	0.659 (0.566–0.743)	50.0	98.3
AA	0.868 (0.739–0.948)	58.3	100	0.721 (0.632–0.799)	55.0	95.0
EPA	0.837 (0.702–0.928)	83.3	70.8	0.739 (0.651–0.815)	55.3	93.3
5-HETE	1.00 (0.926–1.00)	100	100	0.558 (0.465–0.649)	41.67	91.67
5-Meta	1 (0.926–1.000)	100	100	0.904 (0.836–0.950)	86.67	80.00

CAE, coronary artery ectasia; CI, confidence interval; 5-Meta, serum metabolite panel.

hyperpolarization and relaxation of smooth muscle cells (SMC) by activating Ca^{2+}-dependent K^{+} channels and the Na-K-ATPase pathway (Malmsjo et al., 1999). Moreover, CYP450 inducers can regulate SMC hyperpolarization to relax the coronary artery by increasing the synthesis of FA metabolites (Fleming, 2000). Our targeted metabolic profile showed that the FA metabolites level in plasma was significantly increased in patients with CAE compared to those in Controls and patients with CAD. We speculated that those increased metabolites led to a local alteration in coronary tone by an endothelium-independent pathway (Nishikawa et al., 1999).

Fatty acid metabolites are closely associated with nitric oxide (NO) release, while NO overstimulation and medial thinning were important pathological mechanisms leading to CAE (Sorrell et al., 1996). FA metabolites as endothelium-derived hyperpolarizing factors could mediate endothelium-dependent relaxations via promoting endothelial nitric oxide synthase (eNOS) expression and NO release (Zuccolo et al., 2016). Indeed, EPA via upregulation of uncoupling protein 2 activates AMPKα1 resulting in increased endothelial nitric oxide synthase (NOS) phosphorylation and promoted NO release in aortic endothelial cells (Wu et al., 2012). Meanwhile, W. Raphael's study found that mRNA expression level of NOS_2 in leukocytes had a close association with plasma oxylipid concentrations, especially for 9-HODE and 13-HODE, while 13-HODE as a substrate was oxidized to the relatively stable 13-Oxo-ODE (Ramsden et al., 2012; Raphael et al., 2014). Our results showed that higher concentrations of FA metabolites in the peripheral blood of patients with CAE than in that of Controls and CAD might contribute to CAE formation via the NO pathway.

A previous study showed that 10–20% of CEA have been described in association with inflammatory or connective tissue diseases, while FAs and their derivatives link nutrient metabolism to inflammation reaction (Sonnweber et al., 2018). During the early phase of inflammation, AA is predominantly metabolized via 5-lipoxygenase (5-LOX), which produces pro-inflammatory leukotriene, such as leukotriene B4 (LTB4), whereas in the late phase prostaglandin E2, enhance 15-LOX expression, followed by a switch from LTB4 synthesis to 5-LOX and 15-LOX-mediated lipoxin A4 production, which contribute to local inflammation (Ho et al., 2010). A previous study showed that 5-LOX and 15-LOX were crucial enzymes that helped in the conversion of AA to 5-HETE (Sinha et al., 2019). In our study, AA, 17-HDoHE, and 5-HETE had a significant increase in the peripheral blood of patients with CAE compared to patients with CAD and Controls, these metabolites might contribute to CAE formation via an inflammatory pathway.

Another pathological mechanism of CAE is related to the metalloproteinase system (Manginas and Cokkinos, 2006). On the one hand, gene polymorphisms of matrix metalloproteinase (MMP)-3 were significantly different in patients with CAE compared to patients with coronary lesions. On the other hand, cardiac-specific over-expression of MMP-2 could induce CAE in mice (Dahi et al., 2011). 9-hydroxyoctadecadienoic acid (9-HODE) was reported to promoting the expression of metallopeptidase domain 17 to induce SMC apoptosis, extracellular matrix degradation, and necrotic core growth (Garbin et al., 2013; Vendrov et al., 2017). Recent studies have documented that 20-HETE as a CYP450-derived AA metabolite was correlated with increased elastin degradation by activating MMP-12 in Ang II-independent pathways (Soler et al., 2018). In addition to 20-HETE, 15-HETE could also induce MMP expression in vessel endothelial cells *in vivo* and *in vitro* (Prato et al., 2010; Liu et al., 2018). Therefore, FA metabolites may induce CAE formation by activating metalloproteinase.

In summary, the present study shows that the plasma FA profiles of patients with CAE could be seen as biomarkers to distinguish CAE from Controls and patients with CAD. Moreover, the diagnostic accuracy of the metabolic biomarkers was verified in the validation sets. Characterizing the metabolic

profile of FAs in the peripheral blood from patients with CAE may help to comprehend the underlying biological mechanisms of the disease.

DATA AVAILABILITY STATEMENT

The original contributions presented in the study are included in the article/**Supplementary Material**, further inquiries can be directed to the corresponding authors.

ETHICS STATEMENT

The studies involving human participants were reviewed and approved by the protocol was approved by the Institutional Review Board of Fuwai Hospital (Approval No: 2018-1066). All subjects gave written informed consent in accordance with the Declaration of Helsinki. The protocol was approved by the Fuwai Hospital. The patients/participants provided their written informed consent to participate in this study. The animal study was reviewed and approved by the protocol was approved by the Institutional Review Board of Fuwai Hospital (Approval No: 2018-1066). All subjects gave written informed consent in accordance with the Declaration of Helsinki. The protocol was approved by the Fuwai Hospital.

AUTHOR CONTRIBUTIONS

TL, YS, HL, and HX worked on sample preparation, data analysis, and drafted the manuscript. NX, XW, LS, CB, HW, and JG conducted sample management. YZ, WS, and JC worked on experimental design, sample management, data analysis, and manuscript preparation. All authors contributed to the article and approved the submitted version.

FUNDING

This study was funded by a grant from the Beijing Municipal Science and Technology Commission (Grant No. Z151100004015045) and Chinese Academy of Medical Sciences Innovation Found for Medical Sciences (CIFMS) (Grant No. 2020-I2M-C&T-B-056).

SUPPLEMENTARY MATERIAL

The Supplementary Material for this article can be found online at: https://www.frontiersin.org/articles/10.3389/fphys.2021.770223/full#supplementary-material

REFERENCES

Bergman, M. R., Teerlink, J. R., Mahimkar, R., Li, L., Zhu, B. Q., Nguyen, A., et al. (2007). Cardiac matrix metalloproteinase-2 expression independently induces marked ventricular remodeling and systolic dysfunction. *Am. J. Physiol. Heart Circ. Physiol.* 292, H1847–H1860. doi: 10.1152/ajpheart.00434.2006

Bilik, M. Z., Kaplan, I., Yildiz, A., Akil, M. A., Acet, H., Yuksel, M., et al. (2015). Apelin levels in isolated coronary artery ectasia. *Korean Circ. J.* 45, 386–390. doi: 10.4070/kcj.2015.45.5.386

Boles, U., Pinto, R. C., David, S., Abdullah, A. S., and Henein, M. Y. (2017). Dysregulated fatty acid metabolism in coronary ectasia: an extended lipidomic analysis. *Int. J. Cardiol.* 228, 303–308. doi: 10.1016/j.ijcard.2016.11.093

Brash, A. R. (1999). Lipoxygenases: occurrence, functions, catalysis, and acquisition of substrate. *J. Biol. Chem.* 274, 23679–23682. doi: 10.1074/jbc.274.34.23679

Brenna, J. T., Salem, N. Jr., Sinclair, A. J., Cunnane, S. C., and International Society for the Study of Fatty Acids and Lipids, ISSFAL (2009). alpha-Linolenic acid supplementation and conversion to n-3 long-chain polyunsaturated fatty acids in humans. *Prostaglandins Leukot. Essent. Fatty Acids* 80, 85–91. doi: 10.1016/j.plefa.2009.01.004

Buczynski, M. W., Dumlao, D. S., and Dennis, E. A. (2009). Thematic review series: proteomics. An integrated omics analysis of eicosanoid biology. *J. Lipid Res.* 50, 1015–1038. doi: 10.1194/jlr.R900004-JLR200

Dahi, S., Karliner, J. S., Sarkar, R., and Lovett, D. H. (2011). Transgenic expression of matrix metalloproteinase-2 induces coronary artery ectasia. *Int. J. Exp. Pathol.* 92, 50–56. doi: 10.1111/j.1365-2613.2010.00744.x

Demopoulos, V. P., Olympios, C. D., Fakiolas, C. N., Pissimissis, E. G., Economides, N. M., Adamopoulou, E., et al. (1997). The natural history of aneurysmal coronary artery disease. *Heart* 78, 136–141. doi: 10.1136/hrt.78.2.136

Doi, T., Kataoka, Y., Noguchi, T., Shibata, T., Nakashima, T., Kawakami, S., et al. (2017). Coronary artery ectasia predicts future cardiac events in patients with acute myocardial infarction. *Arterioscler. Thromb. Vasc. Biol.* 37, 2350–2355. doi: 10.1161/ATVBAHA.117.309683

Eitan, A., and Roguin, A. (2016). Coronary artery ectasia: new insights into pathophysiology, diagnosis, and treatment. *Coron. Artery Dis.* 27, 420–428. doi: 10.1097/MCA.0000000000000379

ElGuindy, M. S., and ElGuindy, A. M. (2017). Aneurysmal coronary artery disease: an overview. *Glob. Cardiol. Sci. Pract.* 2017:e201726. doi: 10.21542/gcsp.2017.26

Fleming, I. (2000). Cytochrome P450 2C is an EDHF synthase in coronary arteries. *Trends Cardiovasc. Med.* 10, 166–170. doi: 10.1016/s1050-1738(00)00065-7

Garbin, U., Baggio, E., Stranieri, C., Pasini, A., Manfro, S., Mozzini, C., et al. (2013). Expansion of necrotic core and shedding of Mertk receptor in human carotid plaques: a role for oxidized polyunsaturated fatty acids? *Cardiovasc. Res.* 97, 125–133. doi: 10.1093/cvr/cvs301

Ho, K. J., Spite, M., Owens, C. D., Lancero, H., Kroemer, A. H., Pande, R., et al. (2010). Aspirin-triggered lipoxin and resolvin E1 modulate vascular smooth muscle phenotype and correlate with peripheral atherosclerosis. *Am. J. Pathol.* 177, 2116–2123. doi: 10.2353/ajpath.2010.091082

Kawsara, A., Nunez Gil, I. J., Alqahtani, F., Moreland, J., Rihal, C. S., and Alkhouli, M. (2018). Management of coronary artery aneurysms. *JACC Cardiovasc. Interv.* 11, 1211–1223. doi: 10.1016/j.jcin.2018.02.041

Kruger, D., Stierle, U., Herrmann, G., Simon, R., and Sheikhzadeh, A. (1999). Exercise-induced myocardial ischemia in isolated coronary artery ectasias and aneurysms ("dilated coronopathy"). *J. Am. Coll. Cardiol.* 34, 1461–1470. doi: 10.1016/s0735-1097(99)00375-7

Li, J. J., Nie, S. P., Qian, X. W., Zeng, H. S., and Zhang, C. Y. (2009). Chronic inflammatory status in patients with coronary artery ectasia. *Cytokine* 46, 61–64. doi: 10.1016/j.cyto.2008.12.012

Liu, Y., Zhang, H., Yan, L., Du, W., Zhang, M., Chen, H., et al. (2018). MMP-2 and MMP-9 contribute to the angiogenic effect produced by hypoxia/15-HETE in pulmonary endothelial cells. *J. Mol. Cell. Cardiol.* 121, 36–50. doi: 10.1016/j.yjmcc.2018.06.006

Malmsjo, M., Bergdahl, A., Zhao, X. H., Sun, X. Y., Hedner, T., Edvinsson, L., et al. (1999). Enhanced acetylcholine and P2Y-receptor stimulated vascular EDHF-dilatation in congestive heart failure. *Cardiovasc. Res.* 43, 200–209. doi: 10.1016/s0008-6363(99)00062-0

Manginas, A., and Cokkinos, D. V. (2006). Coronary artery ectasias: imaging, functional assessment and clinical implications. *Eur. Heart J.* 27, 1026–1031. doi: 10.1093/eurheartj/ehi725

Nishikawa, Y., Stepp, D. W., and Chilian, W. M. (1999). In vivo location and mechanism of EDHF-mediated vasodilation in canine coronary microcirculation. *Am. J. Physiol.* 277(3 Pt 2), H1252–H1259.

Powell, W. S., and Rokach, J. (2013). The eosinophil chemoattractant 5-oxo-ETE and the OXE receptor. *Prog. Lipid Res.* 52, 651–665. doi: 10.1016/j.plipres.2013.09.001

Prato, M., Gallo, V., Giribaldi, G., Aldieri, E., and Arese, P. (2010). Role of the NF-kappaB transcription pathway in the haemozoin- and 15-HETE-mediated activation of matrix metalloproteinase-9 in human adherent monocytes. *Cell. Microbiol.* 12, 1780–1791. doi: 10.1111/j.1462-5822.2010.01508.x

Ramsden, C. E., Ringel, A., Feldstein, A. E., Taha, A. Y., MacIntosh, B. A., Hibbeln, J. R., et al. (2012). Lowering dietary linoleic acid reduces bioactive oxidized linoleic acid metabolites in humans. *Prostaglandins Leukot. Essent. Fatty Acids* 87, 135–141. doi: 10.1016/j.plefa.2012.08.004

Raphael, W., Halbert, L., Contreras, G. A., and Sordillo, L. M. (2014). Association between polyunsaturated fatty acid-derived oxylipid biosynthesis and leukocyte inflammatory marker expression in periparturient dairy cows. *J. Dairy Sci.* 97, 3615–3625. doi: 10.3168/jds.2013-7656

Roman, R. J. (2002). P-450 metabolites of arachidonic acid in the control of cardiovascular function. *Physiol. Rev.* 82, 131–185. doi: 10.1152/physrev.00021.2001

Sayin, T., Doven, O., Berkalp, B., Akyurek, O., Gulec, S., and Oral, D. (2001). Exercise-induced myocardial ischemia in patients with coronary artery ectasia without obstructive coronary artery disease. *Int. J. Cardiol.* 78, 143–149. doi: 10.1016/s0167-5273(01)00365-5

Schuchardt, J. P., Schmidt, S., Kressel, G., Dong, H., Willenberg, I., Hammock, B. D., et al. (2013). Comparison of free serum oxylipin concentrations in hyper- vs. normolipidemic men. *Prostaglandins Leukot. Essent. Fatty Acids* 89, 19–29. doi: 10.1016/j.plefa.2013.04.001

Sinha, S., Doble, M., and Manju, S. L. (2019). 5-Lipoxygenase as a drug target: a review on trends in inhibitors structural design, SAR and mechanism based approach. *Bioorg. Med. Chem.* 27, 3745–3759. doi: 10.1016/j.bmc.2019.06.040

Soler, A., Hunter, I., Joseph, G., Hutcheson, R., Hutcheson, B., Yang, J., et al. (2018). Elevated 20-HETE in metabolic syndrome regulates arterial stiffness and systolic hypertension via MMP12 activation. *J. Mol. Cell. Cardiol.* 117, 88–99. doi: 10.1016/j.yjmcc.2018.02.005

Sonnweber, T., Pizzini, A., Nairz, M., Weiss, G., and Tancevski, I. (2018). Arachidonic acid metabolites in cardiovascular and metabolic diseases. *Int. J. Mol. Sci.* 19:3285. doi: 10.3390/ijms19113285

Sorrell, V. L., Davis, M. J., and Bove, A. A. (1996). Origins of coronary artery ectasia. *Lancet* 347, 136–137. doi: 10.1016/s0140-6736(96)90335-9

Vendrov, A. E., Stevenson, M. D., Alahari, S., Pan, H., Wickline, S. A., Madamanchi, N. R., et al. (2017). Attenuated superoxide dismutase 2 activity induces atherosclerotic plaque instability during aging in hyperlipidemic mice. *J. Am. Heart Assoc.* 6:e006775. doi: 10.1161/JAHA.117.006775

Watkins, S. M., and Hotamisligil, G. S. (2012). Promoting atherosclerosis in type 1 diabetes through the selective activation of arachidonic acid and PGE(2) production. *Circ. Res.* 111, 394–396. doi: 10.1161/CIRCRESAHA.112.273508

Wu, Y., Zhang, C., Dong, Y., Wang, S., Song, P., Viollet, B., et al. (2012). Activation of the AMP-activated protein kinase by eicosapentaenoic acid (EPA, 20:5 n-3) improves endothelial function in vivo. *PLoS One* 7:e35508. doi: 10.1371/journal.pone.0035508

Yetkin, E., and Waltenberger, J. (2007). Novel insights into an old controversy: is coronary artery ectasia a variant of coronary atherosclerosis? *Clin. Res. Cardiol.* 96, 331–339. doi: 10.1007/s00392-007-0521-0

Yip, H. K., Chen, M. C., Wu, C. J., Hang, C. L., Hsieh, K. Y., Fang, C. Y., et al. (2002). Clinical features and outcome of coronary artery aneurysm in patients with acute myocardial infarction undergoing a primary percutaneous coronary intervention. *Cardiology* 98, 132–140. doi: 10.1159/000066322

Zeldin, D. C. (2001). Epoxygenase pathways of arachidonic acid metabolism. *J. Biol. Chem.* 276, 36059–36062. doi: 10.1074/jbc.R100030200

Zhang, G., Kodani, S., and Hammock, B. D. (2014). Stabilized epoxygenated fatty acids regulate inflammation, pain, angiogenesis and cancer. *Prog. Lipid Res.* 53, 108–123. doi: 10.1016/j.plipres.2013.11.003

Zuccolo, E., Dragoni, S., Poletto, V., Catarsi, P., Guido, D., Rappa, A., et al. (2016). Arachidonic acid-evoked Ca(2+) signals promote nitric oxide release and proliferation in human endothelial colony forming cells. *Vascul. Pharmacol.* 87, 159–171. doi: 10.1016/j.vph.2016.09.005

Conflict of Interest: The authors declare that the research was conducted in the absence of any commercial or financial relationships that could be construed as a potential conflict of interest.

Publisher's Note: All claims expressed in this article are solely those of the authors and do not necessarily represent those of their affiliated organizations, or those of the publisher, the editors and the reviewers. Any product that may be evaluated in this article, or claim that may be made by its manufacturer, is not guaranteed or endorsed by the publisher.

frontiers in Physiology

ORIGINAL RESEARCH
published: 17 December 2021
doi: 10.3389/fphys.2021.762242

Monocyte to High-Density Lipoprotein Cholesterol Ratio at the Nexus of Type 2 Diabetes Mellitus Patients With Metabolic-Associated Fatty Liver Disease

Jue Jia[1], Ruoshuang Liu[1], Weiping Wei[1], Fan Yu[2], Xiawen Yu[1], Yirong Shen[1], Caiqin Chen[1], Zhensheng Cai[1], Chenxi Wang[1], Zhicong Zhao[1], Dong Wang[1], Ling Yang[1] and Guoyue Yuan[1]**

[1] Department of Endocrinology and Metabolism, The Affiliated Hospital of Jiangsu University, Zhenjiang, China, [2] Department of Endocrinology and Metabolism, Jurong Hospital Affiliated to Jiangsu University, Zhenjiang, China

OPEN ACCESS

Edited by:
Dawei Zhang,
University of Alberta, Canada

Reviewed by:
Fabio Lira,
São Paulo State University, Brazil
Carmen De Miguel,
University of Alabama at Birmingham, United States
Ruizhi Feng,
Nanjing Medical University, China

***Correspondence:**
Jue Jia
xibeizijj@aliyun.com
Guoyue Yuan
yuanguoyue@ujs.edu.cn

Specialty section:
This article was submitted to Metabolic Physiology, a section of the journal Frontiers in Physiology

Received: *21 August 2021*
Accepted: *22 November 2021*
Published: *17 December 2021*

Citation:
Jia J, Liu R, Wei W, Yu F, Yu X, Shen Y, Chen C, Cai Z, Wang C, Zhao Z, Wang D, Yang L and Yuan G (2021) Monocyte to High-Density Lipoprotein Cholesterol Ratio at the Nexus of Type 2 Diabetes Mellitus Patients With Metabolic-Associated Fatty Liver Disease. Front. Physiol. 12:762242. doi: 10.3389/fphys.2021.762242

Background: Recently, monocyte to high-density lipoprotein cholesterol ratio (MHR) as a novel inflammatory biomarker has drawn lots of attention. This study was conducted in patients with type 2 diabetes mellitus (T2DM) to investigate the correlation between MHR and metabolic-associated fatty liver disease (MAFLD).

Methods: Totally, 1,051 patients with T2DM from the Affiliated Hospital of Jiangsu University were enrolled and classified as MAFLD ($n = 745$) group and non-MAFLD ($n = 306$) group according to the MAFLD diagnostic criteria. In contrast, patients were also separated into four groups based on MHR quartiles. Anthropometric and biochemical measurements were performed. The visceral fat area (VFA) and subcutaneous fat area (SFA) of participants were measured by dual bioelectrical impedance. Fatty liver was assessed by ultrasonography.

Results: The MHR level of subjects in the MAFLD group was statistically greater than that in the non-MAFLD group ($P < 0.05$). Meanwhile, MHR was higher in the overweight or obese MAFLD group compared with that in the lean MAFLD group ($P < 0.05$). The area under the ROC Curve (AUC) assessed by MHR was larger than that of other inflammatory markers ($P < 0.01$). The cutoff value of MHR was 0.388, with a sensitivity of 61.74% and a specificity of 56.54%. For further study, binary logistic regression analyses of MAFLD as a dependent variable, the relationship between MHR and MAFLD was significant ($P < 0.01$). After adjusting for many factors, the relationship still existed. In the four groups based on MHR quartiles, groups with higher values of MHR had a significantly higher prevalence of MAFLD ($P < 0.05$). The percentage of patients with obese MAFLD increased as the MHR level increased ($P < 0.01$). Among different quartiles of MHR, it showed that with the increasing of MHR, the percentage of patients with MAFLD who had more than four metabolic dysfunction indicators increased, which was 46.39, 60.52, 66.79, and 79.91%, respectively, in each quartile.

Conclusion: Monocyte to high-density lipoprotein cholesterol ratio is a simple and practicable inflammatory parameter that could be used for assessing MAFLD in T2DM. T2DM patients with higher MHR have more possibility to be diagnosed as MAFLD. Therefore, more attention should be given to the indicator in the examination of T2DM.

Keywords: monocyte to high-density lipoprotein cholesterol ratio (MHR), metabolic-associated fatty liver disease, type 2 diabetes mellitus, inflammatory marker, obesity

INTRODUCTION

Currently, owing to the rapidly growing economy and unhealthy lifestyles, non-alcoholic fatty liver disease (NAFLD) has become an epidemic globally (Loomba et al., 2021; Powell et al., 2021). Its prevalence is up to ∼25% (Zhou et al., 2021). It is characterized by hepatic triglyceride (TG) accumulation, and depending on the progress of the disease process, it ranges from liver steatosis to non-alcoholic steatohepatitis (NASH), fibrosis, cirrhosis, till hepatocellular carcinoma, which has taken the serious economic burden to the society (Kumar et al., 2021; Yki-Järvinen et al., 2021). Although the pathogenesis of NAFLD has not been fully clarified, previous studies showed that it shared common pathophysiological mechanisms with type 2 diabetes mellitus (T2DM), such as insulin resistance (IR), impaired lipid metabolism, and inflammation (Ferguson and Finck, 2021; Targher et al., 2021). There are also data showing that the prevalence of NAFLD in subjects with T2DM/glucose intolerance was estimated to be higher (around 40–70%) than that in the general population (Younossi et al., 2019; Mantovani et al., 2020). Meanwhile, NAFLD is often accompanied by serious complications, for instance, cardiovascular diseases and chronic kidney diseases, thus leading to a bad prognosis for patients with T2DM (Mantovani et al., 2020; Nasr et al., 2020). In 2020, NAFLD was renamed metabolic-associated fatty liver disease (MAFLD), which is a sensitive and important indicator of metabolic dysfunction (Eslam et al., 2020).

In recent years, studies indicate that inflammation plays an important role in the pathophysiology of NAFLD (Han et al., 2021; Zhang et al., 2021). Lipotoxicity and release of endogenous factors induce the hepatic inflammatory response (Han et al., 2021). Inflammatory cells, such as neutrophils, lymphocytes, monocytes, macrophages, and Kupffer cells, infiltrated in the liver could mediate hepatic TG storage, regulate the inflammatory response, lead to the phenomena of lipid peroxidation, produce their own reactive oxygen species, and activate nuclear transcription factors, which contribute to hepatocellular damage (Wang et al., 2020; Sakurai et al., 2021; Tacke and Weiskirchen, 2021).

Recently, monocyte to high-density lipoprotein cholesterol ratio (MHR) as a novel inflammatory biomarker, which is largely available in clinical practice, has drawn lots of attention. Elevated MHR has been proved to be associated with many disorders such as cardiovascular diseases, metabolic syndrome (MetS), and polycystic ovary syndrome (PCOS) (Akboga et al., 2016; Uslu et al., 2018; Usta et al., 2018). Studies also investigated that increased MHR was independently related to long-term mortality in patients with coronary artery disease (CAD) who have undergone percutaneous coronary intervention (Zhang et al., 2020). MHR is also a marker that could predict the presence and progression of subclinical carotid atherosclerosis in patients with T2DM (Chen et al., 2019). However, till now, no data exist regarding the association between MHR and T2DM patients with MAFLD. In this study, we aimed to evaluate the association between the inflammatory biomarker MHR and T2DM patients with MAFLD.

METHODS

Study Population

This study upholds the principles of the Declaration of Helsinki, and the study protocol was approved by the Human Research Ethics Committee of the Affiliated Hospital of Jiangsu University. All the patients recruited in this study signed informed consent. A total of 1,368 participants with T2DM were enrolled in the study population from June 2018 to July 2020. T2DM was diagnosed according to the criteria of the American Diabetes Association (American Diabetes Association, 2021). According to the diagnostic criteria of MAFLD (Eslam et al., 2020), the patients were separated into two groups, namely, non-MAFLD group and MAFLD group. The exclusion criteria were as follows: type 1 diabetes, gestational diabetes mellitus, special type diabetes, acute/chronic infection, autoimmune disease, hematological disease, chronic lung disease, tumor, thyroid dysfunction, and those without complete data. Thus, 317 individuals were excluded from this study. Eventually, 1,051 patients were included in the final enrollment (**Figure 1**). In the meantime, on the basis of body mass index (BMI) values (Shin and Lee, 2021), the MAFLD group was separated into lean MAFLD group (BMI < 23 kg/m^2), overweight MAFLD group (BMI, 23.0–24.9 kg/m^2), and obese MAFLD group (BMI ≥ 25.0 kg/m^2). The criteria of metabolic dysfunction were as follows (Lima et al., 2015; Osonoi et al., 2018; Blanquet et al., 2019):

Abbreviations: T2DM, type 2 diabetes mellitus; CAD, coronary artery disease; BMI, body mass index; NC, neck circumference; WC, waist circumference; HC, hip circumference; SBP, systolic blood pressure; DBP, diastolic blood pressure; MAP, mean arterial pressure; VFA, visceral fat area; SFA, subcutaneous fat area; HOMA-IR, homeostasis model assessment of insulin resistance; HOMA-ISI, homeostasis model assessment of insulin sensitivity index; ALT, alanine aminotransferase; AST, aspartate aminotransferase; ALP, alkaline phosphatase; γ-GGT, gamma-glutamyl transferase; TCHOL, total cholesterol; TG, triglyceride; HDL-c, high-density lipoprotein cholesterol; LDL-c, low-density lipoprotein cholesterol; WBC, white blood cell; MHR, monocyte/HDL-c; NHR, neutrophil/HDL-c; NLR, neutrophil/lymphocyte; PLR, platelet/lymphocyte; NFS, non-alcoholic fatty liver disease fibrosis score.

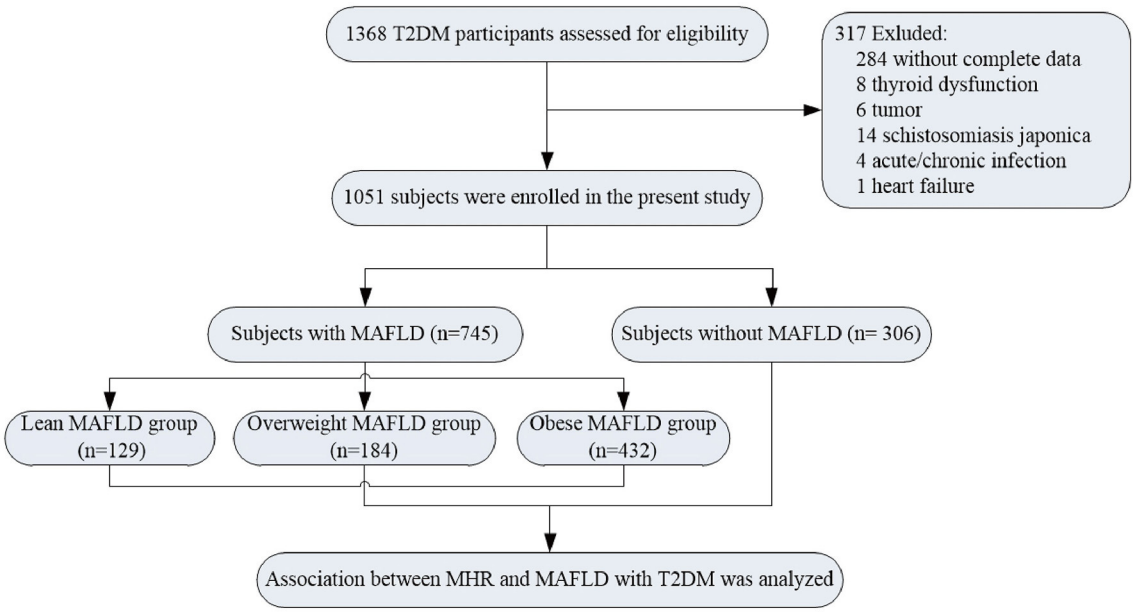

FIGURE 1 | Flowchart describing the selection process of the study population.

(1) waist circumference (WC) ≥ 90 cm for men and ≥ 80 cm for women; (2) systolic blood pressure (SBP) ≥ 130 mmHg or diastolic blood pressure (DBP) ≥ 85 mmHg or treatment of previously diagnosed hypertension; (3) TG levels ≥ 1.70 mmol/L or specific treatment for this lipid abnormalities; (4) high-density lipoprotein cholesterol levels (HDL-c) of <1.0 mmol/L in men and <1.3 mmol/L in women or specific treatment for this lipid abnormalities; (5) fasting plasma glucose of ≥5.60 mmol/L or previously diagnosed T2DM; (6) uric acid levels of ≥420 μmol/L or specific treatment for this abnormalities; and (7) urinary microalbumin (uMA) > 30 mg/L or MA/UCREA > 30 mg/L.

Clinical and Biochemical Parameters

Anthropometric indexes of patients such as height, weight, BMI, neck circumference (NC), WC, hip waist circumference (HC), blood pressure (BP), and heart rate were measured by trained survey personnel in accordance with international standards. After overnight fasting for longer than 8 h, the venous blood samples of subjects were collected. The glucose oxidase method was used to detect fasting blood glucose, and the chemiluminescence method was used to determine fasting plasma insulin and C-peptide. HbA1c was measured by high-performance liquid chromatography (HPLC). Serum lipids and liver function indicators were detected using a BEKMAN AU 5800 automatic biochemical analyzer. Monocyte, neutrophil, and lymphocyte counts were determined using an SYSMEX XN3000 automated blood cell counter.

Homeostasis model assessment was used to estimate insulin resistance (HOMA-IR). HOMA-IR = fasting plasma glucose (mmol/L) × fasting plasma insulin (mIU/L)/22.5. Insulin sensitivity index (ISI) was conducted to estimate insulin sensitivity. ISI = 22.5/fasting plasma glucose (mmol/L) × fasting plasma insulin (mIU/L).

Measurement of Visceral Fat Area

The visceral fat area (VFA) and subcutaneous fat area (SFA) of participants were measured using a dual bioelectrical impedance at the umbilical level (DUALSCAN; OmronHealthcare Co. Ltd, Kyoto, Japan).

Calculation of MHR and Other Inflammatory Markers

The MHR, neutrophil to HDL-c ratio (NHR), neutrophil to lymphocyte ratio (NLR), and platelet to lymphocyte ratio (PLR) were calculated using the following formula, respectively: MHR = monocyte/HDL-c, NHR = neutrophil/HDL-c, NLR = neutrophil/lymphocyte, and PLR = platelet/lymphocyte.

Assessment of Fatty Liver by Ultrasonography

Liver ultrasonography was performed by experienced sonographers. All the patients fasted overnight for 8 h before ultrasound imaging. The diagnostic criteria of hepatic steatosis were based on the following sonographic characteristics: enlarged or slightly normal liver volume, full in shape, and obtuse at both lower margins; increased liver contrast compared with kidney and spleen; flake hypoechoic areas can be seen in some parenchyma; intrahepatic biliary tract is not clearly shown; and the echo of portal vein wall is weakened.

TABLE 1 | The clinical, biochemical, and inflammatory characteristics of patients in MAFLD and non-MAFLD groups.

Variables	MAFLD (n = 745)	Non-MAFLD (n = 306)	P value
Demographic parameters			
Age (years)	**55.00 (47.00, 69.00)**	**60.00 (52.00, 66.00)**	**<0.001**
Male (*n*, %)	454 (60.94)	189 (61.76)	0.803
Smoking (*n*, %)	201 (26.98)	77 (25.16)	0.544
Alcohol intake (*n*, %)	103 (13.83)	36 (11.76)	0.370
Hypertension (*n*, %)	**434 (58.26)**	**137 (44.77)**	**<0.001**
History of CAD (*n*, %)	59 (7.92)	23 (7.52)	0.825
Dyslipidemia (*n*, %)	**663 (88.99)**	**179 (58.50)**	**<0.001**
Antidiabetic drug (*n*, %)	**587 (78.79)**	**265 (86.60)**	**0.003**
Anthropometric parameters			
Height (cm)	**167.00 (160.00, 173.00)**	**165.00 (159.50, 170.50)**	**0.001**
Weight (kg)	**70.70 (63.60, 79.25)**	**62.60 (56.68, 68.3)**	**<0.001**
BMI (kg/m^2)	**25.60 (23.70, 27.73)**	**23.00 (21.40, 25.00)**	**<0.001**
NC (cm)	**39.27 ± 4.75**	**37.00 ± 4.39**	**<0.001**
WC (cm)	**93.67 ± 8.98**	**85.85 ± 8.99**	**<0.001**
HC (cm)	**98.60 ± 7.85**	**94.63 ± 7.17**	**<0.001**
SBP (mmHg)	129.24 ± 16.77	127.06 ± 17.91	0.061
DBP (mmHg)	**76.01 ± 10.29**	**71.84 ± 9.82**	**<0.001**
MAP (mmHg)	**93.75 ± 11.14**	**90.24 ± 10.91**	**<0.001**
VFA (cm^2)	**102.98 ± 34.47**	**66.22 ± 33.56**	**<0.001**
SFA (cm^2)	**190.00 (154.40, 229.75)**	**142.65 (116.00, 177.63)**	**<0.001**
Biochemical parameters			
Fasting plasma glucose (mmol/L)	9.84 (7.87, 12.54)	9.97 (7.24, 12.90)	0.846
Fasting plasma insulin (μIU/mL)	**8.22 (5.08, 11.19)**	**5.38 (3.17, 10.30)**	**<0.001**
Fasting C-peptide (ng/mL)	**2.68 ± 1.01**	**1.82 ± 1.02**	**<0.001**
2 h plasma glucose (mmol/L)	19.16 ± 5.10	19.25 ± 5.51	0.792
2 h plasma insulin (μIU/mL)	**32.87 (18.12, 45.47)**	**26.97 (13.14, 39.17)**	**<0.001**
2 h C-peptide (ng/mL)	**4.91 (3.66, 7.39)**	**3.51 (2.33, 5.02)**	**<0.001**
HbA1c (%)	**9.40 (8.00, 10.80)**	**9.70 (7.98, 11.50)**	**0.027**
HOMA-IR	**3.68 (2.27, 4.92)**	**2.34 (1.41, 3.74)**	**<0.001**
HOMA-ISI	**0.32 (0.20, 0.44)**	**0.51 (0.29, 0.71)**	**<0.001**
ALT (U/L)	**24.00 (16.20, 40.50)**	**16.60 (11.00, 23.25)**	**<0.001**
AST (U/L)	**18.60 (14.20, 26.00)**	**15.20 (12.30, 20.00)**	**<0.001**
ALP (U/L)	71.00 (58.00, 87.00)	71.40 (58.00, 84.00)	0.728
γ-GGT (U/L)	**33.00 (23.00, 52.00)**	**22.00 (15.75, 32.00)**	**<0.001**
Albumin (g/L)	**40.70 (38.70, 42.70)**	**39.40 (37.20, 42.00)**	**<0.001**
Blood urea nitrogen (mmol/L)	**5.13 (4.27, 6.25)**	**5.51 (4.60, 6.87)**	**<0.001**
Creatinine (μmol/L)	59.00 (49.80, 69.50)	60.45 (49.10, 70.80)	0.333
Uric acid (μmol/L)	**298.00 (243.00, 351.50)**	**258.00 (208.50, 310.25)**	**<0.001**
TCHOL (mmol/L)	**4.96 ± 1.14**	**4.77 ± 1.24**	**0.021**
TG (mmol/L)	**2.23 (1.56, 3.25)**	**1.44 (1.00, 1.99)**	**<0.001**
HDL-c (mmol/L)	**1.02 (0.86, 1.21)**	**1.15 (0.97, 1.45)**	**<0.001**
LDL-c (mmol/L)	2.83 ± 0.90	2.79 ± 0.98	0.515
Blood Cells Counts			
WBC (*10^9/L)	6.00 (5.00, 7.10)	5.80 (4.80, 7.20)	0.102
Neutrophil (*10^9/L)	3.30 (2.70, 4.20)	3.30 (2.50, 4.40)	0.909
Monocyte (*10^9/L)	0.47 ± 0.15	0.46 ± 0.16	0.298
Lymphocyte (*10^9/L)	**2.00 (1.60, 2.40)**	**1.80 (1.40, 2.20)**	**<0.001**
Platelet (*10^9/L)	195.26 ± 55.78	190.84 ± 54.47	0.240
Inflammation parameters			
MHR	**0.43 (0.33, 0.58)**	**0.37 (0.27, 0.49)**	**<0.001**
NHR	**3.24 (2.44, 4.29)**	**2.90 (1.99, 4.17)**	**<0.001**
NLR	**1.67 (1.28, 2.20)**	**1.79 (1.40, 2.67)**	**0.002**
PLR	**96.67 (75.29, 122.05)**	**103.10 (79.37, 135.88)**	**0.004**

CAD, coronary artery disease; BMI, body mass index; NC, neck circumference; WC, waist circumference; HC, hip circumference; SBP, systolic blood pressure; DBP, diastolic blood pressure; MAP, mean arterial pressure; VFA, visceral fat area; SFA, subcutaneous fat area; HOMA-IR, homeostasis model assessment of insulin resistance; HOMA-ISI, homeostasis model assessment of insulin sensitivity index; ALT, alanine aminotransferase; AST, aspartate aminotransferase; ALP, alkaline phosphatase; γ-GGT, gamma-glutamyl transferase; TCHOL, total cholesterol; TG, triglyceride; HDL-c, high-density lipoprotein cholesterol; LDL-c, low-density lipoprotein cholesterol; WBC, white blood cell; MHR, monocyte/HDL-c; NHR, neutrophil/HDL-c; NLR, neutrophil/lymphocyte; PLR, platelet/lymphocyte. Continuous variables were described as mean values ± SD and median (interquartile range) according to the distributions of data. Categorical variables were expressed as the number of patients and percentage. $P < 0.05$ (two-sided) was defined as statistically significant. Bold values indicate statistically significance.

TABLE 2 | Subgroup analysis of the clinical and laboratory characteristics based on BMI in patients with MAFLD.

Variables	Lean MAFLD (n = 129) (BMI < 23 kg/m^2)	Overweight MAFLD (n = 184) (BMI 23.0–24.9 kg/m^2)	Obese MAFLD (n = 432) (BMI ≥ 25.0 kg/m2)	P Value
Age (years)	56.00 (50.00, 63.00)	56.00 (48.00, 63.00)	55.00 (45.00, 64.00)	0.279
Male (n, %)	76 (58.91)	112 (60.87)	266 (61.57)	0.863
Smoking (n, %)	30 (23.26)	57 (30.98)	114 (26.39)	0.290
Alcohol intake (n, %)	20 (15.50)	28 (15.22)	55 (12.73)	0.595
Hypertension (n, %)	**58 (44.96)**	**94 (51.09)**	**282 (65.28)**	**<0.001**
History of CAD (n, %)	13 (10.08)	12 (6.52)	34 (7.87)	0.517
Dyslipidemia (n, %)	114 (88.37)	160 (86.96)	389 (90.05)	0.517
Antidiabetic drug (n, %)	108 (83.72)	144 (78.26)	335 (77.55)	0.315
Height (cm)	167.50 (160.50, 174.25)	166.00 (158.50, 173.00)	167.25 (160.00, 173.00)	0.681
Weight (kg)	**60.80 (55.75, 66.50)**	**66.25 (60.48, 72.35)**	**76.95 (69.83, 84.45)**	**<0.001**
NC (cm)	**36.00 (34.00, 39.00)**	**38.00 (36.00, 40.00)**	**40.75 (38.00, 43.00)**	**<0.001**
WC (cm)	**85.00 (80.00, 89.00)**	**89.00 (85.00, 93.00)**	**97.00 (93.00, 103.00)**	**<0.001**
HC (cm)	**93.00 (89.00, 95.00)**	**96.00 (93.00, 98.00)**	**101.00 (98.00, 106.00)**	**<0.001**
SBP (mmHg)	**124.00 (116.00, 135.00)**	**125.00 (115.00, 137.00)**	**130.00 (118.00, 141.75)**	**0.005**
DBP (mmHg)	**74.27 ± 9.60**	**75.14 ± 9.53**	**76.89 ± 10.71**	**0.016**
MAP (mmHg)	**91.46 ± 10.27**	**92.62 ± 10.75**	**94.91 ± 11.42**	**0.002**
VFA (cm^2)	**76.62 ± 25.26**	**86.78 ± 23.50**	**117.75 ± 33.00**	**<0.001**
SFA (cm^2)	**137.10 (116.20, 160.45)**	**162.05 (142.03, 187.60)**	**218.95 (189.00, 260.75)**	**<0.001**
Fasting plasma glucose (mmol/L)	9.07 (7.68, 11.64)	10.16 (7.80, 12.70)	9.90 (7.95, 12.81)	0.140
Fasting plasma insulin (μIU/mL)	**6.59 (4.15, 10.66)**	**6.42 (4.16, 10.09)**	**9.85 (6.17, 12.86)**	**<0.001**
Fasting C-peptide (ng/mL)	**2.40 ± 0.90**	**2.55 ± 0.89**	**2.83 ± 1.07**	**<0.001**
2h plasma glucose (mmol/L)	18.94 ± 5.16	19.44 ± 5.51	19.11 ± 4.90	0.208
2h plasma insulin (μIU/mL)	**30.01 (15.42, 39.59)**	**26.46 (15.77, 40.22)**	**37.78 (20.97, 50.37)**	**<0.001**
2h C-peptide (ng/mL)	4.68 (3.65, 7.22)	4.86 (3.64, 6.62)	5.09 (3.70, 7.54)	0.212
HbA1c (%)	9.50 (8.00, 10.80)	9.60 (8.00, 10.90)	9.20 (7.90, 10.80)	0.646
HOMA-IR	**2.71 (1.70, 4.60)**	**3.00 (1.74, 4.66)**	**4.22 (2.71, 5.76)**	**<0.001**
HOMA-ISI	**0.38 (0.28, 0.59)**	**0.37 (0.23, 0.58)**	**0.27 (0.17, 0.38)**	**<0.001**
ALT (U/L)	**18.80 (13.65, 29.25)**	**22.00 (15.48, 34.45)**	**28.60 (18.55, 45.00)**	**<0.001**
AST (U/L)	**17.10 (13.20, 21.30)**	**17.00 (13.23, 24.48)**	**20.35 (15.60, 27.70)**	**<0.001**
ALP (U/L)	70.00 (55.50, 85.00)	72.00 (57.00, 89.75)	70.50 (58.00, 86.75)	0.628
γ-GGT (U/L)	**27.00 (21.00, 46.54)**	**30.00 (22.00, 44.75)**	**35.00 (24.00, 57.00)**	**0.002**
Albumin (g/L)	40.49 ± 3.51	40.84 ± 4.52	40.80 ± 3.69	0.685
Blood urea nitrogen (mmol/L)	5.24 (4.27, 6.22)	5.07 (4.10, 6.06)	5.15 (4.31, 6.41)	0.461
Creatinine (μmol/L)	58.40 (50.1, 66.15)	59.70 (49.35, 69.68)	59.00 (50.00, 70.25)	0.628
Uric acid (μmol/L)	**286.76 ± 74.89**	**293.86 ± 75.77**	**315.86 ± 92.99**	**0.001**
TCHOL (mmol/L)	4.83 (4.19, 5.75)	4.76 (4.09, 5.60)	4.87 (4.21, 5.61)	0.462
TG (mmol/L)	**2.08 (1.39, 3.18cc)**	**2.11 (1.51, 3.12)**	**2.30 (1.63, 3.33)**	**0.029**
HDL-c (mmol/L)	**1.09 (0.95, 1.28)**	**1.02 (0.86, 1.18)**	**1.00 (0.84, 1.19)**	**0.003**
LDL-c (mmol/L)	2.87 ± 0.95	2.79 ± 0.85	2.83 ± 0.91	0.718
WBC (*10^9/L)	5.70 (4.80, 7.00)	5.90 (4.93, 6.80)	6.20 (5.10, 7.28)	0.119
Neutrophil (*10^9/L)	3.20 (2.60, 4.25)	3.10 (2.60, 3.90)	3.40 (2.70, 4.20)	0.119
Monocyte (*10^9/L)	0.40 (0.40, 0.50)	0.40 (0.33, 0.50)	0.50 (0.0.40, 0.60)	0.074
Lymphocyte (*10^9/L)	1.90 (1.45, 2.30)	2.00 (1.63, 2.40)	2.00 (1.60, 2.40)	0.099
Platelet (*10^9/L)	198.07 ± 53.61	193.93 ± 58.36	194.99 ± 55.40	0.802
MHR	**0.39 (0.31, 0.53)**	**0.40 (0.32, 0.56)**	**0.45 (0.35, 0.60)**	**0.008**
NHR	**3.02 (2.21, 4.27)**	**3.13 (2.38, 4.05)**	**3.33 (2.57, 4.35)**	**0.040**
NLR	**1.75 (1.37, 2.38)**	**1.58 (1.27, 1.96)**	**1.70 (1.24, 2.21)**	**0.025**
PLR	103.64 (78.63, 137.75)	93.33 (71.16, 119.67)	96.98 (75.25, 121.24)	0.056
NFS	**−0.73 ± 1.05**	**−0.68 ± 1.09**	**−0.37 ± 1.12**	**<0.001**
Fibrosis severity scale				
F0–F2	31 (24.03%)	39 (21.20%)	69 (15.97%)	0.071
Indeterminant score	85 (65.89%)	126 (68.48%)	297 (68.75%)	0.825
F3–F4	13 (10.08%)	19 (10.32%)	66 (15.28%)	0.131

CAD, coronary artery disease; BMI, body mass index; NC, neck circumference; WC, waist circumference; HC, hip circumference; SBP, systolic blood pressure; DBP, diastolic blood pressure; MAP, mean arterial pressure; VFA, visceral fat area; SFA, subcutaneous fat area; HOMA-IR, homeostasis model assessment of insulin resistance; HOMA-ISI, homeostasis model assessment of insulin sensitivity index; ALT, alanine aminotransferase; AST, aspartate aminotransferase; ALP, alkaline phosphatase; γ-GGT, gamma-glutamyl transferase; TCHOL, total cholesterol; TG, triglyceride; HDL-c, high-density lipoprotein cholesterol; LDL-c, low-density lipoprotein cholesterol; WBC, white blood cell; MHR, monocyte/HDL-c; NHR, neutrophil/HDL-c; NLR, neutrophil/lymphocyte; PLR, platelet/lymphocyte; NFS, non-alcoholic fatty liver disease fibrosis score. Bold values indicate statistically significance.

TABLE 3 | Correlation of MHR with other parameters in the whole study population or MAFLD patients with T2DM.

	MAFLD group		Total	
	r	*p*	r	*p*
Gender	**−0.344**	**<0.001**	**−0.298**	**<0.001**
Age (years)	**−0.148**	**<0.001**	**−0.159**	**<0.001**
Smoking	**0.228**	**<0.001**	**0.192**	**<0.001**
Alcohol intake	0.050	0.176	0.034	0.274
Hypertension	0.014	0.694	0.030	0.338
History of CAD	0.025	0.499	0.001	0.962
Dyslipidemia	**0.206**	**<0.001**	**0.305**	**<0.001**
Antidiabetic drug	**−0.077**	**0.035**	**−0.077**	**0.012**
Height (cm)	**0.285**	**<0.001**	**0.275**	**<0.001**
Weight (kg)	**0.292**	**<0.001**	**0.316**	**<0.001**
BMI (kg/m^2)	**0.143**	**<0.001**	**0.191**	**<0.001**
NC (cm)	**0.310**	**<0.001**	**0.313**	**<0.001**
WC (cm)	**0.215**	**<0.001**	**0.256**	**<0.001**
HC (cm)	**0.114**	**0.002**	**0.143**	**<0.001**
SBP (mmHg)	0.029	0.428	0.021	0.498
DBP (mmHg)	0.046	0.209	**0.079**	**0.010**
MAP (mmHg)	0.040	0.281	0.060	0.053
VFA (cm^2)	**0.214**	**<0.001**	**0.245**	**<0.001**
SFA (cm^2)	0.059	0.110	**0.128**	**<0.001**
Fasting plasma glucose (mmol/L) (mmol/L)	**0.079**	**0.031**	0.053	0.085
Fasting plasma insulin (μIU/mL)	**0.119**	**0.001**	**0.130**	**<0.001**
Fasting C-peptide (ng/mL)	**0.126**	**0.001**	**0.205**	**<0.001**
2 h plasma glucose (mmol/L)	0.060	0.102	0.053	0.088
2 h plasma insulin (μIU/mL)	0.027	0.455	**0.067**	**0.029**
2 h C-peptide (ng/mL)	0.011	0.763	**0.102**	**0.001**
HbA1c (%)	0.059	0.106	0.036	0.242
HOMA-IR	**0.141**	**<0.001**	**0.155**	**<0.001**
HOMA-ISI	**−0.129**	**<0.001**	**−0.166**	**<0.001**
ALT (U/L)	**0.144**	**<0.001**	**0.158**	**<0.001**
AST (U/L)	0.022	0.549	0.034	0.268
ALP (U/L)	−0.060	0.099	−0.030	0.324
γ-GGT (U/L)	**0.158**	**<0.001**	**0.212**	**<0.001**
Albumin (g/L)	−0.057	0.119	**−0.078**	**0.011**
Blood urea nitrogen (mmol/L)	**0.085**	**0.020**	0.037	0.228
Creatinine (μmol/L)	**0.157**	**<0.001**	**0.132**	**<0.001**
Uric acid (μmol/L)	**0.199**	**<0.001**	**0.215**	**<0.001**
TCHOL (mmol/L)	**−0.177**	**<0.001**	**−0.165**	**<0.001**
TG (mmol/L)	**0.222**	**<0.001**	**0.292**	**<0.001**
HDL-c (mmol/L)	**−0.645**	**<0.001**	**−0.666**	**<0.001**
LDL-c (mmol/L)	**−0.169**	**<0.001**	**−0.123**	**<0.001**
WBC (*10^9/L)	**0.462**	**<0.001**	**0.469**	**<0.001**
Neutrophil (*10^9/L)	**0.365**	**<0.001**	**0.367**	**<0.001**
Monocyte(*10^9/L)	**0.757**	**<0.001**	**0.744**	**<0.001**
Lymphocyte (*10^9/L)	**0.264**	**<0.001**	**0.292**	**<0.001**
Platelet (*10^9/L)	**0.159**	**<0.001**	**0.148**	**<0.001**
NLR	**0.087**	**0.018**	**0.075**	**0.016**
NHR	**0.667**	**<0.001**	**0.669**	**<0.001**
PLR	**−0.117**	**0.001**	**−0.147**	**<0.001**

CAD, coronary artery disease; BMI, body mass index; NC, neck circumference; WC, waist circumference; HC, hip circumference; SBP, systolic blood pressure; DBP, diastolic blood pressure; MAP, mean arterial pressure; VFA, visceral fat area; SFA, subcutaneous fat area; HOMA-IR, homeostasis model assessment of insulin resistance; HOMA-ISI, homeostasis model assessment of insulin sensitivity index; ALT, alanine aminotransferase; AST, aspartate aminotransferase; ALP, alkaline phosphatase; γ-GGT, gamma-glutamyl transferase; TCHOL, total cholesterol; TG, triglyceride; HDL-c, high-density lipoprotein cholesterol; LDL-c, low-density lipoprotein cholesterol; WBC, white blood cell; MHR, monocyte/HDL-c; NHR, neutrophil/HDL-c; NLR, neutrophil/lymphocyte; PLR, platelet/lymphocyte. Bold values indicate statistically significance.

Calculation of the NAFLD Fibrosis Score

The non-alcoholic fatty liver disease fibrosis score (NFS) was used to evaluate the degree of liver fibrosis, and the calculation formula was as follows: NFS = −1.675 + 0.037 × age (years) + 0.094 × BMI (kg/m^2) + 1.13 × impaired fasting glucose/diabetes (yes = 1, no = 0) + 0.99 × AST/ALT ratio − 0.013 × platelet count (×10^9/L) − 0.66 × albumin (g/dl) (Bril et al., 2020).

Advanced fibrosis was explicitly excluded if the NFS was lower than the cutoff point (−1.455), while the diagnosis of advanced fibrosis was established when the NFS was above the cutoff point (0.675) (Bril et al., 2020).

Statistical Analysis

Statistical analyses were performed using SPSS version 22.0 software (SPSS, Inc., Chicago, IL, United States). Continuous variables were described as mean values ± SD or median (interquartile range) according to the distributions of data. Categorical variables were expressed as the number of patients and percentage. The difference between the two groups was examined using Student's *t*-test or Mann-Whitney *U* test, and the difference among the three groups was determined using the one-way ANOVA (normally distributed variables) or Kruskal-Wallis test (non-normally distributed variables). The chi-squared test was used for categorical variables. The relationship between variables was tested by the Pearson or Spearman correlation analysis. Binary logistics regression analyses were performed to explore the association of MHR with MAFLD. The receiver operating characteristic (ROC) curves were operated to identify the optimal value for the assessment of the risk of MAFLD in this population. Optimal cutoffs were derived from maximizing the Yoden index. A p <0.05 (two-sided) was defined as statistically significant.

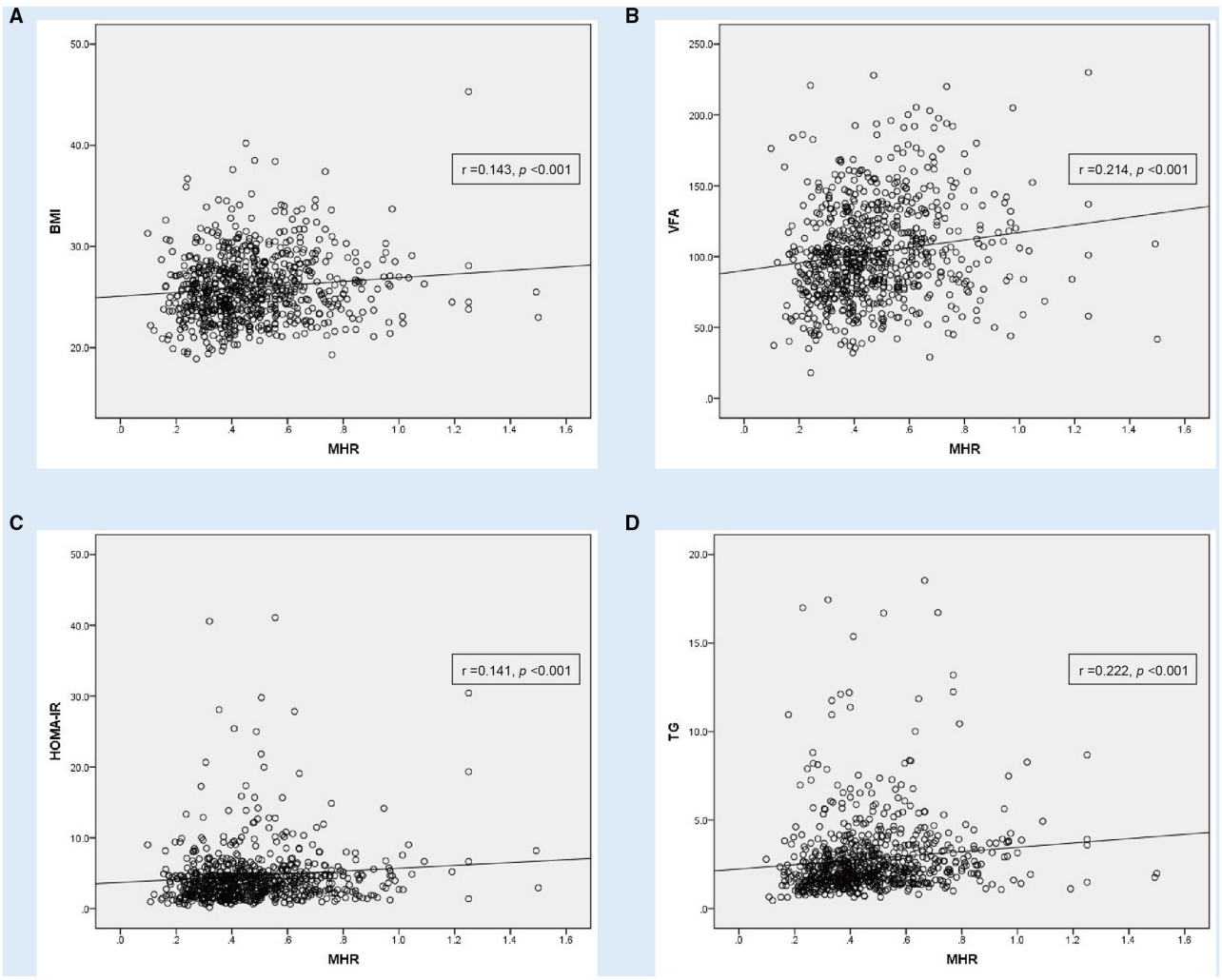

FIGURE 2 | Correlation analysis showing statistically positive correlation between monocyte to HDL cholesterol ratio (MHR) with other parameters in MAFLD patients with T2DM (n = 745). **(A)** body mass index (BMI), **(B)** visceral fat area (VFA), **(C)** homeostasis model assessment of insulin resistance (HOMA-IR) and **(D)** triglyceride (TG).

RESULTS

The Clinical, Biochemical, and Inflammatory Characteristics of Patients

In this current cohort of 1,051 patients (**Supplementary Table 1**), 745 subjects were MAFLD with T2DM, and the prevalence of MAFLD in T2DM was 70.88%. Male patients in both groups were more than 60%. The general characteristics of participants were presented in **Table 1**. With regard to the demographic parameters, patients with MAFLD were younger, showing a higher percentage of hypertension as well as dyslipidemia than those without MAFLD ($P < 0.05$). Regarding anthropometric parameters, the MAFLD group had a remarkably higher level of height, weight, BMI, NC, WC, HC, DBP, MAP, VFA, and SFA than the non-MAFLD group. Regarding biochemical parameters, fasting plasma insulin, fasting C-peptide, 2-h plasma insulin, 2-h C-peptide, HOMA-IR, ALT, AST, γ-glutamyl transpeptidase (γ-GGT), albumin, uric acid, total cholesterol (TCHOL), and TG were significantly augmented in patients with MAFLD compared with those with non-MAFLD, while HbA1c, HOMA-ISI, urea nitrogen, and HDL-c were greatly reduced in subjects with MAFLD ($P < 0.05$). Concerning immune cell counts, lymphocyte counts, MHR, and NHR levels were statistically greater in the MAFLD group than the non-MAFLD group ($P < 0.05$).

Subgroup Analysis of the Clinical and Laboratory Characteristics Based on BMI in Patients With MAFLD

As shown in **Table 2**, the parameters of weight, NC, WC, HC, SBP, DBP, MAP, VFA, SFA, fasting plasma insulin, fasting C-peptide, 2-h plasma insulin, HOMA-IR, HOMA-ISI, ALT, AST, γ-GGT, uric acid, TG, and HDL-c presented a remarkable difference among lean MAFLD group, overweight MAFLD group, and obese MAFLD group ($P < 0.05$). The inflammation markers of MHR and NHR were higher in the overweight or obese MAFLD

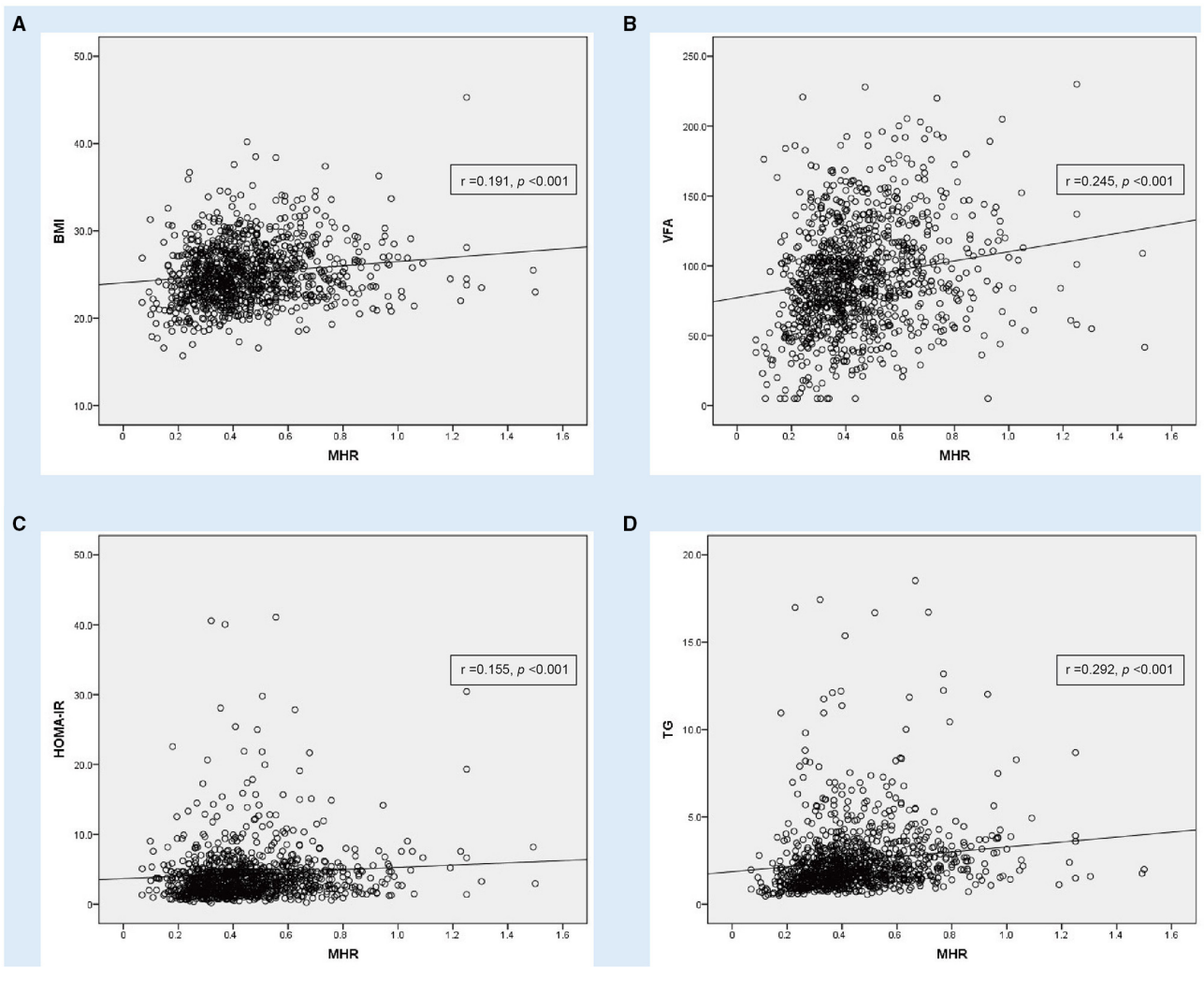

FIGURE 3 | Correlation analysis showing statistically positive correlation between monocyte to HDL cholesterol ratio (MHR) with other parameters in T2DM (n = 1,051). **(A)** Body mass index (BMI), **(B)** visceral fat area (VFA), **(C)** homeostasis model assessment of insulin resistance (HOMA-IR) and **(D)** triglyceride (TG).

group compared with those in the lean MAFLD group ($P < 0.05$). NFS of the highest BMI group increased than that of lower BMI groups ($P < 0.05$), while no difference in fibrosis severity scale was observed in different BMI groups.

Correlation of MHR With Other Parameters in the Whole Study Population or MAFLD With T2DM Patients

In the Pearson or Spearman correlation analysis, MHR presented a significantly positive correlation with smoking, dyslipidemia, height, weight, BMI, NC, WC, HC, VFA, fasting plasma insulin, fasting C-peptide, HOMA-IR, ALT, γ-GGT, creatinine, uric acid, TG, WBC, neutrophil, monocyte, lymphocyte, platelet, NLR, and NHR, and in the meantime, negative correlation with gender, antidiabetic drug usage, age, HOMA-ISI, TCHOL, HDL-c, LDL-c, PLR, and in both, the whole study population and MAFLD with T2DM patients ($P < 0.05$). A significantly positive correlation between MHR and other parameters, such as DBP, SFA, 2-h plasma insulin, and 2-h C-peptide, only existed in the whole population, while a positive correlation between MHR and fasting plasma glucose only existed in MAFLD with T2DM patients ($P < 0.05$). All details are shown in **Table 3**; **Figures 2**, **3**.

Evaluation of the Impact of MHR on MAFLD With T2DM

As **Figure 4** shows the performance for evaluating the endpoint among the inflammatory markers for MAFLD risk, the AUC of the marker is as follows: MHR 0.610 (95% CI: 0.573–0.648), NHR 0.571 (95% CI: 0.531–0.611), NLR 0.438 (95% CI: 0.400–0.477), and PLR 0.443 (95% CI: 0.404–0.482). The result demonstrated that the AUC assessed by MHR was larger than that of the other inflammatory markers ($P < 0.01$). The cutoff value of MHR was 0.388 with a sensitivity of 61.74% and a specificity of 56.54% (**Table 4**).

Then, based on the cutoff point, the whole patients were separated into high MHR group and low MHR group, and the result showed that the high MHR group had a significantly higher level of height, weight, BMI, NC, WC, HC, DBP, VFA, SFA,

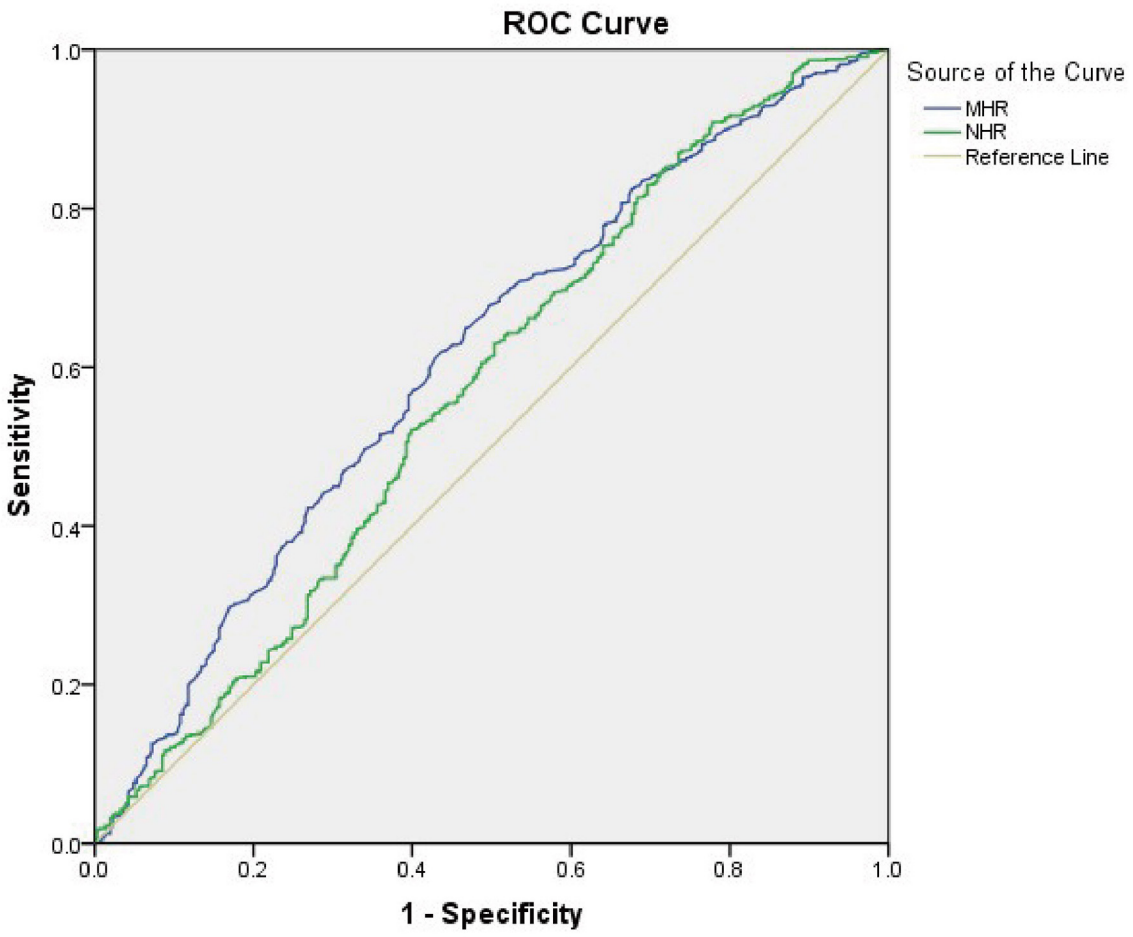

FIGURE 4 | Receiver operating characteristic (ROC) curve analysis of monocyte to HDL cholesterol ratio (MHR) and neutrophil to HDL cholesterol ratio (NHR) to assess the accuracy of these parameters as a biomarker of MAFLD risk in T2DM patients. The area under the ROC curve (AUC) values in the MHR and NHR were 0.610 (95% confidence interval: 0.573–0.648) and 0.571 (95% confidence interval: 0.531–0.611), respectively.

TABLE 4 | ROC curve analysis of MHR in assessing MAFLD risk in patients with T2DM.

Variables	AUC	95%CI	Sensitivity (%)	Specificity (%)	Cut-Off value	Youden Index
MHR	0.610	0.573–0.648	61.74	56.54	0.388	0.183
NHR	0.571	0.531–0.611	86.98	26.47	2.029	0.135
NLR	0.438	0.400–0.477	99.73	0.33	0.574	0.001
PLR	0.443	0.404–0.482	0.40	100	318.036	0.004

MHR, monocyte/HDL-c; NHR, neutrophil/HDL-c; NLR, neutrophil/lymphocyte; PLR, platelet/lymphocyte.

fasting plasma insulin, fasting C-peptide, 2-h plasma insulin, 2-h C-peptide, HOMA-IR, ALT, γ-GGT, creatinine, uric acid, TG, WBC, neutrophil, lymphocyte, platelet, NHR, and NLR than the low MHR group, while HOMA-ISI, TCHOL, HDL-c, LDL-c, and PLR were reduced in the high MHR group than the low MHR group. The prevalence of MAFLD in the high MHR group was higher than that in the low MHR group (77.57 and 62.22%, respectively, **Supplementary Table 2**).

We further performed the binary logistic regression analyses, and the result showed that the risk of MAFLD significantly increased with the increasing of MHR ($P < 0.01$ in every model, **Figure 5**). In the base model, MHR was independently associated with MAFLD ($P < 0.001$). After adjusting for gender and age, MHR and MAFLD were independently correlated ($P < 0.001$ in model 1). After additional correction of smoking, alcohol intake, and hypertension history, MHR and MAFLD still showed an independent correlation ($P < 0.001$ in model 2). Furthermore, the MHR was also an independent determinant of MAFLD after further adjustment of usage of antidiabetic drug, HOMA-IR, TC, HOMA-ISI, and HbA1c ($P = 0.002$ in model 3). This indicates that the high MHR is independently associated with MAFLD in patients with T2DM. We also observed that NHR was independently associated with MAFLD in the unadjusted model ($P = 0.004$) and model 1 ($P = 0.019$), while no significant correlation was found in models 2 and 3 ($P = 0.064$ and $P = 0.072$, respectively).

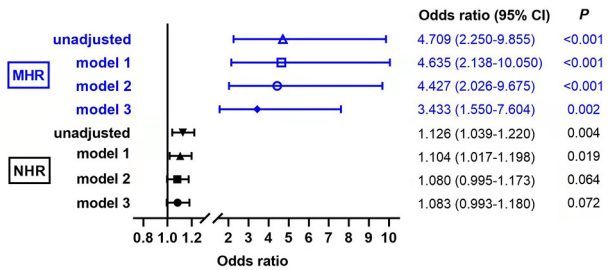

FIGURE 5 | Evaluation of the impact of monocyte to HDL cholesterol ratio (MHR) and neutrophil to HDL cholesterol ratio (NHR) on MAFLD with T2DM by binary logistic regression analyses. Model 1: adjusted for age, gender; Model 2: adjusted for smoking, alcohol intake, hypertension history, in addition to model 1; Model 3: adjusted for use of antidiabetic drug, homeostasis model assessment of insulin resistance (HOMA-IR), total cholesterol (TC), homeostasis model assessment of insulin sensitivity index (HOMA-ISI), HbAlc in addition to model 2.

The Clinical and Biochemical Characteristics According to MHR Quartiles

The study population was divided according to MHR quartiles: Q1 (MHR $\leq$ 0.31, $n = 263$), Q2 (0.31 $<$ MHR $\leq$ 0.41, $n = 266$), Q3 (0.41 $<$ MHR $\leq$ 0.56, $n = 268$), Q4 (MHR $>$ 0.56, $n = 254$), as shown in **Table 5**. ANOVA revealed that groups with higher values of MHR had remarkably higher height, weight, BMI, NC, WC, HC, VFA, SFA, fasting plasma insulin, fasting C-peptide, 2-h plasma insulin, 2-h C-peptide, HOMA-IR, ALT, γ-GGT, creatinine, uric acid, TG, WBC, neutrophil, monocyte, lymphocyte, platelet, NHR, significantly lower age, HOMA-ISI, albumin, TCHOL, HDL-c, LDL-c, and PLR ($P < 0.05$).

The Prevalence of MAFLD Among Different Quartiles of MHR

As illustrated in **Figure 6**, groups with higher values of MHR had a significantly higher prevalence of MAFLD ($P < 0.05$). In each quartile, as shown in **Figure 7**, when the patients with MAFLD were divided into lean MAFLD group, overweight MAFLD group, and obese MAFLD group according to BMI, the number of obese MAFLD patients increased as the MHR level increased.

Distribution of Metabolic Dysfunction in Patients With MAFLD Among Different Quartiles of MHR

We further analyzed the distribution of metabolic dysfunction in patients with MAFLD among different quartiles of MHR, and the result displayed that with the increase of MHR, the percentage of patients with MAFLD who had more than four metabolic dysfunction indicators increased, which was 46.39, 60.52, 66.79, and 79.91%, respectively, in each quartile (**Figure 8**).

DISCUSSION

The prevalence of NAFLD in the T2DM population has been proved to reach approximately 40–70% which is higher than that in the general population (Younossi et al., 2019; Mantovani et al., 2020). The finding in this study is consistent with the previous reports, and the prevalence of MAFLD is reaching 70.88%. The pathogenesis of the two comorbid disorders of NAFLD and T2DM has been studied extensively, while the exact molecular mechanisms are still undiscovered (Wu et al., 2017). It is well-recognized that IR is the core to the pathogenesis of NAFLD and T2DM (Wu et al., 2017). IR could lead to hyperglycemia

TABLE 5 | The clinical and biochemical characteristics according to MHR quartiles.

Variables	Q1 ($n = 263$) (MHR $\leq$ 0.31)	Q2 ($n = 266$) (0.31 < MHR $\leq$ 0.41)	Q3 ($n = 268$) (0.41 < MHR $\leq$ 0.56)	Q4 ($n = 254$) (MHR > 0.56)	*P* value
Age (years)	**58.00 (52.00, 66.00)**	**58.00 (50.00, 66.00)**	**55.50 (46.00, 64.00)**	**54.00 (44.00, 62.25)**	**<0.001**
Male (*n*, %)	**110 (41.83)**	**151 (56.77)**	**171 (63.81)**	**211 (83.07)**	**<0.001**
Smoking (*n*, %)	**42 (15.97)**	**68 (25.56)**	**64 (23.88)**	**104 (40.94)**	**<0.001**
Alcohol intake (*n*, %)	25 (9.51)	36 (13.53)	46 (17.16)	32 (12.60)	0.075
Hypertension (*n*, %)	136 (51.71%)	151 (56.77)	142 (52.99)	142 (55.91)	0.612
History of CAD (*n*, %)	18 (6.84)	26 (9.77)	17 (6.34)	21 (8.27)	0.450
Dyslipidemia (*n*, %)	**161 (61.22)**	**210 (78.95)**	**233 (86.94)**	**238 (93.70)**	**<0.001**
Antidiabetic drug (*n*, %)	**229 (87.07)**	**213 (80.08)**	**215 (80.22)**	**195 (76.77)**	**0.023**
Height (cm)	**162.79 ± 8.48**	**165.88 ± 8.28**	**166.39 ± 8.23**	**169.40 ± 7.87**	**<0.001**
Weight (kg)	**62.90 (57.20, 70.00)**	**67.35 (61.15, 75.80)**	**69.55 (62.43, 77.08)**	**73.85 (65.65, 82.13)**	**<0.001**
BMI (kg/m^2)	**24.00 (22.00, 26.20)**	**24.50 (22.70, 27.13)**	**25.20 (23.23, 27.20)**	**25.63 (23.40, 28.13)**	**<0.001**
NC (cm)	**36.00 (34.00, 39.00)**	**38.00 (36.00, 41.00)**	**39.00 (36.00, 41.38)**	**40.00 (37.88, 42.00)**	**<0.001**
WC (cm)	**87.00 (82.00, 93.00)**	**91.00 (85.00, 97.00)**	**93.00 (86.50, 98.00)**	**94.00 (88.00, 100.00)**	**<0.001**
HC (cm)	**96.00 (92.00, 100.00)**	**97.00 (93.00, 101.00)**	**97.00 (93.00, 103.00)**	**98.00 (94.00, 103.00)**	**<0.001**
SBP (mmHg)	127.00 (117.00, 139.00)	128.00 (114.00, 140.00)	126.00 (116.00, 138.00)	129.00 (117.00, 140.00)	0.760
DBP (mmHg)	74.50 ± 10.54	74.00 ± 10.92	74.52 ± 9.92	76.21 ± 9.78	0.080
MAP (mmHg)	92.59 ± 11.03	92.05 ± 11.97	92.42 ± 10.90	93.92 ± 10.74	0.251
VFA (cm^2)	**78.02 ± 37.32**	**91.33 ± 32.63**	**95.07 ± 36.11**	**105.09 ± 41.14**	**<0.001**
SFA (cm^2)	**174.11 ± 68.95**	**180.16 ± 57.07**	**184.32 ± 63.35**	**197.61 ± 69.94**	**<0.001**
Fasting plasma glucose (mmol/L)	9.68 (7.09, 12.46)	9.69 (7.99, 12.52)	10.06 (7.77, 12.91)	10.03 (8.04, 12.93)	0.257
Fasting plasma insulin (μIU/mL)	**6.89 (3.60, 10.33)**	**6.79 (4.12, 10.66)**	**7.63 (4.59, 11.21)**	**9.31 (5.29, 12.11)**	**<0.001**
Fasting C-peptide (ng/mL)	**2.07 ± 1.11**	**2.40 ± 0.95**	**2.52 ± 1.06**	**2.74 ± 1.13**	**<0.001**
2h plasma glucose (mmol/L)	18.95 ± 5.56	18.87 ± 5.17	19.46 ± 5.10	19.48 ± 5.01	0.383
2h plasma insulin (μIU/mL)	**31.96 (16.61, 44.83)**	**27.08 (15.25, 39.59)**	**30.78 (16.14, 46.59)**	**34.17 (19.66, 46.98)**	**0.037**
2h C-peptide (ng/mL)	**4.31 (2.87, 6.62)**	**4.18 (3.29, 6.15)**	**4.59 (3.22, 6.85)**	**5.09 (3.51, 7.17)**	**0.010**
HbA1c (%)	9.30 (7.50, 11.00)	9.50 (8.00, 10.90)	9.65 (8.10, 11.10)	9.48 (8.00, 11.03)	0.425
HOMA-IR	**2.76 (1.64, 4.28)**	**3.07 (1.77, 4.66)**	**3.43 (1.94, 5.17)**	**3.89 (2.37, 5.43)**	**<0.001**
HOMA-ISI	**0.41 (0.25, 0.61)**	**0.38 (0.23, 0.58)**	**0.35 (0.19, 0.54)**	**0.30 (0.18, 0.44)**	**<0.001**
ALT (U/L)	**19.50 (13.20, 29.70)**	**19.85 (13.30, 32.23)**	**22.10 (15.00, 37.88)**	**24.00 (16.98, 43.85)**	**<0.001**
AST (U/L)	17.30 (14.00, 24.80)	17.00 (13.00, 22.87)	17.85 (13.35, 24.23)	18.50 (13.58, 25.53)	0.309
ALP (U/L)	71.00 (59.00, 86.00)	70.50 (57.00, 90.00)	70.00 (58.00, 83.00)	71.50 (57.00, 86.00)	0.905
γ-GGT (U/L)	**26.00 (16.00, 42.00)**	**26.00 (19.00, 41.00)**	**29.00 (21.00, 47.00)**	**35.00 (25.00, 60.25)**	**<0.001**
Albumin (g/L)	**41.56 ± 5.91**	**40.25 ± 3.86**	**40.27 ± 3.83**	**40.02 ± 3.70**	**0.025**
Blood urea nitrogen (mmol/L)	5.30 ± 1.48	5.69 ± 2.00	5.50 ± 1.70	5.75 ± 2.31	0.239
Creatinine (μmol/L)	**57.00 (47.80, 66.10)**	**58.70 (48.58, 68.58)**	**60.15 (50.13, 70.40)**	**62.80 (53.80, 71.83)**	**0.001**
Uric acid (μmol/L)	**270.02 ± 79.93**	**288.33 ± 90.26**	**295.64 ± 82.77**	**319.71 ± 88.32**	**<0.001**
TCHOL (mmol/L)	**5.04 (4.31, 5.78)**	**4.89 (4.26, 5.64)**	**4.77 (4.15, 5.44)**	**4.49 (3.88, 5.41)**	**<0.001**
TG (mmol/L)	**1.53 (1.06, 2.27)**	**1.91 (1.34, 2.72)**	**2.00 (1.49, 2.98)**	**2.41 (1.67, 3.60)**	**<0.001**
HDL-c (mmol/L)	**1.34 (1.13, 1.60)**	**1.12 (1.01, 1.27)**	**0.99 (0.86, 1.15)**	**0.84 (0.70, 0.98)**	**<0.001**
LDL-c (mmol/L)	**2.94 ± 0.99**	**2.86 ± 0.90**	**2.85 ± 0.85**	**2.61 ± 0.93**	**<0.001**
WBC (*10^9/L)	**5.00 (4.20, 6.10)**	**5.70 (5.00, 6.60)**	**6.00 (5.20, 7.10)**	**7.10 (6.10, 8.43)**	**<0.001**
Neutrophil (*10^9/L)	**2.80 (2.20, 3.70)**	**3.20 (2.68, 3.93)**	**3.30 (2.70, 4.10)**	**4.00 (3.28, 4.93)**	**<0.001**
Monocyte (*10^9/L)	**0.30 (0.30, 0.40)**	**0.40 (0.40, 0.50)**	**0.50 (0.40, 0.50)**	**0.60 (0.50, 0.70)**	**<0.001**
Lymphocyte (*10^9/L)	**1.73 ± 0.55**	**1.94 ± 0.58**	**2.03 ± 0.65**	**2.29 ± 0.91**	**<0.001**
Platelet (*10^9/L)	**187.20 ± 52.61**	**184.18 ± 53.81**	**197.68 ± 56.47**	**207.34 ± 56.02**	**<0.001**
NHR	**2.12 (1.58, 2.90)**	**2.86 (2.31, 3.42)**	**3.30 (2.71, 4.16)**	**4.67 (3.86, 6.00)**	**<0.001**
NLR	1.65 (1.25, 2.20)	1.72 (1.33, 2.36)	1.65 (1.29, 2.25)	1.78 (1.40, 2.45)	0.066
PLR	**110.50 (85.00, 138.33)**	**94.89 (72.36, 125.14)**	**99.37 (77.07, 124.33)**	**92.81 (72.03, 119.02)**	**<0.001**

CAD, coronary artery disease; BMI, body mass index; NC, neck circumference; WC, waist circumference; HC, hip circumference; SBP, systolic blood pressure; DBP, diastolic blood pressure; VFA, visceral fat area; SFA, subcutaneous fat area; HOMA-IR, homeostasis model assessment of insulin resistance; HOMA-ISI, homeostasis model assessment of insulin sensitivity index; ALT, alanine aminotransferase; AST, aspartate aminotransferase; ALP, alkaline phosphatase; γ-GGT, gamma-glutamyl transferase; TCHOL, total cholesterol; TG, triglyceride; HDL-c, high-density lipoprotein cholesterol; LDL-c, low-density lipoprotein cholesterol; WBC, white blood cell; MHR, monocyte/HDL-c; NHR, neutrophil/HDL-c; NLR, neutrophil/lymphocyte; PLR, platelet/lymphocyte. Bold values indicate statistically significance.

and reactive hyperinsulinemia, which in turn could cause lipid accumulation, and finally affects lipid metabolism in the liver (Li P. et al., 2020). Simultaneously, the current result shows that the MAFLD group has higher levels of BMI, NC, WC, HC, VFA, and SFA than the non-MAFLD group, which indicates that patients with T2DM in overweight and obese groups are more likely to be combined with MAFLD. Previous report clarified that obesity could increase the risk of developing IR, T2DM, dyslipidemia, hypertension, and NAFLD (Jung and Choi, 2014). In addition, many studies suggest that chronic inflammation in adipose tissue might play a significant role in the development of obesity-related metabolic dysfunction (Zatterale et al., 2019).

This study observes the effect of MHR on the assessment of MAFLD in T2DM. Our findings manifested that the MHR was higher in T2DM patients with MAFLD, compared with the control group. Concurrently, when the study population was divided according to MHR quartiles, the prevalence of MAFLD

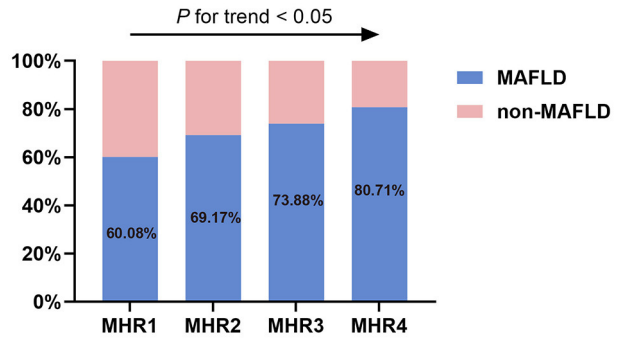

FIGURE 6 | The prevalence of MAFLD in T2DM patients among different quartiles of monocyte to HDL cholesterol ratio (MHR).

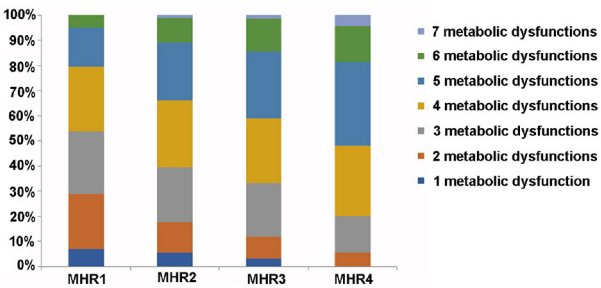

FIGURE 8 | Distribution of metabolic dysfunction in MAFLD patients among different quartiles of monocyte to HDL cholesterol ratio (MHR). Metabolic dysfunction indicators: waist circumference (WC) ≥ 90 cm for men and ≥ 80 cm for women; systolic blood pressure (SBP) ≥ 130 mmHg or diastolic blood pressure (DBP) ≥85 mmHg or treatment of previously diagnosed hypertension; TG levels ≥ 1.70 mmol/L or specific treatment for this lipid abnormalities; high-density lipoprotein cholesterol levels (HDL-c) of < 1.0 mmol/L in men and < 1.3 mmol/L in women or specific treatment for this lipid abnormalities; fasting plasma glucose (FPG) of ≥ 5.60 mmol/L or previously diagnosed T2DM; uric acid (UA) levels of ≥420 μmol/L or specific treatment for this abnormalities; urinary microalbumin (uMA) > 30 mg/L or MA/UCREA > 30 mg/L.

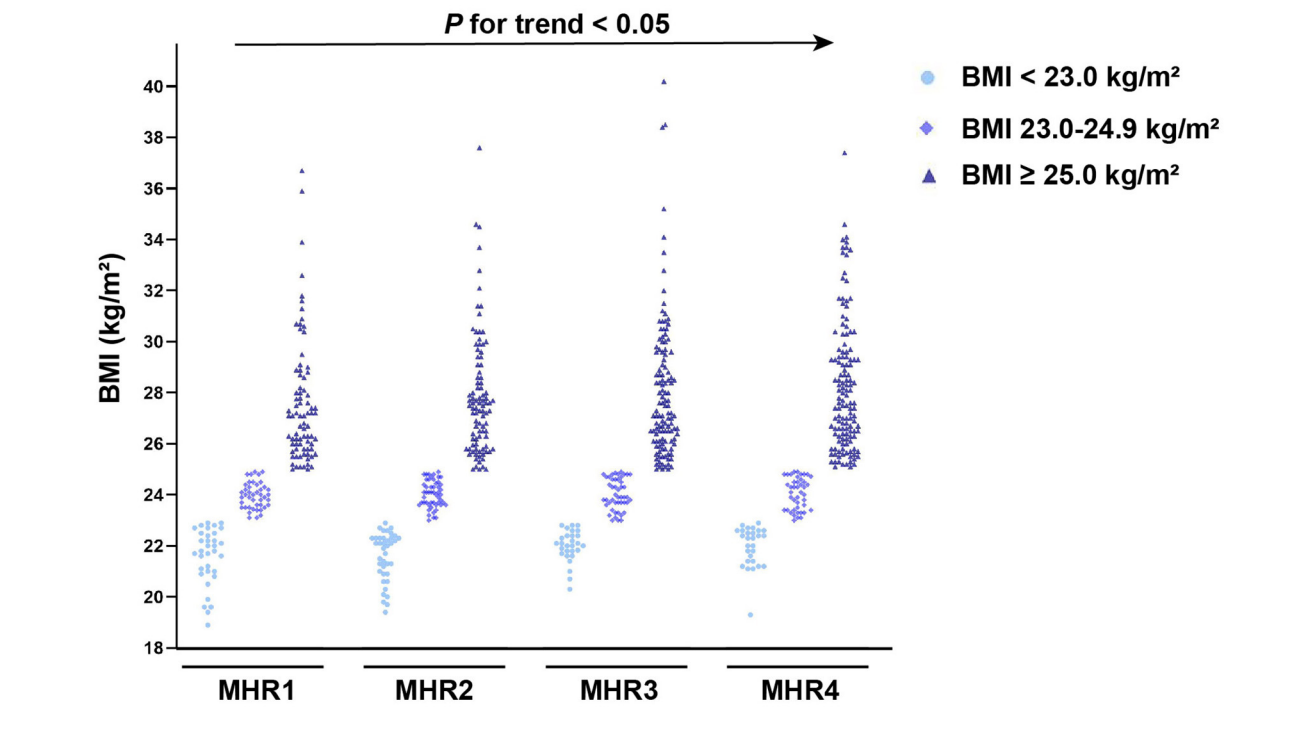

FIGURE 7 | The number of MAFLD patients with T2DM based on body mass index (BMI) among different quartiles of monocyte to HDL cholesterol ratio (MHR).

increased as the values of MHR increased. Meanwhile, in each quartile, the percentage of patients with obese MAFLD increased as the MHR level increased. In patients with MAFLD, Pearson or Spearman correlation analysis demonstrated that the MHR is positively related to BMI, NC, WC, HC, VFA, and HOMA-IR. In recent years, MHR was confirmed to be a novel maker with the integration of pro-inflammatory and anti-inflammatory indices, and it owned comparatively higher clinic practical values since it is convenient to obtain (Chen et al., 2019). Wang et al. demonstrated a linear relation between MHR levels and the odds of ischemic stroke in a large community-based population, and they also found that MHR could be a clinical indicator in risk stratification in subjects with ischemic stroke (Wang et al., 2019). In a metabolic syndrome-related study, the scholars investigated and found out that patients with metabolic syndrome had higher MHR values than healthy controls; moreover, MHR could be an inflammatory marker to evaluate disease severity (Uslu et al., 2018). Cetin et al. demonstrated that MHR might be an independent predictor of the severity of coronary artery disease and future cardiovascular events in patients with acute coronary syndrome (Cetin et al., 2016).

The activation of monocytes and their differentiated forms into lipid-laden macrophages play an important role in promoting immune defenses in patients with chronic inflammatory (Usta et al., 2018). Meanwhile, the activation of monocytes and their differentiated forms into lipid-laden macrophages could be regulated by inflammatory cytokines (Akboga et al., 2016). Previous study shows that the monocyte count is an independent predictor of plaque formation and progression in atherosclerosis (Johnsen et al., 2005). Study also demonstrated that the M1 type macrophage/M2 type macrophage ratio was increased during the progression of liver disease (Ziolkowska et al., 2021). On the contrary, HDL-c has anti-inflammatory, antioxidant, and antithrombotic effects, which has the ability to counteract macrophages migration and remove cholesterol from these cells (Akboga et al., 2016; Usta et al., 2018). HDL-c molecules also play a suppressive role in the control of monocyte activation, as well as in the proliferation and differentiation of the progenitor cells of monocytes, as reported in previous study (Usta et al., 2018). Therefore, monocytes play a pro-inflammatory role, while HDL-c shows a reversal factor during this process (Yilmaz and Kayançiçek, 2018). Higher monocyte counts and lower LDL-c levels act as indirect indicators of inflammation and development of atherosclerosis (Usta et al., 2018). Actually, the relationship between monocyte counts and HDL-c provides a better understanding of inflammation. MAFLD is recognized as the liver disease component of metabolic syndrome, which is mainly associated with obesity, IR, T2DM, and inflammation (Li H. et al., 2020). In this study, the higher MHR in MAFLD patients with T2DM has been confirmed. The ROC curve showed that the evaluative value of MHR for MAFLD risk was 0.610. For further study, with binary logistic regression analyses of MAFLD as a dependent variable, the relationship between MHR and MAFLD was significant. After adjusting for many factors, the relationship still existed. It also demonstrated that with the increasing of the MHR, the percentage of patients with MAFLD who had more than four metabolic dysfunction indicators increased. Above all, the MHR has the advantage as an evaluating indicator of MAFLD in T2DM patients, which is reported for the first time as far as we know.

We also found that the NHR was higher in T2DM patients with MAFLD than that in the non-MAFLD group. Kou et al. recently demonstrated that the NHR was closely related to CAD, and it was an independent predictor of severe coronary stenosis (Huang et al., 2020; Kou et al., 2021). Previous study showed that the NHR had a strong predictive value for predicting metabolic syndrome (Chen et al., 2020). In this study, the ROC curve showed that the evaluative value of the NHR for MAFLD risk was 0.571, with a sensitivity of 86.98% and a specificity of 26.47% only, which was inferior to that of MHR. The increased number of lymphocytes was found in the MAFLD group. This is similar to the previous report that the percentage of lymphocytes is independently and positively correlated with MAFLD (Li H. et al., 2020). ROC curve of the value of lymphocyte for predicting MAFLD risk was analyzed (data were not shown), and the result was also inferior to that of MHR.

Limitation

Several limitations exist in this study. First, this study was a retrospective analysis based on prospectively collected data from a single center in the Chinese population. Second, the golden criteria of MAFLD diagnosis were based on histological examination and imaging techniques. However, these two techniques are invasive, expensive, and unfeasible in clinical work. Third, in this study, the relationship between the MHR level and the severity of MAFLD was not clarified. Further prospective studies should be performed to investigate whether MHR would be an evaluating indicator of improving MAFLD.

CONCLUSION

The MHR is a convenient, simple and cost-effective, parameter that could be used for assessing MAFLD in T2DM. T2DM patients with a higher MHR have more possibility to be diagnosed as MAFLD. Therefore, more attention should be given to the indicator in the examination of T2DM.

DATA AVAILABILITY STATEMENT

The original contributions presented in the study are included in the article/**Supplementary Material**, further inquiries can be directed to the corresponding author/s.

ETHICS STATEMENT

The study protocol was approved by the Human Research Ethics Committee of the Affiliated Hospital of Jiangsu University. The patients/participants provided their written informed consent to participate in this study.

AUTHOR CONTRIBUTIONS

JJ and GY participated in the study design. JJ, RL, WW, XY, YS, ZZ, and CC were involved in the conduct of the study and data collection. JJ, RL, WW, FY, and ZC made contributions to data analysis and result interpretation. JJ, RL, CW, DW, and LY wrote and modified the manuscript and prepared tables and figures. All authors read and approved the final manuscript.

FUNDING

This study was supported by the National Natural Science Foundation of China (81870548, 81570721, and 81500351), the Social Development Project of Jiangsu Province (BE2018692), the Natural Science Foundation of Jiangsu Province (BK20191222), the Youth Medical Talent Project of Jiangsu Province (QNRC2016842), the Jiangsu University Affiliated Hospital 5123 Talent Plan (51232017305), the sixth 169 Talent Project of Zhenjiang, the Science and Technology Commission of Zhenjiang City (FZ2020038), Doctoral Research Initiation Fund (jdfyRC2020010), and Clinical Medical Science and Technology Development Foundation of Jiangsu University (JLY2021209).

ACKNOWLEDGMENTS

The authors appreciate the help and support from all participants who took part in this study.

SUPPLEMENTARY MATERIAL

The Supplementary Material for this article can be found online at: https://www.frontiersin.org/articles/10.3389/fphys.2021.762242/full#supplementary-material

REFERENCES

Akboga, M. K., Balci, K. G., Maden, O., Ertem, A. G., Kirbas, O., Yayla, C., et al. (2016). Usefulness of monocyte to HDL-cholesterol ratio to predict high SYNTAX score in patients with stable coronary artery disease. *Biomark. Med.* 10, 375–383. doi: 10.2217/bmm-2015-0050

American Diabetes Association (2021). 2. classification and diagnosis of diabetes: standards of medical care in diabetes-2021. *Diabetes Care.* 44, S15–S33. doi: 10.2337/dc21-S002

Blanquet, M., Legrand, A., Pélissier, A., and Mourgues, C. (2019). Socio-economics status and metabolic syndrome: a meta-analysis. *Diabetes Metab. Syndr.* 13, 1805–1812. doi: 10.1016/j.dsx.2019.04.003

Bril, F., McPhaul, M. J., Caulfield, M. P., Clark, V. C., Soldevilla-Pico, C., Firpi-Morell, R. J., et al. (2020). Performance of plasma biomarkers and diagnostic panels for nonalcoholic steatohepatitis and advanced fibrosis in patients with type 2 diabetes. *Diabetes Care.* 43, 290–297. doi: 10.2337/dc19-1071

Cetin, M. S., Ozcan Cetin, E. H., Kalender, E., Aydin, S., Topaloglu, S., Kisacik, H. L., et al. (2016). Monocyte to HDL cholesterol ratio predicts coronary artery disease severity and future major cardiovascular adverse events in acute coronary syndrome. *Heart Lung Circ.* 25, 1077–1086. doi: 10.1016/j.hlc.2016.02.023

Chen, J. W., Li, C., Liu, Z. H., Shen, Y., Ding, F. H., Shu, X. Y., et al. (2019). The role of monocyte to high-density lipoprotein cholesterol ratio in prediction of carotid intima-media thickness in patients with type 2 diabetes. *Front Endocrinol (Lausanne).* 10:191. doi: 10.3389/fendo.2019.00191

Chen, T., Chen, H., Xiao, H., Tang, H., Xiang, Z., Wang, X., et al. (2020). Comparison of the value of neutrophil to high-density lipoprotein cholesterol ratio and lymphocyte to high-density lipoprotein cholesterol ratio for predicting metabolic syndrome among a population in the Southern Coast of China. *Diabetes Metab. Syndr. Obes.* 13, 597–605. doi: 10.2147/DMSO.S238990

Eslam, M., Sanyal, A. J., and George, J. (2020). MAFLD: a consensus-driven proposed nomenclature for metabolic associated fatty liver disease. *Gastroenterology.* 158, 1999–2014.e1991. doi: 10.1053/j.gastro.2019.11.312

Ferguson, D., and Finck, B. N. (2021). Emerging therapeutic approaches for the treatment of NAFLD and type 2 diabetes mellitus. *Nat. Rev. Endocrinol.* 17, 484–495. doi: 10.1038/s41574-021-00507-z

Han, Y. H., Lee, K., Saha, A., Han, J., Choi, H., Noh, M., et al. (2021). Specialized proresolving mediators for therapeutic interventions targeting metabolic and inflammatory disorders. *Biomol. Ther. (Seoul)* 29, 455–464. doi: 10.4062/biomolther.2021.094

Huang, J. B., Chen, Y. S., Ji, H. Y., Xie, W. M., Jiang, J., Ran, L. S., et al. (2020). Neutrophil to high-density lipoprotein ratio has a superior prognostic value in elderly patients with acute myocardial infarction: a comparison study. *Lipids Health Dis.* 19:59. doi: 10.1186/s12944-020-01238-2

Johnsen, S. H., Fosse, E., Joakimsen, O., Mathiesen, E. B., Stensland-Bugge, E., Njølstad, I., et al. (2005). Monocyte count is a predictor of novel plaque formation: a 7-year follow-up study of 2610 persons without carotid plaque at baseline the Tromsø Study. *Stroke.* 36, 715–719. doi: 10.1161/01.STR.0000158909.07634.83

Jung, U. J., and Choi, M. S. (2014). Obesity and its metabolic complications: the role of adipokines and the relationship between obesity, inflammation, insulin resistance, dyslipidemia and nonalcoholic fatty liver disease. *Int. J. Mol. Sci.* 15, 6184–6223. doi: 10.3390/ijms15046184

Kou, T., Luo, H., and Yin, L. (2021). Relationship between neutrophils to HDL-C ratio and severity of coronary stenosis. *BMC Cardiovasc. Disord.* 21:127. doi: 10.1186/s12872-020-01771-z

Kumar, S., Duan, Q., Wu, R., Harris, E. N., and Su, Q. (2021). Pathophysiological communication between hepatocytes and non-parenchymal cells in liver injury from NAFLD to liver fibrosis. *Adv. Drug Deliv. Rev.* 176:113869. doi: 10.1016/j.addr.2021.113869

Li, H., Guo, M., An, Z., Meng, J., Jiang, J., Song, J., et al. (2020). Prevalence and risk factors of metabolic associated fatty liver disease in Xinxiang, China. *Int. J. Environ. Res. Public Health* 17:1818. doi: 10.3390/ijerph17061818

Li, P., Fan, C., Cai, Y., Fang, S., Zeng, Y., Zhang, Y., et al. (2020). Transplantation of brown adipose tissue up-regulates miR-99a to ameliorate liver metabolic disorders in diabetic mice by targeting NOX4. *Adipocyte* 9, 57–67. doi: 10.1080/21623945.2020.1721970

Lima, W. G., Martins-Santos, M. E., and Chaves, V. E. (2015). Uric acid as a modulator of glucose and lipid metabolism. *Biochimie* 116, 17–23. doi: 10.1016/j.biochi.2015.06.025

Loomba, R., Friedman, S. L., and Shulman, G. I. (2021). Mechanisms and disease consequences of nonalcoholic fatty liver disease. *Cell.* 184, 2537–2564. doi: 10.1016/j.cell.2021.04.015

Mantovani, A., Scorletti, E., Mosca, A., Alisi, A., Byrne, C. D., and Targher, G. (2020). Complications, morbidity and mortality of nonalcoholic fatty liver disease. *Metabolism* 111s:154170. doi: 10.1016/j.metabol.2020.154170

Nasr, P., Fredrikson, M., Ekstedt, M., and Kechagias, S. (2020). The amount of liver fat predicts mortality and development of type 2 diabetes in non-alcoholic fatty liver disease. *Liver Int.* 40, 1069–1078. doi: 10.1111/liv.14414

Osonoi, T., Gouda, M., Kubo, M., Arakawa, K., Hashimoto, T., and Abe, M. (2018). Effect of canagliflozin on urinary albumin excretion in japanese patients with type 2 diabetes mellitus and microalbuminuria: a pilot study. *Diabetes Technol. Ther.* 20, 681–688. doi: 10.1089/dia.2018.0169

Powell, E. E., Wong, V. W., and Rinella, M. (2021). Non-alcoholic fatty liver disease. *Lancet* 397, 2212–2224. doi: 10.1016/S0140-6736(20)32511-3

Sakurai, Y., Kubota, N., Yamauchi, T., and Kadowaki, T. (2021). Role of Insulin Resistance in MAFLD. *Int. J. Mol. Sci.* 22:4156. doi: 10.3390/ijms22084156

Shin, D., and Lee, K. W. (2021). High pre-pregnancy BMI with a history of gestational diabetes mellitus is associated with an increased risk of type 2 diabetes in Korean women. *PLoS ONE* 16:e0252442. doi: 10.1371/journal.pone.0252442

Tacke, F., and Weiskirchen, R. (2021). Non-alcoholic fatty liver disease (NAFLD)/non-alcoholic steatohepatitis (NASH)-related liver fibrosis: mechanisms, treatment and prevention. *Ann. Transl. Med.* 9:729. doi: 10.21037/atm-20-4354

Targher, G., Corey, K. E., Byrne, C. D., and Roden, M. (2021). The complex link between NAFLD and type 2 diabetes mellitus - mechanisms and treatments. *Nat. Rev. Gastroenterol. Hepatol.* 18, 599-612. doi: 10.1038/s41575-021-00448-y

Uslu, A. U., Sekin, Y., Tarhan, G., Canakc,i N., Gunduz, M., and Karagulle, M. (2018). Evaluation of monocyte to high-density lipoprotein cholesterol ratio in the presence and severity of metabolic syndrome. *Clin. Appl. Thromb. Hemost.* 24, 828–833. doi: 10.1177/1076029617741362

Usta, A., Avci, E., Bulbul, C. B., Kadi, H., and Adali, E. (2018). The monocyte counts to HDL cholesterol ratio in obese and lean patients with polycystic ovary syndrome. *Reprod. Biol. Endocrinol.* 16:34. doi: 10.1186/s12958-018-0351-0

Wang, H. Y., Shi, W. R., Yi, X., Zhou, Y. P., Wang, Z. Q., and Sun, Y. X. (2019). Assessing the performance of monocyte to high-density lipoprotein ratio for predicting ischemic stroke: insights from a population-based Chinese cohort. *Lipids Health Dis.* 18:127. doi: 10.1186/s12944-019-1076-6

Wang, X., Rao, H., Zhao, J., Wee, A., Li, X., Fei, R., et al. (2020). STING expression in monocyte-derived macrophages is associated with the progression of liver inflammation and fibrosis in patients with nonalcoholic fatty liver disease. *Lab. Invest.* 100, 542–552. doi: 10.1038/s41374-019-0342-6

Wu, H., Zhang, T., Pan, F., Steer, C. J., Li, Z., Chen, X., et al. (2017). MicroRNA-206 prevents hepatosteatosis and hyperglycemia by facilitating insulin signaling and impairing lipogenesis. *J. Hepatol.* 66, 816–824. doi: 10.1016/j.jhep.2016.12.016

Yilmaz, M., and Kayançiçek, H. (2018). A new inflammatory marker: elevated monocyte to HDL cholesterol ratio associated with smoking. *J. Clin. Med.* 7:76. doi: 10.3390/jcm7040076

Yki-Järvinen, H., Luukkonen, P. K., Hodson, L., and Moore, J. B. (2021). Dietary carbohydrates and fats in nonalcoholic fatty liver disease. *Nat. Rev. Gastroenterol. Hepatol.* 18, 770-786. doi: 10.1038/s41575-021-00472-y

Younossi, Z. M., Golabi, P., de Avila, L., Paik, J. M., Srishord, M., Fukui, N., et al. (2019). The global epidemiology of NAFLD and NASH in patients with type 2 diabetes: a systematic review and meta-analysis. *J. Hepatol.* 71, 793–801. doi: 10.1016/j.jhep.2019.06.021

Zatterale, F., Longo, M., Naderi, J., Raciti, G. A., Desiderio, A., Miele, C., et al. (2019). Chronic adipose tissue inflammation linking obesity to insulin resistance and type 2 diabetes. *Front. Physiol.* 10:1607. doi: 10.3389/fphys.2019.01607

Zhang, D. P., Baituola, G., Wu, T. T., Chen, Y., Hou, X. G., Yang, Y., et al. (2020). An elevated monocyte-to-high-density lipoprotein-cholesterol ratio is associated with mortality in patients with coronary artery disease who have undergone PCI. *Biosci. Rep.* 40:BSR20201108. doi: 10.1042/BSR20201108

Zhang, Y., Li, K., Kong, A., Zhou, Y., Chen, D., Gu, J., et al. (2021). Dysregulation of autophagy acts as a pathogenic mechanism of non-alcoholic fatty liver disease (NAFLD) induced by common environmental pollutants. *Ecotoxicol. Environ. Saf.* 217:112256. doi: 10.1016/j.ecoenv.2021.112256

Zhou, J., Bai, L., Zhang, X. J., Li, H., and Cai, J. (2021). Nonalcoholic fatty liver disease and cardiac remodeling risk: pathophysiological mechanisms and clinical implications. *Hepatology* 74, 2839–2847. doi: 10.1002/hep.32072

Ziolkowska, S., Binienda, A., Jablkowski, M., Szemraj, J., and Czarny, P. (2021). The interplay between insulin resistance, inflammation, oxidative stress, base excision repair and metabolic syndrome in nonalcoholic fatty liver disease. *Int. J. Mol. Sci.* 22:11128. doi: 10.3390/ijms222011128

Conflict of Interest: The authors declare that the research was conducted in the absence of any commercial or financial relationships that could be construed as a potential conflict of interest.

Publisher's Note: All claims expressed in this article are solely those of the authors and do not necessarily represent those of their affiliated organizations, or those of the publisher, the editors and the reviewers. Any product that may be evaluated in this article, or claim that may be made by its manufacturer, is not guaranteed or endorsed by the publisher.

frontiers in Physiology

MINI REVIEW
published: 14 January 2022
doi: 10.3389/fphys.2021.794629

Fatty Acid Metabolism and Idiopathic Pulmonary Fibrosis

Jing Geng[1†], Yuan Liu[1,2†], Huaping Dai[1] and Chen Wang[1,2*]*

[1] *Department of Pulmonary and Critical Care Medicine, Center of Respiratory Medicine, China-Japan Friendship Hospital, National Clinical Research Center for Respiratory Diseases, Institute of Respiratory Medicine, Chinese Academy of Medical Sciences, Beijing, China,* [2] *Graduate School of Peking Union Medical College, Chinese Academy of Medical Sciences and Peking Union Medical College, Beijing, China*

Fatty acid metabolism, including the *de novo* synthesis, uptake, oxidation, and derivation of fatty acids, plays several important roles at cellular and organ levels. Recent studies have identified characteristic changes in fatty acid metabolism in idiopathic pulmonary fibrosis (IPF) lungs, which implicates its dysregulation in the pathogenesis of this disorder. Here, we review the evidence for how fatty acid metabolism contributes to the development of pulmonary fibrosis, focusing on the profibrotic processes associated with specific types of lung cells, including epithelial cells, macrophages, and fibroblasts. We also summarize the potential therapeutics that target this metabolic pathway in treating IPF.

Keywords: fatty acid synthesis, fatty acid oxidation, idiopathic pulmonary fibrosis, alveolar epithelial cell, myofibroblast, macrophage

OPEN ACCESS

Edited by:
Dawei Zhang,
University of Alberta, Canada

Reviewed by:
Dan Predescu,
Rush University, United States

****Correspondence:***
Huaping Dai
daihuaping@ccmu.edu.cn
Chen Wang
cyh-birm@263.net

[†]These authors have contributed equally to this work

Specialty section:
This article was submitted to Lipid and Fatty Acid Research, a section of the journal Frontiers in Physiology

Received: *13 October 2021*
Accepted: *20 December 2021*
Published: *14 January 2022*

Citation:
Geng J, Liu Y, Dai H and Wang C (2022) Fatty Acid Metabolism and Idiopathic Pulmonary Fibrosis. Front. Physiol. 12:794629. doi: 10.3389/fphys.2021.794629

INTRODUCTION

Idiopathic pulmonary fibrosis (IPF) is a fatal fibrotic disorder of unknown etiology. It is usually associated with worsening respiratory symptoms, lung function decline, and limited responses to therapies. The worldwide incidence of IPF has risen steadily over time (Hutchinson et al., 2015), and disease burdens on the global healthcare system are increasing. Underlying genetic susceptibility, together with environmental insults, is believed to trigger an abnormal wound repair response, leading to the activation of a non-resolving fibrotic cascade. Mechanistic features include epithelial apoptosis, macrophages releasing pro-fibrotic mediators, and the activation of fibroblasts and myofibroblasts.

Although the underlying mechanisms of these dysregulated fibrotic responses are not completely understood, recent evidence indicates that metabolic abnormalities play a critical role. For example, altered glycolysis and glutamine metabolism were found in human lungs with severe IPF (Kang et al., 2016). Additionally, changes in lipid metabolism, specifically leading to the overproduction of profibrotic lipids such as lysophospholipids, sphingolipids, and eicosanoids, contribute to the pathogenesis of IPF [for general review, see Castelino (2012); Mamazhakypov et al. (2019)].

In this brief review, we describe the general concepts in fatty acid (FA) metabolism and the pathology of IPF. We analyze the roles of this metabolic pathway in regulating the function of specific cells and the relevant pathologic cellular responses in IPF, including pro-fibrotic phenotype changes of alveolar epithelial cells and macrophages, and fibroblast/myofibroblast activation. We also discuss potential pulmonary fibrosis therapeutics that target this pathway.

THE FATTY ACID METABOLIC PATHWAY

Fatty acids (FAs) contain a terminal carboxyl group and a hydrocarbon chain, and mostly contain an even number of carbons; they can be saturated or unsaturated. The understanding of the role of FA metabolism in both healthy and disease physiology has recently been greatly advanced (Kuda et al., 2018; Yi et al., 2018). Fatty acids tightly couple glucose and lipid metabolism *via* the *de novo* FA synthesis pathway, supporting cell adaption to environmental changes and generating large amounts of adenosine triphosphate (ATP) through β-oxidation (Bartlett and Eaton, 2004). As well as their role in energy production and as part of the structural "building blocks" of cell membranes, FAs also act individually by converting to FA-derived lipid mediators to regulate biological activities (de Carvalho and Caramujo, 2018) such as signal transduction, cell cycle regulation, apoptosis, and differentiation (**Figure 1**).

Fatty Acid Synthesis

Fatty acid (FAs) in cells derive either from exogenous sources or *de novo* FA synthesis. The FA biosynthesis pathway is highly conserved and occurs in the cytoplasm (Rui, 2014). The TCA cycle intermediator citrate is transported out of mitochondria and cleaved by ATP citrate lyase (ACLY) into acetyl-CoA and oxaloacetate. Acetyl-CoA is then converted to malonyl-CoA by the rate-limiting enzyme acetyl-CoA carboxylase (ACC). Finally, acetyl-CoA and malonyl-CoA are used to produce palmitic acid as an initial product by the action of FA synthase (FASN) (Smith, 1994). Subsequent elongation and desaturation of palmitic acid determine the length and degree of FA saturation, which are critical to their functions and metabolic fates (Guillou et al., 2010). For example, stearate, a long-chain fatty acid, is produced through the actions of a family of enzymes, ELOVL1–7, that add two carbons to the terminal carboxyl group in each reaction cycle. Another family of stearoyl-CoA desaturases (SCDs) catalyzes FA desaturation (Paton and Ntambi, 2009). Fatty acids can also be taken up from extracellular surroundings *via* cell surface receptors, such as CD36 (Wang and Li, 2019), which is a widely expressed transmembrane protein. Once entering the intracellular FA pool, they can be esterified with glycerol or sterol backbones and stored in the form of triglycerides in lipid droplets, or utilized for energy production through FA oxidation (FAO).

Fatty Acid Oxidation

FA oxidation (FAO) is a major pathway for the utilization of FAs to generate biological energy. Free FAs in the cytosol are activated by acyl-CoA synthase to generate acyl-CoA. Acyl-CoA is conjugated to carnitine *via* carnitine palmitoyl transferase 1 (CPT1) activity to form acylcarnitine which is subsequently transported into the mitochondrial matrix by carnitine acylcarnitine translocase (CAT). Acylcarnitine is then converted back to acyl-CoA and carnitine by CPT2 in the mitochondria. Acyl-CoA undergoes β-oxidation, which is a series of enzyme-mediated reactions that yield large amounts of intermediator metabolites that are subsequently utilized in the TCA cycle; carnitines are recycled by being transported out of the mitochondrial matrix (Houten et al., 2016).

Fatty Acid Derivation and Derivatives

Besides anabolism and catabolism pathways in the cytoplasm, some FAs serve as substrates for enzymatic conversation to lipid-derived mediators that are bioactive in tissue inflammation and organ injury. Arachidonic acid is incorporated into cellular phospholipids and is rapidly released from cell membranes by phospholipase A2 enzymes for enzymatic conversion to prostaglandins (PGs) and leukotrienes (Kuehl and Egan, 1980) as well as lipoxins (LXs) (Serhan and Savill, 2005). Prostaglandins and leukotrienes are widely recognized for their important role in injury and inflammation, while LXs, as a family of special pre-resolving mediators (SPMs), are formed by transcellular biosynthesis and have anti-inflammatory and pro-resolving effects. These derivatives underlie the pathology of many prevalent diseases resulting in tissue fibrosis, as typified by kidney (Brennan et al., 2017), liver (Mariqueo and Zúñiga-Hernández, 2020), and lung fibrosis (Bozyk and Moore, 2011; Suryadevara et al., 2020).

ALTERATIONS IN FATTY ACID METABOLISM IN PULMONARY FIBROSIS

An altered content and profile of saturated and unsaturated FAs have been identified in IPF patients and animal models of lung fibrosis; however, there is no consensus on the specific changes. One study observed a 63% increase in serum total FA levels in IPF patients compared with control subjects (Iannello et al., 2002). Others found low levels of saturated long-chain FAs, such as palmitic acid, oleic acid, and stearic acid, in IPF lung tissues and bronchoalveolar lavage fluid (BALF) (Schmidt et al., 2002; Kim et al., 2021). In contrast, Chu et al. (2019) detected significantly higher levels of palmitic and stearic acid in BALF from IPF patients compared with controls.

The chemotherapeutic drug bleomycin is widely used as a means of inducing experimental lung fibrosis in animal models (Fleischman et al., 1971; Adamson and Bowden, 1974; Thrall et al., 1979), including mice, rats, and dogs. Lower levels of free FAs were detected in BALF from rats exposed to bleomycin the previous day, which then reached twice normal levels on days 3–30 before returning to normal on day 120 (Swendsen et al., 1996); however, unsaturated FAs were significantly increased compared with controls between day 3 and 120 (Swendsen et al., 1996). Moreover, abnormal FA compositions were identified in the lung tissue of mice exposed to bleomycin, with high levels of palmitic acid and oleic acid but low levels of the essential polyunsaturated linoleic acid (Sunaga et al., 2013).

ABERRANT FATTY ACID METABOLISM CONTRIBUTES TO IDIOPATHIC PULMONARY FIBROSIS PATHOGENESIS

Extensive changes in FA metabolism have been observed in IPF, suggesting its potential critical role in disease pathophysiology.

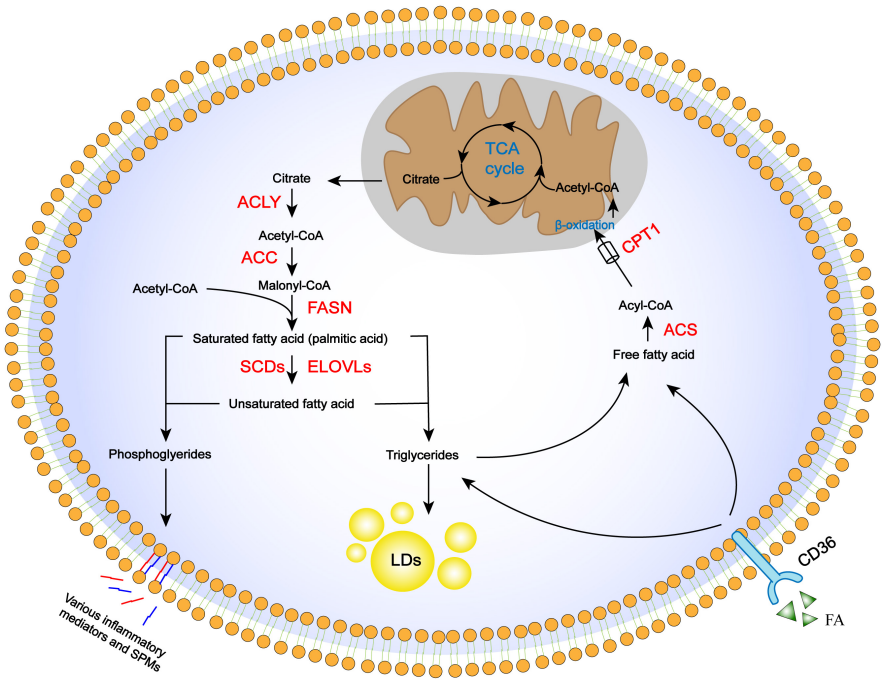

FIGURE 1 | Regulation of FA metabolism pathways, including anabolism, storage, uptake, catabolism, and derivation. *De novo* FA synthesis occurs in the cytoplasm, where citrate is converted in the TCA cycle to the final long-chain saturated or unsaturated FA. These steps involve ACLY, ACC, FASN, and desaturases, as well as elongation proteins. Once synthesized, FA is stored in lipid droplets as triglycerides or mobilized through β-oxidation to provide energy and acetyl-CoA. Acetyl-CoA is used again in the TCA cycle. Essential FAs are incorporated into cellular phospholipids and released from cell membranes to be converted into lipid-derived mediators. FAs from extracellular sources can also be used for storage or β-oxidation through the CD36 receptor.

Various FA metabolism pathways are intricately intertwined, and a perturbation of any of these in the lung may contribute to the development of pro-fibrotic phenotypes in epithelial cells, macrophages, and fibroblasts/myofibroblasts (**Figure 2**).

Impact on Epithelial Cell Switch to a Pro-fibrotic Phenotype

Epithelial cell dysfunction is a central component in IPF pathophysiology. Alveolar type (AT)2 cells are the most active cell of lung lipid metabolism, with an important role in alveolar homeostasis involving surfactant biosynthesis, and as progenitor cells to both self-renew and transdifferentiate into AT1 cells (Barkauskas et al., 2013). AT2 cells, and other lung epithelia, are often susceptible to injury. Thus, repeated genetic or environment stimulation may result in a diverse range of cellular endophenotypes and molecular signatures including endoplasmic reticulum (ER) stress, apoptosis, and inflammatory and profibrotic signaling, which ultimately converge to drive downstream fibrotic remodeling in IPF lungs (Katzen and Beers, 2020).

Fatty acid (FA) synthesis and composition are known to be involved in ER stress (Volmer et al., 2013; Han and Kaufman, 2016; Velázquez et al., 2016). Lipids are required for the export of folded proteins contained in lipid droplets from the ER lumen (Velázquez et al., 2016), and impaired lipid synthesis can increase protein accumulation, resulting in sustained ER stress. Additionally, changes in the ER membrane composition following increased levels of FA saturation may directly activate protein kinase R-like ER kinase and inositol-requiring enzyme 1 (Volmer et al., 2013). Although the mechanism that connects FA metabolism with ER stress in IPF is unclear, studies have reported that lipotoxicity caused by saturated FA accumulation may increase ER stress, leading to apoptosis. For example, Romero et al. (2018) reported that SCD1 expression was reduced in IPF lung tissues by showing that a pharmacological inhibitor of SCD1 induced epithelial cell injury and promoted lung fibrosis by blocking the synthesis of unsaturated FAs. Moreover, a high-fat diet rich in saturated FAs has consistently been shown to induce lung epithelial cell apoptosis by causing ER stress and thereby aggravating bleomycin-induced lung fibrosis (Chu et al., 2019). Additionally, Sunaga et al. (2013) found that ELOVL6 expression was downregulated in the lungs of IPF patients. ELOVL6 catalyzes the elongation of C16 FA and renders it an unsaturated FA (Matsuzaka et al., 2007). Thus, an ELOVL6 deficiency increases the proportion of saturated FAs, thereby worsening pulmonary fibrosis with collagen deposition. Furthermore, treatment with palmitic acid was shown to trigger apoptosis and transforming growth factor (TGF)-β1 expression in cultured AT2 cells (Sunaga et al., 2013).

Although the role of the epithelial–mesenchymal transition (EMT) in IPF remains controversial, recent evidence indicates that multiple inflammatory mediators and essential FA-derived SPMs involved in EMT also function in lung fibrosis.

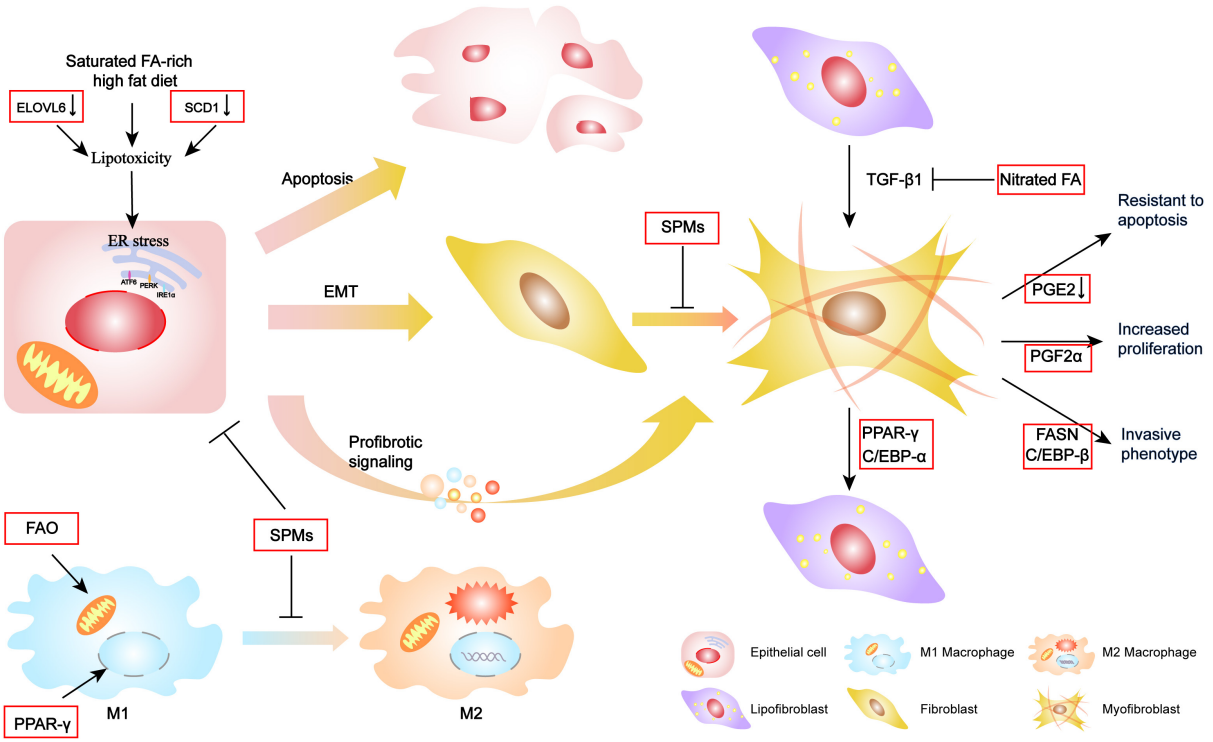

FIGURE 2 | Mechanism of FA metabolism contributing to the pathogenesis of IPF. Alterations in FA metabolism contribute epithelial cellular ER stress toward apoptosis, EMT, or secretion with profibrotic signaling, which further activates fibroblast differentiation. Increasing FAO and activation of PPAR-γ transcription factor may facilitate the transportation of some M2 macrophage target genes and promote M2 polarization. SPMs could protect these cellular endophenotypes changes and fibrotic molecular signature. Additionally, FA and the regulators are also involved in the reversible lipogenic-to-myogenic differentiation and directly contribute to myofibroblast proliferation, invasion, and resistance to apoptosis.

TABLE 1 | Summary of studies evaluating the effects of fatty acid-targeting agents in animal models of lung fibrosis.

Agent	Target and mechanism	Strategy	Animal models	Agent application	Main effects	References
T0901317	Augment expression of several lipid-synthesizing enzyme	curative	Silica, mice (14 days)	Intraperitoneal, daily (days 4–14)	Reduce ER stress and attenuate fibrotic remodeling	Romero et al., 2018
Troglitazone	Activation of the PPAR-r signaling	curative preventive	Bleomycin, mice (21days)	Oral, daily (days -3–21 or days 11–21)	Reduce fibrosis and TGF-β1 levels	Jung et al., 2018
Pioglitazone	Activation of the PPAR-r signaling	preventive	Bleomycin, rats (28 days)	Oral, daily (days -7–28)	Prevent inflammation and collagen synthesis	Genovese et al., 2005
Metformin	Activation of the AMPK and PPAR-r signaling	curative	Bleomycin, mice (28 days)	Supplied *via* drinking water (days 14–28)	Induce lipogenic differentiation in myofibroblast and accelerate resolution of fibrosis	Kheirollahi et al., 2019
Docosahexa-enoic acid	A single n-3 polyunsaturated fatty acid	preventive	Bleomycin, mice (21 days)	Intratracheal, once (days -4–21)	Reduce weight loss and mortality; reduce fibrosis; reduce lung function changes	Kennedy et al., 1989
Dietary essential fatty acids	Rich in omega-3 fatty acid, eicosapentaenoic acid, and docosahexaenoic acid	preventive	Bleomycin, mice (21 days)	Dietary treatment began at 21 days of age and continued for the entire study	Reduce the severity of fibrosis	Zhao et al., 2014

ER, endoplasmic reticulum; PPAR-γ, peroxisome proliferator-activated receptor γ; TGF-β1, transforming growth factor β1, AMPK, AMP-activated protein kinase, ROS, reactive oxidative species; ATP, adenosine triphosphate.

For example, maresin 1 (MaR1), an SPM derived from docosahexaenoic acid, was found to inhibit TGF-β1-induced EMT and prevent the activation of Smad2/3, Akt, and the transcription factor Snail. Additionally, MaR1 treatment attenuated bleomycin-induced lung fibrosis *in vivo* and reduced the generation of TGF-β1 (Wang et al., 2015). Similarly, protein DX, which also derives from docosahexaenoic acid, was reported to suppress inflammatory infiltration and the expression of pro-fibrotic cytokines, and to inhibit the EMT phenotype, which prolonged the survival time of lung fibrosis mice (Li et al., 2017). Other work found that SPMs inhibited apoptosis and promoted wound repair proliferation and the transdifferentiation of AT2 cells in respiratory distress syndrome-related lung fibrosis (Zheng et al., 2018; Yang et al., 2019).

Modulation of Macrophage Polarization

As the most abundant immune cell in the lung, macrophages play a vital role in the pathogenesis of pulmonary fibrosis. Most resident macrophages originate from progenitors in the bone marrow and migrate into different tissues where the local environment and signal cues shape the macrophage phenotype (Shapouri-Moghaddam et al., 2018). Macrophage polarization achieves a phenotypic dichotomy of the pro-inflammatory M1 subtype, which is induced by the Th1 cytokine interferon-γ, and the M2 phenotype, which is induced by the Th2 cytokines interleukin (IL)-4 or IL-13. The M2 phenotype is associated with tissue remodeling and repair and is a vital regulator of fibrogenesis in IPF (Zhang et al., 2018). Upon activation, M2 macrophages produce profibrotic mediators such as TGF-β1, which activates fibroblasts and extracellular matrix (ECM) deposition.

There appears to be a strong relationship between macrophage polarization and its demand for FAs. Fatty acids provide energy to support macrophage polarization and activate signaling pathways to shape it, while FAO generates large quantities of ATP that is thought to promote M2 polarization. Indeed, increased levels of FAO were found in IPF lungs (Gu et al., 2019), suggesting that FAO may be involved in fibrogenesis by promoting M2 macrophage activation. The M2 phenotype is also dependent upon the transcription factor peroxisome proliferator-activated receptor (PPAR)-γ (Namgaladze and Brüne, 2016), which has numerous FAs as its natural ligands (Marion-Letellier et al., 2016). Furthermore, FAs promote expression of the FA receptor CD36, thereby inducing the M2 phenotype *via* the simultaneous escalation of FA uptake and a cycle of self-augmented profibrotic activation. The loss of CD36 was reported to inhibit lung fibrosis and reduce levels of pro-fibrotic Th2 cytokines including IL-9, IL-4, and IL-13 (Parks et al., 2013). Lipoxins also regulate different macrophage subtypes in lung fibrosis, while an aspirin-triggered LX synthetic analog was reported to have the therapeutic ability to decrease cytokine production and restore M2 macrophage populations in established bleomycin-induced lung fibrosis (Martins et al., 2009; Guilherme et al., 2013).

Activation of Fibroblasts/Myofibroblasts

Dysfunctional epithelial cells and polarized macrophages generate large quantities of profibrotic cytokines that induce fibroblast differentiation into myofibroblasts. Myofibroblasts within IPF lungs have a pathologic phenotype (Richeldi et al., 2017), including the ability to secrete excessive amounts of matrix within lung parenchyma, and causing basement membrane disruption. The main source of lung myofibroblasts is resident interstitial lung fibroblasts. Recently, lipofibroblast was suggested as an origin of the activated myofibroblast in pulmonary fibrosis (El Agha et al., 2017). Lipofibroblast is one of the interstitial fibroblasts that contain lipid droplets and are located adjacent to AT2 cells, and likely contribute to surfactant production in quiescent lungs (Rehan and Torday, 2014).

El Agha et al. (2017) used cell lineage tracing to monitor lipogenic or myogenic populations of lung fibroblasts in mice and demonstrated a phenotypic switch between the two populations during the progression and resolution phases of lung fibrosis. Mechanically, they found that this phenotypic shift involves PPAR-γ. Nitrated fatty acids are PPAR-γ agonists which promote the dedifferentiation of myofibroblasts by blocking TGF-β1 effects (Reddy et al., 2014). Additionally, CCAAT enhancer-binding protein (C/EBP) α, which is regulated by FAs and their derivatives in adipogenesis, was found to promote myofibroblast to lipofibroblast dedifferentiation (Liu et al., 2019). Both non-fibrotic controls and IPF-derived fibroblasts/myofibroblasts express LXA4 receptors that enable activation of the ALXR G-protein-coupled receptor to regress a myofibroblastic phenotype to a fibroblastic one by reducing α-SMA expression, actin stress fiber formation, and nuclear Smad2/3 levels (Roach et al., 2015).

Additional characteristic phenotypes of fibroblasts/myofibroblasts that contribute to the development of lung fibrosis include increased proliferation, resistance to apoptosis, and the acquisition of invasive activity (Hinz and Lagares, 2020; Phan et al., 2021). During wound healing, fibroblasts proliferate in response to tissue injury but eventually disappear through apoptosis when the tissue returns to homeostasis. However, IPF fibroblasts demonstrate increased proliferation and resistance to FAS ligand-induced apoptosis (Bamberg et al., 2018). Idiopathic pulmonary fibrosis lungs have also been shown to have an abundance of PGF2α that stimulates the proliferation of lung fibroblasts (Oga et al., 2009), while IPF-derived fibroblasts have reduced PGE2 levels that contribute to their apoptotic resistance (Maher et al., 2010). Indeed, PGE2 limits many of the pathologic features of lung fibroblasts and myofibroblasts, including proliferation, migration, collagen secretion, and TGFβ1-induced differentiation (reviewed in Bozyk and Moore, 2011). These findings suggest that prostaglandins have pleiotropic activities in regulating the fibroblast phenotype in IPF.

Unlike normal fibroblasts, IPF fibroblasts invade the surrounding ECM much like metastatic cancer cells (Ballester et al., 2019). The underlying mechanism for this enhanced invasion may be correlated with *de novo* FA synthesis because the inhibition of *FASN* attenuated the invasive activity of TGFβ1-treated fibroblasts (Jung et al., 2018). Another possibility is the formation of α-smooth muscle actin (α-SMA)-containing

stress fibers. A cognate binding element of C/EBPβ was identified in the α-*SMA* promoter that contributed to its upregulation (Phan, 2012).

POTENTIAL THERAPEUTICS TARGETING THE FATTY ACID METABOLIC PATHWAY IN IDIOPATHIC PULMONARY FIBROSIS TREATMENT

Therapies targeting FA metabolism have been tested in pre-clinical models of lung fibrosis (**Table 1**). Promoting the conversion and formation of FAs with small molecule compounds, such as a liver X receptor agonist (T0901317) and PPAR-γ agonists (e.g., rosiglitazone, pioglitazone, and troglitazone), was found to be beneficial in animal models of lung fibrosis (Genovese et al., 2005; Milam et al., 2008; Aoki et al., 2009; Romero et al., 2018). Metformin also exerts potent antifibrotic effects, including altering the fate of myofibroblasts *via* PPAR-γ activation and inhibiting collagen production *via* AMP-activated protein kinase activation (Kheirollahi et al., 2019; Xiao et al., 2020). Based on the altered content and composition of FAs in IPF lungs and animal models that we describe, it seems a reasonable approach to supplement appropriate FAs for the treatment of this disease. Indeed, dietary essential FAs provide protection from lung fibrosis after bleomycin treatment (Kennedy et al., 1989), while intratracheally delivered FAs have a therapeutic potential for the treatment of lung fibrosis (Zhao et al., 2014).

CONCLUSION

Abnormalities of FA metabolism in pulmonary fibrosis have received increasing attention in recent years. This review describes how the FA metabolism regulates the profibrotic phenotype of alveolar epithelial cells and macrophages, as well as fibroblasts/myofibroblasts activation in the IPF lungs and the lungs of mice with experimental pulmonary fibrosis. Understanding the mechanism of these metabolic abnormalities in IPF will open a new avenue of novel therapeutics.

AUTHOR CONTRIBUTIONS

All authors contributed to the writing of the article and the development of the figures.

FUNDING

This work was supported by the National Natural Science Foundation of China (Grant No. 81800067) and CAMS Innovation Fund for Medical Sciences (CIFMS) (Grant No. 2018-12M-1-001).

SUPPLEMENTARY MATERIAL

The Supplementary Material for this article can be found online at: https://www.frontiersin.org/articles/10.3389/fphys.2021.794629/full#supplementary-material

REFERENCES

Adamson, I. Y., and Bowden, D. H. (1974). The pathogenesis of bleomycin-induced pulmonary fibrosis in mice. *Am. J. Pathol.* 77, 185–197.

Aoki, Y., Maeno, T., Aoyagi, K., Ueno, M., Aoki, F., Aoki, N., et al. (2009). Pioglitazone, a peroxisome proliferator-activated receptor gamma ligand, suppresses bleomycin-induced acute lung injury and fibrosis. *Respiration* 77, 311–319. doi: 10.1159/000168676

Ballester, B., Milara, J., and Cortijo, J. (2019). Idiopathic pulmonary fibrosis and lung cancer: mechanisms and molecular targets. *Int. J. Mol. Sci.* 20:593. doi: 10.3390/ijms20030593

Bamberg, A., Redente, E. F., Groshong, S. D., Tuder, R. M., Cool, C. D., Keith, R. C., et al. (2018). Protein tyrosine phosphatase-N13 promotes myofibroblast resistance to apoptosis in idiopathic pulmonary fibrosis. *Am. J. Respir. Crit. Care Med.* 198, 914–927. doi: 10.1164/rccm.201707-1497OC

Barkauskas, C. E., Cronce, M. J., Rackley, C. R., Bowie, E. J., Keene, D. R., Stripp, B. R., et al. (2013). Type 2 alveolar cells are stem cells in adult lung. *J. Clin. Invest.* 123, 3025–3036. doi: 10.1172/jci68782

Bartlett, K., and Eaton, S. (2004). Mitochondrial beta-oxidation. *Eur. J. Biochem.* 271, 462–469. doi: 10.1046/j.1432-1033.2003.03947.x

Bozyk, P. D., and Moore, B. B. (2011). Prostaglandin E2 and the pathogenesis of pulmonary fibrosis. *Am. J. Respir. Cell Mol. Biol.* 45, 445–452. doi: 10.1165/rcmb.2011-0025RT

Brennan, E. P., Cacace, A., and Godson, C. (2017). Specialized pro-resolving mediators in renal fibrosis. *Mol. Aspects Med.* 58, 102–113. doi: 10.1016/j.mam.2017.05.001

Castelino, F. V. (2012). Lipids and eicosanoids in fibrosis: emerging targets for therapy. *Curr. Opin. Rheumatol.* 24, 649–655. doi: 10.1097/BOR.0b013e328356d9f6

Chu, S. G., Villalba, J. A., Liang, X., Xiong, K., Tsoyi, K., Ith, B., et al. (2019). Palmitic acid-rich high-fat diet exacerbates experimental pulmonary fibrosis by modulating endoplasmic reticulum stress. *Am. J. Respir. Cell Mol. Biol.* 61, 737–746. doi: 10.1165/rcmb.2018-0324OC

de Carvalho, C., and Caramujo, M. J. (2018). The various roles of fatty acids. *Molecules* 23:2583. doi: 10.3390/molecules23102583

El Agha, E., Moiseenko, A., Kheirollahi, V., De Langhe, S., Crnkovic, S., Kwapiszewska, G., et al. (2017). Two-way conversion between lipogenic and myogenic fibroblastic phenotypes marks the progression and resolution of lung fibrosis. *Cell Stem Cell* 20, 261–273.e3. doi: 10.1016/j.stem.2016.10.004

Fleischman, R. W., Baker, J. R., Thompson, G. R., Schaeppi, U. H., Illievski, V. R., Cooney, D. A., et al. (1971). Bleomycin-induced interstitial pneumonia in dogs. *Thorax* 26, 675–682. doi: 10.1136/thx.26.6.675

Genovese, T., Cuzzocrea, S., Di Paola, R., Mazzon, E., Mastruzzo, C., Catalano, P., et al. (2005). Effect of rosiglitazone and 15-deoxy-Delta12,14-prostaglandin J2 on bleomycin-induced lung injury. *Eur. Respir. J.* 25, 225–234. doi: 10.1183/09031936.05.00049704

Gu, L., Larson Casey, J. L., Andrabi, S. A., Lee, J. H., Meza-Perez, S., Randall, T. D., et al. (2019). Mitochondrial calcium uniporter regulates PGC-1α expression to mediate metabolic reprogramming in pulmonary fibrosis. *Redox Biol.* 26:101307. doi: 10.1016/j.redox.2019.101307

Guilherme, R. F., Xisto, D. G., Kunkel, S. L., Freire-de-Lima, C. G., Rocco, P. R., Neves, J. S., et al. (2013). Pulmonary antifibrotic mechanisms aspirin-triggered lipoxin A(4) synthetic analog. *Am. J. Respir. Cell Mol. Biol.* 49, 1029–1037. doi: 10.1165/rcmb.2012-0462OC

Guillou, H., Zadravec, D., Martin, P. G., and Jacobsson, A. (2010). The key roles of elongases and desaturases in mammalian fatty acid metabolism: insights from transgenic mice. *Prog. Lipid Res.* 49, 186–199. doi: 10.1016/j.plipres.2009.12.002

Han, J., and Kaufman, R. J. (2016). The role of ER stress in lipid metabolism and lipotoxicity. *J. Lipid Res.* 57, 1329–1338. doi: 10.1194/jlr.R067595

Hinz, B., and Lagares, D. (2020). Evasion of apoptosis by myofibroblasts: a hallmark of fibrotic diseases. *Nat. Rev. Rheumatol.* 16, 11–31. doi: 10.1038/s41584-019-0324-5

Houten, S. M., Violante, S., Ventura, F. V., and Wanders, R. J. (2016). The biochemistry and physiology of mitochondrial fatty acid β-oxidation and its genetic disorders. *Annu. Rev. Physiol.* 78, 23–44. doi: 10.1146/annurev-physiol-021115-105045

Hutchinson, J., Fogarty, A., Hubbard, R., and McKeever, T. (2015). Global incidence and mortality of idiopathic pulmonary fibrosis: a systematic review. *Eur. Respir. J.* 46, 795–806. doi: 10.1183/09031936.00185114

Iannello, S., Cavaleri, A., Camuto, M., Pisano, M. G., Milazzo, P., and Belfiore, F. (2002). Low fasting serum triglyceride and high free fatty acid levels in pulmonary fibrosis: a previously unreported finding. *MedGenMed* 4:5.

Jung, M. Y., Kang, J. H., Hernandez, D. M., Yin, X., Andrianifahanana, M., Wang, Y., et al. (2018). Fatty acid synthase is required for profibrotic TGF-β signaling. *FASEB J.* 32, 3803–3815. doi: 10.1096/fj.201701187R

Kang, Y. P., Lee, S. B., Lee, J. M., Kim, H. M., Hong, J. Y., Lee, W. J., et al. (2016). Metabolic profiling regarding pathogenesis of idiopathic pulmonary fibrosis. *J. Proteome Res.* 15, 1717–1724. doi: 10.1021/acs.jproteome.6b00156

Katzen, J., and Beers, M. F. (2020). Contributions of alveolar epithelial cell quality control to pulmonary fibrosis. *J. Clin. Invest.* 130, 5088–5099. doi: 10.1172/jci139519

Kennedy, J. I. Jr., Chandler, D. B., Fulmer, J. D., Wert, M. B., and Grizzle, W. E. (1989). Dietary fish oil inhibits bleomycin-induced pulmonary fibrosis in the rat. *Exp. Lung Res.* 15, 315–329. doi: 10.3109/01902148909087861

Kheirollahi, V., Wasnick, R. M., Biasin, V., Vazquez-Armendariz, A. I., Chu, X., Moiseenko, A., et al. (2019). Metformin induces lipogenic differentiation in myofibroblasts to reverse lung fibrosis. *Nat. Commun.* 10:2987. doi: 10.1038/s41467-019-10839-0

Kim, H. S., Yoo, H. J., Lee, K. M., Song, H. E., Kim, S. J., Lee, J. O., et al. (2021). Stearic acid attenuates profibrotic signalling in idiopathic pulmonary fibrosis. *Respirology* 26, 255–263. doi: 10.1111/resp.13949

Kuda, O., Rossmeisl, M., and Kopecky, J. (2018). Omega-3 fatty acids and adipose tissue biology. *Mol. Aspects Med.* 64, 147–160. doi: 10.1016/j.mam.2018.01.004

Kuehl, F. A. Jr., and Egan, R. W. (1980). Prostaglandins, arachidonic acid, and inflammation. *Science* 210, 978–984. doi: 10.1126/science.6254151

Li, H., Hao, Y., Zhang, H., Ying, W., Li, D., Ge, Y., et al. (2017). Posttreatment with Protectin DX ameliorates bleomycin-induced pulmonary fibrosis and lung dysfunction in mice. *Sci. Rep.* 7:46754. doi: 10.1038/srep46754

Liu, W., Meridew, J. A., Aravamudhan, A., Ligresti, G., Tschumperlin, D. J., and Tan, Q. (2019). Targeted regulation of fibroblast state by CRISPR-mediated CEBPA expression. *Respir. Res.* 20:281. doi: 10.1186/s12931-019-1253-1

Maher, T. M., Evans, I. C., Bottoms, S. E., Mercer, P. F., Thorley, A. J., Nicholson, A. G., et al. (2010). Diminished prostaglandin E2 contributes to the apoptosis paradox in idiopathic pulmonary fibrosis. *Am. J. Respir. Crit. Care Med.* 182, 73–82. doi: 10.1164/rccm.200905-0674OC

Mamazhakypov, A., Schermuly, R. T., Schaefer, L., and Wygrecka, M. (2019). Lipids – two sides of the same coin in lung fibrosis. *Cell. Signal.* 60, 65–80. doi: 10.1016/j.cellsig.2019.04.007

Marion-Letellier, R., Savoye, G., and Ghosh, S. (2016). Fatty acids, eicosanoids and PPAR gamma. *Eur. J. Pharmacol.* 785, 44–49. doi: 10.1016/j.ejphar.2015.11.004

Mariqueo, T. A., and Zúñiga-Hernández, J. (2020). Omega-3 derivatives, specialized pro-resolving mediators: promising therapeutic tools for the treatment of pain in chronic liver disease. *Prostaglandins Leukot. Essent. Fatty Acids* 158:102095. doi: 10.1016/j.plefa.2020.102095

Martins, V., Valença, S. S., Farias-Filho, F. A., Molinaro, R., Simões, R. L., Ferreira, T. P., et al. (2009). ATLa, an aspirin-triggered lipoxin A4 synthetic analog, prevents the inflammatory and fibrotic effects of bleomycin-induced pulmonary fibrosis. *J. Immunol.* 182, 5374–5381. doi: 10.4049/jimmunol.0802259

Matsuzaka, T., Shimano, H., Yahagi, N., Kato, T., Atsumi, A., Yamamoto, T., et al. (2007). Crucial role of a long-chain fatty acid elongase, Elovl6, in obesity-induced insulin resistance. *Nat. Med.* 13, 1193–1202. doi: 10.1038/nm1662

Milam, J. E., Keshamouni, V. G., Phan, S. H., Hu, B., Gangireddy, S. R., Hogaboam, C. M., et al. (2008). PPAR-gamma agonists inhibit profibrotic phenotypes in human lung fibroblasts and bleomycin-induced pulmonary fibrosis. *Am. J. Physiol. Lung Cell Mol. Physiol.* 294, L891–L901. doi: 10.1152/ajplung.00333.2007

Namgaladze, D., and Brüne, B. (2016). Macrophage fatty acid oxidation and its roles in macrophage polarization and fatty acid-induced inflammation. *Biochim. Biophys. Acta* 1861, 1796–1807. doi: 10.1016/j.bbalip.2016.09.002

Oga, T., Matsuoka, T., Yao, C., Nonomura, K., Kitaoka, S., Sakata, D., et al. (2009). Prostaglandin F(2alpha) receptor signaling facilitates bleomycin-induced pulmonary fibrosis independently of transforming growth factor-beta. *Nat. Med.* 15, 1426–1430. doi: 10.1038/nm.2066

Parks, B. W., Black, L. L., Zimmerman, K. A., Metz, A. E., Steele, C., Murphy-Ullrich, J. E., et al. (2013). CD36, but not G2A, modulates efferocytosis, inflammation, and fibrosis following bleomycin-induced lung injury. *J. Lipid Res.* 54, 1114–1123. doi: 10.1194/jlr.M035352

Paton, C. M., and Ntambi, J. M. (2009). Biochemical and physiological function of stearoyl-CoA desaturase. *Am. J. Physiol. Endocrinol. Metab.* 297, E28–E37. doi: 10.1152/ajpendo.90897.2008

Phan, S. H. (2012). Genesis of the myofibroblast in lung injury and fibrosis. *Proc. Am. Thorac. Soc.* 9, 148–152. doi: 10.1513/pats.201201-011AW

Phan, T. H. G., Paliogiannis, P., Nasrallah, G. K., Giordo, R., Eid, A. H., Fois, A. G., et al. (2021). Emerging cellular and molecular determinants of idiopathic pulmonary fibrosis. *Cell. Mol. Life Sci.* 78, 2031–2057. doi: 10.1007/s00018-020-03693-7

Reddy, A. T., Lakshmi, S. P., Zhang, Y., and Reddy, R. C. (2014). Nitrated fatty acids reverse pulmonary fibrosis by dedifferentiating myofibroblasts and promoting collagen uptake by alveolar macrophages. *FASEB J.* 28, 5299–5310. doi: 10.1096/fj.14-256263

Rehan, V. K., and Torday, J. S. (2014). The lung alveolar lipofibroblast: an evolutionary strategy against neonatal hyperoxic lung injury. *Antioxid. Redox Signal.* 21, 1893–1904. doi: 10.1089/ars.2013.5793

Richeldi, L., Collard, H. R., and Jones, M. G. (2017). Idiopathic pulmonary fibrosis. *Lancet* 389, 1941–1952. doi: 10.1016/s0140-6736(17)30866-8

Roach, K. M., Feghali-Bostwick, C. A., Amrani, Y., and Bradding, P. (2015). Lipoxin A4 attenuates constitutive and TGF-β1-dependent profibrotic activity in human lung myofibroblasts. *J. Immunol.* 195, 2852–2860. doi: 10.4049/jimmunol.1500936

Romero, F., Hong, X., Shah, D., Kallen, C. B., Rosas, I., Guo, Z., et al. (2018). Lipid synthesis is required to resolve endoplasmic reticulum stress and limit fibrotic responses in the lung. *Am. J. Respir. Cell Mol. Biol.* 59, 225–236. doi: 10.1165/rcmb.2017-0340OC

Rui, L. (2014). Energy metabolism in the liver. *Compr. Physiol.* 4, 177–197. doi: 10.1002/cphy.c130024

Schmidt, R., Meier, U., Markart, P., Grimminger, F., Velcovsky, H. G., Morr, H., et al. (2002). Altered fatty acid composition of lung surfactant phospholipids in interstitial lung disease. *Am. J. Physiol. Lung Cell Mol. Physiol.* 283, L1079–L1085. doi: 10.1152/ajplung.00484.2001

Serhan, C. N., and Savill, J. (2005). Resolution of inflammation: the beginning programs the end. *Nat. Immunol.* 6, 1191–1197. doi: 10.1038/ni1276

Shapouri-Moghaddam, A., Mohammadian, S., Vazini, H., Taghadosi, M., Esmaeili, S. A., Mardani, F., et al. (2018). Macrophage plasticity, polarization, and function in health and disease. *J. Cell Physiol.* 233, 6425–6440. doi: 10.1002/jcp.26429

Smith, S. (1994). The animal fatty acid synthase: one gene, one polypeptide, seven enzymes. *FASEB J.* 8, 1248–1259.

Sunaga, H., Matsui, H., Ueno, M., Maeno, T., Iso, T., Syamsunarno, M. R., et al. (2013). Deranged fatty acid composition causes pulmonary fibrosis in Elovl6-deficient mice. *Nat. Commun.* 4:2563. doi: 10.1038/ncomms3563

Suryadevara, V., Ramchandran, R., Kamp, D. W., and Natarajan, V. (2020). Lipid mediators regulate pulmonary fibrosis: potential mechanisms and signaling pathways. *Int. J. Mol. Sci.* 21:4257. doi: 10.3390/ijms21124257

Swendsen, C. L., Skita, V., and Thrall, R. S. (1996). Alterations in surfactant neutral lipid composition during the development of bleomycin-induced pulmonary fibrosis. *Biochim. Biophys. Acta* 1301, 90–96. doi: 10.1016/0005-2760(96)00023-9

Thrall, R. S., McCormick, J. R., Jack, R. M., McReynolds, R. A., and Ward, P. A. (1979). Bleomycin-induced pulmonary fibrosis in the rat: inhibition by indomethacin. *Am. J. Pathol.* 95, 117–130.

Velázquez, A. P., Tatsuta, T., Ghillebert, R., Drescher, I., and Graef, M. (2016). Lipid droplet-mediated ER homeostasis regulates autophagy and cell survival during starvation. *J. Cell Biol.* 212, 621–631. doi: 10.1083/jcb.201508102

Volmer, R., van der Ploeg, K., and Ron, D. (2013). Membrane lipid saturation activates endoplasmic reticulum unfolded protein response transducers through their transmembrane domains. *Proc. Natl. Acad. Sci. U.S.A.* 110, 4628–4633. doi: 10.1073/pnas.1217611110

Wang, J., and Li, Y. (2019). CD36 tango in cancer: signaling pathways and functions. *Theranostics* 9, 4893–4908. doi: 10.7150/thno.36037

Wang, Y., Li, R., Chen, L., Tan, W., Sun, Z., Xia, H., et al. (2015). Maresin 1 inhibits epithelial-to-mesenchymal transition in vitro and attenuates bleomycin induced lung fibrosis in vivo. *Shock* 44, 496–502. doi: 10.1097/shk.0000000000000446

Xiao, H., Huang, X., Wang, S., Liu, Z., Dong, R., Song, D., et al. (2020). Metformin ameliorates bleomycin-induced pulmonary fibrosis in mice by suppressing IGF-1. *Am. J. Transl. Res.* 12, 940–949.

Yang, Y., Hu, L., Xia, H., Chen, L., Cui, S., Wang, Y., et al. (2019). Resolvin D1 attenuates mechanical stretch-induced pulmonary fibrosis *via* epithelial-mesenchymal transition. *Am. J. Physiol. Lung Cell Mol. Physiol.* 316, L1013–L1024. doi: 10.1152/ajplung.00415.2018

Yi, M., Li, J., Chen, S., Cai, J., Ban, Y., Peng, Q., et al. (2018). Emerging role of lipid metabolism alterations in Cancer stem cells. *J. Exp. Clin. Cancer Res.* 37:118. doi: 10.1186/s13046-018-0784-5

Zhang, L., Wang, Y., Wu, G., Xiong, W., Gu, W., and Wang, C. Y. (2018). Macrophages: friend or foe in idiopathic pulmonary fibrosis? *Respir. Res.* 19:170. doi: 10.1186/s12931-018-0864-2

Zhao, H., Chan-Li, Y., Collins, S. L., Zhang, Y., Hallowell, R. W., Mitzner, W., et al. (2014). Pulmonary delivery of docosahexaenoic acid mitigates bleomycin-induced pulmonary fibrosis. *BMC Pulm. Med.* 14:64. doi: 10.1186/1471-2466-14-64

Zheng, S., Wang, Q., D'Souza, V., Bartis, D., Dancer, R., Parekh, D., et al. (2018). ResolvinD(1) stimulates epithelial wound repair and inhibits TGF-β-induced EMT whilst reducing fibroproliferation and collagen production. *Lab. Invest.* 98, 130–140. doi: 10.1038/labinvest.2017.114

Conflict of Interest: The authors declare that the research was conducted in the absence of any commercial or financial relationships that could be construed as a potential conflict of interest.

Publisher's Note: All claims expressed in this article are solely those of the authors and do not necessarily represent those of their affiliated organizations, or those of the publisher, the editors and the reviewers. Any product that may be evaluated in this article, or claim that may be made by its manufacturer, is not guaranteed or endorsed by the publisher.

frontiers in Physiology

ORIGINAL RESEARCH
published: 20 January 2022
doi: 10.3389/fphys.2021.777386

Acid-Sensing Ion Channel 1/Calpain1 Activation Impedes Macrophage ATP-Binding Cassette Protein A1-Mediated Cholesterol Efflux Induced by Extracellular Acidification

Yuan-Mei Wang[1†], Mo-Ye Tan[2†], Rong-Jie Zhang[1], Ming-Yue Qiu[1], You-Sheng Fu[3], Xue-Jiao Xie[2] and Hong-Feng Gu[1*]*

[1] Hengyang Key Laboratory of Neurodegeneration and Cognitive Impairment and Institute of Neuroscience, Hengyang Medical College, University of South China, Hengyang, China, [2] Department of Zhongjing Theory, College of Chinese Medicine, Hunan University of Chinese Medicine, Changsha, China, [3] Hengyang Hospital of Traditional Chinese Medicine, Hengyang, China

OPEN ACCESS

Edited by:
Jue Wang,
The University of Texas Health Science Center at Tyler, United States

Reviewed by:
Dawei Zhang,
University of Alberta, Canada
Paul "Li-Hao" Huang,
Fudan University, China

***Correspondence:**
Xue-Jiao Xie
9951298@qq.com
Hong-Feng Gu
ghf513@sina.com

[†] These authors have contributed equally to this work and share first authorship

Specialty section:
This article was submitted to Lipid and Fatty Acid Research, a section of the journal Frontiers in Physiology

Received: 15 September 2021
Accepted: 13 December 2021
Published: 20 January 2022

Citation:
Wang Y-M, Tan M-Y, Zhang R-J, Qiu M-Y, Fu Y-S, Xie X-J and Gu H-F (2022) Acid-Sensing Ion Channel 1/Calpain1 Activation Impedes Macrophage ATP-Binding Cassette Protein A1-Mediated Cholesterol Efflux Induced by Extracellular Acidification. Front. Physiol. 12:777386. doi: 10.3389/fphys.2021.777386

Background: Extracellular acidification is a common feature of atherosclerotic lesions, and such an acidic microenvironment impedes ATP-binding cassette transporter A1 (ABCA1)-mediated cholesterol efflux and promotes atherogenesis. However, the underlying mechanism is still unclear. Acid-sensing ion channel 1 (ASIC1) is a critical H^+ receptor, which is responsible for the perception and transduction of extracellular acidification signals.

Aim: In this study, we explored whether or how ASIC1 influences extracellular acidification-induced ABCA1-mediated cholesterol efflux from macrophage-derived foam cells.

Methods: RAW 264.7 macrophages were cultured in an acidic medium (pH 6.5) to generate foam cells. Then the intracellular lipid deposition, cholesterol efflux, and ASIC1/calpain1/ABCA1 expressions were evaluated.

Results: We showed that extracellular acidification enhanced ASIC1 expression and translocation, promoted calpain1 expression and lipid accumulation, and decreased ABCA1 protein expression as well as ABCA1-mediated cholesterol efflux. Of note, inhibiting ASIC1 activation with amiloride or Psalmotoxin 1 (PcTx-1) not only lowered calpain1 protein level and lipid accumulation but also enhanced ABCA1 protein levels and ABCA1-mediated cholesterol efflux of macrophages under extracellular acidification conditions. Furthermore, similar results were observed in macrophages treated with calpain1 inhibitor PD150606.

Conclusion: Extracellular acidification declines cholesterol efflux *via* activating ASIC1 to promote calpain1-mediated ABCA1 degradation. Thus, ASIC1 may be a novel therapeutic target for atherosclerosis.

Keywords: extracellular acidification, foam cells, ASIC1, calpain1, ABCA1, cholesterol efflux

INTRODUCTION

Acidic pH (pH < 7.0) of the intimal fluid in plaques has been regarded as a critical pathological feature of atherosclerosis (Morgan and Leake, 1993; Sneck et al., 2005). The extracellular acidic fluid is mainly resulted from local endometrial hypoxia in atherosclerotic lesions. As we know, under such a hypoxic condition, macrophages will shift their metabolism to anaerobic glycolysis, leading to excessive lactate production and proton extrusion (Zhang et al., 2019). Thus, the acidic intimal fluid is generated in atherosclerotic lesions (Back et al., 2019; Lee-Rueckert et al., 2020). In fact, acidification has been observed both in human and animal atherosclerotic lesions, especially in advanced plaques (Naghavi et al., 2002). Interestingly, extracellular acidification is often observed in the cultured macrophages when the cells are activated or exposed to oxidized low-density lipoprotein (ox-LDL). Recently, extracellular acidification has been confirmed to diminish macrophage cholesterol efflux and promote atherogenesis by unknown mechanisms (Lee-Rueckert et al., 2010). Therefore, clarifying the mechanisms by which extracellular acidification inhibits cholesterol efflux is critical to prevent macrophage-derived foam cells formation and atherosclerotic development.

Acid-sensing ion channel 1 (ASIC1), a member of the ENaC/degenerin family, is activated by elevated extracellular protons (Borg et al., 2020). This channel is widely expressed in nervous and vascular systems and has the unique property to be permeable to calcium (Bouron, 2020). Therefore, activation of ASIC1 enhances calcium influx and initiates intracellular signaling to trigger downstream events, such as inflammation and cell death (Wang and Xu, 2011; Zhang R. J. et al., 2020). ASIC1 plays crucial roles in physiological and pathophysiological processes, including vascular remodeling, cognitive function disorders, pancreatic cancer, and cerebral ischemic injury (Detweiler et al., 2019; Zhou et al., 2019; Zhu et al., 2021). Recently, Ni et al. (2018) reported that ASIC1 activation results in macrophage cell inflammatory response, which impedes ATP-binding cassette protein A1 (ABCA1)-mediated cholesterol efflux from the cells. However, whether the activation of ASIC1 directly influences macrophage cholesterol efflux and foam cell formation is still unclear.

Acid-sensing ion channel 1 is highly expressed in murine macrophages (Ni et al., 2018). Its activation increases intracellular calcium levels, which activates calcium-dependent protease. Calpain1, a calcium-sensitive cysteine protease, has been closely associated with ABCA1-cholesterol efflux (Hanouna et al., 2020). ABCA1 prevents atherogenesis *via* facilitating cholesterol efflux to lipid-free apolipoprotein A1 (ApoA1) from foam cells (Attie, 2007). However, ABCA1 is unstable and prone to be degraded by calpain1, leading to a decrease in ABCA1 expression on the cell surface and a subsequent reduction in cholesterol efflux (Yokoyama et al., 2012). Of note, extracellular acidification obviously decreased ABCA1 protein expression in macrophages and had no significant influence on ABCA1 mRNA levels (Lee-Rueckert et al., 2010, 2020). The discordances between ABCA1 protein and mRNA expression suggest that extracellular acidification decreases ABCA1 protein levels in macrophages *via* promoting its degradation. Given the activated ASIC1 has high permeability for calcium and elevated intracellular calcium increases calpain1 activity (Xiong et al., 2004; Stankowska et al., 2018), we speculate that extracellular acidification results in ASIC1/calpain1 pathway activation and subsequent ABCA1 protein degradation, thereby reducing ABCA1-mediated cholesterol efflux from macrophages.

This study investigated whether ASIC1 activation mediated intracellular lipid deposition and ABCA1 expression and explored the underlying mechanisms in macrophages challenged with acidic culture medium. Our results indicate that extracellular acidification promotes ASIC1 activation and lipid accumulation and decreases ABCA1 protein levels. Mechanistically, ASIC1 activation enhances calpain1 activity and subsequent increases in intracellular lipid deposition through impeding calpain1-mediated ABCA1 cholesterol efflux. Taken together, this study reveals that ASIC1 is critical in linking extracellular acidification to cholesterol efflux and maybe a novel target for atherosclerosis therapy.

MATERIALS AND METHODS

Materials

Oxidized low-density lipoprotein (Ox-LDL) was obtained from Yiyuan Biotechnology (Guangzhou, China). Oil red O (ORO) and RPMI 1640 medium were obtained from Sigma-Aldrich (United States). Recombinant human ApoA1 and CCK-8 kit were provided by Beyotime Biotechnology (Shanghai, China). NBD-cholesterol was purchased from Thermo Fisher Scientific (United States). Anti-ASIC1 antibody was purchased from Alonome (State of Israel). Anti-calpain1 antibody and β-actin antibody were purchased from Proteintech (United States). Anti-ABCA1 antibody was purchased from Abcam (United Kingdom). Goat anti-rabbit antibody was bought from Cell Signaling Technology (United States). Alexa Fluor 488 Goat anti-rabbit antibody was from Jackson TmmunoResearch (United States). DAPI was obtained from Solarbio (Beijing, China). 1,1′-Dioctadecyl-3,3,3′,3′-tetramethylindocarbocyanine perchlorate (Dil) was bought from YEASEN Biotech Co., Ltd. (Shanghai, China). Amiloride was purchased from Sigma-Aldrich (United States), PD150606 was from Abcam Company (United Kingdom). PcTx-1 was acquired from MedChemExpress (United States).

Cell Culture and Treatment

RAW 264.7 macrophages were obtained from the Institute of Cardiovascular Disease, University of South China. To generate foam cells, RAW 264.7 macrophages were incubated in a culture medium of pH 7.4, pH 7.0, or pH 6.5 with 25 μg/ml ox-LDL for 24 h. To sustain a stable extracellular pH, the macrophages were incubated in a CO_2-independent medium (Invitrogen, United States) containing 10% fetal bovine serum (FBS, United States) and 4 mM L-glutamine at 37°C during the experiment (Xu et al., 2011). For pharmacological treatment, the macrophages were cocultured in ASIC inhibitor amiloride,

calpain1 inhibitor PD150606, and ASIC1 inhibitor PcTx1 for 24 h, respectively.

Cell Viability Assay

CCK8 kit (Beyotime Biotechnology, Shanghai, China) was used to detect cell viability and proliferation. Raw 264.7 macrophages were cultured in different pH media supplied with 25 μg/ml ox-LDL in a 96−well plate. After 24 h of treatment, CCK8 (10 μl per well) was incubated with cells for another 4 h at 37°C. Subsequently, the absorbance value of cultured cells was measured using a microplate reader at a wavelength of 450 nm.

Oil Red O Staining

Oil red O staining assay was performed to measure the lipid accumulation in RAW 264.7 macrophages. Those cells were cultured in different pH media supplemented with 25 μg/ml ox-LDL in 6-well plates for 24 h. Then the cultured cells were harvested and fixed using 4% paraformaldehyde for 30 min at room temperature. After being washed three times with phosphate-buffered saline (PBS), the cells were stained with ORO for 15 min. Subsequently, hematoxylin was used to counterstain those samples for 15 s. Lipid accumulation was evaluated using a microscope (Thermo Fisher Scientific, China) and quantified using Image pro plus 7.0 software (Media Cybernetics, Inc., United States).

Western Blot Assay

Cells were collected for protein extraction as described previously (Gu et al., 2017). In brief, after being washed with ice-cold PBS, cell pellets were lysed in RIPA buffer supplemented with protease and phosphatase inhibitors. Protein content was measured using a BCA protein assay kit (Beijing ComWin Biotech, China). Equal amounts of protein samples (10 μg) were loaded on 10% SDS-PAGE for separation. Then, those separated proteins were transferred to polyvinylidene fluoride membranes (Millipore, United States) and blocked with 5% bovine serum albumin for 1 h. Subsequently, the membranes were incubated with primary antibodies against ASIC1 (1:1,000), ABCA1 (1:1,000), calpain1 (1:1,000), and β-actin (1:2,000) overnight at 4°C. After being washed 3 times, the membranes were incubated with second antibodies conjugated with horseradish peroxidase (HRP). Finally, protein bands were visualized using an enhanced chemiluminescence detection system. Image J software was used to quantify the immunoblots.

Real-Time Quantitative PCR

RAW 264.7 macrophages were used to extract total RNA using a TRIzol reagent (Invitrogen) following instructions. The pure and concentrated RNA was then used to synthesize complementary DNA using a cDNA reverse transcription kit (Applied Biosystems, United States). The sequence of ABCA1 primers were 5′-ATGCCAATAACCCTTGCTTCCG -3′ and 5′-ATGTCCCTAATGCTGGTGTC CTT -3′. ABCA1 mRNA level was analyzed using ABI PRISM 7900 sequence detection system (Applied Biosystems).

Detection of Triglycerides and Total Cholesterol Contents

The contents of triglycerides and cholesterol in RAW 264.7 macrophages were determined using a commercially available quantitation kit (Nanjing Jiancheng Bioengineering institute, China). Briefly, RAW 264.7 macrophages were treated with an FBS-free medium. After 12 h, macrophages were cultured in different pH media with or without amiloride (0, 50, and 100 μM). Then, the content of cellular cholesterol and triglycerides was measured following the instructions of the manufacturer.

Immunofluorescent Staining Assay

RAW 264.7 macrophages were stained by immunofluorescence to detect the co-localization of ASIC1 and cellular membrane. RAW 264.7 cells were cultured in different pH media in 6-well plates for 24 h. Then, DiI (1:200) was used to treat cells for 20 min. After being washed three times, the cells were fixed with 4% paraformaldehyde for 30 min at room temperature. Afterward, RAW 264.7 cells were preincubated with 5% goat serum to avoid non-specific antibody binding. Then, the cells were incubated with anti-ASIC1 antibody (1:500) overnight at 4°C. The immune complexes were visualized using Alexa Fluor 488-labeled secondary antibody. DAPI staining was used to indicate the nuclei. Images were obtained using a fluorescence microscope (Thermo Fisher Scientific, China).

ATP-Binding Cassette Protein A1-Mediated Cholesterol Efflux Assay

RAW 264.7 macrophages were incubated with different pH media containing 25 μg/ml ox-LDL in 6-cell plates (1×10^5/cell) for 24 h. Then, the cells were incubated with 5 μmol/L NBD-cholesterol in the phenol red-free RPMI 1640 medium for 4 h to be loaded with cholesterol. After being washed 3 times with PBS, cell layers were incubated in the absence or presence of the indicated concentrations of drugs for an additional 4 h. Finally, cholesterol efflux proceeded for 4 h in a medium containing 20 μg/ml ApoA-1. The fluorescence intensity of the culture medium and cell lysate was determined using a microplate spectrophotometer. The efflux rate was measured by the ratio of medium fluorescence counts to total fluorescence intensity (medium counts + cells lysate counts) × 100%.

Statistical Analysis

All data were shown as mean ± SEM. The Student's *t*-test was used to analyze means between two groups. Differences among the groups were analyzed by one-way ANOVA using SPSS 20 software (International Business Machines Corporation, United States). Statistical significance was considered when $P < 0.05$.

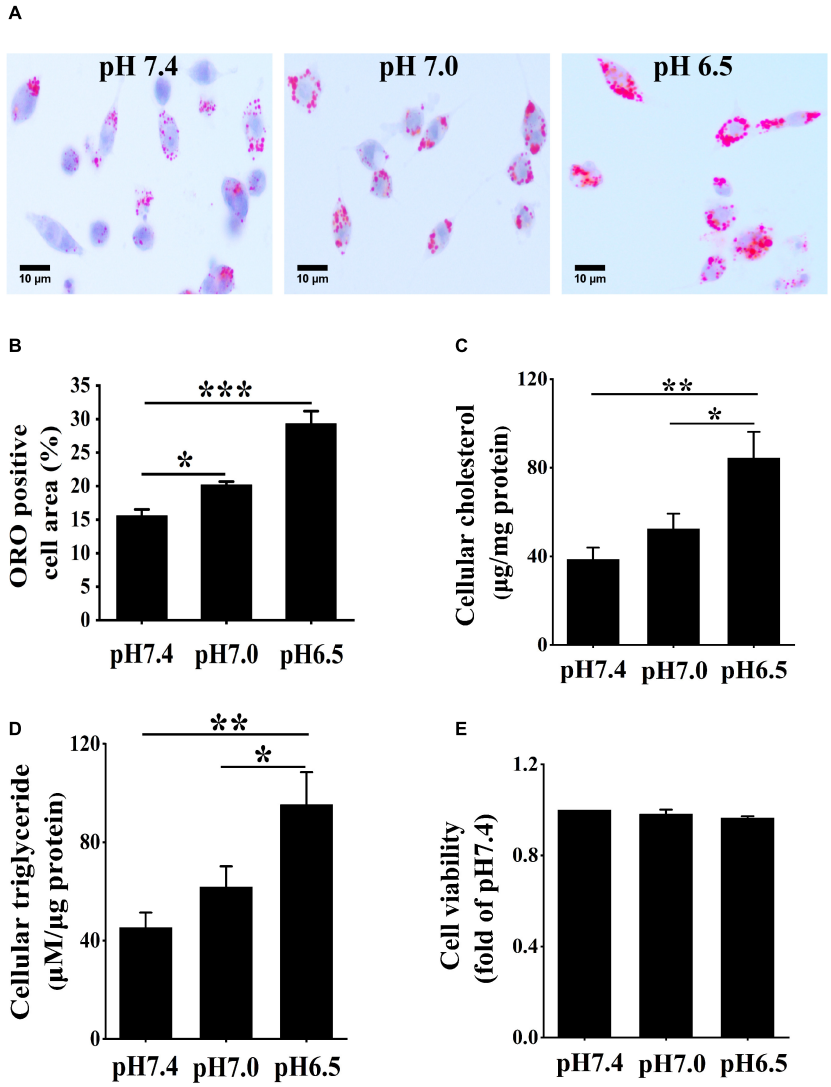

FIGURE 1 | Extracellular acidification aggregates lipid deposition in macrophages. **(A)** RAW 264.7 cells were cultured in 25 μg/ml oxidized low-density lipoprotein (ox-LDL) in different pH media for 24 h. Lipid accumulation was detected by Oil red O (ORO) staining. **(B)** ORO staining positive areas were quantified. **(C,D)** Intracellular cholesterol and triglycerides contents were determined by enzymatic assay. **(E)** CCK-8 kit was used to detect cell viability and proliferation. Results are expressed as the mean ± SEM. Statistical analysis was performed by one-way analysis of variance (ANOVA). $^{*}P < 0.05$; $^{**}P < 0.01$; $^{***}P < 0.001$.

RESULTS

Extracellular Acidification Increases Intracellular Lipid Accumulation

To acquire the role of extracellular acidification in macrophage-derived foam cells, RAW 264.7 macrophage cells were cultured in 25 μg/ml ox-LDL and different acidic pH media for 24 h. ORO staining was used to detect lipid accumulated in the cells under different pH media. Compared with pH 7.4 medium, lipid accumulation was significantly increased in the pH 7.0 group and pH 6.5 group (**Figures 1A,B**). Furthermore, the contents of triglycerides and cholesterol were measured in different pH media (**Figures 1C,D**). The results demonstrated that triglycerides and cholesterol contents were both significantly increased in the pH 7.0 and pH 6.5 groups as compared with the pH 7.4 group. In addition, the results of the CCK-8 assay revealed that pH 7.0 and pH 6.5 culture media had less influence on cell viability (**Figure 1E**). These results demonstrate that extracellular acidification directly promotes lipid accumulation in RAW 264.7 cells.

Extracellular Acidification Promotes the Expressions and Translocation of Acid-Sensing Ion Channel 1 in RAW 264.7 Cells

Next, we explored the potential signaling that could be responsible for the extracellular acidification-induced lipid

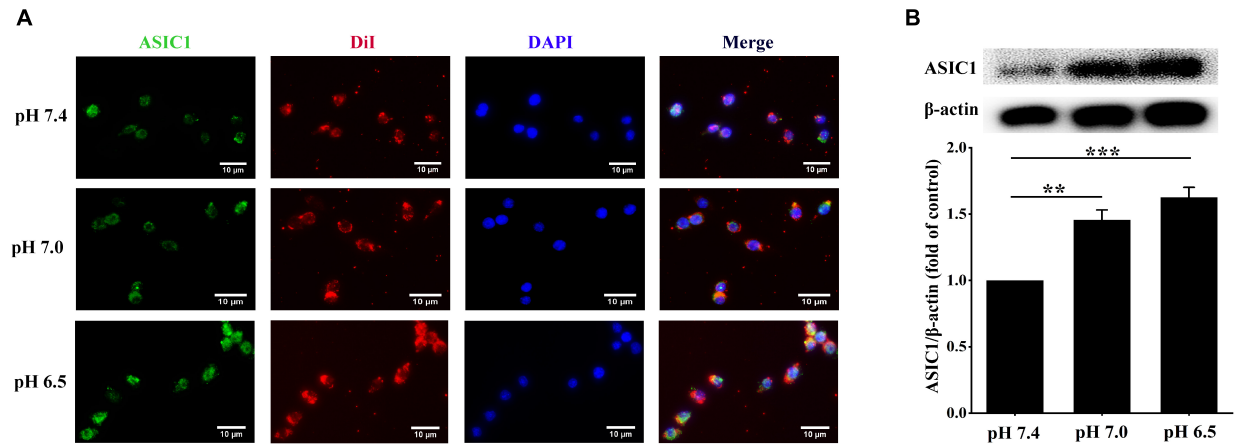

FIGURE 2 | Extracellular acidification promotes acid-sensing ion channel 1 (ASIC1) expression and translocation in macrophages. RAW 264.7 macrophages were incubated with ox-LDL (25 μg/ml) in different pH media for 24 h. **(A)** Representative immunofluorescence of ASIC1 and DiI in RAW 264.7 macrophages. The scale bar is 10 μm. **(B)** The membrane protein levels of ASIC1 were measured using Western blot (WB) analysis. Data were shown as the mean ± SEM from 3 to 4 independent experiments. Statistical analysis was performed by one-way ANOVA. $^{**}P < 0.01$, $^{***}P < 0.001$.

deposition in RAW 264.7 cells. Activation of ASIC1 contributes to neuronal cell death in the contest of tissue acidosis (Borg et al., 2020). We clarified whether similar mechanisms are implicated in increasing lipid accumulation in RAW 264.7 cells. We examined the expression and membrane translocation of ASIC1 in RAW 264.7 cells using immunofluorescent staining and Western blotting, respectively. As indicated in **Figure 2A**, DiI perchlorate (a far-red fluorescent to track cell membrane) was used to stain cellular membranes. The co-localization (indicated by yellow color) of ASIC1 and DiI was much higher in the pH 7.0 and 6.5 groups than those in the pH 7.4 group, respectively. Western blotting results also show that ASIC1 protein expression in the cell plasma membrane of these two acidic pH groups was markedly increased as compared with the pH 7.4 group, respectively (**Figure 2B**). These results suggest that ASIC1 may be associated with lipid accumulation in RAW 264.7 cells induced by extracellular acidification.

Extracellular Acidification Promotes Calpain1 Expression *via* Acid-Sensing Ion Channel 1 Activation

Considerable evidence proves that the ASIC1 activation enhances calcium influx, which results in the activation of calpain1 (Verheijden et al., 2018; Wang et al., 2020). Therefore, we investigated the relationship between ASIC1 and calpain1 expression in RAW 264.7 cells under the extracellular acidification condition. As expected, consistent with the increases in ASIC1 expressions, calpain1 protein levels were significantly elevated in the pH 7.0 group and pH 6.5 group as compared with the control group (**Figure 3A**). Of note, treatment with ASIC1 inhibitor amiloride abolished the increases in calpain1 expression under extracellular acidification conditions (**Figure 3B**). These results illustrate that ASIC1 activation enhances calpain1 expression in RAW 264.7 cells induced by extracellular acidification. Collectively, these results imply that ASIC1/calpain1 activation may involve extracellular acidification-promoted lipid deposition in RAW 264.7 cells.

Extracellular Acidification Inhibits ATP-Binding Cassette Protein A1 Expression and ATP-Binding Cassette Protein A1-Mediated Cholesterol Efflux

ATP-binding cassette transporter A1 protein on the surface of macrophages can easily be degraded by calpain1-mediated proteolysis (Martinez et al., 2003). Given the elevated levels of calpain1 in RAW 264.7 cells, we hypothesized that extracellular acidification might decrease the protein levels of ABCA1. The ABCA1 protein levels were detected using Western blotting, and ABCA1-mediated cholesterol efflux was measured using a high-throughput NBD-labeled cholesterol efflux assay. As expected, Western blotting results indicated that the levels of ABCA1 were much lower at pH 6.5 than at pH 7.0 and pH 7.4, respectively (**Figure 4A**), revealing that extracellular acidification decreased the ABCA1 protein expression in RAW 264.7 cells. Consistent with the lowered expression of ABCA1, cholesterol efflux was markedly reduced in the pH 6.5 group as compared with that in the pH 7.4 group and pH 7.0 group (**Figure 4B**). Altogether, these results demonstrate that extracellular acidification impedes ABCA1-mediated cholesterol efflux, thereby accelerating lipid accumulation in RAW 264.7 cells.

Extracellular Acidification Increases Lipid Accumulation and Decreases ATP-Binding Cassette Protein A1-Mediated Cholesterol Efflux *via* Acid-Sensing Ion Channel 1 Activation

Given that ASIC1 expression is increased in RAW 264.7 macrophages challenged with extracellular acidification, we

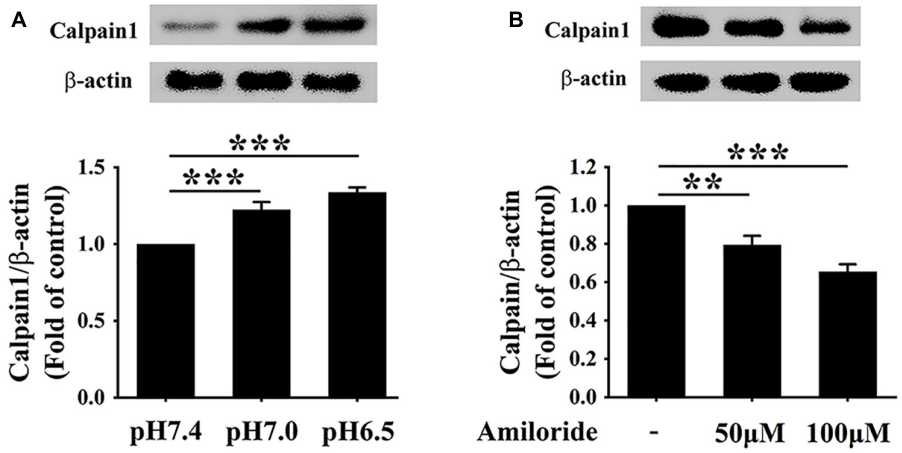

FIGURE 3 | Extracellular acidification enhances calpain1 expression *via* activating ASIC1 in macrophages. **(A)** RAW 264.7 cells were incubated in different pH media with ox-LDL for 24 h, and then the expression of calpain1 was determined using WB analysis. **(B)** RAW 264.7 macrophages were incubated in pH 6.5 medium containing 25 μg/ml ox-LDL with amiloride (0, 50, and 100 μM) for 24 h. Calpain1 expression was determined using WB analysis. Data were shown as the mean ± SEM from 3 to 4 independent experiments. Statistical analysis was performed by one-way ANOVA. $^{**}P < 0.01$; $^{***}P < 0.001$.

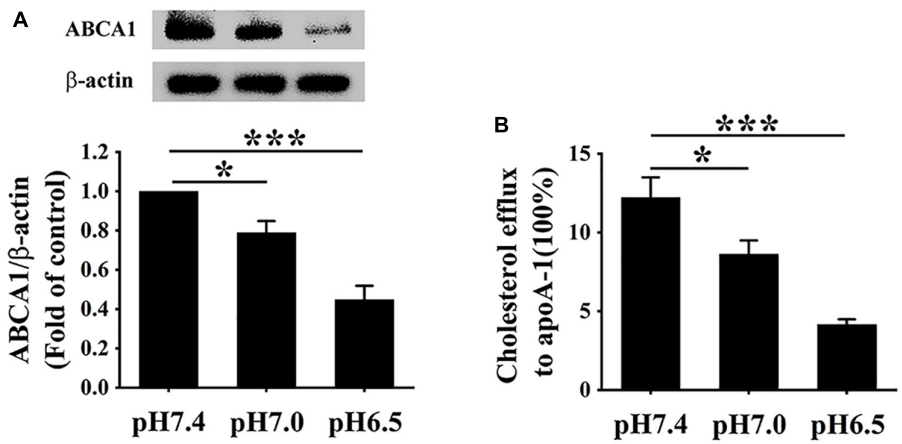

FIGURE 4 | Extracellular acidification decreases ABCA1 protein levels and cholesterol efflux of macrophages. **(A)** RAW 264.7 cells were incubated in different pH media with 25 μg/ml ox-LDL for 24 h. The protein levels of ABCA1 were valued using WB analysis. **(B)** ABCA1-mediated cholesterol efflux was analyzed using an NBD-cholesterol kit. Data were shown as the mean ± SEM from 3 to 4 independent experiments. Statistical analysis was performed by one-way ANOVA. $^{*}P < 0.05$; $^{***}P < 0.001$.

determined the effect of this receptor on lipid accumulation and ABCA1-dependent efflux of the cells. RAW 264.7 cells were exposed to an acidic culture medium (pH 6.5) with or without ASIC1 inhibitor amiloride for 24 h. Lipid deposition, ABCA1 expression, and cholesterol efflux were measured (**Figures 5A–D**). ORO results showed that lipid accumulation (indicated by ORO positive area) was obviously attenuated in groups treated with 50 and 100 μM amiloride as compared with the control group (**Figures 5A,B**), respectively, indicating that ASIC1 activation promotes lipid accumulation induced by acidic pH.

Cholesterol efflux prevents lipid accumulation in macrophage cells. Hence, we further investigated whether inhibition of ASIC1 could reverse the decreases in ABCA1 expression and ABCA1-dependent cholesterol efflux of RAW 264.7 cells under extracellular acidification conditions. Western blotting results showed that ABCA1 protein levels of ASIC1 inhibitor groups were significantly increased as compared with that of the control group (**Figure 5C**). Consistent with the changes in ABCA1 expression, the percentage of cholesterol efflux to ApoA1 was much higher in the ASIC1 inhibitor groups than that of the control group (**Figure 5D**). Taken together, these results demonstrate that extracellular acidification suppresses ABCA1-mediated cholesterol efflux *via* ASIC1 activation, thereby promoting macrophage lipid accumulation.

Moreover, the storage levels of triglycerides and cholesterol were detected in RAW 264.7 macrophages cultured in a pH 6.5 medium with or without amiloride for 24 h (**Figures 5E,F**). The contents of triglycerides and cholesterol were significantly

decreased in 50 and 100 μM amiloride groups compared with those of the control group. These results indicate that ASIC1 activation promotes lipid accumulation.

Extracellular Acidification Promotes Lipid Accumulation and Inhibits ATP-Binding Cassette Protein A1-Mediated Cholesterol Efflux *via* Acid-Sensing Ion Channel 1/Calpain1 Pathway

To further verify whether extracellular acidification increased lipid deposition and decreased cholesterol efflux *via* the activation of ASIC1/calpain1 signaling, RAW 264.7 cells were treated with PcTx-1 (a specific ASIC1 inhibitor) or PD150606 (a specific calpain1 inhibitor). We found that ASIC1 inhibitor PcTx-1 abolished the increases in calpain1 expression and lipid accumulation in RAW 264.7 cells under an acidic microenvironment (**Figures 6A–C**). Moreover, PcTx-1 treatment reversed the influence of extracellular acidification on the inhibition of ABCA1 protein expression and cholesterol efflux (**Figures 6D,E**). Interestingly, similar results were obtained when the cells were treated with calpain1 inhibitor PD150606 (**Figures 6D,E**). Furthermore, real-time PCR (RT-PCR) results indicated that there was no significant difference in the ABCA1 mRNA expression both in PcTx-1 and calpain1 groups as compared with the pH 6.5 group (**Supplementary Figure 1**), suggesting that these two inhibitors had less influence on the ABCA1 mRNA expression. Taken together, these data manifest that the activation of ASIC1/calpain1 signaling contributes to extracellular acidification-promoted lipid accumulation in RAW 264.7 cells.

DISCUSSION

Acid-sensing ion channel 1 has been confirmed to play critical roles in pathophysiological acidosis occurring during neurological disorders, such as ischemic stroke and various neurodegeneration (Friese et al., 2007; Borg et al., 2020). However, the potential roles of ASIC1 in macrophage lipid metabolism under extracellular acidification conditions are unclear. This study shows that an ASIC1-dependent increase in calpain1 activity and reduction in ABCA1 protein levels are evoked in RAW 264.7 cells cultured in an acidic medium. Importantly, inhibiting the activation of the ASIC1/calpain1 pathway by the inhibitors PcTx-1 and PD150606 not only restored ABCA1 protein levels but also significantly facilitated ABCA1-mediated cholesterol efflux and diminished lipid deposition in RAW 264.7 cells exposed to the extracellular acidification. These findings present a novel mechanism that extracellular acidification diminishes ABCA1-dependent cholesterol efflux and ultimately induces foam cell formation *via* activation of the ASIC1/calpain1 pathway.

Acidic intimal fluid pH prevails in local areas of atherosclerotic plaques, where macrophage-derived foam cells locate (Liu et al., 2019). Furthermore, macrophages exposed to modified LDL are capable of generating acidic pericellular environments with pH values even lower than 5.0 (Naghavi et al., 2002; Sluimer et al., 2008). In this study, we first built an extracellular acidification-induced macrophage foam cell model by culturing RAW 264.7 cells in pH 6.5 medium, which may closely mimic the acidic microenvironment-surrounded macrophages within atherosclerotic lesions. Our results confirmed that extracellular acidification notably diminished ABCA1-mediated cholesterol efflux and exacerbated lipid deposition in RAW 264.7 macrophages. Consistently, the acidic extracellular pH also profoundly compromised ABCA1-dependent cholesterol efflux from human monocyte-derived macrophage foam cells (Lee-Rueckert et al., 2020). To clarify the mechanisms underlying extracellular acidification-induced lipid accumulation in RAW 264.7 macrophage cells, we explored the ASIC1/calpain1/ABCA1 signaling in which the acidic extracellular pH involved, including changes in ASIC1 expression and cell membrane translocation, calpain1 and ABCA1 protein levels, and ABCA1-mediated cholesterol efflux.

In this study, we showed the critical role of ASIC1 in extracellular acidification-induced lipid accumulation in RAW 264.7 macrophage cells. ASIC1 is widely expressed in the nervous and cardiovascular systems (Arun et al., 2013; Qiang et al., 2018). Under normal conditions, this protein is primarily expressed in the nucleus. Once exposed to an extracellular acidic pH value, ASIC1 will translocate from nucleus to cell membrane (Zhang Y. et al., 2020), thereby being activated by extracellular protons to trigger downstream signaling cascades such as calpain1 activation and RIP1 interaction (Wang et al., 2015; Stankowska et al., 2018). To explore whether this channel is involved in extracellular acidification-induced lipid accumulation, we first clarified the changes in ASIC1 expression in the membrane when RAW 264.7 cells were cultured in an acidic medium. Our results indicated that ASIC1 is expressed in RAW 264.7 cells and that extracellular acidification significantly promoted its expression and cell membrane translocation. Consistent with the increase in ASIC1 expression in the membrane, intracellular lipid deposition aggregated obviously. Notably, ASIC1-specific inhibitor PcTx-1 treatment significantly attenuated lipid accumulation in the cells under extracellular acidification conditions. These findings reveal that extracellular acidification promoted lipid accumulation in RAW 264.7 cells *via* ASIC1 activation.

ATP-binding cassette transporter A1 impedes foam cell formation and atherogenesis by facilitating cholesterol efflux (Phillips, 2018). Several studies indicate that ABCA1-mediated cholesterol efflux is decreased both in cultured macrophage cells and in atherosclerotic plaques, and this decreased capability is closely related to extracellular acidic pH (Yu et al., 2013; Jin et al., 2018). However, the mechanism underlying extracellular acidification-induced reductions in cholesterol efflux is unknown. Thus, in our study, we explored the influences of ASIC1 activation on the ABCA1 expression in RAW 264.7 cells under extracellular acidification conditions. Our results present that the ABCA1 protein level is decreased under such conditions, coupled with the diminished capability of cholesterol efflux in RAW 264.7 cells. As expected, the decreases both in ABCA1 protein levels and cholesterol efflux were reversed by treatment

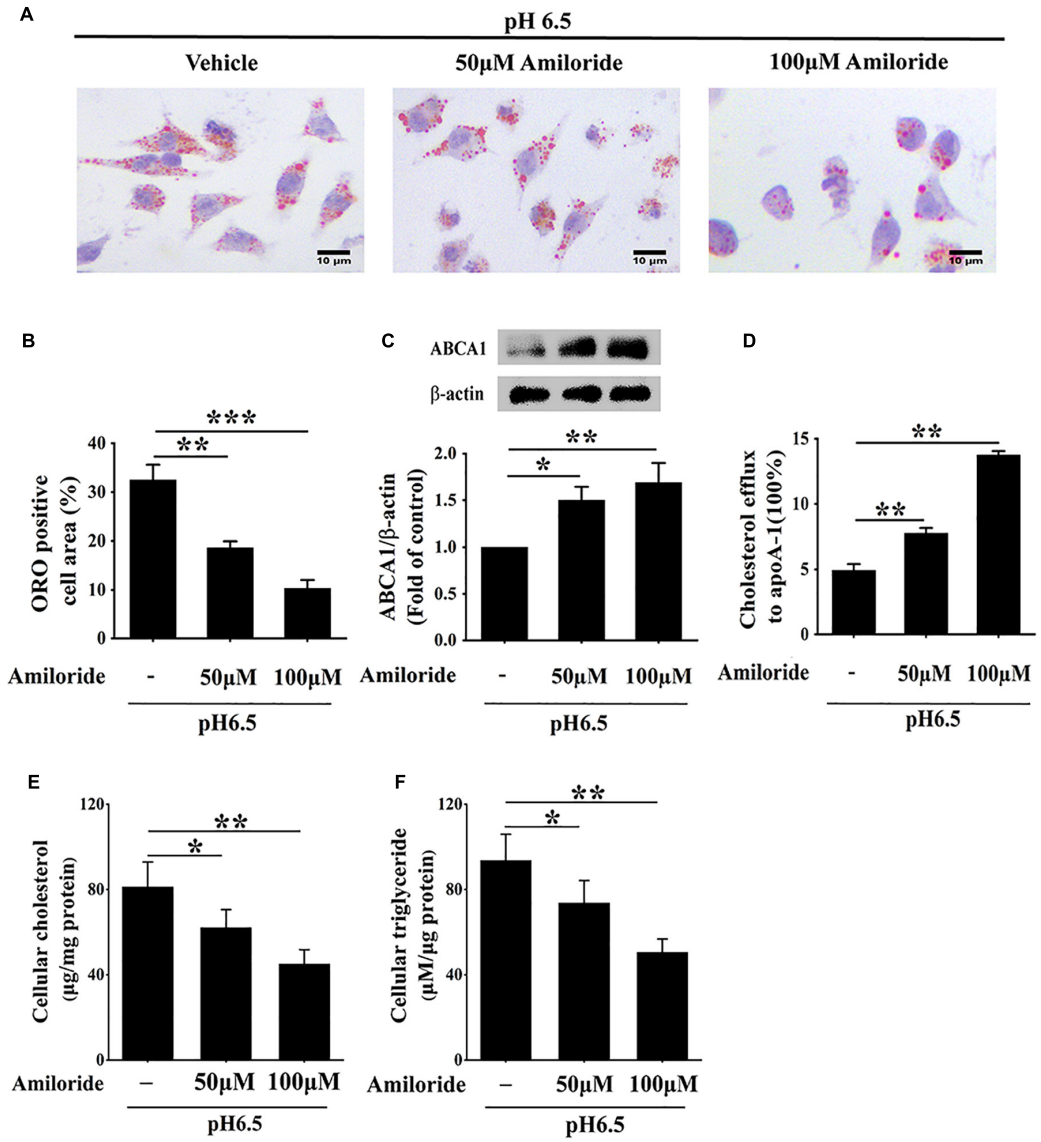

FIGURE 5 | Inhibition of ASIC1 impedes lipid accumulation and promotes ABCA1-mediated cholesterol efflux of macrophages. RAW 264.7 macrophages were cultured in 25 μg/ml ox-LDL and amiloride (0, 50, and 100 μM) under pH 6.5 condition for 24 h. **(A)** Lipid deposition was detected by ORO staining. **(B)** ORO positive areas were quantified. **(C)** ABCA1 protein levels were measured using WB analysis. **(D)** ABCA1-mediated cholesterol efflux was determined using an NBD-cholesterol kit. **(E,F)** Intracellular cholesterol and triglycerides contents were determined by enzymatic assay. Data were shown as the mean ± SEM from 3 to 4 independent experiments. Statistical analysis was performed by one-way ANOVA. $^{*}P < 0.05$; $^{**}P < 0.01$; $^{***}P < 0.001$.

with ASIC1 inhibitors amiloride and PcTx-1. Taken together, these findings demonstrate that ASIC1 activation by extracellular acidification lowers ABCA1 protein levels, thereby decreasing cholesterol efflux from RAW 264.7 macrophages.

The mechanism of extracellular acidification-induced ABCA1 protein degradation results from the activation of the ASIC1/calpain1 pathway. Several lines of evidence have identified that ASIC1 activation enhances calcium influx (Gonzalez Bosc et al., 2016). Calpain1 is a calcium-dependent cysteine protease and its activation promotes the degradation of ABCA1 protein (Martinez et al., 2003; Yokoyama et al., 2012). Therefore, we assumed that extracellular acidification enhanced the activity of calpain1 *via* ASIC1 activation. In fact, the activation of ASIC1 significantly increases the expression of calpain1 in RAW 264.7 macrophages cultured in an acidic medium, indicating that ASIC1/calpain1 pathway is activated in this context. To clarify the role of this signaling activation in extracellular acidification-induced changes in ABCA1 protein levels and cholesterol efflux, we employed specific inhibitors to inhibit ASIC1/calpain1 activation. We found that ASIC1 inhibitor treatments remarkably lowered the levels of calpain1 in RAW 264.7 cells exposed to the acidic culture medium.

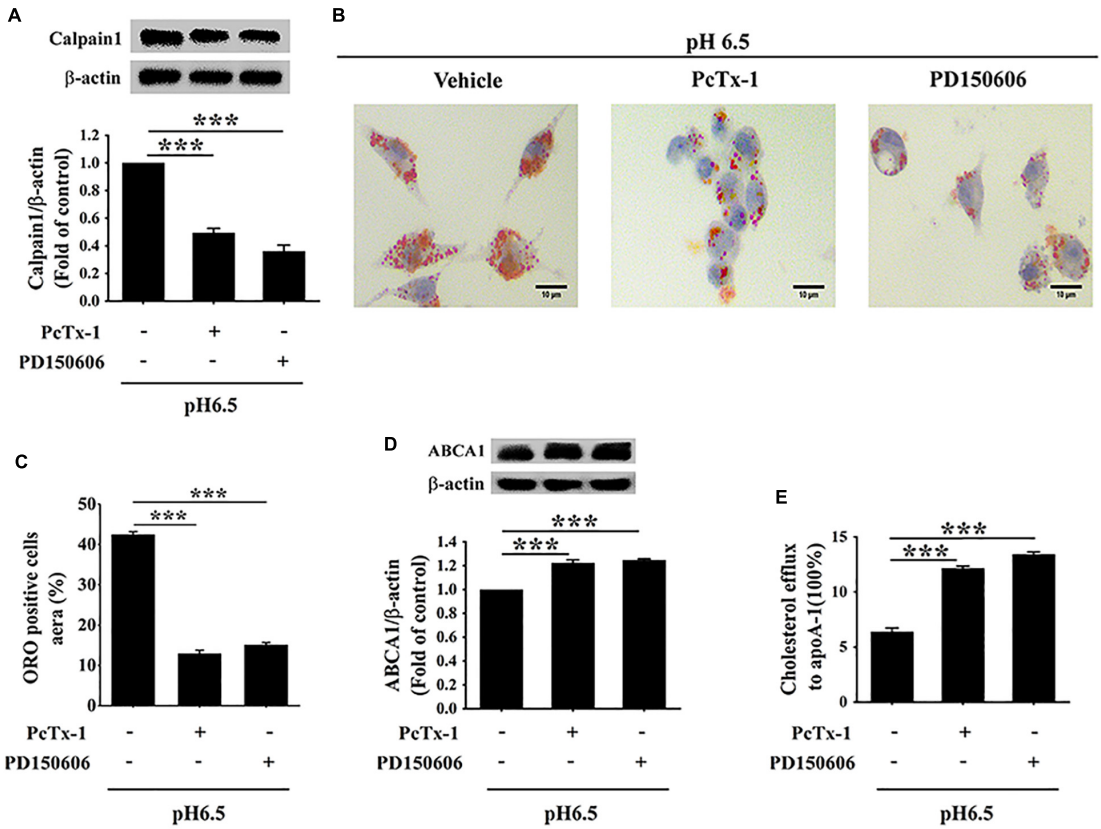

FIGURE 6 | Extracellular acidification increases macrophage lipid deposition *via* activating ASIC1/calpain1 to reduce ABCA1-dependent cholesterol efflux. RAW 264.7 macrophage cells were incubated in pH 6.5 culture medium with or without ASIC1 specific inhibitor PcTx-1 (100 ng/ml) or calpain1 inhibitor PD150606 (50 μM) for 24 h. **(A)** Calpain1 expression was evaluated using WB analysis. **(B)** Lipid deposition was detected using ORO staining. **(C)** ORO staining positive areas were quantified. **(D)** ABCA1 expression was measured using WB analysis. **(E)** ABCA1-mediated cholesterol efflux was measured using the NBD-cholesterol kit. Data were shown as the mean ± SEM from 3 to 4 independent experiments. Statistical analysis was performed by one-way ANOVA. ***$P < 0.001$.

Furthermore, our results confirmed that calpain1 inhibitor PD150606 treatment profoundly elevated ABCA1 protein levels of the cells under extracellular acidification conditions. Accordingly, ABCA1-dependent cholesterol efflux is increased, and lipid accumulation was reduced. Notably, there was no significant difference in ABCA1 mRNA levels between the PcTx-1 group, the PD150606 group, and the pH 6.5 alone group, indicating that activation of ASIC1/calpain1 had no significant influence on the macrophage ABCA1 mRNA expression under acidic conditions. Collectively, these results revealed that the activation of ASIC1 by extracellular acidification increases the calpain1 activity, thereby facilitating calpain1-mediated ABCA1 degradation.

It is undeniable that there are certain limitations in this work. First, in this study, we explored the effect of the ASIC1/calpain1 pathway in extracellular acidification-induced macrophage lipid accumulation only using pharmacological inhibitors and not using siRNA to validate our findings. Second, the pilot study revealed the role of ASIC1/calpain1 activation in macrophage foam cell formation *in vitro*, and its actual atherogenic effect needs to be further verified *in vivo* through ASIC1 knockout and siRNA. Nonetheless, the results provided new insights into the correlation between extracellular acidification and ABCA1-mediated cholesterol efflux impairment, with ASIC1 acting as a link.

CONCLUSION

Extracellular acidification promotes ASIC1 activation and ABCA1 degradation *via* enhancing calpain1 activity, leading to decreased ABCA1 protein levels and diminished cholesterol efflux in macrophages, ultimately causing lipid deposition, and macrophage-derived foam cell formation. Inhibition of ASIC1/calpain1 signaling to restore ABCA1-mediated cholesterol efflux may be a promising therapeutic approach for atherosclerotic diseases.

DATA AVAILABILITY STATEMENT

The original contributions presented in the study are included in the article/**Supplementary Material**, further inquiries can be directed to the corresponding author/s.

AUTHOR CONTRIBUTIONS

Y-MW performed writing the original draft, conception, experimental execution, and investigation. M-YT contributed to data curation, experimental execution, and verification. R-JZ contributed to data curation and experimental execution. M-YQ contributed to investigation. Y-SF performed writing the original draft. X-JX contributed to verification and resources. H-FG contributed to project administration and resources, and edited the draft. All authors contributed to the article and approved the submitted version.

FUNDING

This work was supported by grants from the National Natural Science Foundation of China (Grant No. 81500349), the Natural Science Foundation of Hunan Province, China (Grant Nos. 2020JJ4528 and 2021JJ30510), the key program of the Educational Commission of Hunan Province, China (Grant No. 19A435), program of the Educational Commission of Hunan Province, China (Grant No. 19K069), and the Health and Family Planning Commission of Hunan Province, China (Grant No. B2017048).

SUPPLEMENTARY MATERIAL

The Supplementary Material for this article can be found online at: https://www.frontiersin.org/articles/10.3389/fphys.2021.777386/full#supplementary-material

Supplementary Figure 1 | ASIC1/calpain1 has no effect on the ABCA1 mRNA level. RAW 264.7 macrophage cells were cultured in pH 6.5 medium in the absence or presence of ASIC1 specific inhibitor PcTx-1 (100 ng/ml) or calpain1 inhibitor PD150606 (50 μM) for 24 h. The mRNA level of ABCA1 was measured using real-time PCR (RT-PCR). Data were shown as the mean ± SEM from 3 to 4 independent experiments. Statistical analysis was performed by one-way ANOVA.

REFERENCES

Arun, T., Tomassini, V., Sbardella, E., de Ruiter, M. B., Matthews, L., Leite, M. I., et al. (2013). Targeting ASIC1 in primary progressive multiple sclerosis: evidence of neuroprotection with amiloride. *Brain* 136, 106–115. doi: 10.1093/brain/aws325

Attie, A. D. (2007). ABCA1: at the nexus of cholesterol. HDL and atherosclerosis. *Trends Biochem. Sci.* 32, 172–179. doi: 10.1016/j.tibs.2007.02.001

Back, M., Yurdagul, A. Jr., Tabas, I., Oorni, K., and Kovanen, P. T. (2019). Inflammation and its resolution in atherosclerosis: mediators and therapeutic opportunities. *Nat. Rev. Cardiol.* 16, 389–406. doi: 10.1038/s41569-019-0169-2

Borg, C. B., Braun, N., Heusser, S. A., Bay, Y., Weis, D., Galleano, I., et al. (2020). Mechanism and site of action of big dynorphin on ASIC1a. *Proc. Natl. Acad. Sci. USA* 117, 7447–7454. doi: 10.1073/pnas.1919323117

Bouron, A. (2020). Transcriptomic Profiling of Ca2+ transport systems during the formation of the cerebral cortex in mice. *Cells* 9:9081800. doi: 10.3390/cells9081800

Detweiler, N. D., Herbert, L. M., Garcia, S. M., Yan, S., Vigil, K. G., Sheak, J. R., et al. (2019). Loss of acid-sensing ion channel 2 enhances pulmonary vascular resistance and hypoxic pulmonary hypertension. *J. Appl. Physiol.* 127, 393–407. doi: 10.1152/japplphysiol.00894.2018

Friese, M. A., Craner, M. J., Etzensperger, R., Vergo, S., Wemmie, J. A., Welsh, M. J., et al. (2007). Acid-sensing ion channel-1 contributes to axonal degeneration in autoimmune inflammation of the central nervous system. *Nat. Med.* 13, 1483–1489. doi: 10.1038/nm1668

Gonzalez Bosc, L. V., Plomaritas, D. R., Herbert, L. M., Giermakowska, W., Browning, C., and Jernigan, N. L. (2016). ASIC1-mediated calcium entry stimulates NFATc3 nuclear translocation via PICK1 coupling in pulmonary arterial smooth muscle cells. *Am. J. Physiol. Lung Cell Mol. Physiol.* 311, L48–L58. doi: 10.1152/ajplung.00040.2016

Gu, H. F., Li, H. Z., Xie, X. J., Tang, Y. L., Tang, X. Q., Nie, Y. X., et al. (2017). Oxidized low-density lipoprotein induced mouse hippocampal HT-22 cell damage via promoting the shift from autophagy to apoptosis. *CNS Neurosci. Ther.* 23, 341–349. doi: 10.1111/cns.12680

Hanouna, G., Tang, E., Perez, J., Vandermeersch, S., Haymann, J. P., Baud, L., et al. (2020). Preventing calpain externalization by reducing ABCA1 activity with probenecid limits melanoma angiogenesis and development. *J. Invest. Dermatol.* 140, 445–454. doi: 10.1016/j.jid.2019.06.148

Jin, P., Bian, Y., Wang, K., Cong, G., Yan, R., Sha, Y., et al. (2018). Homocysteine accelerates atherosclerosis via inhibiting LXRalpha-mediated ABCA1/ABCG1-dependent cholesterol efflux from macrophages. *Life Sci.* 214, 41–50. doi: 10.1016/j.lfs.2018.10.060

Lee-Rueckert, M., Lappalainen, J., Leinonen, H., Pihlajamaa, T., Jauhiainen, M., and Kovanen, P. T. (2010). Acidic extracellular environments strongly impair ABCA1-mediated cholesterol efflux from human macrophage foam cells. *Arterioscler. Thromb. Vasc. Biol.* 30, 1766–1772. doi: 10.1161/ATVBAHA.110.211276

Lee-Rueckert, M., Lappalainen, J., Leinonen, H., Plihtari, R., Nordstrom, T., Akerman, K., et al. (2020). Acidic extracellular pH promotes accumulation of free cholesterol in human monocyte-derived macrophages via inhibition of ACAT1 activity. *Atherosclerosis* 312, 1–7. doi: 10.1016/j.atherosclerosis.2020.08.011

Liu, C. L., Zhang, X., Liu, J., Wang, Y., Sukhova, G. K., Wojtkiewicz, G. R., et al. (2019). Na(+)-H(+) exchanger 1 determines atherosclerotic lesion acidification and promotes atherogenesis. *Nat. Commun.* 10:3978. doi: 10.1038/s41467-019-11983-3

Martinez, L. O., Agerholm-Larsen, B., Wang, N., Chen, W., and Tall, A. R. (2003). Phosphorylation of a pest sequence in ABCA1 promotes calpain degradation and is reversed by ApoA-I. *J. Biol. Chem.* 278, 37368–37374. doi: 10.1074/jbc.M307161200

Morgan, J., and Leake, D. S. (1993). Acidic pH increases the oxidation of LDL by macrophages. *FEBS Lett.* 333, 275–279. doi: 10.1016/0014-5793(93)80669-l

Naghavi, M., John, R., Naguib, S., Siadaty, M. S., Grasu, R., Kurian, K. C., et al. (2002). pH Heterogeneity of human and rabbit atherosclerotic plaques; a new insight into detection of vulnerable plaque. *Atherosclerosis* 164, 27–35. doi: 10.1016/s0021-9150(02)00018-7

Ni, L., Fang, P., Hu, Z. L., Zhou, H. Y., Chen, J. G., Wang, F., et al. (2018). Identification and function of acid-sensing ion channels in RAW 264.7 Macrophage Cells. *Curr. Med. Sci.* 38, 436–442. doi: 10.1007/s11596-018-1897-y

Phillips, M. C. (2018). Is ABCA1 a lipid transfer protein? *J. Lipid Res.* 59, 749–763. doi: 10.1194/jlr.R082313

Qiang, M., Dong, X., Zha, Z., Zuo, X. K., Song, X. L., Zhao, L., et al. (2018). Selection of an ASIC1a-blocking combinatorial antibody that protects cells from ischemic death. *Proc. Natl. Acad. Sci. USA* 115, E7469–E7477. doi: 10.1073/pnas.1807233115

Sluimer, J. C., Gasc, J. M., van Wanroij, J. L., Kisters, N., Groeneweg, M., Sollewijn Gelpke, M. D., et al. (2008). Hypoxia, hypoxia-inducible transcription factor, and macrophages in human atherosclerotic plaques are correlated with intraplaque angiogenesis. *J. Am. Coll. Cardiol.* 51, 1258–1265. doi: 10.1016/j.jacc.2007.12.025

Sneck, M., Kovanen, P. T., and Oorni, K. (2005). Decrease in pH strongly enhances binding of native, proteolyzed, lipolyzed, and oxidized low density lipoprotein

particles to human aortic proteoglycans. *J. Biol. Chem.* 280, 37449–37454. doi: 10.1074/jbc.M508565200

Stankowska, D. L., Mueller, B. H. II, Oku, H., Ikeda, T., and Dibas, A. (2018). Neuroprotective effects of inhibitors of Acid-Sensing ion channels (ASICs) in optic nerve crush model in rodents. *Curr. Eye Res.* 43, 84–95. doi: 10.1080/02713683.2017.1383442

Verheijden, K. A. T., Sonneveld, R., Bakker-van Bebber, M., Wetzels, J. F. M., van der Vlag, J., and Nijenhuis, T. (2018). The calcium-dependent protease calpain-1 Links TRPC6 activity to podocyte injury. *J. Am. Soc. Nephrol.* 29, 2099–2109. doi: 10.1681/ASN.2016111248

Wang, K., Kretschmannova, K., Previde, R. M., Smiljanic, K., Chen, Q., Fletcher, P. A., et al. (2020). Cell-type-specific expression pattern of proton-sensing receptors and channels in pituitary gland. *Biophys. J.* 119, 2335–2348. doi: 10.1016/j.bpj.2020.10.013

Wang, Y. Z., Wang, J. J., Huang, Y., Liu, F., Zeng, W. Z., Li, Y., et al. (2015). Tissue acidosis induces neuronal necroptosis via ASIC1a channel independent of its ionic conduction. *Elife* 4:5682. doi: 10.7554/eLife.05682

Wang, Y. Z., and Xu, T. L. (2011). Acidosis, acid-sensing ion channels, and neuronal cell death. *Mol. Neurobiol.* 44, 350–358. doi: 10.1007/s12035-011-8204-2

Xiong, Z. G., Zhu, X. M., Chu, X. P., Minami, M., Hey, J., Wei, W. L., et al. (2004). Neuroprotection in ischemia: blocking calcium-permeable acid-sensing ion channels. *Cell* 118, 687–698. doi: 10.1016/j.cell.2004.08.026

Xu, T., Su, H., Ganapathy, S., and Yuan, Z. M. (2011). Modulation of autophagic activity by extracellular pH. *Autophagy* 7, 1316–1322. doi: 10.4161/auto.7.11.17785

Yokoyama, S., Arakawa, R., Wu, C. A., Iwamoto, N., Lu, R., Tsujita, M., et al. (2012). Calpain-mediated ABCA1 degradation: post-translational regulation of ABCA1 for HDL biogenesis. *Biochim. Biophys. Acta* 1821, 547–551. doi: 10.1016/j.bbalip.2011.07.017

Yu, X. H., Fu, Y. C., Zhang, D. W., Yin, K., and Tang, C. K. (2013). Foam cells in atherosclerosis. *Clin. Chim. Acta* 424, 245–252. doi: 10.1016/j.cca.2013.06.006

Zhang, D., Tang, Z., Huang, H., Zhou, G., Cui, C., Weng, Y., et al. (2019). Metabolic regulation of gene expression by histone lactylation. *Nature* 574, 575–580. doi: 10.1038/s41586-019-1678-1

Zhang, R. J., Yin, Y. F., Xie, X. J., and Gu, H. F. (2020). Acid-sensing ion channels: linking extracellular acidification with atherosclerosis. *Clin. Chim. Acta* 502, 183–190. doi: 10.1016/j.cca.2019.12.027

Zhang, Y., Qian, X., Yang, X., Niu, R., Song, S., Zhu, F., et al. (2020). ASIC1a induces synovial inflammation via the Ca(2+)/NFATc3/ RANTES pathway. *Theranostics* 10, 247–264. doi: 10.7150/thno.37200

Zhou, R., Leng, T., Yang, T., Chen, F., Hu, W., and Xiong, Z. G. (2019). beta-Estradiol protects against acidosis-mediated and ischemic neuronal injury by promoting asic1a (acid-sensing ion channel 1a) protein degradation. *Stroke* 50, 2902–2911. doi: 10.1161/STROKEAHA.119.025940

Zhu, L., Yin, J., Zheng, F., Ji, L., Yu, Y., and Liu, H. (2021). ASIC1 inhibition impairs the proliferation and migration of pancreatic stellate cells induced by pancreatic cancer cells. *Neoplasma* 68, 174–179. doi: 10.4149/neo_2020_200803N811

Conflict of Interest: The authors declare that the research was conducted in the absence of any commercial or financial relationships that could be construed as a potential conflict of interest.

Publisher's Note: All claims expressed in this article are solely those of the authors and do not necessarily represent those of their affiliated organizations, or those of the publisher, the editors and the reviewers. Any product that may be evaluated in this article, or claim that may be made by its manufacturer, is not guaranteed or endorsed by the publisher.

frontiers in Physiology

ORIGINAL RESEARCH
published: 21 March 2022
doi: 10.3389/fphys.2022.859294

Multidrug Resistance-Associated Protein 2 Deficiency Aggravates Estrogen-Induced Impairment of Bile Acid Metabolomics in Rats

*Fatemeh Alaei Faradonbeh[1], Hana Lastuvkova[1], Jolana Cermanova[1], Milos Hroch[2], Zuzana Nova[1], Martin Uher[2], Petra Hirsova[3], Petr Pavek[4] and Stanislav Micuda[1]**

[1]Department of Pharmacology, Faculty of Medicine in Hradec Kralove, Charles University, Hradec Kralove, Czechia, [2]Department of Medical Biochemistry, Faculty of Medicine in Hradec Kralove, Charles University, Hradec Kralove, Czechia, [3]Division of Gastroenterology and Hepatology, Mayo Clinic, Rochester, MN, United States, [4]Department of Pharmacology and Toxicology, Faculty of Pharmacy in Hradec Kralove, Charles University, Hradec Kralove, Czechia

OPEN ACCESS

Edited by:
Da-wei Zhang, University of Alberta, Canada

Reviewed by:
Waddah Alrefai, University of Illinois at Chicago, United States
Jing-Quan Wang, St. John's University, United States

***Correspondence:**
Stanislav Micuda
micuda@lfhk.cuni.cz

Specialty section:
This article was submitted to Lipid and Fatty Acid Research, a section of the journal Frontiers in Physiology

Received: *21 January 2022*
Accepted: *21 February 2022*
Published: *21 March 2022*

Citation:
Alaei Faradonbeh F, Lastuvkova H, Cermanova J, Hroch M, Nova Z, Uher M, Hirsova P, Pavek P and Micuda S (2022) Multidrug Resistance-Associated Protein 2 Deficiency Aggravates Estrogen-Induced Impairment of Bile Acid Metabolomics in Rats. Front. Physiol. 13:859294. doi: 10.3389/fphys.2022.859294

Multidrug resistance-associated protein 2 (Mrp2) mediates biliary secretion of anionic endobiotics and xenobiotics. Genetic alteration of Mrp2 leads to conjugated hyperbilirubinemia and predisposes to the development of intrahepatic cholestasis of pregnancy (ICP), characterized by increased plasma bile acids (BAs) due to mechanisms that are incompletely understood. Therefore, this study aimed to characterize BA metabolomics during experimental Mrp2 deficiency and ICP. ICP was modeled by ethinylestradiol (EE) administration to Mrp2-deficient (TR) rats and their wild-type (WT) controls. Spectra of BAs were analyzed in plasma, bile, and stool using an advanced liquid chromatography–mass spectrometry (LC–MS) method. Changes in BA-related genes and proteins were analyzed in the liver and intestine. Vehicle-administered TR rats demonstrated higher plasma BA concentrations consistent with reduced BA biliary secretion and increased BA efflux from hepatocytes to blood *via* upregulated multidrug resistance-associated protein 3 (Mrp3) and multidrug resistance-associated protein 4 (Mrp4) transporters. TR rats also showed a decrease in intestinal BA reabsorption due to reduced ileal sodium/bile acid cotransporter (Asbt) expression. Analysis of regulatory mechanisms indicated that activation of the hepatic constitutive androstane receptor (CAR)-Nuclear factor erythroid 2-related factor 2 (Nrf2) pathway by accumulating bilirubin may be responsible for changes in BA metabolomics in TR rats. Ethinylestradiol administration to TR rats further increased plasma BA concentrations as a result of reduced BA uptake and increased efflux *via* reduced *Slco1a1* and upregulated Mrp4 transporters. These results demonstrate that Mrp2-deficient organism is more sensitive to estrogen-induced cholestasis. Inherited deficiency in Mrp2 is associated with activation of Mrp3 and Mrp4 proteins, which is further accentuated by increased estrogen. Bile acid monitoring is therefore highly desirable in pregnant women with conjugated hyperbilirubinemia for early detection of intrahepatic cholestasis.

Keywords: Mrp2-deficient rats, estrogen, cholestasis, bile acids, Nrf2

INTRODUCTION

Estrogen-induced cholestasis is regarded clinically as the hepatic disorder in women with increased estrogen levels during pregnancy, or it may develop during estrogen administration as a part of hormonal contraception or hormonal replacement therapy (Rezai et al., 2015). Increased estrogen production contributes to the development of intrahepatic cholestasis of pregnancy (ICP), which is characterized by symptoms including pruritus, abnormal liver function, and raised serum bile acid (BA) levels, occurring especially in the third trimester. Besides unpleasant subjective symptoms, ICP threatens the fetus with a higher incidence of adverse pregnancy outcomes such as iatrogenic preterm delivery, nonreassuring fetal status, meconium staining of the amniotic fluid, and stillbirth. Prophylaxis and effective therapy of ICP are therefore of the highest priority. The need for proper management of ICP is further accentuated by a significant overall incidence of this disorder. The main factor responsible for fetal injury during ICP is elevated BAs, especially when plasma BAs concentration exceeds 40 mM. Therefore, understanding the factors which may predispose to or alleviate the accumulation of BAs during ICP is currently at the center of attention. Furthermore, individual BAs show different characteristics, with hydrophobic ones, such as lithocholic acid or deoxycholic acid, being more toxic than hydrophilic species, such as ursodeoxycholic acid (UDCA), which is even used as first-line therapy in ICP. These BAs also express different potency and efficacy to activate BA receptors, such as farnesoid X receptor (FXR) and pregnane X receptor (PXR). Spectra of BAs must be therefore analyzed to understand pathophysiological consequences.

Multidrug resistance-associated protein 2 (Mrp2) is a major apical efflux pump for biliary secretion of various amphipathic organic anion conjugates, including BAs. Mrp2 creates a key component of BA-independent bile formation by mediating biliary secretion of glutathione (GSH). Homozygous mutations of the gene encoding Mrp2 (ABCC2) cause Dubin-Johnson syndrome, a rare liver disorder that presents with conjugated hyperbilirubinemia (Jemnitz et al., 2010). In contrast, BA metabolomics has not been entirely studied in individuals with Mrp2 deficiency. Douglas et al. (1980) initially reported increased fasting conjugated cholate concentration and prolonged intravenous clearance of sodium glycocholate in a woman with Dubin-Johnson syndrome. Reduced cholic acid (CA) clearance was also detected in sheep exhibiting inherited defects in hepatic bilirubin transport similar to human Dubin-Johnson syndrome (Engelking and Gronwall, 1979). More recent work reports that net plasma concentrations of BAs are often increased in individuals with Mrp2 mutations (Togawa et al., 2018; Junge et al., 2021), although exceptions also exist (Fu et al., 2021). To date, individual BAs in individuals with Mrp2 mutations have not been analyzed. Moreover, several studies have provided evidence that ABCC2 variants are associated with an increased risk of ICP and cholestasis induced by estrogen contraceptives (Sookoian et al., 2008; Dixon et al., 2017; Kularatnam et al., 2017; Huynh et al., 2018; Corpechot et al., 2020), albeit a contradictory report also exists (Meier et al., 2008). The exact mechanisms whereby Mrp2 deficiency modifies BA metabolomics and its relationship to ICP have been poorly studied.

Given this knowledge gap, the present study aimed to elucidate the role of Mrp2 in the development of estrogen-induced cholestasis. We used Mrp2-deficient rats together with their wild-type (WT) controls and induced cholestasis by repeated administration of ethinylestradiol (EE). Previous experimental studies failed to find any alteration of BA biliary secretion in Mrp2-deficient rats after a single dose or 3-day EE regimen (Koopen et al., 1998; Huang et al., 2000). However, impairment of bile flow during ICP is more chronic. Therefore, we used the current standard model of ICP that involves ethinylestradiol administration over a 5-day period. This longer ethinylestradiol treatment worsened cholestasis in Mrp2-deficient rats and significantly altered BA metabolomics accompanied by increased plasma BA concentrations.

MATERIALS AND METHODS

Chemicals

Ethinylestradiol (>98% purity), methanol, acetonitrile, ammonium acetate, acetic acid, formic acid (each in LC/MS grade purity), and D5 CA were purchased from Merck (Prague, Czech Republic). Bile acid standards were purchased from Steraloids, Inc. (Newport, Rhode Island) and Sigma-Aldrich (St. Louis, Missouri).

Animal Study

Multidrug resistance-associated protein 2 deficient (TR, transporter-deficient) Lewis rats or complementary Lewis WT rats were a kind gift from Prof. Ingrid Kloting, Institut für Pathophysiologie, Karlsburg, Germany. All experimental protocols were conducted in accordance with EU Directive 2010/63/EU for animal experiments. The project was approved by the Animal Welfare Bodies of the Faculty of Medicine in Hradec Kralove and the Ministry of Education, Youth and Sports of the Czech Republic (Approval No. MSMT-23573/2015-5). Animals were housed at a constant humidity of 55 ± 10% and a constant temperature of 22 ± 1°C under a 12 h light/dark cycle with free access to water and food. Around 12-week-old female TR and WT rats were randomized to receive either propanediol (vehicle) or EE (5 mg/kg body weight) subcutaneously once daily for 5 consecutive days (six animals/group). Therefore, there were four groups of animals: (i) WT-Ve – WT rats administered with the vehicle; (ii) WT-EE – WT rats receiving ethinylestradiol; (iii) TR-Ve – TR rats administered with the vehicle; and (iv) TR-EE – TR rats receiving ethinylestradiol. The stool was collected over the last 24-h after the last administration of the ethinylestradiol to analyze bile acid fecal elimination. Thereafter, all animals underwent a clearance study performed under general anesthesia induced by pentobarbital (50 mg/kg, i.p.). Herein, the bile duct was cannulated and bile was collected for 60 min. Sample of blood for bile acid analysis was taken in the middle of the collection period from the

cannulated carotid artery. A blood sample for biochemical analysis was taken after bile collection. Animals were then sacrificed by anesthetic overdose, and organs were removed and stored at −80°C for further analysis.

Analytical Methods

Standard biochemical analyses of plasma samples from rats were performed by routine methods in Central laboratories of University Hospital using Modular PP analyzer (Roche, Basel, Switzerland). The analysis of bile acids was performed using the Acquity I-Class UHPLC system (Waters, Milford, United States), implementing separation on YMC Triart C18 column 50 × 2.1 mm (YMC, Japan). The gradient separation was accomplished at flow rate of 0.35 ml.min^{-1} and temperature 45°C with mobile phase composed of solvent A (0.5 mM ammonium acetate, acetic acid 0.001% v/v) and solvent B (methanol:acetonitrile – 75:25 v/v mixture with 0.5 mM ammonium acetate and 0.001% v/v acetic acid). Gradient program was as follows: 0–0.2 min, 40% of solvent B; 0.2–7.0 min, 40–70% of solvent B; 7.0–8.0 min, 70–90% of solvent B; 8.0–8.5 min, 90–95% of solvent B; and 9.0–11 min 40% of solvent B. Xevo-TQ/XS triple quadrupole (Waters, Milford, United States) operated in negative ESI mode was used for detection. Compounds were monitored using multiple reaction monitoring transitions: 375→375 (non-conjugated monohydroxy BA), 391→391 (non-conjugated dihydroxy BA), 407→407 (non-conjugated trihydroxy BA), 432→74 (glycine-conjugated monohydroxy BA), 448→74 (glycine-conjugated dihydroxy BA), 464→74 (glycine-conjugated trihydroxy BA), 482→80 (taurine-conjugated monohydroxy BA), 498→80 (taurine-conjugated dihydroxy BA), and 514→80 (taurine-conjugated trihydroxy BA). Ion source settings were as follows: Capillary voltage 2.5 kV, cone voltage 50 V, desolvation temperature 600°C, desolvation gas 1,000 L/h, and cone gas 350 L/h. MassLynx software was used for LC/MS data acquisition (Version 4.2, Waters, Milford, United States). The concentrations of individual BA were summed to calculate the concentration of conjugated, unconjugated, and total BA. Primary BA: (T/G)CA [(tauro/glyco)cholic acid], (T)CDCA [(tauro)chenodeoxycholic acid], (T)αMCA, and (T)βMCA [(tauro)muricholic acid]; secondary BA: (T)DCA [(tauro)deoxycholic acid], (T)LCA [(tauro)lithocholic acid], (T)UDCA [(tauro)ursodeoxycholic acid], (T)MDCA [(tauro)murideoxycholic acid], THCA (taurohyocholic acid), (T)HDCA [(tauro)hyodeoxycholic acid]; 12α-OH BA: (T)CA and (T)DCA; non12α-OH BA refers to all the remaining BA. Concentrations of reduced GSH and oxidized glutathione (GSSG) were analyzed using a validated HPLC method with fluorescence detection, as described previously (Hirsova et al., 2013).

Quantification of Gene and Protein Expression Levels

Quantitative reverse transcription-PCR (qRT-PCR) and Western blot analyses were completed using previously reported methods (Prasnicka et al., 2017). Individual gene assays are listed in **Table 1** and were purchased from Thermo Fisher Scientific (MA, United States). Antibodies used for Western blot are summarized in **Table 2**.

TABLE 1 | Pre-designed TaqMan® Gene Expression Assay kits (Life Technologies) used for quantitative reverse transcription-PCR (qRT-PCR).

Gene symbol	Protein (when different name from gene)	Life technologies assay ID
Slc10a1	Ntcp	Rn00566894_m1
Abcb11	Bsep	Rn00582179_m1
Cyp7a1		Rn00564065_m1
Cyp8b1		Rn00579921_s1
Cyp27a1		Rn00710298_m1
Cyp2c22		Rn01410778_m1
Abcc2	Mrp2	Rn00563231_m1
Abcc3	Mrp3	Rn01452854_m1
Abcc4	Mrp4	Rn01465702_m1
Oatp1	Slco1a1	Rn00755148_m1
Oatp2	Slco1a4	Rn00756233_m1
Oatp4	Slco1b2	Rn00668623_m1
Abcg2	Bcrp	Rn00710585_m1
Gclc		Rn00689046_m1
Gpx2		Rn00822100_gH
Nqo1		Rn00566528_m1
Asbt	Slc10a2	Rn00691576_m1
Fgf15	Fgf19	Rn00590708_m1
Shp	Nr0b2	Rn00589173_m1
GAPD (*GAPDH*)	4352338E	Rn99999916_s1
Euk 18S rRNA	4333760F	Hs99999901_s1

TABLE 2 | Primary and secondary antibodies used in Western blot.

Protein	Source (cat. number)	Dilution	Secondary antibody dilution
Mrp2	Enzo (ALX-801-037-C125)	1:300	1:2,000
Mrp3	Thermo Fisher (PA5–101482)	1:1,000	1:2,000
Mrp4	Cell signaling (12857S)	1:1,000	1:2,000
Cyp27a1	Thermo Fisher (PA5-27946)	1:1,000	1:2,000
Cyp7a1	Sigma Aldrich (MABD42)	1:1,000	1:2,000
Cyp8b1	Thermo Fisher (PA5–37088)	1:1,000	1:2,000
Cyp2c70	MyBioSource (MBS3223844)	1:1,000	1:2,000
Ntcp	Sigma-Aldrich (SAB2108757)	1:1,000	1:2,000
Bsep	Thermo Fisher (PA5-78690)	1:000	1:2,000
p-SAPK/JNK	Cell signaling (4668S)	1:1,000	1:2,000
p-Erk 1/2 (*P-P44/42*)	Cell signaling (4370S)	1:1,000	1:2,000
RXRa	Cell signaling (5388S)	1:1,000	1:2,000
P65_NFKB	Abcam (ab16502)	1:1,000	1:2,000
Gapdh	Cell signaling (2118)	1:8,000	1:10,000

Statistical Analysis

All statistical analyses were performed using the statistical software GraphPad Prism 6 (San Diego, United States). The results were initially tested for distribution to select the appropriate tests. The data are presented as medians with boxes and whiskers representing the interquartile range and 5th–95th percentiles, respectively. The statistical significance ($p < 0.05$) was determined using either one-way ANOVA for continuous variables or one-way ANOVA on ranks for nonparametric variables.

RESULTS

Mrp2 Deficiency Alters Plasma Biochemical Parameters

To study Mrp2 function during cholestasis, we employed TR rats, which harbor a spontaneous mutation in the Abcc2 gene leading to premature codon termination and Mrp2 deficiency. To induce cholestasis, female TR rats and WT controls received repeated doses of EE. Mrp2 deficiency or ethinylestradiol treatment did not affect the final bodyweight, while liver weight was significantly increased by ethinylestradiol or Mrp2 deficiency (**Figures 1A,B**). Plasma alkaline phosphatase (ALP) activity, a marker of cholestatic injury, was significantly increased by ethinylestradiol, but decreased in TR rats (**Figure 1C**). This unexpected reduction of plasma ALP activity in TR rats may be a consequence of negative interference of the detection method with high bilirubin concentrations (Wang et al., 2014). Mrp2 deficiency increased hepatocellular injury as evident by increased plasma alanine aminotransferase (ALT) activity, though increase in aspartate aminotransferase (AST) did not reach statistical significance (**Figures 1D,E**). Administration of ethinylestradiol did not increase activities of plasma transaminases in either group, which is commonly reported in rodent models of EE-induced cholestasis (Pozzi et al., 2003; Crocenzi et al., 2006; Zhao et al., 2009; Liu et al., 2018). This situation mimics prevailing functional cholestasis without severe hepatocyte injury. TR rats displayed hyperbilirubinemia, which was further exacerbated by ethinylestradiol treatment (**Figure 1F**). Altogether, Mrp2 deficiency increases liver injury and causes severe hyperbilirubinemia in estrogen-induced cholestasis.

Loss of Mrp2 Impairs Biliary Secretion of BAs

Ethinylestradiol administration is a well-established rodent model of intrahepatic cholestasis associated with decreased bile secretion. The ability of ethinylestradiol to alter biliary secretion of bile acids was previously questioned in the Mrp2-deficient rats when ethinylestradiol was applied over 3 days (Koopen et al., 1998). Therefore, we applied ethinylestradiol over a 5-day period, which significantly reduced bile flow in both WT and TR animals (**Figure 2A**). Bile is formed by active biliary secretion of BAs (BA-dependent bile flow) and glutathione (major component of BA-independent bile flow). As expected, the biliary secretion of glutathione was significantly reduced in ethinylestradiol-treated WT rats and vehicle-treated TR group when compared to WT controls (**Figure 2B**). Ethinylestradiol administration did not have any additional effect on biliary glutathione secretion in TR rats when compared to vehicle treatment. Both TR groups also showed increased liver content of reduced glutathione (**Figure 2C**). Ethinylestradiol did not change liver reduced glutathione content in either group. Oxidized glutathione form was significantly increased only in vehicle treated TR rats (**Figure 2D**). Liver ratio of reduced to oxidized form of glutathione was not significantly modified either by ethinylestradiol or Mrp2 deficiency (**Figure 2E**).

Analysis of BAs in the bile showed a significant reduction in their net biliary secretion in ethinylestradiol treated WT rats, reflecting the reduction in 12α-hydroxylated, non-12α-hydroxylated, primary, secondary, and conjugated bile acids (**Figure 3A**). We have detected very low secretion of unconjugated BAs into bile in either group. Biliary secretion of total bile acids was also reduced in vehicle-treated TR rats due to reduced non-12α-hydroxylated, primary, conjugated bile acids. Administration of ethinylestradiol to TR rats did not further reduce biliary secretion of total bile acids but it reduced secretion of 12α-hydroxylated and increased that of non-12α-hydroxylated bile acids compared to vehicle-treated TR rats (**Figure 3A**). As a result, ratio of 12α-hydroxylated to non-12α-hydroxylated bile acids was increased in ethinylestradiol-administered WT rats, and in vehicle-administered TR rats, while it decreased in ethinylestradiol administered TR rats (**Figure 3B**). The biliary ratio of primary to secondary bile acids was reduced only in vehicle-treated TR rats compared to vehicle-treated WT group (**Figure 3B**). Significant discrepancies were noted in biliary secretion of individual bile acids (**Figure 3C**). Ethinylestradiol reduced biliary secretion of taurochenodeoxycholic acid (TCDCA), taurodeoxycholic acid (TDCA), tauro-muricholic acid (TMCA), and taurocholic acid (TCA) in WT rats. Mrp2 deficiency in vehicle-treated TR rats led to reduced biliary secretion of TCDCA and TMCA, and increased secretion of TDCA. Ethinylestradiol-treated TR rats had reduced biliary secretion of glycocholic acid (GCA), TDCA, and TCA, and increased secretion of TUDCA and TMCA compared to control TR rats. These data suggest that Mrp2 deficit indeed impairs biliary secretion of bile acids and their spectra.

Intestinal Reabsorption of BAs Is Reduced in Mrp2-Deficient TR Rats

Bile acids delivered to the intestine *via* bile are metabolized by intestinal microbiota and mainly reabsorbed in the ileum. Reduced reabsorption of BAs from the intestine is one of the compensatory reactions of organism to cholestasis. Reduced reabsorption can be identified as retained stool excretion of BAs, while BA biliary secretion is reduced. This was indeed detected in WT rats administered with ethinylestradiol and in both TR groups (**Figure 4A**). Group analysis of BAs revealed reduced stool excretion of primary and conjugated BAs in vehicle-treated TR rats; and both these changes were restored by administration of ethinylestradiol (**Figure 4A**). Ethinylestradiol significantly reduced ratio of 12α-hydroxylated/non-12α-hydroxylated BAs in both WT and TR rats when compared with corresponding vehicle-treated groups (**Figure 4B**). Vehicle-treated TR rats had also significantly reduced the primary to secondary BA ratio compared with WT animals. This ratio was increased in TR animals by ethinylestradiol administration compared to vehicle-administered TR (**Figure 4B**). Stool excretions of individual BAs were modified only in TR groups (**Figure 4C**). Vehicle-treated TR rats showed significant decrease in stool excretion of TMCA and aMCA. Addition of ethinylestradiol significantly increased fecal content of aMCA, bMCA, and TMCA in TR rats (**Figure 4C**). The altered reabsorption of BAs, especially FXR agonists such as CDCA,

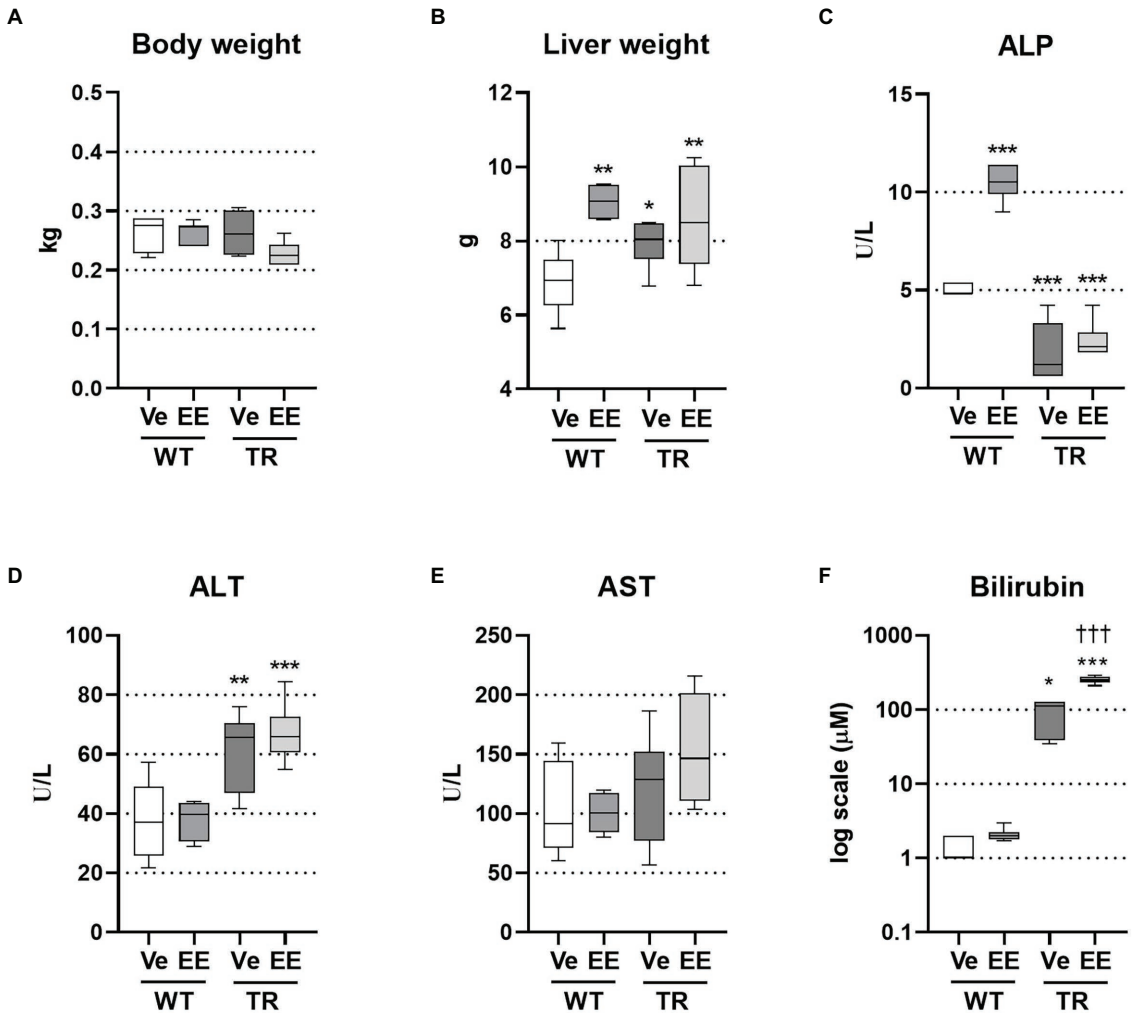

FIGURE 1 | Ethinylestradiol (EE)-induced cholestasis exacerbates hyperbilirubinemia in multidrug resistance-associated protein 2 (Mrp2)-deficient TR rats. Cholestasis was induced by EE administration (5 mg/kg, s.c.) over 5 consecutive days. Experimental groups: WT-Ve, WT rats receiving vehicle; WT-EE, WT rats receiving ethinylestradiol; TR-Ve, TR rats receiving vehicle; and TR-EE, TR rats receiving ethinylestradiol. **(A)** Body weight at the end of the experiment. **(B)** Liver weight. **(C)** Plasma alkaline phosphatase (ALP) activity. **(D)** Plasma alanine aminotransferase (ALT) activity. **(E)** Plasma aspartate aminotransferase (AST) activity. **(F)** Plasma bilirubin concentrations. Data are presented as medians, with boxes and whiskers representing the interquartile range and 5th-95th percentiles, respectively. Significance: $^{*}p < 0.01$, $^{**}p < 0.01$, $^{***}p < 0.001$ compared to vehicle-treated wild-type (WT) rats; $^{\dagger\dagger\dagger}p < 0.001$ compared to vehicle-treated TR rats.

into ileum enterocytes changed the expression of molecules involved in BA homeostasis (**Figure 4D**). The expression of *Slc10a2* (Asbt protein), the apical transporter for BA reabsorption, was significantly reduced in vehicle-treated TR group when compared with vehicle-treated WT rats. The *Slc10a2* also showed tendency toward reduction ($p = 0.075$) in ethinylestradiol-administered WT rats compared with vehicle-treated WT. The major FXR target genes, *Fgf15* and *NR0B2* (Shp) were both suppressed in ethinylestradiol-treated WT rats and in both TR groups compared with vehicle-administered WT rats. Ethinylestradiol significantly increased *Slc10a2* a *NR0B2* expression in Mrp2-deficient rats relative to vehicle administered TR group. These results indicate reduced intestinal reabsorption of BAs in WT and TR rats with reduced FXR receptor activation in ileum of these groups.

Ethinylestradiol Further Increases Already Raised Plasma BA Concentrations in TR Rats

Liquid chromatography–mass spectrometry (LC–MS) analysis of BA spectra in plasma identified significantly increased total BA concentrations in ethinylestradiol-treated WT rats, when compared to vehicle-treated WT group (**Figure 5A**). This increase was due to an increase in 12α-hydroxylated, primary bile acids. Mrp2 deficit in TR rats also led to a significant increase in

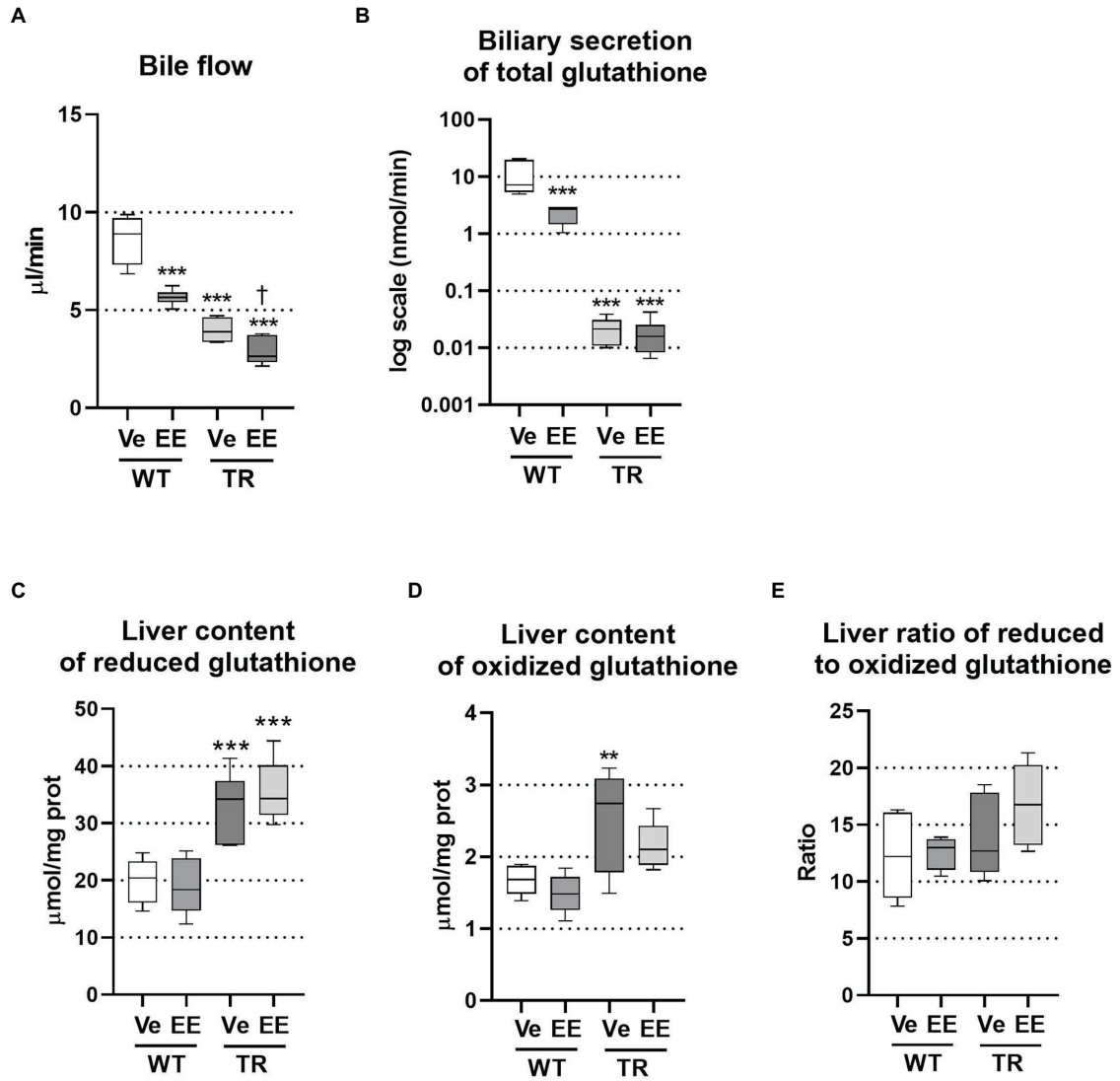

FIGURE 2 | Ethinylestradiol administration reduced bile flow in WT and TR animals. Experimental groups: WT-Ve, WT rats receiving vehicle; WT-EE, WT rats receiving ethinylestradiol; TR-Ve, TR rats receiving vehicle; and TR-EE, TR rats receiving ethinylestradiol. **(A)** Bile flow rate. **(B)** Biliary secretion of glutathione. **(C,D)** Reduced and oxidized glutathione was measured in liver lysates and normalized to protein content. **(E)** Ratio of reduced to oxidized glutathione in the liver. Data are presented as medians, with boxes and whiskers representing the interquartile range and 5th-95th percentiles, respectively. Significance: $^{**}p<0.01$, $^{***}p<0.001$ compared to vehicle-treated WT rats; $^{\dagger}p<0.05$ compared to vehicle-treated TR rats.

total plasma BA concentrations due to an increase in 12α-hydroxylated, primary, secondary but also unconjugated BAs relative to control WT rats. Administration of estrogen to TR rats further increased net plasma BAs by raising 12α-hydroxylated, non-12α-hydroxylated, primary, secondary, and unconjugated BA concentrations. Vehicle-treated TR rats showed increased 12α-hydroxylated/non-12α-hydroxylated ratio compared to vehicle-treated WT group (**Figure 5B**). In contrast, ethinylestradiol reduced 12α-hydroxylated/non-12α-hydroxylated, and increased primary/secondary BA ratios in TR rats (**Figure 5B**). Individual bile acids showed just a tendency for increased plasma concentrations in cholestatic groups (**Figure 5C**). Only the plasma concentration of deoxycholic acid (DCA) was markedly increased in vehicle-treated TR rats compared to control WT, raising thus the 12α-hydroxylated/non-12α-hydroxylated BA ratio. These results indicate accumulation of BAs in plasma of Mrp2-deficient TR rats, which is further worsened by ethinylestradiol.

Executive Pathways of BA Enterohepatic Recycling Are Impaired in TR Rats

To unravel mechanisms of increased plasma BA concentrations in Mrp2-deficient TR rats, we analyzed major enzymes and transporters necessary for BA enterohepatic recycling (**Figure 6A**). As expected, ethinylestradiol administration to WT animals predictably reduced liver protein expression of Na^+-taurocholate

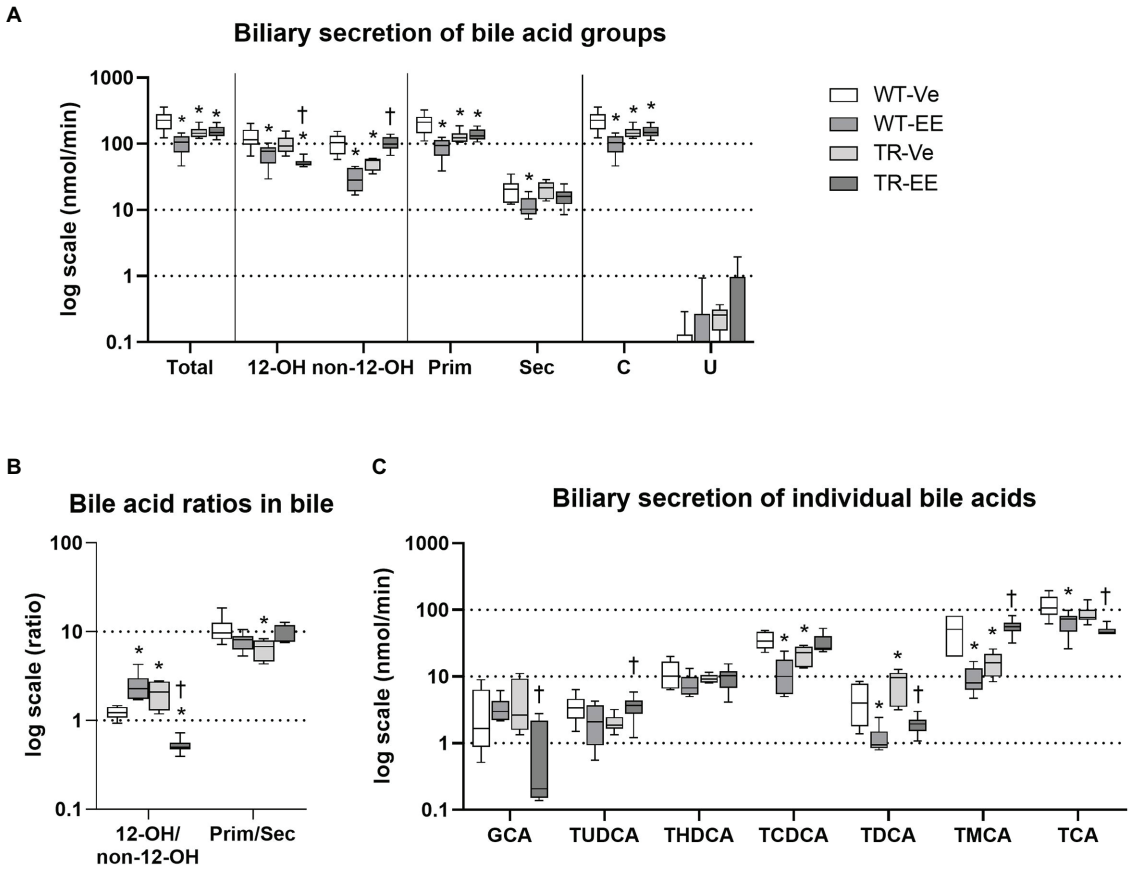

FIGURE 3 | Ethinylestradiol administration reduced biliary secretion of bile acids (BAs) in WT and TR animals. Experimental groups: WT-Ve, WT rats receiving vehicle; WT-EE, WT rats receiving ethinylestradiol; TR-Ve, TR rats receiving vehicle; and TR-EE, TR rats receiving ethinylestradiol. **(A)** Biliary secretion of different types of BAs. **(B)** Biliary ratios of essential bile acid groups. **(C)** Biliary secretion of individual bile acids. Data are presented as medians, with boxes and whiskers representing the interquartile range and 5th-95th percentiles, respectively. Significance: $^{*}p<0.1$ compared to vehicle-treated WT rats; $^{\dagger}p<0.05$ compared to vehicle-treated TR group. BA: 12α-hydroxylated (12-OH), non-12α-hydroxylated (non-12-OH), primary (Prim), secondary (Sec), conjugated (C), glycocholic acid (GCA), ursodeoxycholic acid (UDCA), hyodeoxycholic acid (HDCA), chenodeoxycholic acid (CDCA), deoxycholic acid (DCA), muricholic acid (MCA), and cholic acid (CA), with taurine conjugates TUDCA, taurohyodeoxycholic acid (THDCA), taurochenodeoxycholic acid (TCDCA), taurodeoxycholic acid (TDCA), tauro-muricholic acid (TMCA), and taurocholic acid (TCA).

cotransporting polypeptide (Ntcp; major basolateral transporter for uptake of BAs to hepatocytes), Mrp2, cholesterol 7α-hydroxylase (Cyp7a1; the rate-limiting enzyme for BA synthesis), and sterol 12α-hydroxylase (Cyp8b1; the crucial enzyme for 12α-hydroxylated BA synthesis), and upregulated multidrug resistance-associated protein 4 (Mrp4; transporter responsible for the efflux of BAs from hepatocytes to plasma). As expected, Mrp2-deficient TR rats had negligible protein expression of Mrp2. In addition, these animals had downregulation of Cyp7a1, and upregulation Mrp4 proteins. Ethinylestradiol administration to TR rats downregulated Cyp8b1 and markedly induced Mrp4 efflux protein (**Figure 6A**). Other transporters for BAs such as *Slco1a1*, *Slco1a4*, *Slco1b2*, and *Abcg2* were reduced by ethinylestradiol especially in TR group compared to vehicle-administered controls (**Figure 6B**). Interestingly, the expression of *Slco1a1* and *Abcg2* was unchanged or even increased in WT-EE rats compared to the WT-Ve group indicating different patterns of regulation.

Nrf2 Was the Major Regulatory Pathway of BA Metabolomics Activated in TR Rats

Multiple pathways are involved in the regulation of BA homeostasis (Chiang and Ferrell, 2020). Therefore, we screened the principal ones associated with estrogen-induced cholestasis. Compared to vehicle-treated controls, ethinylestradiol activated FXR-Shp signaling in the liver of WT rats, as apparent from the repressed mRNA of *Cyp7a1*, *Cyp8b1*, *Cyp27a1*, and *Slc10a1* (Ntcp; **Figure 7A**). *Abcb11* (Bsep), *Abcc2* (Mrp2), and *Abcc4* (Mrp4) were not regulated by ethinylestradiol at the transcriptional level (**Figure 7A**). Mrp2 deficiency in vehicle-treated TR rats was associated with reduced mRNA expression of *Cyp7a1* and induced *Abcc3* and *Abcc4* (**Figures 7A,B**). Administration of ethinylestradiol to TR rats reduced mRNA expression of *Cyp8b1*, *Cyp27a1*, and *Cyp2c22* without effect on mRNA of other transporters and enzymes.

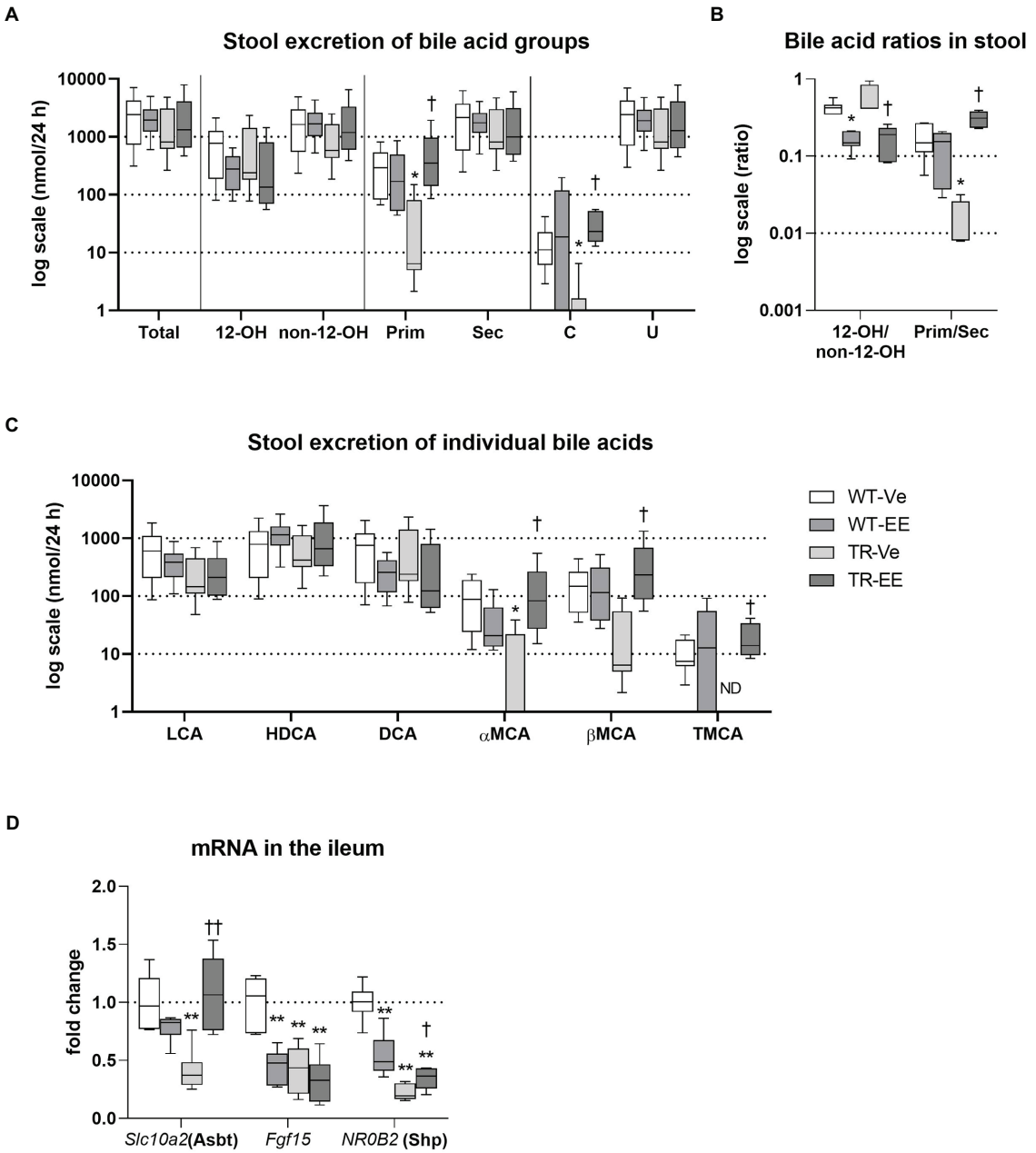

FIGURE 4 | Intestinal homeostasis of bile acids. Experimental groups: WT-Ve, WT rats receiving vehicle; WT-EE, WT rats receiving ethinylestradiol; TR-Ve, TR rats receiving vehicle; and TR-EE, TR rats receiving ethinylestradiol. BAs were analyzed in the feces collected over 24 h. **(A)** Stool excretion of different types of bile acids. **(B)** Ratios of essential bile acid groups in stool. **(C)** Stool excretion of individual bile acids. **(D)** The mRNA expression levels of essential BA transporter and regulators were analyzed in the ileum. Data are presented as median values, with boxes and whiskers representing the interquartile range and 5th-95th percentiles, respectively. Significance: $^{*}p<0.05$ and $^{**}p<0.01$ compared to vehicle-treated WT rats. $^{\dagger}p<0.05$ and $^{\dagger\dagger}p<0.01$ compared to vehicle-treated TR group. BAs are presented as follows: 12-OH, non-12-OH, Prim, Sec, C, unconjugated (U), lithocholic acid (LCA), HDCA, DCA, α muricholic acid (αMCA), β muricholic acid (βMCA), and TMCA.

The mRNA expression of constitutive androstane receptor (CAR) target genes such as *Cyp2b1/2* was reduced in ethinylestradiol administered groups compared with respective vehicle administered animals (**Figure 7B**). Another CAR target, *Abcc3*, was induced by ethinylestradiol in WT group, but unchanged in TR rats. CAR targets were induced in vehicle-treated TR group. Ethinylestradiol-induced Nuclear factor erythroid 2-related factor 2 (Nrf2) target gene expression such as *Nqo1*, *Gclc*, and *Gpx2* in WT animals (**Figure 7C**). Similar induction was detected in vehicle-treated TR rats relative to WT group. In contrast, administration of ethinylestradiol to TR animals reduced mRNA expression of Nrf2 target genes

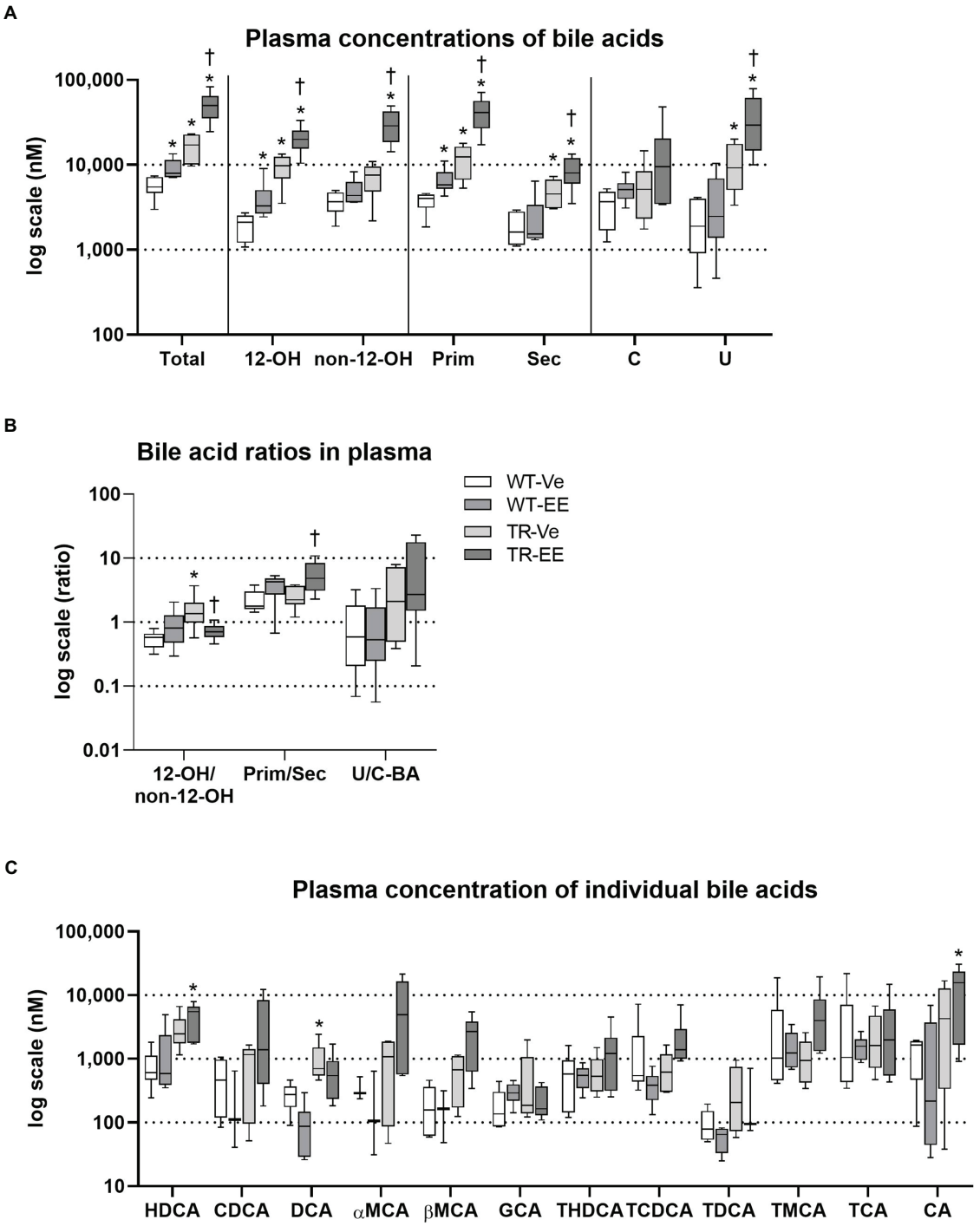

FIGURE 5 | Ethinylestradiol administration increased plasma concentrations of bile acids in WT and TR animals. Experimental groups: WT-Ve, WT rats receiving vehicle; WT-EE, WT rats receiving ethinylestradiol; TR-Ve, TR rats receiving vehicle; and TR-EE, TR rats receiving ethinylestradiol. **(A)** Types of bile acids measured in plasma. **(B)** Ratios of essential bile acid groups in plasma. **(C)** Concentrations of individual bile acids in the plasma. Data are presented as median values, with boxes and whiskers representing the interquartile range and 5th-95th percentiles, respectively. Significance: $^{*}p<0.05$ compared to vehicle-treated WT rats; $^{\dagger}p<0.05$ compared to vehicle-treated TR group. BAs are presented as follows: 12-OH, non-12-OH, Prim, Sec, C, U, HDCA, CDCA, DCA, αMCA, βMCA, GCA, THDCA, TCDCA, TDCA, TMCA, TCA, and CA.

compared to vehicle-treated TR rats. Intracellular MAP kinases, RXRa, and Nuclear factor NF-kappa-B (NF-kB) are another intracellular regulators of bile acid metabolism involved in the response of liver to ethinylestradiol administration. Indeed, tendency toward induction in p-JNK1/2 ($p<0.08$), significantly induced p65-NF-kB and reduced RXRa were detected in WT

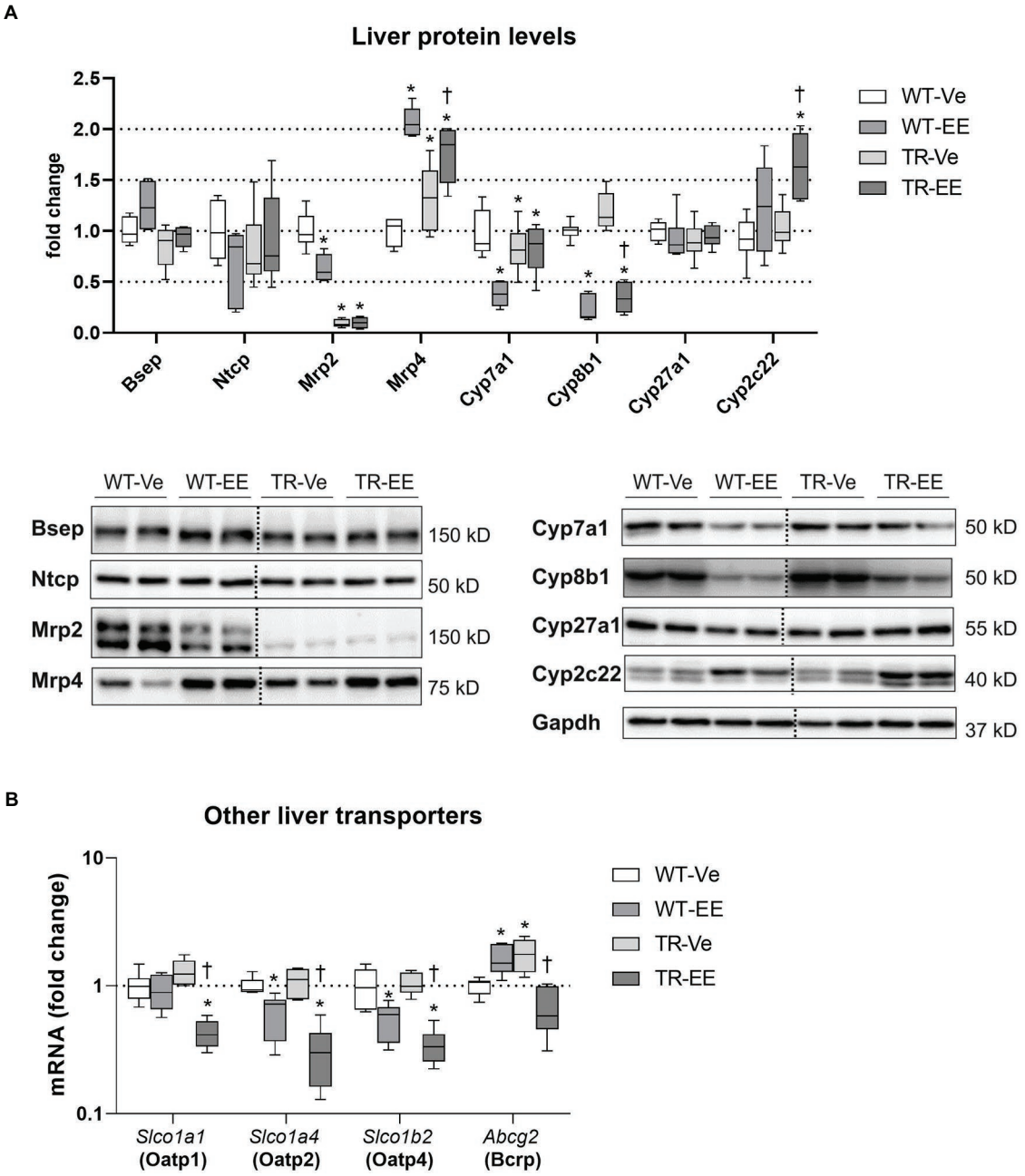

FIGURE 6 | Effect of ethinylestradiol and Mrp2 deficiency on the mRNA and protein expression of bile acid-related genes in the liver. Experimental groups: WT-Ve, WT rats receiving vehicle; WT-EE, WT rats receiving ethinylestradiol; TR-Ve, TR rats receiving vehicle; and TR-EE, TR rats receiving ethinylestradiol. **(A)** The protein expression of crucial bile acid synthetizing and transporting molecules in the liver. Dotted line shows where irrelevant bands were omitted. **(B)** The gene expression of alternative hepatocyte transporters for bile acids. Protein and mRNA levels were normalized to Gapdh expression. Data are presented as medians, with boxes and whiskers representing the interquartile range and 5th-95th percentiles, respectively. Protein and mRNA levels were normalized to Gapdh expression. Significance: $^{*}p < 0.05$, compared to vehicle-treated WT rats; $^{\dagger}p < 0.05$ compared to vehicle-treated TR group.

rats administered with ethinylestradiol (**Figure 7D**). The RXRa was reduced in vehicle-treated TR rats compared with control WT group. Ethinylestradiol administration to TR rats caused further downregulation of RXRa and upregulation of p65-NF-kB relative to vehicle-treated TR animals. These results indicate that there are significant differences in ethinylestradiol-mediated regulation of BA homeostasis between WT and Mrp2-deficient rats.

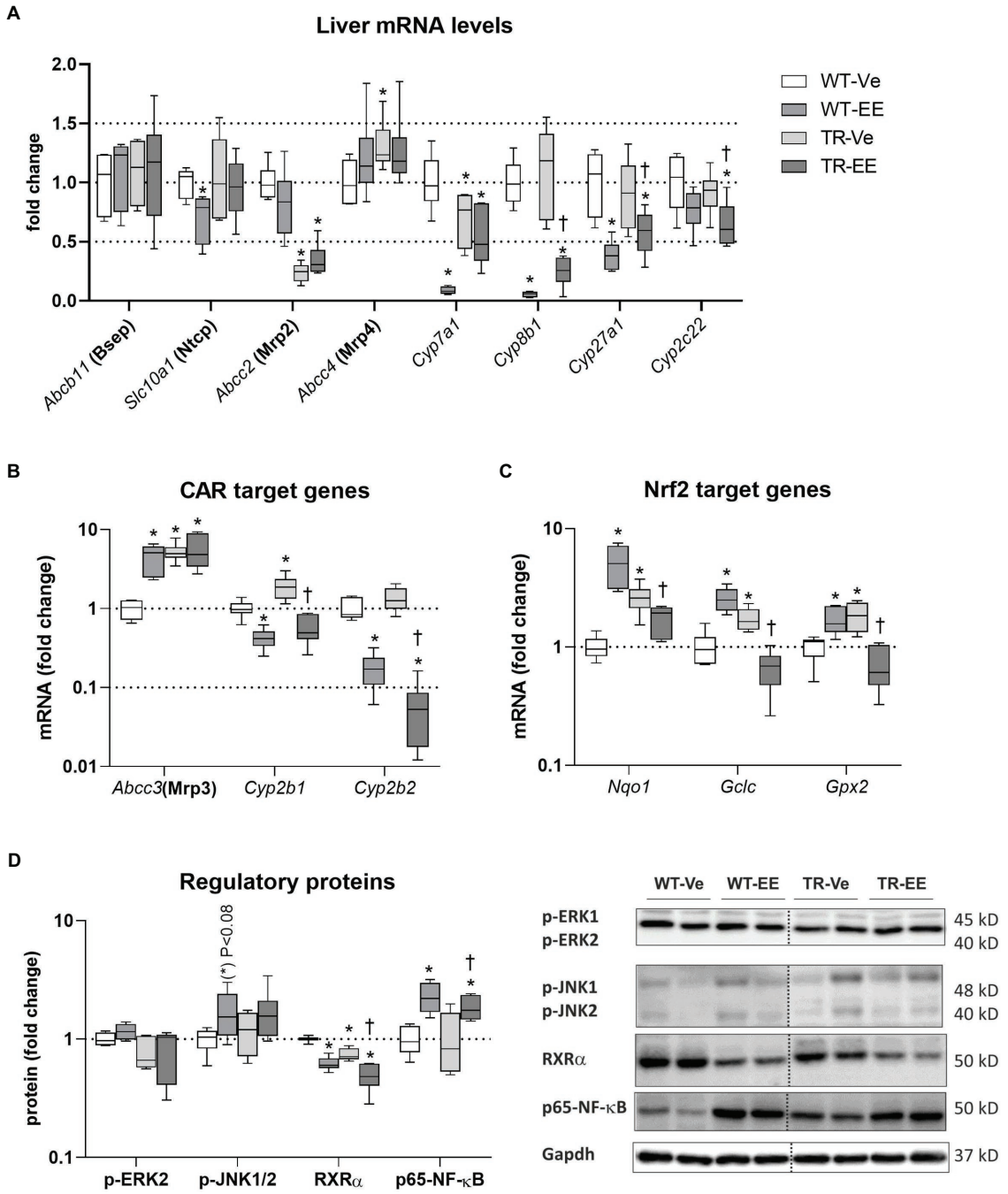

FIGURE 7 | Effect of ethinylestradiol and Mrp2 deficiency on the mRNA or protein expression of pathways regulating bile acid homeostasis in the liver. Experimental groups: WT-Ve, WT rats receiving vehicle; WT-EE, WT rats receiving ethinylestradiol; TR-Ve, TR rats receiving vehicle; and TR-EE, TR rats receiving ethinylestradiol. **(A)** The mRNA expression of crucial bile acid synthetizing and transporting molecules in the liver. **(B)** The expression of genes regulated by constitutive androstane receptor (CAR). **(C)** The expression of Nuclear factor erythroid 2-related factor 2 (Nrf2) target genes. **(D)** Protein expression of key intracellular signaling molecules involved in the regulation of bile acid metabolomics. Protein and mRNA levels were normalized to Gapdh expression. Dotted line shows where irrelevant bands were omitted. Data are presented as medians, with boxes and whiskers representing the interquartile range and 5th-95th percentiles, respectively. Significance: $^{*}p < 0.05$, compared to vehicle-treated WT rats; $^{\dagger}p < 0.05$ compared to vehicle-treated TR group.

DISCUSSION

The major finding of our study is that Mrp2-deficient animals show increased plasma concentrations of BAs and are sensitive to ethinylestradiol-induced cholestatic insult. Measurement of individual BAs in Mrp2-deficient animals was previously performed in one study, where the authors presented only relative peak areas standardized to D4-taurocholic acid using

LC–MS analysis. This analysis showed a 1.6–62.1-fold increase in peak areas of plasma BAs in Mrp2-deficient animals compared to WT animals (Aoki et al., 2011). However, the accuracy of such a standardization method may be altered by different chemical characteristics of individual BAs. Indeed, our LC–MS analysis of absolute BA concentrations in plasma with separate calibrators showed an increased concentration of total BAs in plasma. This was the result of an overall tendency toward an increase for the majority of individual BAs, with the increase in DCA, a secondary 12α-hydroxylated bile acid (12-OH BA), reaching statistical significance. These data suggest a change at the level of net BA transport and synthesis of secondary BAs in Mrp2-deficient TR rats. Importantly, the shift of the plasma BA spectrum toward more lipophilic DCA may imply an increased risk of systemic toxicity.

Our vehicle-treated TR rats showed an expected reduction in BA-independent bile flow *via* reduction in Mrp2-mediated biliary secretion of glutathione. Mrp2 also transports glucuronide- and sulfate-conjugates of BAs, especially TCDCA and TLCA (Kuipers et al., 1988; Takikawa et al., 1991; Akita et al., 2001). Previously, in Mrp2-deficient animals, net biliary secretion of BAs was not changed (Verkade et al., 1993) and concentrations of unconjugated and glycine/taurine-conjugated BAs were not different after administration of radiolabeled ^{14}C-CDCA (Takikawa et al., 1991). However, at the time of these analyses, a sensitive method for BA detection was not available. Indeed, our results achieved by highly sensitive LC–MS analysis showed that biliary secretion of total BAs was reduced at the expense of monoconjugated TCDCA, TMCA, while secretion of TDCA was increased. We identified several factors which may contribute to this effect in Mrp2-deficient TR rats. First, BA synthesis in hepatocytes was reduced *via* repressed Cyp7a1, and BAs underwent increased efflux from hepatocytes to plasma *via* induced multidrug resistance-associated protein 3 (Mrp3) and Mrp4, thus reducing disposition of BAs for biliary secretion. This is consistent with previously described induction of Mrp3 and Mrp4 in Mrp2-deficient rats (Oswald et al., 2006; Gavrilova et al., 2007). As stated previously, Mrp3 level correlates with BA return to plasma (Akita et al., 2002), and Mrp4 transporter may contribute to this effect. Second, stool excretion of BAs was not changed despite the reduced BA intestinal delivery due to reduced BA biliary secretion. This indicates that BA reabsorption is reduced in the ileum, consistent with reduced expression of Asbt, a major absorption transporter for BAs. Therefore, reduced ileum expression of FXR target genes, such as Shp and Fgf15, may be a consequence of decreased reabsorption of FXR agonistic BAs, which was indeed detected for TCDCA. Interestingly, increased biliary secretion was noticed for TDCA. Coupled with unchanged stool excretion of DCA, this indicated that reabsorption of this BA in the ileum is increased. We may only speculate that DCA was reabsorbed by passive diffusion in the large intestine (Chiang and Ferrell, 2020). This may explain increased concentrations of DCA in the plasma of TR rats. Such a shift in the spectrum of BAs reduced the primary to secondary BA ratio in bile and stool of TR rats. It suggests increased conversion of primary BAs into secondary BAs by modified intestinal microbiota as a result of the altered flux of Mrp2 substrates, including BAs, from the liver to the intestine *via* bile. These findings indicate that Mrp2-deficient organism may be predisposed to a more significant increase in plasma BA concentrations upon hormonal cholestatic insult.

Analysis of BA regulatory pathways revealed that liver changes in our Mrp2-deficient rats may be related to the activation of Nrf2 as reflected by increased expression of its target genes, such as *Nqo1*, *Gclc*, and *Gpx2*. Nrf2 plays a critical role in regulating the transcription of cytoprotective genes during oxidative stress. Recently, it was shown that Nrf2 activation induces Mrp3 and Mrp4, represses Cyp7a1, decreases BA concentrations in the liver, and increases BAs in plasma (Aleksunes et al., 2008; Xu et al., 2010; Aleksunes and Klaassen, 2012; Liu et al., 2021), which was also apparent in our study. In addition, repression of Asbt in ileum enterocytes detected in our study was also seen upon Nrf2 activation (Zhang et al., 2020). Activation of Nrf2 may contribute to glutathione accumulation in TR rats due to activation of glutathione synthetizing enzymes in addition to the reduced glutathione biliary secretion due to Mrp2 deficiency. Interestingly, accumulating reduced glutathione and bilirubin provide significant antioxidative activity in the liver of Mrp2-deficient rats, yet Nrf2 is activated. This may be a consequence of CAR activation (Rooney et al., 2019) by accumulated bilirubin, which is a known CAR agonist (Vítek, 2020). Indeed, we observed marked induction of CAR target genes Abcc3, and Cyp2b1. Therefore, one potential mechanism of observed changes in BA homeostasis in TR rats may be bilirubin-mediated activation of CAR-Nfr2 pathway. TR rats also showed decreased RXRa, a versatile dimerization partner (Lefebvre et al., 2010) required for the formation of active heterodimers with orphan nuclear receptors involved in the regulation of BA metabolomics such as FXR (Garcia et al., 2018). Other regulatory pathways seem to have a minor role in TR rats. Fgf15 released from the ileum is a major regulator BA synthesis by suppressing Cyp7a1 expression in the liver through activation of the Fgfr4-JNK (c-Jun-N-terminal kinase) pathway (Chiang and Ferrell, 2020). Reduction of Fgf15 without activation of JNK excludes the contribution of Fgf15 to the observed Cyp7a1 reduction.

The major mechanism responsible for estrogen-induced cholestasis is the activation of ERa receptor with consequent transcriptional repression of basolateral uptake transporters for BAs such as *Slc10a1* (Ntcp), and BA synthetic enzymes such as Cyp7a1 and Cyp8a1 (Geier et al., 2003, 2007; Yamamoto et al., 2006). Ethinylestradiol reduces transactivation of these molecules by decreasing regulatory hepatocyte nuclear factor 1 (HNF1), and RXR: RAR factors, either directly or by induction of inflammatory reactions that activate several intracellular stress pathways including NF-kB, and JNK (Geier et al., 2007). In agreement, our estrogen-treated WT rats showed a decrease in Ntcp, Oatp, Cyp7a1, Cyp8b1, and RXRa and activation of JNK and NF-kB. Similarly to previous results with ethinylestradiol-induced cholestasis, we also detected posttranscriptional reduction of Mrp2 (Trauner et al., 1997; Lee et al., 2000; Wagner et al., 2003; Ruiz et al., 2007; Cermanova et al., 2015), Mrp4 upregulation (Faradonbeh et al., 2021),

and unchanged Bsep protein expression (Ruiz et al., 2007). Cholestasis after ethinylestradiol is typically associated with ERa-JNK-c-JUN mediated (Ruiz et al., 2013) upregulation of Mrp3 basolateral efflux transporter for BAs (Hirsova et al., 2013; Muchova et al., 2015), which all were also reproduced in our study. These mechanisms impede the transcellular transport of BAs and increase their concentrations in plasma. Furthermore, reduced biliary secretion of BAs in ethinylestradiol-treated rats was coupled with unchanged fecal BA elimination. This indicates that reduced BA reabsorption in the intestine represents a compensatory mechanism to restore BA homeostasis during cholestasis (Zhang et al., 2018). In agreement, reduced uptake of FXR agonistic BAs, such as CDCA and DCA, in the ileum led to reduced expression of target genes such as *NR0B2* (Shp) and *Fgf15* as also previously reported (Hirsova et al., 2013; Faradonbeh et al., 2021).

Few earlier studies analyzed estrogen-induced cholestasis in Mrp2-deficient rats. Koopen et al. (1998) showed reduced bile flow in Mrp2-deficient rats after 3-day ethinylestradiol treatment, although biliary secretion of glutathione, bilirubin, and net BAs was not changed. Two other studies with Mrp2-deficient rats failed to find the immediate effect of a single estrogen dose on the bile flow (Huang et al., 2000) or Bsep-mediated taurocholate uptake to canalicular membrane vesicles (Stieger et al., 2000). This was ascribed to the absence of Mrp2-mediated biliary secretion of cholestatic metabolites of ethinylestradiol, such as ethinylestradiol-17-α/β-glucuronide, that consequently block Bsep from the luminal site (Huang et al., 2000; Stieger et al., 2000). However, our 5-day regimen of ethinylestradiol reliably induced cholestasis in the Mrp2-deficient rats. We detected an additional increase of plasma BA concentrations, confirming an increased sensitivity of Mrp2-defective organism to estrogen. Such sensitivity may result from increased exposure of organisms to ethinylestradiol due to altered ethinylestradiol-glucuronide excretion *via* Mrp2 (Zamek-Gliszczynski et al., 2011). Increased plasma BAs were consistent with marked increase in Mrp4-mediated export of BAs back to plasma. In addition, *Slco1a1* and *Abcg2* have been suggested as important hepatocyte transporters for the uptake and secretion of BAs, respectively (Blazquez et al., 2012; Tanaka et al., 2012; Zhang et al., 2012; Jiang et al., 2020). Significant reduction of *Slco1a1* and *Abcg2* in ethinylestradiol administered Mrp2-deficient rats compared with vehicle-treated deficient group contrasts with absence (*Slco1a1*) or even induction (*Abcg2*) of these transporters in ethinylestradiol-treated WT group. However, unchanged biliary secretion of bile acids between Mrp2-deficient groups suggests that the contribution of *Abcg2* to observed changes in BA metabolomics may not be significant. Taking together, reduction of *Slco1a1* expression by ethinylestradiol in Mrp2-deficient rats may contribute to increased BA plasma concentrations in this group *via* decreased BAs uptake into hepatocytes. A compensatory reaction to increased plasma BAs likely involved a decreased expression of Cyp8b1, the rate-limiting enzyme for the synthesis of 12-OH BAs, followed by a generally reduced 12-OH/non-12-OH BA ratio in plasma, bile, and stool. Unlike Cyp7a1, the Cyp8b1 is mainly regulated by liver FXR (Chiang and Ferrell, 2020). Reduced expression of Cyp8b1 may therefore reflect the inhibitory effect of ethinylestradiol on FXR and its cofactor RXRa. In contrast, ethinylestradiol posttranscriptionally induced expression of Cyp2c22, a rat orthologue synthetizing primary muricholic acid (MCA), leading to increased TMCA in bile and stool, and contributing to increased primary/secondary BA ratio in the stool. Unlike in WT rats, ethinylestradiol consistently reduced Nrf2 activation in TR animals by unknown mechanisms.

CONCLUSION

Our findings showed marked modification of BA metabolomics and a significant increase in BA plasma concentrations in Mrp2-deficient rats. The mechanism responsible for this increase was likely related to the increased Mrp3 and Mrp4-mediated efflux of BAs from hepatocytes to plasma. Reduced BA biliary secretion and reabsorption revealed reduced enterohepatic recycling of BAs in Mrp2-deficient animals, except for increased disposition of secondary DCA. Possible alteration of intestinal microbiota in the Mrp2-deficient organism is therefore suggestive but requires further analysis. Accumulation of more lipophilic secondary BAs may threaten the organism with their increased toxicity. Ethinylestradiol administration to Mrp2-deficient TR rats further increased concentrations of BAs in plasma by upregulation of liver Mrp4 efflux pump, and reduced *Slco1a1* uptake transporter. Taken together, our results present mechanisms that may explain the increased sensitivity of Mrp2-deficient organisms to estrogen-induced cholestasis. Bile acid monitoring is therefore highly desirable in pregnant women with conjugated hyperbilirubinemia for early detection of ICP.

DATA AVAILABILITY STATEMENT

The original contributions presented in the study are included in the article/supplementary material, further inquiries can be directed to the corresponding author.

ETHICS STATEMENT

The project was reviewed and approved by the Animal Welfare Bodies of the Faculty of Medicine in Hradec Kralove and the Ministry of Education, Youth and Sports of the Czech Republic.

AUTHOR CONTRIBUTIONS

FAF: methodology, investigation, and writing—original draft. HL, JC, MH, and MU: investigation and methodology. ZN: software. PH: writing—review and editing. PP: validation. SM: supervision, project administration, resources, funding acquisition, and writing—review and editing. All authors contributed to the article and approved the submitted version.

FUNDING

The project was supported by grants Progres Q40/05, SVV 260543/2020, GAUK 5562/18, and GACR 19-14497S, and by the ERDF-Project PERSONMED No. CZ.02.1.01/0.0/0.0/16_048/0007441 and ESF-Project "International mobility of RTAS ChU" No. CZ.02.1.01/0.0/0.0/17_048/0007421. PH received support from the National Institute of Diabetes and Digestive and Kidney Diseases (NIDDK) of the National Institutes of Health (NIH) under the Award Number R01DK130884.

ACKNOWLEDGMENTS

The authors acknowledge contribution of lab technicians: Kristyna Trubacova, Jana Lemfeldova, and Dagmar Jezkova.

REFERENCES

Akita, H., Suzuki, H., Ito, K., Kinoshita, S., Sato, N., Takikawa, H., et al. (2001). Characterization of bile acid transport mediated by multidrug resistance associated protein 2 and bile salt export pump. *Biochim. Biophys. Acta* 1511, 7–16. doi: 10.1016/s0005-2736(00)00355-2

Akita, H., Suzuki, H., and Sugiyama, Y. (2002). Sinusoidal efflux of taurocholate correlates with the hepatic expression level of Mrp3. *Biochem. Biophys. Res. Commun.* 299, 681–687. doi: 10.1016/s0006-291x(02)02723-7

Aleksunes, L. M., and Klaassen, C. D. (2012). Coordinated regulation of hepatic phase I and II drug-metabolizing genes and transporters using AhR-, CAR-, PXR-, PPARalpha-, and Nrf2-null mice. *Drug Metab. Dispos.* 40, 1366–1379. doi: 10.1124/dmd.112.045112

Aleksunes, L. M., Slitt, A. L., Maher, J. M., Augustine, L. M., Goedken, M. J., Chan, J. Y., et al. (2008). Induction of Mrp3 and Mrp4 transporters during acetaminophen hepatotoxicity is dependent on Nrf2. *Toxicol. Appl. Pharmacol.* 226, 74–83. doi: 10.1016/j.taap.2007.08.022

Aoki, M., Konya, Y., Takagaki, T., Umemura, K., Sogame, Y., Katsumata, T., et al. (2011). Metabolomic investigation of cholestasis in a rat model using ultra-performance liquid chromatography/tandem mass spectrometry. *Rapid Commun. Mass Spectrom.* 25, 1847–1852. doi: 10.1002/rcm.5072

Blazquez, A. G., Briz, O., Romero, M. R., Rosales, R., Monte, M. J., Vaquero, J., et al. (2012). Characterization of the role of ABCG2 as a bile acid transporter in liver and placenta. *Mol. Pharmacol.* 81, 273–283. doi: 10.1124/mol.111.075143

Cermanova, J., Kadova, Z., Zagorova, M., Hroch, M., Tomsik, P., Nachtigal, P., et al. (2015). Boldine enhances bile production in rats via osmotic and farnesoid X receptor dependent mechanisms. *Toxicol. Appl. Pharmacol.* 285, 12–22. doi: 10.1016/j.taap.2015.03.004

Chiang, J. Y. L., and Ferrell, J. M. (2020). Up to date on cholesterol 7 alpha-hydroxylase (CYP7A1) in bile acid synthesis. *Liver Res.* 4, 47–63. doi: 10.1016/j.livres.2020.05.001

Corpechot, C., Barbu, V., Chazouillères, O., Broué, P., Girard, M., Roquelaure, B., et al. (2020). Genetic contribution of ABCC2 to Dubin-Johnson syndrome and inherited cholestatic disorders. *Liver Int.* 40, 163–174. doi: 10.1111/liv.14260

Crocenzi, F. A., Pellegrino, J. M., Catania, V. A., Luquita, M. G., Roma, M. G., Mottino, A. D., et al. (2006). Galactosamine prevents ethinylestradiol-induced cholestasis. *Drug Metab. Dispos.* 34, 993–997. doi: 10.1124/dmd.106.009308

Dixon, P. H., Sambrotta, M., Chambers, J., Taylor-Harris, P., Syngelaki, A., Nicolaides, K., et al. (2017). An expanded role for heterozygous mutations of ABCB4, ABCB11, ATP8B1, ABCC2 and TJP2 in intrahepatic cholestasis of pregnancy. *Sci. Rep.* 7:11823. doi: 10.1038/s41598-017-11626-x

Douglas, J. G., Beckett, G. J., Percy-Robb, I. W., and Finlayson, N. D. (1980). Bile salt transport in the Dubin-Johnson syndrome. *Gut* 21, 890–893. doi: 10.1136/gut.21.10.890

Engelking, L. R., and Gronwall, R. (1979). Bile acid clearance in sheep with hereditary hyperbilirubinemia. *Am. J. Vet. Res.* 40, 1277–1280.

Faradonbeh, F. A., Sa, I., Lastuvkova, H., Cermanova, J., Hroch, M., Faistova, H., et al. (2021). Metformin impairs bile acid homeostasis in ethinylestradiol-induced cholestasis in mice. *Chem. Biol. Interact.* 345:109525. doi: 10.1016/j.cbi.2021.109525

Fu, H., Zhao, R., Jia, X., Li, X., Li, G., and Yin, C. (2021). Neonatal Dubin-Johnson syndrome: biochemical parameters, characteristics, and genetic variants study. Pediatr. Res. doi: 10.1038/s41390-021-01583-7 [Epub ahead of print].

Garcia, M., Thirouard, L., Sedès, L., Monrose, M., Holota, H., Caira, F., et al. (2018). Nuclear receptor metabolism of bile acids and Xenobiotics: a coordinated detoxification system with impact on health and diseases. *Int. J. Mol. Sci.* 19:3630. doi: 10.3390/ijms19113630

Gavrilova, O., Geyer, J., and Petzinger, E. (2007). In vivo relevance of Mrp2-mediated biliary excretion of the amanita mushroom toxin demethylphalloin. *Biochim. Biophys. Acta* 1768, 2070–2077. doi: 10.1016/j.bbamem.2007.07.006

Geier, A., Dietrich, C. G., Gerloff, T., Haendly, J., Kullak-Ublick, G. A., Stieger, B., et al. (2003). Regulation of basolateral organic anion transporters in ethinylestradiol-induced cholestasis in the rat. *Biochim. Biophys. Acta* 1609, 87–94. doi: 10.1016/s0005-2736(02)00657-0

Geier, A., Wagner, M., Dietrich, C. G., and Trauner, M. (2007). Principles of hepatic organic anion transporter regulation during cholestasis, inflammation and liver regeneration. *Biochim. Biophys. Acta* 1773, 283–308. doi: 10.1016/j.bbamcr.2006.04.014

Hirsova, P., Karlasova, G., Dolezelova, E., Cermanova, J., Zagorova, M., Kadova, Z., et al. (2013). Cholestatic effect of epigallocatechin gallate in rats is mediated via decreased expression of Mrp2. *Toxicology* 303, 9–15. doi: 10.1016/j.tox.2012.10.018

Huang, L., Smit, J. W., Meijer, D. K., and Vore, M. (2000). Mrp2 is essential for estradiol-17beta(beta-D-glucuronide)-induced cholestasis in rats. *Hepatology* 32, 66–72. doi: 10.1053/jhep.2000.8263

Huynh, M. T., Chrétien, Y., Grison, S., Delaunay, J. L., Lascols, O., Tran, C. T., et al. (2018). Novel compound heterozygous ABCC2 variants in patients with Dubin-Johnson syndrome and intrahepatic cholestasis of pregnancy. *Clin. Genet.* 94, 480–481. doi: 10.1111/cge.13420

Jemnitz, K., Heredi-Szabo, K., Janossy, J., Ioja, E., Vereczkey, L., and Krajcsi, P. (2010). ABCC2/Abcc2: a multispecific transporter with dominant excretory functions. *Drug Metab. Rev.* 42, 402–436. doi: 10.3109/03602530903491741

Jiang, L., Chu, H., Gao, B., Lang, S., Wang, Y., Duan, Y., et al. (2020). Transcriptomic profiling identifies novel hepatic and intestinal genes following chronic plus binge ethanol feeding in mice. *Dig. Dis. Sci.* 65, 3592–3604. doi: 10.1007/s10620-020-06461-6

Junge, N., Goldschmidt, I., Wiegandt, J., Leiskau, C., Mutschler, F., Laue, T., et al. (2021). Dubin-Johnson syndrome as differential diagnosis for neonatal cholestasis. *J. Pediatr. Gastroenterol. Nutr.* 72, e105–e111. doi: 10.1097/mpg.0000000000003061

Koopen, N. R., Wolters, H., Havinga, R., Vonk, R. J., Jansen, P. L., Muller, M., et al. (1998). Impaired activity of the bile canalicular organic anion transporter (Mrp2/cmoat) is not the main cause of ethinylestradiol-induced cholestasis in the rat. *Hepatology* 27, 537–545. doi: 10.1002/hep.510270231

Kuipers, F., Enserink, M., Havinga, R., Van Der Steen, A. B., Hardonk, M. J., Fevery, J., et al. (1988). Separate transport systems for biliary secretion of sulfated and unsulfated bile acids in the rat. *J. Clin. Invest.* 81, 1593–1599. doi: 10.1172/jci113493

Kularatnam, G. A. M., Warawitage, D., Vidanapathirana, D. M., Jayasena, S., Jasinge, E., De Silva, N., et al. (2017). Dubin-Johnson syndrome and intrahepatic cholestasis of pregnancy in a Sri Lankan family: a case report. *BMC. Res. Notes* 10:487. doi: 10.1186/s13104-017-2811-6

Lee, J. M., Trauner, M., Soroka, C. J., Stieger, B., Meier, P. J., and Boyer, J. L. (2000). Expression of the bile salt export pump is maintained after chronic cholestasis in the rat. *Gastroenterology* 118, 163–172. doi: 10.1016/s0016-5085(00)70425-2

Lefebvre, P., Benomar, Y., and Staels, B. (2010). Retinoid X receptors: common heterodimerization partners with distinct functions. *Trends Endocrinol. Metab.* 21, 676–683. doi: 10.1016/j.tem.2010.06.009

Liu, J., Hou, L. L., and Zhao, C. Y. (2018). Effect of YHHJ on the expression of the hepatocellular bile acid transporters multidrug resistance-associated protein 2 and bile salt export pump in ethinylestradiol-induced cholestasis. *Exp. Ther. Med.* 15, 3699–3704. doi: 10.3892/etm.2018.5891

Liu, J., Lickteig, A. J., Zhang, Y., Csanaky, I. L., and Klaassen, C. D. (2021). Activation of Nrf2 decreases bile acid concentrations in livers of female mice. *Xenobiotica* 51, 605–615. doi: 10.1080/00498254.2021.1880033

Meier, Y., Zodan, T., Lang, C., Zimmermann, R., Kullak-Ublick, G. A., Meier, P. J., et al. (2008). Increased susceptibility for intrahepatic cholestasis of pregnancy and contraceptive-induced cholestasis in carriers of the 1331T>C polymorphism in the bile salt export pump. *World J. Gastroenterol.* 14, 38–45. doi: 10.3748/wjg.14.38

Muchova, L., Vanova, K., Suk, J., Micuda, S., Dolezelova, E., Fuksa, L., et al. (2015). Protective effect of heme oxygenase induction in ethinylestradiol-induced cholestasis. *J. Cell. Mol. Med.* 19, 924–933. doi: 10.1111/jcmm.12401

Oswald, S., Westrup, S., Grube, M., Kroemer, H. K., Weitschies, W., and Siegmund, W. (2006). Disposition and sterol-lowering effect of ezetimibe in multidrug resistance-associated protein 2-deficient rats. *J. Pharmacol. Exp. Ther.* 318, 1293–1299. doi: 10.1124/jpet.106.104018

Pozzi, E. J. S., Crocenzi, F. A., Pellegrino, J. M., Catania, V. A., Luquita, M. G., Roma, M. G., et al. (2003). Ursodeoxycholate reduces ethinylestradiol glucuronidation in the rat: role in prevention of estrogen-induced cholestasis. *J. Pharmacol. Exp. Ther.* 306, 279–286. doi: 10.1124/jpet.103.049940

Prasnicka, A., Cermanova, J., Hroch, M., Dolezelova, E., Rozkydalova, L., Smutny, T., et al. (2017). Iron depletion induces hepatic secretion of biliary lipids and glutathione in rats. *Biochim. Biophys. Acta* 1862, 1469–1480. doi: 10.1016/j.bbalip.2017.09.003

Rezai, S., Lam, J., and Henderson, C. E. (2015). Intrahepatic cholestasis of pregnancy: maternal and fetal outcomes associated with elevated bile acid levels. *Am. J. Obstet. Gynecol.* 213:114. doi: 10.1016/j.ajog.2015.03.040

Rooney, J. P., Oshida, K., Kumar, R., Baldwin, W. S., and Corton, J. C. (2019). Chemical activation of the constitutive androstane receptor leads to activation of oxidant-induced Nrf2. *Toxicol. Sci.* 167, 172–189. doi: 10.1093/toxsci/kfy231

Ruiz, M. L., Rigalli, J. P., Arias, A., Villanueva, S. S., Banchio, C., Vore, M., et al. (2013). Estrogen receptor-α mediates human multidrug resistance associated protein 3 induction by 17α-ethynylestradiol. Role of activator protein-1. *Biochem. Pharmacol.* 86, 401–409. doi: 10.1016/j.bcp.2013.05.025

Ruiz, M. L., Villanueva, S. S., Luquita, M. G., Ikushiro, S., Mottino, A. D., and Catania, V. A. (2007). Beneficial effect of spironolactone administration on ethynylestradiol-induced cholestasis in the rat: involvement of up-regulation of multidrug resistance-associated protein 2. *Drug Metab. Dispos.* 35, 2060–2066. doi: 10.1124/dmd.107.016519

Sookoian, S., Castaño, G., Burgueño, A., Gianotti, T. F., and Pirola, C. J. (2008). Association of the multidrug-resistance-associated protein gene (ABCC2) variants with intrahepatic cholestasis of pregnancy. *J. Hepatol.* 48, 125–132. doi: 10.1016/j.jhep.2007.08.015

Stieger, B., Fattinger, K., Madon, J., Kullak-Ublick, G. A., and Meier, P. J. (2000). Drug- and estrogen-induced cholestasis through inhibition of the hepatocellular bile salt export pump (Bsep) of rat liver. *Gastroenterology* 118, 422–430. doi: 10.1016/s0016-5085(00)70224-1

Takikawa, H., Sano, N., Narita, T., Uchida, Y., Yamanaka, M., Horie, T., et al. (1991). Biliary excretion of bile acid conjugates in a hyperbilirubinemic mutant Sprague-Dawley rat. *Hepatology* 14, 352–360.

Tanaka, N., Matsubara, T., Krausz, K. W., Patterson, A. D., and Gonzalez, F. J. (2012). Disruption of phospholipid and bile acid homeostasis in mice with nonalcoholic steatohepatitis. *Hepatology* 56, 118–129. doi: 10.1002/hep.25630

Togawa, T., Mizuochi, T., Sugiura, T., Kusano, H., Tanikawa, K., Sasaki, T., et al. (2018). Clinical, pathologic, and genetic features of neonatal Dubin-Johnson syndrome: a multicenter study in Japan. *J. Pediatr.* 196, 161.e1–167.e1. doi: 10.1016/j.jpeds.2017.12.058

Trauner, M., Arrese, M., Soroka, C. J., Ananthanarayanan, M., Koeppel, T. A., Schlosser, S. F., et al. (1997). The rat canalicular conjugate export pump (Mrp2) is down-regulated in intrahepatic and obstructive cholestasis. *Gastroenterology* 113, 255–264. doi: 10.1016/s0016-5085(97)70103-3

Verkade, H. J., Wolters, H., Gerding, A., Havinga, R., Fidler, V., Vonk, R. J., et al. (1993). Mechanism of biliary lipid secretion in the rat: a role for bile acid-independent bile flow? *Hepatology* 17, 1074–1080.

Vítek, L. (2020). Bilirubin as a signaling molecule. *Med. Res. Rev.* 40, 1335–1351. doi: 10.1002/med.21660

Wagner, M., Fickert, P., Zollner, G., Fuchsbichler, A., Silbert, D., Tsybrovskyy, O., et al. (2003). Role of farnesoid X receptor in determining hepatic ABC transporter expression and liver injury in bile duct-ligated mice. *Gastroenterology* 125, 825–838. doi: 10.1016/s0016-5085(03)01068-0

Wang, Z., Guo, H., Wang, Y., Kong, F., and Wang, R. (2014). Interfering effect of bilirubin on the determination of alkaline phosphatase. *Int. J. Clin. Exp. Med.* 7, 4244–4248.

Xu, S., Weerachayaphorn, J., Cai, S. Y., Soroka, C. J., and Boyer, J. L. (2010). Aryl hydrocarbon receptor and NF-E2-related factor 2 are key regulators of human MRP4 expression. *Am. J. Physiol. Gastrointest. Liver Physiol.* 299, G126–G135. doi: 10.1152/ajpgi.00522.2010

Yamamoto, Y., Moore, R., Hess, H. A., Guo, G. L., Gonzalez, F. J., Korach, K. S., et al. (2006). Estrogen receptor alpha mediates 17alpha-ethynylestradiol causing hepatotoxicity. *J. Biol. Chem.* 281, 16625–16631. doi: 10.1074/jbc.M602723200

Zamek-Gliszczynski, M. J., Day, J. S., Hillgren, K. M., and Phillips, D. L. (2011). Efflux transport is an important determinant of ethinylestradiol glucuronide and ethinylestradiol sulfate pharmacokinetics. *Drug Metab. Dispos.* 39, 1794–1800. doi: 10.1124/dmd.111.040162

Zhang, Y., Lickteig, A. J., Liu, J., Csanaky, I. L., and Klaassen, C. D. (2020). Effects of ablation and activation of Nrf2 on bile acid homeostasis in male mice. *Toxicol. Appl. Pharmacol.* 403:115170. doi: 10.1016/j.taap.2020.115170

Zhang, Y., Limaye, P. B., Lehman-Mckeeman, L. D., and Klaassen, C. D. (2012). Dysfunction of organic anion transporting polypeptide 1a1 alters intestinal bacteria and bile acid metabolism in mice. *PLoS One* 7:e34522. doi: 10.1371/journal.pone.0034522

Zhang, F., Xi, L., Duan, Y., Qin, H., Wei, M., Wu, Y., et al. (2018). The ileum-liver farnesoid X receptor signaling axis mediates the compensatory mechanism of 17α-ethynylestradiol-induced cholestasis via increasing hepatic biosynthesis of chenodeoxycholic acids in rats. *Eur. J. Pharm. Sci.* 123, 404–415. doi: 10.1016/j.ejps.2018.08.005

Zhao, Y., Zhai, D., He, H., Liu, J., Li, T., Chen, X., et al. (2009). Matrine improves 17alpha-ethinyl estradiol-induced acute cholestasis in rats. *Hepatol. Res.* 39, 1144–1149. doi: 10.1111/j.1872-034X.2009.00557.x

Conflict of Interest: The authors declare that the research was conducted in the absence of any commercial or financial relationships that could be construed as a potential conflict of interest.

Publisher's Note: All claims expressed in this article are solely those of the authors and do not necessarily represent those of their affiliated organizations, or those of the publisher, the editors and the reviewers. Any product that may be evaluated in this article, or claim that may be made by its manufacturer, is not guaranteed or endorsed by the publisher.

GLOSSARY

12-OH	12α-hydroxylated bile acid
Abcc2	ATP-binding cassette transporter sub-family C-member 2
Abcg2	ATP-binding cassette transporter sub-family G-member 2
ALT	Alanine aminotransferase
ANOVA	Analysis of variance
Asbt	Ileal sodium/bile acid cotransporter
AST	Aspartate aminotransferase
ATP	Adenosine triphosphate
BA	Bile acid
BADF	Bile acid-dependent bile flow
BAIF	Bile acid-independent bile flow
BE	Biliary excretion
Bsep	Bile salt export pump
CAR	Constitutive androstane receptor
CDCA	Chenodeoxycholic acid
Cyp27a1	Sterol 27-hydroxylase
Cyp2b1	Cytochrome P450 family 2, subfamily b, polypeptide 1
Cyp2c22	Cytochrome P450, family 2, subfamily c, polypeptide 22
Cyp7a1	Cholesterol 7α-hydroxylase
Cyp8b1	Sterol 12α-hydroxylase
CAD5	D5-cholic acid
DCA	Deoxycholic acid
EE	Ethinylestradiol
ERK	Extracellular signal-regulated kinase
Fgf15	Fibroblast growth factor 15
FXR	Farnesoid X receptor
Gapdh	Glyceraldehyde 3-phosphate dehydrogenase
GCA	Glycocholic acid
Gclc	Glutamate-cysteine ligase catalytic subunit
Gpx2	Glutathione peroxidase 2
GSH	Reduced glutathione
GSSG	Oxidized glutathione
HPLC	High-performance liquid chromatography
ICP	Intrahepatic cholestasis of pregnancy
LCA	Lithocholic acid
LC–MS	Liquid chromatography–mass spectrometry
MCA	Muricholic acid
Mrp2	Multidrug resistance-associated protein 2
Mrp3	Multidrug resistance-associated protein 3
Mrp4	Multidrug resistance-associated protein 4
Non-12-OH	Non-12α-hydroxylated
Nqo1	NAD(P)H quinone dehydrogenase 1
Nrf2	Nuclear factor erythroid 2-related factor 2
Ntcp	Na^+-taurocholate cotransporting polypeptide
P65 NF-kB	Nuclear factor NF-kappa-B p65 subunit
p-JNK	Phosphorylated c-Jun N-terminal kinases
PXR	Pregnane X receptor
qRT-PCR	Quantitative reverse transcription-PCR
RXRα	Retinoid X receptor alpha
SHP	Small heterodimer partner
TCA	Taurocholic acid
TCDCA	Taurochenodeoxycholic acid
TDCA	Taurodeoxycholic acid
TLCA	Taurolithocholic acid
TMCA	Tauromuricholic acid
TR rats	Mrp2-deficient rats
UDCA	Ursodeoxycholic acid
WT	Wild-type

frontiers | Frontiers in Physiology

REVIEW
published: 20 June 2022
doi: 10.3389/fphys.2022.921597

Smooth Muscle Cell—Macrophage Interactions Leading to Foam Cell Formation in Atherosclerosis: Location, Location, Location

Pinhao Xiang†, *Valentin Blanchard*† *and Gordon A. Francis* *

Department of Medicine, Centre for Heart Lung Innovation, Providence Research, St. Paul's Hospital, University of British Columbia, Vancouver, BC, Canada

Cholesterol-overloaded cells or "foam cells" in the artery wall are the biochemical hallmark of atherosclerosis, and are responsible for much of the growth, inflammation and susceptibility to rupture of atherosclerotic lesions. While it has previously been thought that macrophages are the main contributor to the foam cell population, recent evidence indicates arterial smooth muscle cells (SMCs) are the source of the majority of foam cells in both human and murine atherosclerosis. This review outlines the timeline, site of appearance and proximity of SMCs and macrophages with lipids in human and mouse atherosclerosis, and likely interactions between SMCs and macrophages that promote foam cell formation and removal by both cell types. An understanding of these SMC-macrophage interactions in foam cell formation and regression is expected to provide new therapeutic targets to reduce the burden of atherosclerosis for the prevention of coronary heart disease, stroke and peripheral vascular disease.

Keywords: atherosclerosis, smooth muscle cells, macrophages, foam cells, human, mouse

OPEN ACCESS

Edited by:
Kai Yin,
Guilin Medical University, China

Reviewed by:
Julian Albarran Juarez,
Aarhus University, Denmark
José Ramón López-López,
University of Valladolid, Spain

***Correspondence:**
Gordon A. Francis
gordon.francis@hli.ubc.ca

†*These authors have contributed equally to this work and share first authorship.*

Specialty section:
This article was submitted to Lipid and Fatty Acid Research, a section of the journal Frontiers in Physiology

Received: *16 April 2022*
Accepted: *30 May 2022*
Published: *20 June 2022*

Citation:
Xiang P, Blanchard V and Francis GA (2022) Smooth Muscle Cell—Macrophage Interactions Leading to Foam Cell Formation in Atherosclerosis: Location, Location, Location. Front. Physiol. 13:921597. doi: 10.3389/fphys.2022.921597

INTRODUCTION

Smooth muscle cells (SMCs) and macrophages form the bulk of the cells in all stages of human and mouse atherosclerosis. Studies since the early 1990's have mostly used mice to study atherogenesis, and have suggested that this process is primarily macrophage-driven, is a consequence of the endothelial damage caused by the severe dyslipidemia required to induce atherosclerosis in these animals, and that SMCs play a lesser role (Libby, 2021). In contrast, the initial stages of human atherogenesis occur on a background of pre-atherosclerotic thickening of the arterial intima believed to be caused by migration and proliferation of medial SMCs early in life in atherosclerosis-prone arteries, prior to lipid deposition (Allahverdian et al., 2018). These SMCs promote the retention of lipids by secreting negatively-charged proteoglycans that bind positively-charged apolipoprotein B (apoB) on atherogenic lipoproteins, before the presence of many monocytes/macrophages in the lesion. The interactions between monocytes/macrophages and SMCs are therefore dependent both on the species being examined and the stage of atherosclerosis. In this review we outline what is known regarding the timing of appearance and proximity of SMCs and macrophages to each other in different stages of human and mouse atherosclerosis, and how this allows interactions between these cell types. Secondly, we review current knowledge about lipid uptake mechanisms and cellular factors secreted by both SMCs and macrophages that may be involved in the formation of foam cells of each cell type, as well as cholesterol removal from these cells. An understanding of these interactions is

expected to identify potential new targets to reduce atherosclerosis for the prevention and treatment of ischemic vascular disease.

APPEARANCE AND ROLE OF SMOOTH MUSCLE CELLS AND MACROPHAGES IN EARLY HUMAN AND MOUSE ATHEROSCLEROSIS

Mice are the most widely used animal model for the study of atherosclerosis, due to their short developmental and life cycle, ease of genetic modification, low-cost rearing, small size and high reproductive rate. However, mice and humans exhibit significant genetic and physiologic differences influencing major steps in the process of atherogenesis.

Wild-type (WT) mice do not develop spontaneous atherosclerosis owing in part to their low-fat diet, low plasma cholesterol and overall atheroprotective lipoprotein metabolism (Nakashima et al., 1994). In particular, mice do not express cholesteryl ester transfer protein (CETP), a plasma protein shuttling cholesteryl esters from high-density lipoproteins (HDL) to apoB-containing lipoproteins including very-low- (VLDL), intermediate- (IDL) and especially low-density lipoproteins (LDL). Consequently, while in humans up to 2/3 of total cholesterol is transported in atherogenic apoB-containing lipoproteins, mice carry most of their cholesterol in atheroprotective HDL particles (Gordon et al., 2015). The induction of atherosclerosis in mice thus requires a susceptible mouse strain (C57BL/6) plus extreme pro-inflammatory and hyperlipemic conditions characterized by an exaggerated elevation of plasma cholesterol levels 6–10 times the levels seen in WT mice (Reddick et al., 1994). These inflammatory conditions mean that initiation of atherosclerosis is primarily immune cell/macrophage-driven in mice. Another major difference is the absence in mice of pre-atherosclerotic thickening of the intima by SMCs and their secreted proteoglycans (Diffuse Intimal Thickening, DIT), a critical precursor required for future development of atherosclerosis in human arteries.

These major differences between may lead to inaccurate assumptions of what drives early as well as later stages of atherosclerosis in humans when comparing results with mice. Hereafter, we describe the appearance and pathological mechanisms involving SMCs and macrophages and their interactions from the pre-atherosclerotic stage to the advanced plaque in these two species.

DISTRIBUTION OF SMCS AND MACROPHAGES IN HUMAN ATHEROSCLEROSIS

Atherosclerosis is a disease of medium and large size arteries that progresses from the initial deposition and accumulation of lipids derived from circulating apoB-containing lipoproteins in the already formed DIT layer of SMCs and proteoglycans of atherosclerosis-prone arteries. Nakashima and co-workers described elegantly the chronological stages of pre-atherosclerotic DIT, lipid infiltration and retention, macrophage recruitment, and pathological intimal thickening (PIT) as the last stage before progression to an advanced lesion (Nakashima et al., 2007).

Initial Lipid Deposition in DIT

Certain mammalian species including humans and non-human primates but not mice, rat or rabbits, exhibit DIT in all atherosclerosis-prone arteries of their vascular system (Stout et al., 1983). The critical role of DIT in atherosclerosis is indicated by the observation that atherosclerotic lesions appear only in arteries exhibiting DIT such as the coronary and carotid arteries and aorta (Nakashima et al., 2002), whereas atherosclerosis-resistant vessels such as the internal thoracic artery lack DIT. DIT devoid of lipid deposition begins in utero, is present in all humans by the age of 2 years (Ikari et al., 1999), and is regarded as a physiological adaptation to changes in artery flow and wall tension (Stary et al., 1994). At this pre-atherosclerotic stage, rare resident patrolling macrophages may be observed near the endothelium but not in deeper layers of the intima (Stary et al., 1992).

SMCs particularly in the deeper intima secrete high levels of the negatively charged proteoglycans biglycan and decorin (Nakashima et al., 2007). According to the response-to-retention hypothesis of atherosclerosis proposed by Williams and Tabas, diffusion of circulating positively-charged apoB-containing lipoproteins into the intima, which is based on non LDL-receptor (LDLR)-dependent mechanisms (Jang et al., 2020), and occurs particularly in the presence of elevated circulating LDL cholesterol (LDL-C) such as in familial hypercholesterolemia, over a lifetime results in their infiltration into and retention in the subendothelial space (Williams and Tabas, 1995). This lipid retention occurs primarily in the deep intima based on the charge-charge interaction between apoB and biglycan and decorin secreted in high amounts by SMCs in this region, and prior to any significant monocyte infiltration in human atherosclerosis (Napoli et al., 1997) (Nakashima et al., 2007). These observations suggest human atherosclerosis occurs primarily as a response to retention of lipids, rather than as a response to injury as in mice.

Fatty Streak to Pathological Intimal Thickening

Fatty streaks are visually recognizable by the deformation and thickening of the intima towards the arterial lumen, though, in this early stage of atherosclerosis, most of this lipid is deposited in the deep intima surrounding SMCs, as well as being internalized in SMC foam cells (Katsuda et al., 1992; Nakashima et al., 2007). Whether a particular phenotype of SMCs in the deep intima are primed to take up the retained lipoproteins concentrated in this region, or are converted to foam cells purely on the basis of being surrounded by these lipoproteins, requires further investigation. Rare macrophages may also migrate from the superficial layer to

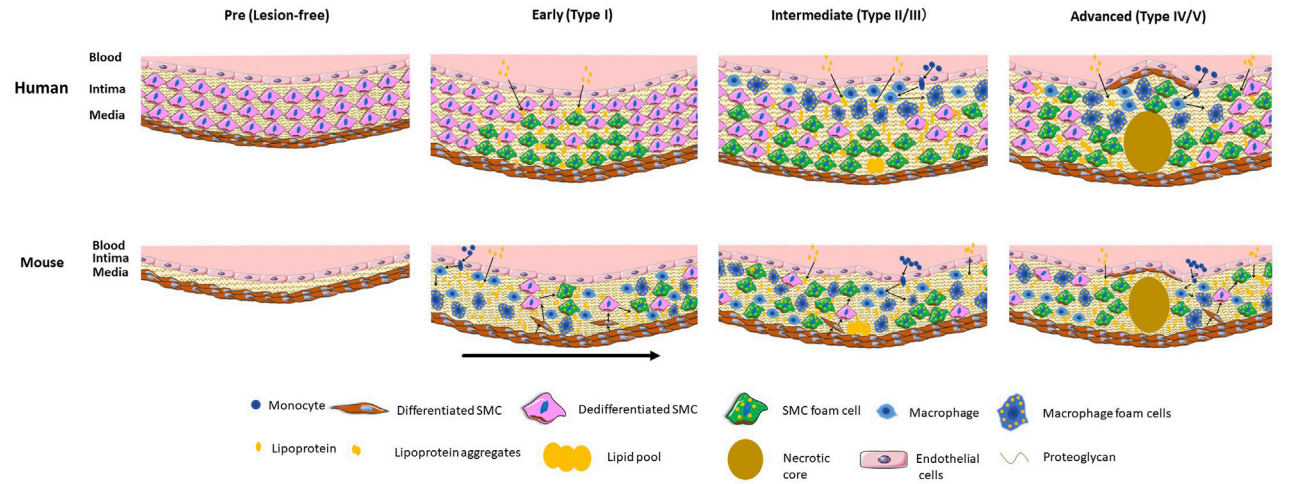

FIGURE 1 | Stages and relative localization and contribution of SMCs and macrophage and their foam cells to human and mouse atherosclerosis. Human atherosclerosis is preceded by the formation of a thick intimal layer composed of SMCs and their secreted proteoglycans, known as diffuse intimal thickening. Atherogenic lipoproteins diffuse into the intima over decades and are deposited primarily in the deep intima, resulting in initial SMC foam cell formation. In intermediate lesions there is expansion of the SMC foam cell pool, and infiltration of circulating monocytes that differentiate to macrophages and take up lipids to become foam cells. In the advanced lesion a large necrotic core forms along with a fibrous cap of SMCs. Direct SMC-macrophage interactions occur primarily in the upper intima where most macrophages are located. Mouse atherosclerosis develops on a background of a healthy artery lacking diffuse intimal thickening. Severe dyslipidemia in mouse models induces endothelial inflammation and influx of lipids and monocytes that differentiate to macrophages and take up lipids to become foam cells. Cytokine-induced SMC migration occurs followed by proliferation and dedifferentiation of SMCs and uptake of lipids to become foam cells. In later early and more advanced mouse lesions SMCs make up the majority of foam cells. Direct as well as indirect macrophage-SMC interactions occur throughout the full thickness of the mouse lesion. The early mouse lesion shows different stages of development with the arrow indicating progression. In both humans and mice macrophage foam cells store cholesteryl ester droplets in the cytoplasm whereas in SMC foam cells the cholesteryl ester droplets appear mainly in lysosomes. Part of the figure was generated using Servier Medical Art, licensed under a Creative Commons Attribution 3.0 unported license.

the middle of the intima at this stage (Guyton and Klemp, 1994) and contribute to the early foam cell formation. Some investigators suggest transmigration of adventitial monocytes at least into the arterial media (Maiellaro and Taylor, 2007). However, these observations have been reported in animal models in the context of restenosis after coronary angioplasty whose intervention completely strips the intima and leads to ruptures in the internal elastic lamina (Shi et al., 1996). To our knowledge, the sole study reporting migration of adventitial cells towards the intima in a context of native atherosclerosis is that of Eriksson, who showed images of migrating cells on the adventitial/intimal border in advanced lesions of apolipoprotein E (apoE) knockout (KO) mice (Eriksson, 2011). In contrast, there is no report of accumulation of adventitial macrophages in the intima of early human lesions.

In pathological intimal thickening (PIT), lipid-laden and non-lipid-laden macrophages may infiltrate more abundantly down to the middle of the intima (Otsuka et al., 2015; Nakagawa and Nakashima, 2018). Interestingly, following the initial population of the human pre-atherosclerotic intima with SMCs early in life, the number of SMCs remains stable from DIT to PIT, and there is no clear evidence of cell death or cell proliferation during this progression (Nakagawa and Nakashima, 2018). This also suggests that the migration rate of SMCs from the media to the intima is very low or non-existent in early lesions including in PIT (Nakagawa and Nakashima, 2018).

Regarding the relative contribution of SMCs and macrophages to the foam cell population, early studies suggested, based on the microscopic appearance of lesions and staining for SMCs and macrophages, that SMCs contribute the majority of these cells in fatty streaks and PIT (Stary, 1985, Stary, 1987; Katsuda et al., 1992). Allahverdian et al. (2014) attempted to quantitate this contribution specifically using immunohistochemistry. They estimated that, conservatively, SMCs are the source of at least 50% of foam cells in intermediate to advanced lesions based on costaining of smooth muscle actin (SMA) and Oil Red O following fixation to identify intracellular lipid localization. The contribution of SMCs to the total human foam cell population is potentially much higher, given that many intimal SMCs express low levels of or no SMA. In general, staining for macrophages including macrophage foam cells indicates the majority of these cells reside primarily in the immediate subendothelial region throughout human atherosclerosis but at later stages can migrate somewhat deeper into the upper-mid intima region where they are in immediate proximity with additional SMCs in the intima. Accurate identification of macrophages requires use of markers that are not known to be expressed by SMCs, such as CD45 (Allahverdian et al., 2014; Wang et al., 2019; Robichaud et al., 2022). Recent studies indicate that markers previously thought to be macrophage-specific, such as CD68, are expressed by a high percentage of intimal SMCs in both human and mouse lesions (Allahverdian et al., 2014; Feil et al., 2014), and should no longer be used to identify macrophages specifically in lesions.

The stages of development and relative contribution of SMCs and macrophages to the foam cell population in humans are indicated in the **Figure 1**.

THE EARLY AND DIRECT INTERACTION BETWEEN SMCS AND MACROPHAGES IN MOUSE LESIONS

The Predominant Role of Macrophages in Early Atherosclerosis in Mice

The genetic manipulation of mice to generate atherosclerosis requires severe dyslipidemia, as achieved in models including apoE- and LDLR-KO mice on a C57BL/6 background who are also fed a high fat and cholesterol diet. The severe circulating dyslipidemia thus created itself represents a highly inflammatory environment for the vascular endothelium, in which immune cells such as monocytes/macrophages are rapidly recruited and have the predominant role in initiating atherogenesis (Swirski et al., 2006, Swirski et al., 2007). The absolute requirement for monocytes/macrophages to stimulate atherosclerosis in mice has been demonstrated by numerous investigators. Smith and co-workers generated apoE KO mice with homozygous or heterozygous mutation in the gene encoding macrophage colony-stimulating factor (MCSF) and fed them an ad libitum chow diet for 16 weeks. Double mutant (MCSF and apoE KO) mice showed an allele-dependent 85% decrease in atherosclerotic lesion areas compared to apoE KO mice expressing MCSF normally, despite a 3-fold increase in total cholesterol level (Smith et al., 1995). Similar findings were obtained on LDLR KO mice homozygous for MCSF mutation and fed an atherogenic diet, with complete absence of atherosclerotic lesions in the aortic arch after 16 weeks (Rajavashisth et al., 1998). Further strong evidence for the role of the immune system in atherogenesis in apoE KO mice comes from an elegant study from the group of Mallat. They combined inhibition of chemokine receptor type 2 (CCR2), C-X3-C motif chemokine receptor 1 (CX3CR1) and C-C motif chemokine receptor 5 (CCR5), three receptors involved in monocytosis of three specific subsets of monocytes, and compared the number of circulating monocytes and the size of lesions with WT mice. They reported a markedly reduced concentration of circulating monocytes accompanied with an almost complete abolition (>90% reduction) of atherosclerosis, despite elevated total cholesterol levels compared to WT mice (Combadière et al., 2008). These studies strongly attest to the predominant and excessive role of immune cells in particular of the myeloid lineage to induce atherosclerosis in mice, and contrast strongly with human atherosclerosis that is mainly induced by the initial SMC-driven retention of lipids in the intima.

Early Macrophage Infiltration and Progressive Medial SMC Influx in Mouse Intima

As indicated above, SMCs, and DIT are not present in the intima of mouse aorta or other arteries, with SMCs only appearing following induction of atherogenesis. Although SMCs are strongly implicated in lipoprotein retention *via* proteoglycan secretion in humans, their absence in mouse intima is not accompanied by the absence of extracellular matrix proteins nor lipid retention. Indeed, in 3 week-old-only apoE KO mice fed a chow diet, Tamminen et al. (1999) reported the presence of individual lipid particles in a reticular network of branching filaments, thought to be proteoglycans, and containing numerous collagen fibrils. Subsequently, the first monocytes were observed in close association with endothelial cells in 5-week-old mice. At 9 weeks of age, the intima contained larger aggregated particles as well as more abundant subendothelial monocytes. This suggests that monocyte recruitment occurs secondarily to lipid retention but prior to SMC migration from the media. In a similar study, sporadic foam cells were observed in the aortic sinus of 11 week-old apoE KO mice fed a chow diet, and multilayered foam cell deposits as well as SMCs were observed in mice of 5–7 months of age (Reddick et al., 1994). Some resident and quiescent macrophages are also present in the lesion-free mouse lesions. However, their limited proliferative capacity and modest contribution in foam cells formation suggest a minor role in atherogenesis (Paulson et al., 2010; Williams et al., 2020; Hernandez et al., 2022). Nakashima also nicely described the development of atherosclerosis in mice with apoE deficiency and fed a Western diet (Nakashima et al., 1994). In their study, monocytes adherent to the endothelial surface and sporadic foam cells in the subendothelial space were observed in 6-week-old mice fed a Western Diet for 1 week. Visible fatty streaks lesions characterized by yellowish-white nodules appeared after 3 and 5 weeks of Western and chow diet, respectively. In mice fed a Western diet for 5–10 weeks, spindle-shaped cells thought to be SMCs were intertwined with foam cells or tended to form a cap around the lesion. By 10 weeks of Western diet (15 weeks of age), some lesions contained fibrous connective tissue with both necrotic cores and foam cells covered by a fibrous cap composed of SMCs.

Our lab has characterized foam cells in the aortic arch of non-lineage tracing and SMC-lineage tracing apoE KO mice using leukocyte-specific markers, neutral lipid staining and flow cytometry. In mice fed a Western diet for just 6 weeks, 70% of total foam cells were SMC- derived (Wang et al., 2019). This was very striking given the absence of SMCs in mouse intima at the onset of atherogenesis. This rapid progression is thought to be due to induction of SMC migration from the mouse arterial medial layer by cytokines secreted by inflamed endothelial cells and macrophages, followed by rapid proliferation and uptake of lipids by SMCs within the intima (Wang et al., 2019). Such a large contribution of SMCs to the foam cell content in mice had not previously been recognized, due to the loss of SMC markers by dedifferentiated SMCs, apparently more so in mice than in humans, and expression of macrophage markers by those same intimal SMCs (Feil et al., 2014; Shankman et al., 2015). Interestingly, in mice fed a lower fat chow diet, SMC-derived foam cells contributed 37% and 75% of the total foam cells at ages 27 and 57 weeks respectively, which emphasizes the gradually increasing role of SMCs in foam cell formation in mice (Wang et al., 2019). This is thought to be due to defects in cholesterol

TABLE 1 | Summary of major lipoprotein uptake mediators driving foam cell formation in macrophages and SMCs.

Cell type	Mediators	Lipoprotein ligands	SR activators
Macrophages	SRA	AcLDL and oxLDL (Kunjathoor et al., 2002b)	MAPK signaling, hyperglycemia (Ben et al., 2009; Zhu et al., 2011)
	CD36	OxLDL (Boullier et al., 2000; Podrez et al., 2002; Nicholson, (2004)	PPARγ, IL-4, Hyperglycemia (Tontonoz et al., 1998; Feng et al., 2000; Nicholson, 2004)
	LOX1	OxLDL (Pirillo et al., 2013)	OxLDL, inflammatory cytokines (Kattoor et al., 2019)
	LRP1	AgLDL (Llorente-Cortés et al., 2007)	SREBP inhibition
	Macropinocytosis/ exophagy	Native or modified LDL (Jones et al., 2000; Kruth et al., 2005)	TLR4 (Kruth et al., 2005; Kruth, 2013)
	Proteoglycan	LDL (Ng et al., 2021)	Inflammatory stimuli or hypoxia stress (Uhlin-Hansen et al., 1993; Asplund et al., 2011)
SMCs	SRA	AcLDL and oxLDL (Mietus-Snyder et al., 2000)	OxLDL, growth factors from macrophages and platelets, IFNγ, MAPK signaling (Gong and Pitas, 1995; Li et al., 1995)
	CD36	OxLDL (Zingg et al., 2002)	PPARγ, VEGF, MAPK signaling, hyperglycemia, oxLDL (Matsumoto et al., 2000; Zingg et al., 2000; Xue et al., 2010; Schlich et al., 2015)
	LOX1	OxLDL (Aoyama et al., 2000)	OxLDL, inflammatory cytokines (Aoyama et al., 2000; Hofnagel et al., 2004)
	LRP1	AgLDL (Llorente-Cortés et al., 2000; Llorente-Cortés et al., 2002; Llorente-Cortés et al., 2006)	P2Y2 receptor (Dissmore et al., 2016)
	Proteoglycan	LDL (Nakashima et al., 2007; Neufeld et al., 2014)	oxLDL, TGFβ, PDGF, SMC dedifferentiation (Camejo et al., 1993; Chang et al., 2000; Doran et al., 2008; Bennett et al., 2016)

efflux from SMC compared to macrophage foam cells, as discussed below. A similar finding of the majority of foam cells being derived from SMCs was recently reported by the Ouimet group in mice injected with an adeno-associated viral (AAV) vector encoding gain-of-function PCSK9 (proprotein convertase subtilisin/kexin type 9) and fed a Western diet to induce hypercholesterolemia. The percentage of non-leukocyte foam cells increased from 60% to 76% between 6 and 25 weeks of Western diet, respectively (Robichaud et al., 2022). In the Wang et al. (2020) study, at 12 weeks of Western diet, both macrophages and SMCs appeared intermingled throughout the whole thickened intima. These studies clearly indicate that macrophage infiltration is followed rapidly by the influx of SMCs from the surrounding media in mice. As macrophages are present in the entire intima following lipid infiltration, migrating SMCs from the media are in direct contact with macrophages as soon as they arrive in the intima. As such, there are marked differences in the localization of SMCs and macrophages in human when compared to mouse lesions, with human lesions maintaining relatively sequestered locations of these two cell types until more advanced lesion stages, whereas in mice macrophages and SMCs are intermingled from very early stages after SMCs soon begin to migrate into the intima.

The stages of development and the relative contribution of macrophages and SMCs to the foam cell population in mice are indicated in the **Figure 1**.

Smooth Muscle Cell—Macrophage Interactions Leading to Foam Cell Formation in Atherosclerosis

While arterial SMCs in humans and mice can express macrophage markers as they dedifferentiate from contractile to synthetic, intimal-type SMCs (Rong et al., 2003; Allahverdian et al., 2014; Feil et al., 2014; Shankman et al., 2015), they never achieve full macrophage function, exhibiting at most 25% of the ability of macrophages to perform phagocytosis and efferocytosis when dedifferentiated (Vengrenyuk et al., 2015). SMCs do, however, like macrophages, express a host of scavenger receptors that can, upon exposure over years to retained lipoproteins in the human intima, or even weeks in the mouse intima, take up these lipoproteins to become foam cells. In the following section, we outline the key mechanisms known to allow macrophages and SMCs to become foam cells, and interactions between these cells that promote foam cell formation by the reciprocal cell type. A Summary of the mediators of lipoprotein uptake promoting foam cell formation by macrophages and SMCs is presented in **Table 1**.

MEDIATORS AND REGULATION OF MACROPHAGE FOAM CELL FORMATION

While circulating levels of LDL-C are tightly associated with atherogenesis and ischemic vascular disease (Yusuf et al., 2004), native LDL is a poor inducer of SMC and macrophage foam cell formation because its main receptor, the LDLR, is downregulated in response to cholesterol loading of cells (Goldstein and Brown, 1977; Goldstein et al., 1977; Brown and Goldstein, 1983). Excess cholesterol derived from LDL inhibits the proteolytic cleavage of sterol regulatory element-binding protein (SREBP) in the endoplasmic reticulum and therefore inhibits migration of the SREBP fragment to the nucleus, which reduces the transcription of the *LDLR* gene (Brown and Goldstein, 1999; Goldstein and Brown, 2009). The key ligands thought to be responsible for foam cell formation *in vivo* are aggregated and oxidized forms of LDL and other apoB-containing lipoproteins (Steinbrecher and Lougheed, 1992). Previous research has indicated the predominant receptors that drive unregulated uptake of these modified apoB-containing lipoproteins are scavenger receptors (SRs) (Brown et al., 1979). SRs are thought to be beneficial in their ability to clear modified lipoprotein accumulation in the artery

wall, but the unregulated uptake of these lipoproteins by SRs leads to overaccumulation of lipoprotein-derived cholesteryl esters, the biochemical hallmark of foam cells. In macrophages, this results in cholesteryl ester droplet accumulation in the cytoplasm with the droplets imparting a "foamy" appearance; excess macrophage foam cells promote inflammation and instability of the plaque. As noted below, SMC foam cells appear to store their excess cholesteryl esters in lysosomes rather than in the cytoplasm, due to relative deficiency of lysosomal acid lipase (LAL) (Dubland et al., 2021) (**Figure 1**).

Scavenger Receptor-Dependent Macrophage Foam Cell Development

There are 12 classes of scavenger receptors identified on membrane surfaces, which are class A-L grouped based on their structural characteristics (PrabhuDas et al., 2017). Among the 12 classes, the class A scavenger receptors A I/II and the class B receptor CD36 are the most studied and believed to be the major receptors taking up modified lipoproteins (Kunjathoor et al., 2002b). Scavenger receptors A I/II (SRA) share a homotrimeric structure composed of a collagen-like domain and a c-type lectin domain. Despite having some structural differences, the two receptors' functions and regulations are similar (Moore and Freeman, 2006). It was reported that in mouse macrophages SRA was responsible for 70% of uptake of the acetylated LDL (acLDL) and 40% of the uptake of oxidized LDL (oxLDL) based on intracellular LDL degradation (Kunjathoor et al., 2002b). A significant reduction (60%–80%) in atherosclerotic lesion area was observed in mouse models with SRA deficiency, confirming this *in vitro* observation (Babaev et al., 2000; Nicholson, 2004). The atherogenic role of SRA was enhanced in hyperglycemic conditions, which upregulates SRA expression (Fukuhara-Takaki et al., 2005). Using mouse RAW264.7 macrophages, it was shown that SRA-mediated endocytosis activated extracellular signal-regulated kinase (ERK) signaling and c-Jun N-terminal kinase (JNK) signaling (Zhu et al., 2011), which are part of the mitogen-activated protein kinase (MAPK) pathway (Ben et al., 2009; Zhu et al., 2011). At the same time, activation of the JNK and ERK signaling pathways cooperatively enhanced SRA transcription factors binding to the promoter, driving a positive feedback loop to enhance SRA receptor gene expression on the cell surface (Moulton et al., 1994). Further studies confirmed that inhibition of protein kinase C (PKC), a kinase in the ERK signaling pathway, and c-Jun, the final transcription factor of JNK signaling, downregulated SRA expression and reduced lipoprotein uptake (Akeson et al., 1991; Moulton et al., 1992).

CD36 belongs to the class B scavenger receptor family, which traverse the plasma membrane twice to form a loop with a heavily glycosylated extracellular portion and an intracellular tail to transmit the signal (Moore and Freeman, 2006). Similar to SRA, CD36 also promotes modified lipoprotein uptake and shows a high affinity to oxidized lipoproteins *in vitro* and in mice (Boullier et al., 2000; Podrez et al., 2002; Nicholson, 2004). CD36 regulation is mediated by peroxisome proliferator-activated receptor (PPARγ), which is upregulated in response to exposure to oxLDL (Tontonoz et al., 1998; Feng et al., 2000; Nicholson, 2004). Similar to SRA, hyperglycemia increases CD36 mRNA abundance and translational efficiency, leading to more scavenger receptors expressed on the membrane (Griffin et al., 2001). Though CD36 and SRA receptors play significant roles in taking up modified lipoproteins, previous research showed macrophages can still become foam cells without CD36 and SRA, indicating there are numerous mediators of foam cell development (Sakr et al., 2001; Kunjathoor et al., 2002b; Manning-Tobin et al., 2009). For example, it was observed that lectin-like oxidized low-density lipoprotein receptor-1 (LOX1) contributed to oxLDL uptake in macrophages, which was upregulated with increased oxidative stress or in the presence of proinflammatory cytokines (Pirillo et al., 2013; Kattoor et al., 2019). Another example is LDLR-related protein-1 (LRP1), knockdown of which reduced cholesteryl ester accumulation from aggregated LDL (agLDL) in macrophages by 95%. Interestingly, the receptor was subjected to negative regulation by sterol regulatory element-binding protein 1 (SREBP1) (Llorente- Cortés et al., 2007). Thus, in hypercholesterolemic conditions, the expression of LRP1 likely remains high as SREBP1 is not delivered to the nucleus, confirming the observation that the receptor can play a significant role in agLDL uptake and foam cell formation. Scavenger receptor B1 (SRB1) usually functions as a SR driving cholesterol efflux (Moore and Freeman, 2006; Hu et al., 2013), but research by Marsche et al. showed that SRBI also mediates the uptake of hypochlorite modified-LDL and HDL, which promoted lipid accumulation while reducing cholesterol efflux, leading to foam cell development (Marsche et al., 2002; Marsche et al., 2003). Other receptors that can take up modified lipoproteins include scavenger receptor expressed by endothelial cells-I (SREC-I) (Shimaoka et al., 2000), C-X-C motif chemokine ligand 16 (CXCL16) (Barlic et al., 2006; Sheikine and Sirsjö, 2008), CD68 (Ramprasad et al., 1996), and CD146 (Luo et al., 2017), which are less well characterized compared to the ones described (Moore and Freeman, 2006; Kzhyshkowska et al., 2012; Checkouri et al., 2021).

Scavenger Receptor-Independent Macrophage Foam Cell Formation

Further research has described mechanisms of macrophage foam cell development independent of lipoprotein receptors. Human-monocyte derived macrophages can take up LDL *via* fluid-phase pinocytosis, which is a receptor-independent uptake mechanism whereby LDL is taken up *via* large vacuoles through micropinocytosis, or *via* small vesicles through micropinocytosis. Though both pathways are equally important in LDL uptake, we have very limited knowledge of the role of micropinocytosis in cholesterol uptake and therefore will focus on macropinocytosis (Kruth, 2013). Macropinocytosis was shown to drive foam cell formation with native LDL or modified LDL (Jones et al., 2000; Kruth et al., 2002, Kruth et al., 2005). It was observed that human monocyte-derived macrophages take up lipoproteins along with fluid in a sealed macropinosome (Kruth et al., 2002, Kruth et al., 2005; Barthwal et al., 2013; Doodnauth et al., 2019). This uptake increased with

increased extracellular lipoprotein concentrations and was subjected to regulation by actin, microtubules, vacuolar-type H + ATPase (V-ATPase), phosphoinositide 3- kinase (PI3K), and spleen tyrosine kinase (SYR) in a toll-like receptor 4 (TLR4) dependent manner (Kruth et al., 2005; Kruth, 2013). Interestingly, a similar mechanism was observed to upregulate exophagy, or extracellular degradation of large elements such as agLDL. Using the mouse macrophages, it was observed that agLDL triggered activation of PI3K and SYR-dependent TLR4 signaling in the macrophage. TLR4 signaling triggered actin polymerization and lysosomal exocytosis to form an acidic lysosomal synapse in the extracellular environment, where lysosomal acid lipase (LAL) degraded the aggregate extracellularly into free cholesterol (Haka et al., 2009; Singh et al., 2016, Singh et al., 2020). Free cholesterol can then be taken up by macrophages to drive foam cell formation. More research is necessary to identify if macropinocytosis is linked to exophagy or if these are two independent pathways subjected to similar regulation.

Proteoglycans are complex macromolecules consisting of the core protein to which linear negatively charged glycosaminoglycan (GAG) molecules are covalently linked (Wight, 2018; Allahverdian et al., 2021). It was observed that the proteoglycan content increases dramatically during early atherosclerosis, which was predominantly composed of versican, biglycan, and decorin in humans (Nakashima et al., 2007, Nakashima et al., 2008; Wight, 2018) and biglycan and perlecan in mice (Kunjathoor et al., 2002a). As noted above, proteoglycans retain apoB- carrying lipoproteins in the subendothelial space through ionic interactions, specifically through the positively charged arginine and lysine residues on apoB and negatively charged sulfates on proteoglycans (Borén et al., 2000; Nakashima et al., 2007; Wight, 2018; Allahverdian et al., 2021). Within the intimal space, retained lipoproteins can undergo enzymatic or chemical modifications, which increases the atherogenicity and subendothelial retention of the lipoproteins (Aviram, 1993; Tabas, 1999). Simultaneously, the presence of proteoglycans can cause irreversible structural disruption of lipoproteins (Camejo et al., 1998). *In vitro* structural analysis and oxidation experiments showed that lipoproteins exposed to chondroitin sulfate had increased exposure of arginine and lysine residues and had greater chance to undergo oxidation, thereby increasing the binding affinity to scavenger receptors on SMCs and macrophages (Hurt-Camejo et al., 1992; Vijayagopal et al., 1993; Ismail et al., 1994; Krettek et al., 1997).

Though SMCs are the major source of proteoglycan secretion in the intima, macrophages can also secrete proteoglycans that contribute to lipoprotein retention (Kolset and Gallagher, 1990; Wight, 2018; Ng et al., 2021). For example, macrophages synthesize chondroitin sulfate proteoglycans, which connect atherogenic LDL and SRA in proximity, promoting more lipoprotein uptake and foam cell development (Christner, 1988; Santiago-García et al., 2003). Analysis of macrophage conditioned medium showed that macrophage colony-stimulating factor (MCSF) could complex with proteoglycans when secreted by macrophages, which promoted monocyte differentiation and lipoprotein retention at the same time, contributing to foam cell development (Chang et al., 1998). Recently, Ng and colleagues also identified that perlecan was the major proteoglycan secreted by human macrophages involved in LDL retention, though perlecan was also suggested to be low in human lesions (Tran et al., 2007; Ng et al., 2021). It was observed that proteoglycan synthesis by macrophages was upregulated when macrophages received inflammatory stimuli or were under hypoxia stress. (Uhlin-Hansen et al., 1993; Asplund et al., 2011).

Influence of Macrophage Polarization on Foam Cell Development

Macrophage phenotype is highly plastic, including levels of SR expression (Yang et al., 2020). For example, interferon-gamma (IFNγ) is a potent cytokine inducing a proinflammatory response in human monocyte-derived macrophages. Proinflammatory macrophages (M1) were shown to have lower CD36 and SRA expression and therefore had reduced uptake of modified lipoproteins (Geng and Hansson, 1992; Zingg et al., 2000; Chu et al., 2013; Murray et al., 2014). In contrast, alternatively activated macrophages (M2), which were polarized by interleukin-4 (IL-4) *in vitro* (Murray et al., 2014), had greater CD36 expression and uptake of modified lipoproteins (Yesner et al., 1996; Chu et al., 2013; Murray et al., 2014). Alternatively activated macrophages also had higher macropinocytosis activity *in vitro*, promoting lipoprotein phagocytosis within the cells (Redka et al., 2018). Different macrophage phenotypes may also secrete different proteoglycans, modulating extracellular lipoprotein retention (Ng et al., 2021). It should be noted that the polarization impact described here focuses on human monocyte-derived macrophages, and the effect may vary depending on the macrophage origin and type (Geng and Hansson, 1992; Fitzgerald et al., 2000).

MEDIATORS AND REGULATION OF SMC FOAM CELL FORMATION

In recent years, since the introduction of mouse models of atherosclerosis, foam cells have been thought to mostly be derived from macrophages, and to have major importance especially in areas where plaques are prone to rupture, such as the fibrous cap or shoulder regions (Ross, 1995; Libby et al., 2011; Bennett et al., 2016; Chistiakov et al., 2017). While macrophage foam cells are undoubtedly important for plaque instability and rupture, recent studies now suggest a major role of SMCs as a source of foam cells in human and mouse atherosclerosis, and as likely predictors of the development and regression of atherosclerotic lesions. Immunostaining of early atherosclerotic lesions showed a large number of SMC foam cells in the deep intima in early atherosclerosis and suggested SMCs are an important source for foam cells (Katsuda et al., 1992; Nakashima et al., 2007). Recent studies using early and advanced coronary artery lesions from mice and humans have indeed confirmed that the majority of foam cells in both early and

advanced lesions are SMC-derived (Allahverdian et al., 2012; Wang et al., 2019).

Scavenger Receptor-Dependent SMC Foam Cell Development

Intima SMCs have higher scavenger receptor activity than medial SMCs, likely due to their innate phenotype and possibly due to exposure to diverse growth factors secreted by macrophages and platelets (Gong and Pitas, 1995). Growth factors can upregulate SRA synergistically up to 7-fold *in vitro* (Gong and Pitas, 1995; Li et al., 1995). Using an *in vitro* SMC model, studies from the Pitas group showed that the presence of oxLDL can activate tyrosine-protein kinase, triggering MAPK signaling cascade and upregulating the c-Jun transcription factor. C-Jun then increased SRA and cyclooxygenase-2 expressions, contributing to acLDL uptake and foam cell formation (Mietus-Snyder et al., 1997, Mietus-Snyder et al., 2000). However, the importance of SRA in SMC foam cells is questionable, as SRA was reported to be dispensable in driving SMC foam cell development (Luechtenborg et al., 2008) and was primarily associated with macrophages in atherosclerotic lesions (Pryma et al., 2019). Interestingly, the regulation of SRA in SMCs appears to be opposite compared to in macrophages. For example, though IFNγ is a negative regulator for macrophage SRA, it can increase SRA mRNA expression and its acLDL degradation activity in cultured SMCs (Li et al., 1995).

CD36 is another scavenger receptor expressed in human SMCs, reported to be responsible for 80% of oxLDL uptake and the uptake of free fatty acids (Zingg et al., 2002; Ma et al., 2011). CD36 is primarily upregulated by its ligand oxLDL, which activates PPARγ to upregulate CD36 transcription (Matsumoto et al., 2000; Zingg et al., 2000). Tyrosine kinase inhibition downregulates CD36 *in vitro* and reduces oxLDL uptake in SMCs (Lin et al., 2015), suggesting that the MAPK signaling pathway is also involved in CD36 positive regulation. Endothelial-1, which is an endogenous factor stimulating SMC proliferation, was shown to reduce CD36 expression in a tyrosine kinase-dependent manner (Kwok et al., 2007). In contrast, the growth factor VEGF that promotes SMC proliferation can increase CD36 expression, suggesting different growth factors might regulate CD36 differently (Schlich et al., 2015). Interestingly, it was observed that CD36 expression on SMCs is upregulated in diabetic patients, triggered by hyperglycemia condition and oxLDL exposure, leading to increased cholesterol influx and SMC foam cell development (Xue et al., 2010; Navas-Madroñal et al., 2020).

Besides the classical SRs, SMCs also express LOX1 and LRP1 when exposed to modified lipoproteins (Pryma et al., 2019; Checkouri et al., 2021). Llorente-Cortés and colleagues showed that LRP1 was responsible for 80% uptake of the agLDL and 65% of versican-modified LDL *in vitro* (Llorente-Cortés et al., 2000; Llorente-Cortés et al., 2002; Llorente-Cortés et al., 2006). Additional research suggested that LRP1 was subjected to P2Y2 receptor regulation in SMCs, a receptor triggering rearrangement of the actin cytoskeleton and cell motility (Dissmore et al., 2016). Similar to macrophages, LOX1 is also present in SMCs and is upregulated in the presence of oxLDL (Aoyama et al., 2000) and inflammatory cytokines (Hofnagel et al., 2004). C-X-C-motif chemokine ligand 16 (CXCL16) (Wågsäter et al., 2004) and receptor for the advanced glycation end products (RAGE) (Bao et al., 2020) were identified to act as scavenger receptors to promote SMC foam cell formation, but further investigation is required to determine the precise role and regulation of the receptors in atherosclerosis. Intriguingly, it was shown *in vitro* that SMCs can ingest lipoproteins modified by trypsin and cholesteryl ester hydrolase *via* calcium-dependent macropinocytosis, but the detailed mechanism and the clinical relevance of macropinocytosis remains to be explored (Chellan et al., 2016).

Scavenger Receptor-Independent SMC Foam Cell Development

As the predominant cell source of proteoglycans in the vascular wall (Wight, 1985; Nigro et al., 2005), SMCs are responsible for the increase in proteoglycan content in early atherosclerosis (Wight, 2018). Among the proteoglycans secreted, biglycan and decorin were shown to have the highest binding affinity towards LDL and were enriched in atherosclerotic lesions in the deep intima, suggesting both proteoglycans were major players in LDL retention in this location (Riessen et al., 1994; O'Brien et al., 1998; Nakashima et al., 2007; Neufeld et al., 2014). Perlecan was shown to be important in mice in promoting lipoprotein retention and increasing vascular permeability but is reduced in human atherosclerotic lesions, likely due to species difference (Tran-Lundmark et al., 2008; Allahverdian et al., 2021). The synthesis of proteoglycans is also governed by lipoproteins that SMCs are exposed to. Using monkey SMCs as an *in vitro* model, oxLDL was shown to induce elongation of glycosaminoglycan chains of biglycan, decorin, and versican, which was not observed with native LDL and could induce 30%–50% more total proteoglycan synthesis compared to native LDL (Camejo et al., 1993; Chang et al., 2000; Doran et al., 2008). In addition, the presence of growth factors that promote SMC proliferation, such as PDGF and TGFβ, promoted the synthesis of versican and biglycan in SMCs in an NF-kb—dependent manner (Schönherr et al., 1993; Chang et al., 2000; Basatemur et al., 2019), contributing to the lipoprotein retention.

Intima SMCs may transit into a synthetic state with a gain of macrophage markers such as CD68 in culture and in atherosclerotic lesions (Bennett et al., 2016; Basatemur et al., 2019). Synthetic SMCs have increased proteoglycan synthesis (Bennett et al., 2016) and phagocytosis activity (Sandison et al., 2016), contributing to excess cholesterol retention and uptake. Interestingly, it was observed that cholesterol uptake (Rong et al., 2003) and proteoglycans in the subendothelial space (Roy et al., 2002; Allahverdian et al., 2021) could be positive feedback regulators that contributed to SMC dedifferentiation *in vitro*, initiating a vicious cycle in driving more lipid uptake in SMCs.

TABLE 2 | Summary of potential SMC-macrophages interactions in foam cell development.

Direct interaction	Macrophage effect on SMCs • Increase SMC phagocytic activity (Vijayagopal and Glancy, 1996) • Delivery of macrophage cholesterol into SMCs (Weinert et al., 2013; He et al., 2020) SMC effect on macrophages • Increase CD36 expression on monocytes
Indirect interaction	Macrophage effect on SMCs • Increase cholesterol uptake and degradation (Aviram, 1989; Nishide et al., 1992; Stein et al., 1994; Mietus-Snyder et al., 2000; Wang et al., 2019) • Transfer cholesterol directly to SMCs (Wolfbauer et al., 1986; He et al., 2018; Hu et al., 2019) • Increase LAL activity (Dubland et al., 2021) SMC effect on macrophages • Increase cholesterol degradation (Aviram, 1989) • Increase CD36 expression on monocytes (Cai et al., 2004)
Limitations	• Limited ability to mimic artery wall milieu (Zuniga et al., 2014; Beck-Joseph and Lehoux, 2021) • Inconsistent SMC and macrophage origins and phenotypes (Murray et al., 2014; Allahverdian et al., 2018)

SMC-MACROPHAGE INTERACTIONS IN FOAM CELL DEVELOPMENT

Immunohistochemistry studies on human and mouse atherosclerotic lesions have indicated macrophages and SMCs are in proximity in early and intermediate stages of atherosclerosis, depending on the species, suggesting that interactions between macrophages and SMCs are important in atherogenesis (Nakashima et al., 2007; Wang et al., 2019). Numerous *in vitro* studies have found that interactions between macrophages and SMCs can promote SMC proliferation (Zhang et al., 1993; Chen et al., 2014), proteoglycan/matrix metalloproteinase synthesis (Edwards et al., 1990; Zhu et al., 2000), migration (Niu et al., 2016), and dedifferentiation into the synthetic state (Beck-Joseph and Lehoux, 2021). In reverse, SMCs can also contribute to monocyte adhesion, recruitment, and survival (Doran et al., 2008; Beck-Joseph and Lehoux, 2021). SMC-macrophage interactions can also heighten inflammation in both cell types and can transform SMCs into a macrophage-like phenotype (Butoi et al., 2014). For this review, we will specifically focus on the interactions between SMCs and macrophages leading to foam cell development in atherosclerosis. A summary of the potential SMC-macrophage interactions in foam cell development is presented in **Table 2**.

Cell-Cell Interactions Between SMCs and Macrophages

In vitro models showed that the direct contact between macrophages and SMCs could promote increased foam cell development in SMCs but the mechanism causing the increase in lipoprotein uptake was not clear.Vijayagopal and Glancy, (1996) reported that the presence of macrophages could increase SMC phagocytic activity and therefore lipoprotein uptake. However, Hu et al. and Weinert et al. (2013) suggested that macrophages can deliver cytosolic and lysosomal cholesterol into SMCs when in close proximity, possibly through cell-cell membrane interactions (He et al., 2020). Though we did not find an *in vitro* study assessing the role of direct cell contact in macrophage foam cell development, it was observed *in vitro* that direct or indirect coculture of human SMCs with monocytes could lead to an increase in CD36 scavenger receptor expression and oxLDL uptake by monocytes. It was shown that monocyte chemoattractant protein-1 (MCP-1) secreted by SMCs was responsible for contact-independent CD36 upregulation in monocytes, while vascular adhesion molecule-1 (VCAM-1) on SMCs was responsible for contact-dependent CD36 upregulation in monocytes (Cai et al., 2004).

Indirect Interactions Between SMCs and Macrophages

Previous studies also assessed the indirect interactions between macrophages and SMCs in foam cell development. By measuring the LDL degradation rate, Aviram's early study showed that conditioned media from macrophages doubled the LDL degradation rate within SMCs while SMC's conditioned media enhanced macrophage LDL degradation by 15%, suggesting that the conditioned media of macrophages and SMCs both promote foam cell development in the other cell type (Aviram, 1989). Similarly, Stein et al. (1994) and Nishide et al. (1992) showed that conditioned media from macrophages triggered a ten-fold increase in cholesterol uptake by SMCs compared to control SMCs. Component analysis by Stein et al. (1994) identified that lipoprotein lipase, apoE, and proteoglycans likely played key roles in lipoprotein adhesion to the SMC surface and therefore in promoting lipoprotein uptake. Using a conditioned media approach, previous research observed that macrophages could release cholesterol-rich particles that can be taken up by SMCs through phagocytosis and promote SMC foam cell formation (Wolfbauer et al., 1986; He et al., 2018; Hu et al., 2019). Similarly, Mietus-Synder et al. (2000) showed that incubation of SMCs with THP-1 macrophage-conditioned media also showed a 25–30-fold increase in the uptake of DiI-labeled acLDL by SMCs, which was not observed if there was no serum or with lipid poor serum in the conditioned media. Using a collagen gel system model, a recent study done by Wang et al. (2019) observed that the presence of mouse macrophage led mouse SMCs to have a 5-fold increase in agLDL uptake without having direct cell-cell contact, confirming the early observations.

In addition, using the conditioned media approach, several articles showed that macrophages might promote cholesterol esterification within SMCs while promoting lipoprotein uptake. Stein et al. showed that after 24 h incubation with macrophage conditioned media, SMCs had a 3-4-fold increase in cholesteryl ester content compared to with SMCs alone, which could be enhanced further by another 3-fold if the conditioned media was from the macrophage foam cells (Stein et al., 1981, Stein et al., 1993, Stein et al., 1994). Recent research by Dubland et al.(2021) also showed that the conditioned media from macrophages could lead to a 2.8-fold increase in SMC LAL activity, indicating the ability of macrophages to influence LAL-dependent cholesterol metabolism in SMCs (discussed further below).

In vitro Models for the Study of SMCs-Macrophages Interactions in Atherosclerosis

Currently, most *in vitro* models utilize direct cell contact models to study direct cell-cell interactions and conditioned media or transwell models to study secreted soluble mediator effects. While the models are relatively simple to set up, they have several limitations. Firstly, most *in vitro* models are 2-dimensional (2D) and therefore cannot capture fully the artery wall structure and dynamics observed *in vivo*, such as blood flow and extracellular matrix (Zuniga et al., 2014; Beck-Joseph and Lehoux, 2021). Previous research attempted to mimic the artery wall using a gel scaffold model, but the composition of the scaffold in healthy and diseased states remains to be determined to ensure the model's physiological relevance (Sukhova et al., 1999; Wight, 2018). Recent engineered tissue designs include microfabricated vessels with biomaterials to mimic the functional blood vessel *in vivo*, but the model remains to be tested to assess its applicability in studying cell-cell interactions and foam cell formation (Moses et al., 2021). Secondly, as different studies utilized cells from different origins, species differences may contribute to the discrepancies observed among studies. The plasticities of both cell types can add a layer of complexity when comparing different co-culture studies (Murray et al., 2014; Allahverdian et al., 2018). Therefore, future studies should characterize the cell phenotypes before performing interaction studies to ensure the reproducibility of the results.

POTENTIAL ROLE OF MACROPHAGE-SMC INTERACTIONS IN PROMOTING CHOLESTEROL EFFLUX FROM FOAM CELLS, AND POTENTIAL THERAPEUTIC INTERVENTIONS

Cholesterol removal from foam cells is dependent on external factors such as reducing the further influx of atherogenic lipoproteins into the artery wall through the use of LDL-lowering medications, and promoting intracellular cholesterol efflux pathways. The latter include secretion of cellular cholesterol to form HDL particles by upregulation of the cholesterol exporter protein ATP-binding cassette transporter A1 (ABCA1), achieved through the action of intracellular oxysterols binding to liver X receptor (LXR) nuclear receptors on the promoter region of the *ABCA1* gene in the nucleus (Oram and Heinecke, 2005). Additional cholesterol efflux pathways include ABCG1, also upregulated by intracellular oxysterols, SR-BI, and passive diffusion of cholesterol from the plasma membrane to preformed HDL particles in the extracellular space (Phillips, 2014). We previously determined that ABCA1 expression is low in arterial SMCs when compared to macrophages in both humans and mice (Allahverdian et al., 2014; Wang et al., 2019); in human SMCs we have also determined their expression of sterol-27-hydroxylase, responsible for production of 27-hydroxycholesterol, the key oxysterol required for upregulation of ABCA1 in the artery wall via LXRα (Björkhem et al., 1994), as well as LXRα itself, are also low when compared to macrophages (Dubland et al., 2021). As such, arterial SMCs have a number of potential reasons for impaired upregulation of ABCA1.

Perhaps most remarkably, arterial SMCs of both humans and mice exhibit inherently low expression of *Lipa*, responsible for LAL expression, when compared to macrophages in both species (Dubland et al., 2021). This results in sequestration of lipoprotein-derived cholesteryl esters within the lysosomes of SMCs, rather than in the cytoplasm as in macrophage foam cells (**Figure 1**). Addition of conditioned medium from macrophages, which contains secreted LAL, or exogenous LAL, is, however, able to correct cholesterol efflux in SMC foam cells, despite lack of a further increase in ABCA1 expression in these cells (Dubland et al., 2021). As such, *in vivo*, it is possible that macrophage-secreted LAL may be taken up and be able to promote cholesterol efflux from nearby SMC foam cells, depending on the proximity of the surrounding macrophages and the ability of secreted LAL to diffuse within the plaque interstitial fluid.

Other potential therapeutics aimed specifically at influencing SMC-macrophage interactions could play an important role in reducing atherosclerosis or inducing its regression. An example is compound NBI-74330, an antagonist for C-X-C motif chemokine receptor 3 (CXCR3) on the surface of macrophages, which blocks SMC-secreted ligand C-X-C motif chemokine ligand 10 (CXCL10) from activating CXCR3 to drive monocyte retention and inflammation (van Wanrooij et al., 2008; van den Borne et al., 2014). *In vivo,* NBI-74330 treatment led to a significant reduction in mouse lesion area (van Wanrooij et al., 2008). An additional target influencing both SMC and macrophage foam cell formation is the lipoprotein-proteoglycan interaction responsible for arterial lipoprotein retention. Antibody chp3R99 has been developed to recognize sulfated glycosaminoglycans, blockage of which inhibits lipoprotein binding and reduces atherosclerotic lesion formation in the rabbit (Soto et al., 2012). Similarly, removing chondroitin sulfate from versican was also shown to reduce lipid retention and monocyte recruitment in a rabbit model (Merrilees et al., 2011). Further investigations are required to determine whether targeting interactions between SMCs and macrophages, as well as recruitment of each cell type to and retention of lipoproteins in the intima, will come to fruition as novel

treatments to prevent residual risk from atherosclerosis not addressed by currently available medications.

CONCLUSION

In both humans and mice, the relative contribution of SMCs and macrophages, the timing of their appearance, and their relative proximity to each other and deposited lipids in the artery wall are all key determinants of the initiation and progression of atherosclerosis. A clearer understanding of these steps and the interactions between SMCs and macrophages that influence foam cell development and regression are likely to provide fertile ground in the years ahead for development of novel treatments that will reduce ischemic vascular disease beyond what is possible with currently available treatments.

AUTHOR CONTRIBUTIONS

All authors contributed to the design, writing and review of the manuscript.

FUNDING

PX is supported by a Frederick Banting and Charles Best Canada Graduate Scholarship- Master's Award. VB is supported by a Canadian Institutes of Health Research Fellowship Award. GF is supported by Canadian Institutes of Health Research Project Grant PJT-180508 and a Michael Smith Health Research BC/ Providence Research Health Professional Investigator Award. Funders had no role in the design, writing or review of the report.

REFERENCES

Akeson, A., Schroeder, K., Woods, C., Schmidt, C., and Jones, W. D. (1991). Suppression of Interleukin-1 Beta and LDL Scavenger Receptor Expression in Macrophages by a Selective Protein Kinase C Inhibitor. *J. Lipid Res.* 32, 1699–1707. doi:10.1016/S0022-2275(20)41655-4

Allahverdian, S., Chaabane, C., Boukais, K., Francis, G. A., and Bochaton-Piallat, M.-L. (2018). Smooth Muscle Cell Fate and Plasticity in Atherosclerosis. *Cardiovasc. Res.* 114, 540–550. doi:10.1093/cvr/cvy022

Allahverdian, S., Chehroudi, A. C., McManus, B. M., Abraham, T., and Francis, G. A. (2014). Contribution of Intimal Smooth Muscle Cells to Cholesterol Accumulation and Macrophage-like Cells in Human Atherosclerosis. *Circulation* 129, 1551–1559. doi:10.1161/CIRCULATIONAHA.113.005015

Allahverdian, S., Ortega, C., and Francis, G. A. (2020). "Smooth Muscle Cell-Proteoglycan-Lipoprotein Interactions as Drivers of Atherosclerosis," in *Handbook of Experimental Pharmacology* (Berlin, Heidelberg: Springer), 1–24. doi:10.1007/164_2020_364

Allahverdian, S., Pannu, P. S., and Francis, G. A. (2012). Contribution of Monocyte-Derived Macrophages and Smooth Muscle Cells to Arterial Foam Cell Formation. *Cardiovasc. Res.* 95, 165–172. doi:10.1093/CVR/CVS094

Aoyama, T., Chen, M., Fujiwara, H., Masaki, T., and Sawamura, T. (2000). LOX-1 Mediates Lysophosphatidylcholine-Induced Oxidized LDL Uptake in Smooth Muscle Cells. *FEBS Lett.* 467, 217–220. doi:10.1016/S0014-5793(00)01154-6

Asplund, A., Fridén, V., Stillemark-Billton, P., Camejo, G., and Bondjers, G. (2011). Macrophages Exposed to Hypoxia Secrete Proteoglycans for Which LDL Has Higher Affinity. *Atherosclerosis* 215, 77–81. doi:10.1016/j.atherosclerosis.2010.12.017

Aviram, M. (1989). Low-density Lipoprotein and Scavenger Receptor Activities Are Modulated by Secretory Products Derived from Cells of the Arterial Wall. *Metabolism* 38, 445–449. doi:10.1016/0026-0495(89)90196-0

Aviram, M. (1993). Modified Forms of Low Density Lipoprotein and Atherosclerosis. *Atherosclerosis* 98, 1–9. doi:10.1016/0021-9150(93)90217-i

Babaev, V. R., Gleaves, L. A., Carter, K. J., Suzuki, H., Kodama, T., Fazio, S., et al. (2000). Reduced Atherosclerotic Lesions in Mice Deficient for Total or Macrophage-specific Expression of Scavenger Receptor-A. *Atvb* 20, 2593–2599. doi:10.1161/01.ATV.20.12.2593

Bao, Z., Li, L., Geng, Y., Yan, J., Dai, Z., Shao, C., et al. (2020). Advanced Glycation End Products Induce Vascular Smooth Muscle Cell-Derived Foam Cell Formation and Transdifferentiate to a Macrophage-like State. *Mediat. Inflamm.* 2020, 1–12. doi:10.1155/2020/6850187

Barlic, J., Zhang, Y., Foley, J. F., and Murphy, P. M. (2006). Oxidized Lipid-Driven Chemokine Receptor Switch, CCR2 to CX3CR1, Mediates Adhesion of Human Macrophages to Coronary Artery Smooth Muscle Cells through a Peroxisome Proliferator-Activated Receptor γ-Dependent Pathway. *Circulation* 114, 807–819. doi:10.1161/CIRCULATIONAHA.105.602359

Barthwal, M. K., Anzinger, J. J., Xu, Q., Bohnacker, T., Wymann, M. P., and Kruth, H. S. (2013). Fluid-Phase Pinocytosis of Native Low Density Lipoprotein Promotes Murine M-CSF Differentiated Macrophage Foam Cell Formation. *PLoS One* 8, e58054. doi:10.1371/journal.pone.0058054

Basatemur, G. L., Jørgensen, H. F., Clarke, M. C. H., Bennett, M. R., and Mallat, Z. (2019). Vascular Smooth Muscle Cells in Atherosclerosis. *Nat. Rev. Cardiol.* 16, 727–744. doi:10.1038/s41569-019-0227-9

Beck-Joseph, J., and Lehoux, S. (2021). Molecular Interactions between Vascular Smooth Muscle Cells and Macrophages in Atherosclerosis. *Front. Cardiovasc. Med.* 8, 1328. doi:10.3389/FCVM.2021.737934

Ben, J., Gao, S., Zhu, X., Zheng, Y., Zhuang, Y., Bai, H., et al. (2009). Glucose-regulated Protein 78 Inhibits Scavenger Receptor A-Mediated Internalization of Acetylated Low Density Lipoprotein. *J. Mol. Cell. Cardiol.* 47, 646–655. doi:10.1016/j.yjmcc.2009.08.011

Bennett, M. R., Sinha, S., and Owens, G. K. (2016). Vascular Smooth Muscle Cells in Atherosclerosis. *Circ. Res.* 118, 692–702. doi:10.1161/CIRCRESAHA.115.306361

Borén, J., Gustafsson, M., Skålén, K., Flood, C., and Innerarity, T. L. (2000). Role of Extracellular Retention of Low Density Lipoproteins in Atherosclerosis. *Curr. Opin. Lipidol.* 11, 451–456.

Boullier, A., Gillotte, K. L., Hörkkö, S., Green, S. R., Friedman, P., Dennis, E. A., et al. (2000). The Binding of Oxidized Low Density Lipoprotein to Mouse CD36 Is Mediated in Part by Oxidized Phospholipids that Are Associated with Both the Lipid and Protein Moieties of the Lipoprotein. *J. Biol. Chem.* 275, 9163–9169. doi:10.1074/jbc.275.13.9163

Brown, M. S., and Goldstein, J. L. (1999). A Proteolytic Pathway that Controls the Cholesterol Content of Membranes, Cells, and Blood. *Proc. Natl. Acad. Sci. U.S.A.* 96, 11041–11048. doi:10.1073/pnas.96.20.11041

Brown, M. S., Goldstein, J. L., Krieger, M., Ho, Y. K., and Anderson, R. G. (1979). Reversible Accumulation of Cholesteryl Esters in Macrophages Incubated with Acetylated Lipoproteins. *J. Cell Biol.* 82, 597–613. doi:10.1083/jcb.82.3.597

Brown, M. S., and Goldstein, J. L. (1983). LIPOPROTEIN METABOLISM IN the MACROPHAGE: Implications for Cholesterol Deposition in Atherosclerosis. *Annu. Rev. Biochem.* 52, 223–261. doi:10.1146/annurev.bi.52.070183.001255

Butoi, E., Gan, A. M., and Manduteanu, I. (2014). Molecular and Functional Interactions Among Monocytes/Macrophages and Smooth Muscle Cells and Their Relevance for Atherosclerosis. *Crit. Rev. Eukaryot. Gene Expr.* 24, 341–355. doi:10.1615/CritRevEukaryotGeneExpr.2014012157

Cai, Q., Lanting, L., and Natarajan, R. (2004). Interaction of Monocytes with Vascular Smooth Muscle Cells Regulates Monocyte Survival and Differentiation through Distinct Pathways. *Atvb* 24, 2263–2270. doi:10.1161/01.ATV.0000146552.16943.5e

Camejo, G., Fager, G., Rosengren, B., Hurt-Camejo, E., and Bondjers, G. (1993). Binding of Low Density Lipoproteins by Proteoglycans Synthesized by Proliferating and Quiescent Human Arterial Smooth Muscle Cells. *J. Biol. Chem.* 268, 14131–14137. doi:10.1016/S0021-9258(19)85218-3

Camejo, G., Hurt-Camejo, E., Wiklund, O., and Bondjers, G. (1998). Association of Apo B Lipoproteins with Arterial Proteoglycans: Pathological Significance and Molecular Basis. *Atherosclerosis* 139, 205–222. doi:10.1016/s0021-9150(98)00107-5

Chang, M. Y., Olin, K. L., Tsoi, C., Wight, T. N., and Chait, A. (1998). Human Monocyte-Derived Macrophages Secrete Two Forms of Proteoglycan-Macrophage Colony-stimulating Factor that Differ in Their Ability to Bind Low Density Lipoproteins. *J. Biol. Chem.* 273, 15985–15992. doi:10.1074/jbc.273.26.15985

Chang, M. Y., Potter-Perigo, S., Tsoi, C., Chait, A., and Wight, T. N. (2000). Oxidized Low Density Lipoproteins Regulate Synthesis of Monkey Aortic Smooth Muscle Cell Proteoglycans that Have Enhanced Native Low Density Lipoprotein Binding Properties. *J. Biol. Chem.* 275, 4766–4773. doi:10.1074/jbc.275.7.4766

Checkouri, E., Blanchard, V., and Meilhac, O. (2021). Macrophages in Atherosclerosis, First or Second Row Players? *Biomedicines* 9, 1214. doi:10.3390/biomedicines9091214

Chellan, B., Reardon, C. A., Getz, G. S., and Hofmann Bowman, M. A. (2016). Enzymatically Modified Low-Density Lipoprotein Promotes Foam Cell Formation in Smooth Muscle Cells via Macropinocytosis and Enhances Receptor-Mediated Uptake of Oxidized Low-Density Lipoprotein. *ATVB* 36, 1101–1113. doi:10.1161/ATVBAHA.116.307306

Chen, T.-C., Sung, M.-L., Kuo, H.-C., Chien, S.-J., Yen, C.-K., and Chen, C.-N. (2014). Differential Regulation of Human Aortic Smooth Muscle Cell Proliferation by Monocyte-Derived Macrophages from Diabetic Patients. *PLOS ONE* 9, e113752. doi:10.1371/journal.pone.0113752

Chistiakov, D. A., Melnichenko, A. A., Myasoedova, V. A., Grechko, A. V., and Orekhov, A. N. (2017). Mechanisms of Foam Cell Formation in Atherosclerosis. *J. Mol. Med.* 95, 1153–1165. doi:10.1007/S00109-017-1575-8

Christner, J. E. (1988). Biosynthesis of Chondroitin Sulfate Proteoglycan by P388D1 Macrophage-like Cell Line. *Arteriosclerosis* 8, 535–543. doi:10.1161/01.atv.8.5.535

Chu, E. M., Tai, D. C., Beer, J. L., and Hill, J. S. (2013). Macrophage Heterogeneity and Cholesterol Homeostasis: Classically-Activated Macrophages Are Associated with Reduced Cholesterol Accumulation Following Treatment with Oxidized LDL. *Biochimica Biophysica Acta (BBA) - Mol. Cell Biol. Lipids* 1831, 378–386. doi:10.1016/j.bbalip.2012.10.009

Combadière, C., Potteaux, S., Rodero, M., Simon, T., Pezard, A., Esposito, B., et al. (2008). Combined Inhibition of CCL2, CX3CR1, and CCR5 Abrogates Ly6C Hi and Ly6C Lo Monocytosis and Almost Abolishes Atherosclerosis in Hypercholesterolemic Mice. *Circulation* 117, 1649–1657. doi:10.1161/CIRCULATIONAHA.107.745091

Dissmore, T., Seye, C. I., Medeiros, D. M., Weisman, G. A., Bradford, B., and Mamedova, L. (2016). The P2Y 2 Receptor Mediates Uptake of Matrix-Retained and Aggregated Low Density Lipoprotein in Primary Vascular Smooth Muscle Cells. *Atherosclerosis* 252, 128–135. doi:10.1016/j.atherosclerosis.2016.07.927

Doodnauth, S. A., Grinstein, S., and Maxson, M. E. (2019). Constitutive and Stimulated Macropinocytosis in Macrophages: Roles in Immunity and in the Pathogenesis of Atherosclerosis. *Phil. Trans. R. Soc. B* 374, 20180147. doi:10.1098/rstb.2018.0147

Doran, A. C., Meller, N., and McNamara, C. A. (2008). Role of Smooth Muscle Cells in the Initiation and Early Progression of Atherosclerosis. *Atvb* 28, 812–819. doi:10.1161/ATVBAHA.107.159327

Dubland, J. A., Allahverdian, S., Besler, K. J., Ortega, C., Wang, Y., Pryma, C. S., et al. (2021). Low LAL (Lysosomal Acid Lipase) Expression by Smooth Muscle Cells Relative to Macrophages as a Mechanism for Arterial Foam Cell Formation. *Atvb* 41, e354–e368. doi:10.1161/ATVBAHA.120.316063

Edwards, I. J., Wagner, W. D., and Owens, R. T. (1990). Macrophage Secretory Products Selectively Stimulate Dermatan Sulfate Proteoglycan Production in Cultured Arterial Smooth Muscle Cells. *Am. J. Pathol.* 136, 609–621.

Ehsan Ismail, N. A., Alavi, M. Z., and Moore, S. (1994). Lipoprotein-proteoglycan Complexes from Injured Rabbit Aortas Accelerate Lipoprotein Uptake by Arterial Smooth Muscle Cells. *Atherosclerosis* 105, 79–87. doi:10.1016/0021-9150(94)90010-8

Eriksson, E. E. (2011). Intravital Microscopy on Atherosclerosis in Apolipoprotein E-Deficient Mice Establishes Microvessels as Major Entry Pathways for Leukocytes to Advanced Lesions. *Circulation* 124, 2129–2138. doi:10.1161/CIRCULATIONAHA.111.030627

Feil, S., Fehrenbacher, B., Lukowski, R., Essmann, F., Schulze-Osthoff, K., Schaller, M., et al. (2014). Transdifferentiation of Vascular Smooth Muscle Cells to Macrophage-like Cells during Atherogenesis. *Circ. Res.* 115, 662–667. doi:10.1161/CIRCRESAHA.115.304634

Feng, J., Han, J., Pearce, S. F. A., Silverstein, R. L., Gotto, A. M., Hajjar, D. P., et al. (2000). Induction of CD36 Expression by Oxidized LDL and IL-4 by a Common Signaling Pathway Dependent on Protein Kinase C and PPAR-γ. *J. Lipid Res.* 41, 688–696. doi:10.1016/S0022-2275(20)32377-4

Fitzgerald, M. L., Moore, K. J., Freeman, M. W., and Reed, G. L. (2000). Lipopolysaccharide Induces Scavenger Receptor A Expression in Mouse Macrophages: a Divergent Response Relative to Human THP-1 Monocyte/macrophages. *J. Immunol.* 164, 2692–2700. doi:10.4049/jimmunol.164.5.2692

Fukuhara-Takaki, K., Sakai, M., Sakamoto, Y.-i., Takeya, M., and Horiuchi, S. (2005). Expression of Class A Scavenger Receptor Is Enhanced by High Glucose *In Vitro* and under Diabetic Conditions *In Vivo*. *J. Biol. Chem.* 280, 3355–3364. doi:10.1074/jbc.M408715200

Geng, Y. J., and Hansson, G. K. (1992). Interferon-gamma Inhibits Scavenger Receptor Expression and Foam Cell Formation in Human Monocyte-Derived Macrophages. *J. Clin. Invest.* 89, 1322–1330. doi:10.1172/jci115718

Goldstein, J. L., Anderson, R. G., Buja, L. M., Basu, S. K., and Brown, M. S. (1977). Overloading Human Aortic Smooth Muscle Cells with Low Density Lipoprotein-Cholesteryl Esters Reproduces Features of Atherosclerosis *In Vitro*. *J. Clin. Invest.* 59, 1196–1202. doi:10.1172/JCI108744

Goldstein, J. L., and Brown, M. S. (2009). The LDL Receptor. *Atvb* 29, 431–438. doi:10.1161/ATVBAHA.108.179564

Goldstein, L. J., and Brown, S. M. (1977). The Low-Density Lipoprotein Pathway and its Relation to Atherosclerosis. *Annu. Rev. Biochem.* 46, 897–930. doi:10.1146/annurev.bi.46.070177.004341

Gong, Q., and Pitas, R. E. (1995). Synergistic Effects of Growth Factors on the Regulation of Smooth Muscle Cell Scavenger Receptor Activity. *J. Biol. Chem.* 270, 21672–21678. doi:10.1074/jbc.270.37.21672

Gordon, S. M., Li, H., Zhu, X., Shah, A. S., Lu, L. J., and Davidson, W. S. (2015). A Comparison of the Mouse and Human Lipoproteome: Suitability of the Mouse Model for Studies of Human Lipoproteins. *J. Proteome Res.* 14, 2686–2695. doi:10.1021/acs.jproteome.5b00213

Griffin, E., Re, A., Hamel, N., Fu, C., Bush, H., McCaffrey, T., et al. (2001). A Link between Diabetes and Atherosclerosis: Glucose Regulates Expression of CD36 at the Level of Translation. *Nat. Med.* 7, 840–846. doi:10.1038/89969

Guyton, J. R., and Klemp, K. F. (1994). Development of the Atherosclerotic Core Region. Chemical and Ultrastructural Analysis of Microdissected Atherosclerotic Lesions from Human Aorta. *Arterioscler. Thromb.* 14, 1305–1314. doi:10.1161/01.atv.14.8.1305

Haka, A. S., Grosheva, I., Chiang, E., Buxbaum, A. R., Baird, B. A., Pierini, L. M., et al. (2009). Macrophages Create an Acidic Extracellular Hydrolytic Compartment to Digest Aggregated Lipoproteins. *MBoC* 20, 4932–4940. doi:10.1091/mbc.e09-07-0559

He, C., Hu, X., Weston, T. A., Jung, R. S., Sandhu, J., Huang, S., et al. (2018). Macrophages Release Plasma Membrane-Derived Particles Rich in Accessible Cholesterol. *Proc. Natl. Acad. Sci. U.S.A.* 115, E8499–E8508. doi:10.1073/pnas.1810724115

He, C., Jiang, H., Song, W., Riezman, H., Tontonoz, P., Weston, T. A., et al. (2020). Cultured Macrophages Transfer Surplus Cholesterol into Adjacent Cells in the Absence of Serum or High-Density Lipoproteins. *Proc. Natl. Acad. Sci. U.S.A.* 117, 10476–10483. doi:10.1073/pnas.1922879117

Hernandez, G. E., Ma, F., Martinez, G., Firozabadi, N. B., Salvador, J., Juang, L. J., et al. (2022). Aortic Intimal Resident Macrophages Are Essential for Maintenance of the Non-thrombogenic Intravascular State. *Nat. Cardiovasc Res.* 1, 67–84. doi:10.1038/s44161-021-00006-4

Hofnagel, O., Luechtenborg, B., Stolle, K., Lorkowski, S., Eschert, H., Plenz, G., et al. (2004). Proinflammatory Cytokines Regulate LOX-1 Expression in Vascular Smooth Muscle Cells. *Atvb* 24, 1789–1795. doi:10.1161/01.ATV.0000140061.89096.2b

Hu, Z., Zhang, Z., Shen, W. J., Yun, C. C., Berlot, C. H., Kraemer, F. B., et al. (2013). Regulation of Expression and Function of Scavenger Receptor ClassB, Type I (SR-BI) by Na+/H+ Exchanger Regulatory Factors (NHERFs). *J. Biol. Chem.* 288, 11416–11435. doi:10.1074/jbc.M112.437368

Hu, X., Weston, T. A., He, C., Jung, R. S., Heizer, P. J., Young, B. D., et al. (2019). Release of Cholesterol-Rich Particles from the Macrophage Plasma Membrane

during Movement of Filopodia and Lamellipodia. *eLife* 8, e50231. doi:10.7554/eLife.50231

Hurt-Camejo, E., Camejo, G., Rosengren, B., López, F., Ahlström, C., Fager, G., et al. (1992). Effect of Arterial Proteoglycans and Glycosaminoglycans on Low Density Lipoprotein Oxidation and its Uptake by Human Macrophages and Arterial Smooth Muscle Cells. *Arterioscler. Thromb.* 12, 569–583. doi:10.1161/01.atv.12.5.569

Ikari, Y., McManus, B. M., Kenyon, J., and Schwartz, S. M. (1999). Neonatal Intima Formation in the Human Coronary Artery. *Atvb* 19, 2036–2040. doi:10.1161/01.atv.19.9.2036

Jang, E., Robert, J., Rohrer, L., von Eckardstein, A., and Lee, W. L. (2020). Transendothelial Transport of Lipoproteins. *Atherosclerosis* 315, 111–125. doi:10.1016/j.atherosclerosis.2020.09.020

Jones, N. L., Reagan, J. W., and Willingham, M. C. (2000). The Pathogenesis of Foam Cell Formation. *Atvb* 20, 773–781. doi:10.1161/01.ATV.20.3.773

Katsuda, S., Boyd, H. C., Fligner, C., Ross, R., and Gown, A. M. (1992). Human Atherosclerosis. III. Immunocytochemical Analysis of the Cell Composition of Lesions of Young Adults. *Am. J. Pathol.* 140, 907–914.

Kattoor, A. J., Goel, A., and Mehta, J. L. (2019). LOX-1: Regulation, Signaling and its Role in Atherosclerosis. *Antioxidants* 8, 218. doi:10.3390/antiox8070218

Kolset, S. O., and Gallagher, J. T. (1990). Proteoglycans in Haemopoietic Cells. *Biochimica Biophysica Acta (BBA) - Rev. Cancer* 1032, 191–211. doi:10.1016/0304-419x(90)90004-k

Krettek, A., Fager, G., Lindmark, H., Simonson, C., and Lustig, F. (1997). Effect of Phenotype on the Transcription of the Genes for Platelet-Derived Growth Factor (PDGF) Isoforms in Human Smooth Muscle Cells, Monocyte-Derived Macrophages, and Endothelial Cells *In Vitro*. *Atvb* 17, 2897–2903. doi:10.1161/01.atv.17.11.2897

Kruth, H. (2013). Fluid-Phase Pinocytosis of LDL by Macrophages: A Novel Target to Reduce Macrophage Cholesterol Accumulation in Atherosclerotic Lesions. *Cpd* 19, 5865–5872. doi:10.2174/1381612811319330005

Kruth, H. S., Huang, W., Ishii, I., and Zhang, W.-Y. (2002). Macrophage Foam Cell Formation with Native Low Density Lipoprotein. *J. Biol. Chem.* 277, 34573–34580. doi:10.1074/jbc.M205059200

Kruth, H. S., Jones, N. L., Huang, W., Zhao, B., Ishii, I., Chang, J., et al. (2005). Macropinocytosis Is the Endocytic Pathway that Mediates Macrophage Foam Cell Formation with Native Low Density Lipoprotein. *J. Biol. Chem.* 280, 2352–2360. doi:10.1074/jbc.M407167200

Kunjathoor, V. V., Chiu, D. S., O'Brien, K. D., and LeBoeuf, R. C. (2002a). Accumulation of Biglycan and Perlecan, but Not Versican, in Lesions of Murine Models of Atherosclerosis. *Atvb* 22, 462–468. doi:10.1161/hq0302.105378

Kunjathoor, V. V., Febbraio, M., Podrez, E. A., Moore, K. J., Andersson, L., Koehn, S., et al. (2002b). Scavenger Receptors Class A-I/II and CD36 Are the Principal Receptors Responsible for the Uptake of Modified Low Density Lipoprotein Leading to Lipid Loading in Macrophages. *J. Biol. Chem.* 277, 49982–49988. doi:10.1074/jbc.M209649200

Kwok, C. F., Juan, C.-C., and Ho, L.-T. (2007). Endothelin-1 Decreases CD36 Protein Expression in Vascular Smooth Muscle Cells. *Am. J. Physiology-Endocrinology Metabolism* 292, E648–E652. doi:10.1152/ajpendo.00084.2006

Kzhyshkowska, J., Neyen, C., and Gordon, S. (2012). Role of Macrophage Scavenger Receptors in Atherosclerosis. *Immunobiology* 217, 492–502. doi:10.1016/j.imbio.2012.02.015

Li, H., Freeman, M. W., and Libby, P. (1995). Regulation of Smooth Muscle Cell Scavenger Receptor Expression *In Vivo* by Atherogenic Diets and *In Vitro* by Cytokines. *J. Clin. Invest.* 95, 122–133. doi:10.1172/JCI117628

Libby, P., Ridker, P. M., and Hansson, G. K. (2011). Progress and Challenges in Translating the Biology of Atherosclerosis. *Nature* 473, 317–325. doi:10.1038/nature10146S

Libby, P. (2021). The Changing Landscape of Atherosclerosis. *Nature* 592, 524–533. doi:10.1038/s41586-021-03392-8

Lin, J., Xu, Y., Zhao, T., Sun, L., Yang, M., Liu, T., et al. (2015). Genistein Suppresses Smooth Muscle Cell-Derived Foam Cell Formation through Tyrosine Kinase Pathway. *Biochem. Biophysical Res. Commun.* 463, 1297–1304. doi:10.1016/j.bbrc.2015.04.155

Llorente-Corte´s, V., Marti´nez-Gonza´lez, J., and Badimon, L. (2000). LDL Receptor-Related Protein Mediates Uptake of Aggregated LDL in Human Vascular Smooth Muscle Cells. *Atvb* 20, 1572–1579. doi:10.1161/01.ATV.20.6.1572

Llorente-Corte´s, V., Otero-Viñas, M., Camino-Lo´pez, S., Costales, P., and Badimon, L. (2006). Cholesteryl Esters of Aggregated LDL Are Internalized by Selective Uptake in Human Vascular Smooth Muscle Cells. *Atvb* 26, 117–123. doi:10.1161/01.ATV.0000193618.32611.8b

Llorente-Corte´s, V., Otero-Viñas, M., Hurt-Camejo, E., Marti´nez-Gonza´lez, J., and Badimon, L. (2002). Human Coronary Smooth Muscle Cells Internalize Versican-Modified LDL through LDL Receptor-Related Protein and LDL Receptors. *Atvb* 22, 387–393. doi:10.1161/hq0302.105367

Llorentecortes, V., Royo, T., Oterovinas, M., Berrozpe, M., and Badimon, L. (2007). Sterol Regulatory Element Binding Proteins Downregulate LDL Receptor-Related Protein (LRP1) Expression and LRP1-Mediated Aggregated LDL Uptake by Human Macrophages. *Cardiovasc. Res.* 74, 526–536. doi:10.1016/j.cardiores.2007.02.020

Luechtenborg, B., Hofnagel, O., Weissen-Plenz, G., Severs, N. J., and Robenek, H. (2008). Function of Scavenger Receptor Class A Type I/II Is Not Important for Smooth Muscle Foam Cell Formation. *Eur. J. Cell Biol.* 87, 91–99. doi:10.1016/j.ejcb.2007.08.004

Luo, Y., Duan, H., Qian, Y., Feng, L., Wu, Z., Wang, F., et al. (2017). Macrophagic CD146 Promotes Foam Cell Formation and Retention during Atherosclerosis. *Cell Res.* 27, 352–372. doi:10.1038/cr.2017.8

Ma, S., Yang, D., Li, D., Tang, B., and Yang, Y. (2011). Oleic Acid Induces Smooth Muscle Foam Cell Formation and Enhances Atherosclerotic Lesion Development via CD36. *Lipids Health Dis.* 10, 53. doi:10.1186/1476-511X-10-53

Maiellaro, K., and Taylor, W. (2007). The Role of the Adventitia in Vascular Inflammation. *Cardiovasc. Res.* 75, 640–648. doi:10.1016/j.cardiores.2007.06.023

Manning-Tobin, J. J., Moore, K. J., Seimon, T. A., Bell, S. A., Sharuk, M., Alvarez-Leite, J. I., et al. (2009). Loss of SR-A and CD36 Activity Reduces Atherosclerotic Lesion Complexity without Abrogating Foam Cell Formation in Hyperlipidemic Mice. *Atvb* 29, 19–26. doi:10.1161/ATVBAHA.108.176644

Marsche, G., Hammer, A., Oskolkova, O., Kozarsky, K. F., Sattler, W., and Malle, E. (2002). Hypochlorite-Modified High Density Lipoprotein, A High Affinity Ligand to Scavenger Receptor Class B, Type I, Impairs High Density Lipoprotein-Dependent Selective Lipid Uptake and Reverse Cholesterol Transport. *J. Biol. Chem.* 277, 32172–32179. doi:10.1074/jbc.M200503200

Marsche, G., Zimmermann, R., Horiuchi, S., Tangon, N. N., Sattler, W., and Malle, E. (2003). Class B Scavenger Receptors CD36 and SR-BI are Receptors for Hypochlorite-Modified Low Density Lipoprotein. *J. Biol. Chem.* 278, 47562–47570. doi:10.1074/jbc.M308428200

Matsumoto, K., Hirano, K.-i., Nozaki, S., Takamoto, A., Nishida, M., Nakagawa-Toyama, Y., et al. (2000). Expression of Macrophage (Mφ) Scavenger Receptor, CD36, in Cultured Human Aortic Smooth Muscle Cells in Association with Expression of Peroxisome Proliferator Activated Receptor-γ, Which Regulates Gain of Mφ-like Phenotype *In Vitro*, and its Implication in Atherogenesis. *Atvb* 20, 1027–1032. doi:10.1161/01.ATV.20.4.1027

Merrilees, M. J., Beaumont, B. W., Braun, K. R., Thomas, A. C., Kang, I., Hinek, A., et al. (2011). Neointima Formed by Arterial Smooth Muscle Cells Expressing Versican Variant V3 Is Resistant to Lipid and Macrophage Accumulation. *Atvb* 31, 1309–1316. doi:10.1161/ATVBAHA.111.225573

Mietus-Snyder, M., Friera, A., Glass, C. K., and Pitas, R. E. (1997). Regulation of Scavenger Receptor Expression in Smooth Muscle Cells by Protein Kinase C. *Atvb* 17, 969–978. doi:10.1161/01.atv.17.5.969

Mietus-Snyder, M., Gowri, M. S., and Pitas, R. E. (2000). Class A Scavenger Receptor Up-Regulation in Smooth Muscle Cells by Oxidized Low Density Lipoprotein. *J. Biol. Chem.* 275, 17661–17670. doi:10.1074/jbc.275.23.17661

Moore, K. J., and Freeman, M. W. (2006). Scavenger Receptors in Atherosclerosis. *Atvb* 26, 1702–1711. doi:10.1161/01.ATV.0000229218.97976.43

Moses, S. R., Adorno, J. J., Palmer, A. F., and Song, J. W. (2021). Vessel-on-a-chip Models for Studying Microvascular Physiology, Transport, and Function *In Vitro*. *Am. J. Physiology-Cell Physiology* 320, C92–C105. doi:10.1152/ajpcell.00355.2020

Moulton, K. S., Semple, K., Wu, H., and Glass, C. K. (1994). Cell-specific Expression of the Macrophage Scavenger Receptor Gene Is Dependent on PU.1 and a Composite AP-1/ets Motif. *Mol. Cell Biol.* 14, 4408–4418. doi:10.1128/mcb.14.7.4408-4418.1994

Moulton, K. S., Wu, H., Barnett, J., Parthasarathy, S., and Glass, C. K. (1992). Regulated Expression of the Human Acetylated Low Density Lipoprotein Receptor Gene and Isolation of Promoter Sequences. *Proc. Natl. Acad. Sci. U.S.A.* 89, 8102–8106. doi:10.1073/pnas.89.17.8102

Murray, P. J., Allen, J. E., Biswas, S. K., Fisher, E. A., Gilroy, D. W., Goerdt, S., et al. (2014). Macrophage Activation and Polarization: Nomenclature and Experimental Guidelines. *Immunity* 41, 14–20. doi:10.1016/J.IMMUNI.2014.06.008

Nakagawa, K., and Nakashima, Y. (2018). Pathologic Intimal Thickening in Human Atherosclerosis Is Formed by Extracellular Accumulation of Plasma-Derived Lipids and Dispersion of Intimal Smooth Muscle Cells. *Atherosclerosis* 274, 235–242. doi:10.1016/j.atherosclerosis.2018.03.039

Nakashima, Y., Chen, Y.-X., Kinukawa, N., and Sueishi, K. (2002). Distributions of Diffuse Intimal Thickening in Human Arteries: Preferential Expression in Atherosclerosis-Prone Arteries from an Early Age. *Virchows Arch.* 441, 279–288. doi:10.1007/s00428-002-0605-1

Nakashima, Y., Fujii, H., Sumiyoshi, S., Wight, T. N., and Sueishi, K. (2007). Early Human Atherosclerosis. *Atvb* 27, 1159–1165. doi:10.1161/ATVBAHA.106.134080

Nakashima, Y., Plump, A. S., Raines, E. W., Breslow, J. L., and Ross, R. (1994). ApoE-deficient Mice Develop Lesions of All Phases of Atherosclerosis throughout the Arterial Tree. *Arterioscler. Thromb.* 14, 133–140. doi:10.1161/01.atv.14.1.133

Nakashima, Y., Wight, T. N., and Sueishi, K. (2008). Early Atherosclerosis in Humans: Role of Diffuse Intimal Thickening and Extracellular Matrix Proteoglycans. *Cardiovasc. Res.* 79, 14–23. doi:10.1093/cvr/cvn099

Napoli, C., D'Armiento, F. P., Mancini, F. P., Postiglione, A., Witztum, J. L., Palumbo, G., et al. (1997). Fatty Streak Formation Occurs in Human Fetal Aortas and Is Greatly Enhanced by Maternal Hypercholesterolemia. Intimal Accumulation of Low Density Lipoprotein and its Oxidation Precede Monocyte Recruitment into Early Atherosclerotic Lesions. *J. Clin. Invest.* 100, 2680–2690. doi:10.1172/JCI119813

Navas-Madroñal, M., Castelblanco, E., Camacho, M., Consegal, M., Ramirez-Morros, A., Sarrias, M. R., et al. (2020). Role of the Scavenger Receptor CD36 in Accelerated Diabetic Atherosclerosis. *IJMS* 21, 7360. doi:10.3390/ijms21197360

Neufeld, E. B., Zadrozny, L. M., Phillips, D., Aponte, A., Yu, Z.-X., and Balaban, R. S. (2014). Decorin and Biglycan Retain LDL in Disease-Prone Valvular and Aortic Subendothelial Intimal Matrix. *Atherosclerosis* 233, 113–121. doi:10.1016/j.atherosclerosis.2013.12.038

Ng, C.-y., Whitelock, J. M., Williams, H., Kim, H. N., Medbury, H. J., and Lord, M. S. (2021). Macrophages Bind LDL Using Heparan Sulfate and the Perlecan Protein Core. *J. Biol. Chem.* 296, 100520. doi:10.1016/j.jbc.2021.100520

Nicholson, A. C. (2004). Expression of CD36 in Macrophages and Atherosclerosis the Role of Lipid Regulation of PPARγ Signaling. *Trends Cardiovasc. Med.* 14, 8–12. doi:10.1016/j.tcm.2003.09.004

Nigro, J., Ballinger, M. L., Survase, S., Osman, N., and J. Little, P. P. (2005). New Approaches to Regulating the Chondroitin/Dermatan Sulfate Glycosaminoglycan Component of the Vascular Extracellular Matrix. *Sci. World J.* 5, 515–520. doi:10.1100/tsw.2005.69

Nishide, T., Morisaki, N., Shirai, K., Saito, Y., and Yoshida, S. (1992). Effect of Conditioning of β-migrating Very Low-Density Lipoprotein with Macrophages on the Accumulation of Cholesteryl Esters in Smooth Muscle Cells. *Scand. J. Clin. Laboratory Investigation* 52, 129–136. doi:10.3109/00365519209088776

Niu, C., Wang, X., Zhao, M., Cai, T., Liu, P., Li, J., et al. (2016). Macrophage Foam Cell-Derived Extracellular Vesicles Promote Vascular Smooth Muscle Cell Migration and Adhesion. *Jaha* 5, e004099. doi:10.1161/JAHA.116.004099

O'Brien, K. D., Olin, K. L., Alpers, C. E., Chiu, W., Ferguson, M., Hudkins, K., et al. (1998). Comparison of Apolipoprotein and Proteoglycan Deposits in Human Coronary Atherosclerotic Plaques. *Circulation* 98, 519–527. doi:10.1161/01.cir.98.6.519

Oram, J. F., and Heinecke, J. W. (2005). ATP-binding Cassette Transporter A1: a Cell Cholesterol Exporter that Protects against Cardiovascular Disease. *Physiol. Rev.* 85, 1343–1372. doi:10.1152/physrev.00005.2005

Otsuka, F., Kramer, M. C. A., Woudstra, P., Yahagi, K., Ladich, E., Finn, A. V., et al. (2015). Natural Progression of Atherosclerosis from Pathologic Intimal Thickening to Late Fibroatheroma in Human Coronary Arteries: A Pathology Study. *Atherosclerosis* 241, 772–782. doi:10.1016/j.atherosclerosis.2015.05.011

Paulson, K. E., Zhu, S.-N., Chen, M., Nurmohamed, S., Jongstra-Bilen, J., and Cybulsky, M. I. (2010). Resident Intimal Dendritic Cells Accumulate Lipid and Contribute to the Initiation of Atherosclerosis. *Circulation Res.* 106, 383–390. doi:10.1161/CIRCRESAHA.109.210781

Phillips, M. C. (2014). Molecular Mechanisms of Cellular Cholesterol Efflux. *J. Biol. Chem.* 289, 24020–24029. doi:10.1074/jbc.R114.583658

Pirillo, A., Norata, G. D., and Catapano, A. L. (20132013). LOX-1, OxLDL, and Atherosclerosis. *Mediat. Inflamm.* 2013, 1–12. doi:10.1155/2013/152786

Podrez, E. A., Poliakov, E., Shen, Z., Zhang, R., Deng, Y., Sun, M., et al. (2002). A Novel Family of Atherogenic Oxidized Phospholipids Promotes Macrophage Foam Cell Formation via the Scavenger Receptor CD36 and Is Enriched in Atherosclerotic Lesions. *J. Biol. Chem.* 277, 38517–38523. doi:10.1074/jbc.M205924200

PrabhuDas, M. R., Baldwin, C. L., Bollyky, P. L., Bowdish, D. M. E., Drickamer, K., Febbraio, M., et al. (2017). A Consensus Definitive Classification of Scavenger Receptors and Their Roles in Health and Disease. *J. I.* 198, 3775–3789. doi:10.4049/jimmunol.1700373

Pryma, C. S., Ortega, C., Dubland, J. A., and Francis, G. A. (2019). Pathways of Smooth Muscle Foam Cell Formation in Atherosclerosis. *Curr. Opin. Lipidol.* 30, 117–124. doi:10.1097/MOL.0000000000000574

Rajavashisth, T., Qiao, J. H., Tripathi, S., Tripathi, J., Mishra, N., Hua, M., et al. (1998). Heterozygous Osteopetrotic (Op) Mutation Reduces Atherosclerosis in LDL Receptor- Deficient Mice. *J. Clin. Invest.* 101, 2702–2710. doi:10.1172/JCI119891

Ramprasad, M. P., Terpstra, V., Kondratenko, N., Quehenberger, O., and Steinberg, D. (1996). Cell Surface Expression of Mouse Macrosialin and Human CD68 and Their Role as Macrophage Receptors for Oxidized Low Density Lipoprotein. *Proc. Natl. Acad. Sci. U.S.A.* 93, 14833–14838. doi:10.1073/pnas.93.25.14833

Reddick, R. L., Zhang, S. H., and Maeda, N. (1994). Atherosclerosis in Mice Lacking Apo E. Evaluation of Lesional Development and Progression. *Arterioscler. Thromb.* 14, 141–147. doi:10.1161/01.ATV.14.1.141

Redka, D. y. S., Gütschow, M., Grinstein, S., and Canton, J. (2018). Differential Ability of Proinflammatory and Anti-inflammatory Macrophages to Perform Macropinocytosis. *MBoC* 29, 53–65. doi:10.1091/mbc.E17-06-0419

Riessen, R., Isner, J. M., Blessing, E., Loushin, C., Nikol, S., and Wight, T. N. (1994). Regional Differences in the Distribution of the Proteoglycans Biglycan and Decorin in the Extracellular Matrix of Atherosclerotic and Restenotic Human Coronary Arteries. *Am. J. Pathol.* 144, 962–974.

Robichaud, S., Rasheed, A., Pietrangelo, A., Doyoung Kim, A., Boucher, D. M., Emerton, C., et al. (2022). Autophagy Is Differentially Regulated in Leukocyte and Nonleukocyte Foam Cells during Atherosclerosis. *Circ. Res.* 130 (6), 831–847. doi:10.1161/CIRCRESAHA.121.320047

Rong, J. X., Shapiro, M., Trogan, E., and Fisher, E. A. (2003). Transdifferentiation of Mouse Aortic Smooth Muscle Cells to a Macrophage-like State after Cholesterol Loading. *Proc. Natl. Acad. Sci. U.S.A.* 100, 13531–13536. doi:10.1073/pnas.1735526100

Ross, R. (1995). Cell Biology of Atherosclerosis. *Annu. Rev. Physiol.* 57, 791–804. doi:10.1146/annurev.ph.57.030195.004043

Roy, J., Tran, P. K., Religa, P., Kazi, M., Henderson, B., Lundmark, K., et al. (2002). Fibronectin Promotes Cell Cycle Entry in Smooth Muscle Cells in Primary Culture. *Exp. Cell Res.* 273, 169–177. doi:10.1006/excr.2001.5427

Sakr, S. W., Eddy, R. J., Barth, H., Wang, F., Greenberg, S., Maxfield, F. R., et al. (2001). The Uptake and Degradation of Matrix-Bound Lipoproteins by Macrophages Require an Intact Actin Cytoskeleton, Rho Family GTPases, and Myosin ATPase Activity. *J. Biol. Chem.* 276, 37649–37658. doi:10.1074/jbc.M105129200

Sandison, M. E., Dempster, J., and McCarron, J. G. (2016). The Transition of Smooth Muscle Cells from a Contractile to a Migratory, Phagocytic Phenotype: Direct Demonstration of Phenotypic Modulation. *J. Physiol.* 594, 6189–6209. doi:10.1113/JP272729

Santiago-Garcı´a, J., Kodama, T., and Pitas, R. E. (2003). The Class A Scavenger Receptor Binds to Proteoglycans and Mediates Adhesion of Macrophages to the Extracellular Matrix. *J. Biol. Chem.* 278, 6942–6946. doi:10.1074/jbc.M208358200

Schlich, R., Lamers, D., Eckel, J., and Sell, H. (2015). Adipokines Enhance Oleic Acid-Induced Proliferation of Vascular Smooth Muscle Cells by Inducing CD36 Expression. *Archives Physiology Biochem.* 121, 81–87. doi:10.3109/13813455.2015.1045520

Schönherr, E., Järveläinen, H. T., Kinsella, M. G., Sandell, L. J., and Wight, T. N. (1993). Platelet-derived Growth Factor and Transforming Growth Factor-Beta 1 Differentially Affect the Synthesis of Biglycan and Decorin by Monkey Arterial Smooth Muscle Cells. *Arterioscler. Thromb.* 13, 1026–1036. doi:10.1161/01.atv.13.7.1026

Shankman, L. S., Gomez, D., Cherepanova, O. A., Salmon, M., Alencar, G. F., Haskins, R. M., et al. (2015). KLF4-dependent Phenotypic Modulation of Smooth Muscle Cells Has a Key Role in Atherosclerotic Plaque Pathogenesis. *Nat. Med.* 21, 628–637. doi:10.1038/nm.3866

Sheikine, Y., and Sirsjö, A. (2008). CXCL16/SR-PSOX-A Friend or a Foe in Atherosclerosis? *Atherosclerosis* 197, 487–495. doi:10.1016/j.atherosclerosis.2007.11.034

Shi, Y., O'Brien, J. E., Fard, A., Mannion, J. D., Wang, D., and Zalewski, A. (1996). Adventitial Myofibroblasts Contribute to Neointimal Formation in Injured Porcine Coronary Arteries. *Circulation* 94, 1655–1664. doi:10.1161/01.cir.94.7.1655

Shimaoka, T., Kume, N., Minami, M., Hayashida, K., Kataoka, H., Kita, T., et al. (2000). Molecular Cloning of a Novel Scavenger Receptor for Oxidized Low Density Lipoprotein, SR-PSOX, on Macrophages. *J. Biol. Chem.* 275, 40663–40666. doi:10.1074/jbc.C000761200

Singh, R. K., Barbosa-Lorenzi, V. C., Lund, F. W., Grosheva, I., Maxfield, F. R., and Haka, A. S. (2016). Degradation of Aggregated LDL Occurs in Complex Extracellular Sub-compartments of the Lysosomal Synapse. *J. Cell Sci.* 129, 1072–1082. doi:10.1242/jcs.181743

Singh, R. K., Haka, A. S., Asmal, A., Barbosa-Lorenzi, V. C., Grosheva, I., Chin, H. F., et al. (2020). TLR4 (Toll-like Receptor 4)-Dependent Signaling Drives Extracellular Catabolism of LDL (Low-Density Lipoprotein) Aggregates. *Atvb* 40, 86–102. doi:10.1161/ATVBAHA.119.313200

Smith, J. D., Trogan, E., Ginsberg, M., Grigaux, C., Tian, J., and Miyata, M. (1995). Decreased Atherosclerosis in Mice Deficient in Both Macrophage Colony-Stimulating Factor (Op) and Apolipoprotein E. *Proc. Natl. Acad. Sci. U.S.A.* 92, 8264–8268. doi:10.1073/pnas.92.18.8264

Soto, Y., Acosta, E., Delgado, L., Pérez, A., Falcón, V., Bécquer, M. A., et al. (2012). Antiatherosclerotic Effect of an Antibody that Binds to Extracellular Matrix Glycosaminoglycans. *Atvb* 32, 595–604. doi:10.1161/ATVBAHA.111.238659

Stary, H. C., Blankenhorn, D. H., Chandler, A. B., Glagov, S., Insull Jr, W., Richardson, M., et al. (1992). A Definition of the Intima of Human Arteries and its Atherosclerosis-Prone Regions. A Report From the Committee on Vascular Lesions of the Council on Arteriosclerosis, American Heart Association. *Arterioscler. Thromb.* 12, 120–134. doi:10.1161/01.atv.12.1.120

Stary, H. C., Chandler, A. B., Glagov, S., Guyton, J. R., Insull, W., Rosenfeld, M. E., et al. (1994). A Definition of Initial, Fatty Streak, and Intermediate Lesions of Atherosclerosis. A Report from the Committee on Vascular Lesions of the Council on Arteriosclerosis, American Heart Association. *Circulation* 89, 2462–2478. doi:10.1161/01.cir.89.5.2462

Stary, H. C. (1985). Macrophage Foam Cells in the Coronary Artery Intima of Human Infantsa. *Ann. N. Y. Acad. Sci.* 454, 5–8. doi:10.1111/j.1749-6632.1985.tb11839.x

Stary, H. C. (1987). Macrophages, Macrophage Foam Cells, and Eccentric Intimal Thickening in the Coronary Arteries of Young Children. *Atherosclerosis* 64, 91–108. doi:10.1016/0021-9150(87)90234-6

Stein, O., Ben-naim, M., Dabach, Y., Hollander, G., and Steina, Y. (1994). Murine Macrophages Secrete Factors that Enhance Uptake of Non-lipoprotein [3H] cholesteryl Ester by Aortic Smooth Muscle Cells. *Biochimica Biophysica Acta (BBA) - Lipids Lipid Metabolism* 1212, 305–310. doi:10.1016/0005-2760(94)90204-6

Stein, O., Dabach, Y., Ben-Naim, M., Hollander, G., and Stein, Y. (1993). Macrophage-conditioned Medium and Beta-VLDLs Enhance Cholesterol Esterification in SMCs and HSFs by LDL Receptor-Mediated and Other Pathways. *Arterioscler. Thromb.* 13, 1350–1358. doi:10.1161/01.ATV.13.9.1350

Stein, O., Halperin, G., and Stein, Y. (1981). Enhancement of Cholesterol Esterification in Aortic Smooth Muscle Cells by Medium of Macrophages Conditioned with Acetylated LDL. *FEBS Lett.* 123, 303–306. doi:10.1016/0014-5793(81)80314-6

Steinbrecher, U. P., and Lougheed, M. (1992). Scavenger Receptor-independent Stimulation of Cholesterol Esterification in Macrophages by Low Density Lipoprotein Extracted from Human Aortic Intima. *Arterioscler. Thromb.* 12, 608–625. doi:10.1161/01.ATV.12.5.608

Stout, L., Whortonjr, E., and Vaghela, M. (1983). Pathogenesis of Diffuse Intimal Thickening (DIT) in Non-human Primate Thoracic Aortas. *Atherosclerosis* 47, 1–6. doi:10.1016/0021-9150(83)90065-5

Sukhova, G. K., Schönbeck, U., Rabkin, E., Schoen, F. J., Poole, A. R., Billinghurst, R. C., et al. (1999). Evidence for Increased Collagenolysis by Interstitial Collagenases-1 and -3 in Vulnerable Human Atheromatous Plaques. *Circulation* 99, 2503–2509. doi:10.1161/01.CIR.99.19.2503

Swirski, F. K., Libby, P., Aikawa, E., Alcaide, P., Luscinskas, F. W., Weissleder, R., et al. (2007). Ly-6Chi Monocytes Dominate Hypercholesterolemia-Associated Monocytosis and Give Rise to Macrophages in Atheromata. *J. Clin. Invest.* 117, 195–205. doi:10.1172/JCI29950

Swirski, F. K., Pittet, M. J., Kircher, M. F., Aikawa, E., Jaffer, F. A., Libby, P., et al. (2006). Monocyte Accumulation in Mouse Atherogenesis Is Progressive and Proportional to Extent of Disease. *Proc. Natl. Acad. Sci. U.S.A.* 103, 10340–10345. doi:10.1073/pnas.0604260103

Tabas, I. (1999). Nonoxidative Modifications of Lipoproteins in Atherogenesis. *Annu. Rev. Nutr.* 19, 123–139. doi:10.1146/annurev.nutr.19.1.123

Tamminen, M., Mottino, G., Qiao, J. H., Breslow, J. L., and Frank, J. S. (1999). Ultrastructure of Early Lipid Accumulation in ApoE-Deficient Mice. *Atvb* 19, 847–853. doi:10.1161/01.atv.19.4.847

Tontonoz, P., Nagy, L., Alvarez, J. G. A., Thomazy, V. A., and Evans, R. M. (1998). PPARγ Promotes Monocyte/Macrophage Differentiation and Uptake of Oxidized LDL. *Cell* 93, 241–252. doi:10.1016/s0092-8674(00)81575-5

Tran, P.-K., Agardh, H. E., Tran-Lundmark, K., Ekstrand, J., Roy, J., Henderson, B., et al. (2007). Reduced Perlecan Expression and Accumulation in Human Carotid Atherosclerotic Lesions. *Atherosclerosis* 190, 264–270. doi:10.1016/j.atherosclerosis.2006.03.010

Tran-Lundmark, K., Tran, P.-K., Paulsson-Berne, G., Friden, V., Soininen, R., Tryggvason, K., et al. (2008). Heparan Sulfate in Perlecan Promotes Mouse Atherosclerosis: Roles in Lipid Permeability, Lipid Retention, and Smooth Muscle Cell Proliferation. *Circulation Res.* 103, 43–52. doi:10.1161/CIRCRESAHA.108.172833

Uhlin-Hansen, L., Wik, T., Kjellen, L., Berg, E., Forsdahl, F., and Kolset, S. (1993). Proteoglycan Metabolism in Normal and Inflammatory Human Macrophages. *Blood* 82, 2880–2889. doi:10.1182/blood.v82.9.2880.bloodjournal8292880

van den Borne, P., Quax, P. H. A., Hoefer, I. E., and Pasterkamp, G. (2014). The Multifaceted Functions of CXCL10 in Cardiovascular Disease. *BioMed Res. Int.* 2014, 1–11. doi:10.1155/2014/893106

van Wanrooij, E. J. A., de Jager, S. C. A., van Es, T., de Vos, P., Birch, H. L., Owen, D. A., et al. (2008). CXCR3 Antagonist NBI-74330 Attenuates Atherosclerotic Plaque Formation in LDL Receptor-Deficient Mice. *Atvb* 28, 251–257. doi:10.1161/ATVBAHA.107.147827

Vengrenyuk, Y., Nishi, H., Long, X., Ouimet, M., Savji, N., Martinez, F. O., et al. (2015). Cholesterol Loading Reprograms the microRNA-143/145-Myocardin axis to Convert Aortic Smooth Muscle Cells to a Dysfunctional Macrophage-like Phenotype. *Atvb* 35, 535–546. doi:10.1161/ATVBAHA.114.304029

Vijayagopal, P., and Glancy, D. L. (1996). Macrophages Stimulate Cholesteryl Ester Accumulation in Cocultured Smooth Muscle Cells Incubated with Lipoprotein-Proteoglycan Complex. *Atvb* 16, 1112–1121. doi:10.1161/01.atv.16.9.1112

Vijayagopal, P., Srinivasan, S. R., Xu, J. H., Dalferes, E. R., Radhakrishnamurthy, B., and Berenson, G. S. (1993). Lipoprotein-proteoglycan Complexes Induce Continued Cholesteryl Ester Accumulation in Foam Cells from Rabbit Atherosclerotic Lesions. *J. Clin. Invest.* 91, 1011–1018. doi:10.1172/jci116257

Wågsäter, D., Olofsson, P. S., Norgren, L., Stenberg, B., and Sirsjö, A. (2004). The Chemokine and Scavenger Receptor CXCL16/SR-PSOX Is Expressed in Human Vascular Smooth Muscle Cells and Is Induced by Interferon γ. *Biochem. Biophysical Res. Commun.* 325, 1187–1193. doi:10.1016/j.bbrc.2004.10.160

Wang, Y., Dubland, J. A., Allahverdian, S., Asonye, E., Sahin, B., Jaw, J. E., et al. (2019). Smooth Muscle Cells Contribute the Majority of Foam Cells in ApoE (Apolipoprotein E)-Deficient Mouse Atherosclerosis. *Atvb* 39, 876–887. doi:10.1161/ATVBAHA.119.312434

Wang, Y., Nanda, V., Direnzo, D., Ye, J., Xiao, S., Kojima, Y., et al. (2020). Clonally Expanding Smooth Muscle Cells Promote Atherosclerosis by Escaping Efferocytosis and Activating the Complement Cascade. *Proc. Natl. Acad. Sci. U.S.A.* 117, 15818–15826. doi:10.1073/pnas.2006348117

Weinert, S., Poitz, D. M., Auffermann-Gretzinger, S., Eger, L., Herold, J., Medunjanin, S., et al. (2013). The Lysosomal Transfer of LDL/cholesterol

from Macrophages into Vascular Smooth Muscle Cells Induces Their Phenotypic Alteration. *Cardiovasc Res.* 97, 544–552. doi:10.1093/cvr/cvs367

Wight, T. N. (1985). Proteoglycans in Pathological Conditions: Atherosclerosis. *Fed. Proc.* 44, 381–385.

Wight, T. N. (2018). A Role for Proteoglycans in Vascular Disease. *Matrix Biol.* 71-72, 396–420. doi:10.1016/j.matbio.2018.02.019

Williams, J. W., Zaitsev, K., Kim, K.-W., Ivanov, S., Saunders, B. T., Schrank, P. R., et al. (2020). Limited Proliferation Capacity of Aortic Intima Resident Macrophages Requires Monocyte Recruitment for Atherosclerotic Plaque Progression. *Nat. Immunol.* 21, 1194–1204. doi:10.1038/s41590-020-0768-4

Williams, K. J., and Tabas, I. (1995). The Response-To-Retention Hypothesis of Early Atherogenesis. *Atvb* 15, 551–561. doi:10.1161/01.atv.15.5.551

Wolfbauer, G., Glick, J. M., Minor, L. K., and Rothblat, G. H. (1986). Development of the Smooth Muscle Foam Cell: Uptake of Macrophage Lipid Inclusions. *Proc. Natl. Acad. Sci. U.S.A.* 83, 7760–7764. doi:10.1073/pnas.83.20.7760

Xue, J.-h., Yuan, Z., Wu, Y., Liu, Y., Zhao, Y., Zhang, W.-p., et al. (2010). High Glucose Promotes Intracellular Lipid Accumulation in Vascular Smooth Muscle Cells by Impairing Cholesterol Influx and Efflux Balance. *Cardiovasc. Res.* 86, 141–150. doi:10.1093/cvr/cvp388

Yang, S., Yuan, H.-Q., Hao, Y.-M., Ren, Z., Qu, S.-L., Liu, L.-S., et al. (2020). Macrophage Polarization in Atherosclerosis. *Clin. Chim. Acta* 501, 142–146. doi:10.1016/J.CCA.2019.10.034

Yesner, L. M., Huh, H. Y., Pearce, S. F., and Silverstein, R. L. (1996). Regulation of Monocyte CD36 and Thrombospondin-1 Expression by Soluble Mediators. *Atvb* 16, 1019–1025. doi:10.1161/01.ATV.16.8.1019

Yusuf, S., Hawken, S., Ôunpuu, S., Dans, T., Avezum, A., Lanas, F., et al. (2004). Effect of Potentially Modifiable Risk Factors Associated with Myocardial Infarction in 52 Countries (The INTERHEART Study): Case-Control Study. *Lancet* 364, 937–952. doi:10.1016/S0140-6736(04)17018-9

Zhang, H., Downs, E. C., Lindsey, J. A., Davis, W. B., Whisler, R. L., and Cornwell, D. G. (1993). Interactions between the Monocyte/macrophage and the Vascular Smooth Muscle Cell. Stimulation of Mitogenesis by a Soluble Factor and of Prostanoid Synthesis by Cell-Cell Contact. *Arterioscler. Thromb.* 13, 220–230. doi:10.1161/01.ATV.13.2.220

Zhu, X.-D., Zhuang, Y., Ben, J.-J., Qian, L.-L., Huang, H.-P., Bai, H., et al. (2011). Caveolae-dependent Endocytosis Is Required for Class A Macrophage Scavenger Receptor-Mediated Apoptosis in Macrophages. *J. Biol. Chem.* 286, 8231–8239. doi:10.1074/jbc.M110.145888

Zhu, Y., Hojo, Y., Ikeda, U., Takahashi, M., and Shimada, K. (2000). Interaction between Monocytes and Vascular Smooth Muscle Cells Enhances Matrix Metalloproteinase-1 Production. *J. Cardiovasc. Pharmacol.* 36, 152–161. doi:10.1097/00005344-200008000-00003

Zingg, J.-M., Ricciarelli, R., Andorno, E., and Azzi, A. (2002). Novel 5′ Exon of Scavenger Receptor CD36 Is Expressed in Cultured Human Vascular Smooth Muscle Cells and Atherosclerotic Plaques. *Atvb* 22, 412–417. doi:10.1161/hq0302.104517

Zingg, J.-M., Ricciarelli, R., and Azzi, A. (2000). Scavenger Receptors and Modified Lipoproteins: Fatal Attractions? *IUBMB Life (International Union Biochem. Mol. Biol. Life)* 49, 397–403. doi:10.1080/152165400410245

Zuniga, M. C., White, S. L. P., and Zhou, W. (2014). Design and Utilization of Macrophage and Vascular Smooth Muscle Cell Co-culture Systems in Atherosclerotic Cardiovascular Disease Investigation. *Vasc. Med.* 19, 394–406. doi:10.1177/1358863X14550542

Conflict of Interest: The authors declare that the research was conducted in the absence of any commercial or financial relationships that could be construed as a potential conflict of interest.

Publisher's Note: All claims expressed in this article are solely those of the authors and do not necessarily represent those of their affiliated organizations, or those of the publisher, the editors and the reviewers. Any product that may be evaluated in this article, or claim that may be made by its manufacturer, is not guaranteed or endorsed by the publisher.

frontiers | Frontiers in Physiology

ORIGINAL RESEARCH
published: 21 June 2022
doi: 10.3389/fphys.2022.921866

Fatty Acid Profiling in Facial Sebum and Erythrocytes From Adult Patients With Moderate Acne

Ke Cao[1†], Ye Liu[1†], Ningning Liang[2†], Xia Shen[2], Rui Li[2], Huiyong Yin[2] and Leihong Xiang[1]**

[1]Department of Dermatology, Huashan Hospital, Fudan University, Shanghai, China, [2]CAS Key Laboratory of Nutrition, Metabolism and Food Safety, Shanghai Institute of Nutrition and Health (SINH), Chinese Academy of Sciences (CAS), Shanghai, China

Fatty acid (FA) metabolism has been involved in acne vulgaris, a common inflammatory skin disease frequently observed in adolescents and adults, but it remains poorly defined whether the distributions or location of FA in facial sebum and those in the circulation differentially correlate with the disease. In a cohort of 47 moderate acne patients and 40 controls, sebum samples from forehead and chin areas were collected using Sebutape adhesive patches, and erythrocytes were separated from the fasting blood. Total FAs were analyzed by the gas chromatograph-mass spectrometry method. Compared to control female subjects, female patients showed increased levels of saturated fatty acids (SFAs) and monounsaturated fatty acids (MUFAs) from both facial areas, whereas decreased levels of polyunsaturated fatty acids (PUFAs) from chin areas were observed. Interestingly, the levels of docosahexaenoic acid (DHA) in the circulating erythrocytes were significantly decreased in male patients compared with control. In addition, DHA levels in erythrocytes were positively correlated with PUFAs from sebum only in male subjects. Furthermore, female patients with moderate acne had more severe sebum abnormity and chin-specific FA profiles, consistent with higher acne incidences than males in adulthood, especially in the chin areas. Importantly, serum insulin-like growth factor 1 (IGF-1) levels were positively correlated with SFAs and MUFAs from sebum only in male subjects. In summary, differential spatial FA distributions in facial sebum and correlation with those in erythrocytes and IGF1 levels in serum may shed some light on the pathology of acne in male and female adults.

Keywords: acne (acne vulgaris), sebum, fatty acid (composition), erythrocyte (human), insulin-like growth factor 1 (IGF1)

OPEN ACCESS

Edited by:
Da-Wei Zhang,
University of Alberta, Canada

Reviewed by:
Shoudong Guo,
Weifang Medical University, China
Kai Yin,
Guilin Medical University, China

****Correspondence:***
Huiyong Yin
hyyin@sibs.ac.cn
Leihong Xiang
flora_xiang@vip.163.com

[†]These authors have contributed equally to this work and share first authorship

Specialty section:
This article was submitted to Lipid and Fatty Acid Research, a section of the journal Frontiers in Physiology

Received: *16 April 2022*
Accepted: *13 May 2022*
Published: *21 June 2022*

Citation:
Cao K, Liu Y, Liang N, Shen X, Li R, Yin H and Xiang L (2022) Fatty Acid Profiling in Facial Sebum and Erythrocytes From Adult Patients With Moderate Acne. Front. Physiol. 13:921866. doi: 10.3389/fphys.2022.921866

INTRODUCTION

Acne vulgaris is a multifactorial skin disease that frequently occurrs after puberty (Skroza et al., 2018). It continues to be a common and stressful skin problem even after teenage years and especially affects females at higher rates than males (Collier et al., 2008). Emerging evidence suggests that increased sebum production and alterations of sebum composition, including skin surface lipids (SSLs), are among the most pivotal factors in the pathogenesis of acne (Zouboulis et al., 2014; Camera et al., 2016; Zhou et al., 2018). SSL in sebum consists of diverse classes of lipids, among which fatty acids (FAs) are primarily responsible for the inflammatory and innate immune responses in the pathogenesis of acne (Ottaviani et al., 2010). Depending on the chemical structures, some FAs have

pro-inflammatory and follicular keratinization properties (Katsuta et al., 2005; Choi et al., 2019), but other FAs show antibacterial and anti-inflammatory effects (Balic et al., 2020). A different ratio between saturated fatty acid (SFA) and monounsaturated fatty acid (MUFA) in the SSL of acne patients (Smith et al., 2008) was reported, suggesting that FA alterations in SSL could be considered causative factors of clinical signs of acne (Ottaviani et al., 2010).

Circulating polyunsaturated fatty acids (PUFAs) are usually detected in different lipoprotein particles, while the levels of erythrocyte PUFAs are known to reflect relatively long-term nutritional status (Arab, 2003) and are highly correlated with PUFA compositions in various tissues (Fenton et al., 2016). Furthermore, PUFA levels in the blood of acne patients are associated with a pro-inflammatory state, while supplementation with PUFA reverses acne lesions (Jung et al., 2014; Aslan et al., 2017). In addition, insulin-like growth factor 1 (IGF1) plays an important role in the pathogenesis of acne by inducing sebum overproduction (Ju et al., 2017). However, it remains to be poorly defined whether FA compositions in SSL in both genders and facial anatomical sites correlate with those in the circulation and IGF1 levels in serum.

In this study, we examined the sebum alteration of the forehead and chin in male and female patients with moderate acne, focusing on the correlations between spatial FA levels in facial sebum and those in blood circulation. Correlation of FA profiles with IGF1 levels was also made. Discovery of these clues on the FA compositions in acne may lay the ground for potential dietary interventions to alter the facial FA in the prevention and treatment of acne.

MATERIALS AND METHODS

Study Population

Forty-seven patients with moderate acne and forty age- and gender-matched controls with normal facial skin were recruited between September and December 2020 in Huashan Hospital with the approval of the Huashan Hospital Ethics Committee, Fudan University, Shanghai, China. Written informed consent was obtained from all patients before the study. All participants were nonsmokers and did not consume alcohol. Patients with acne were selected from participants who had not previously received acne-related treatments for a minimum of 8 weeks prior to the enrollment. The clinical grading of patients and control subjects was assessed by dermatologists who followed the guidelines of acne vulgaris (Zaenglein et al., 2016). Patients of systemic diseases including polycystic ovarian syndrome (PCOS) and other skin disorders were excluded from this study. A survey of food frequency and 24-h dietary recall were conducted using a food frequency questionnaire (FFQ) (Roengritthidet et al., 2021).

Sample Collection

Sebum was collected from the central forehead and chin using a Sebutape® (CuDerm Corporation, Dallas, TX, United States). The Sebutape is an open-celled, microporous, hydrophobic, lipophilic adhesive strip that has been shown to be a reproducible technique for the collection of SSL (Nordstrom et al., 1986). The skin was degreased with a 75% alcohol swab and allowed to dry. A Sebutape that had been pre-weighed beforehand was placed onto the skin for 30 min. The tape was reweighed for the gravimetric assessment of sebum excretion rates (SERs, micrograms per square centimeter per minute). **Table 1** summarizes the average SER for the study groups. The Sebutapes were stored at −80°C until further analysis. In line with the recommendations of the European Group for Efficacy Measurements on Cosmetics and Other Topical Products (Piérard et al., 2000), sebum collections were performed on all participants in the same examination room, where ambient temperature and humidity were kept constant. Sebutapes were applied between 11:00 am and 15:00 pm to avoid diurnal variations of sebum secretion. Peripheral blood was collected and centrifuged, and samples of both erythrocytes and plasma were stored at −80°C until analysis.

TABLE 1 | Demographic details of control subjects and moderate acne patients.

Characteristic	Control subjects (n = 40)	Moderate acne patients (n = 47)
Male, N, (%)	18 (45)	17 (36)
Female, N, (%)	22 (55)	30 (64)
AGE, mean (SD), y	26.72 (3.154)	25.67 (3.273)^{NS}
BMI, mean (SD), kg/m^2	20.86 (1.578)	20.94 (1.570)^{NS}
SER, mean (SD), μg/cm^2/minute		
Total	6.166 (2.931)	6.577 (2.617)^{NS}
Male	6.698 (3.085)	6.907 (2.971)^{NS}
Female	5.711 (2.749)	6.349 (2.407)^{NS}
Forehead	6.221 (2.522)	6.515 (2.666)^{NS}
Chin	6.111 (3.323)	6.640 (2.597)^{NS}
IGF1, mean (SD), μg/L		
Total	167.2 (33.96)	171.65 (33.19)^{NS}
Male	155.5 (28.49)	167.14 (34.31)^{NS}
Female	182.29 (34.5)	174.08 (32.31)^{NS}

BMI, body mass index; SER, sebum excretion rate; IGF1, insulin-like growth factor 1.

Sample Preparation

FAs were extracted according to a previously published protocol from our laboratory (Liu et al., 2021). In brief, a solvent mixture (chloroform/methanol, 2:1 v/v) was added with the addition of 0.025% antioxidant butylated hydroxytoluene and C21:0 (20 μg, internal standard). The extracts were vortexed for 5 min and then centrifuged at 2,000 g for 10 min. After discarding the Sebutapes, the extracts were dried under a gentle N_2 flow and then derivatized to form fatty acid methyl esters (FAMEs) *via* the addition of 2 ml 2% H_2SO_4 in methanol and incubation at 80°C for 1 h. Next, 2 ml hexane and 500 μl ddH_2O were added, and the upper phase was dried under the N_2 flow. The samples were resuspended in 100 μl hexane prior to gas chromatography-mass spectrometry (GC-MS) analysis.

GC-MS Analysis

A Shimadzu QP-2010 Ultra GC-MS was programed with an injection temperature of 250°C, injection split ratio of 1/20, and injection volume of 1 μl sample. The GC column was a 30 m ×

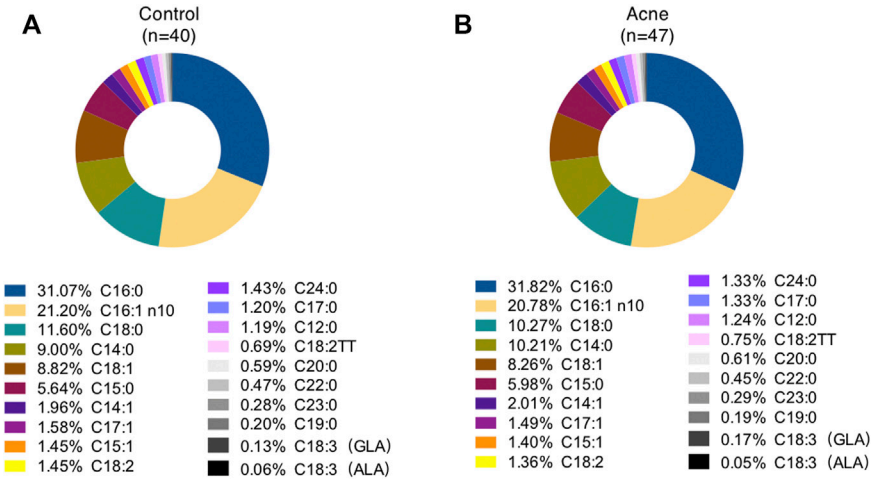

FIGURE 1 | Percentage of total fatty acids in sebum from control subjects **(A)** and acne patients **(B)**. GLA, γ-linolenic acid; ALA, α-linolenic acid.

0.25 mm × 0.25 mm HP-5ms. The amount of FA was quantified by using a standard response curve with the internal standard. The samples were analyzed in a random sequence. Quality control samples and blank control samples were injected for every 15 samples to ensure repeatability.

Statistical Analysis

Statistical analysis was conducted using GraphPad Prism (GraphPad Software) and SPSS, version 26 (IBM Corporation). Continuous variables were expressed as means and standard deviations (SDs) and categorical data as percentage distributions. Student's t test and analysis of variance test were used for quantitative data, and Fisher's test was used to compare categorical data. A statistical probability of $p < 0.05$ was considered significant. Z-score was calculated and presented in a heatmap using the R package ComplexHeatmap v.2.8.0. Red in the heatmap represents that Z-score is more than 0, whereas blue represents that Z-score is less than 0. Spearman's correlation coefficients between sebum within samples in each group were calculated and visualized by R package corrplot 0.9.0. Negative correlations were shown in blue, whereas positive correlations were in red. All the statistical analyses were performed using R v.4.1.0.

RESULTS

Subject Demographics

Participants in the current study were 18–35 years old. Demographics of controls and subjects with acne are described in **Table 1**. Two groups were similarly distributed in terms of gender and age. The body mass index (BMI) in the two groups was within the normal range. To evaluate sebometry, the parameter associated with acne pathogenesis including the SER was determined for each participant. The SER of acne patients was all increased than that of control subjects regardless of the genders and facial sites but did not reach statistical significance. To minimize the effects of SER values on sebum chemometrics, the levels of FA in all samples were normalized to the weight of sebum.

FA Profiles in Sebum

A total of twenty FAs in SSL were quantified in the GC-MS analysis (**Supplementary Table S1**). Palmitic acid (PA, C16:0), sapienic acid (SA, C16:1n-10), stearic acid (C18:0), myristic acid (C14:0), and oleic acid (OA, C18:1) are the top five most abundant FAs in the sebum, accounting for about 31%, 21%, 11%,10%, and 8%, respectively, for control subjects (**Figure 1A**) and acne patients (**Figure 1B**), consistent with previous reports (Akaza et al., 2014). However, none of these FAs between the two groups was statistically significant. Moreover, 11 SFA, five MUFA, and four PUFA were detected in our method. Heatmaps of the average amounts of sebum lipids in the forehead and chin of both genders between the control and acne groups are reported in **Figure 2**. First, comparisons within each group were made. In the control group, SFA (C15:0, C16:0, C17:0, C19:0, C20:0, C22:0, C23:0, C24:0) and MUFA (C15:1, C17:1) from forehead were decreased in female subjects compared to male ones ($^{\#}p < 0.05$). Meanwhile, the levels of SFA (C15:0) and MUFA (C16:1n10, C17:1) from the chin were also lower in female subjects than in males ($^{\#}p < 0.05$). However, these differences in SFA and MUFA between the two genders did not differ within the acne group. Moreover, in the control group, the level of linoleic acid (C18:2, LA) from the chin of both genders was higher than that of the forehead ($^{\$}p < 0.05$). C18:3 (α-linolenic acid, ALA) was also increased in the chin of women ($^{\$}p < 0.05$). However, within the acne group, when gender and site were taken into consideration, only men had higher levels of ALA ($^{\$}p < 0.05$) in the chin than the forehead. Next, comparisons were made between the two groups. Female acne patients had more FA alterations in the sebum (shown as $^{*}p < 0.05$). In detail, in the forehead of female subjects, all detected SFA (except C18:0) and two MUFA (C14:1 and C17:1) were significantly increased compared to those of control females ($^{*}p < 0.05$). Meanwhile, markedly increased levels of SFA (C14:0, C15:0) and MUFA (C16:1n10) and decreased level of PUFA (ALA) were detected in the chin of female acne patients than in control female subjects ($^{*}p < 0.05$). In addition, male patients had lower levels of PUFA (C18:2) in the chin in the acne group than in the control group ($^{*}p < 0.05$). Overall, the FA abnormality of facial sebum in acne patients was mainly found in females in a spatial and gender-specific manner.

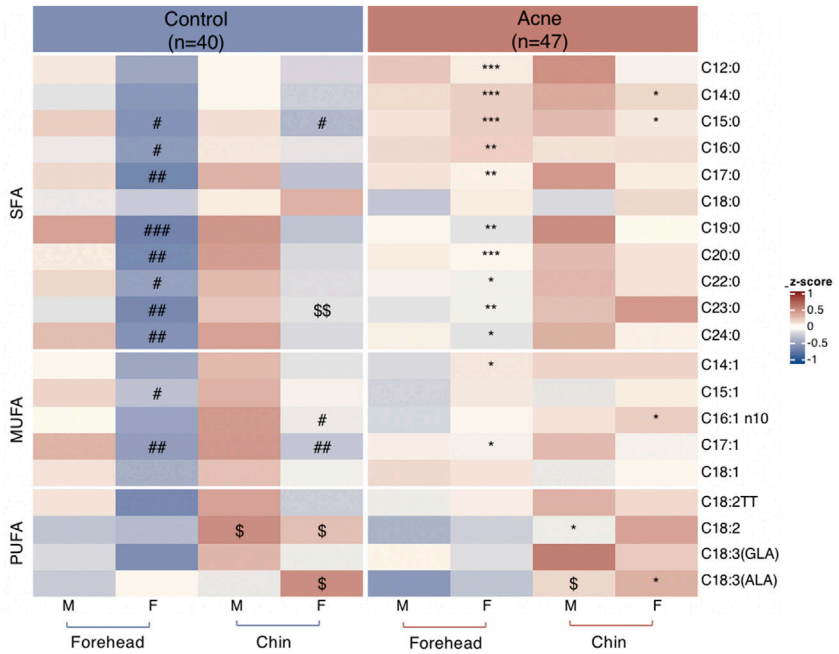

FIGURE 2 | Heatmaps of quantified fatty acids levels normalized by Z-score from sebum on forehead and chin between males (M) and females (F) in control and acne groups. $^{*}p < 0.05$, $^{**}p < 0.01$, and $^{***}p < 0.001$ vs. the gender- and site-matched control group; $^{\#}p < 0.05$, $^{\#\#}p < 0.01$, and $^{\#\#\#}p < 0.001$ vs. site-matched male control group; $^{\$}p < 0.05$ and $^{\$\$}p < 0.01$ vs. gender- and group-matched subjects.

TABLE 2 | Fatty acid profile of erythrocytes between control and acne groups.

FA of erythrocyte (μg/μl, mean ± SD)

	Control subjects (n = 40)		Moderate acne patients (n = 47)	
	Male	**Female**	**Male**	**Female**
C12:0	0.03 ± 0.01	0.05 ± 0.03	0.05 ± 0.03	0.12 ± 0.07
C14:0	0.47 ± 0.12	0.51 ± 0.17	0.50 ± 0.23	0.78 ± 0.37
C15:0	0.24 ± 0.06	0.25 ± 0.08	0.21 ± 0.04	0.37 ± 0.20
C16:0	48.61 ± 6.58	46.68 ± 6.86	46.17 ± 6.04	50.50 ± 6.12
C17:0	0.47 ± 0.05	0.49 ± 0.07	0.38 ± 0.10	0.51 ± 0.07
C18:0	14.63 ± 1.32	14.35 ± 2.58	14.48 ± 2.85	16.33 ± 3.67
C16:1	0.36 ± 0.18	0.37 ± 0.12	0.34 ± 0.29	0.53 ± 0.35
C18:1	33.00 ± 4.74	29.41 ± 5.72	32.28 ± 5.34	32.55 ± 4.35
C18:2	26.44 ± 4.03	24.91 ± 6.34	26.17 ± 2.71	28.22 ± 5.91
C18:3 (ALA)	0.27 ± 0.07	0.22 ± 0.09	0.27 ± 0.07	0.33 ± 0.15
C20:4	9.80 ± 1.27	10.10 ± 1.82	9.45 ± 1.63	10.14 ± 2.18
C20:5	0.57 ± 0.15	0.52 ± 0.15	0.54 ± 0.17	0.77 ± 0.27
C22:6	5.48 ± 0.55	6.25 ± 1.17	4.58 ± 0.51*	7.01 ± 1.26#

*ALA, α-linolenic acid; *p < 0.05 vs. the gender-matched control subjects, #p < 0.05 vs. the group-matched male subjects.*

FA Profile of Erythrocytes in Subjects

We separated blood samples into erythrocytes and plasma fractions. The levels of erythrocytes FA are known to reflect relatively long-term nutritional status (Arab, 2003). Thirteen FAs were detected in erythrocytes, including six SFAs, two MUFAs, and five PUFAs (**Table 2**). We found that levels of docosahexaenoic acid (C22:6, DHA) in erythrocytes were significantly decreased in male patients with moderate acne than in control male subjects ($^{*}p < 0.05$). Interestingly, female patients with acne showed higher levels of DHA than male patients ($^{\#}p < 0.05$). However, none of the FA in plasma had significant differences between control and acne groups in both genders (**Supplementary Table S2**).

Correlation of FA Levels With Those in the Sebum and Blood

As we observed that DHA in erythrocytes had specific differences in males, we further analyzed the correlation of Omega-3 PUFAs in erythrocytes and sebum. In male subjects,

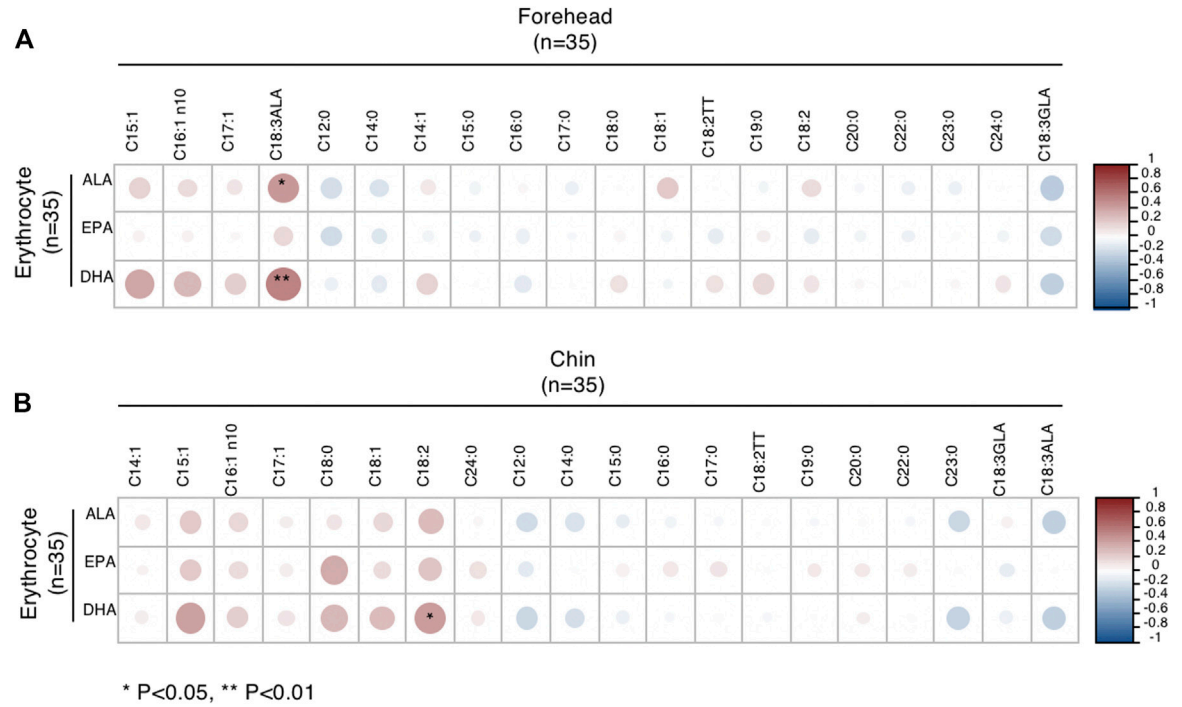

FIGURE 3 | Correlations between Omega-3 PUFA of erythrocytes and FA of sebum from the forehead **(A)** and chin **(B)** in male subjects. *$p < 0.05$ and **$p < 0.01$.

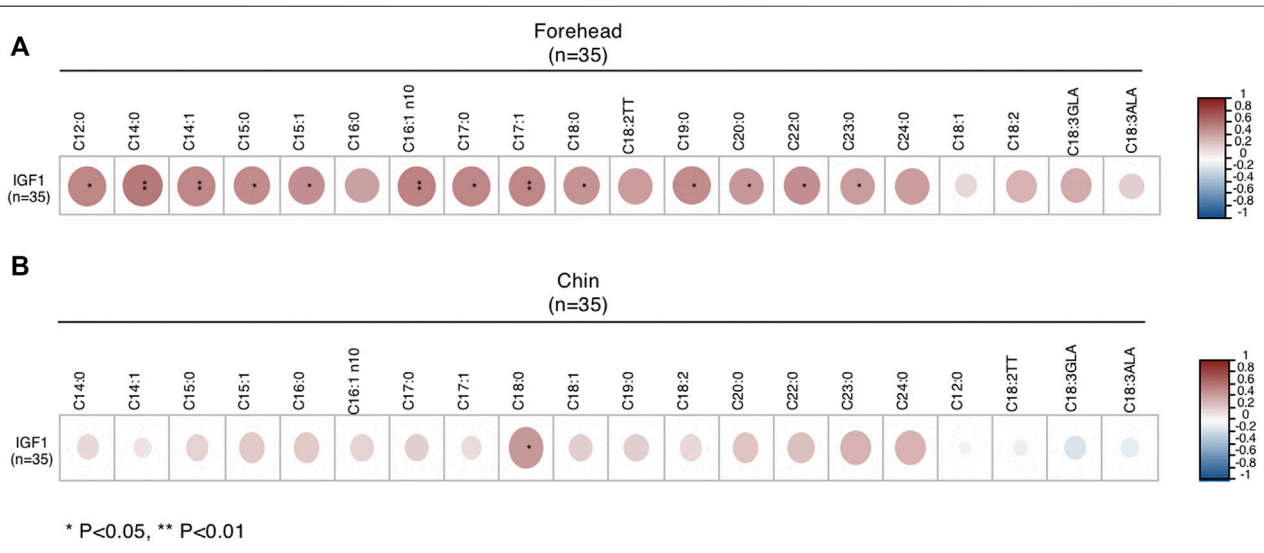

FIGURE 4 | Correlations between IGF1 levels and FA of sebum from forehead **(A)** and chin **(B)** in male subjects. *p < 0.05 and **p < 0.01.

ALA and DHA levels of erythrocytes were positively correlated with ALA levels in sebum from the forehead (**Figure 3A**). Meanwhile, DHA levels of erythrocytes positively correlated with LA levels from the chin (**Figure 3B**). However, the patterns of correlation were different in females (**Supplementary Figure S1**).

Correlation of IGF1 Levels and FA Composition From Sebum

Next, we examined the correlation between IGF1 levels with sebum FAs and found that IGF1 levels were increased in male patients with moderate acne, but it did not reach statistical significance (**Table 1**). We further analyzed the correlation of IGF1 levels and FA

TABLE 3 | Categorical analysis of milk consumption and acne.

Characteristic	Control subjects (*n* = 40)	Moderate acne patients (*n* = 47)	Odds ratio (95% CI)	*p*-value
Any kind of milk, n (%)				
Total				
<250 ml/day	31 (77.5)	29 (61.7)	2.138 (0.793–5.237)	0.163
≥250 ml/day	9 (22.5)	18 (38.3)		
Male				
<250 ml/day	15 (83.3)	9 (52.9)	4.444 (0.959–17.86)	0.075
≥250 ml/day	3 (16.7)	8 (47.1)		
Female				
<250 ml/day	16 (72.7)	20 (66.7)	1.333 (0.417–4.429)	0.765
≥250 ml/day	6 (27.3)	10 (33.3)		

composition from sebum. In male subjects, IGF1 levels were positively correlated with SFA (C12:0, C14:0, C15:0, C17:0, C18:0, C19:0, C20:0, C22:0, C23:0) and MUFA (C14:1, C15:1, C16:1n10, C17:1) levels in sebum from the forehead (**Figure 4A**). Meanwhile, IGF1 levels were positively correlated with SFA (C18:0) levels from the chin (**Figure 4B**). However, IGF1 levels showed no correlation with FA composition from sebum in females (**Supplementary Figure S2**). Previous studies showed that milk consumption was positively associated with circulating IGF-1 levels (Melnik and Schmitz, 2009). We found that the frequent consumption of milk, 250 ml or more per day, was associated with acne in categorical analysis in both genders, although it did not reach statistical significance (**Table 3**).

DISCUSSION

Acne is a common dermatosis characterized by increased sebum production and inflammatory response (Melnik, 2015). It frequently occurs in teenagers and continues to late adolescence or early adulthood (Collier et al., 2008). Teenagers are prone to have numerous inflammatory and non-inflammatory comedonal lesions in T-zone (forehead, nose, and upper cheeks); however, the female type of adult acne presents deep-seated, long-lasting small nodules and cysts in the U-zone (chin, jawline, and neck) (Holzmann and Shakery, 2014; Dreno et al., 2018). Emerging studies have focused an SSL abnormity in both juvenile acne and adult acne (Camera et al., 2016; Zhou et al., 2018) and found that FA variations in sebum play a vital role in the induction of acne inflammation (Zouboulis et al., 2014). Furthermore, FAs in facial sebum can be affected by many factors, including acne severity, age, gender, anatomical site, circadian rhythm, and drug application (Ní Raghallaigh et al., 2012; Cui et al., 2018; Jia et al., 2019; Zhou et al., 2020a; Zhou et al., 2020b; Zhou et al., 2020c). However, the FA alterations in facial sebum remain to be clearly studied. In this study, we systematically analyzed FA levels in facial sebum in the forehead and chin area and in erythrocytes from both male and female acne patients, compared with their gender- and aged-matched control subjects. To the best of our knowledge, this study represents the first study on Chinese populations with moderate acne, who have distinct lifestyles, including dietary habits and environmental exposure, from the Western countries.

FAs can have both pro-inflammatory and anti-inflammatory effects in the context of acne pathogenesis (Balic et al., 2020). SFAs, such as palmitic acid (PA, C16:0), can induce the production of proinflammatory cytokines in sebocytes, keratinocytes, and macrophages (Zhou et al., 2013; Choi et al., 2019). On the other hand, unsaturated fatty acids (UFAs), especially MUFA, including sapienic acid (SA, C16:1n-10), palmitoleic acid (POA, C16:1), and oleic acid (OA, C18:1), have bactericidal activity (Wille and Kydonieus, 2003). However, the potential role of SA which is unique to human sebum in the etiology of acne is still controversial and remains to be elucidated. SA can replace LA and result in comedogenesis besides its antimicrobial function (Stewart et al., 1986; Perisho et al., 1988). Furthermore, POA and OA induce calcium influx into keratinocytes and cause abnormal differentiation of the epidermis that characterizes acne (Katsuta et al., 2005). In the current study, we substantiated that levels of SFA and MUFA from sebum were at higher levels in adult female acne patients than in control females, whereas no significant difference in these FAs was observed in male subjects. These observations might partly explain the increased rates of acne in women than men after puberty (Collier et al., 2008). Furthermore, we observed markedly increased levels of SA in the chin of female patients, consistent with the fact that adult women have a specific appearance of U-zone acne.

Notably, FAs consisted of odd carbon that may come from dairy and intestinal bacteria. For example, pentadecanoic acid (C15:0) and heptadecanoic acid (C17:0), which account for only a small proportion of total saturated fatty acids in milk fat and ruminant meat, can also be synthesized endogenously from gut-derived propionic acid (C3:0) (Pfeuffer and Jaudszus, 2016). Fatty acid desaturase 2 (FADS2), highly expressed in the human sebaceous gland, has been shown to convert C17:0 to C17:1 (Wang et al. 2020).

PUFAs are classified as Omega-3 and Omega-6, such as ALA and LA, respectively (Zouboulis et al., 2014). The therapeutic effect of ALA has been attributed to its anti-inflammatory activity (Balic et al., 2020). LA can attenuate the development of comedonal acne, and topical application of LA reduces microcomedones (Nicolaides et al., 1972; Letawe et al., 1998). Interestingly, we found that in the control group, female subjects have much more ALA and LA in the chin than the forehead, but

this trend disappeared in the acne group. Instead, decreased levels of ALA in the chin of females acne patients compared to control females were observed. These data may partially explain why acne lesions are likely to spread on the chin of adult women (Dreno et al., 2018; Muguet Guenot et al., 2018). Thus, it is tempting to speculate that topical application of ALA or LA may be beneficial specifically in female acne patients.

Erythrocytes FAs are known to reflect relatively long-term dietary status (Arab, 2003) and are highly correlated with FA compositions in various tissues (Fenton et al., 2016). Hence, we also analyzed FA profiles of erythrocytes and plasma in acne patients and control subjects. Our data showed the decreased levels of Omega-3 FA in male patients, especially DHA in erythrocytes, compared to the control. It has been reported that an aggravation of acne and changes of FA in sebum were associated with increased intake of a Western diet that contains more saturated fat (Macdonald, 1964; Burris et al., 2014). The ratio of Omega-6/Omega-3 is 15:1 to 16:1 in a Western diet, while the recommended ratio differs from 1:1 up to 4:1 Balic et al., (2020). A high intake of these "danger signals" can activate the nutrient-sensitive kinase mechanistic target of rapamycin complex 1 (mTORC1), which stimulates sterol response element binding protein-1 (SREBP-1) and then upregulates stearoyl-CoA-desaturase (SCD), enhancing the proportion of MUFA in sebum triglycerides during the pathogenesis of acne (Melnik, 2015). Smith RN et al. (Smith et al., 2008) reported that a low glycemic load diet on acne patients was beneficial because it showed a decreased desaturase activity, contributing to a low level of MUFA in SSL. Furthermore, decreased PUFA (eicosapentaenoic acid, EPA) level in acne reveals the presence of a proinflammatory state (Aslan et al., 2017), while supplementing with EPA may be used as adjuvant treatments for acne patients (Jung et al., 2014). In our study, we tried to correlate FA profiles of erythrocytes and sebum and found a distinct pattern of correlation between females and males, suggesting that dietary intervention can be a viable therapeutic approach for male acne patients.

The relationship between IGF1 and acne remains controversial. Some studies reported that IGF1 levels were increased in acne patients (Agamia et al., 2016), while others showed no significant difference in IGF1 levels between acne patients and controls (Cappel et al., 2005; Aktas Karabay et al., 2020). Moreover, Vora et al. (2008) found that serum IGF1 levels were positively correlated with facial sebum excretion and acne lesion counts. However, the correlation between IGF1 levels and FA compositions of facial sebum has never been reported. In this study, we demonstrated that IGF1 levels were positively correlated with SFA and MUFA levels in sebum from male patients with moderate acne. Interestingly, milk consumption appears to be associated with increased IGF1 levels in serum, consistent with previous reports in which IGF1 was positively associated with acne severity in adults (Norat et al., 2007; Roengritthidet et al., 2021) Our study suggests that diets with high IGF1 should be seriously considered during the outbreak of acne due to their direct effect on FA composition of facial sebum, especially for male acne patients.

There are some limitations in this study. The study population was limited to moderate acne patients after puberty and did not include teenagers and mild and severe acne patients. Because the BMI of the enrolled participants was normal and toward lean bodies, observations from this study may not reflect overweight and obese populations. Due to the low levels of EPA and DHA in sebum, these two essential FAs were below the detection limit in sebum FA profiling. Furthermore, inflammatory parameters were not considered in the study. Milk consumption was not categorized into specific milk types, and other dietary intakes need to be included in the dietary questionnaire. Last, this cross-sectional study does not provide dynamic changes during the pathogenesis of acne, and future longitudinal study with multiple time points for follow-ups may provide more mechanistic insights.

In summary, our study has provided evidence that FA alterations in facial sebum in female acne patients can be partially responsible for their higher incidence than males in adulthood. Moreover, altered FA compositions of different anatomical sites resulted in an increased inflammation environment characteristic of U-zone acne in adult women. In addition, we observed distinct patterns of correlations between Omega-3 PUFA in erythrocytes and sebum and correlations between IGF1 levels in serum and sebum in male acne patients. Overall, our study suggests that gender- and site-specific topical application of FA can be used as sebum-modifying treatments, especially for Omega-3 PUFA.

DATA AVAILABILITY STATEMENT

The original contributions presented in the study are included in the article/**Supplementary Material**; further inquiries can be directed to the corresponding authors.

ETHICS STATEMENT

The studies involving human participants were reviewed and approved by the Huashan Hospital Ethics Committee, Fudan University, Shanghai, China. The patients/participants provided their written informed consent to participate in this study.

AUTHOR CONTRIBUTIONS

KC and YL contributed to the conception and design of the study and organized the sample collection. KC and NL contributed to the methodology. KC, XS, and RL performed the statistical analysis. KC wrote the manuscript. HY and LX contributed to supervision and revision. All authors contributed to manuscript revision, read, and approved the submitted version.

FUNDING

This work is supported by grants from the National Natural Science Foundation of China (Grant Numbers 81803154, 32030053, and 32150710522).

ACKNOWLEDGMENTS

The authors are grateful to acne group members in LX's team in Huashan hospital for the assistance during the enrollment

of acne patients and to group members in HY's laboratory in Shanghai Institute of Nutrition and Health for the support of GC-MS methods instruction, and Minye Dong from Shanghai Jiaotong University for the assistance of statistical methods.

SUPPLEMENTARY MATERIAL

The Supplementary Material for this article can be found online at: https://www.frontiersin.org/articles/10.3389/fphys.2022.921866/full#supplementary-material

REFERENCES

Agamia, N. F., Abdallah, D. M., Sorour, O., Mourad, B., and Younan, D. N. (2016). Skin Expression of Mammalian Target of Rapamycin and Forkhead Box Transcription Factor O1, and Serum Insulin-like Growth Factor-1 in Patients with Acne Vulgaris and Their Relationship with Diet. *Br. J. Dermatol* 174 (6), 1299–1307. doi:10.1111/bjd.14409

Akaza, N., Akamatsu, H., Numata, S., Matsusue, M., Mashima, Y., Miyawaki, M., et al. (2014). Fatty Acid Compositions of Triglycerides and Free Fatty Acids in Sebum Depend on Amount of Triglycerides, and Do Not Differ in Presence or Absence of Acne Vulgaris. *J. Dermatol* 41 (12), 1069–1076. doi:10.1111/1346-8138.12699

Aktas Karabay, E., Saltik, Z. A., and Unay Demirel, O. (2020). Evaluation of Serum FoxO1, mTORC1, IGF-1, IGFBP-3 Levels, and Metabolic Syndrome Components in Patients with Acne Vulgaris: A Prospective Case-Control Study. *Dermatol Ther.* 33 (6), e13887. doi:10.1111/dth.13887

Arab, L. (2003). Biomarkers of Fat and Fatty Acid Intake. *J. Nutr.* 133 Suppl 3 (3), 925S–932S. doi:10.1093/jn/133.3.925S

Aslan, İ., Özcan, F., Karaarslan, T., Kıraç, E., and Aslan, M. (2017). Decreased Eicosapentaenoic Acid Levels in Acne Vulgaris Reveals the Presence of a Proinflammatory State. *Prostagl. Other Lipid Mediat.* 128-129, 1–7. doi:10.1016/j.prostaglandins.2016.12.001

Balic, A., Vlasic, D., Zuzul, K., Marinović, B., and Mokos, Z. B. (2020). Omega-3 versus Omega-6 Polyunsaturated Fatty Acids in the Prevention and Treatment of Inflammatory Skin Diseases. *Int. J. Mol. Sci.* 21 (3), 741. doi:10.3390/ijms21030741

Burris, J., Rietkerk, W., and Woolf, K. (2014). Relationships of Self-Reported Dietary Factors and Perceived Acne Severity in a Cohort of New York Young Adults. *J. Acad. Nutr. Dietetics* 114 (3), 384–392. doi:10.1016/j.jand.2013.11.010

Camera, E., Ludovici, M., Tortorella, S., Sinagra, J.-L., Capitanio, B., Goracci, L., et al. (2016). Use of Lipidomics to Investigate Sebum Dysfunction in Juvenile Acne. *J. Lipid Res.* 57 (6), 1051–1058. doi:10.1194/jlr.m067942

Cappel, M., Mauger, D., and Thiboutot, D. (2005). Correlation between Serum Levels of Insulin-like Growth Factor 1, Dehydroepiandrosterone Sulfate, and Dihydrotestosterone and Acne Lesion Counts in Adult Women. *Archives Dermatology* 141 (3), 333–338. doi:10.1001/archderm.141.3.333

Choi, C. W., Kim, Y., Kim, J. E., Seo, E. Y., Zouboulis, C. C., Kang, J. S., et al. (2019). Enhancement of Lipid Content and Inflammatory Cytokine Secretion in SZ95 Sebocytes by Palmitic Acid Suggests a Potential Link between Free Fatty Acids and Acne Aggravation. *Exp. Dermatol* 28 (2), 207–210. doi:10.1111/exd.13855

Collier, C. N., Harper, J. C., Cantrell, W. C., Wang, W., Foster, K. W., and Elewski, B. E. (2008). The Prevalence of Acne in Adults 20 Years and Older. *J. Am. Acad. Dermatology* 58 (1), 56–59. doi:10.1016/j.jaad.2007.06.045

Cui, L., He, C. f., Fan, L. n., and Jia, Y. (2018). Application of Lipidomics to Reveal Differences in Facial Skin Surface Lipids between Males and Females. *J. Cosmet. Dermatol* 17 (6), 1254–1261. doi:10.1111/jocd.12474

Dreno, B., Bagatin, E., Blume-Peytavi, U., Rocha, M., and Gollnick, H. (2018). Female Type of Adult Acne: Physiological and Psychological Considerations and Management. *JDDG J. der Deutschen Dermatologischen Gesellschaft* 16 (10), 1185–1194. doi:10.1111/ddg.13664

Fenton, J. I., Gurzell, E. A., Davidson, E. A., and Harris, W. S. (2016). Red Blood Cell PUFAs Reflect the Phospholipid PUFA Composition of Major Organs. *Prostagl. Leukot. Essent. Fat. Acids* 112, 12–23. doi:10.1016/j.plefa.2016.06.004

Holzmann, R., and Shakery, K. (2014). Postadolescent Acne in Females. *Skin. Pharmacol. Physiol.* 27 Suppl 1, 3–8. doi:10.1159/000354887

Jia, Y., Zhou, M., Huang, H., Gan, Y., Yang, M., and Ding, R. (2019). Characterization of Circadian Human Facial Surface Lipid Composition. *Exp. Dermatol* 28 (7), 858–862. doi:10.1111/exd.13933

Ju, Q., Tao, T., Hu, T., Karadağ, A. S., Al-Khuzaei, S., and Chen, W. (2017). Sex Hormones and Acne. *Clin. Dermatology* 35 (2), 130–137. doi:10.1016/j.clindermatol.2016.10.004

Jung, J., Kwon, H., Hong, J., Yoon, J., Park, M., Jang, M., et al. (2014). Effect of Dietary Supplementation with Omega-3 Fatty Acid and Gamma-Linolenic Acid on Acne Vulgaris: a Randomised, Double-Blind, Controlled Trial. *Acta Derm. Venerol.* 94 (5), 521–525. doi:10.2340/00015555-1802

Katsuta, Y., Iida, T., Inomata, S., and Denda, M. (2005). Unsaturated Fatty Acids Induce Calcium Influx into Keratinocytes and Cause Abnormal Differentiation of Epidermis. *J. Investigative Dermatology* 124 (5), 1008–1013. doi:10.1111/j.0022-202x.2005.23682.x

Letawe, C., Boone, M., and Piérard, G. E. (1998). Digital Image Analysis of the Effect of Topically Applied Linoleic Acid on Acne Microcomedones. *Clin. Exp. Dermatology* 23 (2), 56–58. doi:10.1046/j.1365-2230.1998.00315.x

Liu, G., Wang, N., Zhang, C., Li, M., He, X., Yin, C., et al. (2021). Fructose-1,6-Bisphosphate Aldolase B Depletion Promotes Hepatocellular Carcinogenesis through Activating Insulin Receptor Signaling and Lipogenesis. *Hepatology* 74 (6), 3037–3055. doi:10.1002/hep.32064

Macdonald, I. (1964). Changes in the Fatty Acid Composition of Sebum Associated with High Carbohydrate Diets. *Nature* 203, 1067–1068. doi:10.1038/2031067b0

Melnik, B. C., and Schmitz, G. (2009). Role of Insulin, Insulin-like Growth Factor-1, Hyperglycaemic Food and Milk Consumption in the Pathogenesis of Acne Vulgaris. *Exp. Dermatol* 18 (10), 833–841. doi:10.1111/j.1600-0625.2009.00924.x

Melnik, B. (2015). Linking Diet to Acne Metabolomics, Inflammation, and Comedogenesis: an Update. *Ccid* 8, 371–388. doi:10.2147/ccid.s69135

Muguet Guenot, L., Vourc'h Jourdain, M., Saint-Jean, M., Corvec, S., Gaultier, A., Khammari, A., et al. (2018). Confocal Microscopy in Adult Women with Acne. *Int. J. Dermatol* 57 (3), 278–283. doi:10.1111/ijd.13910

Ní Raghallaigh, S., Bender, K., Lacey, N., Brennan, L., and Powell, F. C. (2012). The Fatty Acid Profile of the Skin Surface Lipid Layer in Papulopustular Rosacea. *Br. J. Dermatol* 166 (2), 279–287. doi:10.1111/j.1365-2133.2011.10662.x

Nicolaides, N., Fu, H. C., Ansari, M. N. A., and Rice, G. R. (1972). The Fatty Acids of Wax Esters and Sterol Esters from Vernix Caseosa and from Human Skin Surface Lipid. *Lipids* 7 (8), 506–517. doi:10.1007/bf02533016

Norat, T., Dossus, L., Rinaldi, S., Overvad, K., Grønbæk, H., Tjønneland, A., et al. (2007). Diet, Serum Insulin-like Growth Factor-I and IGF-Binding Protein-3 in European Women. *Eur. J. Clin. Nutr.* 61 (1), 91–98. doi:10.1038/sj.ejcn.1602494

Nordstrom, K. M., Schmus, H. G., McGinley, K. J., and Leyden, J. J. (1986). Measurement of Sebum Output Using a Lipid Absorbent Tape. *J. Investigative Dermatology* 87 (2), 260–263. doi:10.1111/1523-1747.ep12696640

Ottaviani, M., Camera, E., and Picardo, M. (2010). Lipid Mediators in Acne. *Mediat. Inflamm.* 2010, 858176. doi:10.1155/2010/858176

Perisho, K., Wertz, P. W., Madison, K. C., Stewart, M. E., and Downing, D. T. (1988). Fatty Acids of Acylceramides from Comedones and from the Skin Surface of Acne Patients and Control Subjects. *J. Investigative Dermatology* 90 (3), 350–353. doi:10.1111/1523-1747.ep12456327

Pfeuffer, M., and Jaudszus, A. (2016). Pentadecanoic and Heptadecanoic Acids: Multifaceted Odd-Chain Fatty Acids. *Adv. Nutr.* 7 (4), 730–734. doi:10.3945/an.115.011387

Piérard, G. E., Piérard-Franchimont, C., Marks, R., Paye, M., and Rogiers, V. (2000). EEMCO Guidance for the *In Vivo* Assessment of Skin Greasiness. The EEMCO Group. *Skin. Pharmacol. Physiol.* 13 (6), 372–389. doi:10.1159/000029945

Roengritthidet, K., Kamanamool, N., Udompataikul, M., Rojhirunsakool, S., Khunket, S., and Kanokrungsee, S. (2021). Association between Diet and Acne Severity: A Cross-Sectional Study in Thai Adolescents and Adults. *Acta Derm. Venereol.* 101 (12), adv00611. doi:10.2340/actadv.v101.569

Skroza, N., Tolino, E., Mambrin, A., Zuber, S., Balduzzi, V., Marchesiello, A., et al. (2018). Adult Acne versus Adolescent Acne: A Retrospective Study of 1,167 Patients. *J. Clin. Aesthet. Dermatol* 11 (1), 21

Smith, R. N., Braue, A., Varigos, G. A., and Mann, N. J. (2008). The Effect of a Low Glycemic Load Diet on Acne Vulgaris and the Fatty Acid Composition of Skin Surface Triglycerides. *J. Dermatological Sci.* 50 (1), 41–52. doi:10.1016/j.jdermsci.2007.11.005

Stewart, M. E., Grahek, M. O., Cambier, L. S., Wertz, P. W., and Downing, D. T. (1986). Dilutional Effect of Increased Sebaceous Gland Activity on the Proportion of Linoleic Acid in Sebaceous Wax Esters and in Epidermal Acylceramides. *J. Investigative Dermatology* 87 (6), 733–736. doi:10.1111/1523-1747.ep12456856

Vora, S., Ovhal, A., Jerajani, H., Nair, N., and Chakrabortty, A. (2008). Correlation of Facial Sebum to Serum Insulin-like Growth Factor-1 in Patients with Acne. *Br. J. Dermatol* 159 (4), 990–991. doi:10.1111/j.1365-2133.2008.08764.x

Wang, Z., Park, H. G., Wang, D. H., Kitano, R., Kothapalli, K. S. D., and Brenna, J. T. (2020). Fatty Acid Desaturase 2 (FADS2) but Not FADS1 Desaturates Branched Chain and Odd Chain Saturated Fatty Acids. *Biochimica Biophysica Acta (BBA) - Mol. Cell Biol. Lipids* 1865 (3), 158572. doi:10.1016/j.bbalip.2019.158572

Wille, J. J., and Kydonieus, A. (2003). Palmitoleic Acid Isomer (C16:1Δ6) in Human Skin Sebum Is Effective against Gram-Positive Bacteria. *Skin. Pharmacol. Physiol.* 16 (3), 176–187. doi:10.1159/000069757

Zaenglein, A. L., Pathy, A. L., Schlosser, B. J., Alikhan, A., Baldwin, H. E., Berson, D. S., et al. (2016). Guidelines of Care for the Management of Acne Vulgaris. *J. Am. Acad. Dermatology* 74 (5), 945–973. doi:10.1016/j.jaad.2015.12.037

Zhou, B. R., Zhang, J. A., Zhang, Q., Permatasari, F., Yang, X., Wu, D., et al. (2013). Palmitic Acid Induces Production of Proinflammatory Cytokines Interleukin-6, Interleukin-1beta, and Tumor Necrosis Factor-Alpha via a NF-kappaB-dependent Mechanism in HaCaT Keratinocytes. *Mediat. Inflamm.* 2013, 530429. doi:10.1155/2013/530429

Zhou, M., Gan, Y., Yang, M., He, C., and Jia, Y. (2020). Lipidomics Analysis of Facial Skin Surface Lipids between Forehead and Cheek: Association between Lipidome, TEWL, and pH. *J. Cosmet. Dermatol* 19 (10), 2752–2758. doi:10.1111/jocd.13345

Zhou, M., Gan, Y., He, C., Chen, Z., and Jia, Y. (2018). Lipidomics Reveals Skin Surface Lipid Abnormity in Acne in Young Men. *Br. J. Dermatol* 179 (3), 732–740. doi:10.1111/bjd.16655

Zhou, M., Wang, H., Yang, M., He, C., Yang, M., Gao, Y., et al. (2020). Lipidomic Analysis of Facial Skin Surface Lipids Reveals an Altered Lipid Profile in Infant Acne. *Br. J. Dermatol* 182 (3), 817–818. doi:10.1111/bjd.18474

Zhou, M., Yang, M., Zheng, Y., Dong, K., Song, L., He, C., et al. (2020). Skin Surface Lipidomics Revealed the Correlation between Lipidomic Profile and Grade in Adolescent Acne. *J. Cosmet. Dermatol* 19 (12), 3349–3356. doi:10.1111/jocd.13374

Zouboulis, C. C., Jourdan, E., and Picardo, M. (2014). Acne Is an Inflammatory Disease and Alterations of Sebum Composition Initiate Acne Lesions. *J. Eur. Acad. Dermatol Venereol.* 28 (5), 527–532. doi:10.1111/jdv.12298

Conflict of Interest: The authors declare that the research was conducted in the absence of any commercial or financial relationships that could be construed as a potential conflict of interest.

Publisher's Note: All claims expressed in this article are solely those of the authors and do not necessarily represent those of their affiliated organizations, or those of the publisher, the editors, and the reviewers. Any product that may be evaluated in this article, or claim that may be made by its manufacturer, is not guaranteed or endorsed by the publisher.

frontiers | Frontiers in Physiology

REVIEW
published: 05 July 2022
doi: 10.3389/fphys.2022.940974

Pathogenesis of Alcohol-Associated Fatty Liver: Lessons From Transgenic Mice

*Afroza Ferdouse and Robin D. Clugston**

Department of Physiology, University of Alberta, Edmonton, AB, Canada

Alcohol-associated liver disease (ALD) is a major public health issue that significantly contributes to human morbidity and mortality, with no FDA-approved therapeutic intervention available. The health burden of ALD has worsened during the COVID-19 pandemic, which has been associated with a spike in alcohol abuse, and a subsequent increase in hospitalization rates for ALD. A key knowledge gap that underlies the lack of novel therapies for ALD is a need to better understand the pathogenic mechanisms that contribute to ALD initiation, particularly with respect to hepatic lipid accumulation and the development of fatty liver, which is the first step in the ALD spectrum. The goal of this review is to evaluate the existing literature to gain insight into the pathogenesis of alcohol-associated fatty liver, and to synthesize alcohol's known effects on hepatic lipid metabolism. To achieve this goal, we specifically focus on studies from transgenic mouse models of ALD, allowing for a genetic dissection of alcohol's effects, and integrate these findings with our current understanding of ALD pathogenesis. Existing studies using transgenic mouse models of ALD have revealed roles for specific genes involved in hepatic lipid metabolic pathways including fatty acid uptake, mitochondrial β-oxidation, *de novo* lipogenesis, triglyceride metabolism, and lipid droplet formation. In addition to reviewing this literature, we conclude by identifying current gaps in our understanding of how alcohol abuse impairs hepatic lipid metabolism and identify future directions to address these gaps. In summary, transgenic mice provide a powerful tool to understand alcohol's effect on hepatic lipid metabolism and highlight that alcohol abuse has diverse effects that contribute to the development of alcohol-associated fatty liver disease.

Keywords: alcohol, alcohol-associated fatty liver disease, steatosis, fatty acid uptake, *de novo* lipogenesis, mitochondrial beta-oxidation, triglyceride metabolism

OPEN ACCESS

Edited by:
Xian-Cheng Jiang,
SUNY Downstate Medical Center, United States

Reviewed by:
Jue Jia,
Nanjing Medical University, China
Qing Miao,
New York University, United States

****Correspondence:***
Robin D. Clugston
clugston@ualberta.ca

Specialty section:
This article was submitted to Lipid and Fatty Acid Research, a section of the journal Frontiers in Physiology

Received: *10 May 2022*
Accepted: *15 June 2022*
Published: *05 July 2022*

Citation:
Ferdouse A and Clugston RD (2022) Pathogenesis of Alcohol-Associated Fatty Liver: Lessons From Transgenic Mice. Front. Physiol. 13:940974. doi: 10.3389/fphys.2022.940974

INTRODUCTION

Chronic excess alcohol consumption is a major public health issue, and one of the leading causes of liver disease (Sherlock and Dooley, 2008; Bruha et al., 2012; WHO, 2018). Excess alcohol consumption is associated with the development of alcohol-associated liver disease (ALD), which includes a well-described spectrum of disease ranging from hepatic fat accumulation (steatosis) to cirrhosis and hepatocellular carcinoma (Miller et al., 2011; Ceni et al., 2014). It is estimated that 1 in 3 people drink alcohol around the world (GBD 2016 Alcohol Collaborators, 2018). While drinking patterns vary from country to country, the overall health burden of alcohol use

TABLE 1 | Summary of study design and key findings from transgenic mouse models of ALD.

Author, year (PMID)	Gene (background)	Sex	Alcohol feeding protocol	ALD phenotype	Putative mechanism
Clugston et al. (2014) (24280415)	*Cd36*$^{-/-}$(C57BL/6)	Male	LDeC, 5.1% (v/v) alcohol, 6 weeks	Alleviated	Impaired FA uptake (?), decreased DNL
Nakajima et al. (2004) (15382117)	*Pparα*$^{-/-}$ (Sv/129)	Male	LDeC, 4.0% (v/v) alcohol, 6 months	Worsened	Impaired mitochondrial β-oxidation
Ji et al. (2006) (16879892)	*Srebp1c*$^{-/-}$ (mixed)	Male	Intragastric infusion, 4.4% (v/v), 4 weeks	Alleviated	Decreased DNL
Lounis et al. (2016) (27477676)	*Scd1*$^{-/-}$ (C57BL/6N)	Male	LDeC, 5.0% (v/v) alcohol, 10 days plus binge (5 g/kg)	Alleviated	Decreased DNL
Zhang et al. (2016) (27062444)	PPARγΔ-Hep (mixed)	Male	LDeC, 5.6% (v/v) alcohol, 8 weeks	Alleviated	Decreased DNL, decreased TG synthesis
Huang et al. (2018) (30192394)	*Dgat1*$^{-/-}$ (C57BL/6)	Male	LDeC, 5.1% (v/v) alcohol, 6 weeks	Alleviated	Decreased TG synthesis
Xu et al. (2016) (27075303)	*Ces1*$^{-/-}$ (C57BL/6J)	Not mentioned	LDeC, 5.0% (v/v) alcohol, 10 days plus binge (3 g/kg)	Worsened	Increased DNL, impaired mitochondrial β-oxidation
Carr et al. (2014) (24831094)	*Plin2*$^{-/-}$ (C57BL/6J)	Male	LDeC, 2.71% (v/of calories from alcohol, 6 weeks	Alleviated	Impaired LD formation

is high, and ranks in the top ten risk factors for death and disability-adjusted life-years (DALYs) GBD 2016 Alcohol Collaborators (2018). Alcohol consumption and abuse are prevalent in North America. In the United States, 85.6% of adults reported drinking alcohol at some point in life, and 25.8% drink heavily (Redlich et al., 1998). In Canada, 78.2% of the total population reported drinking alcohol in the past year and 19.1% reported heavy drinking (Canadian Center on Substance Use and Addiction, 2019). According to the World Health Organization (WHO), global alcohol consumption including that in the United States and Canada is predicted to further increase by 2025 (WHO, 2018). While alcohol has always historically been associated with ALD, this health burden has worsened during the COVID-19 pandemic, which has been associated with a spike in alcohol abuse, and a subsequent increase in hospitalization rates for ALD (Shaheen et al., 2021; Sohal et al., 2021; Stockwell et al., 2021).

Strikingly, there are no FDA-approved therapies for the treatment of ALD (Osna et al., 2017; Singal and Shah, 2019). This represents an unmet need to treat patients with ALD and has its origins in an incomplete understanding of ALD pathogenesis. The initial phase of ALD is the development of hepatic steatosis, which develops in approximately 90%–100% of heavy drinkers (consuming ≥60 g/day of alcohol) and predisposes these individuals to more severe liver disease (Crabb, 1999; Mann et al., 2003; Singal and Shah, 2019). Alcohol is known to have wide-ranging effects on hepatic lipid metabolism leading to the accumulation of hepatic fat, as recently reviewed by others (You and Arteel 2019; Jeon and Carr 2020; Hyun et al., 2021).

The goal of this review is to evaluate the existing literature to gain insight into the pathogenesis of alcohol-associated fatty liver, with a specific emphasis on information garnered from transgenic mouse models (summarized in **Table 1**). This approach allows for a genetic dissection of alcohol's effects on hepatic lipid metabolism, which we integrate with our current understanding of ALD pathogenesis in humans. In addition to reviewing this literature, we aim to discuss the limitations of working with transgenic mouse models, identify current gaps in our understanding of how alcohol abuse impairs hepatic lipid metabolism, and identify future directions to address these gaps.

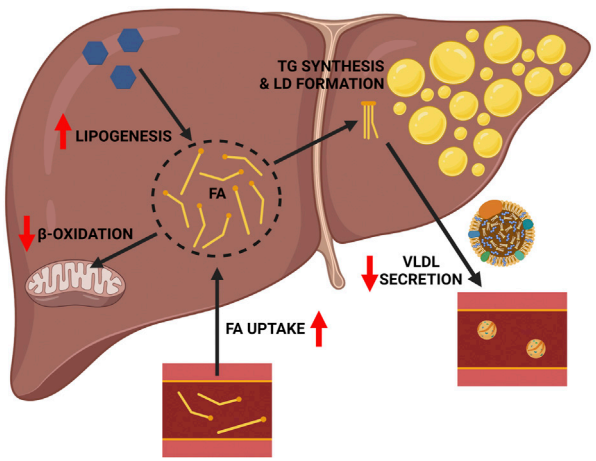

FIGURE 1 | General mechanisms linking chronic alcohol consumption with hepatic lipid accumulation. Chronic alcohol consumption impacts hepatic lipid metabolism and drives the accumulation of hepatic triglycerides in several ways, including: 1) increased FA uptake, 2) decreased mitochondrial β-oxidation, and 3) increased hepatic *de novo* lipogenesis. These effects increase the hepatic FA pool available for esterification into triglyceride and lipid droplet formation. This effect is further compounded by 4) decreased VLDL triglyceride secretion. Red arrows indicate the detrimental effects of alcohol. Image created with BioRender.com.

ALCOHOL'S EFFECTS ON HEPATIC LIPID METABOLISM

The liver is of central importance in whole-body lipid metabolism in mammals (Alves-Bezerra and Cohen, 2017). The liver also serves as the primary organ for alcohol detoxification, the metabolic burden of which directly and indirectly affects the complex and interconnected pathways of hepatic lipid

metabolism, precipitating the development of hepatic steatosis. As reviewed elsewhere (You and Arteel, 2019; Jeon and Carr, 2020), alcohol impacts multiple aspects of hepatic lipid metabolism including increased hepatic fatty acid (FA) uptake, increased hepatic *de novo* lipogenesis (DNL), decreased mitochondrial β-oxidation, and decreased very low density lipoprotein (VLDL) secretion, the net effect of which is increased hepatic lipid accumulation (**Figure 1**). In terms of increased hepatic FA uptake, chronic alcohol consumption increases adipose tissue lipolysis, which leads to an increase in circulatory free FA available for hepatic uptake (Kang et al., 2007; Zhong et al., 2012; Wei et al., 2013). Regarding DNL, the predominant mechanism is alcohol-induced activation of sterol regulatory element binding protein 1 (SREBP1c), a transcriptional regulator of multiple genes in the DNL pathway, including Acetyl CoA Carboxylase (*Acc*), FA Synthase (*Fasn*), and Stearoyl CoA Desaturase 1 (*Scd1*) (You et al., 2002). Alcohol's ability to impair mitochondrial β-oxidation is multifactorial, but is primarily driven by two factors: first, an increase in the hepatic NADH:NAD + ratio secondary to alcohol oxidation, favoring this process over FA oxidation (Lieber, 1988); and second, by decreasing Peroxisome Proliferation Activator Receptor-α (PPARα) activity, a transcriptional regulator of several genes associated with mitochondrial β-oxidation (Nanji et al., 2004). Alcohol's ability to impair VLDL secretion is linked to impaired lipidation of Apo-B, resulting in reduced VLDL particle formation and export of hepatic lipids (Sugimoto et al., 2002; Kharbanda et al., 2012). As noted above, these broad effects of alcohol on hepatic lipid metabolism leads to an increase in the hepatic FA pool, which can be esterified and stored in lipids droplets as triglycerides (TGs). The following sections will further explore each of these pathways, and the importance of using transgenic mice to understand their contribution to ALD.

HEPATIC FA UPTAKE

Chronic alcohol consumption induces the lipolysis of TGs stored in white adipose tissue (WAT), which enter the circulation and can be taken up by the liver (**Figure 1**). Insulin is the major hormone that supresses adipose lipolysis (Stumvoll et al., 2001). Chronic ethanol feeding induces insulin resistance that markedly impairs the anti-lipolytic effects of insulin in WAT, enhancing TG breakdown to release free FA into the circulation (Kang et al., 2007). Circulating free FAs derived from adipose lipolysis are directly taken up by hepatocytes with the help of FA transport proteins (FATPs) or FA translocase/CD36 (Kang et al., 2007; Jeon and Carr, 2020). Among the multiple FATP family members, FATP2 and FATP5 are highly expressed in the liver (Stahl et al., 2001). CD36 expression is normally low in the healthy liver but its expression is induced in the alcohol exposed liver (Ge et al., 2010; Clugston et al., 2011; Ronis et al., 2011; Zhong et al., 2012). This observation led to the hypothesis that alcohol-induced upregulation of CD36 promotes the uptake of circulating FAs, contributing to the development of alcohol-associated fatty liver. Clugston et al. (2014) tested this hypothesis in *Cd36*$^{-/-}$ mice consuming a low-fat/high carbohydrate Lieber-DeCarli (LDeC) liquid diet with 5.1% (v/v) alcohol for 6 weeks. Importantly, the blood alcohol concentration was not different between alcohol fed wild-type (WT) and *Cd36*$^{-/-}$ mice, indicating no effect of CD36 deficiency on ethanol metabolism. Histological and biochemical analysis of hepatic TGs clearly demonstrated that CD36 deficiency had a protective role in the development of alcohol-associated steatosis. However, follow-up analysis indicated that this protective effect was not linked to altered FA uptake, and no compensatory changes in the expression level of *Fatp2* or *Fatp5* were observed in *Cd36*$^{-/-}$ mice. Interestingly, expression studies examining the DNL pathway and *in vivo* kinetic studies indicated that the rate of hepatic DNL was reduced in *Cd36*$^{-/-}$ mice. This data suggested that in alcohol consuming WT mice, a higher rate of DNL provided additional FA for TG synthesis, a finding that was underscored by a significant increase in *Dgat2* expression only in alcohol-fed WT mice, a TG synthesizing enzyme that is known to be coupled to DNL (Wurie et al., 2012). Thus, genotype-specific changes in DNL were the major contributor to the protective effect of CD36 deficiency. Indeed, this link between CD36 and DNL was recently elucidated and linked to CD36's ability to regulate SREBP1c, a key transcriptional regulator of the DNL pathway (Zeng et al., 2022).

In summary, alcohol feeding studies in *Cd36*$^{-/-}$ mice indicate that CD36 is important in the pathogenesis of ALD, although a direct effect on hepatic FA uptake was ruled out (Clugston et al., 2014). It is important to highlight that this study was conducted in mice consuming the low-fat/high carbohydrate formulation of LDeC liquid diets. As discussed below, this lipogenic diet may favor hepatic DNL as a driver of hepatic lipid accumulation as opposed to increased hepatic FA uptake, which might be more associated with the high-fat/low carbohydrate formulation of the LDeC liquid diet. The pathogenesis of ALD in *Cd36*$^{-/-}$ mice consuming the high-fat/low carbohydrate formulation of the LDeC liquid diet has not been reported. The existing literature supports a role for increased hepatic uptake in the pathogenesis of ALD, which is coupled to increased WAT lipolysis (Kang et al., 2007). The importance of this pathway was recently highlighted when it was shown that modulating FA disposal *via* brown adipose tissue impacted the severity of ALD (Shen et al., 2019). The question remains, what is the primary mediator of hepatic FA uptake in the alcohol-exposed liver, and can this be targeted to ameliorate ALD? While FATP2 and FATP5 are possible candidates their role in ALD has not been directly studied and requires further investigation.

MITOCHONDRIAL β-OXIDATION

Alcohol's ability to impair mitochondrial β-oxidation is another mechanism that can contribute to channeling of hepatic FAs toward TGs formation and the development of hepatic steatosis. As reviewed elsewhere (Jeon and Carr, 2020), there are different mechanisms through which alcohol inhibits mitochondrial β-oxidation, although one of the primary ways is thought to be by decreasing PPARα activity (Wan et al., 1995; Galli et al., 2001;

Fischer et al., 2003; Jeon and Carr, 2020). PPARα is an important transcriptional regulator of several genes associated with mitochondrial β-oxidation (Yu et al., 2003), and free FAs and their derivatives serve as ligands for PPARα and activate PPARα signaling to stimulate mitochondrial β-oxidation of hepatic FAs (Keller et al., 1993; Forman et al., 1997).

The central role of PPARα signaling in hepatic lipid metabolism and data linking ALD with altered PPARα activity has led to extensive investigations into the role of PPARα in the pathogenesis of ALD. Indeed, earlier studies in mice showed that ethanol feeding impaired the activity of PPARα resulting in decreased expression of PPARα target genes related to FA β-oxidation (Fischer et al., 2003). Moreover, treatment with a PPARα agonist (Wy14,643) restored the activation of PPARα and target gene expression, thereby increasing FA β-oxidation in alcohol fed mice and preventing steatosis formation (Fischer et al., 2003). Similarly, downregulated PPARα responsive genes have also been reported in alcohol fed rats, which corresponded to increased steatosis and liver injury, and that PPARα activation with Clofibrate restores the expression of PPARα regulated genes, and reduces steatosis severity and markers of ALD (Nanji et al., 2004).

With growing evidence linking altered PPARα activity with ALD, studies leveraging transgenic mice were conducted. In 2004, Nakajima et al. reported that ALD is worsened in *Ppara*$^{-/-}$ mice (Nakajima et al., 2004). These authors fed WT and *Ppara*$^{-/-}$ mice 4% (v/v) ethanol containing LDeC liquid diets for 6 months. At the end of the study period liver injury was markedly more pronounced in alcohol consuming *Ppara*$^{-/-}$ mice, including worsened hepatomegaly and evidence of severe hepatocyte damage, inflammation, and fibrosis that was not observed in WT mice. The authors concluded that loss of PPARα exacerbated ALD through several mechanisms including acetaldehyde accumulation, impaired antioxidant capacity of the liver, and potentiated proinflammatory signaling *via* NF-κB. Regarding steatosis, baseline levels of hepatic TGs were higher in the *Ppara*$^{-/-}$ mice, which is in accord with the phenotype of these mice (Kersten et al., 1999); however, the authors noted that while hepatic TG levels increased to a similar extent after 6 months of alcohol feeding, analysis at earlier time points showed that hepatic TG accumulation was higher in the *Ppara*$^{-/-}$ mice compared to WT. This led the authors to suggest that PPARα's ability to dispose of hepatic FA, *via* mitochondrial β-oxidation, is another important mechanism through which PPARα deficiency exacerbates ALD, and that this pathway may be a significant contributor to the development of steatohepatitis.

With the establishment of *Ppara*$^{-/-}$ mice as a model of severe ALD, this transgenic mouse has been further used to study the pathogenesis of ALD. The importance of oxidative stress in ALD was highlighted in alcohol consuming *Ppara*$^{-/-}$ mice treated with the antioxidant polyenephosphatidylcholine (PPC) (Okiyama et al., 2009). This study showed that PPC treatment ameliorated severe ALD in *Ppara*$^{-/-}$ mice, including reduced markers of hepatocyte damage and death, inflammation, and fibrosis; however, PPC treatment did not improve markers of hepatic steatosis. The beneficial effect of PPC treatment was linked to decreased expression of enzymes associated with the generation of reactive oxygen species (i.e., CYP2E1), and improved markers of hepatic oxidative stress. The link between alcohol's effects on PPARα and hepatic lipid metabolism has also been further explored in *Ppara*$^{-/-}$ mice (Li et al., 2014). Li et al. (2014) confirmed that alcohol consumption is associated with a downregulation of PPARα activity, decreased mitochondrial β-oxidation, and the development of steatosis. The role of PPARα was emphasized by the exacerbation of ALD in *Ppara*$^{-/-}$ mice, as evidenced by increased markers of TG accumulation, inflammation, and fibrosis. The authors of this study concluded that PPARα played a protective role in ALD, that was primarily mediated through enhanced mitochondrial function, including mitochondrial β-oxidation.

As a regulator of mitochondrial β-oxidation, it is clear that altered PPARα activity is an important factor in the pathogenesis of alcohol-associated fatty liver, although it is equally clear that PPARα deficiency exacerbates ALD through multiple mechanisms in addition to impaired FA disposal (Nakajima et al., 2004). In their paper, Nakajima and colleagues highlighted that alcohol fed *Pparα*$^{-/-}$ mice showed many pathogenic hallmarks of ethanol toxicity that mirror human cases of advanced ALD (Nakajima et al., 2004). While data from human ALD is limited, there is evidence of reduced functional PPARα in the human liver, which may partly explain why humans are more susceptible to ethanol-induced liver toxicity than rodents (Tugwood et al., 1996; Hertz and Bar-Tana, 1998; Palmer et al., 1998). Interestingly, although PPARα agonism has shown to ameliorate ALD in rodent models (Fischer et al., 2003; Nanji et al., 2004), this work has not thus far been translated into humans, despite its potential as a novel therapeutic in ALD (Li et al., 2014). Interestingly, while targeting PPARα may have a beneficial effect in the liver, there may be additional benefits to targeting PPARα in the context of human ALD, including reduced ethanol consumption (Barson et al., 2009; Blednov et al., 2015). In closing, while genetic manipulation of PPARα provides key evidence for the importance of FA oxidation in the pathogenesis of ALD, the broad effects of this transcription factor limit the interpretation of this data. To our knowledge, genetic manipulation of other key factors involved in FA oxidation have not been reported.

DE NOVO LIPOGENESIS

The process by which liver synthesizes FA from non-lipid precursor molecules is called DNL. Catabolism of non-lipid precursors such as glucose, and even ethanol, can generate pyruvate to contribute to the TCA cycle, which is subsequently converted to Acetyl CoA and used for the synthesis of FAs (Siler et al., 1999; Yamashita et al., 2001; Ameer et al., 2014; Charidemou et al., 2019). Key transcriptional regulators of DNL include SREBP1c and ChREBP (carbohydrate responsive element binding protein). These transcription factors modulate the expression of key

enzymes in the DNL pathway including *Acc*, *Fasn*, and *Scd1* (Denechaud et al., 2008). As introduced above, it is thought that upregulation of the DNL pathway is one of the contributors to the development of hepatic steatosis in ALD. Indeed, the literature includes reports of increased *Srebp1c*, *Acc*, *Scd1*, and *Fasn* expression in the alcohol exposed liver (Foufelle and Ferre, 2002; Ntambi et al., 2002; You et al., 2002; MacDonald et al., 2008; Huang et al., 2013; Lounis et al., 2016). As discussed below, key insight into the role of altered DNL in ALD comes from alcohol feeding studies in *Srebp1c*$^{-/-}$ and *Scd1*$^{-/-}$ mice.

Evidence From *Srebp1c*$^{-/-}$ Mice

As a transcriptional regulator of multiple key genes in the DNL pathway, analysis of SREBP1c's contribution to the pathogenesis of ALD is important. Indeed, it has been shown that both acute and chronic alcohol consumption can induce SREBP1c protein and its transcript in mice/rodents (You et al., 2002; Yin et al., 2007). Ji et al. (2006) used *Srebp1c*$^{-/-}$ mice to test the hypothesis that ALD is dependent on SREBP1c. These authors performed their study in WT and *Srebp1c*$^{-/-}$ mice on a C57BL/6 background fed alcohol 4.4% (v/v) for 4 weeks by intragastric infusion. Consistent with the hypothesized role of SREBP1c, *Srebp1c*$^{-/-}$ mice were largely protected from ALD, including ameliorated hepatomegaly, hepatic TG accumulation and inflammation. Mechanistically, it was shown that while alcohol consumption induced markers of hepatic DNL (e.g., ACC), this effect was absent in alcohol fed *Srebp1c*$^{-/-}$ mice, leading to the conclusion that the lipogenic pathway was not activated in these mice, protecting them from hepatic lipid accumulation (Ji et al., 2006). Mechanistically, the authors linked the alcohol associated induction of SREBP1c with endoplasmic reticulum stress secondary to alcohol's effect on homocysteine metabolism, and showed that treatment with betaine, which prevents homocysteine accumulation, prevented SREBP1c induction and ALD (Ji et al., 2006).

Evidence From *Scd1*$^{-/-}$ Mice

SCD1 is a δ-9 FA desaturase which catalyses the formation of monounsaturated fatty acids and is an important contributor to hepatic DNL (Cohen et al., 2002). Several studies have shown that SCD1 deficient mice are protected from the development of non-alcoholic fatty liver disease (NAFLD) (Ntambi et al., 2002; MacDonald et al., 2008). In the context of alcohol abuse, it has been shown that both chronic and binge alcohol consumption increases *Scd1* expression in mice (Huang et al., 2013; Zhang et al., 2015). These observations lead to the hypothesis that SCD1 deficiency might protect against ALD, which was tested by Lounis et al. (2016). These authors compared WT and *Scd1*$^{-/-}$ mice using the chronic-binge model of ALD, which consists of mice consuming LDeC diets with 5% (v/v) alcohol for 10 days, followed by a single binge dose of alcohol (5 g/kg body weight) (Bertola et al., 2013). Strikingly, alcohol-fed *Scd1*$^{-/-}$ mice were strongly protected against ALD in comparison to their WT controls. This phenotype included a normalization of hepatic lipid TG levels in alcohol-fed *Scd1*$^{-/-}$, normalized serum liver enzymes (AST and ALT), and decreased markers of hepatic inflammation. Mechanistically, the authors showed a strong induction of the DNL pathway in alcohol-fed WT mice, including increased expression of *Srebp1c*, *Acc*, *Fasn*, and *Scd1*, which was normalized in *Scd1*$^{-/-}$ mice, leading to the conclusion that SCD1 deficiency prevented the upregulation of the DNL pathway and prevented ALD. Interestingly, while alcohol consumption was associated with decreased *Ppar*α and *Cpt1a* expression in WT mice, baseline levels of these genes in *Scd1*$^{-/-}$ mice were elevated and unaffected by alcohol consumption, suggesting that genotype-specific effects on mitochondrial β-oxidation may have also contributed to the protective effect of SCD1 deficiency. Mechanistically, increased mitochondrial β-oxidation may also protect SCD1 deficient mice from NAFLD (Ntambi et al., 2002). Taken together, analysis of alcohol consuming *Scd1*$^{-/-}$ mice provides compelling evidence for the involvement of the DNL pathway in the pathogenesis of ALD.

Taken together, there is strong evidence from *Srebp1c*$^{-/-}$ and *Scd1*$^{-/-}$ mice supporting a role for increased DNL as a significant contributor to hepatic lipid accumulation in ALD. Interestingly, as discussed above the DNL pathway can also be modulated through ChREBP, which links hepatic carbohydrate and lipid metabolism, and it has been repeatedly shown that alcohol can also induce ChREBP (Wada et al., 2008; Liangpunsakul et al., 2013; Marmier et al., 2015; Gao et al., 2016; Zhang et al., 2017; Xue et al., 2021). Thus, while there is clear evidence that alcohol induced activation of DNL *via* SREBP1c contributes to ALD, a role for ChREBP is also likely, although to our knowledge *Chrebp*$^{-/-}$ mice have not been studied in the context of ALD.

TRIGLYCERIDE METABOLISM AND LIPID DROPLET FORMATION

TGs are the major type of neutral lipid that accumulates in the cytosolic lipid droplets of the steatotic liver in ALD (Carr and Ahima, 2016; Jeon and Carr, 2020). This section describes insight gained from transgenic mice targeting different aspects of TG metabolism in the context of ALD, including the transcriptional regulation of hepatic lipogenesis and TG synthesis by peroxisome proliferator-activated receptor gamma (PPARγ), TG synthesis by DGAT1, TG hydrolysis by CES1, and lipid droplet homeostasis by PLIN2. The phenotypes described below emphasize the important insight that can be gained into the pathogenesis of ALD through the study of transgenic mouse models.

Evidence From *Ppar*γ Transgenic Mice

PPARγ belongs to the Type II nuclear hormone receptor superfamily and has pleiotropic effects on hepatic lipid metabolism (Tomita et al., 2004; Pettinelli and Videla, 2011; Zhang et al., 2016). Elevation of hepatic PPARγ expression is a common feature of steatosis in ALD and NAFLD (Schadinger et al., 2005; Pettinelli and Videla, 2011; Yu et al., 2016). Whereas it has also been shown that PPARγ agonists can alleviate liver damage in ALD (Enomoto et al., 2003; Tomita et al., 2004). These studies highlight an important role for hepatic PPARγ signaling in ALD. While whole body deletion of *Ppar*γ is embryonic lethal (Barak et al., 1999), the role of PPARγ in ALD has been studied in

mice using hepatocyte specific PPARγ knock-down (PPARγΔ-Hep) (Zhang et al., 2016). Zhang et al. (2016) generated PPARγΔ-Hep mice by crossing Albumin-Cre transgenic mice and PPARγ$^{flox/flox}$ mice, and experimentally these mice were provided with LDeC diets containing 5.6% (v/v) alcohol for 8 weeks. In agreement with a role for PPARγ signaling in ALD, PPARγΔ-Hep mice were protected from alcohol-induced hepatic steatosis, with a blunted increase in liver TGs in alcohol fed mice. Follow-up studies suggest that this effect was primarily driven by effects on hepatic lipogenesis, with no evidence to support a modulatory effect on FA uptake and oxidation, or VLDL secretion. Regarding DNL, the alcohol-associated induction of SREBP1c and *Fasn* was blunted in PPARγΔ-Hep mice, although surprisingly *Acc* induction was unaffected. Regarding TG synthesis, alcohol's ability to induce both *Dgat1* and *Dgat2* was abolished in PPARγΔ-Hep mice. These data were interpreted to suggest that PPARγ signaling is an important contributor to ALD, which is associated with its ability to promote hepatic lipid accumulation primarily through its effects on DNL and TG synthesis (Zhang et al., 2016).

Evidence From *Dgat1*$^{-/-}$ Mice

DGAT1 and DGAT2 catalyze the final step in TG synthesis and both can have a role in hepatic TG accumulation and steatosis. Studies of partitioning in hepatic TG synthesis suggest that DGAT1 has a substrate preference for exogenous FAs, whereas DGAT2 prefers endogenous FAs produced by DNL (Clugston et al., 2014; Li et al., 2015a). In the context of ALD, both *Dgat1* and *Dgat2* have been shown to be induced in the alcohol-exposed liver leading to hepatic steatosis (Wang et al., 2010; Clugston et al., 2011; Clugston et al., 2014; Zhang et al., 2016). In order to test the hypothesis that DGAT1 contributes to ALD, Huang et al. (2018) conducted a series of alcohol feeding studies in *Dgat1*$^{-/-}$ mice on a C57BL/6 background. These authors provided experimental mice with 5.1% (v/v) alcohol containing LDeC diets for 6 weeks, uniquely using both the high-fat/low carbohydrate formulation of the LDeC diets, and the low-fat/high-carbohydrate formulation. Interestingly, this study revealed that DGAT1 deficiency protects against the development of alcoholic steatosis in mice when alcohol was provided with a high-fat/low carbohydrate, but not low-fat/high-carbohydrate diet, as evidenced by hepatic Oil Red O staining and biochemical measurement of hepatic TGs. This observation led to the conclusion that DGAT1 mediates hepatic steatosis in the context of a high-fat/low carbohydrate diet, presumably coupling with increased exogenous FA supply to the liver, whereas in the context of a low-fat/high-carbohydrate diet that favors DNL, DGAT2 predominates. As discussed above, these differential roles of DGAT1 and DGAT2 are consistent with the existing data (Clugston et al., 2014; Li et al., 2015b; Huang et al., 2018). While this study supports the importance of TG synthesis by DGAT1 in ALD, studies into *Dgat2* transgenic mice are limited because *Dgat2*$^{-/-}$ mice are not viable (Stone et al., 2004).

Evidence From *Ces1*$^{-/-}$ Mice

DGAT1 and DGAT2 are the two enzymes responsible for TG synthesis in the liver, yet there are numerous enzymes that hydrolyse TGs in this organ that have specific physiological functions (Gilham and Lehner, 2004). One such TG hydrolase is Carboxylesterase 1 (CES1), which is a serine esterase that is able to hydrolyze TGs and cholesteryl esters (Quiroga et al., 2012; Xu et al., 2014). There are limited studies on the differential expression of CES1 in ALD, although its expression has been reported to be reduced in alcohol-associated steatohepatitis, and in alcohol consuming mice (Xu et al., 2016). Based on this observation, Xu et al. (2016) tested whether CES1 has a role in the pathogenesis of ALD, showing that *Ces1*$^{-/-}$ mice have worsened ALD. Using *Ces1*$^{-/-}$ mice on a C57BL/6J background, experimental animals were fed 5% (v/v) alcohol containing LDeC diet for 10 days followed by an ethanol binge (3 g/kg body weight). *Ces1*$^{-/-}$ mice were reported to have worsened liver damage and hepatic inflammation in response to alcohol feeding, including elevated liver enzymes, increased expression of inflammatory genes, worsened markers of oxidative stress, and mitochondrial dysfunction. While the authors reported increased hepatic free FA levels in alcohol consuming *Ces1*$^{-/-}$ mice, TG levels were not different, which the authors attributed to possible differences in intestinal alcohol metabolism or absorption. To circumvent this limitation the authors did show increased TG accumulation in alcohol fed mice with hepatic knockdown of *Ces1*, which was linked with increased markers of DNL (Xu et al., 2016). While we have framed these results in the context of TG metabolism, it is important to recognize that loss of CES1 may directly impact hepatic acetaldehyde metabolism, with resultant effects on oxidative stress and metabolism (Xu et al., 2016). Taken together, hepatic CES1 has a protective role in alcohol induced hepatic steatosis and its deficiency worsens hepatic steatosis by inducing DNL and liver injury in ALD.

Evidence From *Plin2*$^{-/-}$ Mice

LDs are enveloped by a phospholipid monolayer associated with LD proteins, in the liver the most abundant LD associated protein is Perilipin 2 (PLIN2) (Itabe et al., 2017). Moreover, it has been shown that PLIN2 expression levels are increased in mice and rat models of ALD (Mak et al., 2008; Straub et al., 2008; Orlicky et al., 2011), and is thought to be a marker of hepatic steatosis development (Carr et al., 2014). Carr et al. (2014) studied *Plin2*$^{-/-}$ mice to test the hypothesis that PLIN2 deficiency would prevent hepatic lipid accumulation in alcohol consuming mice. Using LDeC liquid diets with up to 2.7% (v/v) of alcohol for 6 weeks, this group revealed that PLIN2 deficiency protects against the development of alcohol associated steatosis (Carr et al., 2014). Similar to WT control and *Plin2* $^{-/-}$ control mice, alcohol fed *Plin2* $^{-/-}$ mice showed no histologic evidence of alcoholic steatosis, and hepatic TG levels were not elevated by alcohol consumption. Ceramides derived from the sphingomyelin from LD membranes are known to be elevated in ALD (Liangpunsakul et al., 2010; Longato et al., 2012), and a temporal relationship with PLIN2 upregulation and ceramide accumulation has been reported in ALD (Carr et al., 2013). While alcohol feeding increased C22 and C24 species of ceramide in WT mice, this effect is blunted in alcohol fed *Plin2* $^{-/-}$ mice, indicating that PLIN2 also has a role in alcohol induced hepatic ceramide accumulation. Interestingly, PLIN2 deficiency

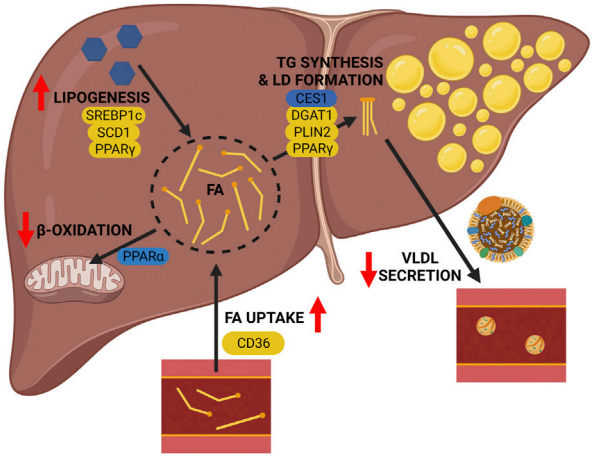

FIGURE 2 | Pathogenesis of alcohol-associated fatty liver: lessons from transgenic mice. Genetic deletion of key genes in lipid metabolic pathways of the liver reveal their contribution to the pathogenesis of ALD. The following pathway-associated genes were found to be important contributors to ALD, including *Cd36* (hepatic FA uptake), *Pparα* (mitochondrial β-oxidation), *De novo* lipogenesis (*Srebp1c*, *Scd1*, and *Pparγ*), and triglyceride metabolism and lipid droplet formation (*Ces1*, *Dgat1*, *Plin2*, and *Pparγ*). Genetic deletion of genes shown in yellow alleviate the effects of alcohol, and genetic deletion of genes shown in blue worsen the effects of alcohol. Image created with BioRender.com.

had a beneficial effect on insulin sensitivity, suggesting that loss of PLIN2 was able to protect against ALD-associated hepatic insulin resistance, an effect that may be secondary to impaired hepatic lipid accumulation in these mice.

Taken together and consistent with alcohol's diverse effects on hepatic lipid metabolism and the central importance of TG metabolism in the development of steatosis, these studies reveal critical regulators of hepatic lipid accumulation in ALD. This includes the protective effect of deficient lipogenic signaling (*Ppara*$^{-/-}$ mice), TG synthesis (*Dgat1*$^{-/-}$), and lipid droplet formation (*Plin2*$^{-/-}$) in ALD, as well as the worsening effect of impaired TG hydrolysis (*Ces1*$^{-/-}$).

CONCLUDING REMARKS

Transgenic mouse models of ALD can help elucidate the mechanisms by which alcohol consumption contributes to alcohol associated fatty liver. It is widely acknowledged that alcohol has multiple effects on hepatic lipid metabolism (**Figure 1**), and through the use of transgenic mouse models we can identify specific key regulators associated with different lipid metabolic pathways that contribute to hepatic lipid accumulation in ALD (summarized in **Figure 2**; **Table 1**). As reviewed herein, gene knock outs in hepatic FA uptake (*Cd36*$^{-/-}$), DNL (*Srebp1c*$^{-/-}$ and *Scd1*$^{-/-}$), and TG metabolism (*Pparγ*$^{-/-}$, *Dgat1*$^{-/-}$, and *Plin2*$^{-/-}$) protect against ALD, whereas gene knocks out in mitochondrial β-oxidation (*Ppara*$^{-/-}$) and TG hydrolysis (*Ces1*$^{-/-}$) exacerbate ALD. Interestingly, although it is accepted that alcohol abuse impacts multiple aspects of hepatic lipid accumulation causing steatosis, the relative importance of these different pathways is unclear. Others have speculated that impaired mitochondrial β-oxidation is the most significant contributor to alcohol associated steatosis (Jeon and Carr 2020; Hyun et al., 2021). While there is strong evidence to support this conclusion, the current review shows that genetic ablation of key components in other metabolic pathways is sufficient to ameliorate ALD independently of mitochondrial β-oxidation. Further study is required to understand the relative contribution of different lipid metabolic pathways to the development of alcohol associated steatosis. It is encouraging that genetic ablation of single genes in different metabolic pathways can ameliorate hepatic lipid accumulation in ALD, as this broadens the potential therapeutic targets to treat ALD in its early stages.

Limitations of Transgenic Mouse Models

While transgenic mouse models are a powerful tool to study ALD, there are inherent weaknesses in their application and gaps in our knowledge remain. At the level of experimental design, it is important to acknowledge that all of the studies reviewed in this manuscript that report sex, only use male mice (**Table 1**). The clinical presentation of ALD is different in men and women, thus it is incumbent upon the research community to include female mice in their study of ALD pathogenesis (Han et al., 2021). Another important aspect of experimental design is the choice of alcohol feeding protocol. The majority of studies reviewed here utilize LDeC liquid diets, with variations in duration and the amount of alcohol (**Table 1**). These models consistently produce hepatic lipid accumulation in response to alcohol, although it is acknowledged that they are limited in their ability to produce severe ALD [e.g., steatohepatitis and fibrosis (Bertola et al., 2013)]. Interestingly, the macronutrient composition of the LDeC liquid diets may have an impact on the predominant pathways leading to hepatic lipid accumulation, with differences dependent on whether FAs are produced endogenously (e.g., *via* DNL), or exogenously (e.g., *via* FA uptake), representing an important consideration when designing studies and translating their results (Li et al., 2015a; Huang et al., 2018). Perhaps one of the most significant limitations in the majority of studies included in this manuscript are the use of global knockouts of genes of interest. While these studies are focused on hepatic lipid metabolism, it should be acknowledged that whole body ablation of specific genes may effect whole body lipid metabolism that might also indirectly impact hepatic lipid metabolism. The use of liver specific knockouts would address this limitation and has the added advantage of circumventing embryonic lethality of specific gene knockouts. For example, Zhang et al. (2016) used liver specific ablation of *Pparγ* to circumvent the lethality of global knockout of this gene. This approach could be used to further study alcohol's effects on hepatic lipid metabolism, for example while *Dgat2*$^{-/-}$ mice are not viable, a liver specific knockout has been described that could be used to dissect the role of this TG synthesizing enzyme in ALD (Stone et al., 2004; Gluchowski et al., 2019). Finally, while transgenic mouse models are a powerful tool to study ALD

pathogenesis, there is an obvious need to translate these studies into humans if a clinical benefit is to be realized. While limited human data is available, there are clear parallels between the effect of alcohol on the mouse and human liver. Indeed, similar to the data generated from mice there are human studies implicating alcohol-induced changes in hepatic FA uptake, mitochondrial β-oxidation, and DNL (Blomstrand et al., 1973; Siler et al., 1999; Rachakonda et al., 2014). Nevertheless, data on molecular mediators of these effects in humans is limited, validating the use of rodent models to gain detailed insight into ALD pathogenesis.

Knowledge Gaps and Future Directions

While the limitations discussed above are important considerations in our interpretation of transgenic mouse data and their potential translation, we also have to acknowledge that significant gaps remain in our understanding of alcohol's effects on hepatic lipid metabolism that could benefit from genetic dissection. As indicated above, each of the major lipid metabolic pathways could be further probed using transgenic mice. For example, given the apparent interaction between CD36 deficiency and DNL (Clugston et al., 2014; Zeng et al., 2022), studies in FATP2 or 5 deficient mice may help better understand the importance of FA uptake in the pathogenesis of ALD. Similarly, genetic targeting of a critical regulator of mitochondria β-oxidation (e.g., *Cpt1a*) would directly probe this pathway separate from the broad effects of *Ppara*$^{-/-}$ mice. Use of *Srebp1c*$^{-/-}$ and *Scd1*$^{-/-}$ mice have provided good coverage of the DNL pathway, but there is also an opportunity to study *Chrebp*$^{-/-}$ mice to better understand alcohol's effect on this regulator of DNL. Moreover, the effect of alcohol on VLDL secretion has been neglected. While genetic targets exist to study this pathway (e.g., *ApoB* or *Mttp*) alcohol feeding studies have not been conducted in transgenic mice targeting these genes.

Conclusion

Transgenic mouse models have been effectively used to study ALD and understand its molecular pathogenesis; however, as discussed above, there is significant opportunity to leverage genetically engineered mouse models targeting different pathways of hepatic lipid accumulation that will provide further insight into ALD. Ultimately, there is consensus in the field that further study of alcohol's effect on hepatic lipid metabolism is warranted to guide the development of much needed treatments for ALD (Jeon and Carr, 2020; Hyun et al., 2021).

AUTHOR CONTRIBUTIONS

AF and RC jointly contributed to all aspects of manuscript preparation including review of the literature, writing, and editing. All authors have read and approved the submitted version of the manuscript.

FUNDING

This work was supported by a Canadian Institutes of Health Research Project Grant (PJT-156226).

REFERENCES

Alves-Bezerra, M., and Cohen, D. E. (2017). Triglyceride Metabolism in the Liver. *Compr. Physiol.* 8 (1), 1–8. doi:10.1002/cphy.c170012

Ameer, F., Scandiuzzi, L., Hasnain, S., Kalbacher, H., and Zaidi, N. (2014). De Novo lipogenesis in Health and Disease. *Metabolism* 63 (7), 895–902. doi:10.1016/j.metabol.2014.04.003

Barak, Y., Nelson, M. C., Ong, E. S., Jones, Y. Z., Ruiz-Lozano, P., Chien, K. R., et al. (1999). PPARγ Is Required for Placental, Cardiac, and Adipose Tissue Development. *Mol. Cell.* 4 (4), 585–595. doi:10.1016/s1097-2765(00)80209-9

Barson, J. R., Karatayev, O., Chang, G.-Q., Johnson, D. F., Bocarsly, M. E., Hoebel, B. G., et al. (2009). Positive Relationship between Dietary Fat, Ethanol Intake, Triglycerides, and Hypothalamic Peptides: Counteraction by Lipid-Lowering Drugs. *Alcohol* 43 (6), 433–441. doi:10.1016/j.alcohol.2009.07.003

Bertola, A., Mathews, S., Ki, S. H., Wang, H., and Gao, B. (2013). Mouse Model of Chronic and Binge Ethanol Feeding (The NIAAA Model). *Nat. Protoc.* 8 (3), 627–637. doi:10.1038/nprot.2013.032

Blednov, Y. A., Benavidez, J. M., Black, M., Ferguson, L. B., Schoenhard, G. L., Goate, A. M., et al. (2015). Peroxisome Proliferator-Activated Receptorsαandγare Linked with Alcohol Consumption in Mice and Withdrawal and Dependence in Humans. *Alcohol Clin. Exp. Res.* 39 (1), 136–145. doi:10.1111/acer.12610

Blomstrand, R., Kager, L., and Lantto, O. (1973). Studies on the Ethanol-Induced Decrease of Fatty Acid Oxidation in Rat and Human Liver Slices. *Life Sci.* 13 (8), 1131–1141. doi:10.1016/0024-3205(73)90380-9

Bruha, R., Dvorak, K., and Petrtyl, J. (2012). Alcoholic Liver Disease. *Wjh* 4 (3), 81–90. doi:10.4254/wjh.v4.i3.81

Canadian Center on Substance Use and Addiction (2019). Alcohol. AvaliableAt: https://www.ccsa.ca/sites/default/files/2019-09/CCSA-Canadian-Drug-Summary-Alcohol-2019-en.pdf (Accessed December 12, 2021).

Carr, R. M., and Ahima, R. S. (2016). Pathophysiology of Lipid Droplet Proteins in Liver Diseases. *Exp. Cell. Res.* 340 (2), 187–192. doi:10.1016/j.yexcr.2015.10.021

Carr, R. M., Dhir, R., Yin, X., Agarwal, B., and Ahima, R. S. (2013). Temporal Effects of Ethanol Consumption on Energy Homeostasis, Hepatic Steatosis, and Insulin Sensitivity in Mice. *Alcohol Clin. Exp. Res.* 37 (7), 1091–1099. doi:10.1111/acer.12075

Carr, R. M., Peralta, G., Yin, X., and Ahima, R. S. (2014). Absence of Perilipin 2 Prevents Hepatic Steatosis, Glucose Intolerance and Ceramide Accumulation in Alcohol-Fed Mice. *PLoS One* 9 (5), e97118. doi:10.1371/journal.pone.0097118

Ceni, E., Mello, T., and Galli, A. (2014). Pathogenesis of Alcoholic Liver Disease: Role of Oxidative Metabolism. *Wjg* 20 (47), 17756–17772. doi:10.3748/wjg.v20.i47.17756

Charidemou, E., Ashmore, T., Li, X., McNally, B. D., West, J. A., Liggi, S., et al. (2019). A Randomized 3-way Crossover Study Indicates that High-Protein Feeding Induces De Novo Lipogenesis in Healthy Humans. *JCI Insight* 4 (12), e124819. doi:10.1172/jci.insight.124819

Clugston, R. D., Jiang, H., Lee, M. X., Piantedosi, R., Yuen, J. J., Ramakrishnan, R., et al. (2011). Altered Hepatic Lipid Metabolism in C57BL/6 Mice Fed Alcohol: a Targeted Lipidomic and Gene Expression Study. *J. Lipid Res.* 52 (11), 2021–2031. doi:10.1194/jlr.m017368

Clugston, R. D., Yuen, J. J., Hu, Y., Abumrad, N. A., Berk, P. D., Goldberg, I. J., et al. (2014). CD36-deficient Mice Are Resistant to Alcohol- and High-Carbohydrate-Induced Hepatic Steatosis. *J. Lipid Res.* 55 (2), 239–246. doi:10.1194/jlr.m041863

Cohen, P., Miyazaki, M., Socci, N. D., Hagge-Greenberg, A., Liedtke, W., Soukas, A. A., et al. (2002). Role for Stearoyl-CoA Desaturase-1 in Leptin-Mediated Weight Loss. *Science* 297 (5579), 240–243. doi:10.1126/science.1071527

Crabb, D. W. (1999). Pathogenesis of Alcoholic Liver Disease. Newer Mechanisms of Injury. *Keio J. Med.* 48 (4), 184–188. doi:10.2302/kjm.48.184

Denechaud, P.-D., Dentin, R., Girard, J., and Postic, C. (2008). Role of ChREBP in Hepatic Steatosis and Insulin Resistance. *FEBS Lett.* 582 (1), 68–73. doi:10.1016/j.febslet.2007.07.084

Enomoto, N., Takei, Y., Hirose, M., Konno, A., Shibuya, T., Matsuyama, S., et al. (2003). Prevention of Ethanol-Induced Liver Injury in Rats by an Agonist of Peroxisome Proliferator-Activated Receptor-γ, Pioglitazone. *J. Pharmacol. Exp. Ther.* 306 (3), 846–854. doi:10.1124/jpet.102.047217

Fischer, M., You, M., Matsumoto, M., and Crabb, D. W. (2003). Peroxisome Proliferator-Activated Receptor α (PPARα) Agonist Treatment Reverses PPARα Dysfunction and Abnormalities in Hepatic Lipid Metabolism in Ethanol-Fed Mice. *J. Biol. Chem.* 278 (30), 27997–28004. doi:10.1074/jbc.m302140200

Forman, B. M., Chen, J., and Evans, R. M. (1997). Hypolipidemic Drugs, Polyunsaturated Fatty Acids, and Eicosanoids Are Ligands for Peroxisome Proliferator-Activated Receptors α and δ. *Proc. Natl. Acad. Sci. U.S.A.* 94 (9), 4312–4317. doi:10.1073/pnas.94.9.4312

Foufelle, F., and Ferré, P. (2002). New Perspectives in the Regulation of Hepatic Glycolytic and Lipogenic Genes by Insulin and Glucose: a Role for the Transcription Factor Sterol Regulatory Element Binding Protein-1c. *Biochem. J.* 366 (Pt 2), 377–391. doi:10.1042/BJ20020430

Galli, A., Pinaire, J., Fischer, M., Dorris, R., and Crabb, D. W. (2001). The Transcriptional and DNA Binding Activity of Peroxisome Proliferator-Activated Receptor α Is Inhibited by Ethanol Metabolism. *J. Biol. Chem.* 276 (1), 68–75. doi:10.1074/jbc.m008791200

Gao, L., Shan, W., Zeng, W., Hu, Y., Wang, G., Tian, X., et al. (2016). Carnosic Acid Alleviates Chronic Alcoholic Liver Injury by Regulating the SIRT1/ChREBP and SIRT1/p66shc Pathways in Rats. *Mol. Nutr. Food Res.* 60 (9), 1902–1911. doi:10.1002/mnfr.201500878

GBD 2016 Alcohol Collaborators (2018). Alcohol Use and Burden for 195 Countries and Territories, 1990-2016: a Systematic Analysis for the Global Burden of Disease Study 2016. *Lancet* 392 (10152), 1015–1035. doi:10.1016/S0140-6736(18)31310-2

Ge, F., Zhou, S., Hu, C., Lobdell, H., and Berk, P. D. (2010). Insulin- and Leptin-Regulated Fatty Acid Uptake Plays a Key Causal Role in Hepatic Steatosis in Mice with Intact Leptin Signaling but Not Inob/obordb/dbmice. *Am. J. Physiology-Gastrointestinal Liver Physiology* 299 (4), G855–G866. doi:10.1152/ajpgi.00434.2009

Gilham, D., and Lehner, R. (2004). The Physiological Role of Triacylglycerol Hydrolase in Lipid Metabolism. *Rev. Endocr. Metab. Disord.* 5 (4), 303–309. doi:10.1023/b:remd.0000045101.42431.c7

Gluchowski, N. L., Gabriel, K. R., Chitraju, C., Bronson, R. T., Mejhert, N., Boland, S., et al. (2019). Hepatocyte Deletion of Triglyceride-Synthesis Enzyme Acyl CoA: Diacylglycerol Acyltransferase 2 Reduces Steatosis without Increasing Inflammation or Fibrosis in Mice. *Hepatology* 70 (6), 1972–1985. doi:10.1002/hep.30765

Han, S., Yang, Z., Zhang, T., Ma, J., Chandler, K., and Liangpunsakul, S. (2021). Epidemiology of Alcohol-Associated Liver Disease. *Clin. Liver Dis.* 25 (3), 483–492. doi:10.1016/j.cld.2021.03.009

Hertz, R., and Bar-Tana, J. (1998). Peroxisome Proliferator-Activated Receptor (PPAR) Alpha Activation and its Consequences in Humans. *Toxicol. Lett.* 102-103, 85–90. doi:10.1016/s0378-4274(98)00290-2

Huang, L.-L., Wan, J.-B., Wang, B., He, C.-W., Ma, H., Li, T.-W., et al. (2013). Suppression of Acute Ethanol-Induced Hepatic Steatosis by Docosahexaenoic Acid Is Associated with Downregulation of Stearoyl-CoA Desaturase 1 and Inflammatory Cytokines. *Prostagl. Leukot. Essent. Fat. Acids* 88 (5), 347–353. doi:10.1016/j.plefa.2013.02.002

Huang, L.-S., Yuen, J. J., Trites, M. J., Saha, A., Epps, C. T., Hu, Y., et al. (2018). Dietary Macronutrient Composition Determines the Contribution of DGAT1 to Alcoholic Steatosis. *Alcohol Clin. Exp. Re* 42 (12), 2298–2312. doi:10.1111/acer.13881

Hyun, J., Han, J., Lee, C., Yoon, M., and Jung, Y. (2021). Pathophysiological Aspects of Alcohol Metabolism in the Liver. *Int. J. Mol. Sci.* 22 (11), 5717. doi:10.3390/ijms22115717

Itabe, H., Yamaguchi, T., Nimura, S., and Sasabe, N. (2017). Perilipins: a Diversity of Intracellular Lipid Droplet Proteins. *Lipids Health Dis.* 16 (1), 83. doi:10.1186/s12944-017-0473-y

Jeon, S., and Carr, R. (2020). Alcohol Effects on Hepatic Lipid Metabolism. *J. Lipid Res.* 61 (4), 470–479. doi:10.1194/jlr.r119000547

Ji, C., Chan, C., and Kaplowitz, N. (2006). Predominant Role of Sterol Response Element Binding Proteins (SREBP) Lipogenic Pathways in Hepatic Steatosis in the Murine Intragastric Ethanol Feeding Model. *J. Hepatology* 45 (5), 717–724. doi:10.1016/j.jhep.2006.05.009

Kang, L., Chen, X., Sebastian, B. M., Pratt, B. T., Bederman, I. R., Alexander, J. C., et al. (2007). Chronic Ethanol and Triglyceride Turnover in White Adipose Tissue in Rats. *J. Biol. Chem.* 282 (39), 28465–28473. doi:10.1074/jbc.m705503200

Keller, H., Dreyer, C., Medin, J., Mahfoudi, A., Ozato, K., and Wahli, W. (1993). Fatty Acids and Retinoids Control Lipid Metabolism through Activation of Peroxisome Proliferator-Activated Receptor-Retinoid X Receptor Heterodimers. *Proc. Natl. Acad. Sci. U.S.A.* 90 (6), 2160–2164. doi:10.1073/pnas.90.6.2160

Kersten, S., Seydoux, J., Peters, J. M., Gonzalez, F. J., Desvergne, B., and Wahli, W. (1999). Peroxisome Proliferator-Activated Receptor α Mediates the Adaptive Response to Fasting. *J. Clin. Invest.* 103 (11), 1489–1498. doi:10.1172/jci6223

Kharbanda, K. K., Todero, S. L., King, A. L., Osna, N. A., McVicker, B. L., Tuma, D. J., et al. (2012). Betaine Treatment Attenuates Chronic Ethanol-Induced Hepatic Steatosis and Alterations to the Mitochondrial Respiratory Chain Proteome. *Int. J. Hepatol.* 2012, 962183. doi:10.1155/2012/962183

Li, C., Li, L., Lian, J., Watts, R., Nelson, R., Goodwin, B., et al. (2015a). Roles of Acyl-CoA:Diacylglycerol Acyltransferases 1 and 2 in Triacylglycerol Synthesis and Secretion in Primary Hepatocytes. *Atvb* 35 (5), 1080–1091. doi:10.1161/atvbaha.114.304584

Li, H.-H., Tyburski, J. B., Wang, Y.-W., Strawn, S., Moon, B.-H., Kallakury, B. V. S., et al. (2014). Modulation of Fatty Acid and Bile Acid Metabolism by Peroxisome Proliferator-Activated ReceptorαProtects against Alcoholic Liver Disease. *Alcohol Clin. Exp. Res.* 38 (6), 1520–1531. doi:10.1111/acer.12424

Li, X., Lian, F., Liu, C., Hu, K.-Q., and Wang, X.-D. (2015b). Isocaloric Pair-Fed High-Carbohydrate Diet Induced More Hepatic Steatosis and Inflammation Than High-Fat Diet Mediated by miR-34a/SIRT1 Axis in Mice. *Sci. Rep.* 5, 16774. doi:10.1038/srep16774

Liangpunsakul, S., Ross, R. A., and Crabb, D. W. (2013). Activation of Carbohydrate Response Element-Binding Protein by Ethanol. *J. Investig. Med.* 61 (2), 270–277. doi:10.2310/jim.0b013e31827c2795

Liangpunsakul, S., Sozio, M. S., Shin, E., Zhao, Z., Xu, Y., Ross, R. A., et al. (2010). Inhibitory Effect of Ethanol on AMPK Phosphorylation Is Mediated in Part through Elevated Ceramide Levels. *Am. J. Physiology-Gastrointestinal Liver Physiology* 298 (6), G1004–G1012. doi:10.1152/ajpgi.00482.2009

Lieber, C. S. (1988). Biochemical and Molecular Basis of Alcohol-Induced Injury to Liver and Other Tissues. *N. Engl. J. Med.* 319 (25), 1639–1650. doi:10.1056/NEJM198812223192505

Longato, L., Ripp, K., Setshedi, M., Dostalek, M., Akhlaghi, F., Branda, M., et al. (2012). Insulin Resistance, Ceramide Accumulation, and Endoplasmic Reticulum Stress in Human Chronic Alcohol-Related Liver Disease. *Oxid. Med. Cell. Longev.* 2012, 479348. doi:10.1155/2012/479348

Lounis, M. A., Escoula, Q., Veillette, C., Bergeron, K.-F., Ntambi, J. M., and Mounier, C. (2016). SCD1 Deficiency Protects Mice against Ethanol-Induced Liver Injury. *Biochimica Biophysica Acta (BBA) - Mol. Cell. Biol. Lipids* 1861 (11), 1662–1670. doi:10.1016/j.bbalip.2016.07.012

MacDonald, M. L. E., Singaraja, R. R., Bissada, N., Ruddle, P., Watts, R., Karasinska, J. M., et al. (2008). Absence of Stearoyl-CoA Desaturase-1 Ameliorates Features of the Metabolic Syndrome in LDLR-Deficient Mice. *J. Lipid Res.* 49 (1), 217–229. doi:10.1194/jlr.m700478-jlr200

Mak, K. M., Ren, C., Ponomarenko, A., Cao, Q., and Lieber, C. S. (2008). Adipose Differentiation-Related Protein Is a Reliable Lipid Droplet Marker in Alcoholic Fatty Liver of Rats. *Alcohol. Clin. Exp. Res.* 32 (4), 683–689. doi:10.1111/j.1530-0277.2008.00624.x

Mann, R. E., Smart, R. G., and Govoni, R. (2003). The Epidemiology of Alcoholic Liver Disease. *Alcohol Res. Health* 27 (3), 209–219.

Marmier, S., Dentin, R., Daujat-Chavanieu, M., Guillou, H., Bertrand-Michel, J., Gerbal-Chaloin, S., et al. (2015). Novel Role for Carbohydrate Responsive Element Binding Protein in the Control of Ethanol Metabolism and Susceptibility to Binge Drinking. *Hepatology* 62 (4), 1086–1100. doi:10.1002/hep.27778

Miller, A. M., Horiguchi, N., Jeong, W.-I., Radaeva, S., and Gao, B. (2011). Molecular Mechanisms of Alcoholic Liver Disease: Innate Immunity and

Cytokines. *Alcohol Clin. Exp. Res.* 35 (5), 787–793. doi:10.1111/j.1530-0277.2010.01399.x

Nakajima, T., Kamijo, Y., Tanaka, N., Sugiyama, E., Tanaka, E., Kiyosawa, K., et al. (2004). Peroxisome Proliferator-Activated Receptor α Protects against Alcohol-Induced Liver Damage. *Hepatology* 40 (4), 972–980. doi:10.1002/hep.1840400428

Nanji, A. A., Dannenberg, A. J., Jokelainen, K., and Bass, N. M. (2004). Alcoholic Liver Injury in the Rat Is Associated with Reduced Expression of Peroxisome Proliferator-α (PPARα)-Regulated Genes and Is Ameliorated by PPARα Activation. *J. Pharmacol. Exp. Ther.* 310 (1), 417–424. doi:10.1124/jpet.103.064717

Ntambi, J. M., Miyazaki, M., Stoehr, J. P., Lan, H., Kendziorski, C. M., Yandell, B. S., et al. (2002). Loss of Stearoyl-CoA Desaturase-1 Function Protects Mice against Adiposity. *Proc. Natl. Acad. Sci. U.S.A.* 99 (17), 11482–11486. doi:10.1073/pnas.132384699

Okiyama, W., Tanaka, N., Nakajima, T., Tanaka, E., Kiyosawa, K., Gonzalez, F. J., et al. (2009). Polyenephosphatidylcholine Prevents Alcoholic Liver Disease in PPARα-Null Mice through Attenuation of Increases in Oxidative Stress. *J. Hepatology* 50 (6), 1236–1246. doi:10.1016/j.jhep.2009.01.025

Orlicky, D. J., Roede, J. R., Bales, E., Greenwood, C., Greenberg, A., Petersen, D., et al. (2011). Chronic Ethanol Consumption in Mice Alters Hepatocyte Lipid Droplet Properties. *Alcohol Clin. Exp. Res.* 35 (6), 1020–1033. doi:10.1111/j.1530-0277.2011.01434.x

Osna, N. A., Donohue, T. M., Jr., and Kharbanda, K. K. (2017). Alcoholic Liver Disease: Pathogenesis and Current Management. *Alcohol Res.* 38 (2), 147–161.

Palmer, C. N. A., Hsu, M.-H., Griffin, K. J., Raucy, J. L., and Johnson, E. F. (1998). Peroxisome Proliferator Activated Receptor-α Expression in Human Liver. *Mol. Pharmacol.* 53 (1), 14–22. doi:10.1124/mol.53.1.14

Pettinelli, P., and Videla, L. A. (2011). Up-Regulation of PPAR-γ mRNA Expression in the Liver of Obese Patients: an Additional Reinforcing Lipogenic Mechanism to SREBP-1c Induction. *J. Clin. Endocrinol. Metab.* 96 (5), 1424–1430. doi:10.1210/jc.2010-2129

Quiroga, A. D., Li, L., Trötzmüller, M., Nelson, R., Proctor, S. D., Köfeler, H., et al. (2012). Deficiency of Carboxylesterase 1/esterase-X Results in Obesity, Hepatic Steatosis, and Hyperlipidemia. *Hepatology* 56 (6), 2188–2198. doi:10.1002/hep.25961

Rachakonda, V., Gabbert, C., Raina, A., Bell, L. N., Cooper, S., Malik, S., et al. (2014). Serum Metabolomic Profiling in Acute Alcoholic Hepatitis Identifies Multiple Dysregulated Pathways. *PLoS One* 9 (12), e113860. doi:10.1371/journal.pone.0113860

Redlich, C. A., Blaner, W. S., Van Bennekum, A. M., Chung, J. S., Clever, S. L., Holm, C. T., et al. (1998). Effect of Supplementation with Beta-Carotene and Vitamin A on Lung Nutrient Levels. *Cancer Epidemiol. Biomarkers Prev.* 7 (3), 211–214.

Ronis, M. J. J., Hennings, L., Stewart, B., Basnakian, A. G., Apostolov, E. O., Albano, E., et al. (2011). Effects of Long-Term Ethanol Administration in a Rat Total Enteral Nutrition Model of Alcoholic Liver Disease. *Am. J. Physiology-Gastrointestinal Liver Physiology* 300 (1), G109–G119. doi:10.1152/ajpgi.00145.2010

Schadinger, S. E., Bucher, N. L. R., Schreiber, B. M., and Farmer, S. R. (2005). PPARγ2 Regulates Lipogenesis and Lipid Accumulation in Steatotic Hepatocytes. *Am. J. Physiology-Endocrinology Metabolism* 288 (6), E1195–E1205. doi:10.1152/ajpendo.00513.2004

Shaheen, A. A., Kong, K., Ma, C., Doktorchik, C., Coffin, C. S., Swain, M. G., et al. (2021). Impact of the COVID-19 Pandemic on Hospitalizations for Alcoholic Hepatitis or Cirrhosis in Alberta, Canada. *Clin. Gastroenterol. Hepatol.* 20, e1170–e1179. doi:10.1016/j.cgh.2021.10.030

Shen, H., Jiang, L., Lin, J. D., Omary, M. B., and Rui, L. (2019). Brown Fat Activation Mitigates Alcohol-Induced Liver Steatosis and Injury in Mice. *J. Clin. Invest.* 129 (6), 2305–2317. doi:10.1172/jci124376

Sherlock, S., and Dooley, J. (2008). *Diseases of the Liver and Biliary System*. Hoboken: Wiley-Blackwell.

Siler, S. Q., Neese, R. A., and Hellerstein, M. K. (1999). De Novo lipogenesis, Lipid Kinetics, and Whole-Body Lipid Balances in Humans after Acute Alcohol Consumption. *Am. J. Clin. Nutr.* 70 (5), 928–936. doi:10.1093/ajcn/70.5.928

Singal, A. K., and Shah, V. H. (2019). Current Trials and Novel Therapeutic Targets for Alcoholic Hepatitis. *J. Hepatology* 70 (2), 305–313. doi:10.1016/j.jhep.2018.10.026

Sohal, A., Khalid, S., Green, V., Gulati, A., and Roytman, M. (2021). The Pandemic within the Pandemic: Unprecedented Rise in Alcohol-Related Hepatitis during the COVID-19 Pandemic. *J. Clin. Gastroenterol.* 56, e171–e175. doi:10.1097/MCG.0000000000001627

Stahl, A., Gimeno, R. E., Tartaglia, L. A., and Lodish, H. F. (2001). Fatty Acid Transport Proteins: a Current View of a Growing Family. *Trends Endocrinol. Metab.* 12 (6), 266–273. doi:10.1016/s1043-2760(01)00427-1

Stockwell, T., Andreasson, S., Cherpitel, C., Chikritzhs, T., Dangardt, F., Holder, H., et al. (2021). The Burden of Alcohol on Health Care during COVID -19. *Drug Alcohol Rev.* 40 (1), 3–7. doi:10.1111/dar.13143

Stone, S. J., Myers, H. M., Watkins, S. M., Brown, B. E., Feingold, K. R., Elias, P. M., et al. (2004). Lipopenia and Skin Barrier Abnormalities in DGAT2-Deficient Mice. *J. Biol. Chem.* 279 (12), 11767–11776. doi:10.1074/jbc.m311000200

Straub, B. K., Stoeffel, P., Heid, H., Zimbelmann, R., and Schirmacher, P. (2008). Differential Pattern of Lipid Droplet-Associated Proteins Andde Novoperilipin Expression in Hepatocyte Steatogenesis. *Hepatology* 47 (6), 1936–1946. doi:10.1002/hep.22268

Stumvoll, M., Wahl, H. G., Löblein, K., Becker, R., Volk, A., Renn, W., et al. (2001). A Novel Use of the Hyperinsulinemic-Euglycemic Clamp Technique to Estimate Insulin Sensitivity of Systemic Lipolysis. *Horm. Metab. Res.* 33 (2), 89–95. doi:10.1055/s-2001-12403

Sugimoto, T., Yamashita, S., Ishigami, M., Sakai, N., Hirano, K.-i., Tahara, M., et al. (2002). Decreased Microsomal Triglyceride Transfer Protein Activity Contributes to Initiation of Alcoholic Liver Steatosis in Rats. *J. Hepatology* 36 (2), 157–162. doi:10.1016/s0168-8278(01)00263-x

Tomita, K., Azuma, T., Kitamura, N., Nishida, J., Tamiya, G., Oka, A., et al. (2004). Pioglitazone Prevents Alcohol-Induced Fatty Liver in Rats through Up-Regulation of C-Met. *Gastroenterology* 126 (3), 873–885. doi:10.1053/j.gastro.2003.12.008

Tugwood, J. D., Aldridge, T. C., Lambe, K. G., Macdonald, N., and Woodyatt, N. J. (1996). Peroxisome Proliferator-Activated Receptors: Stuctures and Function. *Ann. N. Y. Acad. Sci.* 804, 252–265. doi:10.1111/j.1749-6632.1996.tb18620.x

Wada, S., Yamazaki, T., Kawano, Y., Miura, S., and Ezaki, O. (2008). Fish Oil Fed Prior to Ethanol Administration Prevents Acute Ethanol-Induced Fatty Liver in Mice. *J. Hepatology* 49 (3), 441–450. doi:10.1016/j.jhep.2008.04.026

Wan, Y. J., Morimoto, M., Thurman, R. G., Bojes, H. K., and French, S. W. (1995). Expression of the Peroxisome Proliferator-Activated Receptor Gene Is Decreased in Experimental Alcoholic Liver Disease. *Life Sci.* 56 (5), 307–317. doi:10.1016/0024-3205(94)00953-8

Wang, Z., Yao, T., and Song, Z. (2010). Involvement and Mechanism of DGAT2 Upregulation in the Pathogenesis of Alcoholic Fatty Liver Disease. *J. Lipid Res.* 51 (11), 3158–3165. doi:10.1194/jlr.m007948

Wei, X., Shi, X., Zhong, W., Zhao, Y., Tang, Y., Sun, W., et al. (2013). Chronic Alcohol Exposure Disturbs Lipid Homeostasis at the Adipose Tissue-Liver axis in Mice: Analysis of Triacylglycerols Using High-Resolution Mass Spectrometry in Combination with *In Vivo* Metabolite Deuterium Labeling. *PLoS One* 8 (2), e55382. doi:10.1371/journal.pone.0055382

WHO (2018). Global Status Report on Alcohol and Health 2018. AvaliableAt: https://www.who.int/publications-detail-redirect/9789241565639 (Accessed November 03, 2021).

Wurie, H. R., Buckett, L., and Zammit, V. A. (2012). Diacylglycerol Acyltransferase 2 Acts Upstream of Diacylglycerol Acyltransferase 1 and Utilizes Nascent Diglycerides Andde Novosynthesized Fatty Acids in HepG2 Cells. *FEBS J.* 279 (17), 3033–3047. doi:10.1111/j.1742-4658.2012.08684.x

Xu, J., Li, Y., Chen, W.-D., Xu, Y., Yin, L., Ge, X., et al. (2014). Hepatic Carboxylesterase 1 Is Essential for Both Normal and Farnesoid X Receptor-Controlled Lipid Homeostasis. *Hepatology* 59 (5), 1761–1771. doi:10.1002/hep.26714

Xu, J., Xu, Y., Li, Y., Jadhav, K., You, M., Yin, L., et al. (2016). Carboxylesterase 1 Is Regulated by Hepatocyte Nuclear Factor 4α and Protects against Alcohol- and MCD Diet-Induced Liver Injury. *Sci. Rep.* 6, 24277. doi:10.1038/srep24277

Xue, M., Liang, H., Zhou, Z., Liu, Y., He, X., Zhang, Z., et al. (2021). Effect of Fucoidan on Ethanol-Induced Liver Injury and Steatosis in Mice and the Underlying Mechanism. *Food Nutr. Res.* 65, 5384. doi:10.29219/fnr.v65.5384

Yamashita, H., Kaneyuki, T., and Tagawa, K. (2001). Production of Acetate in the Liver and its Utilization in Peripheral Tissues. *Biochim. Biophys. Acta* 1532 (1-2), 79–87. doi:10.1016/s1388-1981(01)00117-2

Yin, H.-Q., Kim, M., Kim, J.-H., Kong, G., Kang, K.-S., Kim, H.-L., et al. (2007). Differential Gene Expression and Lipid Metabolism in Fatty Liver Induced by Acute Ethanol Treatment in Mice. *Toxicol. Appl. Pharmacol.* 223 (3), 225–233. doi:10.1016/j.taap.2007.06.018

You, M., and Arteel, G. E. (2019). Effect of Ethanol on Lipid Metabolism. *J. Hepatology* 70 (2), 237–248. doi:10.1016/j.jhep.2018.10.037

You, M., Fischer, M., Deeg, M. A., and Crabb, D. W. (2002). Ethanol Induces Fatty Acid Synthesis Pathways by Activation of Sterol Regulatory Element-Binding Protein (SREBP). *J. Biol. Chem.* 277 (32), 29342–29347. doi:10.1074/jbc.m202411200

Yu, J. H., Song, S. J., Kim, A., Choi, Y., Seok, J. W., Kim, H. J., et al. (2016). Suppression of PPARγ-Mediated Monoacylglycerol O-Acyltransferase 1 Expression Ameliorates Alcoholic Hepatic Steatosis. *Sci. Rep.* 6, 29352. doi:10.1038/srep29352

Yu, S., Rao, S., and Reddy, J. K. (2003). Peroxisome Proliferator-Activated Receptors, Fatty Acid Oxidation, Steatohepatitis and Hepatocarcinogenesis. *Curr. Mol. Med.* 3 (6), 561–572. doi:10.2174/1566524033479537

Zeng, H., Qin, H., Liao, M., Zheng, E., Luo, X., Xiao, A., et al. (2022). CD36 Promotes De Novo Lipogenesis in Hepatocytes through INSIG2-dependent SREBP1 Processing. *Mol. Metab.* 57, 101428. doi:10.1016/j.molmet.2021.101428

Zhang, M., Wang, C., Wang, C., Zhao, H., Zhao, C., Chen, Y., et al. (2015). Enhanced AMPK Phosphorylation Contributes to the Beneficial Effects of Lactobacillus Rhamnosus GG Supernatant on Chronic-Alcohol-Induced Fatty Liver Disease. *J. Nutr. Biochem.* 26 (4), 337–344. doi:10.1016/j.jnutbio.2014.10.016

Zhang, N., Hu, Y., Ding, C., Zeng, W., Shan, W., Fan, H., et al. (2017). Salvianolic Acid B Protects against Chronic Alcoholic Liver Injury via SIRT1-Mediated Inhibition of CRP and ChREBP in Rats. *Toxicol. Lett.* 267, 1–10. doi:10.1016/j.toxlet.2016.12.010

Zhang, W., Sun, Q., Zhong, W., Sun, X., and Zhou, Z. (2016). Hepatic Peroxisome Proliferator-Activated Receptor Gamma Signaling Contributes to Alcohol-Induced Hepatic Steatosis and Inflammation in Mice. *Alcohol Clin. Exp. Res.* 40 (5), 988–999. doi:10.1111/acer.13049

Zhong, W., Zhao, Y., Tang, Y., Wei, X., Shi, X., Sun, W., et al. (2012). Chronic Alcohol Exposure Stimulates Adipose Tissue Lipolysis in Mice. *Am. J. Pathology* 180 (3), 998–1007. doi:10.1016/j.ajpath.2011.11.017

Conflict of Interest: The authors declare that the research was conducted in the absence of any commercial or financial relationships that could be construed as a potential conflict of interest.

frontiers | Frontiers in Physiology

TYPE Original Research
PUBLISHED 09 August 2022
DOI 10.3389/fphys.2022.870154

OPEN ACCESS

EDITED BY
Da-wei Zhang,
University of Alberta, Canada

REVIEWED BY
Ronaldo Thomatieli-Santos,
Federal University of São Paulo, Brazil
Xiao Zhu,
Guilin Medical University, China

*CORRESPONDENCE
Lachlan Van Schaik,
j.vanschaik@latrobe.edu.au

SPECIALTY SECTION
This article was submitted to Metabolic Physiology,
a section of the journal
Frontiers in Physiology

RECEIVED 06 February 2022
ACCEPTED 05 July 2022
PUBLISHED 09 August 2022

CITATION
Van Schaik L, Kettle C, Green R, Wundersitz D, Gordon B, Irving HR and Rathner JA (2022), Both caffeine and Capsicum annuum fruit powder lower blood glucose levels and increase brown adipose tissue temperature in healthy adult males.
Front. Physiol. 13:870154.
doi: 10.3389/fphys.2022.870154

Both caffeine and *Capsicum annuum* fruit powder lower blood glucose levels and increase brown adipose tissue temperature in healthy adult males

Lachlan Van Schaik [1]*, Christine Kettle [1], Rod Green [1], Daniel Wundersitz [2], Brett Gordon [2], Helen R. Irving [1] and Joseph A. Rathner [1,3]

[1]Department of Rural Clinical Sciences, La Trobe Institute for Molecular Science, La Trobe University, Bendigo, VIC, Australia, [2]Department of Rural Allied Health, Holsworth Research Initiative, La Trobe Rural Health School, La Trobe University, Bendigo, VIC, Australia, [3]Department of Anatomy and Physiology, School of Biomedical Sciences, The University of Melbourne, Melbourne, VIC, Australia

Using a combination of respiratory gas exchange, infrared thermography, and blood glucose (BGL) analysis, we have investigated the impact of *Capsicum annuum (C. annuum)* fruit powder (475 mg) or caffeine (100 mg) on metabolic activity in a placebo controlled (lactose, 100 mg) double-blinded three-way cross-over-design experiment. Metabolic measurements were made on day 1 and day 7 of supplementation in eight adult male participants (22.2 ± 2 years of age, BMI 23 ± 2 kg/m^2, $\bar{x}$ ± SD). Participants arrived fasted overnight and were fed a high carbohydrate meal (90 g glucose), raising BGL from fasting baseline (4.4 ± 0.3 mmol/L) to peak BGL (8.5 ± 0.3 mmol/L) 45 min after the meal. Participants consumed the supplement 45 min after the meal, and both caffeine and *C. annuum* fruit powder restored BGL ($F_{(8,178)} = 2.2$, $p = 0.02$) to near fasting levels within 15 min of supplementation compared to placebo (120 min). In parallel both supplements increased energy expenditure ($F_{(2, 21)} = 175.6$, $p < 0.001$) over the 120-min test period (caffeine = 50.74 ± 2 kcal/kg/min, *C. annuum* fruit = 50.95 ± 1 kcal/kg/min, placebo = 29.34 ± 1 kcal/kg/min). Both caffeine and *C. annuum* fruit powder increased supraclavicular fossa temperature ($F_{(2,42)} = 32$, $p < 0.001$) on both day 1 and day 7 of testing over the 120-min test period. No statistical difference in core temperature or reference point temperature, mean arterial pressure or heart rate was observed due to supplementation nor was any statistical difference seen between day 1 and day 7 of intervention. This is important for implementing dietary ingredients as potential metabolism increasing supplements. Together the results imply that through dietary supplements such as caffeine and *C. annuum*, mechanisms for increasing metabolism can be potentially targeted to improve metabolic homeostasis in people.

KEYWORDS

thermogenesis, substrate utilisation, capsaicin, glucose use, infra-red thermography (IRT), energy expenditure (EE), randomized double-blind placebo and positive-controlled crossover trial

Introduction

Brown adipose tissue (BAT) is activated rapidly in response to cold exposure, and diet, coupled with the potential to improve metabolic homeostasis in people with metabolic dysfunction (Poher et al., 2015; Van Schaik et al., 2021a). BAT is a specialised tissue that consumes energy, turning it into heat through non-shivering thermogenesis (Cannon and Nedergaard, 2004). BAT is a highly metabolically active tissue that participates in glucose homeostasis (Matsushita et al., 2014) and removes triglycerides from the blood (Bartelt et al., 2011; Berbee et al., 2015; Khedoe et al., 2015). In humans, as amounts of BAT decrease with age (Yoneshiro et al., 2011), changing the rate of BAT activity, or inducing BAT recruitment may provide considerable benefits for people with metabolic dysfunction. As such, BAT has the potential to not only be therapeutic but also a preventive mediator in lifestyle-related diseases, particularly diabetes mellitus, due to BAT activation improving whole-body glucose homeostasis and insulin sensitivity in humans (Chondronikola et al., 2014). Previous studies have shown cold acclimation increases BAT mass and BAT thermogenesis by modulating and improving insulin sensitivity in healthy humans (1 month acclimation at 19°C) (Lee et al., 2014) or patients with type 2 diabetes mellitus (10 days at 14–15°C) (Hanssen et al., 2015). These effects could possibly be achieved through dietary ingredients, as it has been shown that diet can stimulate BAT activity (Hibi et al., 2016; Saito et al., 2020), but the extent to which individual nutrients can have comparable effects is not well established.

Caffeine is the psycho-stimulant component of coffee, and other beverages (Smith, 2002). Caffeine increases thermogenesis in both rodents, and humans (Velickovic et al., 2019; Van Schaik et al., 2021b). However, the dose of caffeine is important, as large doses (≥410 mg) are known to have significant adverse effects on heart rate, blood pressure and be anxiogenic in humans (Noordzij et al., 2005; Vilarim et al., 2011). Conversely, acute single doses comparable to a standard cup of coffee in humans (~100 mg), increases interscapular BAT temperature without an adverse cardio dynamic effect in male rats (Van Schaik et al., 2021b). A single ingestion of a caffeine capsule (~375 mg, > 3 cups of coffee) increases the thermogenic activity of BAT in healthy young men and increases energy expenditure in those with only in those who already have high BAT mass compared to those with low BAT mass (Pérez et al., 2021). Glucose homeostasis is altered by acute caffeine ingestion (5 mg/kg) following 2 weeks of daily caffeine consumption in non-caffeine consuming males (Dekker et al., 2007). However, coffee consumption alone is unlikely to elicit significant weight loss in humans due to caffeine-induced lipolysis and catecholamine responses habituation with regular use (Dekker et al., 2007). Together, this suggests that caffeine may not be an anti-obesity therapeutic, but its long-term effect on BAT activity and glucose homeostasis may have considerable benefits for people with metabolic dysfunction. The effects of extensive caffeine use over several days on human BAT activity has not previously been reported.

Red peppers and *Capsicum annuum* (*C. annuum*) fruit are used as spices throughout the world. The major pungent principle of red pepper and *C. annuum* fruit is capsaicin (Saito and Yoneshiro, 2013), which has been reported to elevate body temperature in humans (Hachiya et al., 2007) and stimulate the secretion of catecholamines in rats (Watanabe et al., 1987). Capsaicin or capsinoids activate BAT thermogenesis in BAT positive humans (individuals with active BAT), as measured by [^{18}F] fluorodeoxyglucose positron emission tomography-computed tomography (18F-FDG PET/CT) imaging (Sun et al., 2018). Capsaicin activates transient potential receptor vanilloid 1 (TRPV1), which results in increases in adrenaline secretion (Iwasaki et al., 2008) and energy expenditure (Yoneshiro et al., 2012), while potentiating decreases in body fat in humans (Snitker et al., 2008). In mice, TRPV1 channels attenuate diet induced obesity and insulin resistance (Lee et al., 2015), and TRPV1 activation counters diet induced obesity through BAT activation (Baskaran et al., 2017). Furthermore, dietary capsaicin induces browning of white adipose tissue by activating TRPV1 channels (Baskaran et al., 2016; El Hadi et al., 2019). Prolonged ingestion of capsinoids for 6 weeks increases BAT vascular density and resting energy expenditure in healthy adults (Fuse et al., 2020). Capsaicin and its analog capsinoids, are representative TRPV1 agonists, and as such decrease body fat through the activation and recruitment of BAT, mimicking the effects of cold induced thermogenesis (Saito, 2015). While capsinoids/capsaicin activate BAT, the 18F-FDG PET/CT technique does not quantify the extent of thermogenesis or measure acute uptake of free fatty acids as a substrate for heat production. Infra-red thermography (IRT) is an alternative non-invasive imaging technique (Law et al., 2018; Brasil et al., 2020), employing the heat emitting properties of BAT and the superficial position of the supraclavicular human BAT depot. Several research groups have utilised IRT to show a specific rise in temperature in the supraclavicular fossa (Tscf), after cold stimulus and caffeine treatment (Lee et al., 2011; Symonds et al., 2012; Salem et al., 2016; Velickovic et al., 2019; Pérez et al., 2021).

We have shown in rodents that acute central and systemic administration of stimulatory, but non-anxiogenic doses of

TABLE 1 Participant demographics.

	All participants
n	8
Age, *y*	22 ± 2
Height, cm	176 ± 5
Weight, kg	74 ± 8
BMI, kg/m^2	23 ± 2
Body fat, %	20 ± 8

Values are means ± SD unless otherwise indicated.

caffeine activates key hypothalamic nuclei involved in the regulation of BAT and increases interscapular BAT temperature (Van Schaik et al., 2021b). Although acute consumption of coffee increases supraclavicular temperatures in adult humans (Velickovic et al., 2019; Pérez et al., 2021), there is a gap in the understanding of the effect of longer periods of caffeine ingestion (>1 day) on BAT thermogenesis, energy expenditure, and plasma glucose levels. Both caffeine and *C. annuum* in isolation have previously been shown to activate BAT (Yoneshiro et al., 2012; Velickovic et al., 2019), increase energy expenditure (Yoneshiro et al., 2012; Pérez et al., 2021) and improve glucose handling (Dekker et al., 2007; Chaiyasit et al., 2009), but not all in one study. Therefore, *C. annuum* will be used as a positive control. The primary aim of this study is to test whether longer periods of caffeine ingestion activates BAT thermogenesis, increases energy expenditure, lowers respiratory exchange ratio (RER), and lowers plasma glucose levels following a carbohydrate load. A secondary aim of this study is to test the effects of longer periods of caffeine ingestion on sympathetic activity (heart rate and heart rate variability), blood pressure, fat oxidation, and carbohydrate oxidation. Measuring these outcome variables together in the one study is important as it will enable a more holistic physiological assessment of responses to the supplementation. We hypothesise that caffeine ingestion will increase BAT temperature, energy expenditure, and lower blood glucose levels both acutely and on day seven following daily supplementation.

Research design and methods

The study design and protocol were approved by the University Human Ethics Committee (HEC 19032). Using data published in Acheson (Acheson et al., 2004) the predicated Cohen's d for difference in carbohydrate metabolism between placebo and caffeine in humans is 0.91. Power analysis using a repeated measure model to determine interaction effect (GPower 3.1.7) predicts that a sample size of eight subjects would allow the study to have 84% power to detect an effect size >0.5 between the supplement and control trials ($p < 0.05$).

Participants

Eight lean healthy adult male participants aged 18–28 years who could ingest capsules as well as present themselves for six data collection sessions at the University laboratory were recruited to participate in this study (Table 1). Females were excluded from this study as underlying fluctuations due to menstrual cycles prevent accurate evaluation of their energy expenditure changes using the experimental procedures (Sievers et al., 2019). All participants were screened for health status. Exclusion criteria included diabetes mellitus, participants taking any prescription medication, a body mass index (BMI) of >30 kg/m^2, and an inability to tolerate or experience potential adverse effects from coffee or caffeine containing products.

Study design

This randomized, double-blind, placebo, and positive-controlled crossover study was designed to compare the physiological effects of caffeine and *C. annuum* fruit in healthy adult males. The participants were randomly allocated to an intervention sequence via a random number generator by a researcher not involved in data collection. The investigators were blinded to conditions until completion of all data collection and analysis. All experiments were conducted under thermoneutral conditions (22°C) (van Marken Lichtenbelt et al., 2009; Iwen et al., 2017). The participants received either caffeine (100 mg/day, No Doze, Key Pharmaceuticals) (Velickovic et al., 2019; Van Schaik et al., 2021b), placebo (lactose, Ajax Chemicals), or capsicum positive control [475 mg of *C. annuum* fruit powder (capsaicin = 2.375 mg), Nature's Sunshine] (Lejeune et al., 2003; Johnson, 2007) capsules daily for 7-days each. Each of the interventions are non-prescription supplements and used at the manufacturer's specifications. To blind the participants and researchers to the supplements being ingested, all supplements were repackaged into generic capsules in advance and the capsules were placed in sealed envelopes by an investigator not involved in the data collection. The experimental protocol consisted of three trials (Figure 1), with each trial lasting for 7 days, with a washout period of 7 days between trials (5 weeks in total). Prior to Trial 1, participants were required to water fast for 11 h prior to testing and not perform any vigorous exercise within 24-h before testing. Additionally, participants were asked to abstain from caffeine and caffeinated products for the duration of the experiment. On Day 1 and Day 7 of each trial participants were asked to attend the laboratory water fasted. Participants arrived at the lab at 8 a.m., to control for daily hormone rhythms. Participants' height and weight were measured on each day of testing. At each laboratory visit, cardiovascular parameters, IRT, indirect calorimetry, blood glucose, and core temperature were measured every 15-min over a 120-min period. After baseline

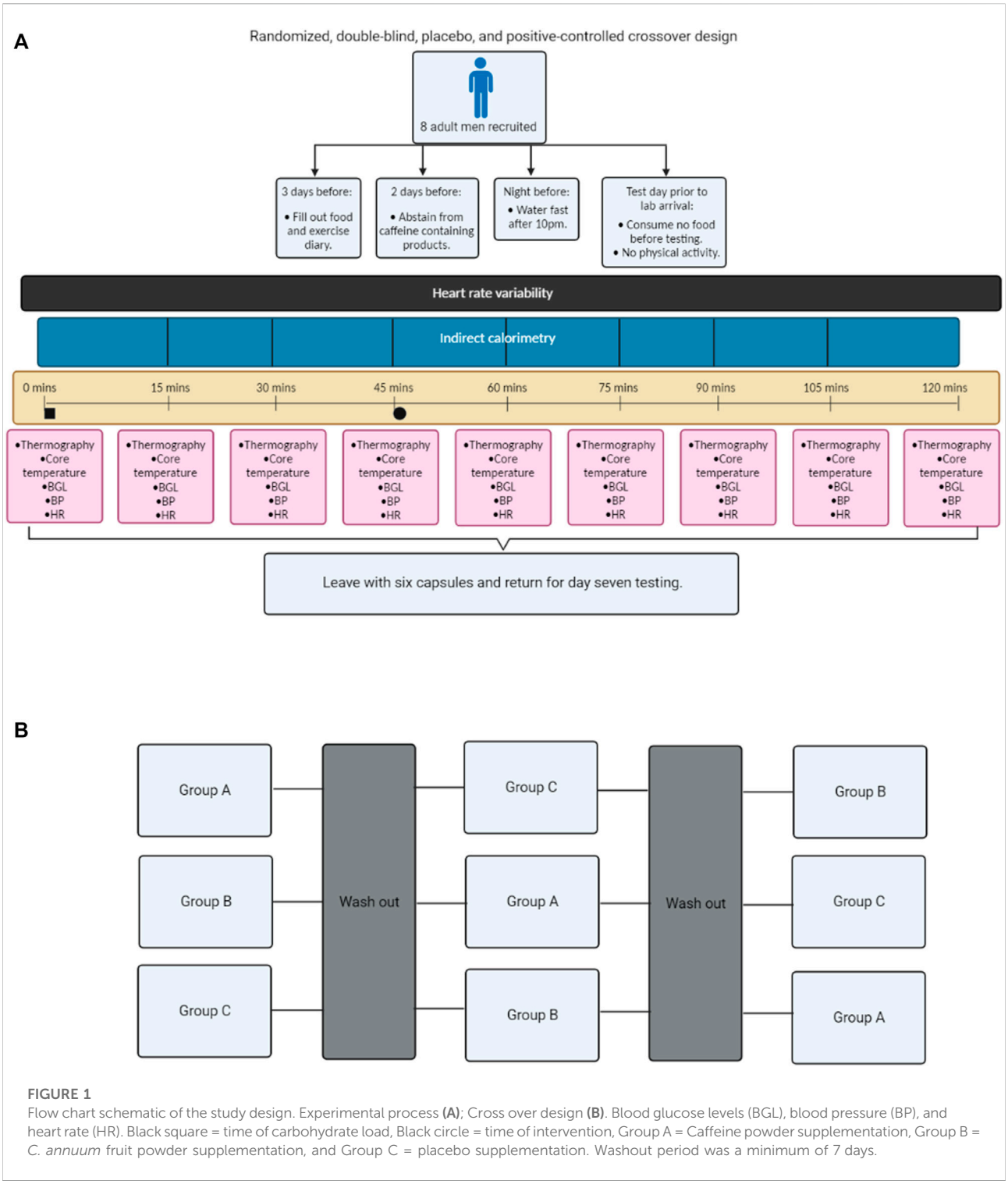

FIGURE 1
Flow chart schematic of the study design. Experimental process **(A)**; Cross over design **(B)**. Blood glucose levels (BGL), blood pressure (BP), and heart rate (HR). Black square = time of carbohydrate load, Black circle = time of intervention, Group A = Caffeine powder supplementation, Group B = *C. annuum* fruit powder supplementation, and Group C = placebo supplementation. Washout period was a minimum of 7 days.

measurements, participants were carbohydrate loaded through consumption of three carbohydrate gels (90 g glucose, Winners Sports Nutrition). In addition, before or after one of the scheduled testing sessions each participant was required to undergo a dual-energy X-ray absorptiometry (DXA; Hologic Horizon, Hologic Inc., Bedford, MA, United States) scan to measure fat mass. Participants filled out food and exercise diaries during the testing protocol. The participants were instructed to maintain their usual dietary intake, and physical activity during the experimental period. On non-testing days,

participants were instructed to consume the supplements in the morning at 9 a.m.

Indirect calorimetry

Substrate utilization and energy expenditure were estimated from expired gas, measured using a ParvoMedics TrueOne 2400 respiratory gas analyser (ParvoMedics Inc., East Sandy, UT, United States). Upon arrival at the laboratory, participants rested quietly on a plinth in the supine position for at least 30-min. Expired O_2 and CO_2 was sampled with 5 s averaging over a 15 min period, energy expenditure, and respiratory exchange ratio were calculated and averaged over the stable final 10 min of this period. Following baseline measurements expired O_2 and CO_2 were sampled in 15 min intervals. Carbohydrate and lipid oxidation rates and total energy expenditure were calculated using the non-protein Weir equations (Cunningham, 1990; Peronnet and Massicotte, 1991):

$$\text{Fat oxidation rate}\left(\text{g/min}^{-1}\right) = 1.695\,VO_2 - 1.701\,VCO_2$$

$$\text{Carbohydrate oxidation rate}\left(\text{g/min}^{-1}\right) = 4.585\,VCO_2 - 3.226\,VO_2$$

$$\text{Energy Expenditure (kcal/min)} = 3.94 \times VO_2 + 1.1 \times VCO_2$$

Core temperature measurements

With participants supine and the head in a neutral position, a non-contact infrared thermometer (Berrcom, JXB-178, Guangdong, China; the stated measurement error of this device is ± 0.2°C) was used to acquire body temperature measurements. Core temperature was not directly measured due to COVID-19 safety restrictions; a non-contact infrared thermometer was used as a measurement of core temperature. The non-contact thermometer was positioned consistently towards the centre of the participant's forehead.

Plasma blood glucose measurements

Blood samples were collected *via* finger (capillary) puncture and blood glucose levels were determined using a glucometer (Freestyle Optium Xceed, Abbott Diabetes Care, Alameda, SK, Canada). Blood glucose readings were conducted after expired gas measurements were completed.

Anthropometric measurements

On each testing day body mass was measured using calibrated scales (Seca 813, Seca, Hamburg, Germany) and followed by measurements of stature using a wall mounted stadiometer (Seca 206, Seca, Hamburg, Germany). Body Mass Index (BMI) was calculated as follows: body mass in kilograms divided by the square of stature in meters (kg/m^2). Body composition (bone mineral density, fat mass, lean mass, total mass, and total body fat percentage) was measured using DXA analysis (Haarbo et al., 1991).

Cardiovascular measurements

Systolic and diastolic blood pressure (mmHg) as well as heart rate (beats/min) were measured using an automated sphygmomanometer (Omron SEM-2 advanced, Omron, Kyoto, Japan) after expired gas measurements were completed, and at a similar time (within 3 min) as blood glucose measurements. Heart rate variability (HRV; square milliseconds) was determined from continuous electrocardiogram (ECG) recordings obtained from a five lead ECG (Medilog AR12 plus; Schiller, Germany) as a measure for central autonomic balance. Participants were required to remove clothing above the waist to allow placement of ECG electrodes (Ambu Blue Sensor R, Malaysia). The recorded ECG was analyzed using Medilog Darwin2 software (Professional; Schiller, Germany) and HRV was determined in the spectral domain using Welch's method, a fast Fourier transform (FFT) width 128 overlap and a 5-min window size. Welch's method and 128 overlap has been shown to provide a smoothed spectral estimate with clearly outlined peaks in low and high frequency bands (Malik, 1998). The calculation includes low frequency bands (LF), high frequency bands (HF), and the log LF/HF ratio as the log LF/HF ratio conforms the data more readily to a normal distribution.

Infrared thermography

Every 15-min, participants were asked to sit up in an upright posture looking straight ahead with the chest area to neck region exposed. A thermal imaging camera (FLIR E60, FLIR Systems Australia, Melbourne, Australia) was used to acquire images of the anterior neck and upper chest region. The camera was positioned on a tripod at the level of the neck 1 m from the subject's face.

Data/statistical analysis

For analysis of the IRT, bilaterally, three regions of the anterior thorax were chosen for analysis of surface temperature, with the skin overlying BAT in the supraclavicular fossa (SCF) and the lateral region of the neck, with the sternal area considered as a control reference point as this area does not contain BAT (van der Lans et al., 2014;

El Hadi et al., 2016). Triangular regions of interest (ROI) were placed in the left and right SCF areas, while a circular ROI was placed over the sternal region. The mean temperature of these ROIs was then extracted for further analysis (van der Lans et al., 2014; El Hadi et al., 2016). The thermal images were analysed to determine mean temperature (°C) using FLIR Research and Development software (FLIR Systems Australia, Melbourne, Australia).

All statistical analysis was conducted using PRISM 9 GraphPad software. Averages from the IRT, core temperature, blood glucose, heart rate, and blood pressure data were taken from the measured single time point. Averages from the RER, fat oxidation, carbohydrate oxidation, and energy expenditure were calculated in 10-min epochs. Averages from HRV were calculated in 5-min epochs. Data are expressed as mean ± SD. To assess if any differences at baseline occurred in each measure in the intervention groups, average baseline IRT temperatures, core temperature and cardiovascular measures prior to supplementation were tested using a one-way ANOVA, Welch's correction. All averages from outcome measurements are expressed as change from baseline for each intervention group. All data were inspected for normality which indicated parametric distribution, furthermore the central limit theorem states that given sufficient samples, sample distribution will be normal, regardless of the underlying population distribution (Kwak and Kim, 2017). The data values were analysed using repeated measures 3-way analysis of variance (ANOVA; day × treatment × time). Each ANOVA assessed differences between treatments (caffeine, capsaicin, and control), day (1 and 7), and time points. For energy expenditure, we summed the rate of energy expenditure for each group and separated it into pre intervention and post intervention for both day 1 and day 7. Data for each group were analysed using separate two-way repeated measures ANOVA for each testing day (day 1 and day 7). Each ANOVA assessed differences between treatments (caffeine, *C. annuum*, and placebo) and time points (pre vs. post intervention).

To assess if the order of treatment impacted on the study, averages from the IRT, core temperature, blood glucose, heart rate, heart rate variability, blood pressure, RER, fat oxidation, carbohydrate oxidation, and energy expenditure values were analysed in the same manner as the 3-way ANOVA described above. However, rather than assessing difference between treatments, day, and timepoints, each ANOVA assessed differences between trial order, day and timepoints (ANOVA; day × trial × time). If a significant interaction or main effect was found, post hoc analysis was conducted *via* a *t*-test between trials to determine where the significance detected by the ANOVA occurred. For multiple comparisons a Bonferroni correction was applied. Values were considered to indicate statistical significance if $p < 0.05$.

Results

Participant's characteristics

A total of eight participants were included in this study. The participants age, stature, mass, BMI, and body fat percentage can be found in Table 1. Each participant's baseline temperature, blood glucose levels, and cardiovascular measures were recorded and no significant differences in any blood glucose, cardiovascular or temperature measures were detected (Tables 2, 3; $p > 0.05$, one-way AVOVA).

Caffeine and *C. annuum* effects on substrate utilization and blood glucose levels

A randomised crossover design administering caffeine, *C. annuum* fruit powder, or placebo interventions to healthy male participants were used to assess any potential differences between acute effects and prolonged daily administration of the interventions after a carbohydrate load on respiratory exchange ratio (RER), substrate utilisation, and blood glucose levels (Figure 1). As this is a crossover study it is important to test if the order of treatment has any influence on the outcomes reported. No effect on the order of treatment was observed in this study (Supplementary Figures S1–S3).

For RER a significant interaction effect ($F_{(9,198)} = 2.8$, $p < 0.001$, Figures 2A,B) was identified. Participants were given a carbohydrate load and then an intervention 45 min later. The caffeine intervention reduced RER from 60 to 105 min, while the *C. annuum* fruit powder intervention lowered RER from 60 to 75 min compared to the placebo at day 1 (Figure 2A). Similar results were seen after 7 days of intervention with the caffeine intervention reducing RER from 60 to 105 min, while *C. annuum* fruit powder improving in efficacy and lowering RER from 60 to 90 min. Reflecting the significant day interactions ($F_{(9.4,198.5)} = 2.8$, $p = 0.003$, Figures 2A,B). The peak day 1 lowering of RER for the caffeine treatment was 60 min after administration (Figure 2A), peak day 7 lowering of RER for the caffeine treatment was 30 min after administration (Figure 2B). The peak day 1 lowering of RER for the *C. annuum* fruit powder treatment was 30 min after administration (Figure 2A). Peak day 7 lowering of RER for *C. annuum* fruit powder treatment was 75 min after administration (Figure 2B).

For fat oxidation a significant interaction effect ($F_{(10,229)} = 8.9$, $p < 0.001$, Figures 2C,D) was found. The caffeine intervention increased levels of fat oxidation from 75 to 105 min, while the *C. annuum* fruit powder intervention increased fat oxidation from 75 to 90 min compared to placebo. After 7 days of intervention with caffeine levels of fat oxidation improved with increases between 60 and 120 min, while *C. annuum* fruit powder increased levels of fat oxidation between 75 min and 90 min

TABLE 2 Average baseline skin and core temperature measures.

	Tscf (°C) day 1	Tscf (°C) day 7	Tcore (°C) day 1	Tcore (°C) day 7	Tref (°C) day 1	Tref (°C) day 7
Caffeine capsule	34.08 ± 0.1	34.03 ± 0.1	36.56 ± 0.3	36.45 ± 0.3	34.16 ± 0.2	34.15 ± 0.1
C. annuum fruit capsule	33.98 ± 0.1	33.09 ± 0.1	36.54 ± 0.3	36.40 ± 0.2	34.14 ± 0.1	34.14 ± 0.2
Placebo capsule	33.95 ± 0.1	33.95 ± 0.1	36.45 ± 0.3	36.20 ± 0.3	34.03 ± 0.1	34.08 ± 0.1
p value	0.12	0.11	0.76	0.13	0.29	0.57

Average baseline skin temperature measures prior to supplementation. Statistical testing (one-way ANOVA, Welch's correction) indicates no significant difference (p value > 0.05) in base line conditions prior to interventions. Values are means ± SD (n = 8 per intervention). Tscf, supraclavicular temperature; Tcore, core temperature; Tref, manubrium temperature.

TABLE 3 Average baseline for cardiovascular and blood glucose measures.

	HR (BPM) day 1	HR (BPM) day 7	MAP (mmHg) day 1	MAP (mmHg) day 7	BGL (mmol/L) day 1	BGL (mmol/L) day 7
Caffeine capsule	63.25 ± 10.2	59.87 ± 7.4	85.26 ± 9.8	89.61 ± 9.5	4.25 ± 0.24	4.13 ± 0.32
C. annuum fruit capsule	58.12 ± 8.6	58.34 ± 6.9	89.8 ± 8.4	85.42 ± 3.6	4.53 ± 0.16	4.41 ± 0.28
Placebo capsule	66.13 ± 8.4	67.31 ± 8.6	88.53 ± 6.5	90.73 ± 6.1	4.42 ± 0.24	4.38 ± 0.18
p value	0.25	0.09	0.92	0.82	0.07	0.22

Average baseline for cardiovascular and blood glucose measures prior to supplementation. Statistical testing indicates no difference in baseline conditions prior to interventions. p value is calculated using a one-way ANOVA, Welch's correction, n = 8 per intervention. Values are means ± SD (n = 8 per intervention). HR, heart rate (beats per minute); MAP, mean arterial pressure (millimetres of Mercury); BGL, blood glucose levels (millimole per litre).

compared to placebo (Figures 2C,D). The peak day 1 increase in fat oxidation for the caffeine treatment was 60 min after administration (Figure 2C), peak day 7 increase in fat oxidation for the caffeine treatment was 45 min after administration (Figure 2D). The peak day 1 increase in fat oxidation for the *C. annuum* fruit powder treatment was 75 min after administration (Figure 2C). Peak day 7 increase in fat oxidation for *C. annuum* fruit powder treatment was 60 min after administration (Figure 2D). No significant day interaction effect was found for fat oxidation.

For carbohydrate oxidation a significant interaction effect ($F_{(8,174)} = 7.1$, $p < 0.001$, Figures 2E,F) was found. The caffeine intervention lowered the rate of carbohydrate oxidation between 60 and 105 min, while the *C. annuum* fruit powder intervention lowered the rate of carbohydrate oxidation between 105 and 120 min compared to placebo on day 1 (Figure 2E). Similar results were seen after 7 days of intervention with the caffeine intervention lowering the rate of carbohydrate oxidation between 60 and 105 min, whereas *C. annum* fruit powder lowered the rate of carbohydrate oxidation between 60 and 75 min compared to placebo on day 7 (Figure 2F). The peak day 1 lowering in carbohydrate oxidation for the caffeine treatment was 75 min after administration (Figure 2E), peak day 7 lowering in carbohydrate oxidation for the caffeine treatment was 75 min after administration (Figure 2F). The peak day 1 lowering of carbohydrate oxidation for the *C. annuum* fruit powder treatment was 75 min after administration (Figure 2E). Peak day 7 increase in fat oxidation for *C. annuum* fruit powder treatment was 75 min after administration (Figure 2F). No significant day interaction effect was found for carbohydrate oxidation.

For BGL a significant interaction effect ($F_{(8,178)} = 2.2$, $p = 0.02$, Figures 2G,H) was found. Participants arrived fasted overnight and were feed a high carbohydrate meal, raising fasting BGL from baseline (4.4 ± 0.3 mmol/L) to peak BGL (8.5 ± 0.3 mmol/L) 45 min after the meal. Participants consumed the supplement at 45 min after the meal, and both caffeine and *C. annuum* fruit powder lowered BGL levels between 60 and 105 min compared to placebo on day 1 and day 7 (Figures 2G,H). Both caffeine and *C. annuum* fruit powder restored BGL to near fasting levels within 15 min of supplementation compared to placebo (120 min) on day 1 and day 7. No significant day interaction effect was found for BGL.

Caffeine and *C. annuum* effects on total energy expenditure

To assess whether caffeine or *C. annuum* fruit powder increased energy expenditure independent of the carbohydrate load we summed the rate of energy expenditure for each group and separated it into pre intervention and post intervention for both day 1 and day 7.

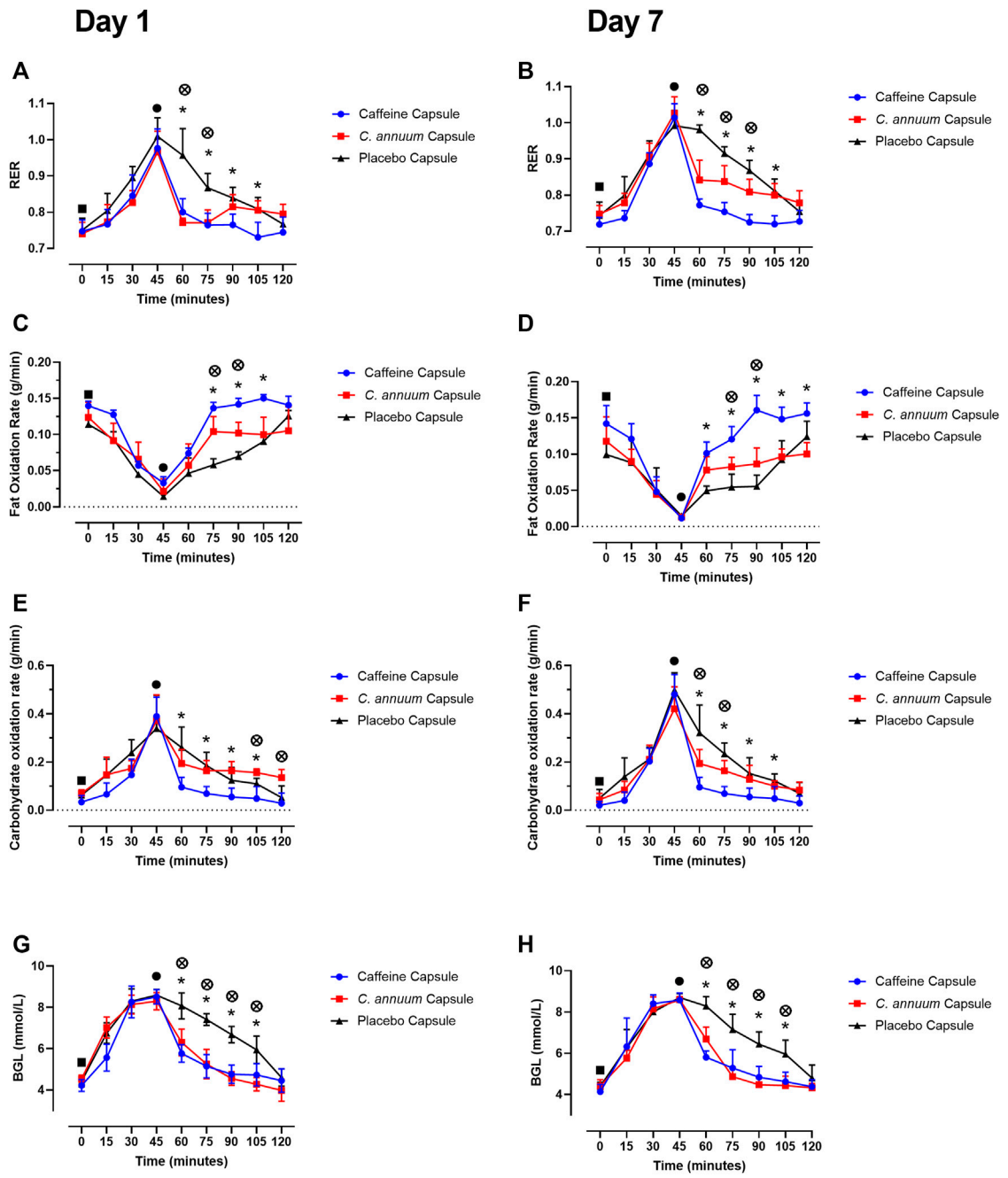

FIGURE 2
Effects of interventions on metabolic measures. Respiratory exchange ratio (RER) **(A)** day 1 and **(B)** day 7. Fat oxidation rate **(C)** day 1 and **(D)** day 7, and carbohydrate oxidation rate **(E)** day 1, **(F)** day 7. Blood glucose levels **(G)** day 1, and **(H)** day 7. Filled black square, time of carbohydrate load; filled black circle, time of intervention; blue circle, caffeine capsule; red square, *C. annuum* fruit powder capsule; black triangle, placebo capsule. Data is expressed as mean ± SD, $n = 8$ per intervention, *represents caffeine interaction effect, ⊗ represents *C. annuum* fruit powder interaction effects (*, ⊗ $p < 0.05$). Data values were analysed using repeated measures 3-way analysis of variance (ANOVA; day × treatment × time). Each ANOVA assessed differences between treatments (caffeine, *C. annuum* fruit powder, control), day (1 and 7), and time points. If a significant interaction or main effect was found, post hoc analysis was conducted *via* a *t*-test between trials. For multiple comparisons a Bonferroni correction was applied.

For day 1 energy expenditure, a significant interaction effect ($F_{(2, 21)} = 175.6$, $p < 0.001$, Figure 3A) was found. Post-hoc analysis revealed that both caffeine (53.2 ± 1 kcal/kg/min) over the 120 min intervention period and *C. annuum* fruit powder (50.95 ± 1 kcal/kg/min over 120 min) significantly increased the rate of energy expenditure compared to placebo (30.14 ±

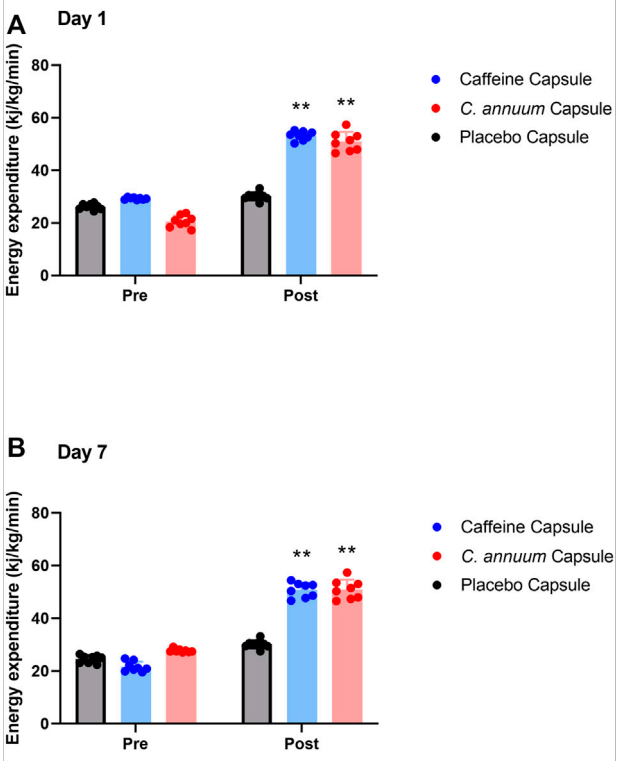

FIGURE 3
Changes in whole-body energy expenditure in participants between pre- and post-administration of interventions in a 120 min period. **(A)** day 1 and **(B)** day 7. Grey bar, placebo capsule; blue bar, caffeine capsule; red bar, *C. annuum* fruit powder capsule. Data is expressed as mean ± SD, n = 8 per intervention, *represents interaction effect (*$p < 0.05$). Data values were analysed using repeated measures 2-way analysis of variance (ANOVA; pre × post). Each ANOVA assessed differences between treatments (caffeine, *C. annuum*, and placebo) and time points (pre vs. post intervention).

2 kcal/kg/min over 120 min). Similarly, for day 7, a significant interaction effect ($F_{(2, 21)} = 98.84$, $p < 0.0001$, Figure 3B) was found. Post-hoc analysis revealed that caffeine (50.74 ± 2 kcal/kg/min) and *C. annuum* fruit powder (50.95 ± 1 kcal/kg/min) significantly increased the rate of energy expenditure compared to placebo (29.34 ± 1 kcal/kg/min; Figures 3A,B). No significant day interaction effect was found for energy expenditure.

Caffeine and *C. annuum* effects on temperature of the supraclavicular region

The supraclavicular region co-locates with BAT in humans (van der Lans et al., 2014; El Hadi et al., 2016), so we utilised IRT to assess whether caffeine or *C. annuum* fruit powder supplementation increased Tscf. Triangular ROIs were placed in the left and right SCF areas, while a circular ROI was placed over the sternal region. IRT images from one participant visually highlights changes in Tscf from baseline (Figure 4A), post carbohydrate load (Figure 4B), and 60 min following caffeine supplementation (Figure 4C). Changes in Tscf following caffeine supplementation are particularly marked (compare Figures 4B,C).

A significant interaction effect ($F_{(2,42)} = 32$, $p < 0.001$, Figures 4D,E) and post-hoc analysis revealed a single capsule of caffeine or *C. annuum* fruit powder consumed acutely on separate occasions increased Tscf region co-locating with BAT in humans (Figure 4D), and this effect was reproduced at the end of the 7-days treatment period (Figure 4E). Caffeine increased Tscf between 60 and 105 min, while *C. annuum* fruit powder increased Tscf between 75 and 105 min compared to placebo on day 1. For day 7, caffeine increased Tscf between 60 and 120 min, and *C. annuum* fruit powder increased Tscf between 60 and 105 min, with no change in temperature for the placebo treatment. The peak day 1 increase in temperature for the caffeine treatment was 30 min after administration (Figure 4D), similarly peak day 7 increase in temperature for the caffeine treatment was 30 min after administration (Figure 4E). The peak day 1 increase in temperature for the *C. annuum* fruit powder treatment was also 30 min after administration (Figure 4D). Likewise, peak day 7 increase in temperature for *C. annuum* fruit powder treatment was 30 min after administration (Figure 4E). Neither caffeine or *C. annuum* fruit powder treatment evoked changes in core temperature ($F_{(2,42)} = 0.5$, $p = 0.5$) for both day one and day seven testing (Figures 4F,G). Additionally, there were no changes in temperature of the manubrium ($F_{(11,240)} = 1$, $p = 0.2$, Figures 4H,I) following treatment of caffeine or *C. annuum* fruit powder on day one and day seven testing. No significant day interaction effect was found for Tscf, core, or manubrium.

Caffeine or *C. annuum* effects on cardiovascular measures

To test whether the dose of caffeine and *C. annuum* fruit powder affected cardiovascular responses, heart rate (HR), mean arterial pressure (MAP), and heart rate variability (HRV) were measured. Neither caffeine or *C. annuum* fruit powder changed HR compared to placebo over time on either day 1 or day 7 testing ($F_{(10,222)} = 0.6$, $p = 0.7$, Figures 5A,B). Similarly, caffeine and *C. annuum* fruit powder had no effect on MAP compared with placebo on both day 1 and day 7 testing ($F_{(12,268)} = 0.8$, $p = 0.5$, Figures 5C,D). No significant day interaction effect was found for HR and MAP.

For HRV, a significant interaction effect was found ($F_{(8,170)} = 1.6$, $p = 0.04$, Figures 5E,F). Caffeine treatment significantly increased HRV compared to placebo on day 1 between 60 and 105 min. Similarly, caffeine increased HRV on day

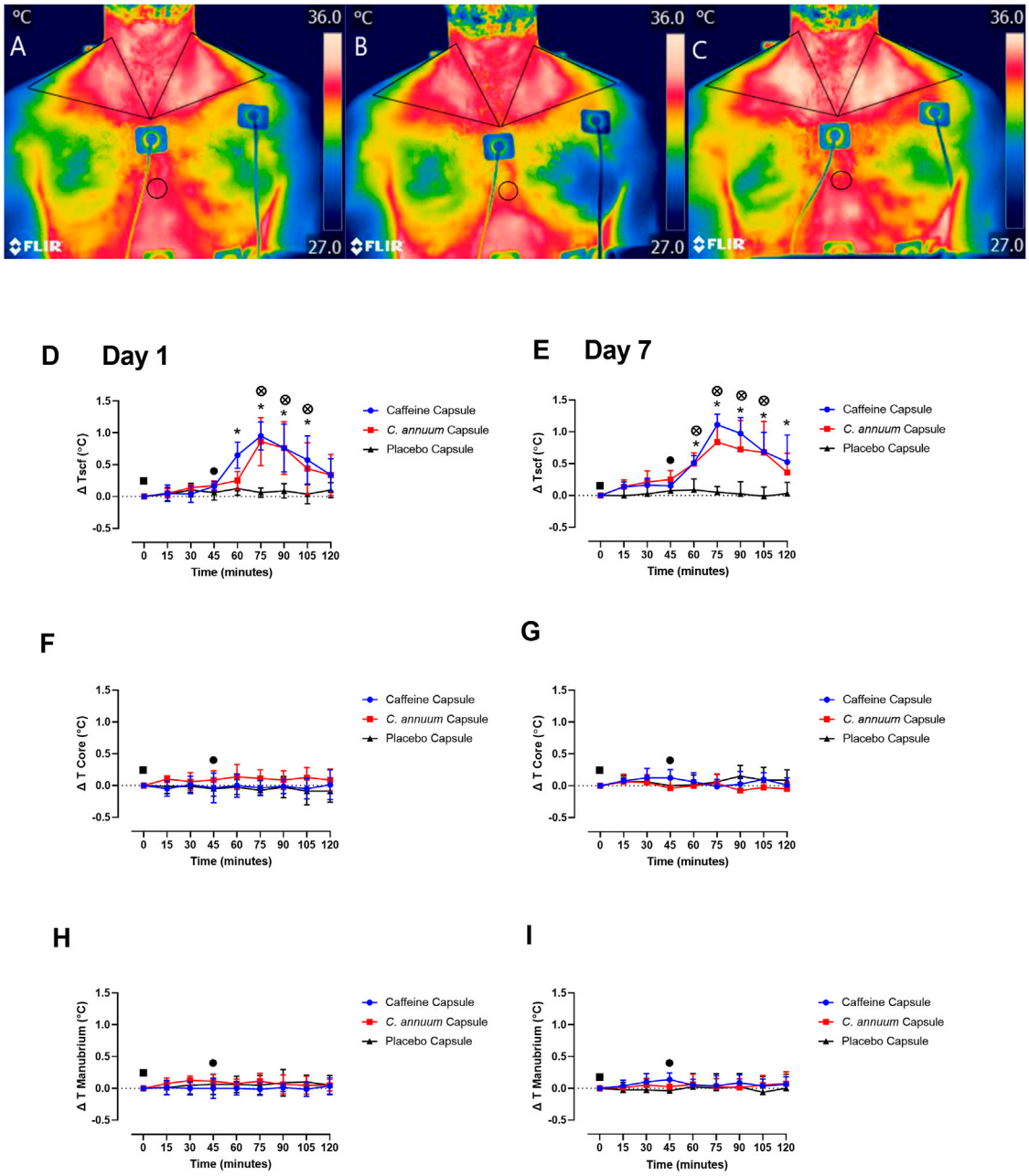

FIGURE 4
Representative example of thermal images of the skin overlying the region of interest (ROI) located at the supraclavicular fossa (SCF) and sternal (circular ROI) area in participants. **(A)** at baseline measurement, **(B)** 15 min post carbohydrate load and **(C)** at 90 min post intervention with caffeine treatment. Changes in temperature (ΔT) of SCF, core and manubrium in participants following a carbohydrate load (time = 0), and administration of a caffeine capsule, *C. annuum* fruit powder capsule, or placebo capsule (time = 45) to 120 min. SCF temperature **(D)** day 1 and **(E)** day 7. Core temperature **(F)** day 1 and **(G)** day 7, and manubrium temperature **(H)** day 1, **(I)** day 7. Filled black square, time of carbohydrate load; filled black circle, time of intervention; blue circle, caffeine capsule; red square, *C. annuum* fruit powder capsule; black triangle, placebo capsule. Error bars represent S.D., $n = 8$ per intervention, *represents caffeine interaction effect, ® represents *C. annuum* fruit powder interaction effects (*, ® $p < 0.05$). The data values were analysed using repeated measures 3-way analysis of variance (ANOVA; day × treatment × time). Each ANOVA assessed differences between treatments (caffeine, *C. annuum* fruit powder, control), day (1 and 7), and time points. If a significant interaction or main effect was found, post hoc analysis was conducted *via* a *t*-test between trials. For multiple comparisons a Bonferroni correction was applied. Values were considered to indicate statistical significance if $p < 0.05$.

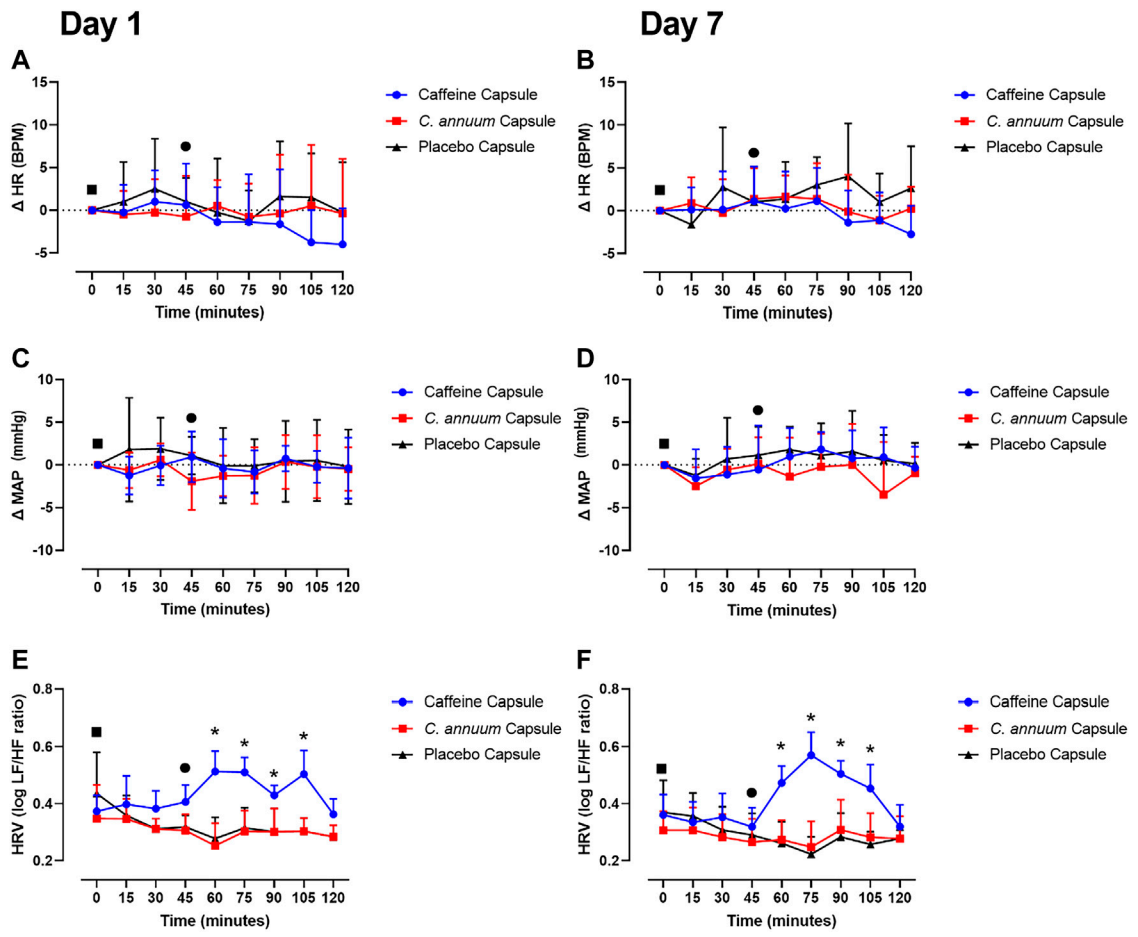

FIGURE 5
Effects of interventions on cardiovascular measures of participants. The cardiovascular measures were made following a carbohydrate load (time = 0), and administration of a caffeine capsule, *C. annuum* fruit powder capsule, or placebo capsule (time = 45) to 120 min. Changes (Δ) in heart rate **(A)** day 1 and **(B)** day 7. Δ in mean arterial pressure (MAP) **(C)** day 1 and **(D)** day 7, and heart rate variability (HRV) **(E)** day 1, **(F)** day 7. Filled black square = time of carbohydrate load, filled black circle = time of intervention, blue circle = caffeine capsule, red square = capsicum capsule, and black triangle = placebo capsule. Error bars represent S.D., n = 8 per intervention, *represents caffeine interaction effect, ⊗ represents capsicum interaction effects (*, ⊗ $p < 0.05$). The data values were analysed using repeated measures 3-way analysis of variance (ANOVA; day × treatment × time). Each ANOVA assessed differences between treatments (caffeine, *C. annuum*, control), day (1, 7), and time points. If a significant interaction or main effect was found, post hoc analysis was conducted using Bonferroni's test. Values were considered to indicate statistical significance if $p < 0.05$.

7 between 60 and 105 min, Figures 5E,F). The peak day 1 increase in HRV for the caffeine treatment was 30 min after administration (Figure 5E), peak day 7 increase in HRV for the caffeine treatment was 30 min after administration (Figure 5F). No significant day interaction effect was found for HRV.

Discussion

This study shows a physiologically significant effect of caffeine and *C. annuum* fruit powder on BAT activation, substrate utilisation, energy expenditure, and blood glucose levels. Here we show that both caffeine (100 mg/day) and *C. annuum* (475 mg/day) taken on separate occasions, lowers blood glucose levels, increases fat oxidation, decreases carbohydrate utilisation, increases total energy expenditure, lowers RER, and increases Tscf after a carbohydrate load. Notably, these effects are sustained in treatments continued over a period of 7 days. To our knowledge this is the first-time measures of energy expenditure, substrate utilisation, blood glucose, and BAT thermogenesis have all together been significantly altered, and this effect has been sustained for a prolonged period.

In this study, we measured thermogenesis as changes in Tscf, a region co-locating with BAT in humans (El Hadi et al., 2016). The increases in Tscf compared to the manubrium

reference point and core body temperature, combined with the changes in RER, fat oxidation, and carbohydrate oxidation is indicative of physiologically meaningful BAT thermogenesis following both caffeine and *C. annuum* supplementation. This is important as cold induced BAT thermogenesis improves insulin sensitivity and whole-body glucose homeostasis in healthy individuals (Chondronikola et al., 2014) and those with type 2 diabetes (Hanssen et al., 2015). These results combined with the blood glucose findings suggest that caffeine supplementation through central and peripheral mechanisms (Van Schaik et al., 2021a; Van Schaik et al., 2021b) and *C. annuum* supplementation through TRPV1 mediated mechanisms (Ahuja et al., 2006; Wang et al., 2012; Saito and Yoneshiro, 2013; Baskaran et al., 2016) may have the potential to target BAT to improve insulin sensitivity in humans. The extent to which individual dietary components can activate BAT in humans is not clear. However, the significant results from this study within 15-min following caffeine or *C. annuum* fruit supplementation, may help in providing some clarity about the mechanisms.

Results from this study show that a single caffeine capsule (100 mg) consumed daily increases energy expenditure, Tscf, lowers RER, and increases fat oxidation acutely and after 7 days of supplementation. Pérez et al. (2021) show that in physically active men a single caffeine capsule of 375 mg resulted in an acute increase in energy expenditure 40-min after supplementation and BAT activation (measured via IRT) after 30 min. Results from Pérez et al. (2021) are similar to a previous study (Yoneshiro et al., 2017) which observed an increase in energy expenditure in participants following ingestion of a tea rich in catechins (natural phenolic compounds found in green teas). Our caffeine treatment results are comparable to Pérez et al. (2021) in terms of change in Tscf, and energy expenditure, but importantly we observe this effect for 7 days and at a lower, more tolerable caffeine dose. However, Pérez et al. (2021) assessed the effects of caffeine in physically active men (Pérez et al., 2021). It should be noted that within our study, participants levels of physical activity were collected through food and exercise diaries, and participants were instructed to maintain regular levels of physical activity, but physical activity was not a needed for inclusion in this study. Given this, results from our study significantly build upon those described by Pérez et al. (2021), as a key part of the protocol is the carbohydrate loading of the participants, which ensures carbohydrate metabolism prior to intervention. This was not done in the Pérez et al. (2021) study. BAT thermogenesis switches metabolism from carbohydrate to free fatty acid as evidence by the decline in RER. Although the preferred substrate for BAT thermogenesis is free fatty acids, substantial uptake of glucose into active BAT is well known (Orava et al., 2011; Ouellet et al., 2012; Chen et al., 2013). Thus, we observe concomitant with BAT thermogenesis a fall in blood glucose levels. Both the change in substrate utilization (RER) and the fall in blood glucose levels would not be observable if the in a fasted state.

Human studies investigating the thermogenic influence of nutrients on BAT activity are limited. This may be due to the long considered gold standard to assess BAT function, 18F-FDG PET/CT (van Marken Lichtenbelt et al., 2009) that requires subjects to be fasted. This is due to feeding induced increases in glucose uptake by muscular tissue, which considerably limits the capacity for this method to detect BAT and BAT function (Roman et al., 2015). Additionally, this method alone cannot quantify the physiological significance or amount of BAT activation. Finally, due to the use of ionizing radiation in PET imaging studies, repeat measure cross over designs are difficult to administer. Our technique of carbohydrate loading subjects prior to measuring BAT temperature and combining indirect calorimetry, and blood glucose levels allows us to quantify the physiological extent of thermogenesis and altered substrate utilization, which would otherwise be masked during a fasted state. Several research groups have utilised IRT to show a specific rise in supraclavicular temperatures, after cold stimulus (Lee et al., 2011; Symonds et al., 2012; Andersson et al., 2019). IRT has the advantage of being able to measure BAT activation in real time and can be used repeatedly in large numbers of healthy or unhealthy subjects, irrespective of age or nutritional status. But IRT of SCF alone is not a suitable measure for BAT activation, as it is indirect, and subject to potential confounding factors such as increased blood flow. Temperatures from other landmarks such as the chest region and core temperature are required to demonstrate any increase in Tscf being suggestive of BAT activation (El Hadi et al., 2016; Andersson et al., 2019; Brasil et al., 2020). We have, therefore, utilized a practical method to detect changes in BAT activity, which can detect adjustments in response to ingestion without requiring exposure to radiation. Also, this technique correlates well with the uptake of 18F-FDG following cold exposure (Law et al., 2018).

Our results indicate energy expenditure increases, RER lowers, which coincides with fat oxidation increasing following ingestion of *C. annuum* (capsaicin). A systematic review and meta-analysis (Jang et al., 2020) examined the effects of *C. annuum* supplementation on components of metabolic syndrome. Metabolic syndrome is characterised by hypertension, dyslipidemia, insulin resistance, and abdominal obesity (McCracken et al., 2018). The meta-analysis found *C. annuum* has a significant effect on LDL-cholesterol and body weight, however the meta-analysis did not show any significant effect of *C. annuum* on diastolic blood pressure, and systolic blood pressure, and no significant effect on glucose levels but the analysis showed considerable heterogeneity between studies (Jang et al., 2020). Another meta-analysis which has examined energy expenditure, fat oxidation, and respiratory quotient (Zsiborás et al., 2018) showed that following consumption of capsaicin energy expenditure increased (245 kJ/day, 58.56 kcal/day) and the

respiratory quotient decreased (by 0.216) indicating a rise in fat oxidation. Furthermore, these metabolic effects of capsaicin are significant in individuals with a BMI greater than 25 kg/m^2 (Zsiborás et al., 2018). Although our study only looked at these measures in healthy individuals with a BMI of <25 kg/m^2, our results are consistent with the findings of this meta-analysis (Figures 2, 3).

Results from this study show that caffeine but not *C. annuum* fruit powder supplement significantly increases HRV (LF/HF ratio) on both testing days. Heart rate variability is the fluctuation in the time intervals between adjacent heartbeats (Ernst, 2017). HRV is a measure of the balance between sympathetic and parasympathetic autonomic drive to the heart (cardiac autonomic activity) (Ernst, 2017). Frequency-domain measurements estimate the distribution of absolute or relative power into four frequency bands. Task Force of the European Society of Cardiology the North American Society of Pacing Electrophysiology (1996) divided heart rate fluctuations into ultra-low-frequency, very-low-frequency, low-frequency (LF), and high-frequency (HF) bands (1996). Essentially, the closer the LF/HF ratio is to one the more sympathetic tone there is, the closer the ratio is to zero the more parasympathetic balance. Results from this study show an increase in HRV (LF/HF ratio) and increased Tscf following caffeine supplementation. This indicates caffeine is acting to increase sympathetic nerve drive systemically in the body (Van Schaik et al., 2021a). Previous rodent studies have shown caffeine works through central mechanisms to activate BAT thermogenesis (Van Schaik et al., 2021b). Notwithstanding the increased sympathetic activity to the heart, the doses of caffeine used in this study had no measurable impact on either HR or MAP. We did not find *C. annuum* to have any effect on HRV (LF/HF ratio). This suggests that the *C. annuum* and caffeine are acting via different pathways to evoke the observed increases in energy expenditure, Tscf and blood glucose removal. We observe that in participants at rest, the LF/HF ratio starts off much lower than we might expect possibly due to participants laying supine rather than sitting upright. This could result in less sympathetic nerve drive required to maintain MAP.

A key strength of this study is that we carbohydrate loaded participants prior to supplementation. Previous studies have used fasted individuals and seen no acute change in substrate utilization, which is masked by the fasted state (Ohnuki et al., 2001; Galgani et al., 2010). By carbohydrate loading the participants we were able to see the oscillation of BGL in response to both carbohydrate loading and supplement intervention along with changes in substrate utilization. Due to COVID-19 safety restrictions core temperature was not measured invasively. As such a non-contact infrared thermometer measuring forehead temperature was used to measure core temperature. These thermometers are calibrated to make clinical measures of fever (Teran et al., 2012). Furthermore, participants in the study laid still at a constant ambient temperature thermoneutral temperature (22°C) (van Marken Lichtenbelt et al., 2009; Iwen et al., 2017), minimising any artefacts due to increased/altered skin blood flow. Evidence suggests that these non-contact thermometers provide good precision in measuring body temperature (Teran et al., 2012; Chen et al., 2020). Although not all studies agree, results from Sullivan et al. (2021) indicate that sensitivity and specificity for predicting a subject's temperature falls significantly once a 38°C threshold is met. While there may be an offset between core and measured forehead temperature, each of these three papers (Teran et al., 2012; Chen et al., 2020; Sullivan et al., 2021) do indicate that non-contact thermometers are able to measure change in core temperature accurately under the conditions in this study.

Dietary interventions are successful in treating the associated risk factors of metabolic syndrome (Barnard et al., 2009), including the reversal of insulin resistance (Dunaief et al., 2012), increasing insulin sensitivity (Barnard et al., 2005), treating hypertension (Najjar et al., 2018), and reducing body weight (Kahleova et al., 2018). However, individuals may find these types of interventions restrictive and difficult to maintain long term. Consequently, identifying pharmacological therapies that may promote weight loss and treat metabolic disease, through increased energy expenditure *via* thermogenesis, may be a way to augment current interventions for long term weight reduction (Ursino et al., 2009; Nedergaard and Cannon, 2010; Dulloo, 2011; Whittle et al., 2013). Various pharmaceuticals, such as mirabegron and formoterol have been shown to increase energy expenditure, fatty acid oxidation and increase thermogenesis in humans (Lee et al., 2012; O'Mara et al., 2020). But participants report palpitation, tremor, a loss of appetite and insomnia with use of formoterol (Lee et al., 2012), and tachycardia, and raised systolic blood pressure have been observed with use of mirabegron (O'Mara et al., 2020). These side effects will likely reduce the use of these drugs clinically. A possible low cost and low risk option is combining both caffeine and capsaicin. Results from this study indicate that such a combination may be extremely beneficial for individuals with markers of metabolic syndrome. Although we did not measure blood markers for insulin, the rapid return of blood glucose to fasting levels following individual supplementation suggests that it is possible we improved insulin signalling. Additionally, the effects of individual supplementation of caffeine or *C. annum* in relation to RER, energy expenditure and substrate utilisation, and no effect on heart rate and mean arterial pressure show a great benefit with little cardiovascular risk. Interestingly we did find an increase in heart rate variability following caffeine supplementation which adds to an ambiguous body of evidence for caffeine effects on heart rate

variability (Rauh et al., 2006; Koenig et al., 2013). A previous study (Yoshioka et al., 2001) examined the combined effects of red pepper and caffeine consumption on 24 h energy balance in subjects given free access to food. Two appetizers (2 × 322 kJ with or without 3 g red pepper) were given before lunch and dinner, and a drink (decaffeinated coffee with or without 200 mg caffeine) was served at all meals and snacks except for the after-dinner snack. An important note is that on the experimental day, 8.6 and 7.2 g red pepper were also added to lunch and dinner respectively. Red pepper and caffeine consumption significantly reduced the cumulative *ad libitum* energy intake and increased energy expenditure. The mean difference in energy balance between both conditions was 4,000 kJ/d (Yoshioka et al., 2001). These results indicate that the consumption of red pepper and caffeine can induce a considerable change in energy balance. Our results are consistent with this observation. There remains potential to replicate the findings from our study, but with the combination of *C. annuum* and caffeine, rather than individual supplementation. Additionally, such a study could be undertaken in healthy subjects or those with metabolic dysfunction.

Conclusion

In conclusion, our results demonstrate that caffeine and *C. annuum* supplementation increase blood glucose removal, energy expenditure, Tscf, and promote a change in substrate oxidation. These results support a physiological role of caffeine and *C. annuum* on metabolic activity and glucose homeostasis and may provide a basis to pharmacologically target BAT through caffeine and *C. annuum* mediated mechanisms to potentially improve metabolic homeostasis in humans. Further research is needed to investigate the effects of combining caffeine and *C. annuum* on markers of metabolic dysfunction, and the mechanisms underlying BAT activation to identify safe and efficacious lifestyle or pharmaceutical interventions that may activate BAT.

Data availability statement

The raw data supporting the conclusion of this article will be made available by the authors, without undue reservation.

Ethics statement

The studies involving human participants were reviewed and approved by the La Trobe University Human Ethics Committee. The patients/participants provided their written informed consent to participate in this study.

Author contributions

JR, CK, and LVS designed the study. LVS performed data collection. RG and LVS performed statistical analysis. DW performed the DEXA scans. LVS, JR, CK, HI, and RG wrote the initial draft of the manuscript. LVS, JR, CK, HI, RG, DW, and BG critically reviewed the study before publication. LVS is the guarantor of this work and, as such, had full access to all the data in the study and takes responsibility for the integrity of the data and the accuracy of the data analysis.

Funding

This study was conducted with the support of the Holsworth Research Initiative, La Trobe University. The Defence Science Institute (DSI, Australia).

Acknowledgments

The authors thank the study participants, and Erryn Smith in running a pilot study which led on to this research. The authors also thank the Holsworth Research Initiative, La Trobe University, and the Defence Science Institute for helping to fund the study

Conflict of interest

The authors declare that the research was conducted in the absence of any commercial or financial relationships that could be construed as a potential conflict of interest.

Publisher's note

Supplementary material

The Supplementary Material for this article can be found online at: https://www.frontiersin.org/articles/10.3389/fphys.2022.870154/full#supplementary-material

References

Acheson, K. J., Gremaud, G., Meirim, I., Montigon, F., Krebs, Y., Fay, L. B., et al. (2004). Metabolic effects of caffeine in humans: lipid oxidation or futile cycling? *Am. J. Clin. Nutr.* 79 (1), 40–46. doi:10.1093/ajcn/79.1.40

Ahuja, K. D., Robertson, I. K., Geraghty, D. P., and Ball, M. J. (2006). Effects of chili consumption on postprandial glucose, insulin, and energy metabolism. *Am. J. Clin. Nutr.* 84 (1), 63–69. doi:10.1093/ajcn/84.1.63

Andersson, J., Lundström, E., Engström, M., Lubberink, M., Ahlström, H., Kullberg, J., et al. (2019). Estimating the cold-induced brown adipose tissue glucose uptake rate measured by 18 F-FDG PET using infrared thermography and water-fat separated MRI. *Sci. Rep.* 9 (1), 12358. doi:10.1038/s41598-019-48879-7

Barnard, N. D., Scialli, A. R., Turner-McGrievy, G., Lanou, A. J., and Glass, J. (2005). The effects of a low-fat, plant-based dietary intervention on body weight, metabolism, and insulin sensitivity. *Am. J. Med.* 118 (9), 991–997. doi:10.1016/j.amjmed.2005.03.039

Barnard, N. D., Cohen, J., Jenkins, D. J., Turner-McGrievy, G., Gloede, L., Green, A., et al. (2009). A low-fat vegan diet and a conventional diabetes diet in the treatment of type 2 diabetes: a randomized, controlled, 74-wk clinical trial. *Am. J. Clin. Nutr.* 89 (5), 1588S–1596S. doi:10.3945/ajcn.2009.26736H

Bartelt, A., Bruns, O. T., Reimer, R., Hohenberg, H., Ittrich, H., Peldschus, K., et al. (2011). Brown adipose tissue activity controls triglyceride clearance. *Nat. Med.* 17 (2), 200–205. doi:10.1038/nm.2297

Baskaran, P., Krishnan, V., Ren, J., and Thyagarajan, B. (2016). Capsaicin induces browning of white adipose tissue and counters obesity by activating TRPV1 channel-dependent mechanisms. *Br. J. Pharmacol.* 173 (15), 2369–2389. doi:10.1111/bph.13514

Baskaran, P., Krishnan, V., Fettel, K., Gao, P., Zhu, Z., Ren, J., et al. (2017). TRPV1 activation counters diet-induced obesity through sirtuin-1 activation and PRDM-16 deacetylation in brown adipose tissue. *Int. J. Obes.* 41 (5), 739–749. doi:10.1038/ijo.2017.16

Berbee, J. F. P., Boon, M. R., Khedoe, P., Bartelt, A., Schlein, C., Worthmann, A., et al. (2015). Brown fat activation reduces hypercholesterolaemia and protects from atherosclerosis development. *Nat. Commun.* 6, 6356. doi:10.1038/ncomms7356

Brasil, S., Renck, A. C., de Meneck, F., Brioschi, M. L., Costa, E. F., and Teixeira, M. J. (2020). A systematic review on the role of infrared thermography in the brown adipose tissue assessment. *Rev. Endocr. Metabolic Disord.* 21, 37–44. doi:10.1007/s11154-020-09539-8

Cannon, B., and Nedergaard, J. (2004). Brown adipose tissue: function and physiological significance. *Physiol. Rev.* 84 (1), 277–359. doi:10.1152/physrev.00015.2003

Chaiyasit, K., Khovidhunkit, W., and Wittayalertpanya, S. (2009). Pharmacokinetic and the effect of capsaicin in Capsicum frutescens on decreasing plasma glucose level. *J. Med. Assoc. Thai* 92 (1), 108–113.

Chen, K. Y., Brychta, R. J., Linderman, J. D., Smith, S., Courville, A., Dieckmann, W., et al. (2013). Brown fat activation mediates cold-induced thermogenesis in adult humans in response to a mild decrease in ambient temperature. *J. Clin. Endocrinol. Metab.* 98 (7), E1218–E1223. doi:10.1210/jc.2012-4213

Chen, H.-Y., Chen, A., and Chen, C. (2020). Investigation of the impact of infrared sensors on core body temperature monitoring by comparing measurement sites. *Sensors (Basel, Switz)* 20 (10), 2885. doi:10.3390/s20102885

Chondronikola, M., Volpi, E., Børsheim, E., Porter, C., Annamalai, P., Enerbäck, S., et al. (2014). Brown adipose tissue improves whole-body glucose homeostasis and insulin sensitivity in humans. *Diabetes* 63 (12), 4089–4099. doi:10.2337/db14-0746

Cunningham, J. (1990). Calculation of energy expenditure from indirect calorimetry: assessment of the Weir equation. *Nutr. (Burbank)* 6 (3), 222–223.

Dekker, M. J., Gusba, J. E., Robinson, L. E., and Graham, T. E. (2007). Glucose homeostasis remains altered by acute caffeine ingestion following 2 weeks of daily caffeine consumption in previously non-caffeine-consuming males. *Br. J. Nutr.* 98 (3), 556–562. doi:10.1017/S0007114507730738

Dulloo, A. G. (2011). The search for compounds that stimulate thermogenesis in obesity management: from pharmaceuticals to functional food ingredients. *Obes. Rev.* 12 (10), 866–883. doi:10.1111/j.1467-789X.2011.00909.x

Dunaief, D. M., Fuhrman, J., Dunaief, J. L., and Ying, G. (2012). Glycemic and cardiovascular parameters improved in type 2 diabetes with the high nutrient density (HND) diet. *Open J. Prev. Med.* 2, 364–371. doi:10.4236/ojpm.2012.23053

El Hadi, H., Frascati, A., Granzotto, M., Silvestrin, V., Ferlini, E., Vettor, R., et al. (2016). Infrared thermography for indirect assessment of activation of brown adipose tissue in lean and obese male subjects. *Physiol. Meas.* 37 (12), N118–N128. doi:10.1088/0967-3334/37/12/N118

El Hadi, H., Di Vincenzo, A., Vettor, R., and Rossato, M. (2019). Food ingredients involved in white-to-Brown adipose tissue conversion and in calorie burning. *Front. Physiol.* 9, 1954. doi:10.3389/fphys.2018.01954

Ernst, G. (2017). Heart-Rate Variability-more than heart beats? *Front. Public Health* 5, 240. doi:10.3389/fpubh.2017.00240

Fuse, S., Endo, T., Tanaka, R., Kuroiwa, M., Ando, A., Kume, A., et al. (2020). Effects of capsinoid intake on Brown adipose tissue vascular density and resting energy expenditure in healthy, middle-aged adults: a randomized, double-blind, placebo-controlled study. *Nutrients* 12 (9), 2676. doi:10.3390/nu12092676

Galgani, J. E., Ryan, D. H., and Ravussin, E. (2010). Effect of capsinoids on energy metabolism in human subjects. *Br. J. Nutr.* 103 (1), 38–42. doi:10.1017/S0007114509991358

Haarbo, J., Gotfredsen, A., Hassager, C., and Christiansen, C. (1991). Validation of body composition by dual energy X-ray absorptiometry (DEXA). *Clin. Physiol.* 11 (4), 331–341. doi:10.1111/j.1475-097x.1991.tb00662.x

Hachiya, S., Kawabata, F., Ohnuki, K., Inoue, N., Yoneda, H., Yazawa, S., et al. (2007). Effects of CH-19 Sweet, a non-pungent cultivar of red pepper, on sympathetic nervous activity, body temperature, heart rate, and blood pressure in humans. *Biosci. Biotechnol. Biochem.* 71 (3), 671–676. doi:10.1271/bbb.60359

Hanssen, M. J., Hoeks, J., Brans, B., van der Lans, A. A., Schaart, G., van den Driessche, J. J., et al. (2015). Short-term cold acclimation improves insulin sensitivity in patients with type 2 diabetes mellitus. *Nat. Med.* 21 (8), 863–865. doi:10.1038/nm.3891

Hibi, M., Oishi, S., Matsushita, M., Yoneshiro, T., Yamaguchi, T., Usui, C., et al. (2016). Brown adipose tissue is involved in diet-induced thermogenesis and whole-body fat utilization in healthy humans. *Int. J. Obes.* 40 (11), 1655–1661. doi:10.1038/ijo.2016.124

Iwasaki, Y., Tanabe, M., Kobata, K., and Watanabe, T. (2008). TRPA1 agonists-allyl isothiocyanate and cinnamaldehyde-induce adrenaline secretion. *Biosci. Biotechnol. Biochem.* 72 (10), 2608–2614. doi:10.1271/bbb.80289

Iwen, K. A., Backhaus, J., Cassens, M., Waltl, M., Hedesan, O. C., Merkel, M., et al. (2017). Cold-induced brown adipose tissue activity alters plasma fatty acids and improves glucose metabolism in men. *J. Clin. Endocrinol. Metab.* 102 (11), 4226–4234. doi:10.1210/jc.2017-01250

Jang, H.-H., Lee, J., Lee, S.-H., and Lee, Y.-M. (2020). Effects of capsicum annuum supplementation on the components of metabolic syndrome: a systematic review and meta-analysis. *Sci. Rep.* 10 (1), 20912. doi:10.1038/s41598-020-77983-2

Johnson, W. (2007). Final report on the safety assessment of capsicum annuum extract, capsicum annuum fruit extract, capsicum annuum resin, capsicum annuum fruit powder, capsicum frutescens fruit, capsicum frutescens fruit extract, capsicum frutescens resin, and capsaicin. *Int. J. Toxicol.* 26, 3–106. doi:10.1080/10915810601163939

Kahleova, H., Dort, S., Holubkov, R., and Barnard, N. D. (2018). A plant-based high-carbohydrate, low-fat diet in overweight individuals in a 16-week randomized clinical trial: the role of carbohydrates. *Nutrients* 10 (9), 1302. doi:10.3390/nu10091302

Khedoe, P. P., Hoeke, G., Kooijman, S., Dijk, W., Buijs, J. T., Kersten, S., et al. (2015). Brown adipose tissue takes up plasma triglycerides mostly after lipolysis. *J. Lipid Res.* 56 (1), 51–59. doi:10.1194/jlr.M052746

Koenig, J., Jarczok, M. N., Kuhn, W., Morsch, K., Schäfer, A., Hillecke, T. K., et al. (2013). Impact of caffeine on heart rate variability: a systematic review. *J. caffeine Res.* 3 (1), 22–37. doi:10.1089/jcr.2013.0009

Kwak, S. G., and Kim, J. H. (2017). Central limit theorem: the cornerstone of modern statistics. *Korean J. Anesthesiol.* 70 (2), 144–156. doi:10.4097/kjae.2017.70.2.144

Law, J., Morris, D. E., Izzi-Engbeaya, C., Salem, V., Coello, C., Robinson, L., et al. (2018). Thermal imaging is a noninvasive alternative to PET/CT for measurement of brown adipose tissue activity in humans. *J. Nucl. Med.* 59 (3), 516–522. doi:10.2967/jnumed.117.190546

Lee, P., Ho, K., Lee, P., Greenfield, J., Ho, K., Greenfield, J., et al. (2011). Hot fat in a cool man: Infrared thermography and brown adipose tissue. *Diabetes Obes. Metab.* 13 (1), 92–93. doi:10.1111/j.1463-1326.2010.01318.x

Lee, P., Day, R. O., Greenfield, J. R., and Ho, K. K. Y. (2012). Formoterol, a highly β2-selective agonist, increases energy expenditure and fat utilisation in men. *Int. J. Obes.* 37 (4), 593–597. doi:10.1038/ijo.2012.90

Lee, P., Smith, S., Linderman, J., Courville, A. B., Brychta, R. J., Dieckmann, W., et al. (2014). Temperature-acclimated brown adipose tissue modulates insulin sensitivity in humans. *Diabetes* 63 (11), 3686–3698. doi:10.2337/db14-0513

Lee, E., Jung, D. Y., Kim, J. H., Patel, P. R., Hu, X., Lee, Y., et al. (2015). Transient receptor potential vanilloid type-1 channel regulates diet-induced obesity, insulin resistance, and leptin resistance. *FASEB J.* 29 (8), 3182–3192. doi:10.1096/fj.14-268300

Lejeune, M. P., Kovacs, E. M., and Westerterp-Plantenga, M. S. (2003). Effect of capsaicin on substrate oxidation and weight maintenance after modest body-weight loss in human subjects. *Br. J. Nutr.* 90 (3), 651–659. doi:10.1079/bjn2003938

Malik, M. (1998). Heart rate variability. *Curr. Opin. Cardiol.* 13 (1), 36–44. doi:10.1097/00001573-199801000-00006

Matsushita, M., Yoneshiro, T., Aita, S., Kameya, T., Sugie, H., Saito, M., et al. (2014). Impact of brown adipose tissue on body fatness and glucose metabolism in healthy humans. *Int. J. Obes.* 38 (6), 812–817. doi:10.1038/ijo.2013.206

McCracken, E., Monaghan, M., and Sreenivasan, S. (2018). Pathophysiology of the metabolic syndrome. *Clin. Dermatol.* 36 (1), 14–20. doi:10.1016/j.clindermatol.2017.09.004

Najjar, R. S., Moore, C. E., and Montgomery, B. D. (2018). A defined, plant-based diet utilized in an outpatient cardiovascular clinic effectively treats hypercholesterolemia and hypertension and reduces medications. *Clin. Cardiol.* 41 (3), 307–313. doi:10.1002/clc.22863

Nedergaard, J., and Cannon, B. (2010). The changed metabolic world with human brown adipose tissue: therapeutic visions. *Cell Metab.* 11 (4), 268–272. doi:10.1016/j.cmet.2010.03.007

Noordzij, M., Uiterwaal, C. S., Arends, L. R., Kok, F. J., Grobbee, D. E., Geleijnse, J. M., et al. (2005). Blood pressure response to chronic intake of coffee and caffeine: a meta-analysis of randomized controlled trials. *J. Hypertens.* 23 (5), 921–928. doi:10.1097/01.hjh.0000166828.94699.1d

Ohnuki, K., Niwa, S., Maeda, S., Inoue, N., Yazawa, S., Fushiki, T., et al. (2001). CH-19 sweet, a non-pungent cultivar of red pepper, increased body temperature and oxygen consumption in humans. *Biosci. Biotechnol. Biochem.* 65 (9), 2033–2036. doi:10.1271/bbb.65.2033

O'Mara, A. E., Johnson, J. W., Linderman, J. D., Brychta, R. J., McGehee, S., Fletcher, L. A., et al. (2020). Chronic mirabegron treatment increases human brown fat, HDL cholesterol, and insulin sensitivity. *J. Clin. Invest.* 130 (5), 2209–2219. doi:10.1172/JCI131126

Orava, J., Nuutila, P., Lidell, M. E., Oikonen, V., Noponen, T., Viljanen, T., et al. (2011). Different metabolic responses of human brown adipose tissue to activation by cold and insulin. *Cell Metab.* 14 (2), 272–279. doi:10.1016/j.cmet.2011.06.012

Ouellet, V., Labbé, S. M., Blondin, D. P., Phoenix, S., Guérin, B., Haman, F., et al. (2012). Brown adipose tissue oxidative metabolism contributes to energy expenditure during acute cold exposure in humans. *J. Clin. Invest.* 122 (2), 545–552. doi:10.1172/JCI60433

Pérez, D. I. V., Soto, D. A. S., Barroso, J. M., dos Santos, D. A., Queiroz, A. C. C., Miarka, B., et al. (2021). Physically active men with high brown adipose tissue activity showed increased energy expenditure after caffeine supplementation. *J. Therm. Biol.* 99, 103000. doi:10.1016/j.jtherbio.2021.103000

Peronnet, F., and Massicotte, D. (1991). Table of nonprotein respiratory quotient: an update. *Can. J. Sport Sci.* 16 (1), 23–29.

Poher, A. L., Altirriba, J., Veyrat-Durebex, C., and Rohner-Jeanrenaud, F. (2015). Brown adipose tissue activity as a target for the treatment of obesity/insulin resistance. *Front. Physiol.* 6 (4), 4. doi:10.3389/fphys.2015.00004

Rauh, R., Burkert, M., Siepmann, M., and Mueck-Weymann, M. (2006). Acute effects of caffeine on heart rate variability in habitual caffeine consumers. *Clin. Physiol. Funct. Imaging* 26 (3), 163–166. doi:10.1111/j.1475-097X.2006.00663.x

Roman, S., Agil, A., Peran, M., Alvaro-Galue, E., Ruiz-Ojeda, F. J., Fernández-Vázquez, G., et al. (2015). Brown adipose tissue and novel therapeutic approaches to treat metabolic disorders. *Transl. Res.* 165 (4), 464–479. doi:10.1016/j.trsl.2014.11.002

Saito, M., and Yoneshiro, T. (2013). Capsinoids and related food ingredients activating brown fat thermogenesis and reducing body fat in humans. *Curr. Opin. Lipidol.* 24 (1), 71–77. doi:10.1097/MOL.0b013e32835a4f40

Saito, M., Matsushita, M., Yoneshiro, T., and Okamatsu-Ogura, Y. (2020). Brown adipose tissue, diet-induced thermogenesis, and thermogenic food ingredients: from mice to men. *Front. Endocrinol.* 11, 222. doi:10.3389/fendo.2020.00222

Saito, M. (2015). Capsaicin and related food ingredients reducing body fat through the activation of TRP and Brown fat thermogenesis. *Adv. Food Nutr. Res.* 76, 1–28.

Salem, V., Izzi-Engbeaya, C., Coello, C., Thomas, D., Chambers, E., Comninos, A., et al. (2016). Glucagon increases energy expenditure independently of brown adipose tissue activation in humans. *Diabetes Obes. Metab.* 18 (1), 72–81. doi:10.1111/dom.12585

Sievers, W., Rathner, J. A., Green, R. A., Kettle, C., Irving, H. R., Whelan, D. R., et al. (2019). The capacity for oestrogen to influence obesity through brown adipose tissue thermogenesis in animal models: a systematic review and meta-analysis. *Obes. Sci. Pract.* 5, 592–602. doi:10.1002/osp4.368

Smith, A. (2002). Effects of caffeine on human behavior. *Food Chem. Toxicol.* 40 (9), 1243–1255. doi:10.1016/s0278-6915(02)00096-0

Snitker, S., Fujishima, Y., Shen, H., Ott, S., Pi-Sunyer, X., Furuhata, Y., et al. (2008). Effects of novel capsinoid treatment on fatness and energy metabolism in humans: possible pharmacogenetic implications. *Am. J. Clin. Nutr.* 89 (1), 45–50. doi:10.3945/ajcn.2008.26561

Sullivan, S. J. L., Rinaldi, J. E., Hariharan, P., Casamento, J. P., Baek, S., Seay, N., et al. (2021). Clinical evaluation of non-contact infrared thermometers. *Sci. Rep.* 11 (1), 22079. doi:10.1038/s41598-021-99300-1

Sun, L., Camps, S. G., Goh, H. J., Govindharajulu, P., Schaefferkoetter, J. D., Townsend, D. W., et al. (2018). Capsinoids activate brown adipose tissue (BAT) with increased energy expenditure associated with subthreshold 18-fluorine fluorodeoxyglucose uptake in BAT-positive humans confirmed by positron emission tomography scan. *Am. J. Clin. Nutr.* 107 (1), 62–70. doi:10.1093/ajcn/nqx025

Symonds, M. E., Henderson, K., Elvidge, L., Bosman, C., Sharkey, D., Perkins, A. C., et al. (2012). Thermal imaging to assess age-related changes of skin temperature within the supraclavicular region co-locating with brown adipose tissue in healthy children. *J. Pediatr.* 161 (5), 892–898. doi:10.1016/j.jpeds.2012.04.056

Task Force of the European Society of Cardiology the North American Society of Pacing Electrophysiology (1996). Heart rate variability: standards of measurement, physiological interpretation, and clinical use. *Circulation* 93 (5), 1043–1065. doi:10.1161/01.cir.93.5.1043

Teran, C., Torrez-Llanos, J., Teran-Miranda, T., Balderrama, C., Shah, N., Villarroel, P., et al. (2012). Clinical accuracy of a non-contact infrared skin thermometer in paediatric practice. *Child. Care Health Dev.* 38 (4), 471–476. doi:10.1111/j.1365-2214.2011.01264.x

Ursino, M. G., Vasina, V., Raschi, E., Crema, F., and De Ponti, F. (2009). The beta3-adrenoceptor as a therapeutic target: current perspectives. *Pharmacol. Res.* 59 (4), 221–234. doi:10.1016/j.phrs.2009.01.002

van der Lans, A. A., Wierts, R., Vosselman, M. J., Schrauwen, P., Brans, B., van Marken Lichtenbelt, W. D., et al. (2014). Cold-activated brown adipose tissue in human adults: methodological issues. *Am. J. Physiol. Regul. Integr. Comp. Physiol.* 307 (2), R103–R113. doi:10.1152/ajpregu.00021.2014

van Marken Lichtenbelt, W. D., Vanhommerig, J. W., Smulders, N. M., Drossaerts, J. M., Kemerink, G. J., Bouvy, N. D., et al. (2009). Cold-activated brown adipose tissue in healthy men. *N. Engl. J. Med.* 360 (15), 1500–1508. doi:10.1056/NEJMoa0808718

Van Schaik, L., Kettle, C., Green, R., Irving, H., and Rathner, J. (2021a). Effects of caffeine on brown adipose tissue thermogenesis and metabolic homeostasis: a review. *Front. Neurosci.* 15, 621356. doi:10.3389/fnins.2021.621356

Van Schaik, L., Kettle, C., Green, R., Sievers, W., Hale, M. W., Irving, H. R., et al. (2021b). Stimulatory, but not anxiogenic, doses of caffeine act centrally to activate interscapular brown adipose tissue thermogenesis in anesthetized male rats. *Sci. Rep.* 11 (1), 113. doi:10.1038/s41598-020-80505-9

Velickovic, K., Wayne, D., Leija, H. A. L., Bloor, I., Morris, D. E., Law, J., et al. (2019). Caffeine exposure induces browning features in adipose tissue *in vitro* and *in vivo*. *Sci. Rep.* 9 (1), 9104. doi:10.1038/s41598-019-45540-1

Vilarim, M. M., Rocha Araujo, D. M., and Nardi, A. E. (2011). Caffeine challenge test and panic disorder: a systematic literature review. *Expert Rev. Neurother.* 11 (8), 1185–1195. doi:10.1586/ern.11.83

Wang, P., Yan, Z., Zhong, J., Chen, J., Ni, Y., Li, L., et al. (2012). Transient receptor potential vanilloid 1 activation enhances gut glucagon-like peptide-1 secretion and improves glucose homeostasis. *Diabetes* 61 (8), 2155–2165. doi:10.2337/db11-1503

Watanabe, T., Kawada, T., Yamamoto, M., and Iwai, K. (1987). Capsaicin, a pungent principle of hot red pepper, evokes catecholamine secretion from the adrenal medulla of anesthetized rats. *Biochem. Biophys. Res. Commun.* 142 (1), 259–264. doi:10.1016/0006-291x(87)90479-7

Whittle, A., Relat-Pardo, J., and Vidal-Puig, A. (2013). Pharmacological strategies for targeting BAT thermogenesis. *Trends Pharmacol. Sci.* 34 (6), 347–355. doi:10.1016/j.tips.2013.04.004

Yoneshiro, T., Aita, S., Matsushita, M., Okamatsu-Ogura, Y., Kameya, T., Kawai, Y., et al. (2011). Age-related decrease in cold-activated Brown adipose tissue and accumulation of body fat in healthy humans. *Obesity* 19 (9), 1755–1760. doi:10.1038/oby.2011.125

Yoneshiro, T., Aita, S., Kawai, Y., Iwanaga, T., and Saito, M. (2012). Nonpungent capsaicin analogs (capsinoids) increase energy expenditure through the activation of brown adipose tissue in humans. *Am. J. Clin. Nutr.* 95 (4), 845–850. doi:10.3945/ajcn.111.018606

Yoneshiro, T., Mami, M., Hibi, M., Tone, H., Takeshita, M., Yasunaga, K., et al. (2017). Tea catechin and caffeine activate brown adipose tissue and increase cold-induced thermogenic capacity in humans. *Am. J. Clin. Nutr.* 105, 873–881. doi:10.3945/ajcn.116.144972

Yoshioka, M., Doucet, E., Drapeau, V., Dionne, I., and Tremblay, A. (2001). Combined effects of red pepper and caffeine consumption on 24 h energy balance in subjects given free access to foods. *Br. J. Nutr.* 85 (2), 203–211. doi:10.1079/BJN2000224

Zsiborás, C., Mátics, R., Hegyi, P., Balaskó, M., Pétervári, E., Szabó, I., et al. (2018). Capsaicin and capsiate could be appropriate agents for treatment of obesity: a meta-analysis of human studies. *Crit. Rev. Food Sci. Nutr.* 58 (9), 1419–1427. doi:10.1080/10408398.2016.1262324

frontiers | Frontiers in Physiology

ORIGINAL RESEARCH
published: 22 August 2022
doi: 10.3389/fphys.2022.921942

A High-Fat Diet Disrupts Nerve Lipids and Mitochondrial Function in Murine Models of Neuropathy

Amy E. Rumora[1,2†], Kai Guo[1,3†], Lucy M. Hinder[1†], Phillipe D. O'Brien[1], John M. Hayes[1], Junguk Hur[1,3] and Eva L. Feldman[1]*

[1]Department of Neurology, University of Michigan, Ann Arbor, MI, United States, [2]Department of Neurology, Columbia University, New York, NY, United States, [3]Department of Biomedical Sciences, University of North Dakota, Grand Forks, ND, United States

As the prevalence of prediabetes and type 2 diabetes (T2D) continues to increase worldwide, accompanying complications are also on the rise. The most prevalent complication, peripheral neuropathy (PN), is a complex process which remains incompletely understood. Dyslipidemia is an emerging risk factor for PN in both prediabetes and T2D, suggesting that excess lipids damage peripheral nerves; however, the precise lipid changes that contribute to PN are unknown. To identify specific lipid changes associated with PN, we conducted an untargeted lipidomics analysis comparing the effect of high-fat diet (HFD) feeding on lipids in the plasma, liver, and peripheral nerve from three strains of mice (BL6, BTBR, and BKS). HFD feeding triggered distinct strain- and tissue-specific lipid changes, which correlated with PN in BL6 mice versus less robust murine models of metabolic dysfunction and PN (BTBR and BKS mice). The BL6 mice showed significant changes in neutral lipids, phospholipids, lysophospholipids, and plasmalogens within the nerve. Sphingomyelin (SM) and lysophosphatidylethanolamine (LPE) were two lipid species that were unique to HFD BL6 sciatic nerve compared to other strains (BTBR and BKS). Plasma and liver lipids were significantly altered in all murine strains fed a HFD independent of PN status, suggesting that nerve-specific lipid changes contribute to PN pathogenesis. Many of the identified lipids affect mitochondrial function and mitochondrial bioenergetics, which were significantly impaired in *ex vivo* sural nerve and dorsal root ganglion sensory neurons. Collectively, our data show that consuming a HFD dysregulates the nerve lipidome and mitochondrial function, which may contribute to PN in prediabetes.

Keywords: dyslipidemia, prediabetes, mitochondria, obesity, neuropathy, lipidomics, high-fat diet, metabolic syndrome

OPEN ACCESS

Edited by:
Da-Wei Zhang,
University of Alberta, Canada

Reviewed by:
Michael Bukowski,
Beltsville Human Nutrition Center (USDA), United States
Mario Ruiz,
University of Gothenburg, Sweden

****Correspondence:***
Amy E. Rumora
aer2219@cumc.columbia.edu

[†]These authors have contributed equally to this work

Specialty section:
This article was submitted to Lipid and Fatty Acid Research, a section of the journal Frontiers in Physiology

Received: *16 April 2022*
Accepted: *24 June 2022*
Published: *22 August 2022*

Citation:
Rumora AE, Guo K, Hinder LM, O'Brien PD, Hayes JM, Hur J and Feldman EL (2022) A High-Fat Diet Disrupts Nerve Lipids and Mitochondrial Function in Murine Models of Neuropathy. Front. Physiol. 13:921942. doi: 10.3389/fphys.2022.921942

Abbreviations: CL, cardiolipin; DG, diacylglycerol; DGAT2, diacylglycerol acyltransferase 2; DRG, dorsal root ganglion; FCCP, carbonyl cyanide-4-(trifluoromethoxy)phenyl-hydrazone; HFD, high-fat diet; IENFD, intraepidermal nerve fiber density; LC-MS/MS, liquid chromatography-tandem mass spectrometry; LPC, lysophosphatidylcholine; LPE, lysophosphatidylethanolamine; NCV, nerve conduction velocity; PC, phosphatidylcholine; PE, phosphatidylethanolamine; PI, phosphatidylinositol; plasmenyl-PE, plasmenyl-phosphatidylethanolamine; plasmenyl-PC, plasmenylphosphatidylcholine; PLS-DA, Partial least squares-discriminant analysis; PN, peripheral neuropathy; PS, phosphatidylserine; SM, sphingomyelin; TG, triglyceride; T2D, type 2 diabetes; VIP, variable importance in projection.

INTRODUCTION

Peripheral neuropathy (PN) is a common and highly morbid complication of prediabetes and type 2 diabetes (T2D) (Feldman et al., 2019). PN presents as a distal to proximal loss of sensation in the extremities with pain as a frequent feature (Feldman et al., 2019). While the pathogenesis of PN is incompletely understood, impaired peripheral nervous system bioenergetics under conditions of excess energy substrate is a central characteristic of PN (Feldman et al., 2017). In parallel, recent clinical studies highlight components of the metabolic syndrome as PN risk factors (Callaghan et al., 2016a; Callaghan et al., 2016b), suggesting lipids, including triglycerides (TGs), contribute to peripheral nervous system energy overload (Wiggin et al., 2009; Andersen et al., 2018).

Murine models of diet-induced obesity develop features of prediabetes and PN like that seen in humans; however, the genetic background of each mouse strain affects the degree of metabolic dysfunction and type of nerve fibers affected (Montgomery et al., 2013). Large nerve fibers confer proprioceptive information related to position and movement whereas small afferent Aδ fibers and unmyelinated C-fibers are responsible for temperature, pain, and nociceptive sensations. Prediabetes and T2D PN result from a combination of large and small fiber dysfunction. We recently reported the effects of high-fat diet (HFD) feeding on three mouse strains (BL6, BTBR, and BKS). Mice on the BL6 background gained weight throughout the 36-weeks study and developed features of the metabolic syndrome as well as large and small fiber PN similar to what is observed in humans with prediabetes (Hinder et al., 2017). In contrast, HFD-fed BTBR mice developed large fiber PN only and gained weight at the same rate as standard diet (SD)-fed BTBR for the first 24 weeks of the study. The final strain of mice fed a HFD, the BKS mice, also developed large fiber PN only but required genetic manipulation of the leptin receptor to gain weight from study onset.

The goal of the current study was to assess the association between disruptions in lipid composition and PN metabolic risk factors and disease severity. Because lipid levels profoundly impact mitochondrial bioenergetics (Rumora et al., 2018), we postulated that distinct nerve lipid levels would associate with PN under varying conditions of metabolic dysfunction. We conducted untargeted lipidomics of nerve, liver and plasma from HFD-fed BL6, BTBR and BKS mice and observed distinct changes in nerve, liver and plasma lipids in all three strains. Unique changes in mitochondrial lipid levels were observed within the nerves of HFD-fed BL6 mice with PN, the only strain that developed both large and small nerve fiber dysfunction. Further evaluation of mitochondrial bioenergetics in *ex vivo* sural nerves and sensory dorsal root ganglion (DRG) neurons from BL6 animals showed impaired mitochondrial bioenergetics, suggesting a role for nerve-specific lipid signatures in the pathogenesis of PN.

MATERIALS AND METHODS

Mouse Model Description

Mouse strains included i) BKS-*wt* (C57BLKS/J #000662, Jackson laboratory, Bar Harbor, ME), ii) B6-*wt* (C57BL/6J #000664, Jackson Laboratory), and iii) BTBR-*wt* (BTBR T+ Itpr3tf/J #002282, Jackson Laboratory). Mice from each strain were randomly assigned to two groups at 4 weeks of age and fed either a standard diet (SD) (#D12450-B, 10% kcal fat, Research Diets, New Brunswick, NJ) or a 54% HFD (#05090701, 54% kcal fat from lard, Research Diets) for 32 weeks, leading to six groups of male mice with 12 mice/group (HFD BKS, SD BKS, HFD B6, SD B6, HFD BTBR, SD BTBR). The fatty acid composition of each diet is provided in **Supplementary Table S1**. At the study end at 36 weeks of age, sciatic nerve, footpads, plasma, and liver samples were collected. Terminal metabolic measurements included body weight, fasting blood glucose, glucose tolerance, and glycated hemoglobin, as well as terminal neuropathy measurements including assessments of sural and sciatic nerve conduction velocities (NCV), measures of large fiber function, and intraepidermal nerve fiber density (IENFD), a measure of small nerve fiber function, were evaluated at 36 weeks of age. Plasma insulin, cholesterol, and triglycerides were also measured by Mouse Metabolic Phenotyping Centers (MMPC; Vanderbilt University, Nashville, TN; University of Cincinnati, Cincinnati, OH). All metabolic and neuropathy measurements were reported previously (Hinder et al., 2017). Herein, we conducted a follow-up untargeted lipidomics analysis on sciatic nerve, plasma, and liver from each group of mice. Mice were housed in a pathogen-free environment and animal husbandry was conducted by the University of Michigan Unit for Laboratory Animal Medicine. Animal protocols followed Diabetic Complications Consortium Guidelines (https://www.diacomp.org/shared/protocols.aspx) and were approved by the University of Michigan University Committee on Use and Care of Animals.

Untargeted Lipidomics Profiling

Four sciatic nerves from each group of mice were selected blindly and submitted to the Michigan Regional Comprehensive Metabolomics Resource Core (MRC2; www.mrc2.umich.edu) for untargeted lipidomics, which was conducted as described previously (Sas et al., 2018). Briefly, lipids were extracted from each sample (plasma, homogenized sciatic nerve, or homogenized liver) according to a modified Bligh-Dyer protocol. Purified lipids from samples and quality controls were analyzed by liquid chromatography-tandem mass spectrometry (LC-MS/MS). LipidBlast (http://fiehnlab.ucdavis.edu/projects/LipidBlast) was used to identify lipids and MultiQuant (SCIEX, Concord, Canada) was used for lipid quantification. A total of 967 lipid species were detected within the sciatic nerve (Positive - 579; Negative—388), 1,339 lipid species were detected in the liver (Positive- 799; Negative—540), and 956 lipid species were detected in the plasma (Positive - 603; Negative—353).

Untargeted Lipidomics Data Preprocessing and Analysis

Missing values in the raw data were imputed with the K-nearest neighbor method and normalized to internal standards using the R package pamr with the function pamr. knnimpute (https://www.rdocumentation.org/packages/pamr/versions/1.55/topics/pamr.knnimpute) (Troyanskaya et al., 2001). Euclidian was used

as the distance metric (Troyanskaya et al., 2001). At least one internal standard for each lipid class was included in the analysis (**Supplementary Tables S2–S4**). Lipid species with a coefficient of variation >30% were removed and then lipid species from positive and negative ion modes were merged into a single dataset. Lipids measured in both positive and negative modes were assigned an average value from both modes. Lipid species with an odd number of carbons were removed because odd-chain lipids are rarely synthesized in mammalian systems and are typically obtained from the diet or by gut microbiota (Venn-Watson et al., 2020; Ampong et al., 2022). We also did not identify any significant changes in branched lipids in this study. To summarize lipid levels per class, the total values of lipid species in each class were summed and then $\log_2$-transformed. Heatmaps were generated to visualize the profiling pattern of each lipid class across different tissue and genetic background groups. Pearson correlation coefficients were calculated for each shared lipid species between different tissues (O'Brien et al., 2020). Lipid heatmaps were not displayed in the figures if the HFD compared to the SD had no significant impact on tissue lipid levels in a particular strain of mice.

Identifying Important Lipid Species

A *t*-test was performed for each lipid species to determine significant differences between the HFD and SD groups. Lipid species with a p-value < 0.05 were deemed significant differential lipids. Partial least squares-discriminant analysis (PLS-DA) was also performed with mixOmics package (Rohart et al., 2017), to identify lipid species that carry the greatest class-separating information, represented by the first latent variable (Brereton and Lloyd, 2014). Tenfold cross-validation was used to select the tuning parameter (the number of components) for PLS-DA with the minimal overall error rate. Once the optimal number of components was decided, the PLS-DA was refit to the full dataset to obtain the final model. Score plots were generated to illustrate the difference between HFD versus SD for each genetic background (BKS, BL6, BTBR). The variable importance in projection (VIP) score for each lipid species was calculated as a weighted sum of the squared correlations between the PLS-DA components and the original lipid species (Galindo-Prieto et al., 2014). Lipid species with a VIP score >1 were selected as the important species, which contribute highly to group separation (Cho et al., 2008). All the above analyses were performed using R v3.5 (https://www.R-project.org/).

Mitochondrial Bioenergetics Analysis

Ex vivo mitochondrial bioenergetics analysis was conducted on whole sural nerve tissue and primary DRG neurons dissected from 20-week HFD- versus SD-fed BL6 mice using an XF24 Extracellular Flux Analyzer (Agilent Technologies, Santa Clara, CA, United States). Bioenergetic analysis was conducted 3–6 h post mortem for both primary DRG neuron cultures and whole sural nerve. Whole sural nerves were dissected from four mice/group, placed in optimized energetics media, and arranged on an islet capture screen (Pooya et al., 2014). For DRG neuron cultures, DRG were extracted, dissociated into a single-cell suspension, and plated on a laminin-coated Seahorse plate, as described previously (Rumora et al., 2018; Rumora et al., 2019a; Rumora et al., 2019b). Whole sural nerves were then challenged by sequential addition of mitochondrial drugs in the following order: i) 12.6 μM oligomycin, ii) 20 μM carbonyl cyanide-4-(trifluoromethoxy)phenyl-hydrazone (FCCP), and iii) 2 μM antimycin A. DRG neurons were challenged with the consecutive injection of i) 1.25 mM oligomycin, ii) 100 or 600 nM FCCP, and iii) 1 mM antimycin A. All bioenergetics measurements were recorded by the Seahorse XF analyzer and bioenergetics parameters were analyzed using mitochondrial drug response curves, as described previously (Rumora et al., 2018). Results were normalized to tissue weight and mitochondrial copy number (see below). Data analysis was conducted on GraphPad Prism using one-way ANOVA with a Tukey *post*-test for multiple comparisons, two-way ANOVA with Bonferroni *post*-test for multiple comparisons, or unpaired *t*-test (Festing and Altman, 2002).

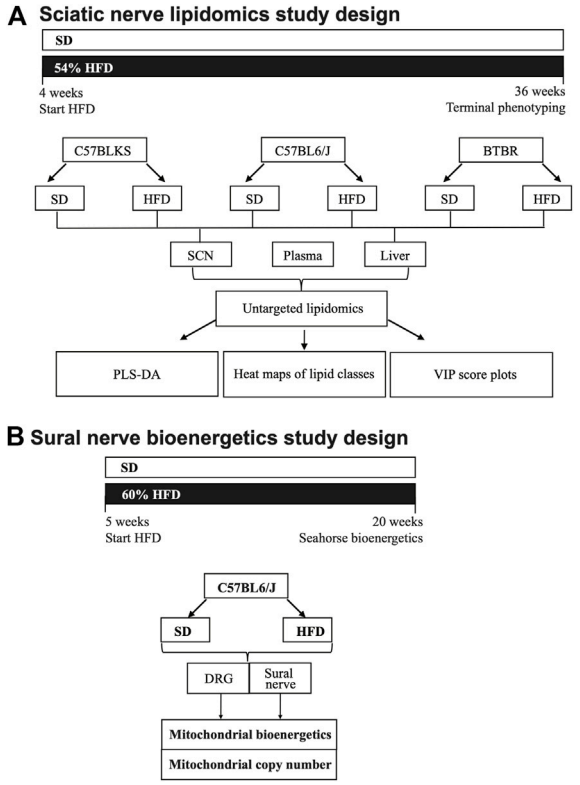

FIGURE 1 | Study paradigm and workflow for lipidomics **(A)** and mitochondrial bioenergetics analysis **(B)**. **(A)** Three strains of mice (C57BLKS/J, C57BL6/J, and BTBR) were divided into two groups per strain and fed either a standard diet (SD) or 54% high-fat diet (HFD). Mice were fed SD or HFD for 32 weeks and phenotyped for metabolic and neuropathy parameters at 36 weeks. At 36 weeks, sciatic nerve, liver, and plasma were collected and processed for LC-MS/MS lipidomics analysis. Lipidomics data were subjected a bioinformatics pipeline including PLS-DA, heat maps, and VIP score plots. **(B)** DRG neuron and sural nerve mitochondrial bioenergetics were evaluated in BL6 mice fed a SD or 60% HFD from 5 to 20 weeks. At 20 weeks of age, mitochondrial bioenergetics and mitochondrial copy number were assessed in DRG neurons and whole sural nerves from HFD BL6 mice compared to SD BL6 mice.

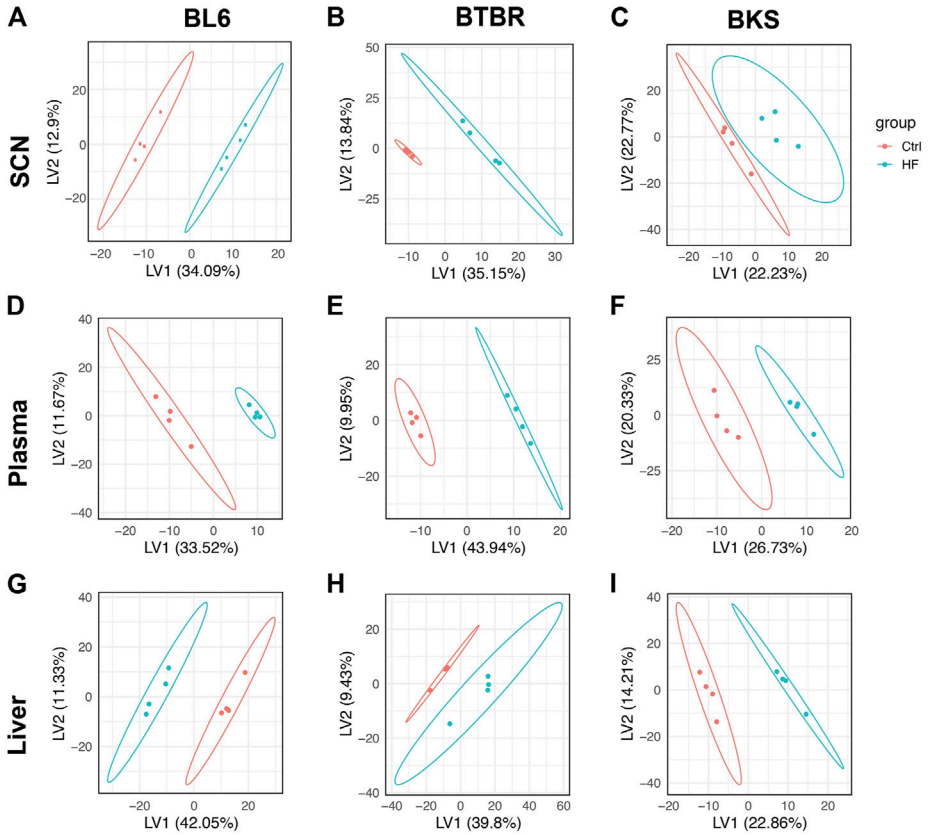

FIGURE 2 | Score plots of lipid changes across species. Partial least squares-discriminant analysis (PLS-DA) showed strain-dependent separation of lipid species between the SD (red) and HFD mice (blue); dots represent individual mice. BL6 mice with weight gain, dyslipidemia, and both large fiber and small fiber PN **(A)** and BTBR mice with weight gain and large-fiber PN **(B)** showed distinct separation of sciatic nerve (SCN) lipids between SD and HFD groups compared to BKS mice with large fiber PN without weight gain **(C)**. Whereas, clear separation between plasma **(D–F)** and liver lipids **(G–I)** was visible across murine strains.

Mitochondrial Copy Number Analysis

The sural nerve mitochondrial copy number was evaluated in HFD- versus SD-fed BL6 mice, as previously described (Rumora et al., 2018). Briefly, DNA was isolated using the AllPrep DNA/RNA Mini Kit (Qiagen, Germantown, MD, United States) from the sural nerves, which were used for mitochondrial bioenergetics analysis. Quantitation of mitochondrial cytochrome b (*cytob*) and nuclear tyrosine 3-monooxygenase/tryptophan five-monooxygenase activation protein (*Ywhaz*) was evaluated using Power SYBR Green PCR Master Mix (Thermo Fisher Scientific) on a StepOnePlus Real-Time PCR system (Thermo Fisher Scientific), as described previously (Rumora et al., 2018). The standard curve method was used for *cytob* and *Ywhaz* gene quantitation.

RESULTS

Tissue Lipidomics Profiling of HFD BL6, BTBR, and BKS Mice

Untargeted lipidomics was performed on the sciatic nerve, plasma, and liver from BL6, BTBR, and BKS mice fed either SD or 54% HFD for 36 weeks (**Figure 1A**). PLS-DA score plots showed a clear separation between lipid species in the sciatic nerve of HFD BL6 mice with large and small fiber PN and HFD BTBR mice with large fiber PN, versus SD BL6 and SD BTBR mice without PN (**Figures 2A,B**). Sciatic nerve lipid profiles from HFD-fed BKS mice that had no weight gain compared to SD-fed animals show less separation between HFD and SD score plots (**Figure 2C**). Elevated plasma insulin levels and large fiber PN, based on slowed sciatic and sural nerve conduction velocities, were present in all strains. However, only BL6 mice fed a HFD had highly significant weight gain throughout the entire study (8-, 16-, 24-, 36- weeks) compared to SD-fed BL6 animals. At the study end, these animals also had statistically elevated cholesterol levels and low IENFDs, a marker of small fiber PN (**Supplementary Table S5**) (Hinder et al., 2017). HFD-fed BTBR mice gained weight at a similar rate as SD-fed animals for the first 24 weeks of the study, and only at the 36-weeks time point were significantly heavier than their SD-fed counterparts. These HFD animals had higher levels of fasting glucose than the SD-fed animals with no changes in lipid levels. In contrast both SD- and HFD-fed BKS mice gained weight at equivalent rates and had no evidence of elevated cholesterol or fasting glucose (**Supplementary Table S5**) (Hinder et al., 2017). The greater separation between the score plots of sciatic nerve lipids from

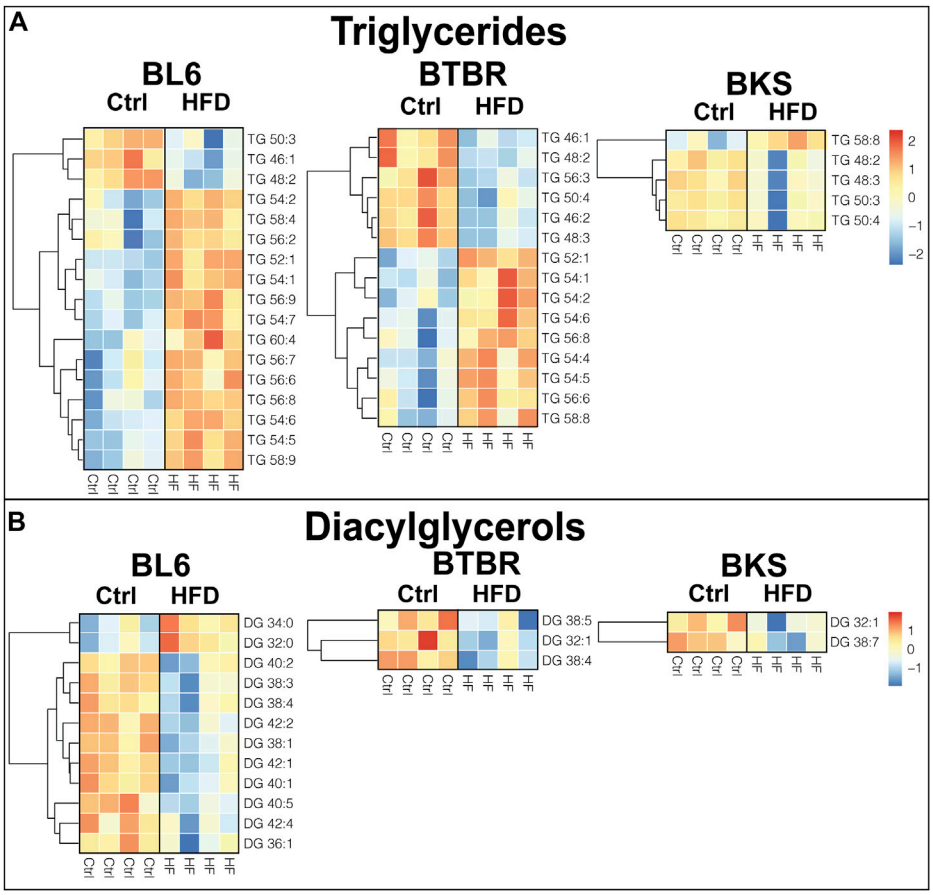

FIGURE 3 | Heat maps of neutral lipids in the sciatic nerve of BL6, BTBR, and BKS mice fed the SD or HFD. **(A)** Sciatic nerve triglyceride (TG) chain length and degree of saturation were significantly altered in HFD sciatic nerve from BL6 and BTBR mice. **(B)** Sciatic nerve diacylglycerols (DGs) were significantly altered by the HFD in all three strains. *t*-test, *p*-value < 0.05.

HFD- vs SD-fed BL6 and BTBR mice shows that changes in nerve lipid composition are associated with distinct PN phenotypes and metabolic changes including weight gain, fasting glucose, and plasma insulin (**Supplementary Table S5**) (Hinder et al., 2017). Unlike the strain-dependent sciatic nerve lipid profiles, the liver and serum lipid profiles had a distinct separation between HFD versus SD groups, regardless of strain (**Figures 2D–I**). These results suggest that tissue-specific sciatic nerve lipid profiles are associated with distinct types of PN as defined by large and small nerve fiber involvement and metabolic dysfunction.

Triglycerides and Diacylglycerols

To identify tissue-specific changes in lipid profiles that associate with PN, we generated heat maps of significantly altered ($p < 0.05$) lipid species in mice fed a HFD compared to SD. Out of a total of 57 detected TG species in the sciatic nerve, 17 were altered in BL6 mice, 15 in BTBR mice, and five in BKS with HFD feeding (**Figure 3A**). The chain length and saturation degree of sciatic nerve TGs were also altered by a HFD. Both BL6 and BTBR strains fed a HFD experienced weight gain by 36 weeks, developed at least two measures of metabolic dysfunction, and exhibited a higher abundance of sciatic nerve long-chain TGs, which contrasted with a higher level of shorter-chain TGs in BL6 and BTBR mice fed a SD. The highly abundant sciatic nerve long-chain TGs in HFD-fed BL6 and BTBR also showed a higher degree of acyl chain unsaturation. These HFD-induced changes in nerve TGs correlated with large fiber PN in both BL6 and BTBR mice. Conversely, sciatic nerve from BKS mice that did not gain weight and developed only one measure of metabolic dysfunction, showed changes in TG level but no distinct changes in TG chain length or saturation.

Diacylglycerols (DGs) were significantly altered in the sciatic nerve of all three strains of mice fed a HFD. A total of 35 DGs were analyzed in the sciatic nerve, of which 12 in BL6, three in BTBR, and two in BKS sciatic nerve were significantly affected by consuming a HFD (**Figure 3B**). Only sciatic nerve from BL6 mice with both large and small fiber PN showed changes in DG chain length, while BTBR and BKS mice had an overall decrease in DGs with HFD feeding compared to their respective SD controls. Interestingly, changes in chain length were opposite in DGs versus TGs, with BL6 sciatic nerve displaying greater shorter-chain and lower longer-chain DG levels in animals fed a HFD compared to animals on a SD. Collectively, these results suggest that elevated long-chain TGs and shorter-chain DGs in sciatic

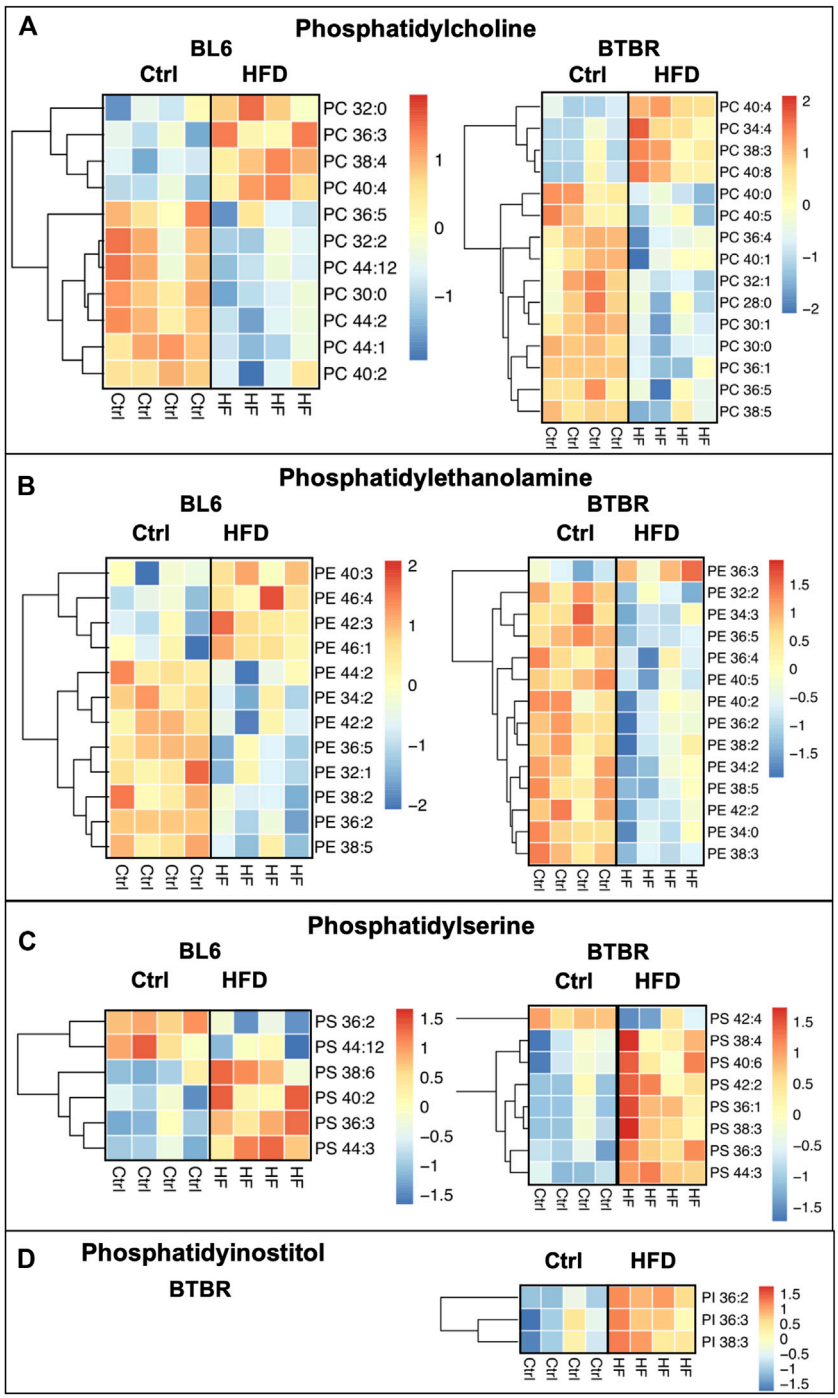

FIGURE 4 | Heat maps of BL6, BTBR, and BKS sciatic nerve phospholipids. All phospholipid levels including **(A)** phosphatidylcholine (PC) **(B)** phosphatidylethanolamine (PE) **(C)** phosphatidylserine (PS) and **(D)** phosphatidylinsotitol (PI) were altered by the HFD in BL6 and BTBR mice. *t*-test, *p*-value < 0.05.

nerves correlate with weight gain, metabolic dysfunction, and large and small fiber PN in HFD BL6 mice after 36 weeks.

Phospholipids

HFD feeding drastically dysregulated phospholipids in the sciatic nerve of BL6 models with large and small fiber PN and BTBR models with large fiber PN, which both experienced weight gain and metabolic dysfunction (**Figure 4**). However, phospholipids were unaffected in the sciatic nerve of HFD-fed BKS mice, the strain that did not gain weight and developed less metabolic dysfunction with a HFD. Collectively, these findings suggest a role for phospholipids in large fiber PN pathogenesis associated with

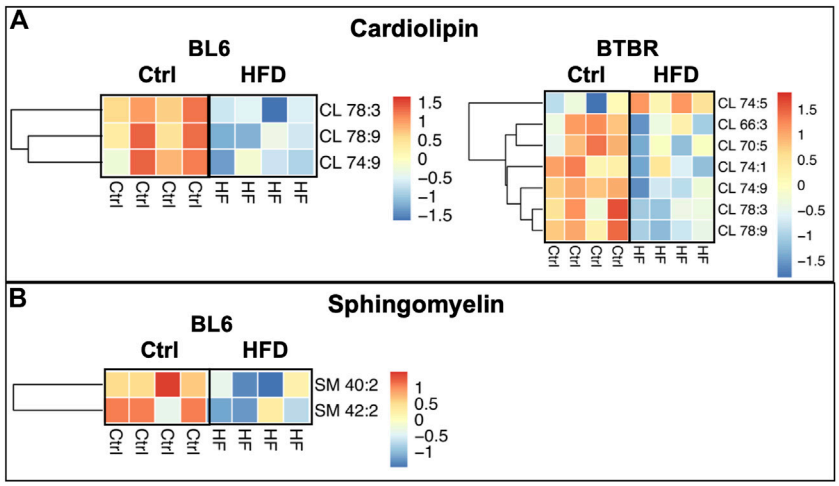

FIGURE 5 | Heat maps of BL6 and BTBR sciatic nerve cardiolipin (CL) and sphingomyelin (SM). HFD BL6 and BTBR mice show global decreases across all **(A)** CL and **(B)** SM lipid species. *t*-test, *p*-value < 0.05.

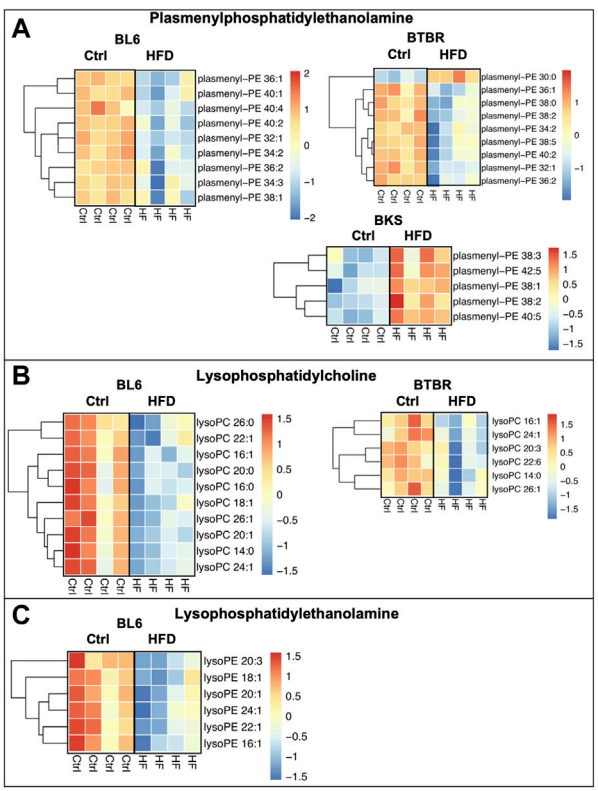

FIGURE 6 | Heat maps of BL6, BTBR, and BKS sciatic nerve plasmalogens and lysophospholipids. **(A)** HFD BL6 and BTBR mice show a global decrease in plasmenyl-phosphatidylethanolamine (plasmenyl-PE) whereas BKS mice have an increase in plasmenyl-PE. **(B)** Lysophosphatidylcholine (LPC) species were also significantly decreased in HFD BL6 and BTBR mice. **(C)** LPE species were decreased exclusively in the sciatic nerve of HFD BL6 mice only. *t*-test, *p*-value < 0.05.

metabolic dysfunction. Within the sciatic nerve, BL6 mice had a higher level of short-chain phosphatidylcholines (PCs) and long-chain phosphatidylethanolamines (PEs) with HFD feeding versus SD mice (**Figures 4A,B**). Although the levels of certain PC and PE species were also affected in HFD-fed BTBR sciatic nerve, there were no distinct changes in the chain length. In both BKS and BTBR mice fed a HFD, levels of specific phosphatidylserine (PS) species were altered, but without discernable changes in chain length (**Figure 4C**). Decreases in phosphatidylinositol (PI) species were exclusive to HFD-fed BTBR sciatic nerve (**Figure 4D**).

Levels of mitochondrial phospholipid cardiolipin (CL) were significantly reduced within the sciatic nerves of BL6 and BTBR mice after HFD feeding whereas sphingomyelin (SM) levels were only reduced in the sciatic nerves from HFD-fed BL6 mice (**Figures 5A,B**). Conversely, a HFD did not affect SM and CL levels in the sciatic nerves of BKS mice. Since CL and SM were only reduced in sciatic nerve from animals that gained weight and were metabolically dysfunctional, these phospholipids may play an important role in PN pathogenesis associated with metabolic dysfunction.

Lysophospholipids and Plasmalogens

The HFD feeding significantly altered lysophospholipid and plasmalogen lipids in the sciatic nerve for all three strains of mice when compared to SD (**Figures 6A–C**). Lysophosphatidylcholine (LPC) and plasmenyl-phosphatidylethanolamine (plasmenyl-PE) lipid species were significantly decreased in the sciatic nerves of BL6 and BTBR mice fed a HFD compared to SD. The HFD-fed BKS mice with no metabolic dysfunction displayed a significant decrease in LPC and an increase in plasmenyl-PE. A reduction in lysophosphatidylethanolamine (LPE) in the sciatic nerve occurred only in BL6 mice fed a HFD, and not the two other

strains, suggesting an association with LPE and both large and small fiber PN in the murine model that most closely replicates the human condition.

Liver and Plasma Lipid Profiles

The sciatic nerve lipidome is modulated by changes in plasma lipid levels, whereas the liver is a major regulator of circulating plasma lipid levels (O'Brien et al., 2017; O'Brien et al., 2020). Therefore, we compared the liver and plasma lipid levels across all murine strains with HFD versus SD feeding and found major changes in lipid profiles regardless of murine strain. Although no significant differences in plasma TG level were detected in all murine strains (**Supplementary Table S5**), the chain length of plasma TGs changed with HFD feeding. The BL6 and BTBR mice, but not the BKS animals, had significant elevations in long-chain TGs in plasma after HFD feeding compared to SD groups (**Supplementary Figure S1**). The levels of several plasma DG and cholesterol ester species were uniquely altered in HFD BTBR mice after HFD feeding (**Supplemental Figure 1B-C**). Plasma phospholipid levels were changed across all murine strains fed the HFD but showed no significant difference in chain length or degree of saturation (**Supplementary Figure S2**). Interestingly, plasma SM levels were elevated in all HFD-fed murine strains including HFD BL6 mice, which contrasted with decreased SM levels in the HFD BL6 sciatic nerve (**Supplementary Figure S3**). The levels of plasma plasmenyl-PE, plasmenylphosphatidylcholine (plasmenyl-PC), LPE, and LPC were also significantly upregulated or downregulated by the HFD feeding depending on the murine strain (**Supplementary Figure S4**).

The liver had distinct changes in neutral lipids including significant increases in TG and DG chain length, as well as an overall decrease in DGs, in BL6 fed a HFD compared to a SD diet (**Supplementary Figure S5**). Conversely, the levels of liver TGs were significantly decreased in BTBR and BKS mice fed a HFD (**Supplementary Figure S5**). Phospholipids were also significantly altered in the liver of all three mouse models. The level of PCs and PEs were significantly decreased in the liver of all three murine strains with HFD feeding (**Supplementary Figure S6**). Other phospholipid groups including PI, PS, phosphatidylglycerol, and phosphatidic acid were also decreased in a strain-dependent manner in the liver of these mice (**Supplementary Figure S6**). As in the sciatic nerve, there was a significant decrease in CL, plasmenyl-PC, LPC, and LPE in the liver of BL6 mice fed a HFD (**Supplementary Figures S7A, S8A–D**). The levels of specific species of SM, plasmalogens, and lysophospholipids were altered in certain strains of HFD mice [SM (BL6, BKS), plasmalogens (BL6, BTBR, BKS), and lysophospholipids (BL6, BTBR)], but there were no distinct changes in chain length or degree of saturation.

Top Lipids Contributing to Peripheral Neuropathy in BL6 HFD-Fed Animals

We have previously reported that HFD feeding of BL6 mice leads to metabolic dysfunction and large and small fiber PN that most closely resembles that seen in humans (Hinder et al., 2017; Rumora et al., 2019b; O'Brien et al., 2020). To determine lipids most significantly linked to pathogenesis of both large and small fiber PN, we identified the lipid species in sciatic nerves, plasma, and liver that contributed the most to diet-induced group separation among BL6 animals by VIP plots and correlation coefficient analysis. A total of 166 sciatic nerve lipids, 141 plasma lipids, and 240 liver lipids had VIP values greater than 1. The top 20 lipids with the highest VIP values were 9 TGs, four PCs, four plasmenyl-PEs, one PS, one PE, and one CL species, which were significantly altered in sciatic nerves (**Figures 7A–C**). Lipid VIP scores for each tissue are provided in **Supplementary Tables S6–S8**. Plasma lipids were also significantly impacted by HFD feeding including five LPCs, five SMs, three PCs, two plasmenyl-PCs, two LPEs, one PE, one CL species, and one cholesterol ester. Important liver lipids affected by HFD feeding included six PEs, 4 TGs, three PCs, two CLs, one LPE, one PS, one phosphatidic acid, one DG, and one phosphatidylglycerol species. We next assessed lipid correlations across tissues and found, among the 35 differentially altered lipids, plasma and liver had greater overlap in shared lipids versus sciatic nerve (**Figure 7D**). Finally, we directly compared the liver, plasma, and sciatic nerve lipid levels in BL6 mice. Interestingly, lipid levels in the sciatic nerve were distinct from lipid levels in the plasma or liver in BL6 mice fed the SD and the HFD (**Supplementary Figures S9A,B**).

To identify lipid changes that contribute to PN in the different mouse strains, we compared sciatic nerve lipids with VIP >1 across the three strains of mice. We identified 33 shared lipid changes between all murine strains, 57 shared lipid changes between sciatic nerve from BL6 and BTBR mice, and 20 shared lipid changes in sciatic nerve from BL6 and BKS mice (**Supplementary Figures S10** and **Supplementary Table S9**). All HFD murine strains developed large fiber neuropathy and had changes in the level of neutral lipids (triglycerides and diacylglycerols) indicating that changes in neutral lipid species may contribute to large nerve fiber damage. HFD BL6 and BTBR mice that developed large fiber neuropathy associated with metabolic dysfunction shared many lipid changes in lysophospholipids and plasmalogens that were less distinct in HFD BKS mice, indicating that these lipid species may contribute to large fiber neuropathy in metabolic dysfunction.

HFD Impairs Mitochondrial Bioenergetics Within DRG Neurons and the Sural Sensory Nerve

Since essential mitochondrial phospholipids, including PE, PC, PI, PS, and CL, were significantly altered in sciatic nerves of BL6 mice fed a HFD, we next evaluated the impact of HFD on *ex vivo* mitochondrial function. Mitochondrial bioenergetic analyses were performed on the DRG sensory neurons and the sural sensory nerve. DRG neurons showed significant increases in basal respiration and ATP production with no discernable change in coupling efficiency at rest (**Figures 8A–C**). DRG neurons from HFD-fed BL6 mice challenged with both 100 and 600 nM FCCP had significantly higher maximum spare respiratory capacity relative to the BL6 DRG neurons from SD, but loss of spare respiratory capacity at 600 nM FCCP (**Figures 8D,E**). Basal ATP production and coupling efficiency were significantly reduced in BL6 sural nerves from

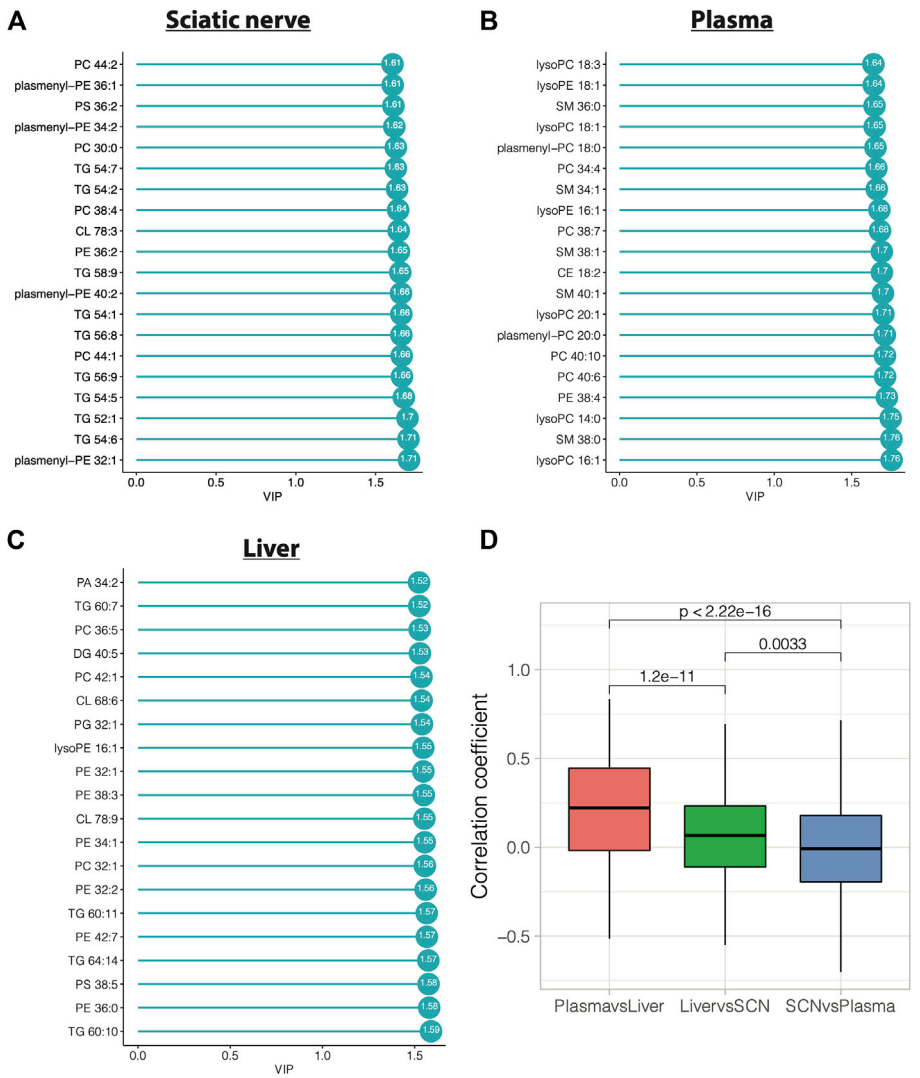

FIGURE 7 | Variable importance in projection (VIP) score plots of the top 20 PLS-DA lipids in **(A)** sciatic nerve, **(B)** plasma, and **(C)** liver, that separate HFD BL6 mice from SD mice. **(D)** Pearson correlation coefficients for each shared lipid species between plasma vs liver, liver vs sciatic nerve, and sciatic nerve vs plasma.

HFD-fed animals, while the basal respiration was not impacted, compared to sural nerves from animals fed a SD (**Figures 8F–H**). Sural nerve mitochondria also showed a significant decrease in maximum respiratory capacity and spare respiratory capacity in HFD-fed versus SD animals (**Figures 8I,J**). Mitochondrial copy number was also significantly lower with HFD feeding in sural nerves but not DRG neurons (**Figure 8K**). These results indicate that a HFD induces DRG and sural nerve mitochondrial dysfunction, correlating with altered mitochondrial lipid levels, which may contribute to the loss of sensory nerve function in PN.

DISCUSSION

Multiple clinical studies identify components of the metabolic syndrome, including dyslipidemia and elevated TGs, as important PN risk factors (Wiggin et al., 2009; Andersen et al., 2018). Preclinical research shows these same risk factors adversely impact axonal mitochondrial trafficking and bioenergetics (Rumora et al., 2018; Rumora et al., 2019a; Sajic et al., 2021) resulting in bioenergetic failure in distal peripheral nerve axons and PN (Feldman et al., 2017). Despite the relevance of lipids, both as PN risk factors and in PN pathogenesis, the precise circulating and nerve lipid species most important to PN remain unknown. Importantly, the correlation of plasma and liver lipidome to nerve lipidome is also incompletely understood, despite the fact that a circulating lipidomic signature correlated to that identified in the nerve could serve as a disease biomarker. Thus, we undertook a systematic study of sciatic nerve, plasma, and liver lipidomics of three HFD-fed mouse models of varying metabolic and neuropathic phenotypes. The first model, HFD-fed BL6 mice, gain weight and develop insulin resistance, dyslipidemia and both large and small fiber PN, metabolic and PN features similar to those reported in humans with prediabetes

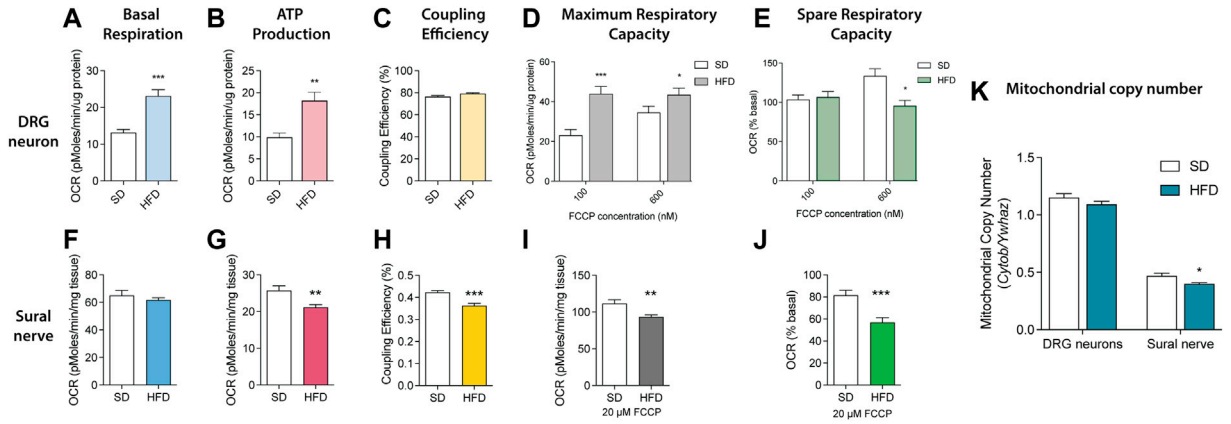

FIGURE 8 | Mitochondrial bioenergetics in SD vs HFD DRG neurons and sural nerves. Resting bioenergetics parameters including **(A)** basal respiration and **(B)** ATP production were significantly increased in DRG neurons from HFD mice compared to SD mice, whereas **(C)** coupling efficiency was unaffected. **(D)** HFD DRG neurons challenged with 100 and 600 nM FCCP had increased maximum respiratory capacity, but significantly diminished spare respiratory capacity with 600 nM FCCP **(E)** relative to SD DRG neurons. The HFD had no effect on sural nerve **(F)** basal respiration but significantly reduced both **(G)** ATP production and **(H)** coupling efficiency compared to the SD sural nerve. Challenging the HFD sural nerve with 20 μM FCCP significantly impaired both **(I)** maximum respiratory capacity and **(J)** spare respiratory capacity compared to SD sural nerves. **(K)** Mitochondrial copy number was reduced in HFD sural nerve. Data mean ± SEM, n = 15 mice/group sural nerves; $^{*}p < 0.05$, $^{**}p < 0.01$, $^{***}p < 0.001$.

(Hinder et al., 2017). The second model, BTBR mice, are resistant to weight gain until 36 weeks but develop insulin resistance, hyperglycemia and large fiber PN. Lastly, the third model, BKS mice fed a HFD diet develop only insulin resistance and large fiber PN without gaining weight. Although large fiber PN was detected in all strains of mice by 36 weeks of age, only BL6 mice consistently developed the diet-induced metabolic dysfunction and sensory PN that closely mimics the human condition. We, therefore, reasoned that comparing the lipid signatures in these different strains with varying metabolic and neuropathic phenotypes would identify tissue-specific lipids important in PN pathogenesis.

We found that score plots of sciatic nerve lipids separated BL6 and BTBR mice fed a HFD from their SD counterparts, aligning with the presence of weight gain and large fiber PN at 36 weeks in these HFD-fed strains. In contrast, BKS animals did not experience this same diet-mediated separation in sciatic nerve lipids and in parallel did not gain weight with a HFD. These data show that nerve-specific lipid changes correlate with weight gain from HFD feeding and support the idea that diet-induced lipid changes impact tissue function, especially in tissues with diverse lipid composition, such as the peripheral nervous system (Surma et al., 2021). We also discovered distinct changes in the sciatic nerve lipidome of HFD-fed BL6 and BTBR mice with large fiber PN, including neutral lipids (TGs, DGs), phospholipids, lysophospholipids, and plasmalogens. However, changes in nerve SMs and LPE levels were unique to HFD-fed BL6 mice who robustly model large and small fiber PN and are the only strain to develop plasma dyslipidemia. These nerve lipid classes may selectively contribute to small fiber nerve damage commonly associated with obesity, the metabolic syndrome, and prediabetes (Palavicini et al., 2020). Liver and plasma lipid profiles, that presumably dictate the sciatic nerve lipidome, also changed significantly in response to a HFD in all mouse strains. Since none of these plasma or liver changes were specific to animals with varying degrees of PN and metabolic dysfunction, it suggests that nerve-specific lipid changes specifically contribute to PN. Many of the nerve lipids identified in BL6 mice fed a HFD are critical for mitochondrial function; indeed, sural nerves from BL6 mice fed a 60% HFD were characterized by a loss of respiratory capacity in both the basal resting and energetically challenged states. Collectively, these results indicate that changes in the peripheral nerve lipidome associate with specific PN phenotypes (large and/or small fiber dysfunction) and likely contribute to mitochondrial dysfunction in PN.

An accumulation of long-chain TGs and short-chain DGs in the sciatic nerve was associated with PN in HFD BL6 mice with small and large fiber PN and in BTBR mice with large fiber PN, indicating that long-chain fatty acids from the diet are incorporated into TGs, mobilized into the plasma, and integrated into the sciatic nerve lipidome (Tracey et al., 2018). These results are consistent with previous studies showing elevated TGs in the sciatic nerve of neuropathic BL6 mice fed 60% HFD (O'Brien et al., 2020). In fact, gene expression of diacylglycerol acyltransferase 2 (DGAT2), the rate-limiting enzyme for TG biosynthesis was significantly increased in the sciatic nerve of these neuropathic BL6 mice fed 60% HFD. DGAT2 was also elevated in sural sensory nerve biopsies from T2D humans with PN, suggesting that nerve TG synthesis is elevated in PN (O'Brien et al., 2020). In the current study, TGs also displayed longer hydrocarbon chains and a greater degree of unsaturation in the HFD BL6 sciatic nerve, consistent with findings in plasma of type 2 diabetic human subjects with dyslipidemia and progressively worsening diabetic complications (Afshinnia et al., 2018; Afshinnia et al., 2019). The increase in TG hydrocarbon chain unsaturation in the sciatic nerve might be a compensatory mechanism to replace saturated TG hydrocarbon chains with polyunsaturated hydrocarbon

chains in an attempt to prevent nerve lipid peroxidation (Bailey et al., 2015; Ackerman et al., 2018). Alternatively, the observed mobilization of long-chain saturated fatty acids from TGs can uncouple the mitochondrial membrane and impair mitochondrial oxidative phosphorylation, which could have contributed to the observed nerve injury (Murray et al., 2011).

In contrast to TGs, saturated DGs, including DGs 30:0–34:0, were significantly elevated in the sciatic nerve of HFD BL6 mice. The predominant DG species in standard rodent sciatic nerve are unsaturated DGs 38:4 (18:0/20:4) and 34:1 (16:0/18:1) (Eichberg and Zhu, 1992). Therefore, our findings indicate that HFD consumption triggers the incorporation of saturated fatty acids, such as palmitic acid and stearic acid, into sciatic nerve DGs in HFD BL6 mice with small and large fiber PN and dyslipidemia. This accumulation of saturated DGs in the sciatic nerve may underlie nerve damage by mediating lipotoxicity, mitochondrial dysfunction, endoplasmic reticulum stress, or apoptosis (Akoumi et al., 2017).

Our findings suggest that redirecting lipid biosynthetic pathways away from TG/DG synthesis could provide a viable therapeutic approach to treating PN. In support of this idea, inhibiting DGAT and lipin1, a DG synthesizing enzyme, promotes axon regeneration in peripheral neurons by reducing TG/DG synthesis and stimulating phospholipid synthesis (Yang et al., 2020). Furthermore, modulating DG levels in the sciatic nerve of STZ-treated rats confers neuroprotection and improves PN measures (Wang et al., 2021). Future preclinical studies focused on nerve-specific TG/DG biology in the setting of dyslipidemia and metabolic dysfunction could facilitate the development of targeted interventions for the treatment of PN.

Phospholipids, including PE, PC, PS, and CL, were significantly altered in the sciatic nerve of both HFD-fed BL6 and BTBR mice but not BKS mice, indicating a major shift in the nerve phospholipid content in response to HFD feeding that correlates with weight gain. These results parallel previous studies in murine models and humans with metabolic syndrome, prediabetes, and T2D (O'Brien et al., 2020; Rumora et al., 2021), suggesting that changes in nerve phospholipids contribute to large fiber PN pathogenesis in these disease states. Phospholipids make up approximately 57% of lipids in the cell bodies and axons of peripheral neurons and 40% of lipids in the myelin sheath (Calderon et al., 1995; Poitelon et al., 2020; Hornemann, 2021). Alterations in phospholipid levels can trigger aberrant changes in cellular signaling (Nishizuka, 1992), cell membrane structure (Kuge et al., 2014), and membrane dynamics in neurons (Tracey et al., 2018). Importantly, phospholipids are a major constituent of the mitochondrial membrane and play an integral role in regulating mitochondrial function.

The most abundant phospholipids in the inner mitochondrial membrane (PE, PC, CL) (Basu Ball et al., 2018) were those most changed in HFD BL6 sciatic nerve in this study, supporting the idea that these phospholipid changes could alter mitochondrial bioenergetics (Schenkel and Bakovic, 2014). Changes in the levels of inner mitochondrial membrane PE, PC, and CL result in the improper assembly of the mitochondrial electron transport supercomplexes, impairing oxidative phosphorylation (Tasseva et al., 2013). Changes in CL are of particular interest since CL is exclusively found in mitochondria and modulates the assembly of respiratory chain supercomplexes III and IV (Zhang et al., 2005), mitochondrial membrane potential (Ghosh et al., 2020), mitochondrial bioenergetics (Paradies et al., 2014), reactive oxygen species production (Falabella et al., 2021), and apoptotic signaling and mitochondrial dynamics (Falabella et al., 2021). The shift in PS and PE lipids, as well as the loss of CL, within the sciatic nerves of HFD BL6 mice may destabilize mitochondrial respiratory chain complexes, thereby reducing the efficiency of oxidative phosphorylation and injuring the peripheral nerves.

The most distinct lipid change was a global decrease in lysophospholipids (LPC, LPE) and plasmenyl-PE in the sciatic nerve of HFD BL6 and BTBR mice compared to BKS mice. A decrease in lysophospholipids was recently reported in both sciatic nerve (O'Brien et al., 2020) and plasma (Guo et al., 2021) from mice and humans, respectively, with PN and metabolic disease. Elevated levels of LPC are also implicated in neuropathic pain associated with chemotherapy-induced neuropathy (Rimola et al., 2020) and other painful neuropathies (Inoue et al., 2008). Lysophospholipids are generated from the hydrolysis of phospholipids (Tan et al., 2020), leading to elevated nitric oxide levels, which may damage peripheral nerves (Wang et al., 2013). Interestingly, LPCs and LPEs, were only decreased in HFD-fed BL6 and HFD-fed BTBR sciatic nerves emphasizing the possibility that sciatic nerve lysophospholipid levels may be strain-dependent (Hinder et al., 2017) and may contribute to the observed differences in PN among the three strains. The HFD BL6 sciatic nerve had the highest number of altered LPC species and was the only strain with HFD-induced alterations in LPE species indicating that altered lysophospholipids levels may contribute to small and large fiber PN associated with metabolic dysfunction. LPC levels are reportedly increased during painful PN (Wang et al., 2013), indicating that a loss of sensory function may be associated with the distinct decrease in LPC species in HFD-fed BL6 mice. Plasmenyl-PE is a plasmalogen, a family of lipids that contain arachidonic acid, a known mediator of nervous system lipid-signaling pathways (Murphy, 2017), membrane trafficking, and inflammatory pathways (Tracey et al., 2018). Critical for the formation of membrane rafts in the nervous system (Poitelon et al., 2020), loss of plasmalogen plasmenyl-PE in peripheral nerves may alter the lipid composition of myelin and ultimately lead to nerve damage.

Only two lipid species, SM and LPE, were dysregulated exclusively in the sciatic nerve from HFD BL6 mice with weight gain, dyslipidemia, and small and large fiber PN that mimics the human condition, compared to sciatic nerve from BTBR or BKS mice. Both SM and LPE were significantly decreased, indicating that the loss of SM and LPE within the sciatic nerve may contribute to small fiber damage within the nerve. This is supported by reports showing decreased plasma SM levels in patients with T2D (Rumora et al., 2021) and obesity (Guo et al., 2021). SM is an important nerve lipid of the myelin sheath, which protects and supports sensory nerve fibers

(Poitelon et al., 2020; Hornemann, 2021). Although the role of LPE in the peripheral nervous system is less studied, changes in LPE levels are reported in other neurological disorders, including Alzheimer's disease (Liu et al., 2021; Llano et al., 2021), emphasizing the importance of this lipid for proper nervous system function.

In the current study, HFD significantly impacted the liver and plasma lipid profile in all three murine strains, irrespective of PN. Since the peripheral nerves rely on both *de novo* lipogenesis and lipid uptake from circulation (Tracey et al., 2018; Poitelon et al., 2020), the saturation and chain length of circulating dietary fatty acids and complex lipids can influence the nerve lipidome. We have shown switching mice from a saturated fatty acid-rich HFD to a monounsaturated fatty acid-rich HFD rich significantly improves nerve function (Rumora et al., 2019b), likely because monounsaturated fatty acids restore mitochondrial function following saturated fatty acid-induced mitochondrial dysfunction (Rumora et al., 2018; Rumora et al., 2019a; Rumora et al., 2019b). Previous studies also describe elevated plasma and liver TGs in HFD-fed BL6 mice with PN, consistent with reports showing higher TGs in plasma of dyslipidemic rodents (Lupachyk et al., 2012), and plasma of diabetic (Wiggin et al., 2009; Callaghan et al., 2011; Smith and Singleton, 2013) and obese subjects with PN (Guo et al., 2021). However, we observed no strain-dependent differences in plasma or liver lipid classes that were unique to the HFD-fed BL6 mice or BTBR HFD-fed animals. These data suggest that nerve-specific lipid changes are a more important driver of PN pathogenesis than plasma or liver lipid signatures. In support of this idea, a recent study showed that statins alter circulating lipid levels in a T2D patient cohort from the ADDITION-Denmark study but have no effect on PN (Kristensen et al., 2020).

Lipids profoundly influence mitochondrial bioenergetics (Hinder et al., 2012; Aon et al., 2014); therefore, we determined whether changes in the peripheral nerve lipidome correlate with mitochondrial function distally in the *ex vivo* sural sensory nerve and proximally in sensory DRG neurons from HFD-fed BL6 mice. Although untargeted lipidomics was conducted on sciatic nerves to provide sufficient tissue for the lipidomic analysis, prediabetic and T2D PN is primarily a sensory neuropathy (Feldman et al., 2017), so mitochondrial bioenergetic analyses were performed on the sural sensory nerve and DRG sensory neurons. Since HFD-fed BL6 mice robustly mimic PN in humans with metabolic dysfunction, we postulated that *ex vivo* sural nerve and DRG neurons from HFD-fed BL6 mice would model changes in mitochondrial function that underlie diet-induced small and large fiber PN pathogenesis. Basal ATP production, coupling efficiency, and mitochondrial copy number were reduced in the sural nerves from HFD-fed animals, suggesting that mitochondrial energy production is compromised due to uncoupling of ATP production from mitochondrial respiration, as well as fewer mitochondria (Chowdhury et al., 2013). Challenging these sural nerves with mitochondrial uncoupler, FCCP, revealed a decrease in both maximum respiratory capacity and spare respiratory capacity, indicating the inability to increase ATP production to match increased energy demand.

In contrast, DRG neurons cultured from HFD-fed BL6 mice had significant increases in basal respiration and ATP production under resting conditions with no changes in coupling efficiency (Rumora et al., 2018), suggesting that mild uncoupling doesn't occur despite the increase in basal respiration. The lack of uncoupling could in part prevent the formation of reactive oxygen species. The loss of spare respiratory capacity suggests the DRG neuron mitochondria are already functioning at maximum capacity and cannot increase energy output to meet increased energy demands. Elevated ATP production in DRG neurons may therefore be a compensatory mechanism to increase mitochondrial content and mitochondrial-derived ATP distally in the sural nerve, to maintain at least partial nerve function (Feldman et al., 2017).

Our study had several limitations. First, we used two different HFD paradigms including a 54% HFD for lipidomics studies versus a 60% HFD for mitochondrial bioenergetics. Since we previously showed lipid changes in the sciatic nerve of mice fed a 60% HFD by 16 weeks of age were similar to mice fed the 54% HFD at 36 weeks of age (O'Brien et al., 2020), we postulated that changes in mitochondrial bioenergetics would be similar across the two HFD paradigms. Future studies will test the effect of the two different HFD paradigms on mitochondrial bioenergetics in whole sural nerve and DRG neurons. Second, we were unable to determine the acyl chain composition of lipids in the untargeted lipidomics analysis. Targeted lipidomics platforms will be used in future studies to identify structural changes in sciatic nerve, liver, and plasma lipid species. It will be interesting to determine whether HFD impacts the identity of the acyl chains of key sciatic nerve lipid species we identified in this study. Further studies are also needed to determine the significance of odd chain lipids in HFD fed mice. Additionally, we will conduct transcriptomics on nerve, liver, and plasma from each mouse strain to assess changes in genes related to *de novo* lipogenesis and other metabolic pathways in each tissue. A third limitation of this study is the use of the sciatic nerve for untargeted lipidomics versus DRG neurons and sural nerve for mitochondrial bioenergetics analysis. Future directions will use targeted lipdomics or MALDI-MSI to correlate changes in mitochondrial bioenergetics function with lipid changes in DRG neurons and sural nerve. A fourth limitation was our limited number of biological samples (4 samples/tissue type) for the untargeted lipidomics analysis. Future studies will evaluate lipidomics changes with a greater number of tissue samples per group and will be analyzed using q-value statistical analysis to show variance across samples.

In conclusion, HFD feeding of different mouse models with varying degrees of PN and metabolic dysfunction produced significant remodeling of the sciatic nerve lipidome and aberrant mitochondrial bioenergetics. Of the three mouse strains (BL6, BTBR, BKS), HFD-fed BL6 mice develop large fiber and small fiber PN and metabolic dysfunction that most closely resembles the human condition. These animals showed significant changes in neutral lipids, phospholipids, lysophospholipids, and plasmalogen levels in the sciatic nerve. Both SM and LPE were significantly altered in sciatic nerves only in the HFD-fed BL6 animals, indicating the importance of these

lipids for maintaining small fiber nerve function. Although plasma and liver lipids were significantly impacted by the HFD across all murine strains, the plasma and liver lipid changes were not biomarkers of PN. The loss of mitochondrial bioenergetics capacity in the sensory sural nerves from HFD-fed BL6 mice differed from HFD-fed BL6 DRG neurons, which showed increased ATP production, potentially as a compensatory mechanism to restore ATP production distally in the injured nerve. Future studies will focus on determining lipid changes that damage specific subsets of nerve fibers, including small and large nerve fibers, as a potential pathogenic mechanism underlying specific PN phenotypes. Additionally, identifying the specific lipid species that drive mitochondrial dysfunction and nerve damage may provide novel therapeutic targets for PN associated with prediabetes and T2D.

DATA AVAILABILITY STATEMENT

The original contributions presented in the study are included in the article/**Supplementary Material**, further inquiries can be directed to the corresponding author. Raw lipidomics data files are publicly available at the DOI: 10.5281/zenodo.6814022.

ETHICS STATEMENT

The animal study was reviewed and approved by the University of Michigan University Committee on Use and Care of Animals.

AUTHOR CONTRIBUTIONS

AR, KG, LH, and EF designed the study; AR, KG, LH, PO'B, and JMH conducted the research and collected data; KG, LH, JMH, and JH performed the statistical analyses; AR and EF wrote the original draft; AR, KG, LH, PO'B, JMH, JH, and EF reviewed and edited the manuscript; EF supervised the manuscript and provided project administration. All authors contributed to the manuscript preparation, edited the manuscript, and approved the submitted manuscript.

FUNDING

This work was provided by U.S. National Institutes of Health (NIH) National Institute of Diabetes and Digestive and Kidney Diseases (NIDDK) Grants R24 DK082841 (to EF), R01 DK107956 (to EF), R21 NS102924 (to EF), K99/R00 DK119366 (to AR) and F32 1F32DK112642 (to AR); the NIDDK DiaComp Award DK076169 (to EF); Novo Nordisk Foundation Grant NNF14OC0011633 (to EF); the American Diabetes Association, the NeuroNetwork for Emerging Therapies at the University of Michigan; and the A. Alfred Taubman Medical Research Institute.

ACKNOWLEDGMENTS

The authors would like Sarah Elzinga for her assistance with making figures and Maegan A. Tabbey for her assistance with data collection and analysis. The authors would also like to thank the Michigan Regional Comprehensive Metabolomics Resource Core (MRC2) for conducting the untargeted lipidomics analysis.

SUPPLEMENTARY MATERIAL

The Supplementary Material for this article can be found online at: https://www.frontiersin.org/articles/10.3389/fphys.2022.921942/full#supplementary-material

REFERENCES

Ackerman, D., Tumanov, S., Qiu, B., Michalopoulou, E., Spata, M., Azzam, A., et al. (2018). Triglycerides Promote Lipid Homeostasis during Hypoxic Stress by Balancing Fatty Acid Saturation. *Cell Rep.* 24 (10), 2596–2605. e2595. doi:10.1016/j.celrep.2018.08.015

Afshinnia, F., Nair, V., Lin, J., Rajendiran, T. M., Soni, T., Byun, J., et al. (2019). Increased Lipogenesis and Impaired β-oxidation Predict Type 2 Diabetic Kidney Disease Progression in American Indians. *JCI Insight* 4 (21). doi:10.1172/jci.insight.130317

Afshinnia, F., Rajendiran, T. M., Soni, T., Byun, J., Wernisch, S., Sas, K. M., et al. (2018). Impaired β-Oxidation and Altered Complex Lipid Fatty Acid Partitioning with Advancing CKD. *J. Am. Soc. Nephrol.* 29 (1), 295–306. doi:10.1681/ASN.2017030350

Akoumi, A., Haffar, T., Mousterji, M., Kiss, R. S., and Bousette, N. (2017). Palmitate Mediated Diacylglycerol Accumulation Causes Endoplasmic Reticulum Stress, Plin2 Degradation, and Cell Death in H9C2 Cardiomyoblasts. *Exp. Cell Res.* 354 (2), 85–94. doi:10.1016/j.yexcr.2017.03.032

Ampong, I., John Ikwuobe, O., Brown, J. E. P., Bailey, C. J., Gao, D., Gutierrez-Merino, J., et al. (2022). Odd Chain Fatty Acid Metabolism in Mice after a High Fat Diet. *Int. J. Biochem. Cell Biol.* 143, 106135. doi:10.1016/j.biocel.2021.106135

Andersen, S. T., Witte, D. R., Dalsgaard, E.-M., Andersen, H., Nawroth, P., Fleming, T., et al. (2018). Risk Factors for Incident Diabetic Polyneuropathy in a Cohort with Screen-Detected Type 2 Diabetes Followed for 13 Years: ADDITION-Denmark. *Diabetes Care* 41 (5), 1068–1075. doi:10.2337/dc17-2062

Aon, M. A., Bhatt, N., and Cortassa, S. C. (2014). Mitochondrial and Cellular Mechanisms for Managing Lipid Excess. *Front. Physiol.* 5, 282. doi:10.3389/fphys.2014.00282

Bailey, A. P., Koster, G., Guillermier, C., Hirst, E. M. A., MacRae, J. I., Lechene, C. P., et al. (2015). Antioxidant Role for Lipid Droplets in a Stem Cell Niche of Drosophila. *Cell* 163 (2), 340–353. doi:10.1016/j.cell.2015.09.020

Basu Ball, W., Neff, J. K., and Gohil, V. M. (2018). The Role of Nonbilayer Phospholipids in Mitochondrial Structure and Function. *FEBS Lett.* 592 (8), 1273–1290. doi:10.1002/1873-3468.12887

Brereton, R. G. L., and Lloyd, G. R. (2014). Partial Least Squares Discriminant Analysis: Taking the Magic Away. *J. Chemom.* 28 (4), 213–225.

Calderon, R. O., Attema, B., and DeVries, G. H. (1995). Lipid Composition of Neuronal Cell Bodies and Neurites from Cultured Dorsal Root Ganglia. *J. Neurochem.* 64 (1), 424–429. doi:10.1046/j.1471-4159.1995.64010424.x

Callaghan, B. C., Feldman, E., Liu, J., Kerber, K., Pop-Busui, R., Moffet, H., et al. (2011). Triglycerides and Amputation Risk in Patients with Diabetes. *Diabetes Care* 34 (3), 635–640. doi:10.2337/dc10-0878

Callaghan, B. C., Xia, R., Banerjee, M., de Rekeneire, N., Harris, T. B., Newman, A. B., et al. (2016a). Metabolic Syndrome Components Are Associated with Symptomatic Polyneuropathy Independent of Glycemic Status. *Diabetes Care* 39 (5), 801–807. doi:10.2337/dc16-0081

Callaghan, B. C., Xia, R., Reynolds, E., Banerjee, M., Rothberg, A. E., Burant, C. F., et al. (2016b). Association between Metabolic Syndrome Components and Polyneuropathy in an Obese Population. *JAMA Neurol.* 73 (12), 1468–1476. doi:10.1001/jamaneurol.2016.3745

Cho, H. W., Kim, S. B., Jeong, M. K., Park, Y., Miller, N. G., Ziegler, T. R., et al. (2008). Discovery of Metabolite Features for the Modelling and Analysis of High-Resolution NMR Spectra. *Int. J. Data Min. Bioinform* 2 (2), 176–192. doi:10.1504/ijdmb.2008.019097

Chowdhury, S. K. R., Smith, D. R., and Fernyhough, P. (2013). The Role of Aberrant Mitochondrial Bioenergetics in Diabetic Neuropathy. *Neurobiol. Dis.* 51, 56–65. doi:10.1016/j.nbd.2012.03.016

Eichberg, J., and Zhu, X. (1992). Diacylglycerol Composition and Metabolism in Peripheral Nerve. *Adv. Exp. Med. Biol.* 318, 413–425. doi:10.1007/978-1-4615-3426-6_37

Falabella, M., Vernon, H. J., Hanna, M. G., Claypool, S. M., and Pitceathly, R. D. S. (2021). Cardiolipin, Mitochondria, and Neurological Disease. *Trends Endocrinol. Metabolism* 32 (4), 224–237. doi:10.1016/j.tem.2021.01.006

Feldman, E. L., Callaghan, B. C., Pop-Busui, R., Zochodne, D. W., Wright, D. E., Bennett, D. L., et al. (2019). Diabetic Neuropathy. *Nat. Rev. Dis. Prim.* 5 (1), 41. doi:10.1038/s41572-019-0092-1

Feldman, E. L., Nave, K.-A., Jensen, T. S., and Bennett, D. L. H. (2017). New Horizons in Diabetic Neuropathy: Mechanisms, Bioenergetics, and Pain. *Neuron* 93 (6), 1296–1313. doi:10.1016/j.neuron.2017.02.005

Festing, M. F. W., and Altman, D. G. (2002). Guidelines for the Design and Statistical Analysis of Experiments Using Laboratory Animals. *ILAR J.* 43 (4), 244–258. doi:10.1093/ilar.43.4.244

Galindo-Prieto, B., Eriksson, L., and Trygg, J. (2014). Variable Influence on Projection (VIP) for Orthogonal Projections to Latent Structures (OPLS). *J. Chemom.* 28 (8), 623–632. doi:10.1002/cem.2627

Ghosh, S., Basu Ball, W., Madaris, T. R., Srikantan, S., Madesh, M., Mootha, V. K., et al. (2020). An Essential Role for Cardiolipin in the Stability and Function of the Mitochondrial Calcium Uniporter. *Proc. Natl. Acad. Sci. U.S.A.* 117 (28), 16383–16390. doi:10.1073/pnas.2000640117

Guo, K., Savelieff, M. G., Rumora, A. E., Alakwaa, F. M., Callaghan, B. C., Hur, J., et al. (2021). Plasma Metabolomics and Lipidomics Differentiate Obese Individuals by Peripheral Neuropathy Status. *J. Clin. Endocrinol. Metab.* 107, 1091–1109. doi:10.1210/clinem/dgab844

Hinder, L. M., O'Brien, P. D., Hayes, J. M., Backus, C., Solway, A. P., Sims-Robinson, C., et al. (2017). Dietary Reversal of Neuropathy in a Murine Model of Prediabetes and the Metabolic Syndrome. *Dis. Model Mech.* 10 (6), 717–725. doi:10.1242/dmm.028530

Hinder, L. M., Vincent, A. M., Burant, C. F., Pennathur, S., and Feldman, E. L. (2012). Bioenergetics in Diabetic Neuropathy: what We Need to Know. *J. Peripher Nerv. Syst.* 17 (Suppl. 2), 10–14. doi:10.1111/j.1529-8027.2012.00389.x

Hornemann, T. (2021). Mini Review: Lipids in Peripheral Nerve Disorders. *Neurosci. Lett.* 740, 135455. doi:10.1016/j.neulet.2020.135455

Inoue, M., Xie, W., Matsushita, Y., Chun, J., Aoki, J., and Ueda, H. (2008). Lysophosphatidylcholine Induces Neuropathic Pain through an Action of Autotaxin to Generate Lysophosphatidic Acid. *Neuroscience* 152 (2), 296–298. doi:10.1016/j.neuroscience.2007.12.041

Kristensen, F. P., Christensen, D. H., Callaghan, B. C., Kahlert, J., Knudsen, S. T., Sindrup, S. H., et al. (2020). Statin Therapy and Risk of Polyneuropathy in Type 2 Diabetes: A Danish Cohort Study. *Diabetes Care* 43 (12), 2945–2952. doi:10.2337/dc20-1004

Kuge, H., Akahori, K., Yagyu, K.-i., and Honke, K. (2014). Functional Compartmentalization of the Plasma Membrane of Neurons by a Unique Acyl Chain Composition of Phospholipids. *J. Biol. Chem.* 289 (39), 26783–26793. doi:10.1074/jbc.M114.571075

Liu, Y., Thalamuthu, A., Mather, K. A., Crawford, J., Ulanova, M., Wong, M. W. K., et al. (2021). Plasma Lipidome Is Dysregulated in Alzheimer's Disease and Is Associated with Disease Risk Genes. *Transl. Psychiatry* 11 (1), 344. doi:10.1038/s41398-021-01362-2

Llano, D. A., Devanarayan, V., and Alzheimer's Disease Neuroimaging, I. (2021). Serum Phosphatidylethanolamine and Lysophosphatidylethanolamine Levels Differentiate Alzheimer's Disease from Controls and Predict Progression from Mild Cognitive Impairment. *J. Alzheimers Dis.* 80 (1), 311–319. doi:10.3233/JAD-201420

Lupachyk, S., Watcho, P., Hasanova, N., Julius, U., and Obrosova, I. G. (2012). Triglyceride, Nonesterified Fatty Acids, and Prediabetic Neuropathy: Role for Oxidative-Nitrosative Stress. *Free Radic. Biol. Med.* 52 (8), 1255–1263. doi:10.1016/j.freeradbiomed.2012.01.029

Montgomery, M. K., Hallahan, N. L., Brown, S. H., Liu, M., Mitchell, T. W., Cooney, G. J., et al. (2013). Mouse Strain-dependent Variation in Obesity and Glucose Homeostasis in Response to High-Fat Feeding. *Diabetologia* 56 (5), 1129–1139. doi:10.1007/s00125-013-2846-8

Murphy, E. J. (2017). Ether Lipids and Their Elusive Function in the Nervous System: a Role for Plasmalogens. *J. Neurochem.* 143 (5), 463–466. doi:10.1111/jnc.14156

Murray, A. J., Knight, N. S., Little, S. E., Cochlin, L. E., Clements, M., and Clarke, K. (2011). Dietary Long-Chain, but Not Medium-Chain, Triglycerides Impair Exercise Performance and Uncouple Cardiac Mitochondria in Rats. *Nutr. Metab. (Lond)* 8, 55. doi:10.1186/1743-7075-8-55

National Diabetes Fact Sheet (2011). National Diabetes Fact Sheet. [Online]. Available at: http://www.cdc.gov/diabetes/pubs/pdf/ndfs_2011.pdf (accessed May 1, 2014).

Nishizuka, Y. (1992). Intracellular Signaling by Hydrolysis of Phospholipids and Activation of Protein Kinase C. *Science* 258 (5082), 607–614. doi:10.1126/science.1411571

O'Brien, P. D., Guo, K., Eid, S. A., Rumora, A. E., Hinder, L. M., Hayes, J. M., et al. (2020). Integrated Lipidomic and Transcriptomic Analyses Identify Altered Nerve Triglycerides in Mouse Models of Prediabetes and Type 2 Diabetes. *Dis. Model Mech.* 13 (2). doi:10.1242/dmm.042101

O'Brien, P. D., Hinder, L. M., Callaghan, B. C., and Feldman, E. L. (2017). Neurological Consequences of Obesity. *Lancet Neurology* 16 (6), 465–477. doi:10.1016/S1474-4422(17)30084-4

Palavicini, J. P., Chen, J., Wang, C., Wang, J., Qin, C., Baeuerle, E., et al. (2020). Early Disruption of Nerve Mitochondrial and Myelin Lipid Homeostasis in Obesity-Induced Diabetes. *JCI Insight* 5 (21). doi:10.1172/jci.insight.137286

Paradies, G., Paradies, V., De Benedictis, V., Ruggiero, F. M., and Petrosillo, G. (2014). Functional Role of Cardiolipin in Mitochondrial Bioenergetics. *Biochimica Biophysica Acta (BBA) - Bioenergetics* 1837 (4), 408–417. doi:10.1016/j.bbabio.2013.10.006

Poitelon, Y., Kopec, A. M., and Belin, S. (2020). Myelin Fat Facts: An Overview of Lipids and Fatty Acid Metabolism. *Cells* 9 (4), 812. doi:10.3390/cells9040812

Pooya, S., Liu, X., Kumar, V. B. S., Anderson, J., Imai, F., Zhang, W., et al. (2014). The Tumour Suppressor LKB1 Regulates Myelination through Mitochondrial Metabolism. *Nat. Commun.* 5, 4993. doi:10.1038/ncomms5993

Rimola, V., Hahnefeld, L., Zhao, J., Jiang, C., Angioni, C., Schreiber, Y., et al. (2020). Lysophospholipids Contribute to Oxaliplatin-Induced Acute Peripheral Pain. *J. Neurosci.* 40 (49), 9519–9532. doi:10.1523/JNEUROSCI.1223-20.2020

Rohart, F., Gautier, B., Singh, A., and Lê Cao, K.-A. (2017). mixOmics: An R Package for 'omics Feature Selection and Multiple Data Integration. *PLoS Comput. Biol.* 13 (11), e1005752. doi:10.1371/journal.pcbi.1005752

Rumora, A. E., Guo, K., Alakwaa, F. M., Andersen, S. T., Reynolds, E. L., Jørgensen, M. E., et al. (2021). Plasma Lipid Metabolites Associate with Diabetic Polyneuropathy in a Cohort with Type 2 Diabetes. *Ann. Clin. Transl. Neurol.* 8 (6), 1292–1307. doi:10.1002/acn3.51367

Rumora, A. E., Lentz, S. I., Hinder, L. M., Jackson, S. W., Valesano, A., Levinson, G. E., et al. (2018). Dyslipidemia Impairs Mitochondrial Trafficking and Function in Sensory Neurons. *FASEB J.* 32 (1), 195–207. doi:10.1096/fj.201700206R

Rumora, A. E., LoGrasso, G., Haidar, J. A., Dolkowski, J. J., Lentz, S. I., and Feldman, E. L. (2019a). Chain Length of Saturated Fatty Acids Regulates Mitochondrial Trafficking and Function in Sensory Neurons. *J. Lipid Res.* 60 (1), 58–70. doi:10.1194/jlr.M086843

Rumora, A. E., LoGrasso, G., Hayes, J. M., Mendelson, F. E., Tabbey, M. A., Haidar, J. A., et al. (2019b). The Divergent Roles of Dietary Saturated and Monounsaturated Fatty Acids on Nerve Function in Murine Models of Obesity. *J. Neurosci.* 39 (19), 3770–3781. doi:10.1523/JNEUROSCI.3173-18.2019

Sajic, M., Rumora, A. E., Kanhai, A. A., Dentoni, G., Varatharajah, S., Casey, C., et al. (2021). High Dietary Fat Consumption Impairs Axonal Mitochondrial Function *In Vivo*. *J. Neurosci.* 41 (19), 4321–4334. doi:10.1523/jneurosci.1852-20.2021

Sas, K. M., Lin, J., Rajendiran, T. M., Soni, T., Nair, V., Hinder, L. M., et al. (2018). Shared and Distinct Lipid-Lipid Interactions in Plasma and Affected Tissues in a Diabetic Mouse Model. *J. Lipid Res.* 59 (2), 173–183. doi:10.1194/jlr.M077222

Schenkel, L. C., and Bakovic, M. (2014). Formation and Regulation of Mitochondrial Membranes. *Int. J. Cell Biol.* 2014–13. doi:10.1155/2014/709828

Smith, A. G., and Singleton, J. R. (2013). Obesity and Hyperlipidemia Are Risk Factors for Early Diabetic Neuropathy. *J. Diabetes its Complicat.* 27 (5), 436–442. doi:10.1016/j.jdiacomp.2013.04.003

Surma, M. A., Gerl, M. J., Herzog, R., Helppi, J., Simons, K., and Klose, C. (2021). Mouse Lipidomics Reveals Inherent Flexibility of a Mammalian Lipidome. *Sci. Rep.* 11 (1), 19364. doi:10.1038/s41598-021-98702-5

Tan, S. T., Ramesh, T., Toh, X. R., and Nguyen, L. N. (2020). Emerging Roles of Lysophospholipids in Health and Disease. *Prog. Lipid Res.* 80, 101068. doi:10.1016/j.plipres.2020.101068

Tasseva, G., Bai, H. D., Davidescu, M., Haromy, A., Michelakis, E., and Vance, J. E. (2013). Phosphatidylethanolamine Deficiency in Mammalian Mitochondria Impairs Oxidative Phosphorylation and Alters Mitochondrial Morphology. *J. Biol. Chem.* 288 (6), 4158–4173. doi:10.1074/jbc.M112.434183

Tracey, T. J., Steyn, F. J., Wolvetang, E. J., and Ngo, S. T. (2018). Neuronal Lipid Metabolism: Multiple Pathways Driving Functional Outcomes in Health and Disease. *Front. Mol. Neurosci.* 11, 10. doi:10.3389/fnmol.2018.00010

Troyanskaya, O., Cantor, M., Sherlock, G., Brown, P., Hastie, T., Tibshirani, R., et al. (2001). Missing Value Estimation Methods for DNA Microarrays. *Bioinformatics* 17 (6), 520–525. doi:10.1093/bioinformatics/17.6.520

Venn-Watson, S., Lumpkin, R., and Dennis, E. A. (2020). Efficacy of Dietary Odd-Chain Saturated Fatty Acid Pentadecanoic Acid Parallels Broad Associated Health Benefits in Humans: Could it Be Essential? *Sci. Rep.* 10 (1), 8161. doi:10.1038/s41598-020-64960-y

Wang, H.-Y., Tsai, Y.-J., Chen, S.-H., Lin, C.-T., and Lue, J.-H. (2013). Lysophosphatidylcholine Causes Neuropathic Pain via the Increase of Neuronal Nitric Oxide Synthase in the Dorsal Root Ganglion and Cuneate Nucleus. *Pharmacol. Biochem. Behav.* 106, 47–56. doi:10.1016/j.pbb.2013.03.002

Wang, M., Xie, M., Yu, S., Shang, P., Zhang, C., Han, X., et al. (2021). Lipin1 Alleviates Autophagy Disorder in Sciatic Nerve and Improves Diabetic Peripheral Neuropathy. *Mol. Neurobiol.* 58, 6049–6061. doi:10.1007/s12035-021-02540-5

Wiggin, T. D., Sullivan, K. A., Pop-Busui, R., Amato, A., Sima, A. A. F., and Feldman, E. L. (2009). Elevated Triglycerides Correlate with Progression of Diabetic Neuropathy. *Diabetes* 58 (7), 1634–1640. doi:10.2337/db08-1771

Yang, C., Wang, X., Wang, J., Wang, X., Chen, W., Lu, N., et al. (2020). Rewiring Neuronal Glycerolipid Metabolism Determines the Extent of Axon Regeneration. *Neuron* 105 (2), 276–292. doi:10.1016/j.neuron.2019.10.009

Zhang, M., Mileykovskaya, E., and Dowhan, W. (2005). Cardiolipin Is Essential for Organization of Complexes III and IV into a Supercomplex in Intact Yeast Mitochondria. *J. Biol. Chem.* 280 (33), 29403–29408. doi:10.1074/jbc.M504955200

Conflict of Interest: The authors declare that the research was conducted in the absence of any commercial or financial relationships that could be construed as a potential conflict of interest.

Publisher's Note: All claims expressed in this article are solely those of the authors and do not necessarily represent those of their affiliated organizations, or those of the publisher, the editors and the reviewers. Any product that may be evaluated in this article, or claim that may be made by its manufacturer, is not guaranteed or endorsed by the publisher.

frontiers | Frontiers in Physiology

TYPE Review
PUBLISHED 30 August 2022
DOI 10.3389/fphys.2022.931931

OPEN ACCESS

EDITED BY
Xian-Cheng Jiang,
Downstate Health Sciences University, United States

REVIEWED BY
Zhongqun Wang,
Jiangsu University, China
Ba-Bie Teng,
University of Texas Health Science Center, United States
Xunde Xian,
Peking University, China

*CORRESPONDENCE
Shou-Dong Guo,
sd-guo@hotmail.com

†These authors have contributed equally to this work

SPECIALTY SECTION
This article was submitted to Lipid and Fatty Acid Research, a section of the journal Frontiers in Physiology

RECEIVED 29 April 2022
ACCEPTED 05 August 2022
PUBLISHED 30 August 2022

CITATION
Qiao Y-N, Zou Y-L and Guo S-D (2022), Low-density lipoprotein particles in atherosclerosis.
Front. Physiol. 13:931931.
doi: 10.3389/fphys.2022.931931

Low-density lipoprotein particles in atherosclerosis

Ya-Nan Qiao†, Yan-Li Zou† and Shou-Dong Guo*

Innovative Drug Research Centre, School of Pharmacy, Institute of Lipid Metabolism and Atherosclerosis, Weifang Medical University, Weifang, China

Among the diseases causing human death, cardiovascular disease (CVD) remains number one according to the World Health Organization report in 2021. It is known that atherosclerosis is the pathological basis of CVD. Low-density lipoprotein (LDL) plays a pivotal role in the initiation and progression of atherosclerotic CVD (ASCVD). LDL cholesterol (LDL-C) is the traditional biological marker of LDL. However, large numbers of patients who have achieved the recommended LDL-C goals still have ASCVD risk. In multiple prospective studies, LDL particle (LDL-P) is reported to be more accurate in predicting CVD risk than LDL-C. LDL-Ps differ in size, density and chemical composition. Numerous clinical studies have proved that the atherogenic mechanisms of LDL-Ps are determined not only by LDL number and size but also by LDL modifications. Of note, small dense LDL (sdLDL) particles possess stronger atherogenic ability compared with large and intermediate LDL subfractions. Besides, oxidized LDL (ox-LDL) is another risk factor in atherosclerosis. Among the traditional lipid-lowering drugs, statins induce dramatic reductions in LDL-C and LDL-P to a lesser extend. Recently, proprotein convertase subtilsin/kexin type 9 inhibitors (PCSK9i) have been demonstrated to be effective in lowering the levels of LDL-C, LDL-P, as well as CVD events. In this article, we will make a short review of LDL metabolism, discuss the discordance between LDL-C and LDL-P, outline the atherogenic mechanisms of action of LDL by focusing on sdLDL and ox-LDL, summarize the methods used for measurement of LDL subclasses, and conclude the advances in LDL-lowering therapies using statins and PCSK9i.

KEYWORDS

LDL particle, PCSK9, atherosclerosis, cardiovascular disease, PCSK9 inhibitor

Introduction

According to the World Health Organization report in 2021, cardiovascular disease (CVD) causes 17.9 million deaths in 2019, representing 32% of total global deaths (WHO, 2021). The pathological basis of CVD is atherosclerosis, a disease of arteries causing myocardial infarction, stroke, and other complications (Libby et al., 2019). Atherosclerosis occurs primarily in the subendothelial space of the middle and large arteries, where blood flow is disturbed and/or bifurcated (Siasos et al., 2018; Kong et al., 2022). Accumulating evidence have demonstrated that many risk factors including hyperlipidemia, hypertension, oxidative stress, inflammation, endothelium dysfunction

as well as high-calorie diet and unhealthy habits, such as smoking, contribute to the initiation and progression of atherosclerotic CVD (ASCVD) (Lee and Cooke, 2011). Epidemiological studies indicate that the elevated levels of low-density lipoprotein (LDL) cholesterol (LDL-C) are the major culprit in the development of atherosclerosis (Matsumoto et al., 2004; Khatana et al., 2020).

Although LDL-C is a well-accepted marker of LDL (Hero et al., 2016), epidemiologic studies and clinical trials using statins and other lipid-lowering drugs have demonstrated that LDL particle (LDL-P) is an alternative indicator and clinical target for treatment of dyslipidemia as well as ASCVD (Sniderman and Kwiterovich, 2013). Cholesterol, triglyceride (TG), and other components of LDL-P are not invariable, but differ greatly from person to person. For instance, lipids carried by LDL-P can be altered by lifestyle changes and lipid-modulatory therapies (Cromwell et al., 2007). In clinical practice, a large proportion of patients who have achieved the recommended LDL-C goals still suffer ASCVD. Therefore, LDL-C alone is not a necessary determinant for ASCVD, while LDL-P is found to be more predictive than any other parameters related to LDL (Kanonidou, 2021). LDL-Ps, the metabolism products of very low-density lipoprotein (VLDL) and intermediate density lipoprotein (IDL), are lipoprotein particles varying in size, components, and density (Maiolino et al., 2013; Ivanova et al., 2017). Of importance, not all LDL-Ps lead to atherosclerosis. Numerous clinical studies have demonstrated that the initiation and progression of atherosclerosis is determined by the number, size, and modification of LDL (Vekic et al., 2022). Particularly, small dense LDL (sdLDL) is widely distributed in the blood of patients with ASCVD and is sensitive to modifications, causing increased occurrence of atherosclerosis (Sekimoto et al., 2021). Moreover, many studies have clearly indicated that oxidized LDL (ox-LDL) and endothelium dysfunction are the main risk factors of atherosclerosis (Chisolm and Steinberg, 2000; Khatana et al., 2020). The measurements and atherogenic mechanisms of action of sdLDL and ox-LDL will be discussed in this review.

Apart from maintaining a healthy lifestyle, pharmaceutical interventions with hypolipidemic drugs, such as statins, are generally recommended for prevention and treatment of ASCVD (Gallego-Colon et al., 2020; Mach et al., 2020). In clinical practice, the effects of non-statin drugs on the outcome of CVD are inferior to those of statins (Visseren et al., 2021). As an add-on-statin therapy, proprotein convertase subtilsin/kexin type 9 (PCSK9) inhibitors (PCSK9i) have shown powerful effect on lowering LDL as well as ASCVD events (Cannon et al., 2015; Chaudhary et al., 2017). In this review, we will make a short review of LDL metabolism, discuss the discordance between LDL-C and LDL-P, outline the atherogenic metabolisms of action of sdLDL and ox-LDL, summarize the methods used for measurement of LDL subfractions, and conclude the current findings of LDL-lowering therapies using statins and PCSK9i. The literature in this article are searching results of the databases including PubMed and Web of Science primarily using "low-density lipoprotein particle or LDL-P" as the keyword.

A brief review of LDL

LDL-P is composed of a lipid core that is primarily consisted of cholesterol, cholesterol ester (CE), and TG, and a shell that is consisted of phospholipids as well as dozens of proteins, such as the dominant apolipoprotein (Apo) B (Prassl and Laggner, 2008). The meaning of LDL varies based on the context. For instance, this term may refer to LDL-C, LDL-P number, or LDL Apo B (Rosenson et al., 2010). LDL-P varies in component, size, and density, while LDL-C specifically represents the cholesterol contained in the LDL-P (El Harchaoui et al., 2007).

LDL metabolism

ApoB100 is the main structural protein of LDL, and there is only one ApoB100 molecule in each LDL-P (Young, 1990). ApoB100 is mostly synthesized in the liver, where Apo B100 is assembled with TG and other lipids as well as proteins to produce TG-rich VLDL particles (Figure 1). In circulation, VLDL particles are converted to IDL and LDL particles by lipoprotein lipase (LPL) and hepatic lipase (HL), which hydrolyze TGs in the core of the ApoB-containing particles including VLDL and chylomicron. As for the origin of LDL subclasses, Berneis and Krauss (2002) proposed two pathways dependent on hepatic TG availability. In case of low TG availability, liver secretes TG-rich VLDL1 and TG-poor IDL2, which are converted to LDLIII and LDLI particles, respectively (Figure 2). In case of high TG availability, liver secretes larger TG-rich VLDL1 and TG-poor VLDL2 particles, which are converted to LDLIV and LDLII, respectively (Figure 2) (Berneis and Krauss, 2002). Of note, cholesteryl ester transfer protein (CETP) mediates lipids exchange (TG and CE) between ApoB-containing lipoproteins and high-density lipoprotein (HDL) particles, contributing to the production of CE-enriched IDL and LDL particles as well as distinct LDL subclasses (Berneis and Krauss, 2002; Hirayama and Miida, 2012; Ivanova et al., 2017; Liu et al., 2021a).

Approximately 40%–60% of the total LDLs in blood are cleared by hepatic LDL receptor (LDLR) through binding the ligand ApoB100 that is carried by LDLs. The rest LDLs in blood are cleared by either hepatic LDLR-related protein (LRP) and heparan sulfate proteoglycan (HPSG) or non-hepatic non-LDLRs that are located at the inner surface of blood vessels (Mehta and Shapiro, 2022). The metabolism of LDL is summarized in Figure 1. Of note, LDLR expression is down-regulated upon increased dietary saturated fat and elevated hepatic uptake of cholesterol through chylomicrons. On the

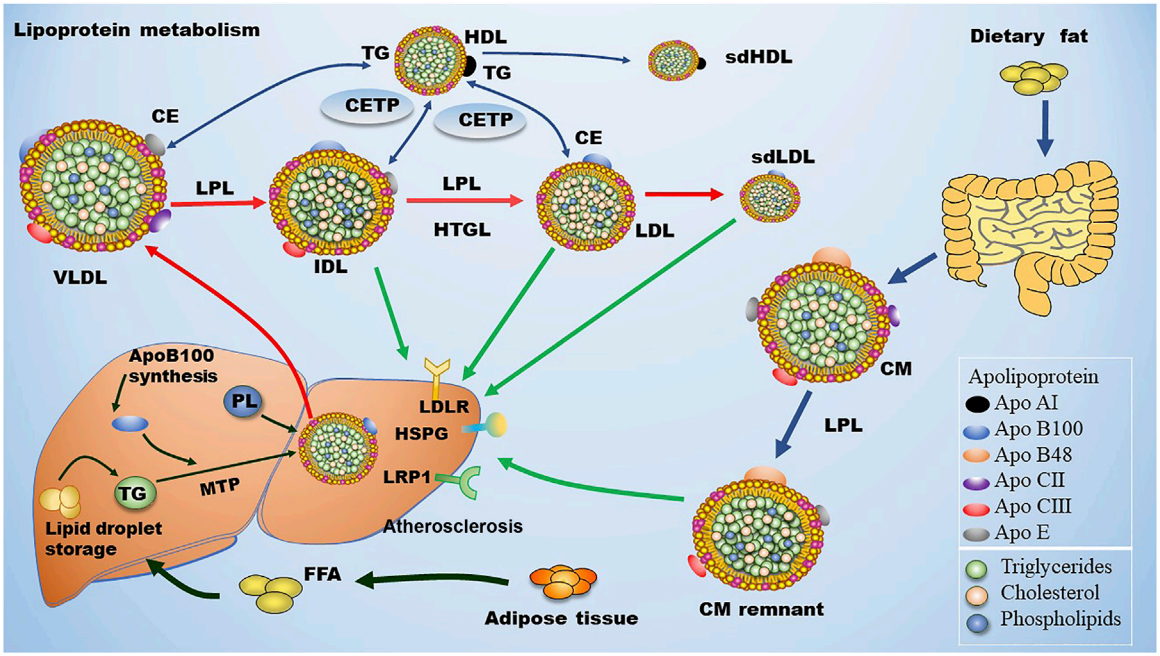

FIGURE 1
Metabolism of LDL. Dietary fat is degraded and then absorbed by intestinal cells for the assembly of chylomicron (CM), which is hydrolyzed by lipoprotein lipase (LPL) in circulation to produce chylomicron remnant (CMR). In the liver, apolipoprotein B (ApoB) 100 is critical for the generation of very low-density lipoprotein (VLDL). In blood, plasma VLDL is converted to intermediate low-density lipoprotein (IDL) and low-density lipoprotein (LDL) *via* hydrolysis of triglycerides (TGs) by LPL and hepatic lipase (HL). Of note, cholesteryl ester transfer protein (CETP) mediates the exchange of cholesterol ester (CE) and TG between high density lipoprotein (HDL) and Apo B-containing lipoprotein, leading to the production of small dense LDL (sdLDL) and small dense HDL (sdHDL), which are atherogenic factors. CMR, IDL, LDL, and sdLDL particles can be cleared by liver through LDL receptor (LDLR), LDLR-related protein 1 (LRP1), heparan sulfate proteoglycan (HSPG), and other potentially unknown receptors. MTP: microsomal triglyceride transfer protein.

contrary, LDLR expression is up-regulated due to reductions in dietary fat and hepatic uptake of cholesterol. Non-hepatic scavenger receptors predominantly located at macrophages are responsible for engulfing the residual LDLs that are not cleared by hepatic receptors. Upon stimulation, monocytes penetrate into the subendothelial space of the artery and turn into macrophages. Next, these macrophages uptake modified LDL particles and become foam cells, initiating the formation of atherosclerotic plaques (Moore et al., 2013). ApoE serves as the ligand for hepatic clearance of ApoB-containing lipoproteins, especially chylomicron, from the blood except for LDL *via* interacting with ApoE receptors including the LRP1 and the VLDL receptor, which are not regulated by cellular cholesterol (Marais, 2019).

LDL-C and LDL-P discordance

Numerous epidemiological studies and clinical trials have confirmed that LDL is a clinical target for treatment of ASCVD (Jeyarajah et al., 2007). In general, LDL levels are indirectly quantified by measurement of LDL-C, the content of cholesterol packaged in LDL-Ps. However, the content of cholesterol and other components in LDL-Ps differ from person to person and change over time due to alterations of lifestyle as well as drug intervention. Many proteins and enzymes can modify the size and components, especially the content of TC and TG, of LDL particles in circulation (Matyus et al., 2014). Of note, the expression of the genes and proteins involved in lipoprotein metabolism also varies among individuals. The above variable factors lead to the fact that LDL-C cannot represent the number of LDL-P at most of the situations.

When LDL-Ps are cholesterol-enriched, the levels of LDL-P number and ApoB will be overestimated by LDL-C levels and vice versa. For instance, subjects with hypertriglyceridemia have increased numbers of sdLDL particles that are relatively poor in cholesterol and CE and rich in TG compared with subjects with normal TG. Under the circumstances, LDL-C levels are sure to underestimate LDL-P numbers as well as Apo B100 levels (Fernández-Cidón et al., 2020). Similarly, LDL-C levels of subjects with more CE-enriched LDL-Ps, are sure to overestimate the number of LDL-P and the level of ApoB100 compared to those with normal or low levels of LDL-CE. The importance of LDL-Ps or ApoB in coronary

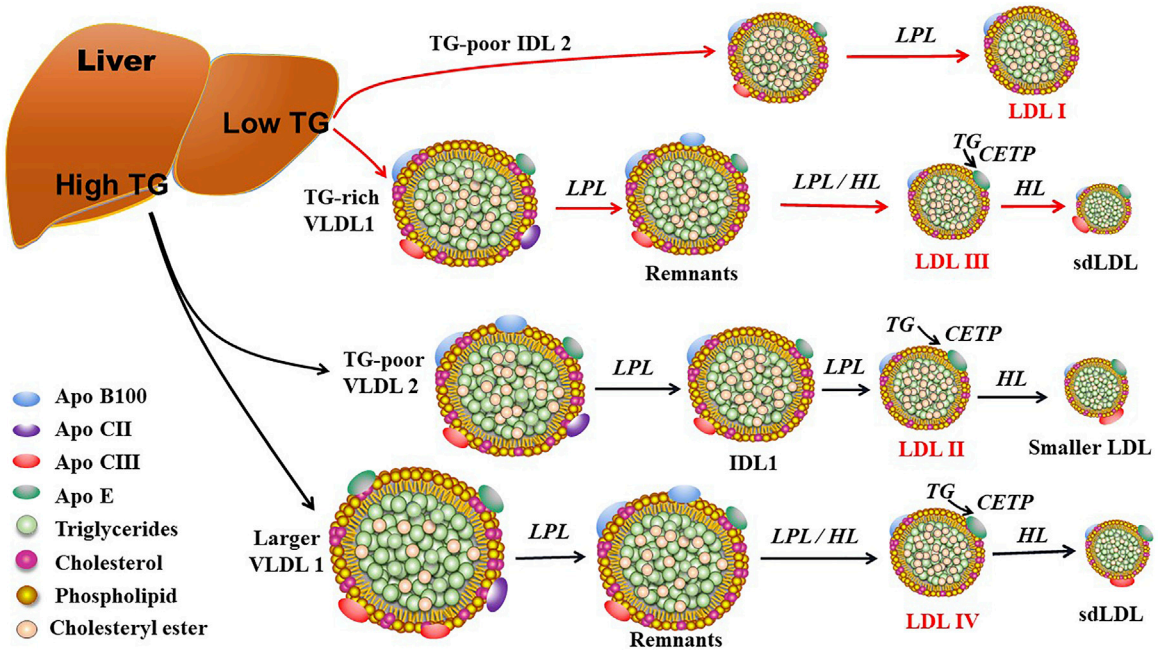

FIGURE 2
The proposed mechanisms for production of LDL subclasses I, II, III, and IV. LDL subclasses II, III, and IV can be further modulated by hepatic lipase (HL) and cholesteryl ester transfer protein (CETP). Of note, LDL subclasses III and IV are responsible for the production of small dense LDL (sdLDL). LPL: lipoprotein lipase; TG: triglyceride; VLDL, very low-density lipoprotein; IDL2: intermediate density lipoprotein 2; IDL1: intermediate low-density lipoprotein 1.

artery disease (CAD) has been vigorously discussed for over 40 years (Sniderman et al., 2019; Sniderman et al., 2022). Dr. Sniderman has devoted his whole clinical and research career since 1973 on the importance of ApoB or LDL-Ps be the parameter to determine the severity of CAD. He is the first person to point out LDL-Ps per se, but not LDL-C as the determinate of CAD. Now, in 2022 the debate is over as written by Allan D. Sniderman et al. (2022).

Studies have indicated that the level of ApoB100 is a superior indicator of CVD risk compared with LDL-C (Sniderman et al., 2012; Sniderman et al., 2019). Each LDL-P consists of one molecule of ApoB100 (Young, 1990). Thus, the level of ApoB100 is well-correlated with the number of LDL-P. Alternatively, LDL-P level is a more convincing predictor of CVD risk compared with other parameters including LDL-C. LDL-P number, size, and modification are all important risk factors for atherosclerosis. The risk of atherosclerosis is aggravated when both the number and size of LDL-P are abnormal (Allaire et al., 2017). LDL-Ps with small size are easier to penetrate the vascular subendothelial space, where they are engulfed by macrophages, accelerating the formation of foam cells. Of note, the relationship between LDL-P size and atherosclerosis risk is affected by LDL-P number. LDL size becomes a non-causal risk factor for coronary heart disease (CHD) when LDL-P number is normal (Allaire et al., 2017). There are certain circumstances, such as inflammation and infections, cause the modification of native LDL. These modified LDLs also induce the formation of foam cells through scavenger receptor-mediated endocytosis (Rafieian-Kopaei et al., 2014). Collectively, LDL-P number, size, and modification are interconnected and contribute to the development of atherosclerosis together.

Detection of LDL subclasses

As shown in Figures 2, 3, LDL-Ps can be divided into three or four subclasses. The size (diameter) of large (LDL I) and intermediate (LDL II) LDL ranges from 26.0 to 28.5 nm and from 25.5 to 26.4 nm, respectively, while the size of sdLDL (LDL III and LDL IV) is generally less than 25.5 nm on average (Berneis et al., 2005; Hirayama and Miida, 2012). LDL-Ps can be divided into different subclasses according to their density, size, electric charge as well as protein composition. Based on their physical and chemical properties as listed above, LDL particles can be separated by different laboratory methods including ultracentrifugation, gradient gel electrophoresis (GGE), high-performance liquid chromatography (HPLC), as well as nuclear magnetic resonance (NMR). In general, results of LDL subclasses obtained using different methods cannot be compared

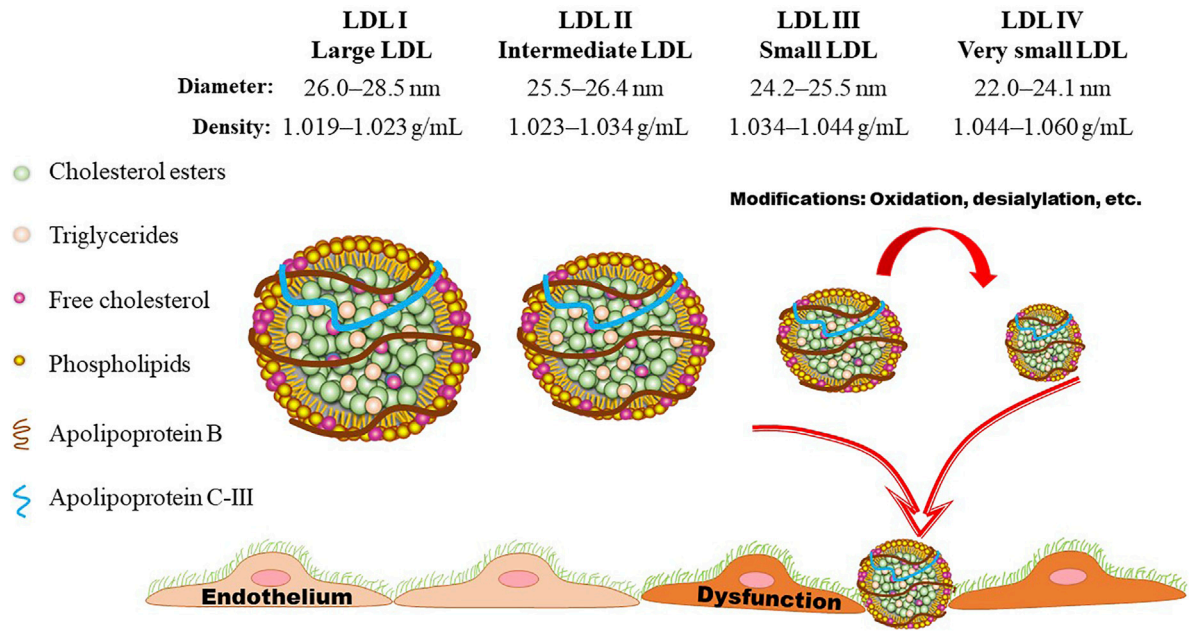

FIGURE 3
LDL subclasses. Based on the flotation rate, LDL particles can be divided into four subclasses by means of ultracentrifugation. Gradient gel electrophoresis is another commonly used method for separation of LDL subclasses according to the size, shape, and electric charge. LDL particles are generally divided into three or four subclasses according to their size (diameter). Presently, LDL III and LDL IV are generally assigned as small dense LDL (sdLDL), which is lack of anti-oxidant component and easily to be oxidized, initiating the onset and progression of atherosclerotic cardiovascular disease.

directly due to the distinct characteristics including size and charge of these particles originated from the different classification principles.

Ultracentrifugation

As shown in Figure 3, the density of LDL-Ps ranges from 1.019 to 1.060 g/ml. Ultracentrifugation is one of the mostly used method for separation of LDL-Ps according to their density (Ivanova et al., 2017). However, the density ranges of LDL subclasses have been designated differently by distinct groups (Teng et al., 1983). Differing from the values shown in Figure 3, the density range of LDL IV is also designated as 1.060–1.063 g/ml (Hirayama and Miida, 2012; Kanonidou, 2021), and the density range of LDL I and LDL III are also defined as 1.016–1.028 mg/ml and 1.028–1.043 mg/ml, respectively (Ivanova et al., 2017). Of note, the traditional gradient ultracentrifugation is time-consuming, while the vertical auto profile technique can identify four LDL subclasses simultaneously in less than an hour (Kulkarni, 2007). It is worth noting that the density of the obtained LDL subclasses varies mildly among different ultracentrifugation methods. For example, the density of the LDL subfractions obtained by iodixanol gradient ultracentrifugation is lower than that separated by traditional salt gradient ultracentrifugation (Davies et al., 2003; Yee et al., 2008). Although ultracentrifugation can separate LDL with high resolution, this method has low throughput and may cause overlap of LDL subclasses as well as destructive alterations due to the centrifugal forces as recently summarized by Kanonidou (Kanonidou, 2021).

Gradient gel electrophoresis

GGE enables the prepared electrophoretic gel to form pore gradients from large to small, so that each component in the sample can pass through the gel with a decreasing pore size during the electrophoresis process, in order to obtain better separation (Kanonidou, 2021). GGE is widely used for separation of LDL subfractions based on size, shape, and electric charge. In this method, a 2%–16% sodium dodecyl sulfate-polyacrylamide gradient (SDS-PAGE) gel is generally used to separation LDL-Ps under non-denaturing conditions (Ensign et al., 2006). According to the peak diameter, LDL subclasses are separated into four subclasses including LDL I (26.0–28.5 nm), LDL II (25.5–26.4 nm), LDL III (24.2–25.5 nm), and LDL IV (22.0–24.1 nm) based on the calibration curve made by the standards that run in parallel with samples (Ivanova et al., 2017; Kanonidou, 2021). Furthermore, the LDL-Ps can be

defined as pattern A (large and intermediate, > 25.5) and pattern B (small and very small LDL, ≤ 25.5 nm) (Ivanova et al., 2017). Similar to ultracentrifugation, GGE is also time-consuming and has a low throughput. Furthermore, this method needs standards for calibration. The polyacrylamide gel tube electrophoresis method is better for separation of LDL-Ps than the traditional GGE method. With the help of specific software, LDL-Ps can be separated into seven subclasses within 1 hour (Hirany et al., 2003).

Two-dimensional gel electrophoresis (2D-GE) is also used to separate LDL particles. In general, 300–500 μg of proteins are first isoelectric focused on immobilised gradient strips (pH 3–10). After equilibration, the strips are subjected to 2D-GE on a gradient SDS-PAGE gel (such as 8%–16%) (Sun et al., 2010; Ljunggren et al., 2019). This method can identify the alterations of proteins carried by LDL-Ps, even modifications of these proteins, in combination with MALDI mass spectrometry, thereby providing another way for examination of changes associated with ASCVD (Karlsson et al., 2005; Ke et al., 2020).

Nuclear magnetic resonance

In the ^{1}H-NMR spectrum, the terminal methyl protons of lipids under different chemical environments may exhibit distinct chemical shifts, which can be used to determine the LDL subclasses by comparation with the data documented in the libraries (Jeyarajah et al., 2007). According to the ^{1}H-NMR data, the concentration of the LDL subclasses can be calculated as well as their size and lipid mass (Aru et al., 2017; Kanonidou, 2021). However, the LDL-P size measured by NMR (18.0–20.5 nm) is smaller than that determined by GGE. Therefore, the data obtained by different methods cannot be directly compared with each other (Kanonidou, 2021). Compared to ultracentrifugation and GGE, NMR can analyze samples within minutes without inducing destructive alterations. Based on the standardized protocols, the variation of NMR data performed by different labs is far less than 1% (Centelles et al., 2017). Therefore, NMR method is time-saving and reproducible and has the characteristic of high throughput.

Fast protein liquid chromatography

Fast protein liquid chromatography (FPLC) method for detection of lipoprotein subclasses including LDL subclasses have been reviewed by Okazaki and Yamashita (Okazaki and Yamashita, 2016) and Kanonidou (Kanonidou, 2021). In combination with gel permeation columns and post-column reactions, this method can detect LDL-P size, LDL-P number as well as the levels of cholesterol and TG at a single run (Okazaki and Yamashita, 2016). Based on the previous report, FPLC method is feasible and straightforward.

Clinical chemistry methods

Some commercially available kits and reference reagents have been developed and released by different companies, such as Quest and LabCorp in the United States. Traditional lipid testing measures the amount of LDL-C present in the blood, but it does not evaluate the number of LDL-P. LDL-P is often used to get a more accurate measure of LDL due to the variability of cholesterol content within a given LDL. Studies have shown that LDL-P more accurately predicts risk of CVD than LDL-C (Mora et al., 2014; Sniderman et al., 2022). These products have the characteristic of high throughput and have been used for common clinical assays in some countries.

Quest diagnostics released a series of advanced testing lipid panels, which go beyond standard lipid panels to assess lipoprotein and apolipoprotein risk factors (https://www.questdiagnostics.com/healthcare-professionals/about-our tests/cardiovascular/advanced-lipid). Quest provides advanced lipid testing including LDL-P number, small and medium LDL, LDL pattern, LDL peak size, and pholipase A2 (Ajala et al., 2020; Farukhi et al., 2020; Dugani et al., 2021). LabCorp also released several advanced testing lipid panels to assess the risk of developing CVD and monitor the treatment of unhealthy lipid levels (https://www.labcorp.com/help/patient-test-info/lipid-panel). These methods include LDL-P, ApoB, ApoA-I, lipoprotein (a), HDL particles, and cardiac risk assessment, which may provide deeper insights into the residual risk of patients with CVD (Ajala et al., 2020; Siddiqui et al., 2020). Furthermore, these companies provide methods for NMR analysis, such as the Lipo-Profile-3 algorithm (LabCorp) (Porter Starr et al., 2019; Lo et al., 2022). It is thought that these values may more accurately reflect heart disease risk in certain people.

LDL-P testing evaluates LDL particles according to their concentration in the blood. It may provide useful information to further evaluate an individual's CVD risk if one has a personal or family history of heart disease at a young age, especially if one's TC and LDL-C values are not significantly elevated. Furthermore, Cardio IQ® is one of advanced cardiovascular testing methods from Quest, which can uncover hidden risk for heart attack and stroke help and improve the management of cardiovascular patients by testing emerging biomarkers such as LDL-P number and subclasses using ion mobility method. The ion mobility method for measuring lipoprotein subfraction concentrations is unique in its capability of directly determining concentrations of the full lipoprotein spectrum (VLDL, IDL, LDL, and HDL) independent of the particles' cholesterol composition (Kanonidou, 2021). Ion mobility determines particle number after separating lipoprotein

particles by size using gas-phase electrophoresis and directly counting the size-separated particles (Caulfield et al., 2008; Mora et al., 2015). Ion mobility method is commercially available from companies such as Quest.

Other methods

The electrospray differential mobility analysis is also used for quantification of non-HDL particles. However, the machine needs to be daily calibrated by the reference standards, whose nature and composition should be close to the interested samples (Clouet Foraison et al., 2017). ApoB and non-HDL particles can also be detected by liquid-chromatography tandem mass spectrometry, but this method can't provide information on lipoprotein subclasses at present (Delatour et al., 2018). Additionally, the research interest in the electrochemical immunosensors for the LDL detection has been constantly growing. Aptamers including oligonucleotides or peptides have characteristics of high reproducibility and high throughput. However, these immunosensors cannot detect the LDL subclasses at present (Rudewicz-Kowalczyk and Grabowska, 2021).

Atherogenic mechanisms of LDL

LDL behaves as a chief risk factor in the initiation and progression of ASCVD (Ivanova et al., 2017). Of note, the number, size, as well as modifications of LDL play pivotal roles in the development of atherosclerosis (Packard, 2006; Rizzo and Berneis, 2006). Herein, we focus on two kinds of specific LDLs, sdLDL and ox-LDL, which have great atherogenic effects.

sdLDL in atherosclerosis

As shown in Figure 3, the size of LDL-Ps ranges from large to small, and sdLDL is generally designated as small and very small LDL subclasses (Rosenson et al., 2010). It has been demonstrated that sdLDL is more atherogenic than large and intermediate LDL subclasses (Nikolic et al., 2013; Ivanova et al., 2017). Elevated levels of sdLDL are linked to atherosclerosis in many conditions, such as hyperlipidemia, metabolic syndrome, diabetes, and other disorders (Toledo et al., 2006; Cali et al., 2007; Fukushima et al., 2011). For instance, the proportion of sdLDL can be used to predict the elevated intima-media thickness (IMT) as well as insulin resistance in patients with diabetes (Gerber et al., 2013). The size of LDL-Ps decreases as insulin resistance becomes more severe (Garvey et al., 2003; Bonilha et al., 2021). Of note, the elevated levels of carotid IMT and sdLDL are correlated with other well-known risk factors of CVD including sex, age, genetics, as well as unhealthy habits such as smoking. Furthermore, sdLDL cholesterol is reported to be a superior indicator of CVD risk compared to other risk factors as listed above (Shen et al., 2015). The convincing correlation between sdLDL cholesterol and CHD is established in a prospective study involving 11,419 participants (Hoogeveen et al., 2014). Another study also indicates that sdLDL cholesterol is a better predictor of CHD than LDL-C (Ivanova et al., 2017).

Compared with large and intermediate LDL subclasses, sdLDL particles are more atherogenic. The small size makes sdLDL easily penetrate into the subendothelial space, where they bind more avidly to the glycosaminoglycans and are engulfed by macrophages to promote the formation of atherosclerotic plaques (Sniderman et al., 2019). Compared to large LDL-P, the longer circulation time of sdLDL provides more chances for its penetration into the subendothelial space (Carmena et al., 2004; Ivanova et al., 2017). *In vitro*, sdLDL particles are easier to be engulfed by macrophages compared with larger and less dense LDL-Ps. The potential reasons are: 1) sdLDL is more sensitive to oxidation; 2) sdLDL has a stronger binding ability to proteoglycans located at the endothelium lining (Alsaweed, 2021). Furthermore, the elevated plasma levels of sdLDL are generally accompanied with reduced levels of HDL-C and Apo A-I, and elevated levels of TG and ApoB. It has been well-documented that HDL and Apo A-I are atheroprotective, while TG- and ApoB-containing lipoproteins are atherogenic (Diffenderfer and Schaefer, 2014; Zhang et al., 2022).

Ox-LDL in atherosclerosis

The higher the amount of LDL being trapped in the subendothelium, the faster the atherosclerotic plaque evolves (Rosenson and Underberg, 2013; Liu et al., 2021b; Lin et al., 2021). It is worth noting that only after modifications, such as oxidation and desialylation, LDL particles become atherogenic. Of note, ox-LDL has been a major risk factor in atherosclerosis (Mitra et al., 2011; Ahmadi et al., 2021; Lin et al., 2021).

Reactive oxygen species (ROS) and reactive nitrogen species are important contributors of LDL oxidation. In the vessels, reactive species can be produced by nicotinamide adenine dinucleotide phosphate (NADPH) oxidase, xanthine oxidase, lipoxygenases, cyclooxygenase, myeloperoxidases, nitric oxide synthase, and uncoupled endothelial nitric oxide synthetase, dysfunctional mitochondria as well as metal ion catalysis (Kattoor et al., 2017; Malekmohammad et al., 2019). The subendothelial space is the presumed site of LDL oxidation (Matsuura et al., 2008). Lipids of LDL are the primary targets of reactive species. Lipid peroxidation includes peroxidation of phospholipid and CE at the polyunsaturated fatty acid moieties. This process generates more reactive aldehyde products and metabolites including malondialdehyde and 4-hydroxynoneal which are linked to ApoB, phosphatidylserine, and

phosphatidylethanolamine, through building adduct with Schiff-base lysine residue (Niki and Noguchi, 1997; Khatana et al., 2020). In general, CE 18:2 hydroperoxide, CE 18:2 hydroxide, phosphatidylcholine hyderoperoxide, ketone, oxidized ApoB, oxidized sphingomyelin, and 7-ketocholesterol are major oxidized components of ox-LDL (Yoshida and Kisugi, 2010; Khatana et al., 2020). The mechanisms of action of LDL oxidation have been reviewed by distinct groups (Yoshida and Kisugi, 2010; Khatana et al., 2020; Koschinsky and Boffa., 2022). A recent *in vitro* study suggests that riboflavin-sensitized photooxidation is also a potential mechanism of LDL oxidation and this process is critical for the development of CVD (Yeo and Shahidi, 2021). However, the above novel mechanism needs to be verified *in vivo* in future.

Some antioxidants are found to counteract the oxidation process. The enzymatic antioxidants in the blood vessels are superoxide dismutase, glutathione peroxidase, catalase, paraoxonase, and thioredoxin reductase (Kattoor et al., 2017). The non-enzymatic antioxidants include glutathione, coenzyme Q/coenzyme QH2, uric acid, bilirubin, lipoic acid, Vitamin E, and Vitamin C (Siekmeier et al., 2007; Malekmohammad et al., 2019). These antioxidants exert important protective functions against oxidation. For instance, glutathione, a cofactor for glutathione peroxidase scavenges hydroxide, hypochlorous acid, and peroxinitrite, thus modulates atherosclerosis (Pastore and Piemonte, 2013). Coenzyme Q improves endothelial function by scavenging peroxyl radicals (Moss and Ramji, 2016). The mechanisms of action of these antioxidants have been well documented by Malekmohammad et al. (2019) and Kattoor et al. (2017).

Of importance, ox-LDL and macrophages are involved in the whole process of atherosclerosis from plaque initiation to plaque progression, rupture, or even regression (Liu et al., 2021a; Lin et al., 2021). Ox-LDL elicits atherosclerotic events right from their production in the subendothelium. Ox-LDL, *via* lectin-like ox-LDL receptor (LOX1) and other factors, activates endothelium for a number of events: adherence of LDL, monocytes, and platelets; secretion of chemokines and growth factors; production of ROS; impairing NO secretion; and so on. Scavenger receptors, CD36, and LOX1 assist the uptake of ox-LDL by monocyte-derived macrophages in the subendothelium (Kattoor et al., 2019). Growth factors mediate proliferation of smooth muscle cell and formation of extracellular matrix. Platelet adherence and accumulation are also, in part elicited by ox-LDL which result into a rupture prone thrombus (Kruth et al., 2002; Yoshida, 2010; Khatana et al., 2020; Liu et al., 2021b; Lin et al., 2021). The mechanisms of action of ox-LDL-induced atherosclerosis have been well-documented (Matsuura et al., 2008; Khatana et al., 2020; Jiang et al., 2022).

The plasma level of ox-LDL is positively associated with the severity of CVD, suggesting ox-LDL is a valuable biomarker of CVD (Ivanova et al., 2017). Presently, several immunological techniques with high sensitivity and reproducibility have been developed for measurement of ox-LDL (Kohno et al., 2000; Fang et al., 2002). The methods using antibodies that are specifically binds to the oxidized components of LDL are sure to improve the detection efficiency and accuracy of ox-LDL. However, these methods are different in principle and operation procedures. Controversial results may be obtained *via* distinct detection methods (Itabe and Ueda, 2007).

Therapies targeting LDL-P

The 2022 American College of Cardiology (ACC)/American Heart Association (AHA)/American Heart Failure Society (HFSA) guidelines support the use of statins to prevent CVD events (Heidenreich et al., 2022). In clinical practice, "the lower the better" is still a widely accepted principle for lowering LDL-C. Except for statins, other hypolipidemic agents are also applied for treatment of dyslipidemias. Presently, the overall effect of non-statins is inferior to that of statins. However, PCSK9i show attractive lipid-lowering and anti-atherosclerotic effects in practice (Cannon et al., 2015; Chaudhary et al., 2017; Guo et al., 2020). As we reviewed recently, angiopoietin-like protein (ANGPTL), such as ANGPTL3, plays a key in regulation of both cholesterol and TG *via* inhibition of LPL (Zhang et al., 2022). The antisense oligonucleotide of ANGPTL3 has been applied to familial hypercholesterolemia and is now in phase 3 clinical trial (Graham et al., 2017). In the following, we will briefly review the hypolipidemic effects and mechanisms of action of statins and PCSK9i.

Statin therapy

Mechanistically, statins primarily reduce the serum level of cholesterol by inhibiting the activity of HMG-CoA reductase. HMG-CoA reductase is the rate-limiting enzyme for cholesterol formation in the liver and other tissues. By inhibiting HMG-CoA reductase, statins reduce the hepatocyte cholesterol content, stimulate the expression of LDLR, and ultimately enhance removal of LDL-C from the circulation (Toth, 2010). Except for lowering LDL-C, recent studies suggest that statins can effectively reduce the number of LDL-P (Folse et al., 2014; Heidenreich et al., 2022). However, statins are more effective in reducing LDL-C than lowering LDL-P. Furthermore, hepatic LDLR is not effective in clearance of sdLDL compared to normal-sized LDL. Therefore, a proportion of patients treated with statins remain high levels of LDL-P due to the discordance between LDL-C and LDL-P (Folse et al., 2014). The inefficiency of statins in reduction of LDL-P may explain, at least in part, the residual CVD risk in patients who have achieved the recommended LDL-C goals (Wong et al., 2017). A series of study have suggested that statin therapy guided by reductions in LDL-P can further decrease the CVD risk compared with that

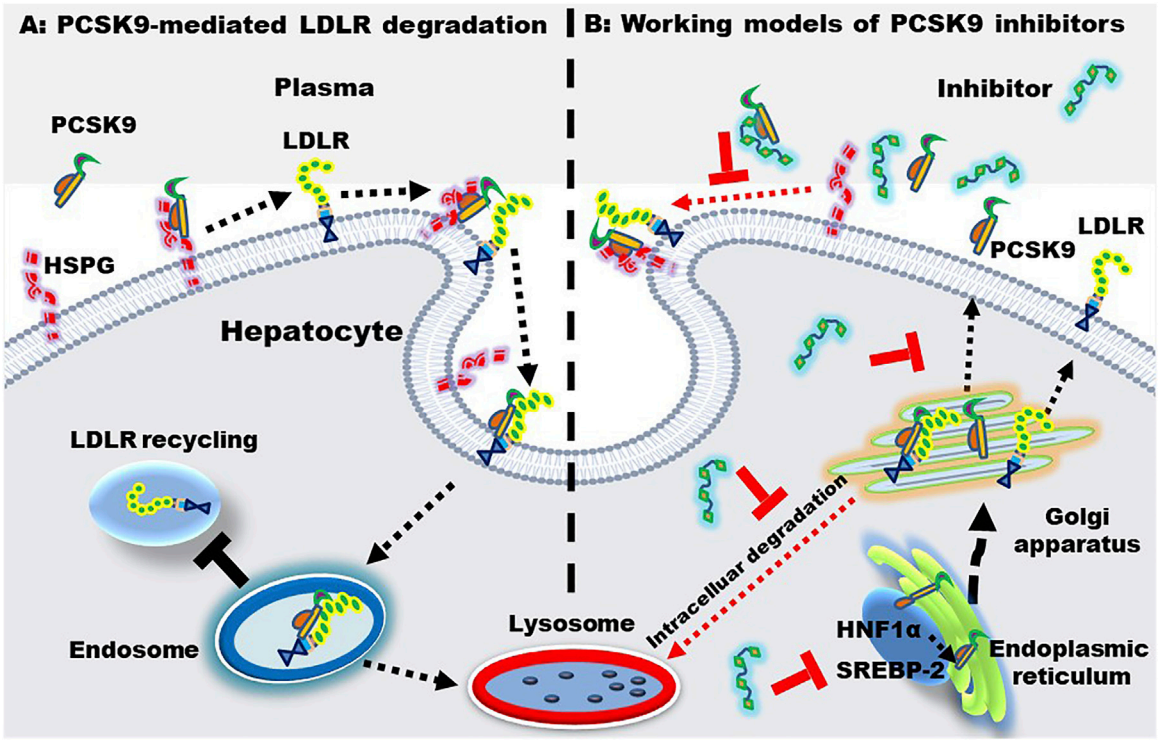

FIGURE 4
PCSK9-mediated LDLR degradation and the working models of PCSK9 inhibitors. **(A)** PCSK9-mediated LDLR degradation. Heparan sulfate proteoglycan (HSPG) located at the hepatic surface captures PCSK9, enhancing the binding between PCSK9 and LDLR. Upon binding, the PCSK9-LDLR complex is internalized and transferred to endosome, where PCSK9 binds LDLR with an even higher affinity. Finally, the complex is transported to the lysosome for degradation. **(B)** working models of PCSK9 inhibitors. PCSK9 inhibitors may inhibit PCSK9-LDLR interactions, PCSK9 production, transcription, and secretion. The PCSK9 expression is regulated by sterol regulatory binding protein-2 (SREBP-2) and hepatocyte nuclear factor 1α (HNF-1α).

guided by LDL-C alone in high-risk patients. Thus, LDL-P guided therapy is an effective way to reduce the residual CVD risk. Furthermore, statin therapy is reported to reduce the level of plasma ox-LDL in patients with different diseases such as acute ischemic stroke (Tsai et al., 2014; Mansouri et al., 2022). As reviewed recently, statins are found to modulate the nuclear factor erythroid two related factor 2/heme oxygenase-1 signaling pathway in different diseases (Mansouri et al., 2022).

Most LDL-Ps are cleared by LDLR that located at the surface of hepatocytes. Upon binding, LDL-P and LDLR are combined to form a complex that is endocytosed by hepatocytes. In general, the LDL and LDLR complex will separate in endosome and the released LDLR is transported back to the surface of hepatocytes to capture LDL-Ps again, further reducing the plasma LDL level. LDL-Ps, on the other hand, are degraded in lysosomes. These mechanisms of action of LDLR are summarized in Figure 4A. Of note, statins upregulate LDLR through sterol regulatory binding protein-2, which also enhance the expression of PCSK9. Accumulating evidence have demonstrated that PCSK9 induces the formation of LDLR-PCSK9 complex, leading to the degradation of LDLR in lysosomes, thereby reducing LDLR recycling and LDL-P clearance (Guo et al., 2020; Kong et al., 2022).

PCSK9i

Statin intervention is associated with side effects as well as intolerability. Of importance, a proportion of patients with hyperlipidemias fail to meet the targeted LDL-C levels even using the maximum tolerated dose of statin (De Backer et al., 2019). Furthermore, clinical data have displayed that > 70% of patients with ASCVD fail to reach the recommended level of LDL-C < 70 mg/dl (Adhyaru and Jacobson, 2018). Of note, PCSK9 inhibition enhances the amount of hepatic LDLRs, leading to a substantial decrease of LDL-Ps in circulation. PCSK9i can be divided into three categories: 1) monoclonal antibodies or mimic antibody proteins which directly inhibit PCSK9 protein from binding to LDLR; 2) small interfering RNA (siRNA) and antisense oligonucleotides which inhibit PCSK9 production *via* gene silencing; 3) small molecules with multiple modulatory functions. The mechanisms of action of

PCSK9i are shown in Figure 4B. Of importance, PCSK9i reduce the production of LDL-Ps, while statins do not change the production rate of LDL-Ps (Sniderman et al., 2017). As mentioned previously, statins increase the level of PCSK9 which reduces LDLR recycling and LDL-P clearance. Therefore, PCSK9i have different LDL-P-lowering effects and mechanisms compared to statins.

Besides, PCSK9i play a potential role in modulating the production of ox-LDL. Several studies demonstrated that elevated circulating PCSK9 directly enhances platelet activation, which induces CVD (Cammisotto et al., 2020; Qi et al., 2021). PCSK9i treatment inhibits platelet activation by modulating ox-LDL production and ox-LDL-mediated signaling pathway (Cammisotto et al., 2021). As reviewed recently, PCSK9 enhances the expression of NADPH oxidase and promotes the production of ROS and ox-LDL; PCSK9i can reduce oxidative stress *via* improving the activity of antioxidants such as glutathione peroxidase, superoxide dismutase, and catalase, thereby counteracting lipid peroxidation, the production of ox-LDL as well as cell damage (Cammisotto et al., 2022). Of note, pre-clinical trials have reported an independent association between plasma levels of PCSK9 and small LDL subfractions in patients with established CVD (Zhang et al., 2015; Lankin et al., 2018). A novel PCSK9 inhibitor RG7652 is reported to reduce both the small and large LDL-Ps, but the median percentage change is lower for the smaller LDL-Ps compared to the larger LDL-Ps (−43% vs. −81% from baseline), and 11 of the 45 patients showed an increase in the small LDL-Ps at the end of the study (Baruch et al., 2017). The PCSK9 monoclonal antibodies, alirocumab and evolocumab, are also reported to reduce larger LDL-Ps more powerfully than small LDL-Ps (Koren et al., 2015; Wu et al., 2017). To summarize, PCSK9 inhibitors seem to be effective at lowering all LDL subfractions, but with a trend towards a more efficient lowering of the larger LDL subfractions.

The development of PCSK9 monoclonal antibodies including evolocumab and alirocumab have been demonstrated to lower LDL-C levels as well as CVD risks (Hadjiphilippou and Ray, 2017; Schwartz et al., 2018). However, the biweekly or monthly subcutaneous injection of these antibodies has been a major concern for patient compliance. The siRNA, inclisiran, is developed to target and reduce the gene expression of PCSK9 by approximately 80% in all three Phase III ORION studies (Hardy et al., 2021; Henney et al., 2021). Inclisiran markedly reduces hepatic generation of PCSK9, causing a profound decrease in LDL-C level > 50% compared with control. Of note, this synthetic siRNA can maintain its pharmacological effects within half a year. However, whether inclisiran can reduce CVD outcomes is still being evaluated at present (ORION-4). Additionally, assessment of the long-term tolerability, efficacy, and safety of inclisiran needs to be continued based on a larger group of patients (Mereép et al., 2022). The gene therapy targeting PCSK9 has been reviewed recently by different research groups (Henney et al., 2021; Miname et al., 2021; Katzmann et al., 2022).

Cost-effective small-molecules with specific PCSK9 inhibition activity is an attractive research field. The advances of these inhibitors including derivatives of guanidine, berberine, piperidine, imidazole, and benzimidazole, have been well-documented recently by Ahamad et al. (2022). Of note, accumulating evidence have demonstrated that natural products are an important resource for discovery of PCSK9i. These natural products include berberine, lupin, quercetin, resveratrol, and others as reviewed by several groups (Ahamad et al., 2022; Waiz et al., 2022). Mechanistically, these small molecules may directly inhibit PCSK9-LDLR interactions, PCSK9 production, transcription, and secretion (Ahamad et al., 2022). Although some advances have been achieved, none of these small-molecule PCSK9i has been approved by the Food and Drug Administration of any country.

Conclusion and future perspetive

Recent studies have demonstrated that LDL-P is a superior indicator of ASCVD risk than LDL-C. Of note, LDL-Ps are divided into various subclasses which vary in atherogenicity. SdLDL and ox-LDL are found to be more atherogenic compared with other LDL-Ps. However, study of the roles of these LDL subclasses, such as sdLDL, in the development of ASCVD is not easy because distinct methods may obtain different LDL subclasses with distinct physiochemical properties. At present, it is still early to determine which of the available methods is the most accurate and suitable for clinical use. Therefore, it is impelled to explore standard methods for preparation and evaluation of these LDL subclasses. Quest and LabCorp in the United states have established some commercially available methods for clinical assays with high throughput.

Statins are effective in reducing LDL-C level and even in decreasing LDL-P number. However, statin intervention is associated with side effects as well as intolerability. Furthermore, a large number of patients fail to reach the desirable LDL-C goals even with the maximum tolerated doses of statins. Furthermore, statin intervention enhances the levels of PCSK9, which accelerates LDLR degradation, causing the reduced ability of statins for lowering LDL-P number. Of note, PCSK9 monoclonal antibodies increase the expression of LDLR proteins, leading to profound reductions in plasma levels of LDL-P. Although PCSK9 siRNA therapy exhibits powerful effects, the long-term tolerability, efficacy, and safety need to be investigated in more participants. At present, the usage of PCSK9i is restricted to secondary prevention in patients with high CVD risks due to the high expense. In the future, the cost-effective small-molecules with specific PCSK9 inhibitory ability

may reduce the manufacturing costs and promote the usage of PCSK9i for primary prevention of ASCVD.

Author contributions

Y-NQ and Y-LZ collected the literature using PubMed and Web of Science and wrote this manuscript; S-DG prepared the figures and further revised this manuscript.

Funding

National Natural Science Foundation of China (Nos. 82070469, 81770463, and 82104031).

Conflict of interest

The authors declare that the research was conducted in the absence of any commercial or financial relationships that could be construed as a potential conflict of interest.

Publisher's note

All claims expressed in this article are solely those of the authors and do not necessarily represent those of their affiliated organizations, or those of the publisher, the editors and the reviewers. Any product that may be evaluated in this article, or claim that may be made by its manufacturer, is not guaranteed or endorsed by the publisher.

References

Adhyaru, B. B., and Jacobson, T. A. (2018). Safety and efficacy of statin therapy. *Nat. Rev. Cardiol.* 15 (12), 757–769. doi:10.1038/s41569-018-0098-5

Ahamad, S., Mathew, S., Khan, W. A., and Mohanan, K. (2022). Development of small-molecule PCSK9 inhibitors for the treatment of hypercholesterolemia. *Drug Discov. Today* 27 (5), 1332–1349. doi:10.1016/j.drudis.2022.01.014

Ahmadi, A., Panahi, Y., Johnston, T. P., and Sahebkar, A. (2021). Antidiabetic drugs and oxidized low-density lipoprotein: A review of anti-atherosclerotic mechanisms. *Pharmacol. Res.* 172, 105819. doi:10.1016/j.phrs.2021.105819

Ajala, O. N., Demler, O. V., Liu, Y., Farukhi, Z., Adelman, S. J., Collins, H. L., et al. (2020). Anti-inflammatory HDL function, incident cardiovascular events, and mortality: A secondary analysis of the jupiter randomized clinical trial. *J. Am. Heart Assoc.* 9 (17), e016507. doi:10.1161/JAHA.119.016507

Allaire, J., Vors, C., Couture, P., and Lamarche, B. (2017). LDL particle number and size and cardiovascular risk: Anything new under the sun? *Curr. Opin. Lipidol.* 28 (3), 261–266. doi:10.1097/mol.0000000000000419

Aru, V., Lam, C., Khakimov, B., Hoefsloot, H. C. J., Zwanenburg, G., Lind, M. V., et al. (2017). Quantification of lipoprotein profiles by nuclear magnetic resonance spectroscopy and multivariate data analysis. *TrAC Trends Anal. Chem.* 94, 210–219. doi:10.1016/j.trac.2017.07.009

Baruch, A., Mosesova, S., Davis, J. D., Budha, N., Vilimovskij, A., Kahn, R., et al. (2017). Effects of RG7652, a monoclonal antibody against PCSK9, on LDL-C, LDL-C subfractions, and inflammatory biomarkers in patients at high risk of or with established coronary heart disease (from the phase 2 EQUATOR study). *Am. J. Cardiol.* 119 (10), 1576–1583. doi:10.1016/j.amjcard.2017.02.020

Berneis, K., Jeanneret, C., Muser, J., Felix, B., and Miserez, A. R. (2005). Low-density lipoprotein size and subclasses are markers of clinically apparent and non-apparent atherosclerosis in type 2 diabetes. *Metabolism.* 54 (2), 227–234. doi:10.1016/j.metabol.2004.08.017

Berneis, K. K., and Krauss, R. M. (2002). Metabolic origins and clinical significance of LDL heterogeneity. *J. Lipid Res.* 43 (9), 1363–1379. doi:10.1194/jlr.r200004-jlr200

Bonilha, I., Hajduch, E., Luchiari, B., Nadruz, W., Le Goff, W., and Sposito, A. C. (2021). The reciprocal relationship between lDL metabolism and type 2 diabetes mellitus. *Metabolites* 11 (12), 807. doi:10.3390/metabo11120807

Cali, A. M., Zern, T. L., Taksali, S. E., de Oliveira, A. M., Dufour, S., Otvos, J. D., et al. (2007). Intrahepatic fat accumulation and alterations in lipoprotein composition in obese adolescents: A perfect proatherogenic state. *Diabetes Care* 30 (12), 3093–3098. doi:10.2337/dc07-1088

Cammisotto, V., Baratta, F., Castellani, V., Bartimoccia, S., Nocella, C., D'Erasmo, L., et al. (2021). Proprotein convertase subtilisin kexin type 9 inhibitors reduce platelet activation modulating ox-LDL pathways. *Int. J. Mol. Sci.* 22 (13), 7193. doi:10.3390/ijms22137193

Cammisotto, V., Baratta, F., Simeone, P. G., Barale, C., Lupia, E., Galardo, G., et al. (2022). Proprotein convertase subtilisin kexin type 9 (PCSK9) beyond lipids: The role in oxidative stress and thrombosis. *Antioxidants (Basel)* 11 (3), 569. doi:10.3390/antiox11030569

Cammisotto, V., Pastori, D., Nocella, C., Bartimoccia, S., Castellani, V., Marchese, C., et al. (2020). PCSK9 regulates Nox2-mediated platelet activation via CD36 receptor in patients with atrial fibrillation. *Antioxidants (Basel)* 9 (4), 296. doi:10.3390/antiox9040296

Cannon, C. P., Blazing, M. A., Giugliano, R. P., McCagg, A., White, J. A., Theroux, P., et al. (2015). Ezetimibe added to statin therapy after acute coronary syndromes. *N. Engl. J. Med.* 372 (25), 2387–2397. doi:10.1056/NEJMoa1410489

Carmena, R., Duriez, P., and Fruchart, J.-C. (2004). Atherogenic lipoprotein particles in atherosclerosis. *Circulation* 109, III2–7. doi:10.1161/01.CIR.0000131511.50734.44

Caulfield, M. P., Li, S., Lee, G., Blanche, P. J., Salameh, W. A., Benner, W. H., et al. (2008). Direct determination of lipoprotein particle sizes and concentrations by ion mobility analysis. *Clin. Chem.* 54 (8), 1307–1316. doi:10.1373/clinchem.2007.100586

Centelles, S., Hoefsloot, H., Khakimov, B., Ebrahimi, P., Lind, M., Kristensen, M., et al. (2017). Toward reliable lipoprotein particle predictions from NMR spectra of human blood: An Interlaboratory Ring Test. *Anal. Chem.* 89 (15), 8004–8012. doi:10.1021/acs.analchem.7b01329

Chaudhary, R., Garg, J., Shah, N., and Sumner, A. (2017). PCSK9 inhibitors: A new era of lipid lowering therapy. *World J. Cardiol.* 9 (2), 76–91. doi:10.4330/wjc.v9.i2.76

Chisolm, G. M., and Steinberg, D. (2000). The oxidative modification hypothesis of atherogenesis: An overview. *Free Radic. Biol. Med.* 28 (12), 1815–1826. doi:10.1016/S0891-5849(00)00344-0

Christian, A., and Nagar, K. (2021). Understanding patients experiences living with diabetes mellitus: A qualitative study, Gujarat, India. *J. Pharm. Res. Int.* 33 (58), 464–471. doi:10.9734/jpri/2021/v33i58A34139

Clouet Foraison, N., Gaie-Levrel, F., Coquelin, L., Ebrard, G., Gillery, P., and Delatour, V. (2017). Absolute quantification of bionanoparticles by electrospray differential mobility analysis: An application to lipoprotein particle concentration measurements. *Anal. Chem.* 89 (4), 2242–2249. doi:10.1021/acs.analchem.6b02909

Cromwell, W. C., Otvos, J. D., Keyes, M. J., Pencina, M. J., Sullivan, L., Vasan, R. S., et al. (2007). LDL particle number and risk of future cardiovascular disease in the framingham offspring study - implications for LDL management. *J. Clin. Lipidol.* 1 (6), 583–592. doi:10.1016/j.jacl.2007.10.001

Davies, I. G., Graham, J. M., and Griffin, B. A. (2003). Rapid separation of LDL subclasses by iodixanol gradient ultracentrifugation. *Clin. Chem.* 49 (11), 1865–1872. doi:10.1373/clinchem.2003.023366

De Backer, G., Jankowski, P., Kotseva, K., Mirrakhimov, E., Reiner, Ž., Rydén, L., et al. (2019). Management of dyslipidaemia in patients with coronary heart disease: Results from the ESC-EORP EUROASPIRE V survey in 27 countries. *Atherosclerosis* 285, 135–146. doi:10.1016/j.atherosclerosis.2019.03.014

Delatour, V., Clouet Foraison, N., Gaie-Levrel, F., Santica, M., Hoofnagle, A., Kuklenyik, Z., et al. (2018). Comparability of lipoprotein particle number concentrations across ES-DMA, NMR, LC-MS/MS, immunonephelometry, and VAP: In search of a candidate reference measurement procedure for ApoB and non-

HDL-P standardization. *Clin. Chem.* 6410, 1485–1495. doi:10.1373/clinchem.2018.288746

Diffenderfer, M., and Schaefer, E. (2014). The composition and metabolism of large and small LDL. *Curr. Opin. Lipidol.* 25, 221–226. doi:10.1097/MOL.0000000000000067

Dugani, S. B., Moorthy, M. V., Li, C., Demler, O. V., Alsheikh-Ali, A. A., Ridker, P. M., et al. (2021). Association of lipid, inflammatory, and metabolic biomarkers with age at onset for incident coronary heart disease in women. *JAMA Cardiol.* 6 (4), 437–447. doi:10.1001/jamacardio.2020.7073

El Harchaoui, K., van der Steeg, W. A., Stroes, E. S. G., Kuivenhoven, J. A., Otvos, J. D., Wareham, N. J., et al. (2007). Value of low-density lipoprotein particle number and size as predictors of coronary artery disease in apparently healthy men and women: The EPIC-Norfolk Prospective Population Study. *J. Am. Coll. Cardiol.* 49 (5), 547–553. doi:10.1016/j.jacc.2006.09.043

Ensign, W., Hill, N., and Heward, C. B. (2006). Disparate LDL phenotypic classification among 4 different methods assessing LDL particle characteristics. *Clin. Chem.* 52 (9), 1722–1727. doi:10.1373/clinchem.2005.059949

Fang, J. C., Kinlay, S., Behrendt, D., Hikita, H., Witztum, J. L., Selwyn, A. P., et al. (2002). Circulating autoantibodies to oxidized LDL correlate with impaired coronary endothelial function after cardiac transplantation. *Arterioscler. Thromb. Vasc. Biol.* 22 (12), 2044–2048. doi:10.1161/01.atv.0000040854.47020.44

Farukhi, Z. M., Demler, O. V., Caulfield, M. P., Kulkarni, K., Wohlgemuth, J., Cobble, M., et al. (2020). Comparison of nonfasting and fasting lipoprotein subfractions and size in 15, 397 apparently healthy individuals: An analysis from the Vitamin D and OmegA-3 Trial. *J. Clin. Lipidol.* 14 (2), 241–251. doi:10.1016/j.jacl.2020.02.005

Fernández-Cidón, B., Candás-Estébanez, B., Ribalta, J., Rock, E., Guardiola-Guionnet, M., Amigó, N., et al. (2020). Precipitated sdLDL: An easy method to estimate LDL particle size. *J. Clin. Lab. Anal.* 34 (7), e23282. doi:10.1002/jcla.23282

Folse, H. J., Goswami, D., Rengarajan, B., Budoff, M., and Kahn, R. (2014). Clinical- and cost-effectiveness of LDL particle-guided statin therapy: A simulation study. *Atherosclerosis* 236 (1), 154–161. doi:10.1016/j.atherosclerosis.2014.06.027

Fukushima, Y., Hirayama, S., Ueno, T., Dohi, T., Miyazaki, T., Ohmura, H., et al. (2011). Small dense LDL cholesterol is a robust therapeutic marker of statin treatment in patients with acute coronary syndrome and metabolic syndrome. *Clin. Chim. Acta.* 412 (15), 1423–1427. doi:10.1016/j.cca.2011.04.021

Gallego-Colon, E., Daum, A., and Yosefy, C. (2020). Statins and PCSK9 inhibitors: A new lipid-lowering therapy. *Eur. J. Pharmacol.* 878, 173114. doi:10.1016/j.ejphar.2020.173114

Garvey, W. T., Kwon, S., Zheng, D., Shaughnessy, S., Wallace, P., Hutto, A., et al. (2003). Effects of insulin resistance and type 2 diabetes on lipoprotein subclass particle size and concentration determined by nuclear magnetic resonance. *Diabetes* 52 (2), 453–462. doi:10.2337/diabetes.52.2.453

Gerber, P. A., Thalhammer, C., Schmied, C., Spring, S., Amann-Vesti, B., Spinas, G. A., et al. (2013). Small, dense LDL particles predict changes in intima media thickness and insulin resistance in men with type 2 diabetes and prediabetes--a prospective cohort study. *PLoS ONE* 8 (8), e72763. doi:10.1371/journal.pone.0072763

Graham, M. J., Lee, R. G., Brandt, T. A., Tai, L.-J., Fu, W., Peralta, R., et al. (2017). Cardiovascular and metabolic effects of ANGPTL3 antisense oligonucleotides. *N. Engl. J. Med.* 377 (3), 222–232. doi:10.1056/NEJMoa1701329

Guo, S., Xia, X. D., Gu, H. M., and Zhang, D. W. (2020). Proprotein convertase subtilisin/kexin-type 9 and lipid metabolism. *Adv. Exp. Med. Biol.* 1276, 137–156. doi:10.1007/978-981-15-6082-8_9

Hadjiphilippou, S., and Ray, K. K. (2017). Evolocumab and clinical outcomes in patients with cardiovascular disease. *J. R. Coll. Physicians Edinb.* 47 (2), 153–155. doi:10.4997/jrcpe.2017.212

Hardy, J., Niman, S., Pereira, E., Lewis, T., Teid, J., Choksi, R., et al. (2021). A critical review of the efficacy and safety of inclisiran. *Am. J. Cardiovasc. Drugs* 21 (6), 629–642. doi:10.1007/s40256-021-00477-7

Heidenreich, P. A., Bozkurt, B., Aguilar, D., Allen, L. A., Byun, J. J., Colvin, M. M., et al. (2022). 2022 AHA/ACC/HFSA guideline for the management of heart failure: Executive summary: A report of the American College of Cardiology/American heart association joint committee on clinical practice guidelines. *Circulation* 145, e876–e894. doi:10.1161/cir.0000000000001062106210.1161/cir.0000000000001062

Henney, N. C., Banach, M., and Penson, P. E. (2021). RNA silencing in the management of dyslipidemias. *Curr. Atheroscler. Rep.* 23 (11), 69. doi:10.1007/s11883-021-00968-7

Hero, C., Svensson, A. M., Gidlund, P., Gudbjörnsdottir, S., Eliasson, B., and Eeg-Olofsson, K. (2016). LDL cholesterol is not a good marker of cardiovascular risk in Type 1 diabetes. *Diabet. Med.* 33 (3), 316–323. doi:10.1111/dme.13007

Hirany, S., Othman, Y., Kutscher, P., Rainwater, D., Jialal, I., and Devaraj, S. (2003). Comparison of low-density lipoprotein size by polyacrylamide tube gel electrophoresis and polyacrylamide gradient gel electrophoresis. *Am. J. Clin. Pathol.* 119, 439–445. doi:10.1309/H4E6KTYUFFF23HFN

Hirayama, S., and Miida, T. (2012). Small dense LDL: An emerging risk factor for cardiovascular disease. *Clin. Chim. Acta.* 414, 215–224. doi:10.1016/j.cca.2012.09.010

Hoogeveen, R. C., Gaubatz, J. W., Sun, W., Dodge, R. C., Crosby, J. R., Jiang, J., et al. (2014). Small dense low-density lipoprotein-cholesterol concentrations predict risk for coronary heart disease: The atherosclerosis risk in communities (ARIC) study. *Arterioscler. Thromb. Vasc. Biol.* 34 (5), 1069–1077. doi:10.1161/ATVBAHA.114.303284

Itabe, H., and Ueda, M. (2007). Measurement of plasma oxidized low-density lipoprotein and its clinical implications. *J. Atheroscler. Thromb.* 14, 1–11. doi:10.5551/jat.14.1

Ivanova, E. A., Myasoedova, V. A., Melnichenko, A. A., Grechko, A. V., and Orekhov, A. N. (2017). Small dense low-density lipoprotein as biomarker for atherosclerotic diseases. *Oxid. Med. Cell. Longev.* 2017, 1273042. doi:10.1155/2017/1273042

Jeyarajah, E., Cromwell, W., and Otvos, J. (2007). Lipoprotein particle analysis by nuclear magnetic resonance spectroscopy. *Clin. Lab. Med.* 26, 847–870. doi:10.1016/j.cll.2006.07.006

Jiang, H., Zhou, Y., Nabavi, S. M., Sahebkar, A., Little, P. J., Xu, S., et al. (2022). Mechanisms of oxidized LDL-mediated endothelial dysfunction and its consequences for the development of atherosclerosis. *Front. Cardiovasc. Med.* 9, 925923. doi:10.3389/fcvm.2022.925923

Kanonidou, C. (2021). Small dense low-density lipoprotein: Analytical review. *Clin. Chim. Acta.* 520, 172–178. doi:10.1016/j.cca.2021.06.012

Karlsson, H., Leanderson, P., Tagesson, C., and Lindahl, M. (2005). Lipoproteomics I: Mapping of proteins in low-density lipoprotein using two-dimensional gel electrophoresis and mass spectrometry. *Proteomics* 5 (2), 551–565. doi:10.1002/pmic.200300938

Kattoor, A. J., Kanuri, S. H., and Mehta, J. L. (2019). Role of ox-LDL and LOX-1 in atherogenesis. *Curr. Med. Chem.* 26 (9), 1693–1700. doi:10.2174/0929867325666180508100950

Kattoor, A. J., Pothineni, N. V. K., Palagiri, D., and Mehta, J. L. (2017). Oxidative stress in atherosclerosis. *Curr. Atheroscler. Rep.* 19 (11), 42. doi:10.1007/s11883-017-0678-6

Katzmann, J. L., Cupido, A. J., and Laufs, U. (2022). Gene therapy targeting PCSK9. *Metabolites* 12 (1), 70. doi:10.3390/metabo12010070

Ke, L. Y., Chan, H. C., Chen, C. C., Chang, C. F., Lu, P. L., Chu, C. S., et al. (2020). Increased APOE glycosylation plays a key role in the atherogenicity of L5 low-density lipoprotein. *FASEB J.* 34 (7), 9802–9813. doi:10.1096/fj.202000659R

Khatana, C., Saini, N. K., Chakrabarti, S., Saini, V., Sharma, A., Saini, R. V., et al. (2020). Mechanistic insights into the oxidized low-density lipoprotein-induced atherosclerosis. *Oxid. Med. Cell. Longev.* 2020, 5245308. doi:10.1155/2020/5245308

Kohno, H., Sueshige, N., Oguri, K., Izumidate, H., Masunari, T., Kawamura, M., et al. (2000). Simple and practical sandwich-type enzyme immunoassay for human oxidatively modified low density lipoprotein using antioxidized phosphatidylcholine monoclonal antibody and antihuman apolipoprotein-B antibody. *Clin. Biochem.* 33 (4), 243–253. doi:10.1016/S0009-9120(00)00065-5

Kong, P., Cui, Z. Y., Huang, X. F., Zhang, D.-D., Guo, R. J., and Han, M. (2022). Inflammation and atherosclerosis: Signaling pathways and therapeutic intervention. *Signal Transduct. Target. Ther.* 7, 131. doi:10.1038/s41392-022-00955-7

Koren, M. J., Kereiakes, D., Pourfarzib, R., Winegar, D., Banerjee, P., Hamon, S., et al. (2015). Effect of PCSK9 inhibition by alirocumab on lipoprotein particle concentrations determined by nuclear magnetic resonance spectroscopy. *J. Am. Heart Assoc.* 4 (11), e002224. doi:10.1161/jaha.115.002224

Koschinsky, M. L., and Boffa, M. B. (2022). Oxidized phospholipid modification of lipoprotein(a): Epidemiology, biochemistry and pathophysiology. *Atherosclerosis* 349, 92–100. doi:10.1016/j.atherosclerosis.2022.04.001

Kruth, H. S., Huang, W., Ishii, I., and Zhang, W. Y. (2002). Macrophage foam cell formation with native low density lipoprotein. *J. Biol. Chem.* 277 (37), 34573–34580. doi:10.1074/jbc.M205059200

Kulkarni, K. (2007). Cholesterol profile measurement by vertical auto profile method. *Clin. Lab. Med.* 26, 787–802. doi:10.1016/j.cll.2006.07.004

Lankin, V. Z., Tikhaze, A. K., Viigimaa, M., and Chazova, I. (2018). PCSK9 Inhibitor causes a decrease in the level of oxidatively modified low-density lipoproteins in patients with coronary artery diseases. *Ter. Arkh.* 90 (9), 27–30. doi:10.26442/terarkh201890927-30

Lee, J., and Cooke, J. P. (2011). The role of nicotine in the pathogenesis of atherosclerosis. *Atherosclerosis* 215 (2), 281–283. doi:10.1016/j.atherosclerosis.2011.01.003

Libby, P., Buring, J. E., Badimon, L., Hansson, G. K., Deanfield, J., Bittencourt, M. S., et al. (2019). Atherosclerosis. *Nat. Rev. Dis. Prim.* 5 (1), 56. doi:10.1038/s41572-019-0106-z

Lin, P., Ji, H. H., Li, Y. J., and Guo, S. D. (2021). Macrophage plasticity and atherosclerosis therapy. *Front. Mol. Biosci.* 8, 679797. doi:10.3389/fmolb.2021.679797

Liu, N., Si, Y., Zhang, Y., Guo, S., and Qin, S. (2021a). Human cholesteryl ester transport protein transgene promotes macrophage reverse cholesterol transport in C57BL/6 mice and phospholipid transfer protein gene knockout mice. *J. Physiol. Biochem.* 77 (4), 683–694. doi:10.1007/s13105-021-00834-9

Liu, N., Zhang, B. H., Sun, Y. L., Song, W. G., and Guo, S. D. (2021b). Macrophage origin, phenotypic diversity, and modulatory signaling pathways in the atherosclerotic plaque microenvironment. *Vessel Plus* 5, 43. doi:10.20517/2574-1209.2021.25

Ljunggren, S., Bengtsson, T., Karlsson, H., Starkhammar Johansson, C., Palm, E., Nayeri, F., et al. (2019). Modified lipoproteins in periodontitis: A link to cardiovascular disease? *Biosci. Rep.* 39 (3), BSR20181665. doi:10.1042/BSR20181665

Lo, T., Lee, Y., Tseng, C. Y., Hu, Y., Connelly, M. A., Mantzoros, C. S., et al. (2022). Daily transient coating of the intestine leads to weight loss and improved glucose tolerance. *Metabolism.* 126, 154917. doi:10.1016/j.metabol.2021.154917

Mach, F., Baigent, C., Catapano, A. L., Koskinas, K. C., Casula, M., Badimon, L., et al. (2020). 2019 ESC/EAS guidelines for the management of dyslipidaemias: Lipid modification to reduce cardiovascular risk. *Eur. Heart J.* 41 (1), 111–188. doi:10.1093/eurheartj/ehz455

Maiolino, G., Rossitto, G., Caielli, P., Bisogni, V., Rossi, G. P., and Calò, L. A. (2013). The role of oxidized low-density lipoproteins in atherosclerosis: The myths and the facts. *Mediat. Inflamm.* 2013, 714653. doi:10.1155/2013/714653

Malekmohammad, K., Sewell, R. D. E., and Rafieian-Kopaei, M. (2019). Antioxidants and atherosclerosis: Mechanistic aspects. *Biomolecules* 9 (8), 301. doi:10.3390/biom9080301

Mansouri, A., Reiner, Ž., Ruscica, M., Tedeschi-Reiner, E., Radbakhsh, S., Bagheri Ekta, M., et al. (2022). Antioxidant effects of statins by modulating Nrf2 and Nrf2/HO-1 signaling in different diseases. *J. Clin. Med.* 11 (5), 1313. doi:10.3390/jcm11051313

Marais, A. D. (2019). Apolipoprotein E in lipoprotein metabolism, health and cardiovascular disease. *Pathol. (Phila.)* 51 (2), 165–176. doi:10.1016/j.pathol.2018.11.002

Matsumoto, T., Takashima, H., Ohira, N., Tarutani, Y., Yasuda, Y., Yamane, T., et al. (2004). Plasma level of oxidized low-density lipoprotein is an independent determinant of coronary macrovasomotor and microvasomotor responses induced by bradykinin. *J. Am. Coll. Cardiol.* 44, 451–457. doi:10.1016/j.jacc.2004.03.064

Matsuura, E., Hughes, G. R., and Khamashta, M. A. (2008). Oxidation of LDL and its clinical implication. *Autoimmun. Rev.* 7 (7), 558–566. doi:10.1016/j.autrev.2008.04.018

Matyus, S. P., Braun, P. J., Wolak-Dinsmore, J., Jeyarajah, E. J., Shalaurova, I., Xu, Y., et al. (2014). NMR measurement of LDL particle number using the Vantera® Clinical Analyzer. *Clin. Biochem.* 47 (16), 203–210. doi:10.1016/j.clinbiochem.2014.07.015

Mehta, A., and Shapiro, M. D. (2022). Apolipoproteins in vascular biology and atherosclerotic disease. *Nat. Rev. Cardiol.* 19 (3), 168–179. doi:10.1038/s41569-021-00613-5

Merćep, I., Friščić, N., Strikić, D., and Reiner, Ž. (2022). Advantages and disadvantages of inclisiran: A small interfering ribonucleic acid molecule targeting PCSK9-a narrative review. *Cardiovasc. Ther.* 2022, 8129513. doi:10.1155/2022/8129513

Miname, M. H., Rocha, V. Z., and Santos, R. D. (2021). The role of RNA-targeted therapeutics to reduce ASCVD risk: What have we learned recently? *Curr. Atheroscler. Rep.* 23 (8), 40. doi:10.1007/s11883-021-00936-1

Mitra, S., Deshmukh, A., Sachdeva, R., Lu, J., and Mehta, J. L. (2011). Oxidized low-density lipoprotein and atherosclerosis implications in antioxidant therapy. *Am. J. Med. Sci.* 342 (2), 135–142. doi:10.1097/MAJ.0b013e318224a147

Moore, K. J., Sheedy, F. J., and Fisher, E. A. (2013). Macrophages in atherosclerosis: A dynamic balance. *Nat. Rev. Immunol.* 13 (10), 709–721. doi:10.1038/nri3520

Mora, S., Buring, J. E., and Ridker, P. M. (2014). Discordance of low-density lipoprotein (LDL) cholesterol with alternative LDL-related measures and future coronary events. *Circulation* 129 (5), 553–561. doi:10.1161/CIRCULATIONAHA.113.005873

Mora, S., Caulfield, M. P., Wohlgemuth, J., Chen, Z., Superko, H. R., Rowland, C. M., et al. (2015). Atherogenic lipoprotein subfractions determined by ion mobility and first cardiovascular events after random allocation to high-intensity statin or placebo: The justification for the use of statins in prevention: An intervention trial evaluating rosuvastatin (JUPITER) trial. *Circulation* 132 (23), 2220–2229. doi:10.1161/circulationaha.115.016857

Moss, J. W., and Ramji, D. P. (2016). Nutraceutical therapies for atherosclerosis. *Nat. Rev. Cardiol.* 13 (9), 513–532. doi:10.1038/nrcardio.2016.103

Niki, E., and Noguchi, N. (1997). Dynamics of oxidation of LDL and its inhibition by antioxidants. *Biofactors* 6 (2), 201–208. doi:10.1002/biof.5520060214

Nikolic, D., Katsiki, N., Montalto, G., Isenovic, E. R., Mikhailidis, D. P., and Rizzo, M. (2013). Lipoprotein subfractions in metabolic syndrome and obesity: Clinical significance and therapeutic approaches. *Nutrients* 5 (3), 928–948. doi:10.3390/nu5030928

Okazaki, M., and Yamashita, S. (2016). Recent advances in analytical methods on lipoprotein subclasses: Calculation of particle numbers from lipid levels by gel permeation HPLC using "Spherical Particle Model". *J. Oleo Sci.* 65, 265–282. doi:10.5650/jos.ess16020

Packard, C. (2006). Small dense low-density lipoprotein and its role as an independent predictor of cardiovascular disease. *Curr. Opin. Lipidol.* 17, 412–417. doi:10.1097/01.mol.0000236367.42755.c1

Pastore, A., and Piemonte, F. (2013). Protein glutathionylation in cardiovascular diseases. *Int. J. Mol. Sci.* 14 (10), 20845–20876. doi:10.3390/ijms141020845

Porter Starr, K. N., Connelly, M. A., Orenduff, M. C., McDonald, S. R., Sloane, R., Huffman, K. M., et al. (2019). Impact on cardiometabolic risk of a weight loss intervention with higher protein from lean red meat: Combined results of 2 randomized controlled trials in obese middle-aged and older adults. *J. Clin. Lipidol.* 13 (6), 920–931. doi:10.1016/j.jacl.2019.09.012

Prassl, R., and Laggner, P. (2008). Molecular structure of low density lipoprotein: Current status and future challenges. *Eur. Biophys. J.* 38 (2), 145–158. doi:10.1007/s00249-008-0368-y

Qi, Z., Hu, L., Zhang, J., Yang, W., Liu, X., Jia, D., et al. (2021). PCSK9 (proprotein convertase subtilisin/kexin 9) enhances platelet activation, thrombosis, and myocardial infarct expansion by binding to platelet CD36. *Circulation* 143 (1), 45–61. doi:10.1161/circulationaha.120.046290

Rafieian-Kopaei, M., Setorki, M., Doudi, M., Baradaran, A., and Nasri, H. (2014). Atherosclerosis: Process, indicators, risk factors and new hopes. *Int. J. Prev. Med.* 5 (8), 927–946.

Rizzo, M., and Berneis, K. (2006). Low-density lipoprotein size and cardiovascular risk assessment. *Q. J. Med.* 99, 1–14. doi:10.1093/qjmed/hci154

Rosenson, R. S., Davidson, M. H., and Pourfarzib, R. (2010). Underappreciated opportunities for low-density lipoprotein management in patients with cardiometabolic residual risk. *Atherosclerosis* 213 (1), 1–7. doi:10.1016/j.atherosclerosis.2010.03.038

Rosenson, R. S., and Underberg, J. A. (2013). Systematic review: Evaluating the effect of lipid-lowering therapy on lipoprotein and lipid values. *Cardiovasc. Drugs Ther.* 27 (5), 465–479. doi:10.1007/s10557-013-6477-6

Rudewicz-Kowalczyk, D., and Grabowska, I. (2021). Detection of low density lipoprotein-comparison of electrochemical immuno- and aptasensor. *Sensors* 21 (22), 7733. doi:10.3390/s21227733

Schwartz, G. G., Steg, P. G., Szarek, M., Bhatt, D. L., Bittner, V. A., Diaz, R., et al. (2018). Alirocumab and cardiovascular outcomes after acute coronary syndrome. *N. Engl. J. Med.* 379 (22), 2097–2107. doi:10.1056/NEJMoa1801174

Sekimoto, T., Koba, S., Mori, H., Sakai, R., Arai, T., Yokota, Y., et al. (2021). Small dense low-density lipoprotein cholesterol: A residual risk for rapid progression of non-culprit coronary lesion in patients with acute coronary syndrome. *J. Atheroscler. Thromb.* 28 (11), 1161–1174. doi:10.5551/jat.60152

Shen, H., Xu, L., Lu, J., Hao, T., Ma, C., Yang, H., et al. (2015). Correlation between small dense low-density lipoprotein cholesterol and carotid artery intima-media thickness in a healthy Chinese population. *Lipids Health Dis.* 14 (1), 137. doi:10.1186/s12944-015-0143-x

Siasos, G., Sara, J. D., Zaromytidou, M., Park, K. H., Coskun, A. U., Lerman, L. O., et al. (2018). Local low shear stress and endothelial dysfunction in patients with nonobstructive coronary atherosclerosis. *J. Am. Coll. Cardiol.* 71 (19), 2092–2102. doi:10.1016/j.jacc.2018.02.073

Siddiqui, M. S., van Natta, M. L., Connelly, M. A., Vuppalanchi, R., Neuschwander-Tetri, B. A., Tonascia, J., et al. (2020). Impact of obeticholic acid on the lipoprotein profile in patients with non-alcoholic steatohepatitis. *J. Hepatol.* 72 (1), 25–33. doi:10.1016/j.jhep.2019.10.006

Siekmeier, R., Steffen, C., and März, W. (2007). Role of oxidants and antioxidants in atherosclerosis: Results of *in vitro* and *in vivo* investigations. *J. Cardiovasc. Pharmacol. Ther.* 12 (4), 265–282. doi:10.1177/1074248407299519

Sniderman, A. D., De Graaf, J., and Couture, P. (2012). Low-density lipoprotein-lowering strategies: Target versus maximalist versus population percentile. *Curr. Opin. Cardiol.* 27 (4), 405–411. doi:10.1097/hco.0b013e328353fed5

Sniderman, A. D., Kiss, R. S., Reid, T., Thanassoulis, G., and Watts, G. F. (2017). Statins, PCSK9 inhibitors and cholesterol homeostasis: A view from within the hepatocyte. *Clin. Sci. (Lond.)* 131 (9), 791–797. doi:10.1042/cs20160872

Sniderman, A. D., Navar, A. M., and Thanassoulis, G. (2022). Apolipoprotein B vs low-density lipoprotein cholesterol and non-high-density lipoprotein cholesterol as the primary measure of apolipoprotein B lipoprotein-related risk. The debate is over. *JAMA Cardiol.* 7 (3), 257–258. doi:10.1001/jamacardio.2021.5080

Sniderman, A. D., Thanassoulis, G., Glavinovic, T., Navar, A. M., Pencina, M., Catapano, A., et al. (2019). Apolipoprotein B particles and cardiovascular disease: A narrative review. *JAMA Cardiol.* 4 (12), 1287–1295. doi:10.1001/jamacardio.2019.3780

Sniderman, A., and Kwiterovich, P. O. (2013). Update on the detection and treatment of atherogenic low-density lipoproteins. *Curr. Opin. Endocrinol. Diabetes Obes.* 20 (2), 140–147. doi:10.1097/MED.0b013e32835ed9cb

Sun, H. Y., Chen, S. F., Lai, M. D., Chang, T. T., Chen, T. L., Li, P. Y., et al. (2010). Comparative proteomic profiling of plasma very-low-density and low-density lipoproteins. *Clin. Chim. Acta.* 411 (5-6), 336–344. doi:10.1016/j.cca.2009.11.023

Teng, B., Thompson, G. R., Sniderman, A. D., Forte, T. M., Krauss, R. M., and Kwiterovich, P. O. (1983). Composition and distribution of low density lipoprotein fractions in hyperapobetalipoproteinemia, normolipidemia, and familial hypercholesterolemia. *Proc. Natl. Acad. Sci. U. S. A.* 80 (21), 6662–6666. doi:10.1073/pnas.80.21.6662

Toledo, F., Sniderman, A., and Kelley, D. (2006). Influence of hepatic steatosis (fatty liver) on severity and composition of dyslipidemia in type 2 diabetes. *Diabetes Care* 29, 1845–1850. doi:10.2337/dc06-0455

Toth, P. P. (2010). Drug treatment of hyperlipidaemia: A guide to the rational use of lipid-lowering drugs. *Drugs* 70 (11), 1363–1379. doi:10.2165/10898610-000000000-00000

Vekic, J., Zeljkovic, A., Cicero, A. F. G., Janez, A., Stoian, A. P., Sonmez, A., et al. (2022). Atherosclerosis development and progression: The role of atherogenic small, dense LDL. *Med. Kaunas.* 58 (2), 299. doi:10.3390/medicina58020299

Visseren, F. L. J., Mach, F., Smulders, Y. M., Carballo, D., Koskinas, K. C., Bäck, M., et al. (2021). 2021 ESC guidelines on cardiovascular disease prevention in clinical practice. *Eur. Heart J.* 42 (34), 3227–3337. doi:10.1093/eurheartj/ehab484

Waiz, M., Alvi, S. S., and Khan, M. S. (2022). Potential dual inhibitors of PCSK-9 and HMG-R from natural sources in cardiovascular risk management. *Excli J.* 21, 47–76. doi:10.17179/excli2021-4453

Who (2021). Cardiovascular diseases (CVDs). Available at: https://www.who.int/en/news-room/fact-sheets/detail/cardiovascular-diseases-(cvds.

Wong, N. D., Zhao, Y., Quek, R. G. W., Blumenthal, R. S., Budoff, M. J., Cushman, M., et al. (2017). Residual atherosclerotic cardiovascular disease risk in statin-treated adults: The Multi-Ethnic Study of Atherosclerosis. *J. Clin. Lipidol.* 11 (5), 1223–1233. doi:10.1016/j.jacl.2017.06.015

Wu, L., Bamberger, C., Waldmann, E., Stark, R., Henze, K., and Parhofer, K. (2017). The effect of PCSK9 inhibition on LDL-subfractions in patients with severe LDL-hypercholesterolemia. *J. Am. Coll. Cardiol.* 69, 1719. doi:10.1016/S0735-1097(17)35108-2

Yee, M. S., Pavitt, D. V., Tan, T., Venkatesan, S., Godsland, I. F., Richmond, W., et al. (2008). Lipoprotein separation in a novel iodixanol density gradient, for composition, density, and phenotype analysis. *J. Lipid Res.* 49 (6), 1364–1371. doi:10.1194/jlr.D700044-JLR200

Yeo, J., and Shahidi, F. (2021). Riboflavin-sensitized photooxidation of low-density-lipoprotein (LDL) cholesterol: A culprit in the development of cardiovascular diseases (CVDs). *J. Agric. Food Chem.* 69 (14), 4204–4209. doi:10.1021/acs.jafc.0c08088

Yoshida, H. (2010). Front line of oxidized lipoproteins: Role of oxidized lipoproteins in atherogenesis and cardiovascular disease risk. *Rinsho Byori.* 58 (6), 622–630.

Yoshida, H., and Kisugi, R. (2010). Mechanisms of LDL oxidation. *Clin. Chim. Acta.* 411 (23-24), 1875–1882. doi:10.1016/j.cca.2010.08.038

Young, S. G. (1990). Recent progress in understanding apolipoprotein B. *Circulation* 82 (5), 1574–1594. doi:10.1161/01.cir.82.5.1574

Zhang, B. H., Yin, F., Qiao, Y. N., and Guo, S. D. (2022). Triglyceride and triglyceride-rich lipoproteins in atherosclerosis. *Front. Mol. Biosci.* 9, 909151. doi:10.3389/fmolb.2022.909151

Zhang, Y., Xu, R. X., Li, S., Zhu, C. G., Guo, Y. L., Sun, J., et al. (2015). Association of plasma small dense LDL cholesterol with PCSK9 levels in patients with angiographically proven coronary artery disease. *Nutr. Metab. Cardiovasc. Dis.* 25 (4), 426–433. doi:10.1016/j.numecd.2015.01.006

Glossary

Apo B apolipoprotein B
ASCVD atherosclerotic cardiovascular disease
CAD coronary artery disease
CE cholesterol ester
CETP cholesteryl ester transfer protein
CHD coronary heart disease
CVD cardiovascular disease
FPLC fast protein liquid chromatography
GGE gradient gel electrophoresis
HDL high-density lipoprotein
HPLC high-performance liquid chromatography
HPSG heparan sulfate proteoglycan
IDL intermediate density lipoprotein
IMT intima media thickness
LDL low-density lipoprotein
LDL-C low-density lipoprotein cholesterol
LDL-P low-density lipoprotein particle
LDLR low-density lipoprotein receptor
LOX1 lectin-like ox-LDL receptor
LRP-1 low-density lipoprotein receptor-related protein 1
MTP microsomal triglyceride transfer protein
NADPH nicotinamide adenine dinucleotide phosphate
NMR nuclear magnetic resonance
ox-LDL oxidized low-density lipoprotein
PCSK9 proprotein convertase subtilsin/kexin type 9
PCSK9i proprotein convertase subtilsin/kexin type 9 inhibitor
ROS reactive oxygen species
sdLDL small dense low-density lipoprotein;
siRNA small interfering RNA
TG triglyceride
VLDL very low-density lipoprotein
WHO World Health Organization
2D-GE two-dimensional gel electrophoresis

Advantages of publishing in Frontiers

OPEN ACCESS
Articles are free to read for greatest visibility and readership

FAST PUBLICATION
Around 90 days from submission to decision

HIGH QUALITY PEER-REVIEW
Rigorous, collaborative, and constructive peer-review

TRANSPARENT PEER-REVIEW
Editors and reviewers acknowledged by name on published articles

Frontiers
Avenue du Tribunal-Fédéral 34
1005 Lausanne | Switzerland

Visit us: www.frontiersin.org
Contact us: frontiersin.org/about/contact

REPRODUCIBILITY OF RESEARCH
Support open data and methods to enhance research reproducibility

DIGITAL PUBLISHING
Articles designed for optimal readership across devices

FOLLOW US
@frontiersin

IMPACT METRICS
Advanced article metrics track visibility across digital media

EXTENSIVE PROMOTION
Marketing and promotion of impactful research

LOOP RESEARCH NETWORK
Our network increases your article's readership